Frascati Physics Series Vol. XXVIII (2002), pp.003-016
HQ & L 2002 – Vietri s/m, May 27th - June 1st, 2002

HEAVY FLAVOUR PRODUCTION

Paolo Nason
INFN, Sez. di Milano, Milan, Italy

ABSTRACT

Recent progress in Heavy Flavour Production phenomenology are discussed. In particular, the long-standing discrepancy of the Tevatron b production data is considered. It is shown that a better use of e^+e^- data in constraining the effect of fragmentation reduces the discrepancy considerably.

1 Introduction

The phenomenology of heavy flavour production has been so far a mixed success. Although the order of magnitude of the total cross sections, and the shape of differential distribution is reasonably predicted, large discrepancy are present, especially for b production.

The theoretical framework for the description of heavy flavour production is the QCD improved parton model. Besides the well-established NLO correc-

tions to the inclusive production of heavy quark in hadron-hadron [1, 2, 3, 4], hadron-photon [5, 6, 7], and photon-photon collisions [8], much theoretical work has been done in the resummation of contributions enhanced in certain regions of phase space: the Sudakov region, the large transverse momentum region and the small-x region.

The theoretical effort involved is justified by the large variety of applications that heavy quark production physics has, in top, bottom and charm production. Besides the need of modeling these processes, heavy quark production is an important benchmark for testing QCD and parton model ideas, due to the relative complexity of the production process, the large range of masses available, and the existence of different production environments, like e^+e^- annihilation, hadron, photon-hadron and photon-photon collisions.

2 Total cross section for top and bottom

Top production [9, 10] has been a most remarkable success of the theoretical model. The measured cross section has been found in good agreement with theoretical calculations, as shown in fig. 1. Resummation of soft gluon effects

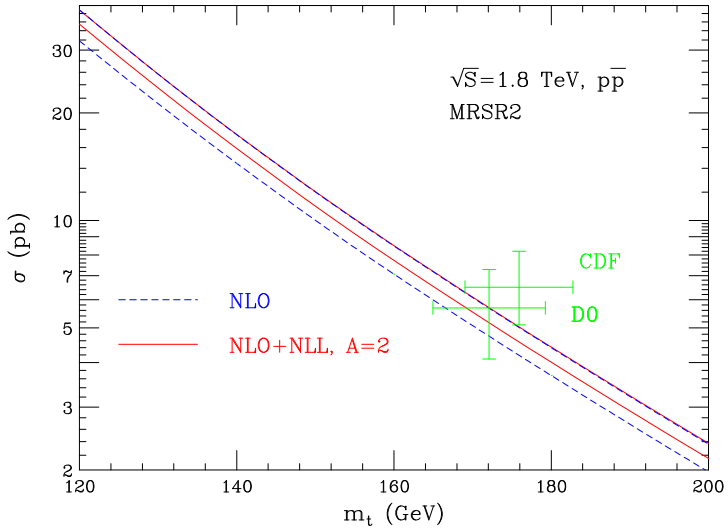

Figure 1: *Results on top cross sections at the Tevatron.*

[11] reduces the theoretical uncertainty in the cross section, pushing it toward the high side of the theoretical band. It remains, however, inside the theoretical band of the fixed order calculation, thus showing consistency with the estimated error.

Recently, the HERA-B experiment has provided a new measurement of the $b\bar{b}$ total cross section [12]. Their result is in good agreement with previous findings [13, 14]. This experiment is sensitive to the moderate transverse momentum region, where the bulk of the total cross section is concentrated. Since the production is (in a certain sense) close to threshold, resummation of Sudakov effects is useful also in this case. A comparison of the HERA-b

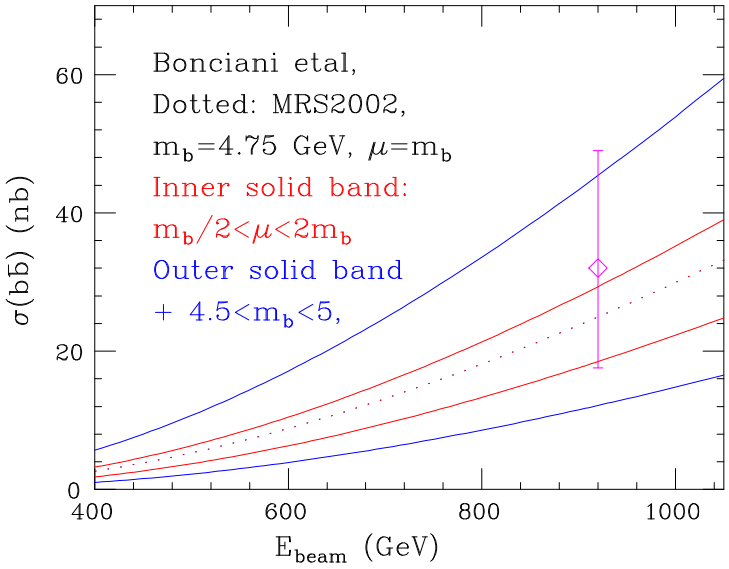

Figure 2: *$b\bar{b}$ total cross section versus theoretical predictions, including resummation of soft gluons.*

measurement with a theoretical calculation is shown in fig. 2. The HERA-b result is compatible with the central value prediction, with the b pole mass around 4.75 GeV. Higher precision may constrain further the b quark mass.

3 Differential distributions

CDF has a longstanding disagreement with QCD in b production. A very recent publication of the B^+ differential cross section [15] has quantified the disagreement as a factor of $2.9 \pm 0.2 \pm 0.4$ in the ratio of the measured cross section over the theoretical prediction. This discrepancy has been present since a long time, and it has been observed both in CDF and D0. Some authors [16] have argued that the discrepancy could be interpreted as a signal for Supersimmetry.

Because of the large theoretical uncertainties, this discrepancy has been often downplayed. In fact, several effects may conspire to raise the b cross section to an appropriate value. It was early recognized that small-x effects may be important in b production at the Tevatron [1]. Resummation of these effects [17, 18] leads to an increase of the cross section of the order of 30%. Threshold effects are small in this case [11], being below 15%, but they are nevertheless positive. Resummation of large $\log p_{\mathrm{T}}$ yields an increase in the p_{T} spectrum of the order of 20% in the intermediate p_{T} region [19]. The presence of many possible enhancements should not lead, however, to excessive optimism. First of all, it is not clear whether these effect can be added up without overcounting. Furthermore, they are all higher order effects, and thus should not push the cross section too far out of the theoretical band, which includes estimates of unknown higher order effects.

It has been observed since some time that an improper understanding of fragmentation effects may be one of the causes of the Tevatron discrepancy. This possibility stems from the fact that b quark cross sections are in reasonable agreement with the Tevatron measurements of the B meson spectrum, while the cross section obtained by applying a standard fragmentation function of the Peterson form [20] with $\epsilon = 0.006$ to the quark cross section yields too soft a spectrum, as can be seen in fig. 3. In ref. [21] it was suggested to study b quark jets rather than B meson's distributions. In fact, the jet momentum should be less sensitive to fragmentation effects than the hadron momentum. A D0 study [22] has demonstrated that by considering b jets instead of B hadrons the agreement between theory and data improves considerably (see fig. 4).

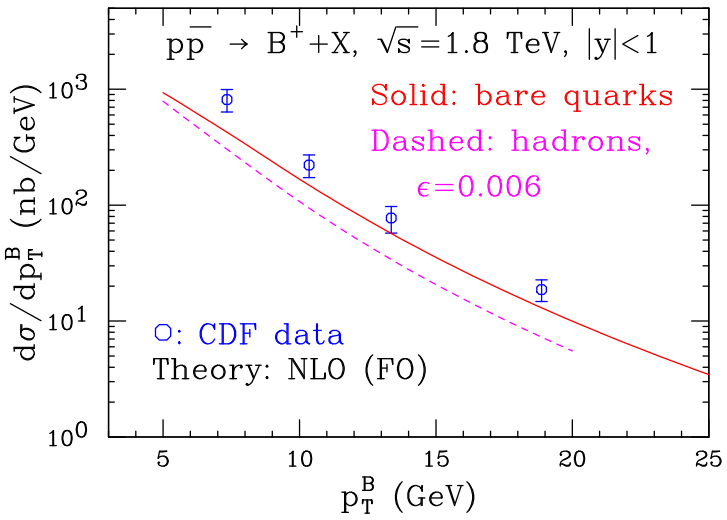

Figure 3: *Quark versus Hadron differential cross section compared to CDF data. The Hadron cross section is obtained by convoluting the quark cross section with a Peterson fragmentation function, with* $\epsilon = 0.006$.

4 Fragmentation

If fragmentation effects are so important, they should be assessed very carefully before claiming a discrepancy with data. Non-perturbative fragmentation is usually introduced by writing the hadron-level cross section for B mesons as

$$\frac{d\sigma^B}{dp_{\rm T}} = \int d\hat{p}_{\rm T} dz \frac{d\sigma^b}{d\hat{p}_{\rm T}} D(z)\, \delta(p_{\rm T} - z\hat{p}_{\rm T}) \,, \tag{1}$$

where $p_{\rm T}$ is the hadron, and $\hat{p}_{\rm T}$ is the quark transverse momentum. Traditionally, $D(z)$ is given by the Peterson form [20]

$$D(z) \propto \frac{z(1-z)^2}{((1-z)^2 + \epsilon z)^2} \,. \tag{2}$$

Strictly speaking, this procedure is justifiable only in the limit of large transverse momenta (i.e. $p_T \gg m_b$). It can however be consider a rough model of the effect of fragmentation at moderate and small transverse momenta, as long

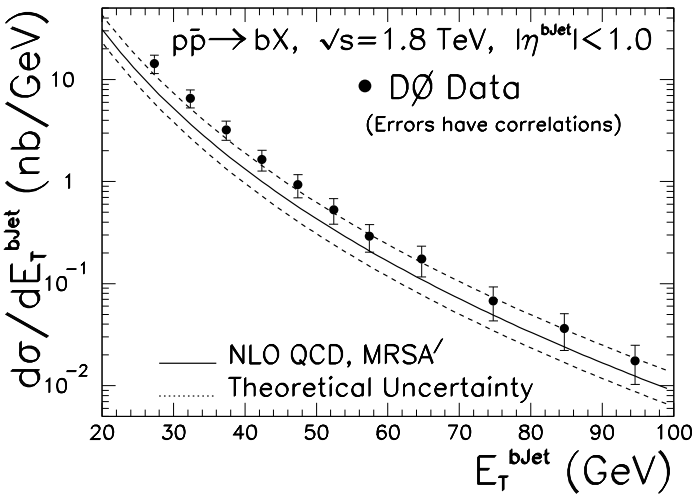

Figure 4: *D0 b-jet data compared with the calculation of ref.* [21].

as the variable z is referred to the momentum or the kinetic energy, rather than the energy or the + component, of the quark momentum.

Eq. (2) is often used with $\epsilon = 0.006$ for bottom and $\epsilon = 0.06$ for charm, in conjunction with shower Montecarlo programs. These values of ϵ were obtained from fits to inclusive heavy flavour production distributions in e^+e^- collisions. The shower Montecarlo accounts for hard fragmentation effects (i.e. hard gluon radiation), where hard means from the typical transverse momentum of the process down to some cutoff, of the order of the hadron mass. This accounts for scaling violation in the inclusive cross section for the production heavy quarks[1].

It has become common practice to adopt the value $\epsilon = 0.006$ also in conjunction with NLO calculations of b production cross sections. This practice is not totally justified, since the procedure used to obtain this value of ϵ does not

[1]The inclusive cross section for single particle production in e^+e^- collisions is sometimes also called fragmentation function, which is often a source of confusion

match the accuracy of the NLO calculation. A better approach is possible; one can use NLL resummation of transverse momentum logarithms in the context of e^+e^- data in order to extract an appropriate non-perturbative fragmentation function, and supplement NLO heavy flavour production calculations with NLL resummation, in order to correctly account for scaling violation. The theoretical tools to do this are in fact available in the literature:

1 Single inclusive particle production in hadronic collisions [23]. Single hadron production are described in term of NLO single parton cross section convoluted with a NLL fragmentation function;

2 Heavy quark Fragmentation Function [24]; a method for the computation of the heavy quark fragmentation function at all orders in perturbation theory is developed, and applied at NLL. Several applications in e^+e^- physics have appeared [25, 26, 27, 28].

3 Single inclusive heavy quark production at large p_T [29]; item 1 and 2 are combined to give a NLL resummation of transverse momentum logarithms in heavy quark production;

4 FONLL calculation of single inclusive heavy quark production; item 3 is merged without overcounting with standard NLO calculations. This procedure has been implemented both in hadroproduction [19] and in photoproduction [30, 31].

When using these ingredients, it was found that the CDF discrepancy is considerably reduced [32]. It can be quantified as a factor of 1.7 ± 0.5 (theory) $\pm$ 0.5 (expt). Reduction in the discrepancy is due to four basic points:

1 FONLL calculation brings about a 20% increase in the intermediate p_T region.

2 The fragmentation step for going from a "perturbative" b quark to a B hadron seems to be too strong at small p_T in the CDF implementation. We get a 20% increase in the small p_T region.

3 A Peterson fragmentation function with $\epsilon = 0.006$ is too soft (present e^+e^- data favour values around 0.002); this is a 20% effect.

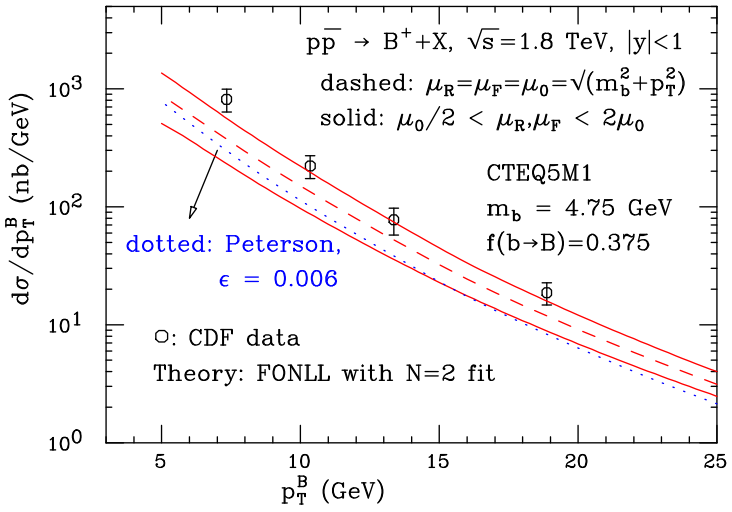

Figure 5: *Comparison of CDF data with the calculation of ref.* [32].

4 A more accurate use of e^+e^- input data on the fragmentation function, described in the following section, brings about another 20% effect.

The net effect is $1.2^3 = 1.7$ and $2.9/1.7 = 1.7$, so that the 2.9 CDF discrepancy becomes our 1.7.

5 A better use of e^+e^- data on b fragmentation

$D(z)$ is extracted from fits to e^+e^- data. One has

$$\underbrace{\frac{d\sigma(e^+e^- \to B+X)}{dp}}_{\text{measured}} = \int d\hat{p}\, dz\, \underbrace{\frac{d\sigma(e^+e^- \to b+X)}{d\hat{p}}}_{\text{computed}} \underbrace{D(z)}_{\text{fitted}}\, \delta(p - z\hat{p}) \qquad (3)$$

From the above equation it is easy to show that

$$\langle x_B^{N-1} \rangle = \langle x_b^{N-1} \rangle\, D_N \qquad (4)$$

where

$$x_B = \frac{p}{p_{\max}}, \qquad x_b = \frac{\hat{p}}{\hat{p}_{\max}}, \qquad D_N = \int dz z^{N-1} D(z). \qquad (5)$$

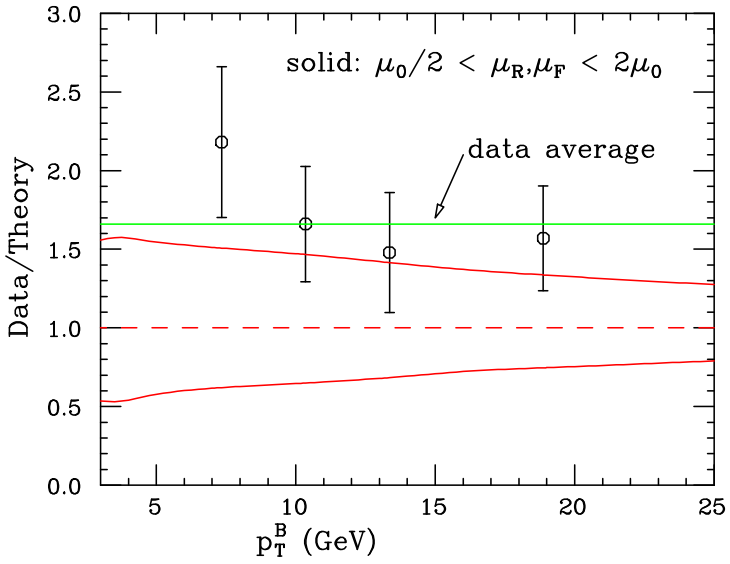

Figure 6: *As in fig. 5, ratios of data to theory.*

It turns out that for the computation of the hadronic cross sections, only the first few moments of the fragmentation function are important. This follows from the fact that the heavy quark hadroproduction cross section is a steeply falling function of the transverse momentum, following roughly a power law. Assuming the form

$$\frac{d\sigma(H_1H_2 \to b + X)}{d\hat{p}_T} \approx A\hat{p}_T^{-n} \tag{6}$$

one finds

$$\frac{d\sigma(H_1H_2 \to b + X)}{dp_T} \approx \int dz d\hat{p}_T\, D(z)\frac{A}{\hat{p}_T^n}\,\delta(p_T - z\hat{p}_T) = \frac{A}{p_T^n}D_n = \frac{d\sigma}{d\hat{p}_T}D_n\ . \tag{7}$$

This simple fact was noticed long ago [33, 34]. The exponent n ranges from 3 to 5 in hadronic collisions. In ref. [34] it was shown that eq. (7) is also an excellent approximation to the exact convolution.

When fitting the non-perturbative fragmentation function from e^+e^- data, the low moments relevant for hadroproduction are not well fitted. The Peterson form with $\epsilon = 0.002$ gives a good fit to the shape of the inclusive

cross section, but not to the moments. For the purpose of predicting hadronic cross section it is instead better to make sure that the first few moments are accurately fitted. In fig. 7, it is shown that a fit to the second moment alone with the simple form $x(1-x)^\beta$, yields a good fit to all moments in the interesting region (i.e. between 3 and 5). We also notice that the second moment fit ($N = 2$ fit from now on), the $\epsilon = 0.002$ and the $\epsilon = 0.006$ fits differ by 20% around the $N = 4$ moment.

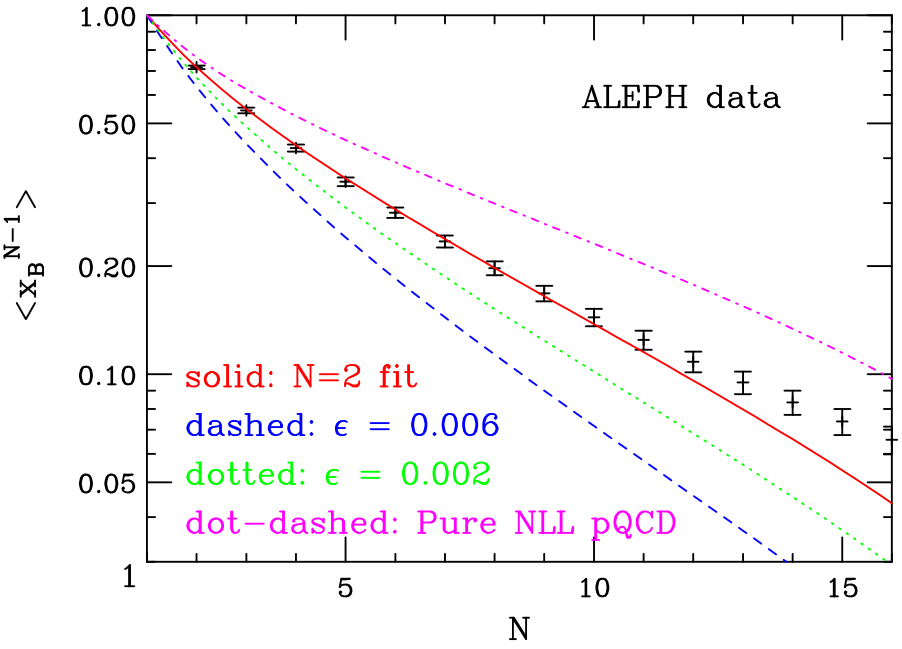

Figure 7: The measured $\langle x_B^{N-1} \rangle$, compared with the perturbative NLL calculation supplemented with different non-perturbative fragmentation forms. The solid line is obtained using a one-parameter form fitted to the second moment.

The reason why x fits do not yield good fits to moments is easy to explain. The large x region in the inclusive production of heavy flavoured hadrons in e^+e^- annihilation is a very difficult region to model. It is in fact affected by large perturbative (i.e. Sudakov) and non-perturbative effects. It is unlikely that the simple forms used commonly for the non-perturbative fragmentation

function can accurately model these complex effects. Thus, the large x region is usually excluded from the fits. On the other hand, this region is the most important one for moments.

From fig. 7, another important fact becomes apparent. When using NLL calculations for the perturbative part of the fragmentation function, the importance of the non-perturbative effects on moments is greatly reduced. This can be taken as an indication of the fact that the heavy quark fragmentation function is, to a considerable extent, perturbatively calculable.

6 Other B production data

The procedure of ref. [32] may affect other b production data at hadron colliders. Here I consider, as an example, the inclusive muon cross section in the central and forward region, where the muons come from the semileptonic decays of the b flavoured hadrons. These distributions were measured by the D0 [35] experiment, and found to be higher than theoretical prediction by up to a factor of 4 in the forward region. The result of the calculation performed with the method of ref. [32] is reported in fig. 8. As one can see, the agreement with data is now quite remarkable.

7 Conclusions

The theory of heavy flavour production seems to give a good qualitative description of the available data. In the case of top production, the comparison between theory and experiment is satisfactory also at a quantitative level.

Recent progress has taken place in the field of b hadroproduction. The HERA-b experiment has provided a cross section for b production at relatively low CM energy. Some progress in understanding the role of fragmentation has considerably reduced the longstanding problem of the b momentum spectrum at the Tevatron.

Major problems do remain in the (perhaps less developed) areas of bottom production in $\gamma\gamma$ and γp collisions. A discussion of these problems is given in ref. [36].

References

1. P. Nason, S. Dawson and R. K. Ellis, *Nucl. Phys.* **B303** (1988) 607.

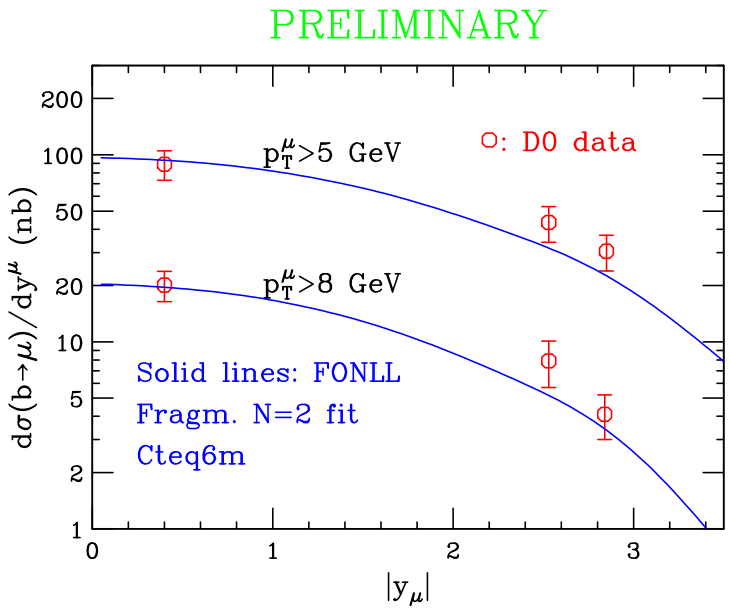

Figure 8: *D0 forward muon data compared with a calculation performed using the method of ref.* [32].

2. P. Nason, S. Dawson and R. K. Ellis, *Nucl. Phys.* **B327** (1989) 49–92.

3. W. Beenakker, W. L. van Neerven, R. Meng, G. A. Schuler and J. Smith, *Nucl. Phys.* **B351** (1991) 507–560.

4. M. L. Mangano, P. Nason and G. Ridolfi, *Nucl. Phys.* **B373** (1992) 295–345.

5. R. K. Ellis and P. Nason, *Nucl. Phys.* **B312** (1989) 551.

6. J. Smith and W. L. van Neerven, *Nucl. Phys.* **B374** (1992) 36–82.

7. S. Frixione, M. L. Mangano, P. Nason and G. Ridolfi, *Nucl. Phys.* **B412** (1994) 225–259, `hep-ph/9306337`.

8. M. Drees, M. Kramer, J. Zunft and P. M. Zerwas, *Phys. Lett.* **B306** (1993) 371–378.

9. **CDF** Collaboration, T. Affolder *et. al.*, *Phys. Rev.* **D64** (2001) 032002, hep-ex/0101036.

10. **D0** Collaboration, V. M. Abazov *et. al.*, hep-ex/0205019.

11. R. Bonciani, S. Catani, M. L. Mangano and P. Nason, *Nucl. Phys.* **B529** (1998) 424–450, hep-ph/9801375.

12. **HERA-B** Collaboration, I. Abt *et. al.*, hep-ex/0205106.

13. D. M. Jansen *et al.*, Phys. Rev. Lett. **74** (1995) 3118.

14. T. Alexopoulos *et al.* [E771 Collaboration], Phys. Rev. Lett. **82** (1999) 41.

15. **CDF** Collaboration, D. Acosta *et. al.*, *Phys. Rev.* **D65** (2002) 052005, hep-ph/0111359.

16. E. L. Berger *et. al.*, *Phys. Rev. Lett.* **86** (2001) 4231–4234, hep-ph/0012001.

17. S. Catani, M. Ciafaloni and F. Hautmann, *Nucl. Phys.* **B366** (1991) 135–188.

18. J. C. Collins and R. K. Ellis, *Nucl. Phys.* **B360** (1991) 3–30.

19. M. Cacciari, M. Greco and P. Nason, *JHEP* **05** (1998) 007, hep-ph/9803400.

20. C. Peterson, D. Schlatter, I. Schmitt and P. M. Zerwas, *Phys. Rev.* **D27** (1983) 105.

21. S. Frixione and M. L. Mangano, *Nucl. Phys.* **B483** (1997) 321–338, hep-ph/9605270.

22. **D0** Collaboration, B. Abbott *et. al.*, *Phys. Rev. Lett.* **85** (2000) 5068–5073, hep-ex/0008021.

23. F. Aversa, M. Greco, P. Chiappetta and J. P. Guillet, *Phys. Rev. Lett.* **65** (1990) 401–403.

24. B. Mele and P. Nason, *Nucl. Phys.* **B361** (1991) 626–644.

25. G. Colangelo and P. Nason, *Phys. Lett.* **B285** (1992) 167–171.

26. M. Cacciari, M. Greco, S. Rolli and A. Tanzini, *Phys. Rev.* **D55** (1997) 2736–2740, `hep-ph/9608213`.

27. M. Cacciari and M. Greco, *Phys. Rev.* **D55** (1997) 7134–7143, `hep-ph/9702389`.

28. P. Nason and C. Oleari, *Nucl. Phys.* **B565** (2000) 245–266, `hep-ph/9903541`.

29. M. Cacciari and M. Greco, *Nucl. Phys.* **B421** (1994) 530–544, `hep-ph/9311260`.

30. M. Cacciari, S. Frixione and P. Nason, *JHEP* **03** (2001) 006, `hep-ph/0102134`.

31. S. Frixione and P. Nason, *JHEP* **03** (2002) 053, `hep-ph/0201281`.

32. M. Cacciari and P. Nason, `hep-ph/0204025`.

33. S. Frixione, M. L. Mangano, P. Nason and G. Ridolfi, *Adv. Ser. Direct. High Energy Phys.* **15** (1998) 609–706, `hep-ph/9702287`.

34. P. Nason *et. al.*, "Bottom Production", in the "1999 CERN Workshop on Standard Model Physics (and more) at the LHC", CERN, Geneva, Switzerland, 25 - 26 May 1999 - CERN, Geneva, 2000, [CERN-2000-004] - pp.231-304 (1999), `hep-ph/0003142`.

35. **D0** Collaboration, B. Abbott *et. al.*, *Phys. Rev. Lett.* **84** (2000) 5478–5483, `hep-ex/9907029`.

36. P. Nason, Invited talk at 20th International Symposium on Lepton and Photon Interactions at High Energies (LP 01), Rome, Italy, 23-28 Jul 2001, `hep-ph/0111024`.

Frascati Physics Series Vol. XXVIII (2002), pp.017-030
HQ & L 2002 – Vietri s/m, May 27th - June 1st, 2002

BEAUTY, CHARM AND HYPERON PRODUCTION AT FIXED-TARGET EXPERIMENTS

Erik E. Gottschalk
Fermilab, P.O. Box 500, Batavia, IL 60510, USA

ABSTRACT

Over the years fixed-target experiments have performed numerous studies of particle production in strong interactions. The experiments have been performed with different types of beam particles of varying energies, and many different target materials. Since the physics of particle production is still not understood, ongoing research of phenomena that we observe as beauty, charm and strange-particle production is crucial if we are to gain an understanding of these fundamental processes. It is in this context that recent results from fixed-target experiments on beauty, charm, and hyperon production will be reviewed.

1 Introduction

Fixed-target experiments have a long history that covers a broad spectrum of physics research. One area of research that has received considerable attention

for the past 50 years is particle production in strong interactions. In its infancy, the research was based on cosmic-ray data. Shortly thereafter fixed-target experiments began to study strange-particle production, followed by studies of charm and beauty production in later years. The research continues today, since an understanding of the underlying production mechanisms remains elusive.

Quantum chromodynamics (QCD) is widely accepted as the correct description of the strong interaction. The properties of strong interactions that involve hard processes, which are associated with large momentum transfer, can be calculated in QCD using perturbation theory. Perturbative QCD is applicable to beauty production in fixed-target experiments, however, the experiments are challenged by relatively low beauty production cross sections. Perturbative QCD is also applicable to charm production. Here theoretical calculations are plagued by larger uncertainties (compared to beauty production), while experiments have acquired large charm samples that have been, and continue to be, used to study different aspects of charm production. The studies often focus on effects that appear to fall outside the realm of perturbative QCD, thereby making theoretical interpretations more difficult. However, it is noteworthy that non-perturbative effects in charm production have remarkable similarities to effects observed in hyperon production. Perhaps the similarities and differences observed in studies of beauty, charm, and strange-particle production can be exploited more effectively to gain a better understanding of the underlying production mechansims.

2 Overview of Experiments and Results

Table 1 lists fixed-target experiments with results that are relevant for this conference. The table shows that the experiments cover a range of beam energies, use a variety of beam particles, and use many different target materials.

Results that are included for this conference are recent results that are unpublished or were published after the last *Heavy Quarks at Fixed Target* conference, held in Rio de Janeiro, 9-12 October 2000. The unpublished results are being prepared for publication. One of these results reports a possible observation of doubly-charmed baryons by SELEX. The SELEX result that was presented at this conference is based on an earlier analysis of SELEX data, while a new result from an updated analysis was presented a few days later at Fermilab. In this paper, the more recent SELEX result will be presented.

Table 1: *Overview of Fixed-Target Experiments*

Experiment	p_{beam} (GeV/c)	Beam	Target
HERA-B	920	p	C, Al, Ti, W
E690	800	p	LH_2
E771	800	p	Si
E866/NuSea E789 and E772	800	p	LH_2, LD_2, C, Ca, Fe, W, Ag, Au, and Cu dump
E769	250	$\pi^{\pm}$, $K^{\pm}$, p	Be, Al, Cu, and W
E781/SELEX	600	Σ^- and π^-	C and Cu
	572	p	C and Cu
E791	500	π^-	C and Pt
E687	220	γ	Be
E831/FOCUS	170	γ	BeO and Si
E835	<8.9	$\overline{p}$	hydrogen gas jet
WA89	340	Σ^- and π^-	C and Cu
	260	n	C and Cu

The measurements that are presented here are arranged by topic as follows:

- $\sigma(b\overline{b})$ cross section measurement
- bottomonium polarization
- kinematic correlations in charm-pair events
- observation of doubly-charmed baryons
- asymmetry measurements comparing particle/antiparticle production
- hyperon production (asymmetries, kinematic correlations, polarization)

Topics that have not been included are measurements of the A-dependence in heavy-quark production, charm production with neutrinos (see Pasquale Migliozzi's contribution to the conference), and a recent measurement [1)] of the mass and width of the χ_{c0} from experiment E835 (see Matteo Negrini's contribution to the conference). Results that are presented in this paper are arranged by flavor starting with beauty, then charm, and ending with results on hyperon production.

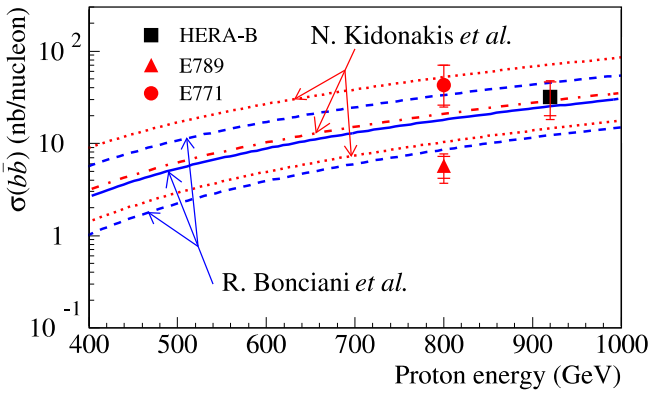

Figure 1: *HERA-B $\sigma(b\bar{b})$ measurement compared to measurements from E771 and E789, and theoretical predictions from R. Bonciani et al.* [5] *updated with the NNLL parton distribution function in* [7] *(solid line: central value, dashed lines: upper and lower bounds) and N. Kidonakis et al.* [6] *(dot-dashed line: central value, dotted lines: upper and lower bounds).*

3 Beauty Production

Measurements of beauty production continue to be a challenge for fixed-target experiments. Despite large theoretical and experimental uncertainties, the measurements are important in that they probe heavy quark production in a regime where perturbative QCD calculations are applicable. Results on beauty production from two experiments are presented here. The first is a preliminary measurement of the $b\bar{b}$ production cross section from HERA-B, the second is a published result on bottomonium polarization from NuSea.

Measuring $\sigma(b\bar{b})$ in a fixed-target experiment is a challenge. HERA-B measures the cross section for 920 GeV proton-nucleus interactions by placing wire targets in the halo of the HERA proton beam. For this measurement, HERA-B reconstructs $J/\psi \to \mu^+\mu^-$ and $J/\psi \to e^+e^-$ decay vertices. J/ψ's that satisfy detachment cuts with respect to the wire targets are used to determine the number of $b-$hadrons decaying to J/ψ, as distinguished from the large prompt J/ψ background. The background comes from J/ψ production in the targets, and HERA-B uses the background events to normalize $\sigma(b\bar{b})$ relative to prompt J/ψ production measurements from two fixed-target exper-

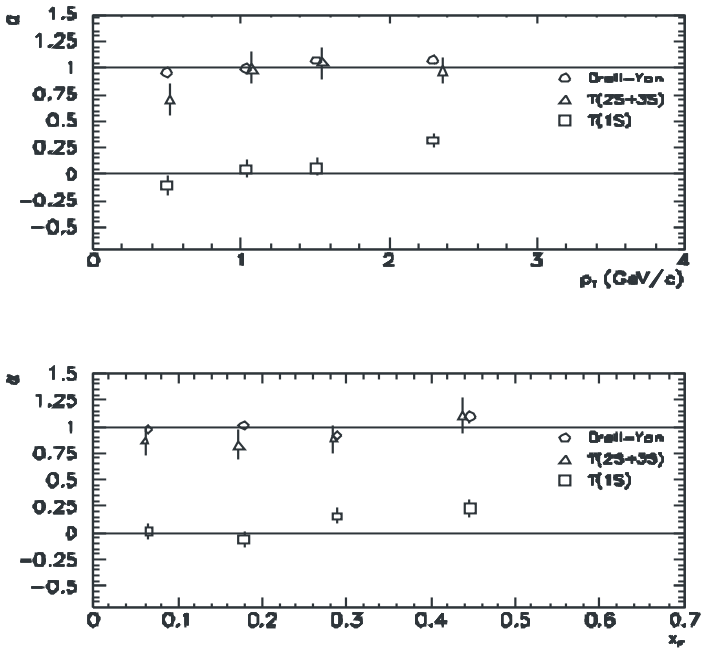

Figure 2: *NuSea data on bottomonium polarization. a) α versus p_T for Drell-Yan sidebands (8.1 < $m_{\mu^+\mu^-}$ < 8.45 GeV and 11.1 < $m_{\mu^+\mu^-}$ < 15.0 GeV), Υ(1S) (8.8 < $m_{\mu^+\mu^-}$ < 10.0 GeV), and Υ(2S+3S) (10.0 < $m_{\mu^+\mu^-}$ < 11.1 GeV). b) α versus x_F for the same mass regions. The error bars show statistical errors only. There is an additional systematic error (not shown) of 0.02 in α for Drell-Yan polarizations, and 0.06 in α for onium polarizations.*

iments [2), 3)]. A correction for the atomic number dependence of the target material is based on a measurement from NuSea [4)].

HERA-B obtains two samples of events, one with 2880 ± 60 $J/\psi \to \mu^+\mu^-$ decays and the other with 5710 ± 380(stat) $\pm$ 280(sys) $J/\psi \to e^+e^-$ decays. The number of events that satisfy detachment cuts are $1.9\ ^{+2.2}_{-1.5}$ and $8.6\ ^{+3.9}_{-3.2}$ for the $\mu^+\mu^-$ and e^+e^- channels, respectively. The two channels are combined in a simultaneous unbinned maximum likelihood fit that is used to obtain the measurement for $\sigma(b\overline{b})$. The result is $32\ ^{+14}_{-12}\ (stat)\ ^{+6}_{-7}\ (sys)$ nb/nucleon, which is shown in Fig. 1 along with the latest QCD calculations [5), 6)] beyond next-to-leading order (NLO). HERA-B has submitted this measurement for publication since the precision of the measurement is comparable to existing measurements

from experiments E771 [8] and E789 [9] (also shown in Fig. 1). In an upcoming run, HERA-B expects to get significantly more data, which will be used to obtain a more precise determination of $\sigma(b\overline{b})$.

The second result on beauty production is a measurement of bottomonium polarization at $\sqrt{s} = 38.8$ GeV from NuSea [10]. The result is compared to predictions from Non-Relativistic Quantum Chromodynamics (NRQCD). This is important to help resolve the issue of color octet contributions to onium production. Fig. 2 shows the NuSea data points as a function of p_T and x_F. The data points for Drell-Yan dimuons are included to show that they are consistent with 100% transverse polarization, as expected for Drell-Yan virtual photons that are produced transversely polarized. The data for $\Upsilon(1S)$ show almost no polarization at small p_T and x_F, which disagrees with an NRQCD calculation [11] that predicts a value of 0.28 to 0.31 averaged over p_T and x_F. The data for $\Upsilon(2S)$ and $\Upsilon(3S)$ are combined in Fig. 2, since NuSea is unable to resolve the two states. The figure shows that the polarization of the cross-section-weighted average of the $2S + 3S$ states is much larger than the polarization of the $1S$ state for all values of p_T and x_F. This is different from polarization measurements in the charmonium system from CDF [12].

4 Charm Production

Studies of charm production benefit from the large data samples that have been collected by several fixed-target experiments. Four new results are presented in this paper. The results come from Fermilab experiments that acquired data during the 1991 fixed-target run, and a subsequent run in 1996-97. In the 1991 run the hadroproduction experiment E791 collected a large charm sample using a 500 GeV/c π^- beam, and a recent publication [13] presents their analysis of Λ_c production asymmetries. A study of Λ_c production asymmetries was also published recently [14] by SELEX, another hadroproduction experiment that ran in 1996-97 with π^-, Σ^-, and proton beams. In addition to studies of Λ_c asymmetries, SELEX may have observed doubly charmed baryons for the first time. The fourth charm production result, on $D\overline{D}$ correlations, comes from FOCUS, a photoproduction experiment that ran with a photon beam that had an average energy of 170 GeV.

FOCUS has extracted a large sample of 7066 ± 119 $D\overline{D}$ events from the data recorded in 1996-97. Each event has two D candidates. Both D candidates

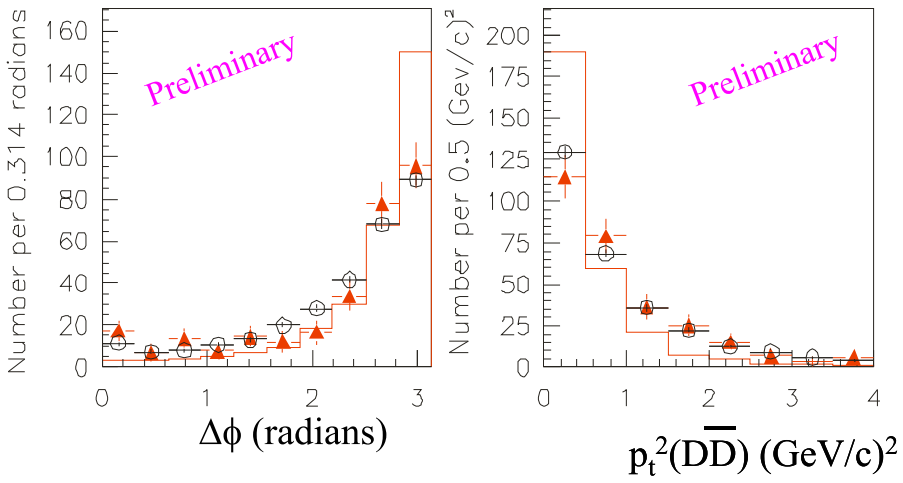

Figure 3: *$D\overline{D}$ correlations for FOCUS data (circles) and E687 data (triangles) compared to PYTHIA version 5.6 (solid line). The plot on the left shows the angle, $\Delta\phi$, between the D and $\overline{D}$ in the plane transverse to the beam, and the plot on the right shows the transverse momentum squared for the $D\overline{D}$ pair.*

are fully reconstructed. The decay modes that are considered for the analysis are $D^0 \to K^-\pi^+$, $D^+ \to K^-\pi^+\pi^+$, $D^0 \to K^-\pi^+\pi^+\pi^-$, and charge conjugate modes. By reconstructing both the D and the $\overline{D}$ in an event, FOCUS is able to study $D\overline{D}$ correlations. Fig. 3 shows $\Delta\phi$, the angle between the D and $\overline{D}$ in the plane transverse to the beam, and the transverse momentum squared for the $D\overline{D}$ pair. These distributions are important with regard to heavy-quark production in QCD [15]. At leading order in QCD the c and $\overline{c}$ quarks are produced back-to-back with $\Delta\phi = 0$ and $p_T(c\overline{c}) = 0$. NLO corrections introduce a broadening of these distributions, but the data tend to disagree with NLO calculations and suggest significant contributions from non-perturbative effects.

Fig. 3 shows a comparison of FOCUS and E687 [16] data compared to PYTHIA version 5.6 [17] with default settings. The FOCUS data, which are preliminary, show good agreement with the published E687 data. Both the FOCUS data and E687 data show a significant discrepancy compared to PYTHIA 5.6, in that PYTHIA distributions are more sharply peaked compared to the data. In Fig. 4 the FOCUS data are compared to a more recent version

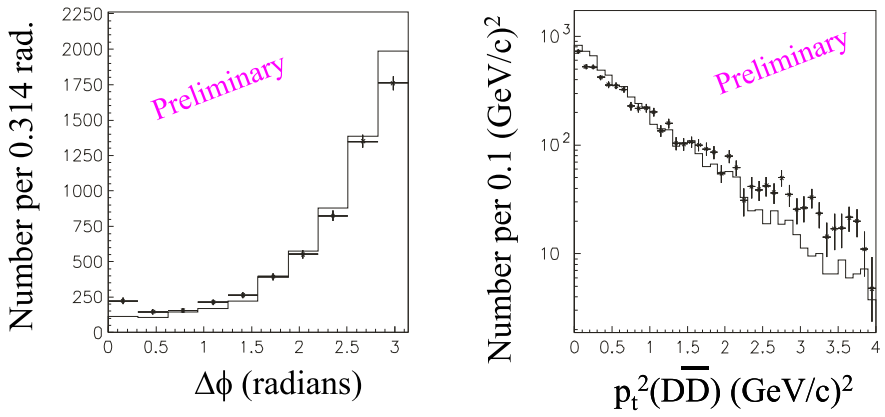

Figure 4: *FOCUS data (points with error bars) compared to PYTHIA version 6.203 (solid line). $\Delta\phi$ is the angle between the D and $\overline{D}$ in the plane transverse to the beam, and p_t^2 is the square of the transverse momentum of the $D\overline{D}$ pair.*

of PYTHIA (version 6.203) [18]. Here the agreement between data and the new version of PYTHIA has improved significantly. One of the reasons for the improvement is that the new version has a larger value for intrinsic k_T in the generator, which introduces a larger transverse momentum for initial partons. However, the new value for intrinsic k_T (PYTHIA 6.203 sets $< k_T^2 > = 1$ GeV^2) does not account for all of the improvement in these comparisons with data, and other changes in PYTHIA are believed to play a role. FOCUS is currently preparing these results for publication.

Another new result that is being prepared for publication is the possible observation of doubly charmed baryons by SELEX. SELEX observes three significant peaks (see Fig. 5) in $\Lambda_c^+ K^- \pi^+$ and $\Lambda_c^+ K^- \pi^+ \pi^+$ mass distributions. The three peaks are believed to be the ccd^+, ccu^{++}, and ccu^{*++} doubly-charmed baryons. One of the questions that has been raised by this analysis with regard to charm production concerns the number of reconstructed Λ_c^+ decays in the SELEX data. The data suggest that about half of all Λ_c^+'s come from the decay of these doubly-charmed baryons. This seems high. For comparison, FOCUS has looked for doubly-charmed baryons and sees no signal [19]. One possible explanation is the higher beam energy in SELEX compared to FOCUS, and another might be that the production of doubly-charmed baryons

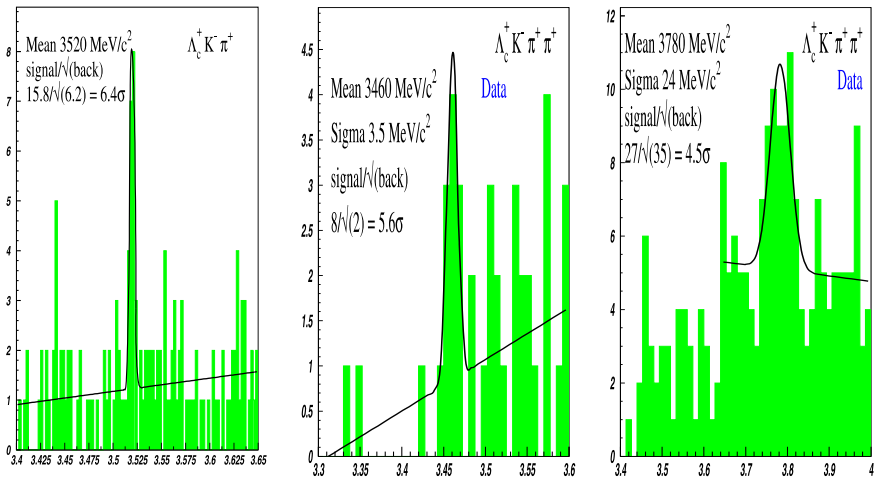

Figure 5: *SELEX invariant mass distributions for* $\Lambda_c^+ K^- \pi^+$ *in the range [3.4, 3.65] GeV (left),* $\Lambda_c^+ K^- \pi^+ \pi^+$ *in the range [3.3, 3.6] GeV (center), and* $\Lambda_c^+ K^- \pi^+ \pi^+$ *in the range [3.4, 4.0] GeV (right).*

is enhanced for a baryon beam, or more specifically a hyperon beam. In either case, if SELEX has observed doubly-charmed baryons, the implications for charm production are significant.

One of the most striking features observed in charm production is the *leading particle effect*. The effect is observed as an enhancement in the production rate of particles that have one or more valence quarks in common with an initial state hadron (either a beam hadron or a target hadron) compared to the corresponding antiparticle production rate. The effect is usually presented as an asymmetry distribution as a function of x_F and p_T^2. For each bin of x_F and p_T^2 the asymmetry parameter A is defined as

$$A \equiv \frac{N - \overline{N}/r}{N + \overline{N}/r}, \qquad r = \frac{\overline{\epsilon}}{\epsilon}, \tag{1}$$

where N ($\overline{N}$) is the number of particles (antiparticles) in the bin, and ϵ ($\overline{\epsilon}$) is an efficiency that accounts for geometrical acceptance, and trigger and reconstruction efficiencies. The leading particle effect is not limited to charm production, since it is also observed in light hadron production (see the next section on

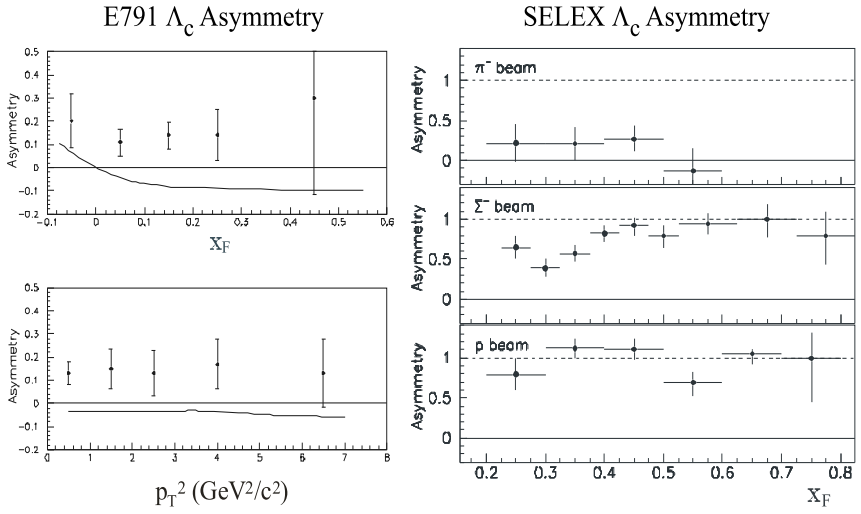

Figure 6: *a) E791 Λ_c asymmetry (data points with error bars) as a function of x_F (top left) and p_T^2 (bottom left) compared to PYTHIA 5.7 (solid lines). b) SELEX Λ_c asymmetry as a function of x_F (shown on the right) for three types of beam particles (top: π^- beam, middle: Σ^- beam, bottom: proton beam).*

hyperon production, for example). However, for charm production the data are compared to next-to-leading-order perturbative QCD calculations. Perturbative QCD predicts that particle/antiparticle asymmetries should be very small. The data, on the other hand, have indicated large asymmetries, which are usually attributed to non-perturbative QCD effects.

Two hadroproduction experiments, E791 and SELEX, have recently published results on Λ_c asymmetry measurements. Fig. 6 shows the E791 asymmetry measurement as a function of x_F and p_T^2 for a π^- beam on the left, and the SELEX measurements as a function of x_F for π^-, Σ^-, and proton beams on the right. The E791 results are compared to PYTHIA version 5.7. In PYTHIA there is an increase in the asymmetry for negative x_F as one would expect for the leading particle effect associated with the valence quarks in the target. In the forward x_F region, on the other hand, one does not expect an enhancement in the Λ_c asymmetry, since both particle and antiparticle share one valence quark with the incident pion beam, and PYTHIA distributions appear to be

qualitatively correct. However, the E791 data have a positive asymmetry that differs from the PYTHIA predictions. This suggests that some effect that is not in PYTHIA or differs from the PYTHIA prediction may be involved, such as associated production of charmed mesons and baryons. Note that the energy threshold is higher for $\overline{\Lambda_c^+}$ production since an additional baryon-antibaryon pair must be produced to satisfy baryon number conservation. When the E791 results are compared to the SELEX asymmetry measurements, one observes the following. First, the SELEX data for the π^- beam are consistent with E791. Second, the asymmetry for baryon beams (both Σ^- and proton beams) is significantly higher. This is a good example of the leading particle effect, in that baryon beams tend to produce baryons, not antibaryons.

Although many of the recent results on charm production emphasize non-perturbative effects such as fragmentation, associated production, and the leading particle effect, there is recent work on a theoretical model that addresses the leading particle effect in the context of perturbative QCD. Recent papers [20), 21)] show that the leading particle effect can be described by a heavy-quark recombination mechanism for data that have been studied so far.

5 Hyperon Production

The same kinds of non-perturbative effects that are observed in charm production also appear in hyperon production data. Moreover, many results on hyperon production are still not represented adequately by models and Monte Carlo programs. Recent results are no exception.

E791 has published results on Λ, Ξ^-, and Ω^- production asymmetries [22)] that display discrepancies that are similar to the Λ_c asymmetries described in the previous section. Fig. 7 shows the asymmetries as a function of x_F and p_T^2 with comparisons to PYTHIA 5.7. The x_F distributions show evidence for the leading particle effect for Λ hyperons with $x_F < 0$, and for Ξ^- hyperons with $x_F < 0$ and $x_F > 0$ (the Ξ^- shares a valence quark with the π^- beam and with the target). Although PYTHIA describes some of the features of the data qualitatively, the model predicts smaller values of the asymmetries for x_F and p_T^2 ranges shown in Fig. 7. As was the case for charm production asymmetries, E791 suggests that the discrepancies in hyperon asymmetries could be due to associated production of strange baryons and mesons.

Experiment WA89 has two new results. They have published a thor-

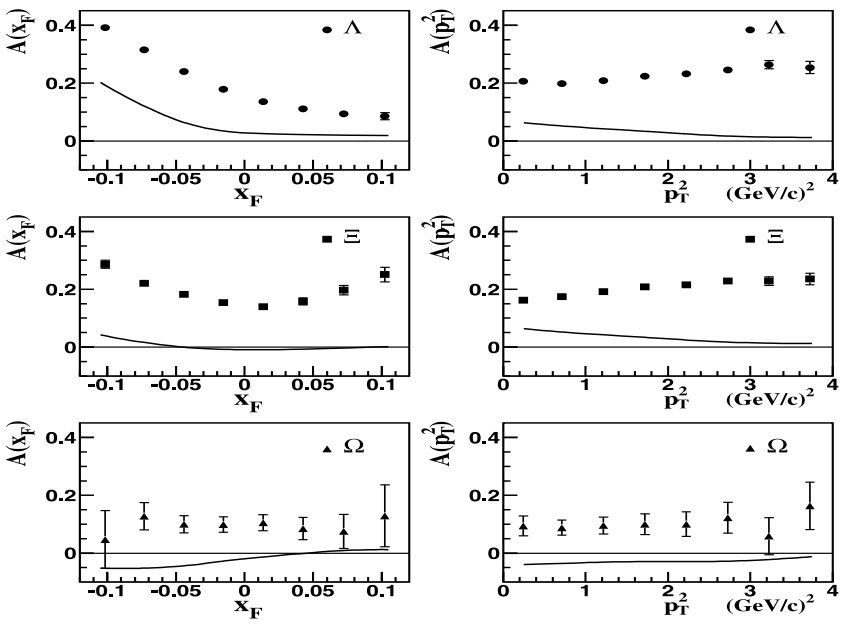

Figure 7: *E791 hyperon asymmetries (data points with error bars) as a function of x_F (left) and p_T^2 (right) compared to PYTHIA 5.7 (solid lines).*

ough investigation [23] of $\Sigma^{\pm}$, $\Sigma^{*\pm}$, and $\overline{\Sigma}^{-}_{1385}$ production with comparisons to PYTHIA and the quark-gluon-string model (QGSM) [25], and a study [24] of Λ and $\overline{\Lambda}$ correlations. The first publication presents numerous distributions and comparisons to models with some striking discrepancies between data and the models. The second publication presents an analysis of kinematic correlations for identical hyperons, showing how momentum-conservation constraints can affect x_F distributions for the hyperons.

The final result on hyperon production presented at this conference comes from a recent publication [26] on Λ polarization in fully reconstructed $pp \rightarrow p\Lambda K^+$ events from E690. E690 sees variations in Λ polarization that appear to be associated with structure in the invariant mass ($M_{\Lambda K}$) distribution for the ΛK^+ system. For small values of $M_{\Lambda K}$, E690 observes large positive polarization, which has not been seen by other experiments. For large values of $M_{\Lambda K}$ the E690 data agree with measurements from a previous experiment [27].

6 Concluding Remarks

Recent measurements from fixed-target experiments on beauty, charm, and hyperon production represent an ongoing effort to understand production mechanisms in strong interactions. Collectively, the measurements provide a wide range of QCD probes that include studies of perturbative QCD predictions and non-perturbative effects. Similarities and differences between heavy-quark and light-quark production characteristics should be exploited to improve our understanding of the underlying production mechanisms. Each quark flavor represents an opportunity to study production in strong interactions with an emphasis on its own physics regime.

7 Acknowledgements

I would like to thank the following people for contributions that made this review of beauty, charm and hyperon production possible: Jeff Appel (E791), Dave Christian (E690), Peter Cooper (SELEX), Brad Cox (E771), Michael Leitch (NuSea), Thomas Mehen (Duke University), Michael Medinnis (HERA-B), Josef Pochodzalla (WA89), and Stephen Pordes (E835). I would also like to thank the local organizers for a successful and enjoyable HQ&L conference, with special thanks to Franco Grancagnolo and Gabriella Cataldi.

References

1. S. Bagnasco *et al.*, Phys. Lett. B **533**, 237 (2002).
2. T. Alexopoulos *et al.*, Phys. Rev. D **55**, 3927 (1997).
3. M.H. Schub *et al.*, Phys. Rev. D **52**, 1307 (1995).
4. M.J. Leitch *et al.*, Phys. Rev. Lett. **84**, 3256 (2000).
5. R. Bonciani *et al.*, Nucl. Phys. B **529**, 424 (1998).
6. N. Kidonakis *et al.*, Phys. Rev. D **64**, 114001 (2001).
7. A.D. Martin, R.G. Roberts, W.J. Stirling and R.S. Thorne, hep-ph/0201127.
8. T. Alexopoulos *et al.*, Phys. Rev. Lett. **82**, 41 (1999).

9. D.M. Jansen *et al.*, Phys. Rev. Lett. **74**, 3118 (1995).

10. C.N. Brown *et al.*, Phys. Rev. Lett. **86**, 2529 (2001).

11. A. Kharchilava *et al.*, Phys. Rev. D **59**, 094023 (1999); A. Tkabladze, Phys. Lett. B **462**, 319 (1999).

12. T. Affolder *et al.*, Phys. Rev. Lett. **85**, 2886 (2000).

13. E.M. Aitala *et al.*, Phys. Lett. B **495**, 42 (2000).

14. F.G. Garcia *et al.*, Phys. Lett. B **528**, 49 (2002).

15. S. Frixione, M.L. Mangano, P. Nason, G. Ridolfi, Adv. Ser. Direct. High Energy Phys. **15**, 609 (1998).

16. P. Frabetti *et al.*, Phys. Lett. B **308**, 193 (1993).

17. H.U. Bengtsson, T. Sjostrand, Comput. Phys. Commun. **46**, 43 (1987).

18. T. Sjostrand *et al.*, Comput. Phys. Commun. **135**, 238 (2001).

19. *http* : *//www.hep.vanderbilt.edu/*∼*stenson/xicc/xicc_focus.html*

20. E. Braaten, Y. Jia, T. Mehen, hep-ph/0108201.

21. E. Braaten, Y. Jia, T. Mehen, hep-ph/0111296.

22. E.M. Aitala *et al.*, Phys. Lett B **496**, 9 (2000).

23. M.I. Adamovich *et al.*, Eur. Phys. J. C **22**, 255 (2001).

24. M.I. Adamovich *et al.*, Phys. Rev. C **65**, 042202 (2002).

25. A.B. Kaidalov, K.A. Ter-Martirosyan, Sov. J. Nucl. Phys. **39**, 1545 (1984); A.I. Veselov, O.I. Piskunova, K.A. Ter-Martirosyan, Phys. Lett. B **158**, 175 (1985); A.B. Kaidalov, O.I. Piskunova, Z. Phys. C **30**, 145 (1986); A.B. Kaidalov, Sov. J. Nucl. Phys. **45**, 1450 (1987).

26. J. Felix *et al.*, Phys. Rev. Lett. **88**, 061801 (2002).

27. T. Henkes *et al.*, Phys. Lett. B **283**, 155 (1992).

Frascati Physics Series Vol. XXVIII (2002), pp.031-044
HQ & L 2002 – Vietri s/m, May 27th - June 1st, 2002

PRODUCTION OF HEAVY FLAVOURS IN ee, ep AND pp SCATTERING

Leonid Gladilin
DESY, Notkestr. 85, 22603 Hamburg, Germany

ABSTRACT

Recent results on heavy flavour production in ee, ep and pp scattering and their comparisons to pQCD predictions are discussed.

1 Introduction

Production of heavy quarks (c, b and t) is one of the most attractive laboratories for QCD prediction tests. Heavy quark masses are much larger than the dimensional QCD parameter $\Lambda_{\rm QCD} \sim 200 - 300\,{\rm MeV}$ that provides a means of calculating cross sections using the perturbative expansion. The perturbative QCD (pQCD) predictions agree with the measured $t\bar{t}$ production cross sections [1, 2]. Some recent results on charm and beauty production in ee, ep and pp scattering and their comparisons to pQCD predictions are discussed in next sections.

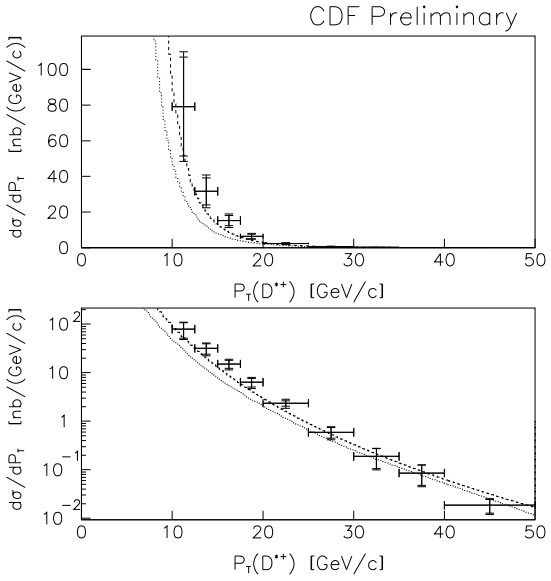

Figure 1: *The differential cross-section $d\sigma/dP_T$ for $D^{*\pm}$ production at Tevatron shown in linear (upper plot) and logarithmic (lower plot) scales.*

2 Charm production in *ee*, *ep* and *pp* scattering

2.1 Charm production in *pp* scattering

The only available measurement of open charm production in *pp* collisions with $\sqrt{s} = 1.8\,\text{TeV}$ at Tevatron was performed by the CDF Collaboration [3]. The open charm was detected in the decay channel $D^{*+} \to D^0\pi^+ \to (K^-\mu^+X)\pi^+$ (+c.c.). The integrated $D^{*\pm}$ production cross section was measured to be $347 \pm 65(\text{stat}) \pm 58(\text{syst})\,\text{nb}$ for the rapidity range of $|\eta(D^{*\pm})| < 1.0$ and the transverse momentum range of $P_T(D^{*\pm}) > 10\,\text{GeV}$. Fig. 1 compares the measured differential cross section $d\sigma/dP_T(D^{*\pm})$ with two pQCD predictions. The lower curve corresponds to the next-to-leading-order (NLO) calculation [4] and the upper curve represents the fixed-order plus next-to-leading-logarithmic (FONLL) calculation [5]. The integrated cross section from the latter calcula-

tion is 240 nb. Both predictions underestimate the measured cross section at lower $P_T(D^{*\pm})$ values.

2.2 Charm production in *ep* scattering

Extensive measurements of charm production in *ep* scattering with $\sqrt{s} = 300 - 318$ GeV at HERA were made by the H1 and ZEUS Collaborations [6, 7, 8, 9, 10]. In the photoproduction regime, i.e. for the exchanged photon virtuality $Q^2 \approx 0$, the measured cross sections of the inclusive $D^{*\pm}$ and $D_s^{\pm}$ production [8, 10] generally lie above the NLO QCD predictions [11], in particular in the proton direction. Recently, the FONLL calculations for charm photoproduction at HERA have become available [12]. However, the FONLL predictions do not provide a better description of the data than does the NLO calculation [13].

The charm photoproduction differential cross section was also measured as a function of the variable $x_\gamma^{\rm obs}$ [8], which is the fraction of the photon momentum contributing to the production of two jets with the highest transverse energies within the accepted pseudorapidity range. This variable provides an experimental separation of direct (point-like) photon processes, in which the photon couples directly to a parton in the proton, and resolved (hadron-like) photon processes, where the photon acts as a source of partons, one of which participates in the hard scattering process. Charm and beauty quarks present in the parton distributions of the photon, as well as of the proton, lead to processes like $cg \rightarrow cg$ and $bg \rightarrow bg$, which are called heavy flavor excitation processes. A comparison of the $x_\gamma^{\rm obs}$ distribution with LO Monte Carlo (MC) simulations indicated the existence of charm excitation in the photon parton density. Recently, the ZEUS Collaboration has performed new measurements of charm dijet photoproduction [14]. The angle between the jet-jet axis and the beam axis in the dijet rest frame has been approximated by the variable $\cos\theta^*$, which is a function of the pseudorapidities of the two jets:

$$\cos\theta^* = \tanh(\frac{\eta^{jet1} - \eta^{jet2}}{2}).$$

The relative differential cross sections as a function of $|\cos\theta^*|$ are compared in Fig. 2 separately for the resolved enriched ($x_\gamma^{\rm obs} < 0.75$) and direct enriched ($x_\gamma^{\rm obs} > 0.75$) samples with the various Monte Carlo (MC) simulations. An enhancement at high values of $|\cos\theta^*|$ is seen for the resolved photon sample, both in the data and in all MC simulations. The direct photon events

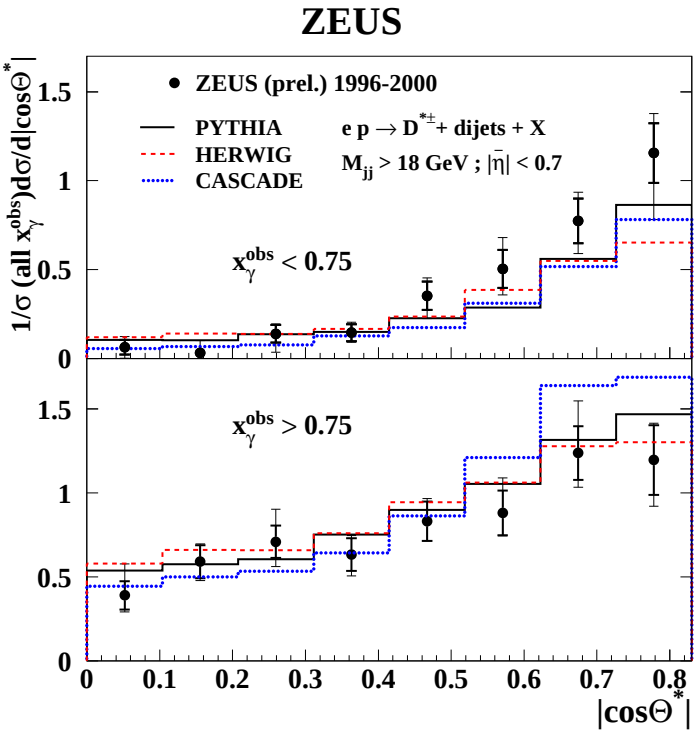

Figure 2: *Relative differential cross sections as a function of* $|\cos\theta^*|$ *compared with various simulations. Results are given separately for enriched resolved photon events* ($x_\gamma^{\rm obs} < 0.75$) *and for enriched direct photon events* ($x_\gamma^{\rm obs} > 0.75$).

exhibit a milder rise towards high $|\cos\theta^*|$. This observation is consistent with a significant gluon-exchange contribution and, consequently, with a significant contribution of charm excitation processes to charm photoproduction at HERA energies. The $D^{*\pm}$ cross section measured at $x_\gamma^{\rm obs} < 0.75$ [8] is higher then the NLO QCD calculation [11].

In deep inelastic scattering (DIS) with $Q^2 > 1\,\mathrm{GeV}^2$, the measured $D^{*\pm}$ differential cross sections were compared with the NLO predictions [15] based on DGLAP [16] formalism and with predictions based on CCFM [17] formalism as implemented in the CASCADE model [18]. The predictions made using DGLAP formalism tend to undershoot the data, particularly for small $D^{*\pm}$

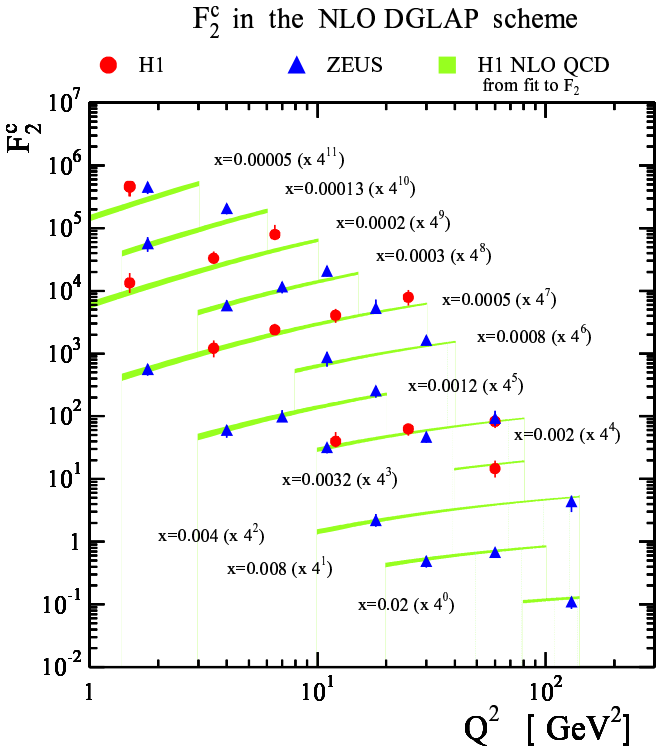

Figure 3: *F_2^c as derived from the inclusive $D^{*\pm}$ meson production cross section as a function of Q^2 for different values of x. The shaded bands represent the prediction of the NLO DGLAP evolution based on the fit to the inclusive F_2.*

transverse momenta and in the proton direction. The expectations of the CCFM based model are in better agreement with the data. The measured cross sections were used to extract the charm contribution $F_2^c(x, Q^2)$ to the proton structure function [7, 9]. The extracted contribution of charm production to the inclusive F_2 exceeds 25% for $Q^2 > 25\,\mathrm{GeV}^2$. Figure 3 shows F_2^c as a function of Q^2 for different values of x. The shaded bands represent the prediction of the NLO DGLAP evolution based on the fit to the inclusive F_2 [19]. The data show a steep rise of F_2^c with Q^2. The steep rise is reasonably well reproduced by the NLO DGLAP calculations. At low x values data tend to be higher and steeper than the predictions.

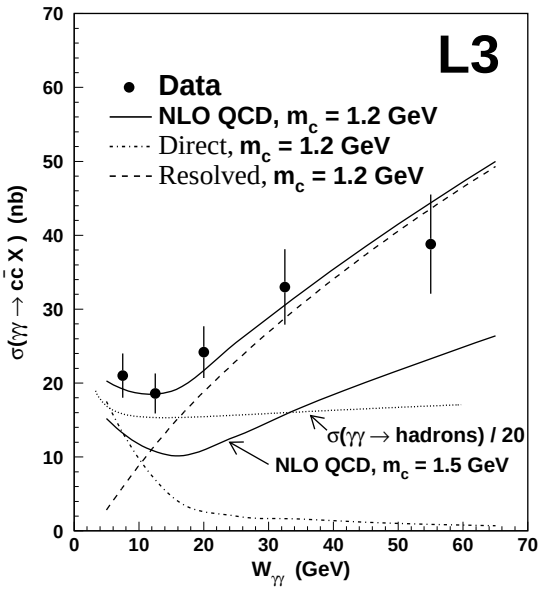

Figure 4: *The cross section* $\sigma(\gamma\gamma \rightarrow c\bar{c}X)$ *as a function of* $W_{\gamma\gamma}$. *The dotted curve is the total cross section* $\sigma(\gamma\gamma \rightarrow hadrons)$ [26] *scaled by an arbitrary factor* $1/20$. *The continuous line is the NLO QCD prediction, while the dashed-dotted and dashed curves show the direct and resolved process, respectively.*

2.3 Charm production in *ee* scattering

Charm production in $\gamma\gamma$ collisions was extensively studied at LEP using *ee* scattering with $\sqrt{s} = 183 - 209\,\text{GeV}$. The measured cross sections of the inclusive $D^{*\pm}$ production [20, 21, 22, 23] are in agreement with the NLO QCD predictions [24] within rather large theory prediction uncertainty.

Using the high statistics electron sample of 2434 events, the L3 Collaboration measured the charm cross section $\sigma(\gamma\gamma \rightarrow c\bar{c}X)$ as a function of the two-photon centre-of-mass energy, $W_{\gamma\gamma}$ [25]. Figure 4 compares the data with the NLO QCD calculations [24]. Using the charm mass $m_c = 1.2\,\text{GeV}$, the NLO QCD predictions reproduce well the energy dependence and the normalization. The calculation with $m_c = 1.5\,\text{GeV}$ results in about 50% lower cross section values.

Using $D^{*\pm}$ production in deep-inelastic electron-photon scattering, the

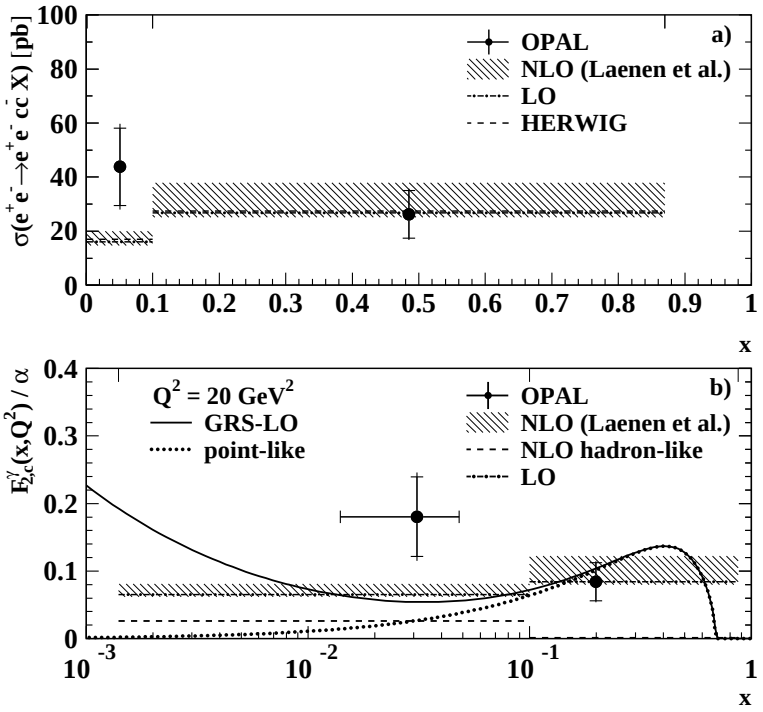

Figure 5: *OPAL results for a) the cross-section* $\sigma(e^+e^- \rightarrow e^+e^-c\bar{c}X)$ *with* $5 < Q^2 < 100\,GeV^2$ *and for b) the charm contribution to the photon structure function divided by the fine structure constant,* $F^{\gamma}_{2,c}/\alpha$*, at* $Q^2 = 20\,GeV^2$.

OPAL Collaboration measured the cross-section $\sigma(e^+e^- \rightarrow e^+e^-c\bar{c}X)$ and the charm contribution $F^{\gamma}_{2,c}$ to the photon structure function in the region $0.0014 < x < 0.87$ and $5 < Q^2 < 100\,\mathrm{GeV}^2$ [27]. Figure 5 compares the data to the calculations [28] performed in LO and NLO. For $x > 0.1$, dominated by the point-like component, the NLO calculation agrees well with the data. For $x < 0.1$ the measured cross-section is $43.8 \pm 14.3 \pm 6.3 \pm 2.8\,\mathrm{pb}$ with the NLO prediction of $17.0^{+2.9}_{-2.3}\mathrm{pb}$. Given the good agreement at large x between the data and the NLO prediction, the NLO point-like prediction has been subtracted from the measured values. For $x < 0.1$ the remaining hadron-like contribution to $F^{\gamma}_{2,c}/\alpha$ amounts $0.154 \pm 0.059 \pm 0.029$, to be compared with the NLO prediction of $0.026^{+0.007}_{-0.005}$.

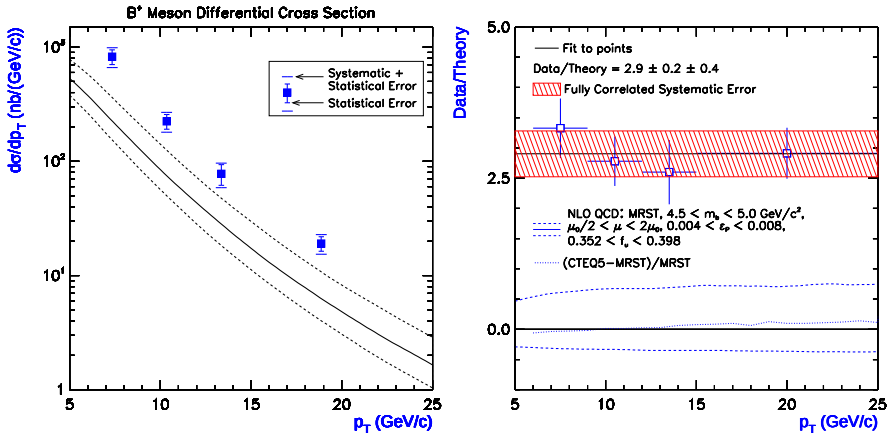

Figure 6: *B^+ meson differential cross section compared to the theoretical prediction (left) and data/theory(NLO) ratio (right). The solid curve is the theoretical prediction for $m_b = 4.75\ GeV$, $\mu_0 = \sqrt{m_b^2 + p_T^2}$, $\epsilon = 0.006$ and $f_u = 0.375$ (the parameters are discussed in [31]). The dashed lines illustrate the changes in the theory once the parameters are varied as indicated in the right plot.*

3 Beauty production in *ee*, *ep* and *pp* scattering

3.1 Beauty production in *pp* scattering

The pQCD calculations are assumed to be more reliable for beauty production than for charm because the heavier b-quark mass provides a harder scale. However, the beauty cross sections measured at Tevatron [29, 30] significantly exceed the predictions. Recently, the CDF Collaboration published new results on the $B^{\pm}$ inclusive production in pp scattering [31]. The $B^{\pm}$ mesons were reconstructed from the decay channels $B^{\pm} \to J/\psi\ K^{\pm}$ with $J/\psi \to \mu^+\mu^-$. Figure 6 compares the measured differential cross-section $d\sigma/dp_T(B^+)$ to the NLO QCD calculation [32]. The fragmentation is modelled using the Peterson fragmentation function [33]. The calculation agrees with the data in shape. However, the absolute rate is underestimated by the calculation. A scale factor for data/theory(NLO) is $2.9 \pm 0.2 \pm 0.4$. These data were compared to the FONLL [5] calculation in [34]. Using the Kartvelishvili fragmentation function [35] tuned to describe moments of the measured B meson fragmentation function [36], the ratio data/theory(FONLL) is $1.7 \pm 0.5(exp) \pm 0.5(theor)$.

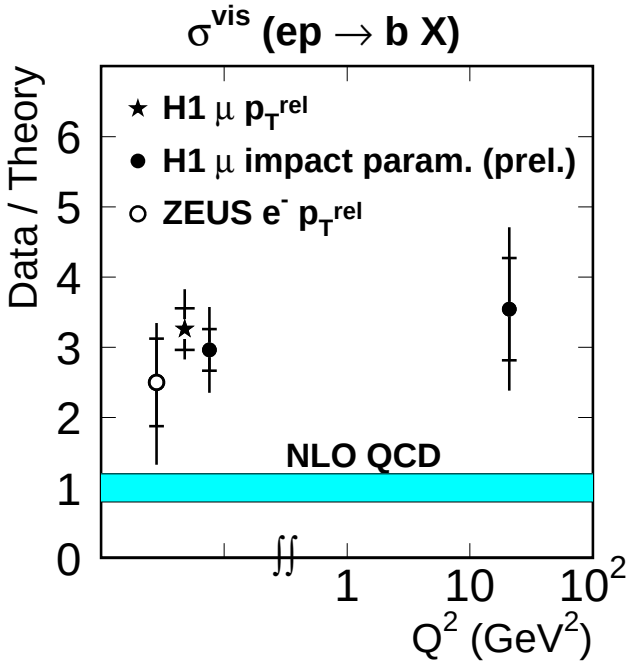

Figure 7: *Ratio of measured b production cross sections at HERA to the NLO QCD predictions. Three left points represent the b production measurements in the photoproduction regime ($Q^2 \approx 0$); right point shows the ratio for beauty production in DIS ($2 < Q^2 < 100\ GeV^2$).*

3.2 Beauty production in ep scattering

Beauty production cross sections in ep scattering at HERA were measured by the H1 and ZEUS Collaborations using events with at least two jets and a lepton in the final state [37, 38, 39, 40]. The beauty signals were extracted by fitting the lepton $p_T^{\rm rel}$ and impact parameter distributions, where $p_T^{\rm rel}$ is the transverse momentum of the lepton relative to the axis of the associated jet. Figure 7 shows the ratio of the measured cross sections to the NLO QCD expectations [11, 15]. The NLO predictions are below the measured cross sections in both photoproduction ($Q^2 \approx 0$) and DIS ($2 < Q^2 < 100\,\mathrm{GeV}^2$).

Recent measurements of the beauty differential cross sections [41] and the production of beauty quarks decaying to a muon and $D^{*\pm}$ [42] were not yet compared to the NLO QCD predictions.

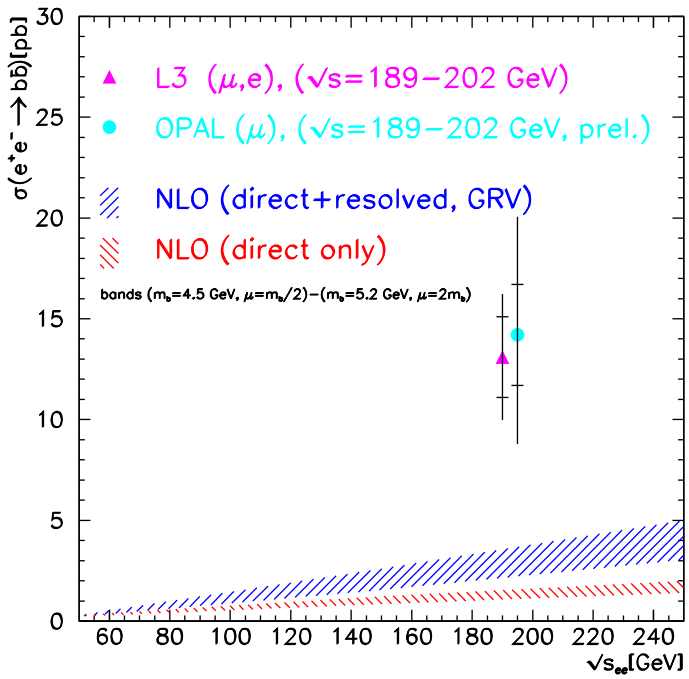

Figure 8: *Total beauty production cross-section* $\sigma(e^+e^- \rightarrow e^+e^- b\bar{b}X)$ *compared to the NLO QCD calculations.*

3.3 Beauty production in ee scattering

The beauty production in $\gamma\gamma$ collisions was measured by the L3 [43] and OPAL [44] Collaborations using ee scattering at LEP with $\sqrt{s} = 189 - 202$ GeV. The beauty signals were extracted using muons or electrons and the $p_T^{\rm rel}$ method. Figure 8 compares the total cross-section $\sigma(e^+e^- \rightarrow e^+e^- b\bar{b}X)$ to the NLO QCD calculations [45]. The theory prediction for the resolved (hadron-like) process is calculated with the GRV parton density function [46]. The direct (point-like) contribution is shown separately. The hatched bands illustrate the changes in the theory once the mass of b quark is varied between 4.5 and 5.2 GeV. The NLO QCD prediction underestimates the data significantly.

4 Summary

Charm production cross sections measured at Tevatron, HERA and LEP generally lie above the NLO and FONLL QCD predictions with central choice of parameters. However in most of cases, the predictions can match the data within rather large theory prediction uncertainty. The predictions underestimate the data significantly in the kinematic ranges where a large contribution from the resolved (hadron-like) photon processes is expected.

Beauty production cross sections measured at Tevatron, HERA and LEP are a factor ∼2–3 higher than the NLO QCD predictions. The excess is rather significant since the theory prediction uncertainty is relatively small for beauty production. Using the Kartvelishvili fragmentation function tuned to describe moments of the measured B meson fragmentation function, the FONLL QCD predictions are in reasonable agreement with B meson cross sections measured at Tevatron.

References

1. T. Affolder et al. (CDF Collaboration), Phys. Rev. **D64**, 032002 (2001).
2. V. M. Abazow et al. (D0 Collaboration), hep-ex/0205019, submitted to Phys. Rev. **D**.
3. T. Nakaya (for the CDF Collaboration), Charmed meson and onium production at the Tevatron, FERMILAB-CONF-00-307-E, in: Proc. XXXVth Rencontres de Moriond (Les Arcs, France, March 2000).
4. M.L. Mangano, P. Nason, G. Ridolfi, Nucl. Phys. **B373**, 295 (1992).
5. M. Cacciari, M. Greco, P. Nason, JHEP **05**, 007 (1998).
6. C. Adloff et al. (H1 Collaboration), Nucl. Phys. **B545**, 21 (1999).
7. C. Adloff et al. (H1 Collaboration), Phys. Lett. **B528**, 199 (2002).
8. J. Breitweg et al. (ZEUS Collaboration), Eur. Phys. J. **C6**, 67 (1999).
9. J. Breitweg et al. (ZEUS Collaboration), Eur. Phys. J. **C7**, 609 (1999).
10. J. Breitweg et al. (ZEUS Collaboration), Phys. Lett. **B481**, 213 (2000).

11. S. Frixione et al., Nucl. Phys. **B454**, 3 (1995);
S. Frixione et al., Phys. Lett. **B348**, 633 (1995).

12. M. Cacciari, S. Frixione, P. Nason, JHEP **0103**, 006 (2001).

13. S. Frixione and P. Nason, JHEP **0203**, 053 (2002).

14. S. Padhi (for the ZEUS Collaboration), Charm fragmentation and dijet angular distributions, hep-ex/0207023, to be published in: Proc. DIS 2002 (Cracow, Poland, April-May 2002).

15. B. W. Harris and J. Smith, Phys. Rev. **D57**, 2806 (1998).

16. V. N. Gribov and L. N. Lipatov, Sov. J. Nucl. Phys. **15**, 438 (1972);
V. N. Gribov and L. N. Lipatov, Sov. J. Nucl. Phys. **15**, 675 (1972);
L. N. Lipatov, Sov. J. Nucl. Phys. **20**, 94 (1975);
G. Altarelli and G. Parisi, Nucl. Phys. **B126**, 298 (1977);
Y. L. Dokshitzer, Sov. Phys. JETP **46**, 1216 (1977).

17. M. Ciafaloni, Nucl. Phys. **B296**, 49 (1988);
S. Catani, F. Fiorani and G. Marchesini, Phys. Lett. **B336**, 49 (1990);
G. Marchesini, Nucl. Phys. **B445**, 49 (1995).

18. H. Jung and G. P. Salam, Eur. Phys. J. **C19**, 351 (2001).

19. C. Adloff et al. (H1 Collaboration), Eur. Phys. J. **C21**, 33 (2001).

20. ALEPH Collaboration, contrib. paper to ICHEP 2000, Abstract 268 (Osaka, Japan, July 2000).

21. M. Chapkin, V. Obraztsov and A. Sokolov (for the DELPHI Collaboration), Inclusive D-meson and Λ_c production in two photon collisions at LEP, in: Proc. PHOTON 2000 (ed. A. J. Finch , Ambleside, UK, August 2000), 252 (Melville, AIP, 2001).

22. P. Achard et al. (L3 Collaboration), Phys. Lett. **B535**, 59 (2002).

23. G. Abbiendi et al. (OPAL Collaboration), Eur. Phys. J **C16**, 579 (2000).

24. S. Frixione, M. Krämer and E. Laenen, Nucl. Phys. **B571**, 169 (2000).

25. P. Acciarri et al. (L3 Collaboration), Phys. Lett. **B514**, 19 (2001).

26. P. Acciarri et al. (L3 Collaboration), Phys. Lett. **B408**, 450 (1997).

27. G. Abbiendi et al. (OPAL Collaboration), CERN-EP-2002-031, accepted by Phys. Lett. **B**.

28. E. Laenen et al., Phys. Rev. **D49**, 5753 (1994);
E. Laenen and S. Riemersma, Phys. Lett. **B376**, 169 (1996).

29. F. Abe et al. (CDF Collaboration), Phys. Rev. Lett. **71**, 500 (1993);
F. Abe et al. (CDF Collaboration), Phys. Rev. Lett. **75**, 1451 (1995);
F. Abe et al. (CDF Collaboration), Phys. Rev. Lett. **79**, 572 (1997).

30. B. Abbot et al. (D0 Collaboration), Phys. Lett. **B487**, 264 (2000);
B. Abbot et al. (D0 Collaboration), Phys. Rev. Lett. **85**, 5068 (2000).

31. D. Acosta et al. (CDF Collaboration), Phys. Rev. **D65**, 052005 (2002).

32. P. Nason, S. Dawson, and R. K. Ellis, Nucl. Phys. **B303**, 607 (1988), erratum *ibid.* **B327**, 49 (1989);
P. Nason, S. Dawson, and R. K. Ellis, Nucl. Phys. **B335**, 260 (1989);
W. Beenakker et al., Nucl. Phys. **B351**, 507 (1991).

33. C. Peterson et al., Phys. Rev. **D27**, 105 (1983).

34. M. Cacciari and P. Nason, hep-ph/0202025, submitted Phys. Rev. Lett.;
P. Nason, these proceedings.

35. V. G. Kartvelishvili, A. K. Likhoded, and V. A. Petrov, Phys. Lett. **B78**, 615 (1978).

36. A. Heister et al. (ALEPH Collaboration), Phys. Lett. **B512**, 30 (2001).

37. C. Adloff et al. (H1 Collaboration), Phys. Lett. **B467**, 156 (1999), erratum *ibid.* **B518**, 331 (2001).

38. J. Breitweg et al. (ZEUS Collaboration), Eur. Phys. J. **C18**, 625 (2001).

39. H1 Collaboration, contrib. paper no. 311 to ICHEP 2000 (Osaka, Japan, July 2000).

40. H1 Collaboration, contrib. paper to EPS 2001, Abstract 807 (Budapest, Hungary, July 2001).

41. ZEUS Collaboration, contrib. paper to EPS 2001, Abstract 496 (Budapest, Hungary, July 2001).

42. J. Wagner (for the H1 Collaboration), $D^*\mu$ correlations and D production in ep scattering at HERA, to be published in: Proc. of DIS 2002 (Cracow, Poland, April-May 2002).

43. P. Acciarri et al. (L3 Collaboration), Phys. Lett. **B503**, 10 (2001).

44. À. Csilling (for the OPAL Collaboration), Charm and bottom production in two-photon collisions with OPAL, hep-ex/0010060, in: Proc. PHOTON 2000 (ed. A. J. Finch , Ambleside, UK, August 2000), 276 (Melville, AIP, 2001).

45. M. Drees et al., Phys. Lett. **B306**, 371 (1993).

46. M. Glück, E. Reya and A. Vogt, Phys. Rev. **D46**, 1973 (1992).

Frascati Physics Series Vol. XXVIII (2002), pp.045-058
HQ & L 2002 – Vietri s/m, May 27th - June 1st, 2002

HEAVY QUARK PRODUCTION WITH HIGH ENERGY NEUTRINO BEAMS

Pasquale Migliozzi
INFN, Sezione Napoli, Italy

ABSTRACT

We review existing data on charm-production in neutrino scattering, describing the theoretical aspects of neutrino charm-production and the main features of the experiments where charm has been looked for. We focus our attention on charm-production through inclusive and exclusive channels such as quasi-elastic, diffractive and associated charm production. We discuss the slow-rescaling model and the extraction of the charm-quark mass. The impact of charm studies on the extraction of the CKM matrix elements is also reported. Moreover, we review existing data on the hadronization of the charm-quark to charmed hadrons. Finally, we give future prospects of charm-production induced by neutrinos and our conclusions.

1 Introduction

The first evidence of charmed hadron production in neutrino interactions became available in 1974 through the observation of opposite sign dimuons in a calorimeter experiment [1]. Since that time, it has been assessed that high energy neutrino interactions produce charmed hadrons at the level of a few percent and therefore they represent a powerful tool to study heavy quark production mechanisms and dynamics. In particular, the charm-production offers the possibility to study the strange-quark content of the nucleon, to measure "directly" the CKM matrix element V_{cd} and to test models for charm-production and subsequent hadronization. Moreover, unlike colliding beams, neutrinos produce charmed hadrons also via specific processes like quasi-elastic and diffractive scattering which provide an unique tool for exclusive charm studies. Furthermore, charm-quark pairs can also be produced, although with considerable suppression, allowing for the investigation of higher order mechanism through which charm-quarks can be produced. Recently, new results from the electronic detector experiments NOMAD at CERN [2, 3] and NuTeV at FNAL [4, 5], as well as from the emulsion experiment CHORUS at CERN [6] became available and will be reviewed in this paper. Finally, we give future prospects of charm-production induced by neutrinos and our conclusions.

The paper is organised as follow: in Section 2 we give a short theoretical introduction on the charm-production in deep-inelastic neutrino interactions and of the hadronization mechanism of the charm-quark to charmed hadrons; the experimental techniques used to study charm-production induced by neutrino and the cross-section measurements are briefly reviewed in Section 3 and Section 4, respectively; results on charm hadronization are discussed in Section 5. Results from dimuon analyses, as well as from low multiplicity and associated charm-production, are discussed in Sections 6, 7 and 8, respectively. Finally future prospects of charm physics by using high-energy neutrino beams are outlined and our conclusions are presented.

2 Charm-production in deep-inelastic neutrino interactions

2.1 Leading-order (LO) charm-production

At leading order, only the Born diagram (the first diagram in Fig. 1a)) is considered for charm-production and only the s- and d-quarks of the nucleon

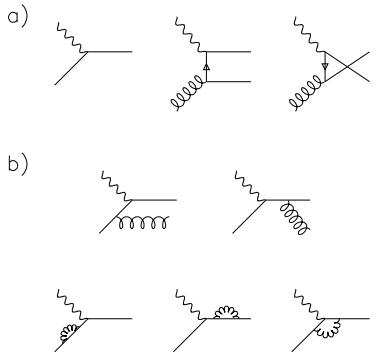

Figure 1: *Diagrams contributing to neutrino production of charm-quark up to* $\mathcal{O}(\alpha_S)$. **a)** *The dominant diagrams: the leading order quark-initiated diagram and the next-to-leading order t-channel and u-channel gluon-initiated diagrams.* **b)** *The radiative-gluon and self-energy diagrams.*

are involved. In terms of the quark distributions, for an isoscalar target the c production cross-section can be written as

$$\begin{aligned}\frac{d^2\sigma(\nu N \to c\mu^-)}{d\xi dy} &= \frac{G_F^2 ME}{\pi(1+Q^2/M_W^2)^2} \\ &\times \left\{ \left[u(\xi,\mu^2) + d(\xi,\mu^2)\right] \mid V_{cd} \mid^2 + 2s(\xi,\mu^2) \mid V_{cs} \mid^2 \right\} \\ &\times \left[\frac{1+R(\xi,\mu^2)}{1+\left(\frac{2M\xi}{Q}\right)^2} \left(1 - y - \frac{Mxy}{2E} + \frac{xy}{\xi}\right) \right] \end{aligned} \quad (1)$$

where M is the nucleon mass, E is the neutrino energy, Q^2 is the negative square of the four-momentum transfer, y is the inelasticity, R is a longitudinal structure function which accounts for violation of the Callan-Gross relation, ξ is the momentum fraction of the struck quark and μ^2 is the scale at which quark momentum distributions are given. The dependence of the parton distributions on the scale μ^2 is specified by QCD [7]. ξ is related to the Bjorken scaling variable x through the relation

$$\xi = x\left(1 + \frac{m_c^2}{Q^2}\right)\left(1 - \frac{x^2M^2}{Q^2}\right)$$

For charm-production induced by $\bar{\nu}$ Eq. 1 holds with substitution of quarks with anti-quarks. The LO expression illustrates the sensitivity of the

process to the strange quark sea. Charm (anti-charm) production from scattering off $d(\bar{d})$-quarks is Cabibbo suppressed. In the case of charm-quark produced by neutrinos, approximately 50% is due to scattering from s-quarks, even though the d-quark content of the proton is approximately ten times larger. In the case of anti-neutrino scattering, where only sea $\bar{d}$-quarks contribute, roughly 90% is due to scattering off $\bar{s}$-quarks.

2.2 Next-to-leading order (NLO) corrections

Because charm-production at LO is a process dominated by sea quark contributions, the gluon-initiated contributions are expected to be significant although they are nominally at NLO [7]. The gluon distribution, which is an order of magnitude larger than the sea quark distribution, compensates for the extra power of α_s involved in the diagram (see Fig. 1).

Calculations including the NLO formalism have recently become available [8].

2.3 Hadronization of charm-quarks to charmed hadrons

In the previous sections we discussed the charm-production at the quark level, whereas the experiments only observe hadrons. The problem of building hadrons (the so-called hadronization) out of the quarks emerging from a hard scattering process is characterized by a relatively low scale, of the order of typical hadron masses, so that perturbative QCD is not applicable. However, the factorization theorem is not limited to the perturbative region and is applicable to the hadronization process in the same way it is used when describing the initial state hadron.

Just as the parton distribution functions are universal, independent of the scattering process through which they are probed, we may expect the fragmentation description to be universal. In particular, one can assume that the quarks emerging from $e^+e^- \to q\bar{q}$ scattering form a hadronic final state through processes which are similar, if not identical, to the processes which build the hadronic final state in lepton-nucleon scattering.

The differential cross-section for charmed-hadron production can be written as

$$\frac{d\sigma(\nu N \to \mu^- CX)}{dxdydzdp_T^2} = \frac{d\sigma(\nu N \to \mu^- cX)}{dxdy} \times \sum_h f_h \times D_c^h(z, p_T^2) \qquad (2)$$

Here, $D_c^h(z, p_T^2)$ is the probability distribution for the charm-quark to fragment into a charmed hadron of type $h(= D^0, D^+, D_s^+, \Lambda_c^+)$ carrying a fraction z of the quark longitudinal momentum and transverse momentum p_T with respect to the quark direction. The number f_h is the mean multiplicity of the hadron h in neutrino charm-production. A similar expression holds for $\bar{\nu}$.

Since only one c-quark is produced in a CC interaction, one can set the normalization conditions as

$$\int_0^1 dz \int_0^\infty D_c^h(z, p_T^2) dp_T^2 = 1 \quad \text{and} \quad \sum_h f_h = 1\,. \qquad (3)$$

Usually, $D_c^h(z, p_T^2)$ is written as

$$D_c^h(z, p_T^2) \propto D(z) \times e^{-bp_T^2} \qquad (4)$$

where $D(z)$ is commonly parameterized either as [10]

$$D(z) \propto \frac{1}{z\left(1 - \frac{1}{z} - \frac{\varepsilon_P}{1-z}\right)} \qquad (5)$$

or as [11]

$$D(z) \propto \frac{\frac{1-z}{z} + \frac{\varepsilon_C(2-z)}{1-z}}{1 - \frac{1}{z} - \frac{\varepsilon_C}{1-z}} \times (1 + z^2) \qquad (6)$$

Qualitatively, the shape of the $D(z)$ can be understood as follows. The charm-quark emerges from the hard scattering process and is relatively energetic. Attaching a light anti-quark $\bar{q}$ to it to form a charmed meson decelerates the heavy quark only slightly, so that we expect the variable z to be peaked towards 1. The ε parameter will be different for different mesons, but it can be expected to scale as $1/m_Q^2$, with m_Q the mass of the heavy quark.

Finally, we want to stress that all the parameters discussed above (f_h, b, ε_P, ε_C) cannot be predicted theoretically and must be determined experimentally.

3 Experimental techniques

3.1 Charm-production studies with di-leptons

In the case of neutrino scattering, the underlying process is a neutrino charged-current (CC) interaction with an s- or d-quark, producing a charm-quark that fragments into a charmed hadron. The charmed hadron may decay semi-leptonically producing opposite sign di-leptons through the process:

$$\begin{aligned} \nu_\mu + \mathrm{N} \longrightarrow \mu^- + c + \mathrm{X} \\ \hookrightarrow s + l^+ + \nu_l \end{aligned} \tag{7}$$

Analogously an anti-neutrino can interact with a $\bar{s}$- or $\bar{d}$-quark, producing a charm anti-quark that fragments into a charmed hadron, again leading to a final state with two oppositely charged leptons.

Since 1974, several experiments have used this technique to study charm-production. Calorimetric and bubble chamber experiments, have exploited the muonic and electronic decay of the charmed hadron, respectively.

For a detailed discussion of the available statistics, of the detection techniques and of the data selection, we refer to [7, 9].

3.2 Charm-production studies with nuclear emulsions

So far only two experiments, E531 [12, 13] and CHORUS [6], have searched for inclusive charm-production through the direct observation of charmed hadron decays in nuclear emulsions. The main advantage of nuclear emulsions is that, being the charmed particle identified through its decay, no kinematical cuts are applied. This translates into a very good sensitivity to the slow-rescaling threshold behavior and consequently to the charm-quark mass. For a detailed discussion of the analysis techniques used in emulsion experiments we refer to [9].

The final E531 data sample consists of 3855 neutrino interactions among which 122 charmed-particle decays have been found [12, 13]. The estimated background is 0.2 and 3.6 events for neutral and charged charmed-particle decays, respectively. The present CHORUS statistics consists of about 1000 charmed-particle decays fully measured in the emulsions. The analysis is still in progress and a final statistics of $3000 \div 4000$ events is expected.

4 Cross-section measurements

The inclusive charm-production cross-section can only be measured in emulsion experiments. The relative charmed-particle production rate measured by the E531 experiment is: $\sigma(\nu_\mu N \to c\mu^- X)/\sigma(\nu_\mu N \to \mu^- X) = 4.9^{+0.7}_{-0.6}\%$.

The inclusive D^0 production rate has been measured by the CHORUS experiment [6] and it amounts to $\sigma(\nu_\mu N \to D^0\mu^- X)/\sigma(\nu_\mu N \to \mu^- X) = 2.18 \pm 0.14 \pm 0.19\%$[1].

Recently, a combined analysis of di-lepton and nuclear emulsion results has been performed to extract a world averaged single-charm production cross-section for both neutrino and anti-neutrino. For the statistical approach used and on the obtained results, we refer to [9].

5 Charm-hadronization studies

5.1 Charmed fractions and semi-muonic branching ratio

The charmed fractions f_h have been measured directly only by the E531 experiment [12]. In checking over the E531 results, a bias was detected in the extraction of the charmed fractions. Therefore, the data was refit with the bias removed [14].

Usually one assumes that f_h's are universal. Therefore, neutrino measurements could be checked against similar fractions measured in e^+e^- experiments with similar kinematics. This assumption is not entirely true, having neutrinos the peculiarity to undergo not only deep-inelastic interactions, but also to induce diffractive and quasi-elastic charm-production (see Section 7).

By using the energy dependence of the charmed fractions reported in Ref. [14] and the semi-muonic branching ratios (BR) reported in [15], I derived the following average semi-muonic BR:

$$E_\nu > 5 \text{ GeV} \quad \bar{B}_\mu = (8.1 \pm 0.8)\% \tag{8}$$

$$E_\nu > 20 \text{ GeV} \quad \bar{B}_\mu = (8.6 \pm 0.9)\% \tag{9}$$

$$E_\nu > 30 \text{ GeV} \quad \bar{B}_\mu = (9.3 \pm 1.0)\% \tag{10}$$

[1] I derived this rate starting from the CHORUS results and accounting for the fact that the only the product $(\sigma(D^0)/\sigma_{CC}) \times [BR(D^0 \to V2) + BR(D^0 \to V4)]$ was measured.

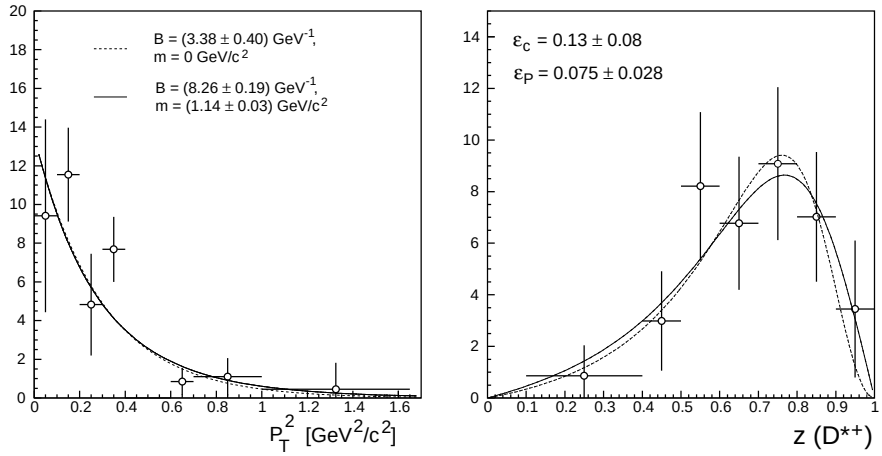

Figure 2: *NOMAD results for $D^\star$ mesons. Left: p_T^2 distribution; the result of a fit by using the function $exp[-b(m^2+p_T^2)]$, where m and b are free parameters, is also shown. Right: z distribution; the results of fits with the functions (5) and (6) are also shown.*

Recently, a direct measurement of $\bar{B}_\mu$ has been performed by CHORUS by using a statistics of about 1000 charm events reconstructed in the nuclear emulsions [16]. Out of these, $(88 \pm 10 \pm 8)$ dimuon events have been reconstructed, which correspond to

$$\bar{B}_\mu = (9.3 \pm 0.9 \pm 0.9)\%$$

which is in agreement with previous indirect measurements.

5.2 p_T^2 distribution

The p_T^2 distribution of charmed hadrons with respect to the direction of the hadronic system has been measured only by two neutrino experiments: E531 [12] and NOMAD [2]. An example of p_T^2 distribution is given in Figure 2. The results of the fits to the p_T^2 distribution from E531 and NOMAD are consistent and the averaged value of b is 3.31 ± 0.27 GeV^{-2}.

The CHORUS experiment is currently analysing about 1000 events with a charmed hadron in the final state. By the end of the year should provide a new insight in the understanding of the p_T^2 distribution of charmed hadrons.

Collaboration	ε_P	ε_C	Comments
E531 [12]	0.076 ± 0.014	—	All charmed hadrons are used
NOMAD [2]	0.075 ± 0.046	0.13 ± 0.14	Only D^{*+} are used
CDHS [20]	$[0.02 \div 0.14]$	—	
CCFR (LO) [23]	0.22 ± 0.05	0.88 ± 0.12	All charmed hadrons are used
CHARM II [22]	0.072 ± 0.017	—	All charmed hadrons are used
NuTeV	—	2.07 ± 0.31	All charmed hadrons are used
CLEO+ARGUS [15]	0.14 ± 0.01	—	Only D^0 are used
CLEO+ARGUS [27]	0.156 ± 0.022	—	Only D^+ are used
CLEO+ARGUS [27]	0.10 ± 0.02	—	Only D_s are used
CLEO+ARGUS [15]	0.25 ± 0.03	—	Only Λ_c are used
CLEO+ARGUS [15]	0.078 ± 0.008	—	Only D^{*+} are used

Table 1: Summary of all available determinations of ε. For comparison results from e^+e^- (CLEO+ARGUS) experiments are also given.

5.3 Fragmentation studies

The parameter ε which characterizes the fragmentation functions of heavy quarks can be determined by using two different approaches:

- Direct measurements: the z distribution is reconstructed and fitted in order to extract the parameter ε. Such analysis has been performed by E531, NOMAD (see Fig. 2) and is currently in progress in CHORUS;
- Indirect measurements: ε is left as one of the free parameters of the fit to the dimuon data. Dimuon analysis has been performed by CDHS, CCFR, CHARM II and NuTeV (see Section 6).

The available results from both approaches are summarized in Table 1, together with the results from e^+e^- experiments (CLEO and ARGUS) at $\sqrt{s} =$ 10.55 GeV.

Collaboration	$B_\mu \mid V_{cd} \mid^2$	κ	m_c
FMMF [19]	$(0.427 \pm 0.167) \times 10^{-2}$	0.479 ± 0.130	1.91 ± 0.57
CDHS [20]	$(0.41 \pm 0.07) \times 10^{-2}$	0.402 ± 0.109	—
Foudas et al. [21]	— —	0.521 ± 0.228 0.44 ± 0.09	1.31 ± 0.56
CHARM II [22]	$(0.442 \pm 0.049) \times 10^{-2}$	0.388 ± 0.095	1.79 ± 0.38
NOMAD [3]	$(0.48 \pm 0.17) \times 10^{-2}$	—	1.3 ± 0.4
CCFR (LO) [23]	$(0.509 \pm 0.036) \times 10^{-2}$	0.373 ± 0.048	1.31 ± 0.24
CCFR (NLO) [24]	$(0.534 \pm 0.060) \times 10^{-2}$	—	
CCFR (F-fit) [25]	—	0.453 ± 0.123	
Average value	$(0.483 \pm 0.024) \times 10^{-2}$	0.406 ± 0.033	1.45 ± 0.16
CCFR (NLO)) [24]		0.553 ± 0.099 0.477 ± 0.051 0.468 ± 0.059	1.70 ± 0.19

Table 2: Summary of all available results obtained from a fit to the dimuon data.

6 Dimuon analyses

The dimuon analyses performed in the past suffer of the limit that the results depend on the model assumptions and on the experimental technique (see in particular [17]). The usual analysis proceeds in two steps: first the s-PDF and charm-production models are parameterized in the Monte Carlo, then a fit of the Monte Carlo parameters to dimuon distributions (z_{vis} , x_{vis} , y_{vis}) is performed to extract the charm-production model and the s-PDF parameters. Results on m_c, $B_\mu \mid V_{cd} \mid^2$ and κ (the nucleon's strange content) from LO and NLO analyses are given in Table 2. By using the latest values of B_μ (see Section 5.1) and of $V_{cs} = 0.996 \pm 0.024$ [18], and the average value of $B_\mu \mid V_{cd} \mid^2$ reported in Table 2, we extracted $V_{cd} = 0.228 \pm 0.014$ as well the weighted average of κ. The measured value of V_{cd} has to be compared with the one obtained by imposing the unitarity constraint in fitting the CKM matrix $V_{cd} = 0.219 \div 0.225$ [15].

Recently, a method for a model independent analysis of dimuon data has been proposed by the NuTeV Collaboration. For a detailed discussion of the

method we refer to [4]. Preliminary results have been presented at the Neutrino 2002 Conference [26].

7 Low multiplicity charm-production

We classify as "low multiplicity" those processes (diffractive $D_s^{(*)}$ and quasi-elastic (QE) charm-production) with at most two particles produced at the primary vertex besides the charmed hadron.

In the following we focus on the quasi-elastic charm-production, as this process is particularly interesting to measure the absolute BR of the Λ_c [28]. In the past several experiments studied this process, but with a small statistics (less than 10 events) [29]. Presently, the CHORUS experiment is performing a dedicated search and several events consistent with a QE topology have been already measured. With the final statistics of a few hundred events, CHORUS will measure for the first time both the differential cross-section of the process and the absolute BR of the Λ_c.

8 Associated charm-production neutral-current (NC) and charged-current (CC) interactions

Associated charm-production in NC interactions proceeds through a gluon-boson fusion process. Only one event has been "directly" observed so far by the E531 experiment [13], while an indirect observation has been recently published by the NuTeV experiment [5]. Both experiments measured a rate of the order of 10^{-3}, normalized to CC events.

In CC interactions charm pairs originate from the splitting of a gluon emitted through the bremsstrahlung of a light quark. In the past indirect evidence for this process was obtained by studying trimuon and same-sign dimuon events [30]. Note that, the observed rate of trimuons and same-sign dimuons was larger than theoretical predictions [31] by more than one order of magnitude. Given the small statistics and the uncertainties related to the background subtraction, the result was not conclusive. Recently a direct search for this process has started in the emulsions of the CHORUS experiment. So far the observation of one event [32] has been reported.

9 Conclusions and future prospects

New results on studies of the hadronization of charm-quark to charmed hadrons have been presented. In particular, a direct determination of the semi-muonic branching ratio $B_\mu = (9.3 \pm 0.9 \pm 0.9)\%$ and a direct measurement of fragmentation variables z and p_T^2 are now available. A reanalysis of all available dimuon data has been presented which gives an estimate of $V_{cd} = 0.228 \pm 0.014$. Finally, results on associated charm-production are available.

In the near future final results from CHORUS, NOMAD and NuTeV experiments should allow:

- detailed studies of threshold behavior of the charm-production cross-section;
- a better understanding and determination of charm-quark hadronization;
- model independent extraction of strange-sea PDF at the NLO;
- model independent determination of absolute Λ_c branching ratios;
- better direct determination of V_{cd};
- high statistic study of associated charm-production both in neutral- and charged-current interactions.

In the long term future, Neutrino Factories have the potentiality to provide an enormous amount of neutrino-induced events with charmed particles in the final state. Moreover, at a neutrino factory it will be possible to also produce bottom-quark. For details on the potentiality of a neutrino factory to study heavy-quarks we refer to [29, 33]

References

1. A. C. Benvenuti *et al.*, Phys. Rev. Lett. **34** (1975) 419.
2. P. Astier *et al.* [NOMAD Collaboration], Phys. Lett. B **526** (2002) 278.
3. P. Astier *et al.* [NOMAD Collaboration], Phys. Lett. B **486** (2000) 35.
4. M. Goncharov *et al.* [NuTeV Collaboration], Phys. Rev. D **64** (2001) 112006 [arXiv:hep-ex/0102049].

5. A. Alton *et al.* [NuTeV Collaboration], Phys. Rev. D **64** (2001) 012002 [Int. J. Mod. Phys. A **16S1B** (2001) 764] [arXiv:hep-ex/0008068].

6. A. Kayis-Topaksu *et al.* [CHORUS Collaboration], Phys. Lett. B **527** (2002) 173.

7. J. M. Conrad, M. H. Shaevitz and T. Bolton, Rev. Mod. Phys. **70** (1998) 1341 [arXiv:hep-ex/9707015].

8. S. Kretzer, D. Mason and F. Olness, Phys. Rev. D **65**, 074010 (2002) [arXiv:hep-ph/0112191].

9. G. De Lellis, A. Marotta and P. Migliozzi, J. Phys. G **28** (2002) 713 [Erratum-ibid. **G28** (2002) 1515] [arXiv:hep-ph/0201050].

10. C. Peterson, D. Schlatter, I. Schmitt and P. M. Zerwas, Phys. Rev. D **27** (1983) 105.

11. P. D. Collins and T. P. Spiller, J. Phys. G **11** (1985) 1289.

12. N. Ushida *et al.* [Fermilab E531 Collaboration], Phys. Lett. B **206** (1988) 380.

13. N. Ushida *et al.* [Fermilab E531 Collaboration], Phys. Lett. B **206** (1988) 375.

14. T. Bolton, arXiv:hep-ex/9708014.

15. D. E. Groom *et al.* [Particle Data Group Collaboration], Eur. Phys. J. C **15** (2000) 1.

16. B. Van de Vyver [CHORUS Collaboration], "Determination of the semi-leptonic branching fraction of neutrino-induced charm hadrons using nuclear emulsion," CERN-THESIS-2002-024.

17. V. Barone, C. Pascaud and F. Zomer, Eur. Phys. J. C **12** (2000) 243 [arXiv:hep-ph/9907512].

18. M. Bargiotti *et al.*, Riv. Nuovo Cim. **23N3** (2000) 1 [arXiv:hep-ph/0001293].

19. B. Strongin *et al.*, Phys. Rev. D **43** (1991) 2778.

20. H. Abramowicz *et al.*, Z. Phys. C **15** (1982) 19.

21. C. Foudas *et al.*, Phys. Rev. Lett. **64** (1990) 1207.

22. P. Vilain *et al.* [CHARM II Collaboration], Eur. Phys. J. C **11** (1999) 19.

23. S. A. Rabinowitz *et al.*, Phys. Rev. Lett. **70** (1993) 134.

24. A. O. Bazarko *et al.* [CCFR Collaboration], Z. Phys. C **65** (1995) 189 [arXiv:hep-ex/9406007].

25. J. Yu *et al.* [CCFR/NuTeV Collaboration], FERMILAB-CONF-98-304-E *Published in the proceedings of 29th International Conference on High-Energy Physics (ICHEP 98), Vancouver, Canada, 23-29 Jul 1998.*

26. Talk presented by D. Naples [CCFR/NuTeV Collaboration], *To be published in the proceedings of Neutrino 2002 Conference, Munich, Germany, 25-30 May 2002.*

27. O. Biebel, P. Nason and B. R. Webber, arXiv:hep-ph/0109282.

28. P. Migliozzi, G. D'Ambrosio, G. Miele and P. Santorelli, Phys. Lett. B **462** (1999) 217 [arXiv:hep-ph/9906219].

29. M. L. Mangano *et al.*, arXiv:hep-ph/0105155.

30. P. H. Sandler *et al.*, Z. Phys. C **57** (1993) 1.

31. K. Hagiwara, Nucl. Phys. B **173** (1980) 487.

32. A. Kayis-Topaksu *et al.* [CHORUS Collaboration], CERN-EP/2002-036.

33. I. Bigi *et al.*, BNL-67404

Frascati Physics Series Vol. XXVIII (2002), pp.059-059
HQ & L 2002 – Vietri s/m, May 27th - June 1st, 2002

HEAVY FLAVOUR PRODUCTION IN DEEP INELASTIC SCATTERING PROCESS *

Stephan Paul
TU Muenchen, Germany

* Written contribution not received

Frascati Physics Series Vol. XXVIII (2002), pp.061-071
HQ & L 2002 – Vietri s/m, May 27th - June 1st, 2002

E835 AT FNAL: STUDY OF CHARMONIUM STATES IN $\bar{p}p$ ANNIHILATIONS

Matteo Negrini
University of Ferrara and INFN, 44100 Ferrara, Italy
on behalf of the E835 Collaboration [1)]

ABSTRACT

Experiment E835 at the Fermilab Antiproton Accumulator has collected a large sample of charmonium states formed in $\bar{p}p$ annihilations, providing precision measurements of mass, width and branching ratios of all the observed $\bar{c}c$ states. A summary of recent results of charmonium spectroscopy in $\bar{p}p$ annihilation will be presented, as well as some E835 preliminary results. Also a measurement of the proton form factor in the time-like region at high momentum transfer can be performed.

1 Introduction

The charmonium spectroscopy of the states below the $\overline{D}D$ threshold has proved to be a good testing ground for QCD and effective theories recently developed, such as Non Relativistic QCD (NRQCD) and Heavy Quark Effective Theory

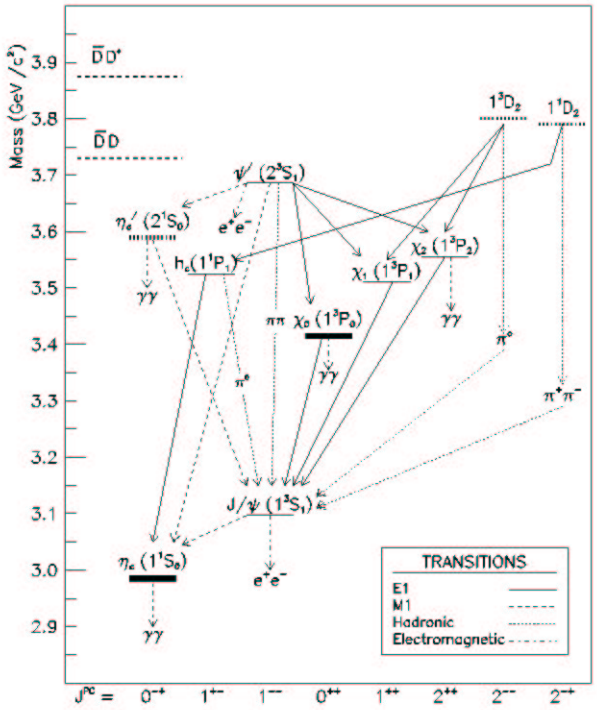

Figure 1: *The charmonium spectrum.*

(HQET). The two heavy quarks in the bound state have $\beta^2 \simeq 0.3$, for this reason the charmonium spectrum is reasonably well described by non-relativistic potential models. Also the decay partial widths can be calculated; the measured values can be used to probe the QCD. However, some features of the charmonium spectrum need more precise measurements. Figure 1 shows the charmonium spectrum. There are still open questions: the η_c' (2^1S_0) and the h_c (1^1P_1) states, for example, were observed only once, respectively by Crystall Ball [2] and Fermilab E760 [3] experiment and still need further confirmation.

From the experimental point of view, masses and widths of all the observed $\bar{c}c$ states can be measured with good precision: the relative error on the mass measurement is at the level of 10^{-4} or better but for the widths it is of

the order of $\sim 10 - 20\%$; an improvement on the width measurements might be helpful to test theoretical predictions.

At e^+e^- colliders, only $J^{PC} = 1^{--}$ states can be directly formed via annihilation of the lepton pair in a virtual photon; the J/ψ (1^3S_1) and the ψ' (2^3S_1) are deeply investigated whith this technique. All the other states can be studied in cascade decays or in two virtual photon interaction in high energy e^+e^- colliders.

The formation of charmonium states in $\overline{p}p$ annihilation is a good method to perform precision measurement of charmonium spectroscopy. With this technique all charmonium states are directly accessible so it is possible to perform precision studies of all known states by direct scan; another advantage is that the total energy of the particles in the final state is known with very good precision from the beam parameters: it is not related to the detector resolution.

The technique was pioneered by CERN experiment R704 [4] at the CERN Intersecting Storage Rings, that proved the feasibility of the experiment by measuring the mass of the χ_{c1} and χ_{c2} and the total width of the χ_{c2} [5]; it was exploited later by the Fermilab experiment E760 [6], that was able to perform high precision measurements of all charmonium states, in particular the first measurement of the χ_{c1} width, and to observe the h_c resonance.

The experiment E835, the upgraded successor of E760, recently completed the data taking program for charmonium spectroscopy in $\overline{p}p$ annihilation at Fermilab. During the first period of data taking, in 1996-97, a luminosity of 143 pb^{-1} was collected for the detailed study of all the $\overline{c}c$ states below the $\overline{D}D$ threshold. During the second period of data taking, in year 2000, 113 pb^{-1} of data were collected, mainly for the detailed study of the χ_{c0} and ψ' states and to confirm the h_c.

2 Experimental technique

The purpose of the E835 experiment at Fermilab is the precision study of the charmonium spectroscopy of charmonium states formed in $\overline{p}p$ annihilations.

Let's consider the process:

$$a + b \to R \to c + d,$$

the Breit-Wigner formula describing the center of mass energy (E) dependence

of the resonant part of the cross section is:

$$\sigma_{BW}(E) = \frac{\pi}{k^2}\frac{(2J+1)}{(2s_a+1)(2s_b+1)}\frac{\Gamma_{ab}\Gamma_{cd}}{(M_R-E)^2+\Gamma_R^2/4}, \quad (1)$$

where $\Gamma_{ab,cd}$ are the partial widths for the two processes $R \to a+b$, $R \to c+d$, k is the proton momentum in CM system and M_R, Γ_R are the mass and the total width of the resonance.

The observed excitation curve is the convolution of (1) with the antiproton beam energy distribution $G(E'-E)$:

$$\sigma(E) = \epsilon\alpha\int_0^\infty \sigma_{BW}(E')G(E'-E)dE', \quad (2)$$

where ϵ and α are the detection efficiency and geometrical acceptance for the selected final state.

The resonance is scanned by moving the antiproton beam energy and measuring the number of observed events N_i at each energy point E_i:

$$N_i = \int dt\mathcal{L}(t)[\sigma(E_i)+\sigma_{bkg}(E_i)], \quad (3)$$

where $\mathcal{L}(t)$ is the instantaneous luminosity and $\sigma_{bkg}(E)$ the background cross section.

The resonance parameters and branching ratios are then obtained from the observed N_i after deconvolution of the beam energy spectrum from the measured resonance profile (2).

A detailed description of the E835 experimental setup can be found in [7].

3 Recent results on χ_{c0}

E835 obtained the first evidence of the formation of the χ_{c0} in $\bar{p}p$ annihilations [8] and recently published the most precise measurement of the χ_{c0} mass, width and branching ratio $\mathcal{B}(\chi_0 \to \overline{p}p)$ [9]. This result is based on a 33 pb^{-1} data sample collected during the year 2000 data taking.

E835 studied the χ_{c0} through the reaction:

$$\overline{p}p \to \chi_0 \to J/\psi\gamma \to e^+e^-\gamma.$$

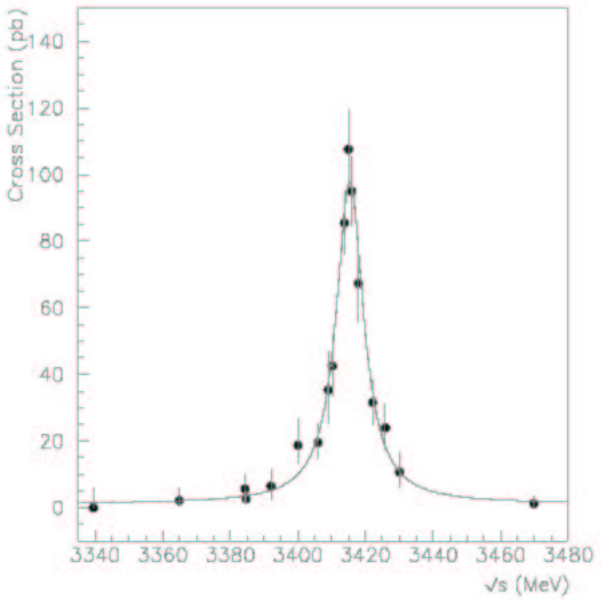

Figure 2: χ_{c0} *scan: measured cross section.*

The events are selected requiring a pair of identified e^+e^- and a photon satisfying the $e^+e^-\gamma$ kinematics. Figure 2 shows the measured cross section. Table 1 summarizes the results of E835 year 2000 data and previous experiment results.

Our value obtained for $\mathcal{B}(\chi_{c0} \to \overline{p}p)$ is larger than $\mathcal{B}(\chi_{c1,2} \to \overline{p}p) \sim 1 \times 10^{-4}$, so there is no evidence of the suppression of spin 0 $\overline{c}c$ states in $\overline{p}p$ annihilation, as suggested by hadron helicity conservation rule in massless QCD.

The leading order theoretical predictions [13, 14] for the ratio:

$$R = \frac{\Gamma(\chi_{c0} \to gg)}{\Gamma(\chi_{c2} \to gg)} = \frac{15}{4} \times \frac{1 + 3.12\alpha_s}{1 - 0.3\alpha_s} = 8.5 \pm 0.5, \qquad (4)$$

obtained using $\alpha_s = 0.33 \pm 0.03$ [15], can be compared with the experimental

Table 1: *χ_{c0} mass, width and branching ratio to $\overline{p}p$ measured by E835 and comparison with recent results from other experiments.*

	$M(\chi_{c0})$ (MeV/c^2)	$\Gamma(\chi_{c0})$ (MeV)	$\mathcal{B}(\overline{p}p) \times 10^4$
E835-II	$3415.4 \pm 0.4 \pm 0.2$	$9.8 \pm 1.0 \pm 0.1$	$4.1 \pm 0.3^{+1.6}_{-0.9}$
E835-I [8]	$3417.4^{+1.8}_{-1.9} \pm 0.2$	$16.6^{+5.2}_{-3.7} \pm 0.1$	$4.8^{+0.9+2.1}_{-0.8-1.1}$
BES [10, 11]	$3414.1 \pm 0.6 \pm 0.8$	$14.3 \pm 2.0 \pm 3.0$	$1.59 \pm 0.43 \pm 0.53$
CBAL [12]	$3417.8 \pm 0.4 \pm 4$	$13.5 \pm 3.3 \pm 4.2$	-

value, which can be determined by the following expression [16, 17]:

$$R = \frac{\Gamma(\chi_{c0} \to had) - \Gamma(\chi_{c1} \to had)}{\Gamma(\chi_{c2} \to had) - \Gamma(\chi_{c1} \to had)}. \tag{5}$$

Assuming that $\Gamma(\chi_{cJ} \to had)$ can be obtained by subtracting the radiative width $\Gamma(\chi_{cJ} \to J/\psi\gamma)$ from the total resonance width $\Gamma(\chi_{cJ})$, using the widths in the PDG [15] and the last E835 $\Gamma(\chi_{c0})$ measurement, we obtained $R = 8.3 \pm 2.1$, in very good agreement with (4).

4 Two photon decays of charmonium states

The $\gamma\gamma$ final state is the main channel for the study of the η_c and η_c' resonances for E835.

E835 collected 18 pb^{-1} in the η_c energy region. The analysis is still under way but some preliminary results for its mass, width and branching ratio into $\gamma\gamma$ are:

$$M(\eta_c) = 2985.4 \pm 2.1 \pm 2\text{MeV/c}^2, \tag{6}$$

$$\Gamma(\eta_c) = 21.6^{+7.5}_{-6.2}\text{MeV}, \tag{7}$$

$$\Gamma_{\gamma\gamma}(\eta_c) = 3.9^{+1.5}_{-1.3}\text{keV}, \tag{8}$$

where (8) has been obtained using $\mathcal{B}(\eta_c \to \overline{p}p) = (1.2 \pm 0.4) \times 10^{-3}$ from the PDG [15]. $M(\eta_c)$ is in agreement with the PDG average [15] and with previous experiments at e^+e^- colliders; the total width is larger than the world average $\Gamma(\eta_c) = 13.2^{+3.8}_{-3.2}$keV [15] but it is in agreement with a recent result from CLEO [18].

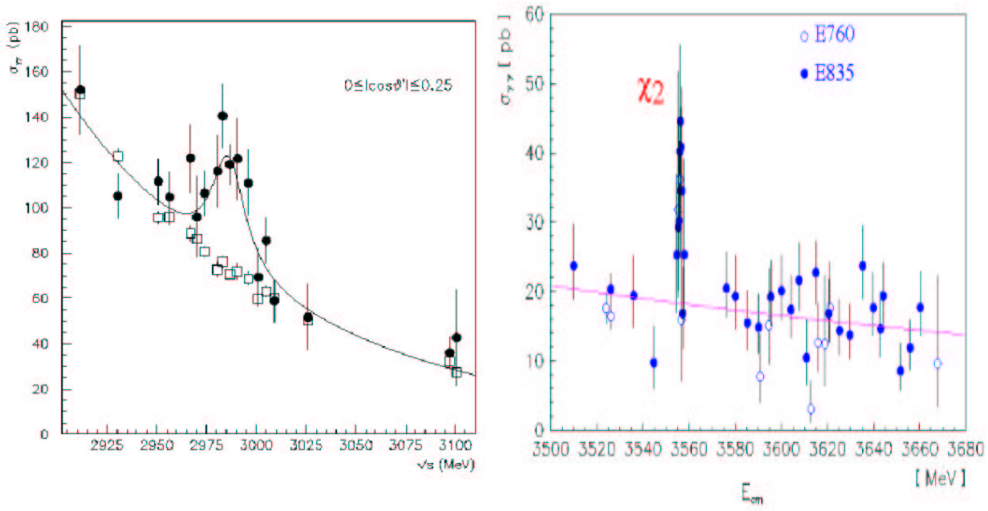

Figure 3: η_c *scan and search for the* η_c' *in the* $\gamma\gamma$ *channel (preliminary result).*

The first observation of the η_c' candidate comes from Crystal Ball [2) 1], they measured its mass and gave a limit for the width:

$$M(\eta_c') = 3594 \pm 5\text{MeV/c}^2, \quad (9)$$

$$\Gamma(\eta_c') < 8.0\text{MeV (C.L. 95\%)}. \quad (10)$$

E835 performed a scan in the energy region from 3570 MeV to 3660 MeV looking for the decay $\eta_c' \to \gamma\gamma$ but the results do not confirm the presence of the resonance (see figure 3) [20].

The analysis of $\gamma\gamma$ final state allowed also the measurement of the branching ratios $\mathcal{B}(\chi_{c0,2} \to \gamma\gamma)$. E835 collected in the first run 3.4 pb^{-1} in the χ_{c0}

[1]Recently Belle experiment observed a η_c' candidate in exclusive $B \to KK_SK^-\pi^+$ decays, with $M(\eta_c') = 3654 \pm 6 \pm 8\text{MeV/c}^2$ and $\Gamma(\eta_c') < 55\text{MeV}$ (C.L. 90%) [19].

Table 2: *ψ' branching ratios values for different channels as measured by E760* [22] *and E835 (1996-97)* [23].

Chan	E760	E835
e^+e^-	$(8.3 \pm 0.5 \pm 0.7) \times 10^{-3}$	$(7.4 \pm 0.2 \pm 0.7) \times 10^{-3}$
$J/\psi\pi^0\pi^0$	$0.184 \pm 0.019 \pm 0.013$	$0.187 \pm 0.009 \pm 0.013$
$J/\psi\pi^+\pi^-$	$0.283 \pm 0.021 \pm 0.020$	–
$J/\psi\eta$	$0.032 \pm 0.010 \pm 0.002$	$0.041 \pm 0.003 \pm 0.005$

energy region and 8.4 pb^{-1} for the χ_{c2} and measured [21]:

$$\mathcal{B}(\chi_{c0} \to \gamma\gamma) = (0.97 \pm 0.50 \pm 0.28) \times 10^{-4}, \quad (11)$$

$$\mathcal{B}(\chi_{c2} \to \gamma\gamma) = (1.35 \pm 0.25 \pm 0.12) \times 10^{-4}. \quad (12)$$

The (12) is by far the most precise evaluation of $\mathcal{B}(\chi_{c2} \to \gamma\gamma)$.

The analysis of the χ_{c0} data taken in the second run period is under way. The much higher luminosity collected on this resonance will allow a new measurement of $\mathcal{B}(\chi_{c0} \to \gamma\gamma)$ with higher statistics and improved precision.

5 ψ' branching ratios

The identification of e^+e^- pairs in the final state allows the selection of the cannels:

$$\overline{p}p \to \psi' \to e^+e^-,$$

$$\overline{p}p \to \psi' \to J/\psi X \to e^+e^- X.$$

The measurement of the branching ratios for these ψ' decay channels was performed by E760 [22] and later by E835 [23], that confirmed the E760 results but with much higher statistics. The results by the two experiments are summarized in table 2.

During year 2000 E835 collected 15 pb^{-1} of data in the ψ' energy region. The analysis of this data is still in progress.

6 Proton e. m. form factors in the time-like region

E760 and E835 also measured the proton form factor in the time-like region by selecting the non resonant exclusive reaction:

$$\overline{p}p \to e^+e^-.$$

The differential cross section for this process can be expressed as a function of the proton electric and magnetic form factors $G_E(s)$ and $G_M(s)$:

$$\frac{d\sigma}{d\Omega} = \frac{\alpha^2}{4\beta_p s}\left[|G_M|^2(1+\cos^2\theta^*) + \frac{4m_p^2}{s}|G_E|^2\sin^2\theta^*\right]. \tag{13}$$

From the total cross section is then possible to use the (13) to extract $|G_M|$.

The asymptotic QCD prediction is given by:

$$\frac{|G_M|}{\mu_p} = \frac{C}{s^2}\cdot\ln\left(\frac{s}{\Lambda^2}\right)^{-2}, \tag{14}$$

where C and Λ are free parameters to be used in the data fit.

Figure 4 shows the preliminary result for $|G_M|$, in the $|G_E| = |G_M|$ approximation, together with previous measurements. Preliminary results for the fit of all the experimental data with (14) are: $C = 57^{+12}_{-9}$ and $\Lambda = 0.30 \pm 0.05$, with a $\chi^2/n.d.f. = 1.7$.

References

1. M. Andreotti[2], S. Bagnasco[3], W. Baldini[2], D. Bettoni[2], G. Borreani[7], A. Buzzo[3], R. Calabrese[2], R. Cester[7], G. Cibinetto[2], P. Dalpiaz[2], G. Garzoglio[1], K. Gollwitzer[1], M. Graham[5], M. Hu[1], D. Joffe[6], J. Kasper[6], G. Lasio[4], M. Lo Vetere[3], E. Luppi[2], M. Macrì[3], M. Mandelkern[4], F. Marchetto[7], M. Marinelli[3], E. Menichetti[7], Z. Metreveli[6], R. Mussa[7], M. Negrini[2], M. Obertino[7], M. Pallavicini[3], N. Pastrone[7], C. Patrignani[3], S. Pordes[1], E. Robutti[3], W. Roethel[4], J. Rosen[6], P. Rumerio[6], R. Rusack[5], A. Santroni[3], J. Schultz[4], S. H. Seo[5], K. K. Seth[6], G. Stancari[2], M. Stancari[2] A. Tomaradze[6], T. Vidnovic III[5], S. Werkema[1] and P. Zweber[6]. [1] *Fermi National Accelerator Laboratory, Batavia, Illinois 60510*, [2] *University of Ferrara and INFN, 44100 Ferrara, Italy*, [3] *University of Genova and INFN, 16146 Genova, Italy*, [4] *University of California at Irvine, California 92697*,

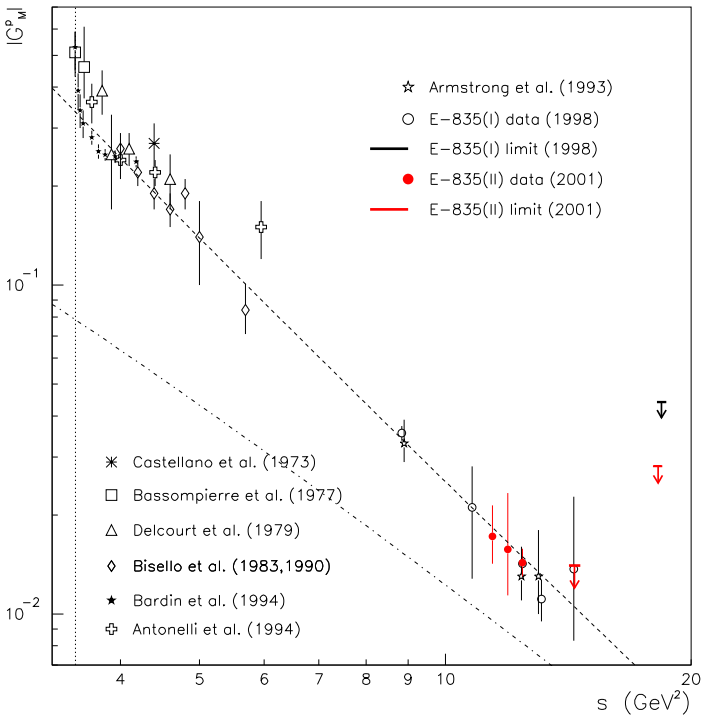

Figure 4: *Proton magnetic form factor in the time-like region (preliminary result). The dot-dashed line represents the dipole behavior of the form factor in the space-like region.*

[5] *University of Minnesota, Minneapolis, Minnesota 55455,* [6] *Northwestern University, Evanston, Illinois 60208,* [7] *University of Torino and INFN, 10125 Torino, Italy.*

2. C. Edwards *et al.*, Phys. Rev. Lett. **48**, 70 (1982).

3. T. A. Armstrong *et al.*, Phys. Rev. Lett. **69**, 2337 (1992).

4. C. Baglin *et al.*, CERN proposal CERN/ISRC/80-14 (1980) (unpublished).

5. C. Baglin *et al.*, Phys. Lett. B **172**, 455 (1986).

6. V. Bharadwaj *et al.*, Fermilab proposal P760 (1985) (unpublished).

7. M. Ambrogiani *et al.*, Experiment E835 at Fermilab (in preparation). To be submitted to NIM.

8. M. Ambrogiani *et al.*, Phys. Rev. Lett. **83**, 2902 (1999).
9. S. Bagnasco *et al.*, Phys. Lett. B **533**, 237 (2002).
10. J. Z. Bai *et al.*, Phys. Rev. D **60**, 072001 (1999).
11. J. Z. Bai *et al.*, Phys. Rev. Lett. **81**, 3091 (1998).
12. J. Gaiser *et al.*, Phys. Rev. D **34**, 711 (1986).
13. Y. A. Novikov *et al.*, Physics Reports **41**, 1 (1978).
14. R. Barbieri *et al.*, Nucl. Phys. B **192**, 61 (1981).
15. D. E. Groom *et al.*, Eur. Phys. J. C **15**, 1 (2000).
16. G. Bodwin, E. Braaten and G. Lepage, Phys. Rev. D **46**, 1914 (1992).
17. M. Mangano and A. Petrelli, Phys. Lett. B **352**, 445 (1995).
18. G. Brandenburg *et al.*, Phys. Rev. Lett. **85**, 3095 (2000).
19. S. K. Choi *et al.*, hep-ex/0206002 (2002) (submitted to Phys. Rev. Lett.)
20. M. Ambrogiani *et al.*, Phys. Rev. D **64**, 052003 (2001).
21. M. Ambrogiani *et al.*, Phys. Rev. D **62**, 052002 (2000).
22. T. A. Armstrong *et al.*, Phys. Rev. D **55**, 1153 (1997).
23. M. Ambrogiani *et al.*, Phys. Rev. D **62**, 032004 (2000).
24. T. A. Armstrong *et al.*, Phys. Rev. Lett. **70**, 1212 (1993).
25. M. Ambrogiani *et al.*, Phys. Rev. D **60**, 032002 (1999).

Frascati Physics Series Vol. XXVIII (2002), pp.075-075
HQ & L 2002 – Vietri s/m, May 27th - June 1st, 2002

SUSY EFFECTS IN NEUTRAL MESON SYSTEM *

Guido Martinelli
Universitá di Roma La Sapienza, Italy

* Written contribution not received

Frascati Physics Series Vol. XXVIII (2002), pp.077-088
HQ & L 2002 – Vietri s/m, May 27th - June 1st, 2002

V_{us} determination and chiral dynamics in K decays

Gilberto Colangelo
Institut für Theoretische Physik der Universität Zürich
Winterthurerstr. 190, CH–8057 Zürich

ABSTRACT

We discuss the present situation of the determination of V_{us} from K_{e3} decays, and emphasize recent developments both on the theory side, where a complete analysis of isospin breaking corrections has become available, and on the experimental side, where preliminary data of a new, more precise measurement of the K_{e3} branching ratio have appeared. Other K decays for which new data have recently been published and where some interesting chiral dynamics takes place are also briefly discussed.

1 Introduction

The low–energy interactions of the pseudoscalar mesons are strongly constrained by the chiral symmetry of QCD. For this reason the term chiral dynamics is often used to indicate the strong interactions in this energy regime. Actually,

the big progress made in recent years in dealing with hadrons at low energy has shown that we need to take into account more than the pure dynamics of the Goldstone bosons in the chiral limit, if we want to reach the necessary level of accuracy. The two examples I will discuss here will clearly show that. On the other hand, the effective Lagrangian framework of chiral perturbation theory (CHPT) is extremely useful in analyzing all these effects, whether they are of chiral, or nonchiral nature. In the following I will illustrate this with the help of two kaon decays for which there are new data available.

2 The Lagrangian of chiral perturbation theory

At lowest order the Lagrangian of CHPT is remarkably simple[1] [1, 2]:

$$\begin{aligned} \mathcal{L}^{(2)} &= \frac{F^2}{4}\langle D_\mu U D^\mu U^\dagger + U\chi^\dagger + \chi U^\dagger\rangle + C\langle QUQU^\dagger\rangle \\ &+ c_2\langle \lambda_6 D_\mu U^\dagger D^\mu U\rangle + c_3(27_L, 1_R) \ , \end{aligned} \tag{1}$$

where

$$\begin{aligned} D_\mu U &= \partial_\mu U - i r_\mu U + i U l_\mu \quad \chi = 2B(M + s + ip) \\ M &= \mathrm{diag}(m_u, m_d, m_s) \quad Q = e\cdot \mathrm{diag}(2/3, -1/3, -1/3) \ , \end{aligned} \tag{2}$$

where U is the usual exponential of the matrix containing the octet of the Goldstone bosons, while r_μ, l_μ, s and p are matrices of external fields. $\langle A\rangle$ stands for the trace of A. The simplicity of this Lagrangian is particularly remarkable in view of the variety of phenomena that it describes: the first two terms describe the strong interactions of the octet of the pseudoscalars between themselves and with external sources. The third, proportional to C describes the electromagnetic effects due to the exchanges of one virtual photon, while the remaining terms account for the effects generated by virtual exchanges of a W or a Z between quarks.

The five constants which appear in the Lagrangian are not fixed by the symmetry but are easily determined in the comparison to the simplest of the observables:

$$F_\pi = F + O(m) \ , \quad M^2_{\pi^0} = B(m_u + m_d) \ ,$$

[1] For simplicity's sake I do not write down explicitly the 27plet, nor the the CP–odd part of the weak Lagrangian.

$$M^2_{\pi^+} - M^2_{\pi^0} \;=\; 2e^2\frac{C}{F^2}\;,\quad A^{(1/2)}_{K\to\pi\pi} \sim c_2 - \frac{2}{3}c_3\;,\quad A^{(3/2)}_{K\to\pi\pi} \sim c_3\;. \qquad (3)$$

Having fixed these constants, we can now calculate any other new observable, and make a prediction. For example the $\pi\pi$ scattering amplitude and the K_{l3} form factors are given by:

$$A(s,t,u) = \frac{s-M^2_\pi}{F^2_\pi} \Rightarrow a^0_0 = \frac{7M^2_\pi}{32\pi F^2_\pi} = 0.16\;, \qquad (4)$$

$$\begin{aligned}\langle\pi^-(p)|V_\mu|K^0(k)\rangle &= (k+p)_\mu f_+(t) + (k-p)_\mu f_-(t)\;\;,\quad t=(k-p)^2\\ f_+(t) &= 1\;,\quad f_-(t) = 0\;.\end{aligned} \qquad (5)$$

2.1 The Lagrangian at next–to–leading order and beyond: strong sector

In the strong sector the situation is the following:

$$\begin{aligned}O(p^2) &\Rightarrow \frac{F^2}{4}\langle D_\mu U D^\mu U^\dagger + U\chi^\dagger + \chi U^\dagger\rangle\;,\\ O(p^4) &\Rightarrow \text{10 new LEC, Gasser and Leutwyler } {}^{2)},\; L_i\;,\\ O(p^6) &\Rightarrow \text{96 new LEC, Fearing, Scherer, Bijnens, G.C., Ecker } {}^{3)}\;,\; C_i\;.\end{aligned}$$

For all the ten L_i's we have either a good phenomenological determination, or a sound theoretical estimate. In order to get a prediction at order p^4 in this sector one simply needs to do the one–loop calculation, remove the divergences with the help of the counterterms, and insert the numerical values of the finite parts from the most recent estimates. At this level the situation is almost as good as at order p^2. This is best seen with a couple of examples, like the $\pi\pi$ scattering lengths and the K_{e3} form factors, that we have seen before at leading order. The next–to–leading order corrections are [2, 4]

$$\begin{aligned}a^0_0 &= \frac{7M^2_\pi}{32\pi F^2_\pi}\left[1 + \frac{M^2_\pi}{3}\langle r^2\rangle^\pi_S + \frac{200\pi F^2_\pi M^2_\pi}{7}(a^0_2+2a^2_2) + \frac{M^2_\pi}{16\pi^2F^2_\pi}\Delta^0_0\right]\\ &= 0.16\cdot[1.25] = 0.20\;,\end{aligned} \qquad (6)$$

$$f_+(t) \;=\; f_+(0)\left(1+\lambda_+\frac{t}{M^2_\pi}\right)\;,\; \lambda_+ = \frac{M^2_\pi}{6}\langle r\rangle^\pi_V + \Delta_+ = 0.031\;. \qquad (7)$$

The formulae above neatly illustrate the beauty of the method: the S–wave scattering lengths and the K_{e3} form factors are expressible in terms of other

observables (like the scalar and vector radii, $\langle r^2\rangle_S^\pi$ and $\langle r\rangle_V^\pi$, respectively, the two D–wave scattering lengths, $a_2^{0,2}$), plus other small corrections (indicated by the Δ symbols). The relation between these observables is exact up to order p^4, and will get corrections if we want to increase the precision of the calculation. By inserting the most recent values for the observables on the right–hand sides, one gets the numerical predictions given above. We will discuss the situation for the $\pi\pi$ scattering lengths in detail below. As for the K_{e3} form factors, the slope λ_+ is quite well known, and the PDG [5] reports a number which is in excellent agreement with the one loop calculation above: $\lambda_+ = 0.0286 \pm 0.0022$.

If we move up to order p^6 the situation worsens considerably, and it becomes impossible to write down expressions as nice as those in Eq. (67). We have to give expressions in terms of the new low–energy constants C_i's, and since we know practically nothing about them, it is an obvious question whether these calculations represent an improvement at all in the final numerical predictions. Before discussing the matter in more detail in the following sections, we can already anticipate an answer at the intuitive level: The low–energy constants parametrise our ignorance of the dynamics which is not explicitly present in the formalism. They contain contributions from all the physics above the scale of the pseudoscalar mesons – the most prominent effect is the one due to the lowest–lying resonances, as it has been explicitly shown [6] at order p^4. Whenever a resonance or any other "high–energy" phenomenon is expected to influence substantially a low–energy quantity, one should expect a very important role of the low–energy constants, and a serious difficulty in making a precise prediction. On the other hand, observables dominated by the dynamics of the pseudoscalar, can be very well calculated within CHPT, and it makes good sense to push the calculations to order p^6, as one can expect the contribution of the low–energy constants to be suppressed. Explicit examples of both situations are given below.

2.2 The Lagrangian at next–to–leading order and beyond: weak and electromagnetic sectors

Both in the electromagnetic and weak sector, the situation becomes unpleasant already at next–to–leading order, where the number of constants immediately gets too large in comparison to the available experimental input:

E.m. sector:

$O(p^2)$ $\Rightarrow$ $C\langle QUQU^\dagger\rangle$,

$O(p^4)$ $\Rightarrow$ 14 LECs, Urech, Neufeld and Rupertsberger [7], K_i ,

+ leptons:

$O(p^4)$ $\Rightarrow$ 7 new LECs, Knecht et al. [8]

Weak sector:

$O(p^2)$ $\Rightarrow$ $c_2\langle\lambda_6 D_\mu U^\dagger D^\mu U\rangle$

$O(p^4)$ $\Rightarrow$ 37 LECs, Kambor, Missimer, Wyler, Ecker [9], N_i .

In both cases, given the practical unfeasibility of a determination of all the available constants, the typical strategy has been to focus on a few selected processes where the same constants occur. One can then exploit the experimental information on some processes to make predictions in other. There are plenty of examples in the literature. A fairly comprehensive review of the situation in the weak sector (especially for the radiative decays), including a list of the new experimental measurements that are possible at a Φ factory can be found in Ref. [10].

3 The extraction of V_{us} from K_{e3} decays

The matrix element and decay rate for K_{e3} decays can be expressed in terms of the two form factors that determine the matrix element of the vector current between a pion and a kaon, which we already introduced above (5)

$$\begin{aligned} \mathcal{M} &= \frac{G_F}{\sqrt{2}} V_{us}^* C \left[f_+(t)(k+p)_\mu + f_-(t)(k-p)_\mu \right] L^\mu \\ \Gamma(K_{e3}) &= \frac{G_F^2}{192\pi^3} M_K^5 |V_{us}|^2 C^2 |f_+(0)|^2 I(f_+, f_-) \end{aligned} \tag{8}$$

where C is a normalization factor, equal to 1 ($1/\sqrt{2}$) for neutral (charged) kaon decays, L^μ is the usual leptonic part of the matrix element, and $I(f_+, f_-)$ is the result of the phase space integration. If one wants to extract V_{us} from the experimental determination of the K_{e3} decay rate one needs:

1. the treatment of photonic radiative corrections;
2. an accurate evaluation of $f_+(0)$, including strong isospin violations;
3. an evaluation (or measurement, if available) of the momentum dependence of $f_\pm(t)$.

The first analysis that included all these ingredients was performed by Leutwyler and Roos [11]. In summary they

1. relied on previous work on the photonic radiative corrections, both for the short– (Sirlin [12]) and the long–distance (Ginsberg [13]) part of this contribution. They estimated an effect in the rate of the form $(1+\delta)$, $\delta \simeq \pm 1\%$;

2. relied on CHPT to $O(p^4)$ for the evaluation of $f_+(0)$, and on a quark model for the estimate of higher–order corrections, obtaining $f_+^{K^0\pi^-}(0) = 0.961 \pm 0.008$ and $f_+^{K^+\pi^0}(0)/f_+^{K^0\pi^-}(0) = 1.022$;

3. relied on CHPT at $O(p^4)$ for the evaluation of λ;

and obtained

$$V_{us} = 0.2196 \pm 0.0023 \tag{9}$$

A recent numerical update of the same analysis was performed by Calderon and Lopez-Castro [14], with substantially an unchanged numerical value. New analytical ingredients where brought to this kind of analysis by Cirigliano et al. [15], who did a complete $O(p^4, \epsilon p^2)$ analysis of the isospin breaking corrections in the framework of CHPT (ϵ stands for both e^2 and $m_u - m_d$). The first observation is that in the presence of these corrections the very structure of the amplitude is modified, both because the form factors now depend on another kinematical variable $f_\pm(t) \longrightarrow f_\pm(t, q^2)$, and because new local contributions, due to the Urech LECs appear. The final result, however, is compatible with that of Leutwyler and Roos:

$$f_+^{K^+\pi^0}(0) = 0.998(\mathrm{LR}) \;\Rightarrow\; 1.0034 \pm 0.0027(\mathrm{CKNRT}) \;. \tag{10}$$

In addition to these changes to the amplitude, one is also forced to take into account the contribution from soft photons, which then change the integration over the phase space. Their result can be summarized by

$$\begin{aligned} f_+(t) &= f_+(0)\left(1 + \lambda_+ t/M_\pi^2\right) \Rightarrow I(f_+, f_-) = I(\lambda_+, \alpha) \\ I(\lambda_+, \alpha) &= I(\lambda_+, 0)(1 + \Delta I(\lambda+)) \quad \Delta I(\lambda+) = -1.3\% \end{aligned}$$

Apart from the exact numerical value of these corrections (which, in order to be evaluated very precisely, must also take into account some details of the specific

experimental setup), the important message arising from this calculation is that these corrections are small and under very good control.

Concerning the higher order corrections to $f_+(0)$, the situation has not improved substantially after Leutwyler and Roos analysis. Here we summarize what is known about these. We write the form factor in a chiral expansion whose first two terms are very well known (the Ademollo–Gatto theorem forbids the presence of local terms in f_2, which is given in terms of masses and decay constants)

$$f_+(0) = f_0 + f_2 + f_4 \ , \quad f_0 = 1 \, , \quad f_2^{K^0\pi^+} = -0.023 \ .$$

As for f_4 the situation is much less clear:

- Leutwyler–Roos on the basis of general arguments (within the framework of a light–cone description of the pion and kaon wavefunctions), came up with the estimate
$$f_4 = -0.016 \pm 0.008$$

- Various quark–model calculations [16] roughly confirm this estimate (sign and size), although some indicate that the error might be a bit too small (or that one should intepret it as gaussian error, as suggested by Leutwyler and Roos, rather than a strict theoretical boundary);

- Bijnens, Ecker and myself [17], calculated the double chiral logs contribution to this quantity, and obtained
$$|f_4| \leq 0.5\%$$

- Post–Schilcher recently completed a full two–loop evaluation and obtained [18]
$$f_4 = 1.8\%$$
by putting to zero all the relevant $O(p^6)$ LECs at $\mu = M_K$. Notice the sign difference with respect ot Leutwyler and Roos. In order to make full use of the latter very important and difficult calculation a more complete numerical analysis, which includes an estimate of the $O(p^6)$ LECs is certainly needed.

This brief summary clearly indicates the need for more theoretical work on this issue. We need an assessment of the central value and uncertainty of f_4. For the time being, however, the best choice is probably to stick to Leutwyler and Roos' estimate. This is what Cirigliano et al. have also done, and, putting together all the elements of their analysis, obtained [15]

$$V_{us} = 0.2201 \pm 0.0013(\Delta\Gamma) \pm 0.0008(\Delta\lambda_+) \pm 0.0019(\Delta f_+(0)) \ . \qquad (11)$$

As it is well known, the determination of V_{ud},and requirement that the CKM matrix be unitary lead to a constraint for V_{us} (the contribution of V_{ub} to the unitarity condition is negligible. The present PDG value for V_{ud} requires

$$V_{us} = 0.2287 \pm 0.0034 \ , \qquad (12)$$

which is about two standard deviations away from the direct determination.

However, only few days before this conference, at the meeting of the Division of Particles and Fields of the American Physical Society, the E865 collaboration of Brookhaven has announced [19] new preliminary data on the K_{e3} branching ratio, which is higher than the previous PDG value

$$\begin{aligned} BR(K^+_{e3}) &= (5.13 \pm 0.02 \pm 0.08 \pm 0.04)\% \quad \text{E865} \\ BR(K^+_{e3}) &= (4.82 \pm 0.06)\% \qquad\qquad\qquad\quad \text{PDG fit} \end{aligned} \qquad (13)$$

If we simply multiply the value of V_{us} above (11) by the square root of the ratio of the E865 to the old PDG branching ratio, we get

$$V_{us} = 0.2271 \pm 0.0024$$

which is in excellent agreement with CKM unitarity (12). Of course, since this number is based on a preliminary experimental result, and on a very naive numerical analysis, it should be considered only as a very preliminary indication of a new value for V_{us}. We eagerly await the outcome of a full–fledged numerical analysis, which also explicitly takes into account the treatment of the real photon emission.

This very timely good news about V_{us} has been counterbalanced by another timely news: on the 27 May 2002 issue of Physical Review Letters the result of a new measurement of the ratio of g_A/g_V from neutron beta decay has appeared [20]. The value for V_{ud} derived from this measurement is

$$V_{ud} = 0.9713 \pm 0.0013 \ , \qquad (14)$$

which would make the problem of unitarity come back again, even with the newly measured K_{e3} branching ratio. This value of V_{ud} is to be compared to the average of older measurement from the neutron β decay, $V_{ud} = 0.9790 \pm 0.0016$, and to the results of measurements from nuclear superallowed Fermi transitions as summarized by the PDG, $V_{ud} = 0.9740 \pm 0.0010$. The only conclusion one can draw from this list of numbers is that the issue of unitarity for the first row of the CKM matrix is still open. More on the neutron and nuclear beta decay can be found in Kleinknecht's contribution to this volume [21].

4 Analysis of $K \to \pi\gamma\gamma$ up to order p^6.

Assuming CP conservation the $A(K_L \to \pi^0\gamma\gamma)$ is determined by two invariant amplitudes, $A(s,\nu)$ and $B(s,\nu)$, $s = (q_1+q_2)^2, \nu = p_K \cdot (q_1 - q_2)$, where $q_{1,2}$ are the momenta of the two photons, and p_K that of the kaon. At order p^2: $A = B = 0$. At order p^4 [22]: $A = 4/s(s - M_\pi^2)F(s/M_\pi^2) + \ldots$, and $B = 0$, where $F(x)$ is a loop function generated by the $\pi\pi$ intermediate state in the s channel, that represents the dominant effect at this order, and the ellipsis stands for other less important contributions. Although the shape of the spectrum was nicely confirmed by the first two experiments that could measure this decay [23], the branching ratio was found to be a factor three too small. Recently there have been two new and much more precise measurements of this decay [27, 28], which give a slightly smaller branching ratio, which is still, however, about a factor two larger than the $O(p^4)$ chiral prediction:

$$BR = \begin{cases} 0.67 \times 10^{-6} & O(p^4) \\ (1.7 \pm 0.3) \times 10^{-6} & (\text{NA31}) \\ (1.86 \pm 0.60 \pm 0.60) \times 10^{-6} & (\text{E731}) \\ (1.68 \pm 0.07 \pm 0.08) \times 10^{-6} & (\text{KTeV}) \\ (1.36 \pm 0.03 \pm 0.03 \pm 0.03) \times 10^{-6} & (\text{NA48}) \end{cases} \qquad (15)$$

A large $O(p^6)$ contribution is very clearly needed. The calculations at order p^6 [24] have considered only the (possibly dominant) corrections to the pion loops, and added to this a polynomial contribution:

$$\begin{aligned} A &= \frac{4}{s}(s - M_\pi^2)\tilde{F}\left(\frac{s}{M_\pi^2}\right) + 4a_V \frac{3M_K^2 - s - M_\pi^2}{M_K^2} + \ldots \\ B &= \tilde{G}\left(\frac{s}{M_\pi^2}\right) - 8a_V + \ldots \ , \end{aligned}$$

where $\tilde{F}(x)$ and $\tilde{G}(x)$ also come from the $\pi\pi$ intermediate state in the s channel. To get into agreement with the experiment one needed to have a large and negative a_V: $BR = 0.83 \times 10^{-6}$ with $a_V = 0$ and $BR = 1.60 \times 10^{-6}$ with $a_V = -0.9$. An accurate measurement of the spectrum, as done in the two most recent measurement, allows a rather precise determination of a_V. According to NA48 the best fit is obtained with

$$a_V = -0.46 \pm 0.03 \pm 0.04 \ , \tag{16}$$

which is quite larger than what dimensional analysis would suggest $|a_V| \sim 0.1$. On the other hand D'Ambrosio and Portolés [25] have shown that this large value can be explained in a model with vector meson exchanges: this decay has the very interesting feature of showing one aspect (the spectrum) which is dominated by chiral dynamics (pion rescattering), and another aspect (the branching ratio) which is dominated by resonance exchange. The analysis of NA48 also shows that the more freedom allowed by Gabbiani and Valencia [26] in their analysis is not really necessary, and that the VMD model does describe accurately enough the data.

A very important consequence of this measurement is that one can now put a boundary on the CP conserving part of the $K_L \to \pi^0 e^+ e^-$ decay, which is a very rare decay where new physics has still a chance to show up. According to NA48

$$BR(K_L \to \pi^0 e^+ e^-)_{CPC} = (4.7 \pm 2.2) \times 10^{-13} \ . \tag{17}$$

5 Conclusions

K decays are a very important source of information on the CKM matrix and on flavour physics. In order to understand them and extract from experiments the information on the Standard Model parameters we must make use of the chiral symmetry constraints – and this is best done using CHPT. At the level of precision we have reached, both on the experimental and on the theoretical side, CHPT must often be pushed to higher orders – the number of completed two–loop calculations is steadily increasing – and moreover, must be supplemented by various other theoretical tools, like dispersion relations, large N_C arguments, models for resonance exchanges etc. I have discussed here a couple of examples where new and very precise data force us theorists to use all the tools we have available to extract the important information which is hidden in the data.

Acknowledgements

Many thanks to Alexander Sher and Peter Truöl for communications about the new E865 results, and to the organizers for the invitation to this very interesting conference. This work is partly supported by Schweizerische Nationalfonds.

References

1. S. Weinberg, PhysicaA **96** (1979) 327.
2. J. Gasser and H. Leutwyler, Annals Phys. **158** (1984) 142; Nucl. Phys. B **250** (1985) 465.
3. H. W. Fearing and S. Scherer, Phys. Rev. D **53** (1996) 315 [arXiv:hep-ph/9408346]. J. Bijnens, G. Colangelo and G. Ecker, JHEP **9902** (1999) 020; Annals Phys. **280** (2000) 100.
4. J. Gasser and H. Leutwyler, Nucl. Phys. **B250** (1985) 517.
5. D. E. Groom *et al.*, Eur. Phys. J. **C15** (2000) 1.
6. G. Ecker, J. Gasser, A. Pich and E. de Rafael, Nucl. Phys. **B321** (1989) 311.
7. R. Urech Nucl. Phys. B **433** (1995) 234 [arXiv:hep-ph/9405341]. H. Neufeld and H. Rupertsberger Z. Phys. C **71** (1996) 131 [arXiv:hep-ph/9506448].
8. M. Knecht, H. Neufeld, H. Rupertsberger and P. Talavera, Eur. Phys. J. C **12** (2000) 469 [arXiv:hep-ph/9909284].
9. J. Kambor, J. Missimer, and D. Wyler, Nucl. Phys. B **346** (1990) 17; G. Ecker, J. Kambor, and D. Wyler, Nucl. Phys. B **394** (1993) 101.
10. G. D'Ambrosio, G. Ecker, G. Isidori and H. Neufeld, in "The Second DAΦNE Physics Handbook", L. Maiani, G. Pancheri, N. Paver (eds.).
11. H. Leutwyler and M. Roos, Z. Phys. C **25** (1984) 91.
12. A. Sirlin, Nucl. Phys. B **196** (1982) 83, and references therein.
13. E. S. Ginsberg, Phys. Rev. D **1** (1970) 229.

14. G. Calderon and G. Lopez Castro, Phys. Rev. D **65** (2002) 073032 [arXiv:hep-ph/0111272].

15. V. Cirigliano, M. Knecht, H. Neufeld, H. Rupertsberger and P. Talavera, Eur. Phys. J. C **23** (2002) 121 [arXiv:hep-ph/0110153].

16. H. M. Choi and C. R. Ji, Phys. Rev. D **59** (1999) 034001 [arXiv:hep-ph/9807500], and references therein.

17. J. Bijnens, G. Colangelo and G. Ecker, Phys. Lett. B **441** (1998) 437 [arXiv:hep-ph/9808421].

18. P. Post and K. Schilcher, arXiv:hep-ph/0112352.

19. A. Sher (E865 Collaboration), talk given at the DPF 2002 meeting. Transparencies are available on–line: `http://www.dpf2002.org`.

20. H. Abele *et al.*, Phys. Rev. Lett. **88** (2002) 211801 [arXiv:hep-ex/0206058].

21. K. Kleinknecht, these proceedings.

22. G. Ecker, A. Pich, and E. de Rafael, Phys. Lett. B **189** (1987) 363. G. Cappiello, and G. D'Ambrosio, Nuovo Cim. A **99** (1988) 155.

23. V. Papadimitriou et al. (E731) Phys. Rev. **D44**, 573 (1991).
G.D. Barr et al. (NA31) Phys. Lett. **B 284**, 440 (1992).

24. G. Cappiello, and G. D'Ambrosio, and M. Miragliuolo Phys. Lett. B **298** (1993) 423. A. Cohen, G. Ecker, and A. Pich, Phys. Lett. B **304** (1993) 347. J. Kambor, and B.R. Holstein, Phys. Rev. D **49** (1994) 2346 [arXiv:hep-ph/9310324].

25. G. D'Ambrosio, and J. Portolés, Nucl. Phys. B **492** (1997) 417 [arXiv:hep-ph/9610244].

26. F. Gabbiani and G. Valencia, Phys. Rev. D **64** (2001) 094008 [arXiv:hep-ph/0105006].

27. A. Alavi-Harati *et al.* [KTeV Collaboration], Phys. Rev. Lett. **83** (1999) 917 [arXiv:hep-ex/9902029].

28. A. Lai *et al.* [NA48 Collaboration], Phys. Lett. B **536** (2002) 229 [arXiv:hep-ex/0205010].

Frascati Physics Series Vol. XXVIII (2002), pp.089-100
HQ & L 2002 – Vietri s/m, May 27th - June 1st, 2002

TESTS OF CHIRAL PERTURBATION THEORY IN RARE KAON DECAYS

Rainer Wanke
Institut für Physik, Universität Mainz, D-55099 Mainz, Germany

ABSTRACT

The neutral Kaon decays $K_S \to \gamma\gamma$ and $K_L \to \pi^0\gamma\gamma$ are very sensitive to higher order loop effects of Chiral Perturbation Theory (ChPT). New measurements of the NA48 experiment show that ChPT contributions of $\mathcal{O}(p^6)$ cannot be neglected in these modes. In addition a new measurement of the related decay $K_L \to \gamma\gamma$ and an upper limit of the rate of $K_S \to \pi^0\gamma\gamma$ are presented.

1 Introduction

Chiral Perturbation Theory (ChPT) has been proven as an extremely successful effective theory for low energy hadron dynamics. Nevertheless, the knowledge of higher order effects is rather scarse at present. The decays $K_S \to \gamma\gamma$ and $K_L \to \pi^0\gamma\gamma$ are well suited for investigation of higher order contributions. In

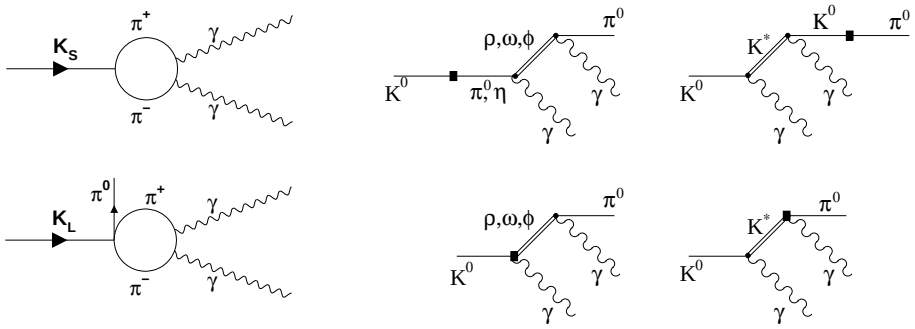

Figure 1: *Left:Examples of $\mathcal{O}(p^4)$ loop diagrams for $K_S \to \gamma\gamma$ and $K_L \to \pi^0\gamma\gamma$. Right: Vector meson exchange diagrams for $K_L \to \pi^0\gamma\gamma$.*

both cases the lowest order $\mathcal{O}(p^2)$ vanishes [1] and the next order $\mathcal{O}(p^4)$ can precisely been calculated, since no counter-terms exist [2, 3] (Fig. 1 (left)).

The $\mathcal{O}(p^4)$ prediction of the $K_S \to \gamma\gamma$ branching ratio is $\mathrm{Br}(K_S \to \gamma\gamma) = 2.1 \times 10^{-6}$ to an accuracy of about 5% [2]. Calculations of the next order $\mathcal{O}(p^6)$ do not exist up to now. The measured value of $\mathrm{Br}(K_S \to \gamma\gamma) = (2.6 \pm 0.5) \times 10^{-6}$ [4] is in agreement with this prediction, however, the experimental errors were still too large to allow an accurate comparison.

For $K_L \to \pi^0\gamma\gamma$ it is known that $\mathcal{O}(p^4)$ alone underestimates the observed branching fraction by about a factor of three [3, 5, 6]. At $\mathcal{O}(p^6)$ the rate can be reproduced by adding a vector meson exchange contribution [7] (Fig. 1 (right)) via the coupling constant a_V [8]. However, the parameter a_V has to be measured experimentally. Additional interest in measuring $K_L \to \pi^0\gamma\gamma$ arises, since it can constrain the CP conserving amplitude of the direct CP violating decay $K_L \to \pi^0 e^+ e^-$. The VMD mechanism could enhance the size of this amplitude, depending on the value of a_V [9].

2 Experimental Method

With KTeV and NA48 mainly two experiments have investigated neutral kaon decays into neutral final states in the recent years. Both experiments were built to perform precise measurements on the parameter ϵ'/ϵ of direct CP violation. Both are fixed target experiments with the neutral kaon beams being produced by high-energetic proton beams.

2.1 The NA48 Experiment

The NA48 experiment, located at the SPS accelerator at CERN, has been taking data for the $\mathrm{Re}(\epsilon'/\epsilon)$ measurement in the years $1997 - 1999$ and 2001. In addition to the regular ϵ'/ϵ data taking, several runs with a high intensity K_S beam have been taken, where the K_S intensity has been increased by more than a factor of 200 with respect to the ϵ'/ϵ runs. In the year 2000, the spectrometer has not been available. In this year half of the data taking took place under ϵ'/ϵ conditions while the second half of the run period was performed with a high intensity K_S beam.

2.2 The KTeV Experiment

The KTeV experiment is located at the TeVatron at Fermilab. It has been taking data in the years 1996, 1997, and 1999 with runs dedicated to determine $\mathrm{Re}(\epsilon'/\epsilon)$ and runs for measuring rare K_L and hyperon decays. The data from the last year of data taking are mostly still being analyzed.

2.3 Reconstruction of Neutral Decays

For detecting the photons in the final states of the decays discussed here, NA48 and KTeV use a quasi-homogeneous liquid krypton and, respectively, a CsI crystal electromagnetic calorimeter. By assuming a kaon decay, the z position (along the beam pipe) of the decay vertex can be calculated to

$$z_{\mathrm{vertex}} \;=\; z_{\mathrm{calorimeter}} \;-\; \frac{1}{m_K}\sqrt{\sum_{i>j} E_i E_j d_{ij}^2}\,,$$

with the shower energies $E_{i,j}$, distances d_{ij}, and the nominal kaon mass m_K. If photons are lost, the missing energy shifts the vertex position down-stream towards the calorimeter. If the decay contains one or more intermediate π^0, background can be suppressed by requiring the π^0 decay vertex to be consistent with the kaon decay vertex.

3 $K_{\mathrm{S,L}} \to \gamma\gamma$

For a decay rate measurement of $K_\mathrm{S} \to \gamma\gamma$ in a fixed-target experiment an irreducible background of $K_\mathrm{L} \to \gamma\gamma$ events has to be subtracted. Therefore, a precise determination of $K_\mathrm{L} \to \gamma\gamma$ is necessary while the current world average

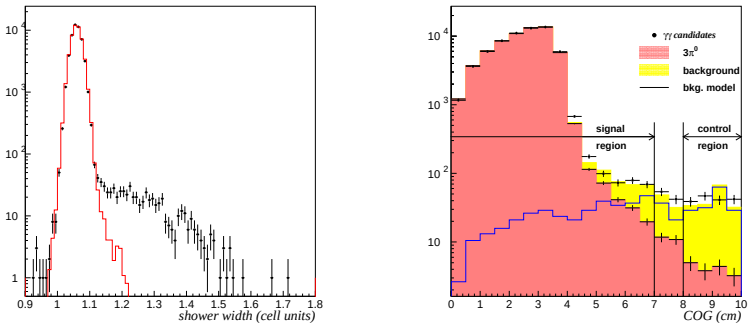

Figure 2: *Shower width (left) and center-of-gravity distribution (right) of the NA48 $K_{\rm L} \to \gamma\gamma$ candidates.*

on $\mathrm{Br}(K_{\rm L} \to \gamma\gamma)$ has a relative error of about 3% [10]. For this reason the NA48 experiment has used a different method for subtracting $K_{\rm L} \to \gamma\gamma$ events: In using the $K_{\rm L}$ target run in 2000 with a very similar experimental set-up the relative rate $\Gamma(K_{\rm L} \to \gamma\gamma)/\Gamma(K_{\rm L} \to 3\pi^0)$ is measured. By also measuring the $K_{\rm L} \to 3\pi^0$ rate in the high intensity $K_{\rm S}$ run 2000, the number of background $K_{\rm L} \to \gamma\gamma$ events can then be accurately subtracted.

3.1 $K_{\rm L} \to \gamma\gamma$

The NA48 $K_{\rm L}$ target run of the year 2000 has provided very clean conditions to measure $K_{\rm L} \to \gamma\gamma$ decays. Backgrounds from $K_{\rm L} \to 2\pi^0$ or other $K_{\rm L}$ decays are completely negligible, in particular $K_{\rm L} \to e^+e^-\gamma$ Dalitz decays are swept out by the spectrometer magnet. The only remaining background source is hadronic activity, e.g. from Λ decay products, which in rare cases might enter the decay volume via the $K_{\rm L}$ beam line. To estimate this background the sidebands in the shower width and center-of-gravity distributions are evaluated (Fig. 2). By using both methods, the hadronic background is determined to $(0.6 \pm 0.3)\%$, where the error reflects the difference of the two estimations.

The normalization channel $K_{\rm L} \to 3\pi^0$, which needs three good $\pi^0 \to \gamma\gamma$ combinations to be selected, is virtually background-free. Both, signal and normalization channel have trigger efficiencies larger than 99%. For the analyis only 25% of the $K_{\rm L}$ target run data were used which already provides sufficient statistics. Evaluating the event numbers in the vertex region -1 m $< z <$ 5 m

(measured from the K_S collimator) and taking the acceptance ratio from Monte Carlo simulation, NA48 finds

$$\frac{\Gamma(K_L \to \gamma\gamma)}{\Gamma(K_L \to 3\pi^0)} = (2.81 \pm 0.01_{stat} \pm 0.02_{syst}) \times 10^{-3}$$

The systematic error is dominated by uncertainties in the $\gamma\gamma/3\pi^0$ acceptance ratio. This result improves the current world average by about a factor of four.

3.2 $K_S \to \gamma\gamma$

In addition to the irreducible $K_L \to \gamma\gamma$ decays more background sources have to be taken into account when selecting $K_S \to \gamma\gamma$ candidates:

$K_S \to 2\pi^0$ with lost and/or overlapping photons may fake a good $\gamma\gamma$ event. Since in these cases energy is lost, the neutral vertex is shifted downstream. Background from $K_S \to 2\pi^0$ can therefore be efficiently rejected by restricting the allowed vertex range to be within -1 and 5 m behind the final collimator. Doing so, the remaining background from $K_S \to 2\pi^0$ is estimated to $(0.8 \pm 0.2)\%$, where the uncertainty is arising from the shower overlap probabilities being different in the simulation as in the data.

Further background sources are hadronic events (originating e.g. from scattering at the collimator) or from accidentally overlapping events. The first is determined by a sideband subtraction in the shower width distribution, the latter by a sideband subtraction in the time difference of the two showers (Fig. 3). From this, the total background from hadronic and accidental activity is estimated to $(0.8 \pm 0.3)\%$.

Finally, Dalitz decays $\pi^0 \to e^+e^-\gamma$ and $K^0 \to e^+e^-\gamma$ have to be taken into account. In the high intensity K_S running in 2000, the NA48 experiment had no magnetic field in the detector. Therefore, many Dalitz e^+e^- pairs did not separate and were overlapping in the calorimeter. From Monte Carlo Simulation, the probability of a Dalitz decay misidentified as $\gamma\gamma$ pair was estimated to about 30%. With Dalitz decay probabilities assumed to be equal for $K^0 \to \gamma\gamma$ and $\pi^0 \to \gamma\gamma$, the effect is twice as big for the $K_S \to 2\pi^0$ normalization than in the $K^0 \to \gamma\gamma$ events and results in a relative correction to the $K_S \to \gamma\gamma$ branching ratio of $(+1.5 \pm 0.3)\%$.

The decay vertex distribution of the NA48 $\gamma\gamma$ candidates is shown in Fig. 4 together with the estimated contributions of $K_S \to \gamma\gamma$, $K_L \to \gamma\gamma$ and $K_S \to 2\pi^0$

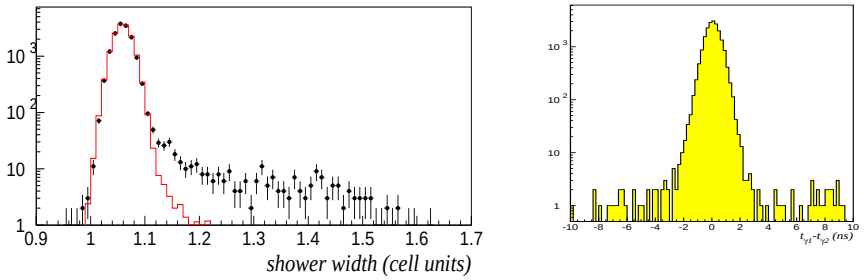

Figure 3: *Distributions of the normalized shower width (left) and the cluster time difference (right) of the NA48 $K_S \to \gamma\gamma$ candidates.*

background. The $K_S \to 2\pi^0$ background contribution has been normalized to the absolute K_S flux. In the fiducial region between -1 and 5 m about 20000 $\gamma\gamma$ candidates were found. Subtracting all background contributions and normalizing to fully reconstructed $K_S \to 2\pi^0$ events, the branching fraction was determined to

$$\mathrm{Br}(K_S \to \gamma\gamma) \;=\; (2.78 \pm 0.06_{\mathrm{stat}} \pm 0.04_{\mathrm{syst}}) \times 10^{-6}.$$

The systematic uncertainty is dominated by the branching fraction of the $K_S \to 2\pi^0$ normalization ($\pm 0.9\%$), the estimation of the hadronic and accidental background ($\pm 0.7\%$) and the Monte Carlo statistics ($\pm 0.6\%$).

This new result significantly improves the previous measurements and is in clear discrepancy with the $\mathcal{O}(p^4)$ based theoretical predictions.

4 $K_L \to \pi^0\gamma\gamma$

With four photons in the final state the decay $K_L \to \pi^0\gamma\gamma$ has almost the same signature as the CP-violating decay $K_L \to 2\pi^0$, which is one of the signal decays for the $\mathrm{Re}(\epsilon'/\epsilon)$ measurement of the KTeV and NA48 experiments. Therefore the decay $K_L \to \pi^0\gamma\gamma$ can be taken in parallel with regular ϵ'/ϵ data taking. Moreover, both signal and normalization ($K_L \to 2\pi^0$) have practically identical trigger efficiencies. However, the analysis of $K_L \to \pi^0\gamma\gamma$ events has to fight strong backgrounds, in particular $K_L \to 3\pi^0$ events with lost and/or

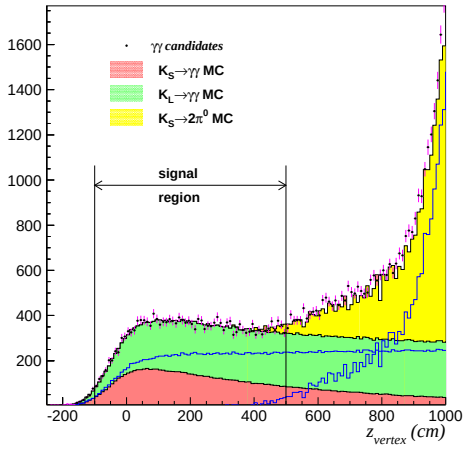

Figure 4: *z vertex distribution of $\gamma\gamma$ candidates.*

overlapping photons, badly reconstructed $K_{\rm L} \to 2\pi^0$ events, and accidentally overlapping events.

The NA48 analysis [11], which is described more detailed in the following, is based on the NA48 data of the years 1998 and 1999. The suppression of background from $K_{\rm L} \to 3\pi^0$ with overlapping or lost photons is done by cutting on the shower width in the calorimeter. As shown in Fig. 5 (left), overlapping photons produce on average a much wider shower and can clearly be separated from the signal. To suppress the $K_{\rm L} \to 3\pi^0$ background even further, a variable $z_{\rm max}$ is constructed as estimate of the real kaon vertex under the assumption of a misidentified $K_{\rm L} \to 3\pi^0$ event. For real background events this variable should be in the physical region down-stream of the collimator (Fig. 5 (right)). By rejecting events with $z_{\rm max} > -5$ m, the $K_{\rm L} \to 3\pi^0$ background is reduced to $(2.7 \pm 0.4)\%$. However, the signal acceptance is also reduced by 54%.

A second source of background are misidentified $K_{\rm L} \to 2\pi^0$ events. They are rejected by requiring the invariant mass $m(\gamma_3\gamma_4)$ of the photons not coming from the π^0 to be outside a window of ± 25 MeV/c^2 around the nominal π^0 mass. By using $K_{\rm S} \to 2\pi^0$ events from both ϵ'/ϵ and high intensity $K_{\rm S}$ runs, the remaining background from $K_{\rm L} \to 2\pi^0$ is estimated to $(0.2 \pm 0.1)\%$.

Finally, good $\pi^0\gamma\gamma$ candidates may be mimicked by accidentally overlap-

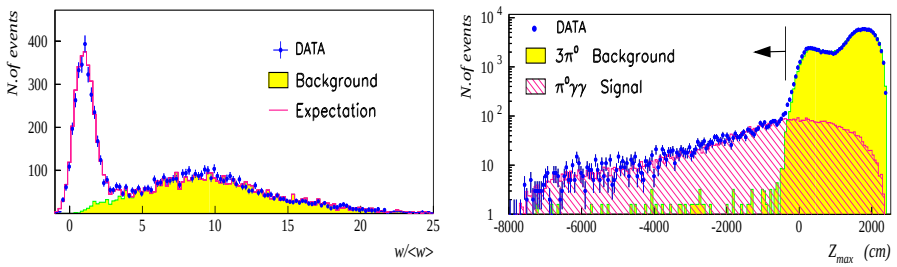

Figure 5: *Distributions of shower width (left) and $z_{\max}$ (right) of the selected $K_{\mathrm{L}} \to \pi^0\gamma\gamma$ candidates of the NA48 experiment. Shown are the data (crosses), the $K_{\mathrm{L}} \to 3\pi^0$ background expectation from Monte Carlo simulation (shaded), and the total expectation (histogram).*

ping events. This background is estimated by extrapolating events with high transverse momentum into the signal region to $(0.3 \pm 0.2)\%$.

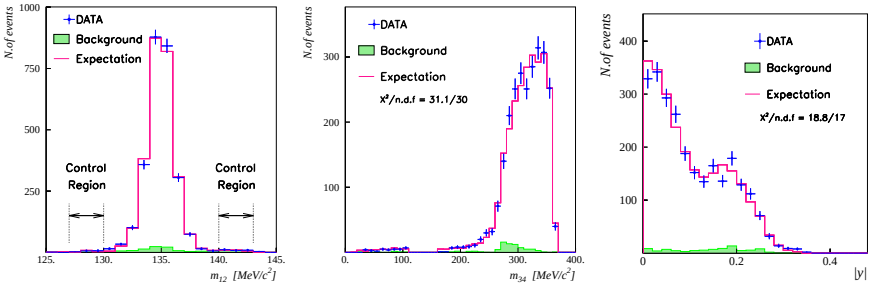

Figure 6: *Distributions of $m(\gamma_1\gamma_2)$ (left), $m(\gamma_3\gamma_4)$ (center) and $y = |E_3 - E_4|/m_K$ (right) of the selected NA48 $K_{\mathrm{L}} \to \pi^0\gamma\gamma$ candidates.*

The invariant mass $m(\gamma_1\gamma_2)$ of the two photons originating from the π^0 is shown in Fig. 6 (left). NA48 finds 2558 $K_{\mathrm{L}} \to \pi^0\gamma\gamma$ candidates with an estimated background of 82 ± 12 events, which are used for the branching ratio measurement. For the fit of the VMD parameter a_V, 345 ambigous events which allow two possible $\pi^0 \to \gamma\gamma$ assignments are excluded. The parameter a_V is fitted using the distributions of both kinematic decay variables $m(\gamma_3\gamma_4)$ and $y = |E_3 - E_4|/m_K$ (Fig. 6). The result of the fit is

$$a_V \;=\; -0.46 \pm 0.03_{\mathrm{stat}} \pm 0.04_{\mathrm{syst}} \qquad (\mathrm{NA48}, 2002),$$

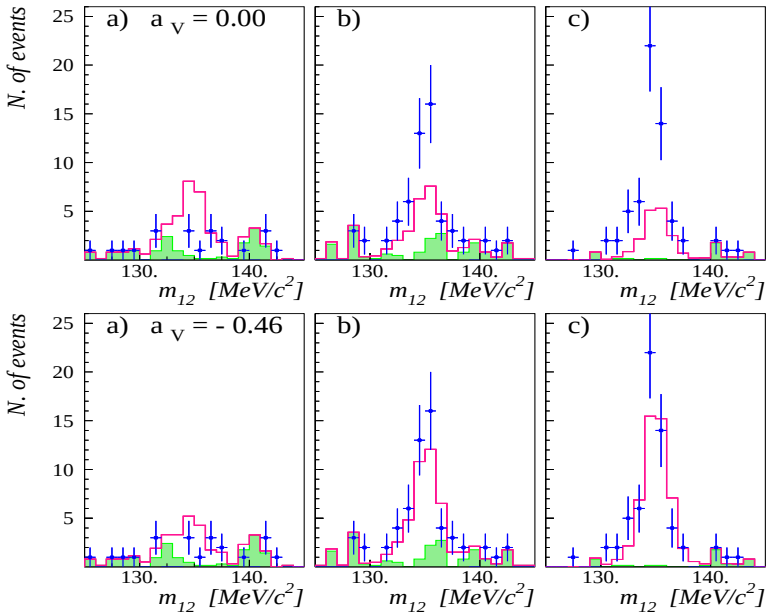

Figure 7: *NA48 data (crosses) and expected background (shaded) in regions with small $m(\gamma_3\gamma_4)$ together with the expectation of a) $a_V = 0.0$ and b) $a_V = 0.46$ (histograms).*

with the systematic error being dominated by uncertainties of the acceptance evaluation (± 0.03) and the parametrization of the $K_{\rm L} \to 3\pi^0$ vertex [12] (± 0.02).

For low $m(\gamma_3\gamma_4)$ the distributions of the π^0 signal $m(\gamma_1\gamma_2)$ are shown in Fig. 7. There is no significant signal of $K_{\rm L} \to \pi^0\gamma\gamma$ events for $m(\gamma_1\gamma_2) < 110$ MeV/c^2, as expected for $a_V \approx -0.46$ due to cancellation effects. Nevertheless, in the region $160 < m(\gamma_3\gamma_4) < 240$ MeV/c^2 a clear signal shows up, which is evidence for a sizeable $\mathcal{O}(p^6)$ contribution to the $K_{\rm L} \to \pi^0\gamma\gamma$ amplitude.

However, an analysis of the KTeV experiment using the data of the years 1996 and 1997, comes to a different result [6]. Performing a similar analysis as described above, KTeV finds 884 signal candidates with estimated 111 ± 12 background events. Fitting both the $m(\gamma_3\gamma_4)$ and y distributions (Fig. 8) the measured value of a_V is

$$a_V \;=\; -0.72 \pm 0.05_{\rm stat} \pm 0.06_{\rm syst} \qquad \text{(KTeV, 1999)},$$

also measuring a large $\mathcal{O}(p^6)$ contribution, but about 2.8 standard devia-

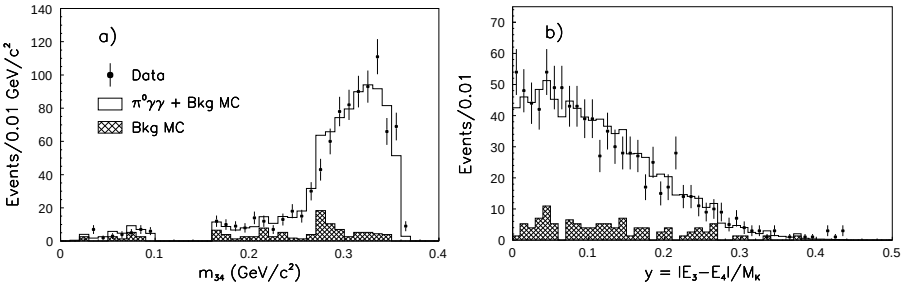

Figure 8: *Distributions of $m(\gamma_3\gamma_4)$ (left) and $y = |E_3 - E_4|/m_K$ (right) of the selected $K_{\rm L} \to \pi^0\gamma\gamma$ candidates of the KTeV experiment.*

tions different from the NA48 result. The systematics are dominated by the knowledge of the $3\pi^0$ background. While NA48 has finished the analysis on $K_{\rm L} \to \pi^0\gamma\gamma$, the KTeV collaboration plans to additionally analyze the data from the 1999 data taking period, which might help to understand the different results of the two experiments.

The two experiments also arrive at different measurements of the $K_{\rm L} \to \pi^0\gamma\gamma$ branching fraction, which can partially be explained by the strong dependence of the detector acceptances on $m(\gamma_3\gamma_4)$:

$$\text{NA48 (2002)}: \quad \mathrm{Br}(K_{\rm L} \to \pi^0\gamma\gamma) = (1.36 \pm 0.03_{\rm stat} \pm 0.04_{\rm syst}) \times 10^{-6}$$

$$\text{KTeV (1999)}: \quad \mathrm{Br}(K_{\rm L} \to \pi^0\gamma\gamma) = (1.68 \pm 0.07_{\rm stat} \pm 0.08_{\rm syst}) \times 10^{-6}$$

The NA48 a_V measurement indicates a negligible CP-conserving amplitude of the (yet to be observed) direct CP-violating decay $K_{\rm L} \to \pi^0 e^+ e^-$ [9]. However, this does not hold for the a_V value measured by KTeV.

5 $K_{\rm S} \to \pi^0\gamma\gamma$

The decay $K_{\rm S} \to \pi^0\gamma\gamma$ is dominated by the pion pole in $K_{\rm S} \to 2\pi^0$.To be able to distinguish this decay from the dominating $K_{\rm S} \to 2\pi^0$, a minimum two-gamma invariant mass of $z = m(\gamma_3\gamma_4)^2/m_K^2 > 0.2$ is required. One theoretical investigation based on ChPT exists [3], predicting the shape of the $m(\gamma_3\gamma_4)$ distribution together with a branching fraction of $\mathrm{Br}(K_{\rm S} \to \pi^0\gamma\gamma)|_{z \geq 0.2} = 3.8 \times 10^{-8}$. No experimental observation or limit has been published so far.

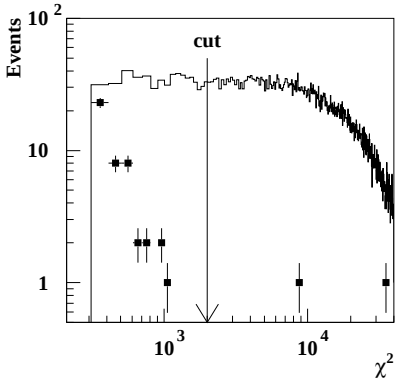

Figure 9: *Right:* $\chi^2_{2\pi^0}$ *distribution of* $K_S \to \pi^0\gamma\gamma$ *candidates under* $K_S \to 2\pi^0$ *hypothesis (crosses). The histogram shows the expected signal distribution.*

Using the data of a two-day high intensity K_S run in 1999, the NA48 experiment has performed a search for the decay $K_S \to \pi^0\gamma\gamma$. In this run about 3×10^8 K_S decays took place in the fiducial detector volume.

Because of the smallness of the expected branching fraction, the main experimental problem is the background suppression. Any non-γ activity in the photon anti-counters, drift chambers, and hadron calorimeter is vetoed. To suppress $K_S \to 2\pi^0$ events, the $\chi^2_{2\pi^0}$ of the event for being a $K_S \to 2\pi^0$ decay is required to be larger than 2000. In this way, only 0.1 ± 0.1 mismeasured $K_S \to 2\pi^0$ events are expected, as determined from Monte Carlo simulation. The main background then comes from $K_S \to 2\pi^0$ decays with one lost and one accidentally in-time photon. This background is estimated by simulated and randomly triggered events to 2.1 ± 0.1 events. The irreducible background coming from $K_L \to \pi^0\gamma\gamma$ decays accounts for another 0.1 expected background event.

The $\chi^2_{2\pi^0}$ distribution of the remaining events is shown in Fig. 9. Only two events above $\chi^2_{2\pi^0} = 2000$ survive the selection, compatible with the background expectation of 2.3 ± 0.2 events. Using $K_S \to 2\pi^0$ decays for normalization, the limit on the branching fraction set by NA48 is

$$\mathrm{Br}(K_S \to \pi^0\gamma\gamma)|_{z \geq 0.2} \; < \; 4.4 \times 10^{-7} \quad \text{at 90\% CL.}$$

This is the first limit set on the decay width of $K_S \to \pi^0\gamma\gamma$. However, it is still about one order of magnitude above the theoretical expectation.

References

1. M.K. Gaillard and B.W. Lee, Phys. Rev. Lett. **33** (1974) 108.
2. G. D'Ambrosio and D. Espriu Phys. Lett. **B 175** (1986) 237; J.L. Goity, Z. Phys **C 34** (1987) 341.
3. G. Ecker, A. Pich, and E. De Rafael, Phys. Lett. **B 189** (1987) 363.
4. A. Lai *et al* (NA48 Collab.), Phys. Lett. **B 493** (2000) 29.
5. G.D. Barr *et al* (NA31 Collab.), Phys. Lett. **B 242** (1990) 523; V. Papadimitriou *et al* (E731 Collab.), Phys. Rev. **D 284** (1991) 573; G.D. Barr *et al* (NA31 Collab.), Phys. Lett. **B 284** (1992) 440.
6. A. Alavi-Harati *et al* (KTeV Collab.), Phys. Rev. Lett. **83** (1999) 917.
7. G. D'Ambrosio and J. Portoles, Nucl. Phys. **B 492** (1997) 417; G. Ecker, A. Pich, and E. De Rafael, Phys. Lett. **B 237** (1990) 481; P. Heiliger and L.M. Sehgal, Phys. Rev. **D 47** (1993) 4920.
8. A.G. Cohen, G. Ecker, and A. Pich, Phys. Lett. **B 304** (1993) 417; L. Cappiello, G. D'Ambrosio, and M. Miragliuolo, Phys. Lett. **B 298** (1993) 423; J. Kambor and B. Holstein, Phys. Rev. **D 49** (1994) 2346.
9. J.F. Donoghue and F. Gabbiani, Phys. Rev. **D 51** (1995) 2187; F. Gabbiani and G. Valencia, Phys. Rev. **D 64** (2001) 094008.
10. D.E. Groom *et al* (Particle Data Group), Eur. Phys. J. **C 15** (2000) 1.
11. A. Lai *et al* (NA48 Collab.), Phys. Lett. **B 536** (2002) 229.
12. J. Kambor, J. Missimer, and D. Wyler, Phys. Lett. **B 261** (1991) 496.

Frascati Physics Series Vol. XXVIII (2002), pp.101-111
HQ & L 2002 – Vietri s/m, May 27th - June 1st, 2002

KLOE RESULTS ON KAON DECAYS AND ϕ RADIATIVE DECAYS

Erika De Lucia
Sezione INFN di Roma
Università "La Sapienza"
P.le A.Moro n.2, Roma, Italy
on behalf of the KLOE Collaboration [1)]

ABSTRACT

The KLOE experiment has been collecting data since April 1999 at the DAΦNE e^+-e^- collider at a center of mass energy equal to the ϕ-meson mass. A total amount of 5×10^7 ϕ decays have been analyzed. Results concerning the measurement of the semileptonic branching ratio of the K_S, the measurement of the ratio $BR(K_S \to \pi^+\pi^-)/BR(K_S \to \pi^0\pi^0)$ and the study of the radiative decays of the ϕ involving η, $\eta^{'}$, $f_0(980)$ and $a_0(980)$ are presented.

1 Introduction

The KLOE [2)] detector at DAΦNE [3)], the Frascati ϕ-factory, started data taking in april 1999. The DAΦNE e^+-e^- collider operates at the center of mass of the $\phi(1020)$ meson producing almost monochromatic K^0_S and K^0_L pairs, K^+ and K^- pairs and all other ϕ decay products. Moreover at DAΦNE kaons

are produced with a $\sim 110 - 125$ MeV/c momentum and their decay lengths are $\lambda_S \sim 0.6$ cm, $\lambda_L \sim 340$ cm and $\lambda_\pm \sim 90$ cm. The unique feature of a ϕ-factory is the *tagging*: the detection of a long lived neutral kaon guarantees the presence of a K^0_S of given momentum and direction and viceversa, the same holds for charged kaons.
In the following we present the first KLOE results on K^0_S decays and ϕ radiative decays based on 17 pb^{-1} of integrated luminosity collected during the year 2000, corresponding to $\simeq 5 \times 10^7$ ϕ decays.
At present DAΦNE reaches a peak luminosity of $\simeq 5 \times 10^{31}$ cm^{-2}s^{-1} and delivers $\simeq 2.5$ pb^{-1}/day and its performances are constantly improving.

2 The KLOE detector

The KLOE detector [2, 4] consists of a large cylindrical drift chamber surrounded by a hermetic electromagnetic calorimeter. A superconducting coil and an iron yoke surrounding the whole detector provide a 0.52 T magnetic field.
The drift chamber [5] (DC) with 4 m diameter and 3.3 m length, has a total number of 52140 wires, arranged in 12582 cells distributed over 58 concentric layers and with an all-stereo geometry. In order to maximize transparency to photons and reduce K^0_L regeneration, the mechanical support of the drift chamber is made of carbon fiber-epoxy composite and the operating gas mixture is 90 % helium - 10 % isobutane. The achieved position resolution is $\sigma_{r\phi} \sim 150\mu m$ and $\sigma_z \sim 2mm$ while vertices are reconstructed with a resolution $\sigma_v \sim 3mm$. The momentum resolution is $\sigma(p_\perp)/p_\perp \sim 0.4\%$.
The electromagnetic calorimeter [4, 6] (EmC) is a lead-scintillating fibers sampling calorimeter made of 88 modules, divided into a barrel section and two C-shaped end-caps, ensuring 98% coverage of the solid angle. The read-out of the modules is performed on both ends with $\sim 4.4 \times 4.4 cm^2$ granularity for a total of 4880 photomultipliers. The calorimeter has to detect with very high efficiency photons with energies down to 20 MeV and to accurately measure their energy and time of flight. The achieved energy resolution is $5.7\%/\sqrt{E(GeV)}$, with a linearity in energy response better than 1% above 80 MeV and better than 4% between 20 to 80 MeV. The time resolution is σ_t=$(54/\sqrt{(}E(GeV) \oplus$ 50) ps.
At the present luminosity the KLOE trigger system [7] works at data acquisition

rate of $\sim$ 2.5 kHz, resulting in a throughput to the DAQ system [8] of $\sim$ 3 Mbytes/s.

3 K^0_S decays

The determination of the ratio of the partial decay widths into two charged and into two neutral pions is presented. This ratio represents the first step towards the measurement of the double ratio from which $\mathrm{Re}(\epsilon'/\epsilon)$, the CP violation parameter in the neutral kaon system, is derived. Moreover, if the radiation of soft photons in the charged decay is properly taken into account [9], this ratio should allow the extraction of isospin I=0 and I=2 decay amplitudes.
The measurement of the branching ratio of the decay $K^0_S \to \pi^\pm e^\mp \bar{\nu}(\nu)$ is also presented. If CPT invariance and $\Delta S = \Delta Q$ hold, the Standard Model can predict $\mathrm{BR}(K^0_S \to \pi^\pm e^\mp \bar{\nu}(\nu))$ using the K^0_S and K^0_L lifetimes and $\Gamma(K^0_S \to \pi^\pm e^\mp \bar{\nu}(\nu)) = \Gamma(K^0_L \to \pi^\pm e^\mp \bar{\nu}(\nu))$. Therefore a precise measurement of this decay is a test of the $\Delta S = \Delta Q$ rule.
Neutral kaons from ϕ meson decays are produced in a pure quantum state ($J^{PC} = 1^{--}$) therefore the final kaon pair is always K^0_S-K^0_L and the observation of a K^0_L *tags* the presence of the K^0_S in the opposite hemisphere. We use the time of flight identification of K^0_L interacting in the EmC ("K^0_Lcrash"), characterized by a neutral cluster with rather slow velocity ($\beta \approx 0.22$) in the event, as K^0_S tagging strategy. The K^0_S momentum is obtained from the position of the K^0_L cluster and the ϕ-meson momentum (at DAΦNE the ϕ has a momentum of $\sim$ 12.5 MeV/c due to the beams crossing angle). About one half of the K^0_L 's reach the calorimeter before decaying, thus the "K^0_L-crash" tag provides a particularly clean and abundant K^0_S mesons sample. Moreover from the measurement of the K^0_L velocity in the ϕ-meson rest frame we can measure the center of mass energy of DAΦNE with 1 MeV accuracy.

3.1 $K^0_S \to \pi^+\pi^-(\gamma)$ and $K^0_S \to \pi^0\pi^0$ decays

The K^0_S decaying into two neutral pions events are selected by requiring the presence of at least three neutral prompt clusters in the EmC with energy larger than 20 MeV. A prompt photon must satisfy $|t_{CL} - |\vec{r}_{CL}|/c| \leq 5 \times \sigma_t$, with t_{CL} being the cluster time, $|\vec{r}_{CL}|$ its position and σ_t the energy dependent time resolution. The photon detection efficiency for given energy/angle has

been evaluated from data using γ's of the decays $\phi \to \pi^+\pi^-\pi^0$. The final selection efficiency for the $K^0_S \to \pi^0\pi^0$ decay channel is ϵ_{00}=(90.1±0.2)% and is dominated by acceptance. The selection of $K^0_S \to \pi^+\pi^-(\gamma)$ events requires two tracks with opposite charge, originating in a cylinder of 4 cm radius and 10 cm length around the interaction point, with polar angle in the interval $30° < \theta < 150°$ and reaching the EmC. A further cut is applied on the measured momenta to remove the residual background due to charged kaon tracks: 120 < p(MeV/c)< 300. No photons are required in EmC therefore this is a fully inclusive measurement. The track reconstruction efficiency as a function of the momentum and polar angle is measured from data samples. The final selection efficiency is ϵ_{+-}=(57.6±0.2)%, again dominated by acceptance. The trigger efficiency and the probability for having at least one good cluster to determine the t_0 of the event are evaluated for both decay types using data. We obtain (99.69 ± 0.04)% for the neutral decay and (97.9 ± 0.03)% for the charged one. Background levels are kept well below 1% for both decay types.
The final result is [10]:

$$\frac{\Gamma(K^0_s \to \pi^+\pi^-(\gamma))}{\Gamma(K^0_s \to \pi^0\pi^0)} = 2.236 \pm 0.003_{\rm stat} \pm 0.015_{\rm syst} \qquad (1)$$

This value has to be compared with the present PDG (particle data group) value of 2.197 ± 0.026. It is worthwhile to note that the experiments contributing to the PDG value do not have a clear indication of the cut on the photon energy and the corresponding efficiency, while we present a fully inclusive measurement of $K^0_S \to \pi^+\pi^-(\gamma)$.

3.2 $K^0_S \to \pi^\pm e^\mp \bar{\nu}(\nu)$ decays

The $K^0_S \to \pi^\pm e^\mp \bar{\nu}(\nu)$ decay candidates are selected asking for events with a "K^0_Lcrash", and two tracks of opposite charge with associated EmC clusters and forming a vertex in the previously defined cylinder around the interaction point. In order to reject the background from $K^0_S \to \pi^+\pi^-$ decays, further cuts are applied on the two tracks invariant mass, evaluated in the pion mass hypothesis, and on the resulting K^0_S momentum in the ϕ rest frame. Electrons and pions discrimination is performed with time of flight measurement, exploiting the excellent time performances of EmC. The vertex reconstruction efficiency and fiducial cuts are estimated by Monte Carlo and checked with a high-purity data sample of K^0_L's decaying into $\pi e\nu$ before the DC internal

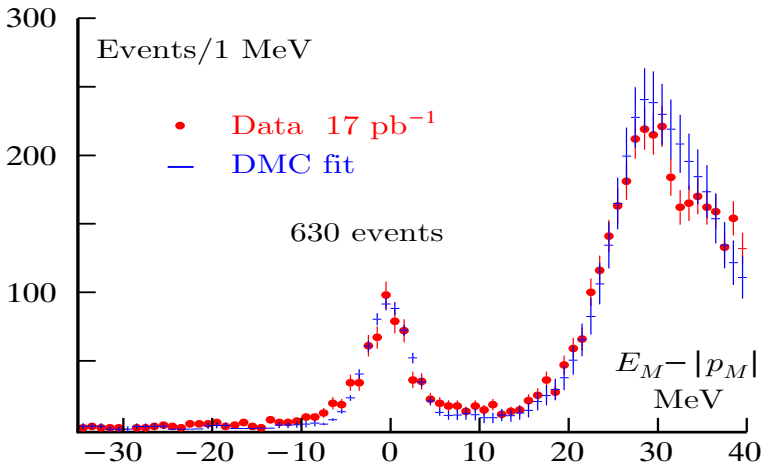

Figure 1: *Distribution of the difference between missing energy and missing momentum for* $K^0_S \to \pi^{\pm}e^{\mp}\bar{\nu}(\nu)$ *candidates. The peak at zero is the signal. The fit to the distribution uses the Monte Carlo for signal and background in the range -40 MeV + 40 MeV.*

wall. The track reconstruction efficiency is evaluated using both Monte Carlo and data from $K^0_S \to \pi^+\pi^-$sample. The efficiencies related to trigger, track to cluster association, t_0 determination, are measured directly from data using $K^0_L \to \pi^{\pm}e^{\mp}\bar{\nu}(\nu)$, $\phi \to \pi^+\pi^-\pi^0$ and $K^0_S \to \pi^+\pi^-$subsamples. Concerning the time of flight identification efficiency this is estimated using the high-purity data sample of K^0_L's decaying into $\pi e\nu$ before the DC internal wall. The overall efficiency for the signal selection is (20.8 ± 0.4) %. Finally for the events passing the previous cuts, we evaluate the missing energy (E_{miss}) and the missing momentum (p_{miss}). $K^0_S \to \pi^{\pm}e^{\mp}\bar{\nu}(\nu)$ events have to satisfy $E_{miss} - p_{miss} = 0$. Figure 1 shows the distribution of $E_{miss} - p_{miss}$ with a clean peak of the signal around zero. The fit to the distribution is done using Monte Carlo spectra for both signal and background.

The measured yield is $N(K^0_S \to \pi^{\pm}e^{\mp}\bar{\nu}(\nu)) = 627 \pm 30$ events. The total number of events is then divided by the number of observed $K^0_S \to \pi^+\pi^-$ events, to give [11]:

$$BR(K^0_s \to \pi^{\pm}e^{\mp}\bar{\nu}(\nu)) = (6.92 \pm 0.34_{stat} \pm 0.15_{syst}) \times 10^{-4}. \qquad (2)$$

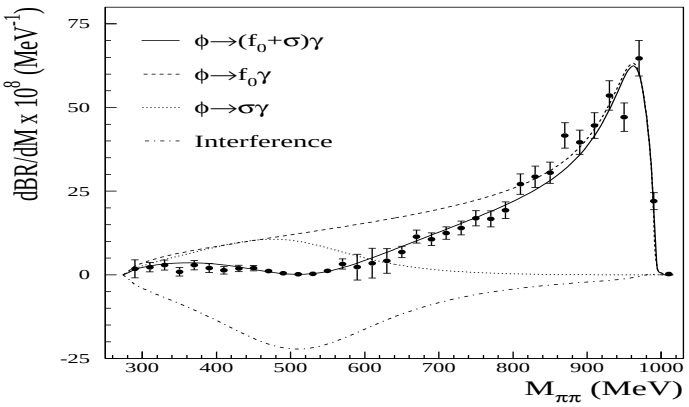

Figure 2: *dBR/dM as a function of $M_{\pi\pi}$ from $\phi \to f_0\gamma$ and $f_0 \to \pi^0\pi^0$. Points are data. The solid line is the fit result assuming contributions from f_0, σ and the interference between them. Individual contributions are also shown.*

This result is in agreement with the Standard Model expectation of $\mathrm{BR}(\mathrm{K}^0_S \to \pi^\pm e^\mp \bar{\nu}(\nu)) = (6.70 \pm 0.07)\times 10^{-4}$, obtained using the K^0_S and K^0_L lifetimes and $\Gamma(\mathrm{K}^0_S \to \pi^\pm e^\mp \bar{\nu}(\nu))$=$\Gamma(\mathrm{K}^0_L \to \pi^\pm e^\mp \bar{\nu}(\nu))$ which follows from CPT invariance and $\Delta S = \Delta Q$.

4 Radiative ϕ decay : $\phi \to f_0\gamma \to \pi^0\pi^0\gamma$ and $\phi \to a_0\gamma \to \eta\pi^0\gamma$.

Various models exist for the description of the nature of the f_0 and a_0 mesons (ordinary qq meson, qqqq state, KK molecule). These models make different predictions [12, 13] for $\mathrm{BR}(\phi \to f_0\gamma)$, $\mathrm{BR}(\phi \to a_0\gamma)$ and their mass spectra, therefore a precise measurement of these quantities would clarify the interpretation on the nature of these mesons. The f_0 meson has been studied in the following decay chain: $\phi \to f_0\gamma$ with $f_0 \to \pi^0\pi^0$. Concerning the a_0 we have investigated the channel: $\phi \to a_0\gamma$ with $a_0 \to \eta\pi^0$ and the following decays of the η: $\eta \to \gamma\gamma$ and $\eta \to \pi^+\pi^-\pi^0$. These final states are characterized by 5 prompt γ's and this is the first observation of events with $a_0 \to \eta\pi^0$ and $\eta \to \pi^+\pi^-\pi^0$. The main background processes are: $e^+e^- \to \omega\pi^0$ with $\omega \to \pi^0\gamma$ or $\omega \to \eta\gamma$, and the resonant process $\phi \to \rho^0\pi^0$ with $\rho^0 \to \pi^0\gamma$ or $\rho^0 \to \eta\gamma$. On the other

hand the $a_0\gamma$ final state with $\pi^+\pi^-5\gamma$ has a unique signature with negligible physical background.
The events are identified by requiring five prompt photons within loose acceptance cuts. Then a first kinematic fit is performed requiring total energy and momentum conservation with the additional constraint $\beta = 1$ for all photons. The best photon pairing is found by matching the $\gamma\gamma$ invariant masses to the intermediate particles masses, either $2\pi^0$ or $\eta\pi^0$, and then a second kinematic fit is performed constraining the masses. Background events are rejected by means of cuts on kinematic variables and on the χ^2 probability values obtained in the kinematic fits.
The overall detection efficiency is obtained by tuning the MC to reproduce the observed $M_{\pi^0\pi^0}$ and $M_{\eta\pi^0}$ invariant mass distributions in case of $\phi \to \pi^0\pi^0\gamma$ and $\phi \to \eta\pi^0\gamma$ events, respectively.
Final result on the branching ratio of $\phi \to \pi^0\pi^0\gamma$ is:

$$BR\left(\phi \to \pi^0\pi^0\gamma\right) = (1.08 \pm 0.03_{stat} \pm 0.05_{syst}) \times 10^{-4} \tag{3}$$

For the branching ratio of $\phi \to \eta\pi^0\gamma$ we measure from the $\eta \to \gamma\gamma$ sample:

$$BR\left(\phi \to \eta\pi^0\gamma\right) = (8.5 \pm 0.5_{stat} \pm 0.6_{syst}) \times 10^{-5} \tag{4}$$

and from the $\eta \to \pi^+\pi^-\pi^0$ sample:

$$BR\left(\phi \to \eta\pi^0\gamma\right) = (8.0 \pm 0.6_{stat} \pm 0.4_{syst}) \times 10^{-5}. \tag{5}$$

In order estimate the contribution to BR($\phi \to \pi^0\pi^0\gamma$) and BR($\phi \to \eta\pi^0\gamma$) from $\phi \to f_0\gamma$ and $\phi \to a_0\gamma$ respectively, we have performed a fit to the invariant mass spectra $M_{\pi^0\pi^0}$ and $M_{\eta\pi^0}$.
In the $\phi \to \pi^0\pi^0\gamma$ mode the process $\phi \to S\gamma$, with a scalar meson S (f_0 or σ) decaying into $\pi^0\pi^0$, and the process $\phi \to \rho^0\pi^0$, with $\rho^0 \to \pi^0\gamma$, contribute to the $M_{\pi^0\pi^0}$ spectrum [12]. To fit the dipion spectrum, together with the f_0 we have to include also the contribution of the σ [14] and a strong destructive interference between these two terms (fig.2). The contribution from the $\phi \to \rho^0\pi^0$ channel comes out to be negligible.
Integrating the f_0 component of the spectrum [12] we obtain:

$$BR\left(\phi \to f_0\gamma \to \pi^0\pi^0\gamma\right) = (1.49 \pm 0.07) \times 10^{-4}. \tag{6}$$

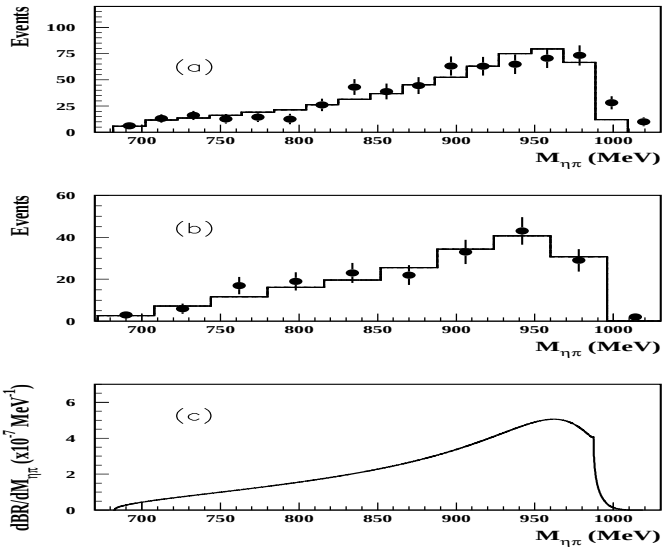

Figure 3: *The background subtracted $M_{\eta\pi}$ spectra resulting from $\phi \to a_0\gamma$ and $a_0 \to \eta\pi$. Points in plot (a) and (b) are data, (a) for the case where $\eta \to 2\gamma$, (b) for case where $\eta \to \pi^+\pi^-\pi^0$. Histograms are results of the fit and (c) is the theoretical curve for the a_0.*

Concerning the $\phi \to \eta\pi^0\gamma$ case, we performed a simultaneous fit of the two $M_{\eta\pi^0}$ spectra (fig 3), from the $\eta \to \gamma\gamma$ and $\eta \to \pi^+\pi^-\pi^0$ samples. The a_0 mass parameter has been set to the PDG value of 984.8 MeV.
From the fit we obtain [13]:

$$BR\left(\phi \to a_0\gamma, a_0 \to \eta\pi^0\right) = (7.4 \pm 0.7) \times 10^{-5}. \tag{7}$$

5 Radiative ϕ decay : $\phi \to \eta'\gamma$ and $\phi \to \eta\gamma$.

Precise measurements of the branching ratios of $\phi \to \eta'\gamma$ and $\phi \to \eta\gamma$ are of particular interest in probing the $|s\bar{s}\rangle$ and gluonium content of the η'. Moreover the ratio of these two branching ratios is related to the $\eta-\eta'$ mixing parameters

predictable in the chiral perturbation theory frame. The decay chain for the $\eta^{'}$ selection is: $\phi \to \eta^{'}\gamma$ with $\eta^{'} \to \pi^+\pi^-\eta$ and then $\eta \to \gamma\gamma$ [15]. The η is selected through the chain $\phi \to \eta\gamma$ with $\eta \to \pi^+\pi^-\pi^0$. The final state $(\pi^+\pi^-\gamma\gamma\gamma)$ is the same for the two selections therefore several systematic errors cancel in the measurement of the ratio BR$(\phi \to \eta^{'}\gamma)$/BR$(\phi \to \eta\gamma)$. The selection for both channels requires: the presence of three prompt photons with energy larger than 7 MeV and two tracks of opposite charge with a vertex near the interaction region. Then a preliminary kinematic fit is performed imposing total energy and momentum conservation, the constraint $\beta = 1$ for all photons, without any invariant mass constraint on intermediate particles. Simple kinematic cuts eliminate the background mainly due to $\phi \to \pi^+\pi^-\pi^0$ events with an extra photon and to $\phi \to K_L K_S \to \pi^+\pi^-\pi^0\pi^0$ events with one photon lost. The number of signal events is $N_{ev} = 120 \pm 12_{stat} \pm 5_{syst}$. Normalizing the signal events to the number of observed $\phi \to \eta\gamma$ events and correcting for detection efficiency estimated from MC, we measure the ratio of the two branching ratios [15]:

$$\frac{BR\left(\phi \to \eta^{'}\gamma\right)}{BR\left(\phi \to \eta\gamma\right)} = (4.70 \pm 0.47_{stat} \pm 0.31_{syst}) \times 10^{-3}. \qquad (8)$$

From this ratio we obtain the following value for the pseudoscalar mixing angle φ_p in the flavour basis: $\varphi_p = (41.8\ ^{+1.9}_{-1.6})^o$.
Moreover making use of the BR$(\phi \to \eta\gamma)$ value from PDG, we obtain [15]:

$$BR(\phi \to \eta^{'}\gamma) = (6.8 \pm 0.6_{stat} \pm 0.5_{syst}) \times 10^{-5}. \qquad (9)$$

This is the most precise determination to date.

6 Conclusions

Results on ϕ radiative decays have been presented, together with precision measurements on two K^0_S decay channels, based on the statistics of about 200 pb^{-1} collected in year 2000 from the KLOE experiment at DAΦNE .

References

1. A. Aloisio, F. Ambrosino, A. Antonelli, M. Antonelli, C. Bacci, G. Bencivenni, S. Bertolucci, C. Bini, C. Bloise, V. Bocci, F. Bossi, P. Branchini,

S. A. Bulychjov, R. Caloi, P. Campana, G. Capon, G. Carboni, M. Casarsa, V. Casavola, G. Cataldi, F. Ceradini, F. Cervelli, F. Cevenini, G. Chiefari, P. Ciambrone, S. Conetti, E. De Lucia, G. De Robertis, P. De Simone, G. De Zorzi, S. Dell'Agnello, A. Denig, A. Di Domenico, C. Di Donato, S. Di Falco, A. Doria, M. Dreucci, O. Erriquez, A. Farilla, G. Felici, A. Ferrari, M. L. Ferrer, G. Finocchiaro, C. Forti, A. Franceschi, P. Franzini, C. Gatti, P. Gauzzi, S. Giovannella, E. Gorini, F. Grancagnolo, E. Graziani, S. W. Han, M. Incagli, L. Ingrosso, W. Kluge, C. Kuo, V. Kulikov, F. Lacava, G. Lanfranchi, J. Lee-Franzini, D. Leone, F. Lu, M. Martemianov, M. Matsyuk, W. Mei, L. Merola, R. Messi, S. Miscetti, M. Moulson, S. Müller, F. Murtas, M. Napolitano, A. Nedosekin, F. Nguyen, M. Palutan, L. Paoluzi, E. Pasqualucci, L. Passalacqua, A. Passeri, V. Patera, E. Petrolo, L. Pontecorvo, M. Primavera, F. Ruggieri, P. Santangelo, E. Santovetti, G. Saracino, R. D. Schamberger, B. Sciascia, A. Sciubba, F. Scuri, I. Sfiligoi, T. Spadaro, E. Spiriti, G. L. Tong, L. Tortora, E. Valente, P. Valente, B. Valeriani, G. Venanzoni, S. Veneziano, A. Ventura, G. Xu, G. W. Yu.

2. The KLOE Collaboration, A general purpose detector for DAΦNE , LNF-92/019 (1992).

3. S.Guiducci et al., Proc. of the 2001 Particle Accelerator Conference (Chicago,Illinois,USA), P.Lucas S.Weber ed., 353, (2001)

4. The KLOE Collaboration, The KLOE detector, Technical Proposal, LNF-93/002 (1993).

5. The KLOE Collaboration, The Tracking detector of the KLOE experiment, LNF-01/016 (P) (2001), to be published on Nucl. Inst. Meth. A.

6. The KLOE Collaboration, The KLOE electromagnetic calorimeter, *Nucl. Inst. Meth.* A **482** 363 (2002)

7. The KLOE Collaboration, The KLOE Trigger System, LNF-02/02 (P) (2002), Submitted to Nucl. Inst. Meth. A.

8. The KLOE Collaboration, The KLOE Data Acquisition System, LNF-95/014 (1995).

9. V. Cirigliano, J.F. Donoghue, E. Golowich, *EPJ* C **18**, 83, (2000).
10. The KLOE collaboration, *Phys. Lett.* B **538** 21,(2002)
11. The KLOE collaboration, *Phys. Lett.* B **535** 37,(2002)
12. The KLOE collaboration, *Phys. Lett.* B **537** 21,(2002)
13. The KLOE collaboration, *Phys. Lett.* B **536** 209,(2002)
14. E.M.Aitala et al., *Phys. Rev. Lett* **86** 770 (2001)
15. The KLOE collaboration, hep-ex/0206010, submitted to Phys. Lett. B

Frascati Physics Series Vol. XXVIII (2002), pp.115-115
HQ & L 2002 – Vietri s/m, May 27th - June 1st, 2002

TWO-BODY MODES OF CHARM *

Franco Buccella
Universitá di Napoli "Federico II", Napoli, Italy

* Written contribution not received

Frascati Physics Series Vol. XXVIII (2002), pp.117-129
HQ & L 2002 – Vietri s/m, May 27th - June 1st, 2002

LEPTONIC, SEMILEPTONIC AND HADRONIC DECAYS OF CHARMED MESONS

Nancy Marinelli
Imperial College, Blackett Laboratory
Prince Consort Road, London SW7 2BW, UK
E-mail: n.marinelli@ic.ac.uk

ABSTRACT

A review of the latest results about charmed meson decays available from various experiments (ALEPH, BABAR, CLEO, FOCUS), operating with different beam conditions (LEP, SLAC, fixed target) is presented.

1 Introduction

The physics of charmed mesons is a field so rich that it is hard to give an exhaustive overview of all recent results. In this paper a few, selected topics are presented, from the experiments which can perform studies in the charm sector. The LEP experiments, where, accurate results are still being produced; the b-factories, which are now in full operation and the fixed-target experiments which collected a large amount of data a few years ago and are now finalizing their analyses.

The paper is organized in four main sections; three of them are dedicated to leptonic, semileptonic and hadronic processes respectively. In each case a brief reminder about the experiment and the specific measurement being presented will be given as well as the results.

The last section is devoted to future perspectives in the study of charmed meson physics with a discussion of some of the achievable improvements on the existing results and of the possibility of new measurements.

2 Leptonic Decays

Leptonic decays of heavy quarks are in general easy to access experimentally thanks to the large branching fractions and peculiar signature. They are especially interesting because of the absence of strong interactions between the final state particles. The interpretation of the measurement is then straightforward and allows the improvement of the knowledge of the strong interaction of the constituent quarks of the meson.

The observable leptonic decays in the charm sector are $D^+ \to \ell\nu$ and $D_s \to \ell\nu$. The former has a very small decay rate since it is Cabibbo forbidden, while the latter is larger and can be studied.

The leptonic decay $D_s \to \ell\nu$ is the second generation analogue of the charged pion leptonic decay, $\pi^+ \to \ell^+\nu$ and it proceeds via the Cabibbo allowed annihilation of the c and $\bar{s}$ quarks in the D_s meson. Standard Model predictions are based on the following expression:

$$\frac{G_F^2}{8\pi}\tau_{D_s} f_{D_s}^2 |V_{cs}|^2 m_{D_s} m_\ell^2 \left(1 - \frac{m_\ell^2}{m_{D_s}^2}\right)^2, \qquad (1)$$

where τ_{D_s} is the mean lifetime of the D_s, $|V_{cs}|$ is the relevant CKM matrix element, m_{D_s} is the D_s mass, m_ℓ is the mass of the lepton and f_{D_s} is the decay constant. Extracting f_{D_s} from the measurement of the branching fraction is the ultimate purpose of this analysis because it describes the internal structure of the D_s meson and it allows verification of various theoretical calculations. Lattice QCD is believed to be the more reliable method and it predicts $f_{D_s} = 255 \pm 30$ MeV [1]. In the lattice QCD framework the decay constants are used to evaluate the third-generation CKM matrix elements. Constraints on the CKM matrix elements are obtained from experimental values of $B^0 - \bar{B}^0$ mixing but

they rely on theoretical predictions of f_B, as this is not yet experimentally accessible. Thus it is important to measure f_{D_s} and compare with theory.

Standard Model predictions for the branching fractions $BR(D_s \to \tau\nu)$, $BR(D_s \to \mu\nu)$ and $BR(D_s \to e\nu)$ are 5.2%, 0.54% and 1.3×10^{-7} respectively, the latter being strongly helicity suppressed. The first two have been measured in ALEPH.

2.1 *Measurement of* f_{D_s} *from* $D_s \to \ell\nu$ *at ALEPH*

The most recent result obtained for f_{D_s} comes from the ALEPH experiment at the LEP machine (e^+e^- collisions at the Z resonance energy). The general strategy for selecting events in the $D_s \to \tau\nu$ channel ($\tau \to e\nu\bar{\nu}$ or $\tau \to \mu\nu\bar{\nu}$) is by searching for hemispheres containing a high momentum lepton associated with large missing energy. ALEPH [2] looks for the decay chain $e^+e^- \to c\bar{c}$, $c \to D_s$, with $D_s \to \tau\nu$ or $D_s \to \mu\nu$.

The selection is optimized for $Z \to c\bar{c}$ events and rejects $Z \to b\bar{b}$ events where the D_s mesons have a softer energy spectrum and are harder to reconstruct. The rejection of the background, mostly due to semileptonic decays from $Z \to c\bar{c}$ and $Z \to b\bar{b}$ events, is mainly achieved by cutting on the reconstructed D_s energy. Lifetime based variables are used to discriminate the signal from the b background, exploiting the fact that in charm hemispheres containing a $D_s \to \ell\nu$ decay all particles but the lepton originate from the primary vertex. In the analysis the physical background from $D^+ \to \ell\nu$ is totally indistinguishable from the $D_s \to \ell\nu$ so it is treated as signal and related to f_{D_s} using the prediction $f_{D_s}/f_{D^+} = 1.11^{+0.006}_{-0.05}$ [3].

The background due to $b\bar{b}$, $c\bar{c}$ and light flavoured ($Z \to u\bar{u}, d\bar{d}, s\bar{s}$) events still present in the selected sample has to be subtracted in order to extract the $D_s \to \tau\nu$ component. Use is made of a linear combination of hemisphere variables suitably chosen according to their discriminant power (Linear Discriminant Variables Technique). Two variables, U_c and U_b, are optimized in order to discriminate the signal from background in $b\bar{b}$ and $c\bar{c}$ events respectively, as shown in Fig. 1 (left side plot).

A fit is then performed to the data consisting of a signal plus three background (uds, $c\bar{c}$ and $b\bar{b}$) components. The relative normalization of the various contributions are fixed according to Eq. 1, the measured charmed production rates [4, 5], the predicted f_{D_s}/f_{D^+} ratio [3] and other quantities (R_c and R_b

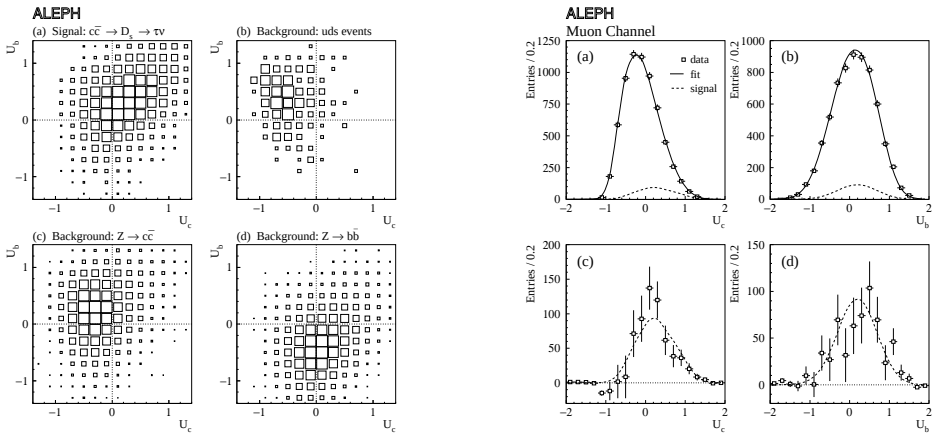

Figure 1: *(Left side) Monte Carlo* U_b *versus* U_c *distributions in the electron channel for the* $D_s \to \tau\nu$ *analysis. (a) signal,* $c\bar{c} \to D_s \to \tau\nu$*; (b) uds background; (c)* $c\bar{c}$ *background; (d)* $b\bar{b}$ *background. The distributions are shown with arbitrary normalization. (Right side) projections of the fit to the data in the muon channel for the* $D_s \to \tau\nu$ *analysis. (a)* U_c *distribution; (b)* U_b *distribution. Squares with error bars represent the data. The solid lines are the fitted distributions while the dashed lines shown the signal contributions. The bottom pair of plots show the fit after the background subtraction.*

from the Standard Model fit in [4], $|V_{cs}|$, $|V_{cd}|$, the D_s and D^+ lifetimes and particle masses from [6]).

In Fig. 1 (right side), the result of the fit in the (U_c,U_b) plane, is shown by projecting the result in the two variables. In Fig. 2 the plots of the purity in both electron and muon channels are shown.

ALEPH has also observed for the first time the presence of signal in the channel $D_s \to \mu\nu$. The analysis technique follows that for the $D_s \to \tau\nu$ channel except that also the M($\mu\nu$) invariant mass is calculated and used as a third discriminant variable together with the pair U_c,U_b optimized to distinguish $c\bar{c} \to D_s \to \mu\nu$ from the background. This analysis is also sensitive to $D_s \to \tau\nu$ decays so the resulting branching fraction has to be interpreted as a measurement of the combined signal.

The main source of systematic error, common to both analyses, is the uncertainty on the charm hadron production rates, mostly the BR(c$\to$ D_s), since

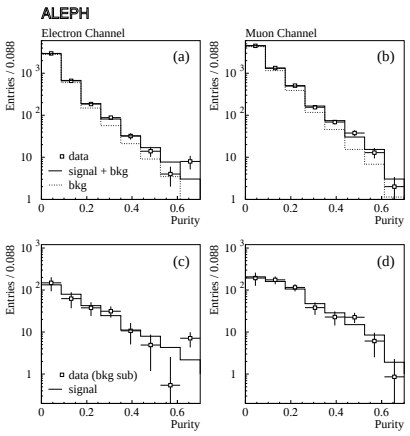

Figure 2: *Distributions of the purity P, in (a) the electron channel and (b) the muon channel for the* $D_s \to \tau\nu$ *analysis. The histograms show the Monte Carlo background and the total signal plus background. In the plots (c),(d) the same distributions after background subtraction are shown.*

it directly affects the number of D_s present in the sample. Other important sources of systematic error are the detector resolution which affects the reconstructed energy of the charmed hadron and the fragmentation of the charm quark.

The measured branching fractions are listed in Table 1 and compared with previous LEP measurements. The extracted values of f_{D_s} are shown in Fig. 3. The quoted ALEPH result is obtained by combining $f_{D_s} = (273 \pm 18 \pm 42)$ MeV from the $D_s \to \tau\nu$ analysis and $f_{D_s} = (291 \pm 25 \pm 38)$ from the $D_s \to \mu\nu$ analysis.

3 Semileptonic Decays

Transition amplitudes in semileptonic decays are proportional to the product of leptonic and hadronic currents, where the latter are represented by three analytic functions, the form factors $A_1(q^2)$,$A_2(q^2)$ and $V(q^2)$ [7].

Theoretical calculations of the form factors are not straightforward in the QCD framework, because of large non-perturbative contributions to the process nor in the HQET [8, 9, 10] because c to s transitions do not satisfy the basic

Table 1: *Summary of the* $D_s \to \ell\nu$ *measurements performed at LEP.*

Experiment	BR($D_s \to \tau\nu$)
ALEPH $\tau \to e\nu\bar{\nu}$	(5.86±1.18±2.16)%
ALEPH $\tau \to \mu\nu\bar{\nu}$	(5.78±0.85±1.81)%
ALEPH combined	(5.79±0.77±1.84)%
DELPHI	(8.5±4.2±2.6)%
L3	(7.4±2.8±2.4)%
	BR($D_s \to \mu\nu$)
ALEPH	(0.68±0.11±0.18)%

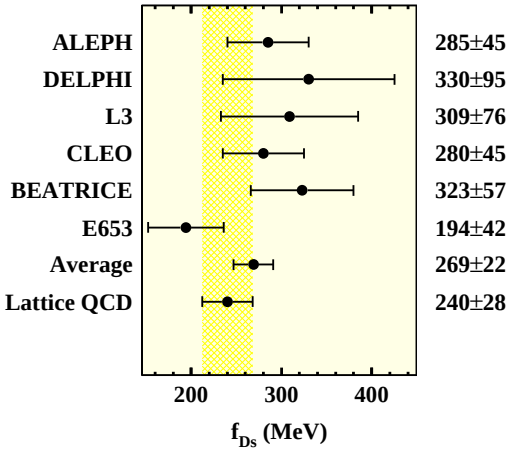

Figure 3: *Summary of the presently available experimental values of* f_{D_s}.

assumptions of the theory. Accurate measurements of the charmed meson leptonic branching ratios and hence of the form factors is therefore important.

3.1 *BR*($D^+ \to \bar{K}^{0\star}\ell^+\nu_\ell$) *at CLEO*

The CLEO experiment, at CESR (Cornell Electron Storage Ring), has recently released a new measurement of the BR($D^+ \to \bar{K}^{0\star}\ell^+\nu_\ell$) [11]. Most of the data analysed ($\sim$ 9.13 fb^{-1}) come from e^+e^- collisions at the $\Upsilon(4S)$ resonance energy but they have also used $\sim$4.4 fb^{-1} taken below the $B\bar{B}$ pair production threshold. The chain $D^{\star+} \to D^+\pi^0$, $D^+ \to \bar{K}^{0\star}\ell^+\nu_\ell$, $\bar{K}^{0\star} \to K^-\pi^+$ is reconstructed; the direction of the D meson is approximated by the thrust

axis and various methods are used to reconstruct the momentum of the ν. Two quantities are used to extract the number of signal events, M(Kπ) and $\delta m = m(\mathrm{K}\pi\ell\nu\pi^0) - m(\mathrm{K}\pi\ell\nu)$. Data are divided into bins of δm and a fit to M(Kπ) is performed extracting the number of $\bar{\mathrm{K}}^{0\star}$s for each bin. The yields obtained are then studied as a function of δm and a fit gives the number of signal events (Fig. 4). The ratios $R_e^+ = \frac{B(\mathrm{D}^+\to\bar{\mathrm{K}}^{0\star}e^+\nu_e)}{B(\mathrm{D}^+\to\mathrm{K}^-\pi^+\pi^+)}$, $R_\mu^+ = \frac{B(\mathrm{D}^+\to\bar{\mathrm{K}}^{0\star}\mu^+\nu_\mu)}{B(\mathrm{D}^+\to\mathrm{K}^-\pi^+\pi^+)}$ and $R_\ell^+ = \frac{B(\mathrm{D}^+\to\bar{\mathrm{K}}^{0\star}\ell^+\nu_\ell)}{B(\mathrm{D}^+\to\mathrm{K}^-\pi^+\pi^+)}$ are measured (Fig. 5). Using the value $\mathrm{BR}(\mathrm{D}^+ \to \mathrm{K}^-\pi^+\pi^+) = (9.0 \pm 0.6)\%$ [6] the resulting branching fractions are $\mathrm{BR}(\mathrm{D}^+ \to \bar{\mathrm{K}}^{0\star}e^+\nu_e) = (6.7 \pm 0.4 \pm 0.5 \pm 0.4)\%$, $\mathrm{BR}(\mathrm{D}^+ \to \bar{\mathrm{K}}^{0\star}\mu^+\nu_\mu) = (6.5 \pm 0.9 \pm 0.5 \pm 0.4)\%$, and $\mathrm{BR}(\mathrm{D}^+ \to \bar{\mathrm{K}}^{0\star}\ell^+\nu_\ell) = (6.7 \pm 0.4 \pm 0.5 \pm 0.4)\%$.

These results and the ratios between the form factors measured by E791 [12] give the following values of the form factors $A_1(0)$=0.69±0.07, $A_2(0) = 0.48 \pm 0.08$ and $V(0) = 1.25 \pm 0.15$.

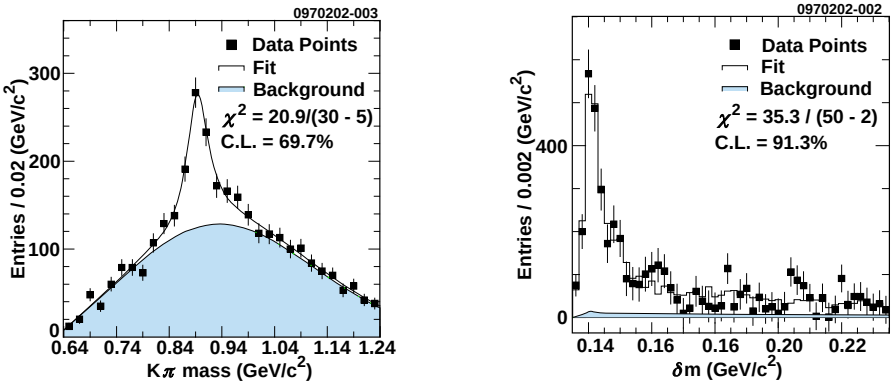

Figure 4: *(left) Kπ mass distribution in the third δm bin of the* $\mathrm{D}^+ \to \bar{\mathrm{K}}^{0\star}e^+\nu_e$ *channel; (right) The δm distribution for the* $\mathrm{D}^+ \to \bar{\mathrm{K}}^{0\star}e^+\nu_e$ *channel.*

3.2 *BR*($\mathrm{D}^+ \to \mathrm{K}^-\pi^+\mu^+\nu_\mu$) *at FOCUS*

The analysis summarized here is based on data collected by FOCUS at Fermilab in 1996-97, during a fixed-target run (photons with 180 GeV average energy incident on a BeO target). The data correspond to about 120K tagged D*s. The results are relevant for the preceeding CLEO analysis as FOCUS [13] has recently observed a discrepancy between the decay intensity for the decay $\mathrm{D}^+ \to \mathrm{K}^-\pi^+\mu^+\nu_\mu$ and that expected for pure $\mathrm{D}^+ \to \bar{\mathrm{K}}^{0\star}\mu^+\nu_\mu$. They find that

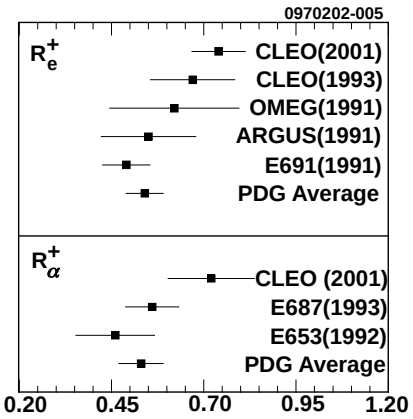

Figure 5: *The latest CLEO measurement of* R_e^+ *and* R_μ^+ *from* $D^+ \to \bar{K}^{0\star}\ell^+\nu_\ell$ *is compared with all the available measurements.*

the decay angular distribution for $D^+ \to K^-\pi^+\mu^+\nu_\mu$ does not agree with that predicted for $D^+ \to \bar{K}^{0\star}\mu^+\nu_\mu$ on the basis of the existing form factor values [6].

Five kinematical variables are needed to fully describe the $D^+ \to K^-\pi^+\mu^+\nu_\mu$ decay; $M(K^-\pi^+)$ the $K^-\pi^+$ invariant mass, the q^2 of the $\mu\nu$ system plus three angles, θ_V, the angle between the π and the D direction in the $K^-\pi^+$ rest frame, θ_ℓ, the angle between the neutrino and the D direction in the $\mu\nu$ rest frame and χ, the acoplanarity between the two decay planes. In Fig. 6 the $K^-\pi^+$ invariant mass peak is shown.

A substantial ($\sim$15%) forward–backward asymmetry in $\cos\theta_V$ is observed for $D^+ \to K^-\pi^+\mu^+\nu_\mu$ events with $M(K^-\pi^+)$ below the $\bar{K}^{0\star}$ pole, as shown in Fig. 7. The explanation for such an observation would be the presence of interference between a broad s–wave amplitude and the Breit–Wigner amplitude describing the $\bar{K}^{0\star}$. In particular this interference creates a term in the decay intensity that, when averaging over the acoplanarity, is proportional to $\cos\theta_V$, while only terms proportional to even powers of $\cos\theta_V$ are expected for pure $D^+ \to \bar{K}^{0\star}\mu^+\nu_\mu$. In Fig. 8 the asymmetry is shown versus $M(K^-\pi^+)$. The asymmetry is well explained if an s-wave amplitude of $0.36\exp(i\pi/4)(\mathrm{GeV}^{-1})$ is assumed which corresponds to $\sim$7% of the $\bar{K}^{0\star}$ Breit–Wigner amplitude at the pole mass.

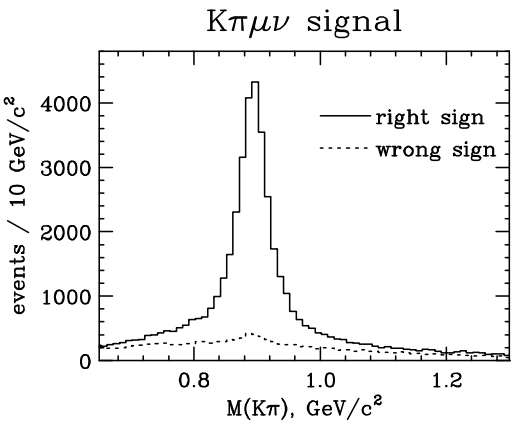

Figure 6: $D^+ \to K^-\pi^+\mu^+\nu_\mu$ *signal; right-sign and wrong-sign components are shown. In the mass window 0.8-1.0 GeV/c^2 the right-sign excess is about 27.2K events.*

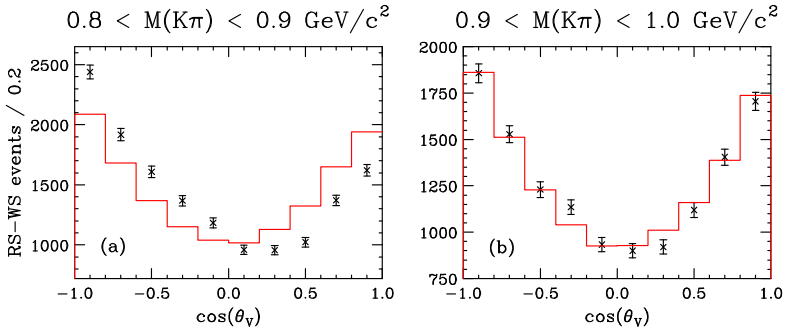

Figure 7: *Distribution in cos* θ_V *for the signal events sample; events with* $M(K^-\pi^+)$ *(a) below and (b) above the* $\bar{K}^{0\star}$ *pole. The points with error bars are FOCUS data wrong-sign background subtracted; the solid line is the FOCUS Monte Carlo prediction including the present values of form factors.*

4 Hadronic Decays

Hadronic decays of charmed mesons are a reach source of information about the underlying QCD and resonant analyses provide information about light resonances. In these section only a brief review of some recent results is given.

A number of new hadronic decay channels have been observed at FOCUS

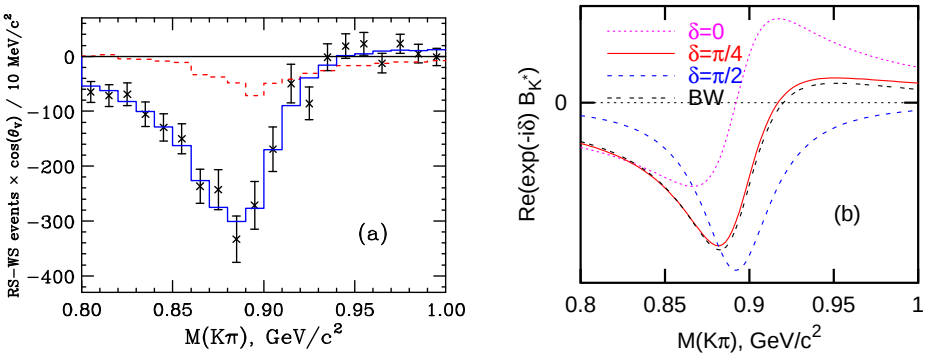

Figure 8: *Asymmetry in the $M(K^-\pi^+)$ distribution. (a) The dashed line is the FOCUS Monte Carlo with no interfering s-wave amplitude; the solid line is the Monte Carlo containing an s-wave amplitude of $\sim 0.36(GeV)^{-1}$ and a phase of $\pi/4$. (b) Theoretical expectations for an s-wave with different phases.*

as summarized in Table 2.

Interesting results in this field are expected soon from BABAR ($B\bar{B}$ pair production threshold with asymmetric beam). About 60 fb^{-1} of data have been collected since the start of data taking. With an $e^+e^- \to c\bar{c}$ cross section of ∼1.3 nb that corresponds to already 80 millions of charm pairs, with ∼ 150K tagged D*s. In Fig.9 an example of resonant analysis in the channel $D_s^+ \to K_S^0 K_S^0 \pi^\pm$ is shown; these studies have just started and the development of Dalitz fits is underway.

5 Future plans and expectations: CLEO-c

A very wide scenario on the charm physics opens with the CLEO-c program. This started this year, 2002, with runs below the $B\bar{B}$ pair production threshold, at the $\Upsilon(1S)$, $\Upsilon(2S)$ and $\Upsilon(3S)$.

About ∼ 1-2 fb^{-1} have been taken at each energy point collecting about 10-20 times the world existing data set available for spectroscopy and matrix element studies. The programs is due to continue in three further stages with a run at $\Psi(3770)$ in 2003 (∼ 3 fb^{-1}), a run at $\sqrt{(}s) \sim 4100$ MeV in 2004 (∼ 1 fb^{-1}), and a run at $\Psi(3100)$ in 2005 (∼ 1 fb^{-1}). These three periods of data taking aim to collect respectively 30 millions of DD events, with 6 million tagged D decays, 1.5 million D_sD_s events including 0.3 million tagged

Table 2: *Summary of hadronic decay modes studied at FOCUS. The channels marked with a star are first observations.*

Decay Mode	Norm. mode	BR (%)	Status
$D^+ \to K^0\pi^+$	$D^+ \to K^-\pi^+\pi^+$	30.60±0.46±0.32	hep-ex/0109022
$D^+ \to \bar{K}^0K^+$	$D^+ \to K^-\pi^+\pi^+$	6.04±0.35±0.30	hep-ex/0109022
$D^+ \to K^+K^-\pi^+\pi^+\pi^-(\star)$		*seen*	Preliminary
$D^+ \to K_SK^-\pi^+\pi^-$	$D^+ \to K_S\pi^-\pi^+\pi^+$	7.68±0.41±0.32	PRL 87,162001
$D^+ \to K_SK^+\pi^+\pi^-(\star)$	$D^+ \to K_S\pi^-\pi^+\pi^+$	5.62 ± 0.39 ± 0.40	PRL 87,162001
$D^+ \to K_SK^+K^-\pi^+(\star)$	$D^+ \to K_S\pi^-\pi^+\pi^+$	0.77 ± 0.15 ± 0.09	PRL 87,162001
$D^+ \to K^+K^+K^-(\star)$	$D^+ \to K^-\pi^+\pi^+$	0.114 ± 0.024	Preliminary
$D^0 \to K^+\pi^-$	$D^0 \to K^-\pi^+$	0.404±0.085±0.025	PRL 86,2955
$D^0 \to K^+K^-K^-\pi^+$	$D^0 \to K^-\pi^+\pi^+\pi^-$	0.306±0.047	Preliminary
$D_s^+ \to K^+K^+K^-(\star)$		*seen*	Preliminary
$D_s^+ \to K_SK^+\pi^+\pi^-(\star)$	$D_s^+ \to K_SK^-\pi^+\pi^+$	58.6 ± 5.2 ± 4.3	PRL 87,162001

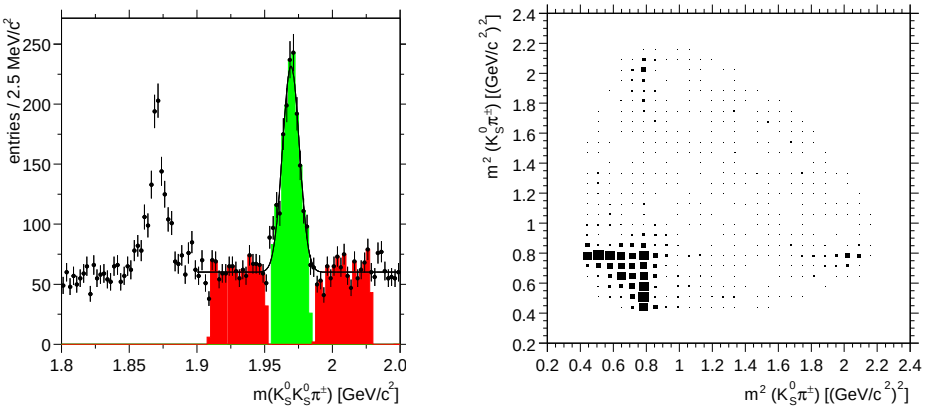

Figure 9: *Very preliminary BABAR resonant analysis in the channel* $D_s^+ \to K_S^0K_S^0\pi^\pm$.

D_s decays and 10^9 J/ψ decays. Overall an unprecedented amount of charm data. Some of the results foreseen for the decay constants and branching ratios are summarized in Table 3.

6 Acknowledgements

I wish to thank S. Bianco (FOCUS), D. Cinabro, T. Coan (CLEO), S. Wasserbaech (ALEPH) and D. Williams (BABAR) who provided me with the results

Table 3: *Summary of some of the results expected from the CLEO-c program in the field of leptonic, semileptonic and hadronic decays of charmed mesons.*

Decay Constant	Decay channel	PDG 2000 ($\delta f/f$)	CLEO-c ($\delta f/f$)
f_{D_s}	$D_s \to \mu\nu$	17%	1.9%
f_{D_s}	$D_s \to \tau\nu$	33%	1.6%
f_{D^+}	$D^+ \to \mu\nu$	UL	2.3%

Decay channel	PDG 2000 ($\delta BR/BR(\%)$)	CLEO-c ($\delta BR/BR(\%)$)
$D^0 \to K\ell\nu$	5	0.4
$D^0 \to \pi\ell\nu$	16	1.0
$D^+ \to \pi\ell\nu$	48	2.0
$D_s \to \phi\ell\nu$	25	3.1
$D^0 \to K^+\pi^-$	2.4	0.5
$D^+ \to K^-\pi^+\pi^-$	7.2	1.5
$D_s \to \phi\pi$	25	1.9

presented here.

References

1. C. Bernard, Nucl. Phys. (Proc. Suppl.) **94**, (2001) 159, hep-lat/00110644.
2. ALEPH Collaboration, Phys. Lett. **B 528**, (2002) 1 .
3. T. Draper, Nucl. Phys. (Proc. Suppl.) **73**, (1999) 43.
4. LEP Collaborations, LEP Electroweak Working Group, SLD Heavy Flavour and Electroweak Groups, "A combination of Preliminary Electroweak Measurements and Constraints on the Standard Model", CERN-EP/2000-016.
5. ALEPH Collaboration, Phys. Lett. **B 388** (1996) 648.
6. Particle Data Group, Eur. Phys. J. **C 15** (2000) 1.
7. B. Stech, Proc. 5^{th} Moriond Workshop, "Flavour Mixing and CP-Violation", (1985) 151.
8. N. Isgur and M.B. Wise, Phys. Lett. **B 232** (1989) 113; N. Isgur and M.B. Wise, Phys. Lett. **B 237** (1990) 257.

9. E. Eichten and B. Hill, Phys. Lett. **B 243** (1990) 427; H. Georgi, Phys. Lett. **B 240** (1990) 447.

10. M. Neubert, Phys. Rep. **245** (1994) 259.

11. CLEO Collaboration, hep-ex/0203030.

12. R. Zaliznyak, Ph.D. Thesis, Stanford University (1998).

13. FOCUS Collaboration, hep-ex/0203031.

Frascati Physics Series Vol. XXVIII (2002), pp.131-142
HQ & L 2002 – Vietri s/m, May 27th - June 1st, 2002

LIGHT MESON SPECTROSCOPY FROM CHARM DECAYS

Jussara M. de Miranda
Centro Brasileiro de Pesquisas Fisicas- CBPF
Xavier Sigaud, 150 - Rio de Janeiro, Brazil

ABSTRACT

We discuss recent achievements in light scalar mesons spectroscopy through amplitude analysis of charm particle decay and its consequences. The high statistics clean samples of charmed mesons, in addition to it's definite J^P and mass, is turning these decays into a new important environment to study light meson physics. We give special attention to the scalar sector favored by a high coupling to charm.

1 Introduction

Most mesons are well understood in the context of the quark model. This is not true just for the scalar sector, that for long has been a source of controversy. For the latest 30 years a great deal of experimental effort have been made but in many cases the experimental results do not converge to compatible outputs. In

production experiments, observing the scalar resonant states is difficult due to a large contribution of the non-resonant background. Moreover, light scalars are too numerous within a relatively short mass interval. The absence of a unique analysis procedure, especially regarding the interference of the background with the resonances results in conflicting measurements. In this sense the wider and lighter the state the worse, and this is the case of the two states $\sigma(500)$ and κ that will be discussed here.

The theoretical interpretation of the lightest scalar meson have also been unclear. Many objects – glueballs, KK molecules, multiquark compact states – are expected to populate the area. In a recent review article F. Close and N. A. Törnqvist [1)] discuss the scalars from both experimental end theoretical points of view. They suggest that the scalars be organized not in one but two nonets. The "standard" quark model $q\bar{q}$ nonet, distorted by a glueball predicted by lattice QCD, is enough to explain the region above $\sim$ 1 GeV. This nonet is composed by $a_0(\sim\ 1400), f_0(1370), K(1430), f_0(1500)$ and $f_0(1710)$. The states below $\sim$ 1GeV – $f_0(980), a_0(980)$ and possibly $\sigma(500)$ and κ – by arguments based on QCD attractive forces in S-wave, would also form a nonet. The interpretation of such nonet would be more complex, of the type meson-meson. In the article, they stress the importance of charm decay as "opening up a new experimental window for understanding light meson spectroscopy and specially the controversial scalar meson which are copiously produced in these decays".

The use of charm decay is an alternative to the traditional production experiments to study lighter resonant particles. It was made possible by the large clean samples of charm now available and which are attributed to mankind effort but also, and more important, by what can be seen as nature's gifts:

1) Non-leptonic charm decays are preferentially two body or quasi-two body, through the formation of intermediate resonant states. With a small non-resonant (NR) component one avoids having to deal with model dependent amplitudes and its interference with the resonant amplitudes. This feature is particularly important for the wide scalars because their amplitudes and the NR (usually taken as constant) can become very similar. We return to this issue later in the text.

2) Charm couple strongly with scalars. This empirical fact is present in the decays discussed here where the contribution to scalars dominates all

processes.

3) We are dealing with a well defined initial state; (charm meson mass, M and J^P)

The first light resonant parameters extracted from charm data use D meson decays to three charged pseudo-scalars. In the following session we summarize the Dalitz plot amplitude formalism used. The parameterization of the overall amplitude consists of a coherent sum of all contributions (NR flat and resonant as relativistic Breit-Wigners modulated by angular momentum conservation functions and form factors) with complex coefficients obtained from the fit. The magnitude of the coefficients are proportional to each relative contribution and the phases accommodate in an effective way the final state interactions. It should be pointed out as the a great pro of these analysis the very good description that such simple model give to the data. Alternative descriptions for the decay amplitude are being tried, for example Focus experiment is using K-matrix to parameterize the light scalars contribution, but we shall not discuss those, still preliminary, results. Also expected for the near future are Focus four-body amplitude analysis.

2 Three body hadronic decay formalism

We describe here the analysis procedure used by the E791 collaboration in their D^+ and $D_s^+ \to \pi^+\pi^-\pi^+$ [2) 3)] and $D^+ \to K^-\pi^+\pi^+$ [4)], from which was measured masses and widths of $\sigma(500)$, $f_0(980)$, $f_0(1370)$, κ and $K_0^*(1430)$.

The decay of a scalar hadron of mass M into 3 spinless daughter particles is completely specified with two degrees os freedom, conveniently chosen as two Dalitz plot variables, m_{12}^2 and m_{23}^2. The Dalitz plot density distribution is proportional to the invariant decay amplitude $\mathcal{A}$ squared and reflects the dynamics of the decay process. A simple analytical model for $\mathcal{A}$ is given by a coherent of all intermediate states contributing, resonant or not:

$$\mathcal{A} = a_{NR} e^{i\delta_{NR}} \mathcal{A}_{NR} + \sum_{j=1}^{n} a_j e^{i\delta_j} \mathcal{A}_j \qquad (1)$$

The parameters a give the various relative contributions and the phases δ are accounts for final state interactions. The non-resonant amplitude $\mathcal{A}_{NR}$ is represented by a constant. Which is a reasonable assuption if we imagine that it is dominantly S-wave, in any case, the impact of this choice in the results is

reduced due to a small NR contribution observed. The decay through resonant intermediate states, j (that then decay to the observed k and l hadrons), are viewed as s-channel processes where the resonance plays the role of massive propagators, represented by relativistic Breit-Wigner functions, BW_j [1] . Momentum dependent form factors, F_D and F_R describe the non-pointlike nature of the D meson and the resonance respectively and depend on the resonance spin, J and the radii of the relevant mesons. The angular momentum conservation is taken care by the function $\mathcal{M}_j^J$. Each resonant amplitude, $\mathcal{A}_j$ is written as:

$$\mathcal{A}_j = BW_j \times F_D \times F_R \times \mathcal{M}_j^J \tag{2}$$

$$BW_j = \frac{1}{m_{kl}^2 - m_0^2 + im_0\Gamma_j(m_{kl})} \tag{3}$$

with

$$\Gamma(m_{kl}) = \Gamma_0 \frac{m_0}{m_{kl}} \left(\frac{p^*}{p_0^*}\right)^{2J+1} \frac{F_R^2(p^*)}{F_R^2(p_0^*)} \tag{4}$$

Above m_{kl}^2 is the the Dalitz plot variable, i.e. the invariant mass of the two hadrons forming a spin-J resonance. Detailed expression of all the above functions are found in the references [2, 3, 4]. Combinatorics background, detector efficiency and Bose symmetrization are also considered in a maximum likelihood fit to the data to extract the parameters. In most cases the masses, m_0, and widths, Γ_0 of the resonances are fixed by values listed in PDG. Only for new or poorly measure states they are allowed to float in the fit.

[1] For the $f_0(980)\pi^+$ E791 uses a coupled channel Breit-Wigner, following the parameterization used by the WA76 Collaboration [6],

$$BW_{f_0(980)} = \frac{1}{m_{kl}^2 - m_0^2 + im_0(\Gamma_\pi + \Gamma_K)}, \text{with}$$

$$\Gamma_\pi = g_\pi \sqrt{m_{kl}^2/4 - m_\pi^2}, \text{and}$$

$$\Gamma_K = \frac{g_K}{2} \left(\sqrt{m_{kl}^2/4 - m_{K^+}^2} + \sqrt{m_{kl}^2/4 - m_{K^0}^2}\right)$$

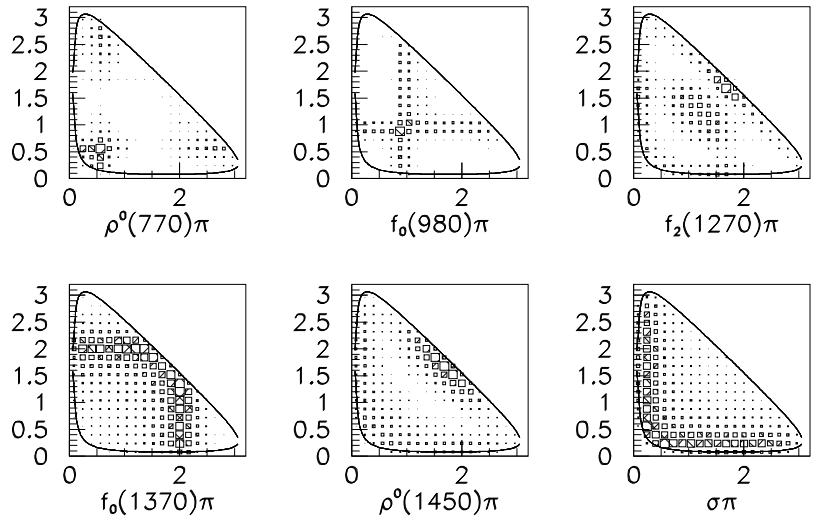

Figure 1: *Dalitz-plot of the individual resonant contributions to the* $D^+ \to \pi^-\pi^+\pi^+$ *decay.*

Figure 1 shows , as an example, Monte Carlo simulation Dalitz-plot of each individual resonant state that contributes in the $D^+ \to \pi^-\pi^+\pi^+$ decay. Notice that being coefficients and the individual amplitudes complex quantities, interference effects will take place when all the pieces act together.

The above described produces a quite stringent model and obtaining acceptable fits is usually a difficult task. To access the quality of each fit a fast Monte Carlo (MC) program was developed which produces Dalitz plot event densities accounting for signal and background PDF's, including detector efficiency and resolution. Comparing the MC density distribution generated using parameters extracted from a given fit with that for the data, it is produced a χ^2 distribution. When comparing two possible models, the best discriminating power test requires ensembles of Monte Carlo "experiments". In the κ discussion below we illustrate the technique.

3 The f_0's resonances

We have chosen to start the results sessions with the f_0 because of the extremely clear signal seen in the $D_s^+ \to \pi^+\pi - \pi^+$ decay, figure 2. There are dozens of measurements listed in PDG [7] for this state and they converge to a reasonably well defined mass, 980 ± 10 MeV but the estimation for width is from 40 to 100 MeV.

For the best E791 fit 5 resonant channels contributes significantly: $\rho^0(770)\pi^+$, $\rho^0(1450)\pi^+$, $f_0(980)\pi^+$, $f_2(1270)\pi^+$, and $f_0(1370)\pi^+$, plus a NR that contributed with a fraction of only $0.5 \pm 0.2\%$. The fit have $\chi^2/dof = 71.8/68$ with a confidence level of 35%. The dominant contributions comes from $f_0(980)\pi^+$, $56.5 \pm 6.4\%$, and $f_0(1370)\pi^+$, $32.4 \pm 7.9\%$ from which they measure: $m_{f_0(980)} = 977 \pm 3.6$ MeV/c^2, $g_\pi = 0.09 \pm 0.01$, $g_K = 0.02 \pm 0.05$, $m_{f_0(1370)} = 1434 \pm 20$ MeV/c^2 and $\Gamma_{f_0(1370)} = 172 \pm 33$ MeV/c^2. There is no evidence of a third higher mass scalar state, $f_0(1500)$.

Previous production experiments claim a large contribution of the $K\bar{K}$ channel by estimation a large value of the parameter g_K [6] [5]. These results do not agree with the value measured by E791 that, in fact, finds that a simple Breit-Wigner 3 is sufficient to represent the data. From the small but clear preliminary signal BES collaboration measure $m_{f_0} = 0.980 \pm 0.009$ GeV and $\Gamma_{f_0} = 0.045 \pm 0.30$ GeV [9]. In figure 3 we compare various results and conclude that in charm decay the resonance $f_0(980)$ presents a narrower signal.

4 The $\sigma(500)$

The 1999 the Workshop on Hadron Spectroscopy [8] devoted one entire session to the meson $\sigma(500)$, " What do we know about the σ?". By that time E791 had not published their observation of the meson σ in the decay of $D^+ \to \pi^+\pi^-\pi^+$ [3]. Today charm decay is viewed as a tool for studying the light spectroscopy.

In figure 4 we show the projection of the E791 Dalitz plot where a clear peak at low mass can be seen. The figure compares the best fit achieved with all possible well established resonances available at the time, *a*) (Fit 1), to their solution including a low mass scalar state, *b*) (Fit 2). They measured $m_\sigma = 478 \pm 29$ MeV/c^2 and $\Gamma_\sigma = 324 \pm 46$ MeV/c^2 and the inclusion of the state took them from an unacceptable solution of $\chi^2/dof = 254/162$ with a

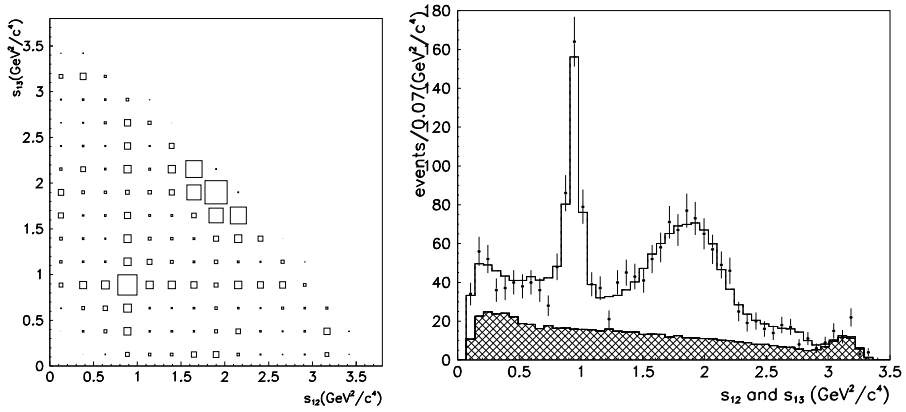

Figure 2: *E791* $D_s^+ \to \pi^+\pi - \pi^+$ *Dalitz plot and* $m^2_{\pi^+\pi^-}$ *projection*

confidence level less than 10^{-5} to a very good fit with $\chi^2/dof = 138/162$ and confidence level of 90%. In Fit 1 the NR contribution is dominant with 38% and in Fit 2 following the trend of charm decays it dropped to 7.8% whereas the $\sigma\pi^+$ dominates with 46%. E791 perform a series of alternative fits and tests to be sure that no other model would as well describe the data.

Studying the channel $J/\Psi \to w\pi^+\pi^-$ BES experiment observe a signal of the mesons σ and measure their parameters [10]; $m_\sigma = 490^{+60}_{-36}$ MeV/c^2 and $\Gamma_\sigma = 282^{+77}_{-50}$ MeV/c^2. In figure 5 we show their final fit and scans for the σ mass and width measurements.

5 The κ

As a last result we consider the κ resonance observed in E791 Cabibbo favored decay $D^+ \to K^-\pi^+\pi^+$. Despite the large statistics available in this channel, no previous experiment [11] [12] have been able to provide a convincing explanation for this decay. E687 [12] best model for their sample of almost 9000 events have $\chi^2/dof = 87/29$. The solution have the NR contribution dominating with

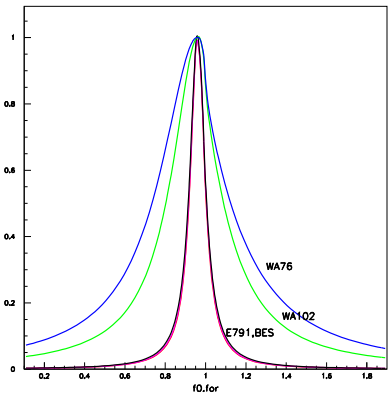

Figure 3: *Comparison of several* $f_0(980)$ *results.*

a fraction of 99%. Large interference pattern is produced with all fractions summing 147%. In contrast to the σ where a clear bump is seen in the $m^2_{\pi^+\pi^-}$ projection, no evidence for a missing piece in the low $m^2_{K^-\pi^+}$ region can be easily observed (figure 6b). On the other hand the very large statistics and small number of possible intermediate states provide strong evidence of the need for an extra low mass wide resonance contributing for the decay.

The first approach tried by E791 [4] was to include all established states; $\bar{K}^*(892)\pi^+, \bar{K}^*_0(1430)\pi^+, \bar{K}^*_2(1430)\pi^+, \bar{K}^*(1680)\pi^+$ plus a NR (they have studied also the possibility of a non-flat NR contribution without success). In general the result agree with previous studies including the bad quality of the fit. At this point they measured mass and width of the scalar $K^*_0(1430)$ to be 1416±27 and 250 ± 21 MeV/c^2 respectively, which agree with PDG values.

Next they include an additional scalar named "κ" for which they measure respectively mass and width of 797± 47 and 410± 97 MeV/c^2. In the same fit the parameters relative to $K^*_0(1430)$ were measured to be 1459±9 and 175±17 MeV/c^2. This new model describes very well the data with a $\chi^2/dof = 46/63$,

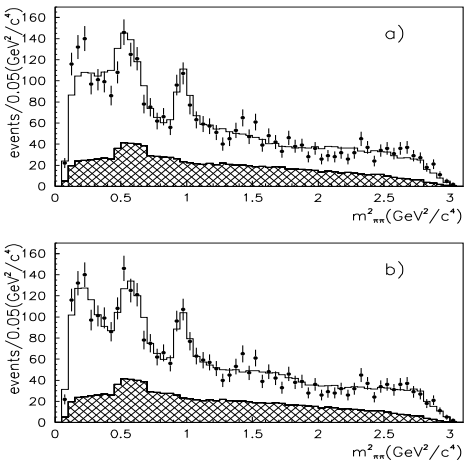

Figure 4: *E791* $D^+ \to \pi^+\pi - \pi^+$ $m^2_{\pi^+\pi^-}$ *projections for data (error bars) and model (solid line). Shaded area is the background. a) solution for Fit 1, and b) Fit 2.*

confidence level of 95%. The contribution of the new state is dominant with 48± 12% of the total fraction and the NR contribution is of 13±7 %. The sum of all fractions dropped from 134% in the fit without κ to 88% indicating a smaller degree of interferences.

In the amplitude analysis described here one do not measure directly a Breit-Wigner phase, instead it is assumed and consistency tests have to be performed to verify if alternative models are able to represent the data. This was done for this analysis; a toy-model (consisting of a Breit-Wigner amplitude without a phase variation), a vector and a tensor alternative models were tried, none producing a satisfying solutions. When comparing two possible models A and B the best figure of merit to be used is given by the Neyman-Person [13] lema: $\Delta w_{A,B} \equiv -2(ln\mathcal{L}_A - ln\mathcal{L}_B)$, where $\mathcal{L}_{A,B}$ are the likelihood for a given set of events calculated with the parameters obtained from fits to the data with

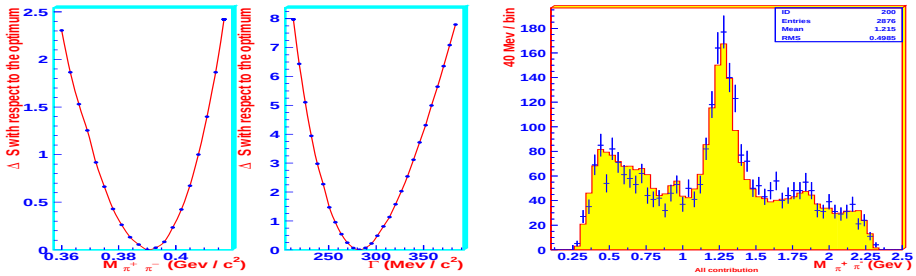

Figure 5: *LEFT: Mass scan on σ; MIDDLE:width scan on σ; RIGHT: final global fit (error bar is real data and histogram is fit)*

models A and B. Ensembles of 1000 Monte Carlo "experiments" were generated with the parameters extracted from fits to the data for the two models A and B. For each of such experiments the quantity $\Delta w_{A,B}$ was calculated and plotted in figure 7, where the model with the scalar κ is compared with model without it; with the toy-model κ or with the vectorial κ. The discriminating power of the exercise is obvious by the separation of the distributions. The value of $\Delta w_{A,B}$ for the data is signed by the triangle showing the clear preference of the data to the model of the scalar κ.

6 Conclusion

In conclusion, charm decay is, as said by F.Close and Törnqvist, a new window for studying light mesons. We discussed some of its remarkable contributions. With the already available data sets and the richness of charm decays, we hope to see in the near future confirmations and better measurements for some of the resonances, like the κ.

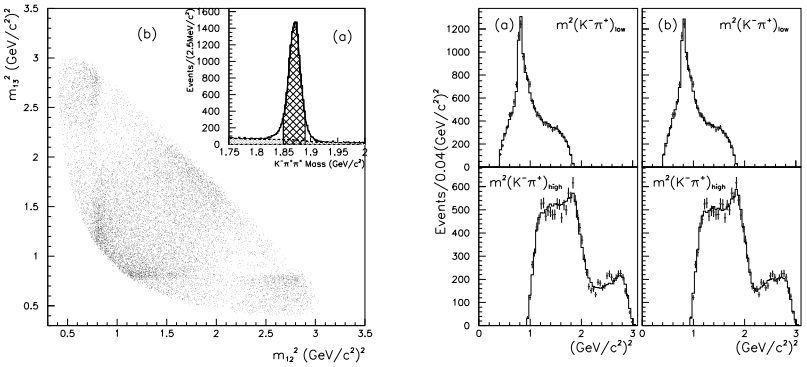

Figure 6: *LEFT: E791 $D^+ \to K^-\pi^+\pi^+$ Dalitz plot ; RIGHT: projections for data (error bars) a)without κ b)with κ*

References

1. Frank E. Close and Nils A. Törnqvist, Scalar mesons above and below 1 GeV,hep-ph/0204205
2. E791 Collaboration, E.M. Aitala *et al.*, Phys. Rev. Lett. **86** 765 (2001).
3. E791 Collaboration, E.M. Aitala *et al.*, Phys. Rev. Lett. **86** 770 (2001).
4. E791 Collaboration, E.M. Aitala *et al.*, hep-ex/0204018. Submitted to PRL.
5. WA102 Collaboration, Barberies, D. *et al.*, Phys. Lett. **453 B**,332 (1999).
6. WA76 Collaboration, T.A. Armstrong *et al.*, Z. Phys. **C** 51, (1991) 351.
7. Particle Data Group, C. Caso *et al.*, Eur. Phys. J. C **15**, 1 (2000).
8. T.Bressani, A. Feliciello and A. Filippi, Proceedings of the Workshop on Hadron Spectroscopy, Frascati Physics Series **XV**, (1999).
9. Daniela Paluselli, representing BES Collaboration " $\Psi(2S) \to wX$ and ϕX" at DPF meeting - Williamsburg, Virginia (2002).

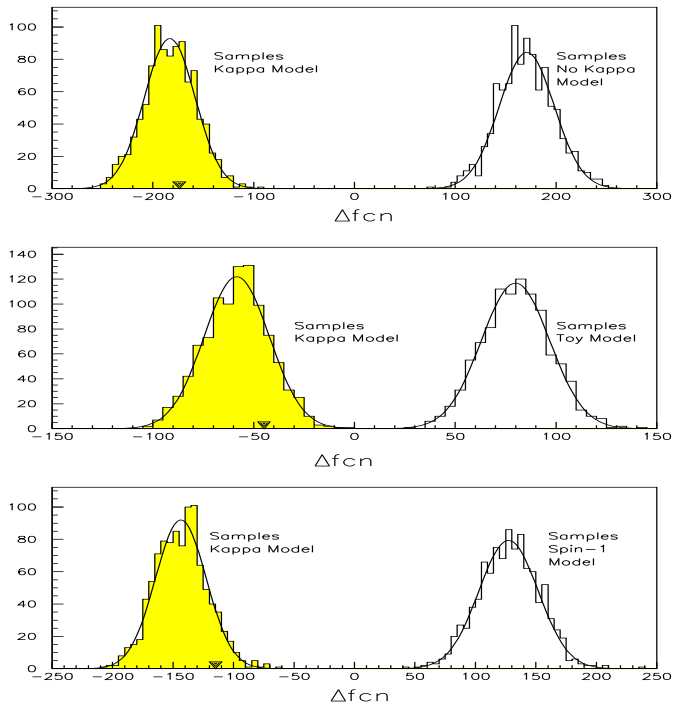

Figure 7: *Comparison of several models to fit E791* $D^+ \to K^-\pi^+\pi^+$ *data. Histogram of* $\Delta w_{A,B}$*, described in the text, for ensembles of Monte Carlo "experiments" and the data point, solid triangle.*

10. Ning Wu, "BES R measurements and J/Ψ decays",hep-ex/0104050

11. E691 Collaboration, J.C. Anjos *et al.*, Phys. Rev. D**48**, 56(1993)

12. E687 Collaboration, P.L. Frabetti *et al.*, Phys. Lett. B **331**, 217 (1994)

13. Glen Cowan,"Statistical Data Analysis", Oxford Univ. Press, 1998;

Frascati Physics Series Vol. XXVIII (2002), pp.143-152
HQ & L 2002 – Vietri s/m, May 27th - June 1st, 2002

CHARMED HADRON SPECTROSCOPY

Luigi Benussi
Laboratori Nazionali di Frascati - INFN

ABSTRACT

The aim of this paper is to try to give an almost comprehensive summary of the most recent experimental results on D and D_s mesons spectrum and a comparison between some theoretical predictions and experimental data.

1 Present status of D and D_s experimental data

Although heavy quark spectroscopy is almost an old subject of studies, the excitation spectrum of heavy-light mesons (D, D_s, B and B_s) still remains to be completely theoretically understood. From the experimental point of view a great part of those spectrum has still to be observed. While the narrow states are well established, the evidence for the broad states (both in the c-quark and in the b-quark sector) is scarce. Focusing our attention on charmed heavy

light meson (D and D_s) the experimental data available, reported in the 2001 edition of the PGD [1], are summarized in tables 1 and 2.

Table 1: *D meson masses and widths as PDG 2001.*

	Mass (MeV/c^2)	Width(MeV/c^2)
$D_0 1/2(0^-)$	1864.5 $\pm$0.5	
$D^{\pm} 1/2(0^-)$	1869.3 $\pm$0.5	
$D^{*0} 1/2(1^-)$	2006.7 $\pm$0.5	< 2.7
$D^{*\pm} 1/2(1^-)$	2010.0 $\pm$0.5	< 0.131
$D_1^0 1/2(1^+)$	2422.2 $\pm$ 1.8	$18.9^{+4.6}_{-3.5}$
$D_1^{\pm} 1/2(?^?)$	2427 $\pm$ 5	28 $\pm$ 8
$D_2^{*0} 1/2(2^+)$	2458.9 $\pm$ 2.0	23 $\pm$ 5
$D_2^{*\pm} 1/2(2^+)$	2459 $\pm$ 4	25^{+8}_{-7}
$D_0^{*0} 1/2(2^+)$	Seen by Focus	–
$D_0^{*+} 1/2(2^+)$	Seen by Focus	–
$D_1 1/2(2^+)$	Seen by Cleo	–
$D^{*'} 1/2(?^?)$	2637 $\pm 2 \pm 6$	< 15
$D^{'} 1/2(?^?)$	Not seen	–

Table 2: *D_s meson masses and widths as PDG 2001.*

	Mass (MeV/c^2)	Width(MeV/c^2)
$D_s 0(0^-)$	1968.6 $\pm$0.6	
$D_{s1}^{\pm}$	Not seen	–
$D_s^* 0(?^?)$	2112.4 $\pm$0.7	< 1.9
$D_s^{*\pm}$	Not seen	–
D_{s1}^0	Not seen	–
$D_{s1}^{\pm}$	2535.35 $\pm$ 0.34	< 2.3
D_{s2}^{*0}	Not seen	–
$D_{s2}^{*\pm} 0(?^?)$	2573.5 $\pm$ 1.7	15^{+5}_{-4}
D_{s0}^{*0}	Not seen	–
D_{s0}^{*+}	Not seen	–
D_{s1}	Not seen	–
$D_s^{*'}$	Not seen	–
$D_s^{'}$	Not seen	–

Although in tables 1 and 2 are also reported new states, claimed to be observed by experimentalists, is however evident that, mainly for charmed-

strange mesons, the experimental spectra are almost incomplete. Moreover, for the well established excreted states the mass and width measurements are effected by large errors, and for some of the observed states the quantum number are still to be confirmed. In Addiction to this picture there is the so called $D^{*'}$ puzzle. In 1998 Delphi collaboration claims an evidence of the 1st radially excited charmed meson [2]. In the following years no other experiments have seen this state, [3], [5] and [4]. Moreover the $D^{*'}$ width measured by Delphi is too narrow with respect to theoretical predictions for a radial excited state as reported by authors of [7] and [6], which also suggest an interpretation of the state seen by Delphi as and L=2 orbital excited state. Moreover the first radial excited state D' is still missing.

1.1 Recent experimental data

New experimental data not yet included into the latest PDG edition came from CLEO and FOCUS collaborations. A detailed discussion of the analysis procedures performed in the search of these states overcome the purpose of this paper. The interested reader can find such details in the referred papers. The new data reported are the first measurement of $D_1 1/2(2^+)$ mass and width performed by Cleo [5], the D^*_{2s}, D^1_s [8] and D^*_2 [9] masses and widths improved measurements performed by Focus, and the evidence of the D^*_0 signal claimed by Focus [9]. In table 3 are reported masses and widths of these states.

Table 3: *New D and D_s masses and width measurements.*

	Mass (MeV/c^2)	Width(MeV/c^2)
$D^{*0}_2 1/2(2^+)$	2462.5±1.1±1.8	25±1.5±1.5
$D^{*+}_2 1/2(2^+)$	2467.2±1.5±1.9	24.9±2.0±0.5
$D^{*0}_0 1/2(2^+)$	2436.6±4.1±9.1	169.7±12.5±54.8
$D^{*+}_0 1/2(2^+)$	2418.3±5.5±9.2	232±13.7±45.1
$D_1 1/2(2^+)$	$2461\ ^{+0.041}_{-0.034} \pm 0.010 \pm 0.032$	$290^{+101}_{-79} \pm 26 \pm 36$
$D^{\pm}_{s1}$	2535.1± 0.3	1.6±1.0
$D^{*\pm}_{s2} 0(?^?)$	$2567.3^{+1.3}_{-1.2}$	$28^{+4.8}_{-4.0}$

The observation of the D^*_0 broad state, if confirmed, is crucially for the understanding of the L=1 states mass splitting, as will be discussed in below. The $D^{'}$ radially excited state is still missing, as well as the confirmation of the $D^{*'}$. No new states have been observed in the D_s spectrum which remains

almost incomplete.

2 Models

In the limit of infinite heavy-quark mass, heavy-light hadron physics can be described by an effective theory (HQET), which is invariant under changes of the flavor and spin of the heavy-quark [10], [11] [12]. The consequences of this heavy-quark symmetry (HQS) for spectroscopy have been worked out in [13]. Further detail about theoretical works can be found in ref. [14]

The basic idea of HQET is that, for an infinite heavy quark mass, the heavy-light (Qq) meson behaves in analogy to the hydrogen atom. With this assumption the heavy quark motion progressively slow down and the system can be described by a non-relativistic Schrödinger equation with a generic two-body potential V = V_C+V_{SS}+V_{SO} where V_C is the central potential plus a linear confining term, V_{SS} is the spin-spin potential plus color hyperfine interaction term and V_{SO} is the spin-orbit potential plus color magnetic term. Assuming the heavy-quark mass M_Q infinite, the system properties are described by the light quark (m_q) properties, i.e. the spin s_q and orbital L. Within this approximation good quantum numbers are the heavy-quark spin S_Q and light-quark total momentum $j_q = s_q + L$ as well as the total angular momentum of the system $J^P = (j_q + S_Q)^P$ where P is the parity of the system. Predicted excited states are formed by combining S_Q and j_q. For $L = 1$ (P-wave mesons) we have $j_q = 1/2$ and $j_q = 3/2$ which, combined with S_Q, provide prediction for two $j_q = 1/2$ (J=0,1) states, and two $j_q = 3/2$ (J=1,2) states. These four states are named respectively D_0^*, $D_1(j_q = 1/2)$, $D_1(j_q = 3/2)$ and D_2^*. In this picture states with same j_q (3/2 or 1/2) are degenerate. Finally, parity and angular momentum conservation favor the ($j_q = 1/2$) states to decay to the ground states mainly via S-wave transitions (broad width), while ($j_q = 3/2$) states would decay via D-wave (narrow width).

Nevertheless the heavy quark masses is non infinite even with respect to the lighter quarks (u and d). However due to the fact that M_Q is still large compared to QCD scale ($M_Q >> \Lambda_{QCD}$) HQET can be corrected introducing terms as $1/M_Q$ and $1/M_Q^2$ to take into account relativistic effects arising from the heavy-quark mass. These corrections make the Hamiltonian of the system no more diagonal and cause the splitting of L=1 states. An example of D spectrum [15] with the decay modes of the states is shown in fig.1.

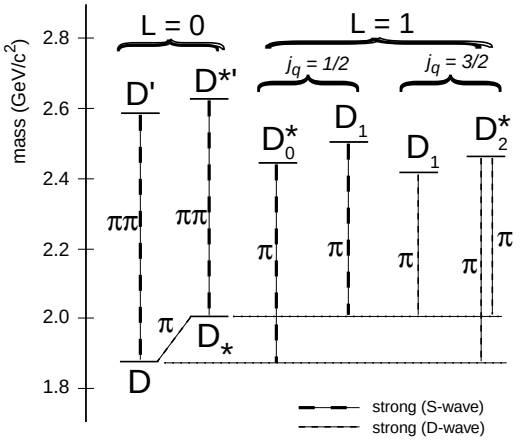

Figure 1: *The D meson spectrum as calculated by* [15].

Lattice QCD calculations have greatly helped the understanding of heavy-quark systems [20]. In the case of one heavy quark ,i.e. D mesons, the dynamics can by written in powers of $1/M_Q$. Calculation are performed in discrete space-time lattice with a lattice spacing $<< 1/M_Q$, which requires high computational capabilities that can be be reduced by introducing a "quenched" lattice (NRQCD) adopting the approximations of HQET (Lewis - woloshyn). If the charm quark is sufficiently heavy, then lattice NRQCD is an efficient computational method for obtaining the spectrum of mesons with a single charm quark.

2.1 P-wave charmed heavy meson

Although the lattice QCD calculation have been very useful to evaluate heavy-light quarks system behavior and improvements have been made in HQET calculations, the P-wave mesons splitting is still a open issue. The levels relative amplitude is not large in comparison to the typical scale of non-perturbative QCD that make the level splitting difficult to evaluate within lattice QCD. Improvement have been made in this direction, but, even if the uncertainties are reduced, the levels patterns is still not unequivocally described. For example, the models of refs. [16] and [18] predict the traditional hydrogen-like ordering of P-waves, where the D_0^* is the lightest meson, the D_2^* is the heaviest, and the

D_1 states lie in between. The authors of [17] find, from lightest to heaviest, D_0^*, $D_1(3/2)$, D_2^*, $D_1(1/2)$ while [13] predicts a dramatic inversion where the D_0^* is heavier than the D_2^* by 100 MeV, but the D_1 states are the absolute lightest and heaviest. Reference [19] claims very small splittings (tens of MeV) where the $D_1(1/2)$ and $D_1(3/2)$ doublets overlap to produce different orderings for the D and Ds systems.

3 Experimental data and theoretical predictions

In this section some theoretical predictions are compared with experimental data. In fig.2 is shown the D meson spectrum expressed in the excitation energy, defined as the mass difference with respect to the ground state D.

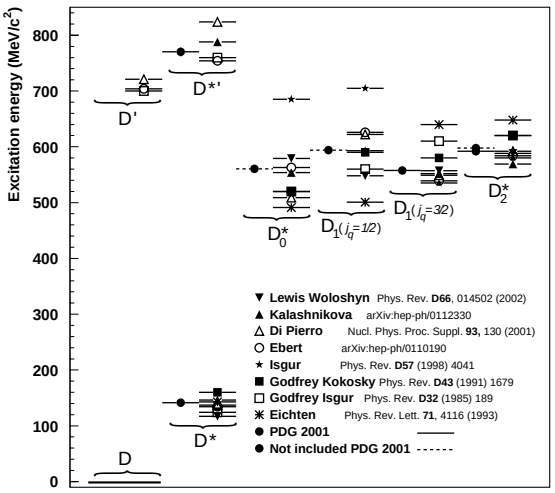

Figure 2: *D meson spectrum expressed in the excitation energy, defined as the mass difference with respect to the ground state D.*

In figure are also included the recently observed $D^*{}_0$ and D_1 states together with some theoretical (both HQET and Lattice QCD) predictions of the experimental states. Theoretical predictions of the low lying excited states fit reasonably well the experimental data while the predictions of the L=1 states, besides the huge discrepancies between different approach already discussed, seem to be not able to describe the experimental patter of data. It' s

worthwhile to underline the great relevance of the two broad states recently observed, that, if confirmed will clarify the problem of the orbital excited states. Assuming the mass values reported in table 1 and table 3 and considering the s_q ($\uparrow$), L ($\Uparrow$) and S_Q ($\updownarrow$) vectors of the four P-wave mesons it is possible to define the following schema (mass units MeV/c^2):

$$\underset{\uparrow\Uparrow\updownarrow}{D_2\ (2462.9)} \quad \underset{\downarrow\Uparrow\updownarrow}{D_1(1/2)\ (2461)} \quad \underset{\uparrow\Uparrow\downarrow}{D_0\ (2427.5)} \quad \underset{\downarrow\Uparrow\downarrow}{D_1(3/2)\ (2424.6)}$$

This schema is not reproduced by any of the theoretical works discussed in this papers. Moreover the experimental relative position of the P-wave mesons seems to suggest that the main spin coupling is between S_Q, L as suggested by the fact that the P-wave mesons are seem to be grouped in the two " *doublets*" ($D_2(3/2)$ - $D_1(1/2)$) and ($D_0(1/2)$ - $D_1(3/2)$). Nonetheless as to be notice that the energy difference between the states of the same "*doublets*" is of few MeV/c^2 that could be associated to the spin flip of the s_q vector.

Similarly as for fig. 2, in fig. 3 is shown the D_s spectrum in term of excitation energy relative to the D_s ground state.

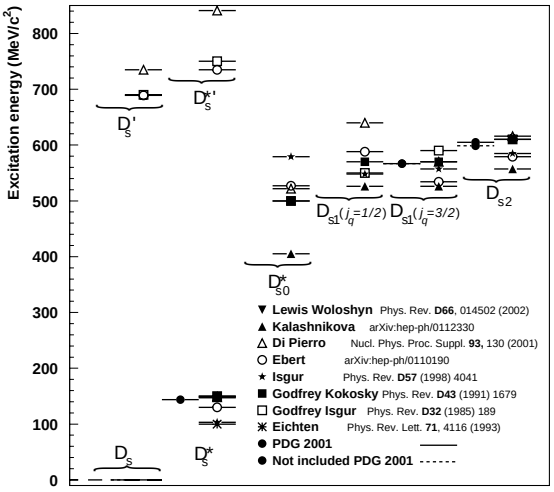

Figure 3: *D_s meson spectrum expressed in the excitation energy, defined as the mass difference with respect to the ground state D_s.*

In figure are plotted data of table 2 and 3 together with theoretical predictions. As said in section 1, the experimental data available for the charmed-strange mesons are very scare. The L=1 states are not complete and no radial excited state candidates has been observed up to now. Analogous considerations done for D mesons can be repeated for fig.3 also for what concern the capability of the different models to describe the "poor" experimental data.

4 Conclusions

Despite of the interest of this topic, heavy-light mesons spectroscopy is still far to be fully understood. Charmed-mesons experimental data are scare and in most case with large errors both for masses and widths. In the D mesons spectrum new states are claimed to be observed by experimentalist that, if confirmed, will complete the L=1 mesons states and open a discussion about their splittings and relative amplitude. No new radial state has been observed since the controversial $D^{*'}$ seen by Delphi. On the D_s site only improved mass and width measurements for already observed states are available and many of the orbital and excited states are still missing.

5 Acknowledgments

Thanks are addressed to my friends F. L. Fabbri and S. Bianco for the help they gave me during the realization of this paper. I want also thanks the organizing committee of HQ&L to invite me at the 2002 edition of the conference.

References

1. D.E. Groom *et al.*, The European Physical Journal **C15**, 1 (2000).
2. P. Abreu. *et al* (DELPHI Coll.) Phys. Lett. **B426**, 231 (1998)
3. G. Abbiendi *et al.* [OPAL Collaboration], Eur. Phys. J. C **20**, 445 (2001) [arXiv:hep-ex/0101045].
4. F. Sefkow [H1 Collaboration], arXiv:hep-ex/0011034.
5. J. L. Rodriguez [CLEO Collaboration], arXiv:hep-ex/9901008. arXiv:hep-ex/9901008

6. D. Melikhov and O. Pene, Phys. Lett. B **446**, 336 (1999) [arXiv:hep-ph/9809308].

7. Y. S. Kalashnikova and A. V. Nefediev, arXiv:hep-ph/0112330.

8. R. K. Kutschke [FOCUS Collaboration], *Prepared for 5th Workshop on Heavy Quarks at Fixed Target (HQ2K), Rio de Janeiro, Brazil, 9-12 Oct 2000.*

9. F. L. Fabri *et al.* [FOCUS Collaboration], arXiv:hep-ex/0011044.

10. N. Isgur and M.B. Wise, Phys. Rev. Lett. **66**, 1130 (1991);

11. E. J. Eichten, C. T. Hill and C. Quigg, Phys. Rev. Lett. **71**, 4116 (1993);

12. H. Georgi Phys. Lett. **B240** 447 (1990);

13. N. Isgur, Phys. Rev. D **57**, 4041 (1998).

14. R. Barbieri, R. Kogerler, Z. Kunszt and R. Gatto, Nucl. Phys. B **105**, 125 (1976). S. Godfrey and N. Isgur, Phys. Rev. **D32**, 189 (1985); S. Godfrey and R. Kokoski, Phys. Rev. **D43**, 1679 (1991); J. Bartelt and S. Shukla, Annu. Rev. Nucl. Part. Sci 1995 **45** 133-61. U. Kilian, J. G. Körner and D. Pirjol, Phys. Lett. B **288**, 360 (1992). M. Di Pierro and E. Eichten, Nucl. Phys. Proc. Suppl. **93**, 130 (2001) T. A. Lahde and D. O. Riska, arXiv:hep-ph/0112223. A. F. Falk and M. E. Luke, Phys. Lett. B **292**, 119 (1992)

15. D. Ebert, R. N. Faustov and V. O. Galkin, arXiv:hep-ph/0110190.

16. S. Godfrey and R. Kokoski, Phys. Rev. D **43**, 1679 (1991). Y. b. Dai, C. S. Huang and H. Y. Jin, Phys. Lett. B **331**, 174 (1994). S. N. Gupta and J. M. Johnson, Phys. Rev. D **51**, 168 (1995) [arXiv:hep-ph/9409432].

17. A. H. Orsland and H. Hogaasen, Eur. Phys. J. C **9**, 503 (1999) [arXiv:hep-ph/9812347].

18. T. A. Lahde, C. J. Nyfalt and D. O. Riska, Nucl. Phys. A **674**, 141 (2000) [arXiv:hep-ph/9908485]. Phys. Lett. **76B**, 461 (19yy).

19. D. Ebert, V. O. Galkin and R. N. Faustov, Phys. Rev. D **57**, 5663 (1998) [Erratum-ibid. D **59**, 019902 (1999)] [arXiv:hep-ph/9712318].

20. Y. S. Kalashnikova and A. V. Nefediev, arXiv:hep-ph/0112330. J. Hein *et al.*, Phys. Rev. D **62**, 074503 (2000) [arXiv:hep-ph/0003130]. N. Mathur, R. Lewis and R. M. Woloshyn, Phys. Rev. D **66**, 014502 (2002) [arXiv:hep-ph/0203253]. B. A. Thacker and G. P. Lepage, Phys. Rev. D **43**, 196 (1991). A. X. El-Khadra, A. S. Kronfeld and P. B. Mackenzie, Phys. Rev. D **55**, 3933 (1997) [arXiv:hep-lat/9604004]. G. P. Lepage, L. Magnea, C. Nakhleh, U. Magnea and K. Hornbostel, Phys. Rev. D **46**, 4052 (1992) [arXiv:hep-lat/9205007].

Frascati Physics Series Vol. XXVIII (2002), pp.155-155
HQ & L 2002 – Vietri s/m, May 27th - June 1st, 2002

STATUS OF HQ EXPANSION AND HQ PARAMETERS *

Nikolai Uraltsev
INFN Milano, Italy

* Written contribution not received

Frascati Physics Series Vol. XXVIII (2002), pp.157-168
HQ & L 2002 – Vietri s/m, May 27th - June 1st, 2002

CHIRAL DYNAMICS AND $B \to 3\pi$ DECAY

Ulf-G. Meißner
Forshungszentrum Jülich, Institut für Kernphysik (Theorie)
D-52425 Jülich, Germany
and
Karl-Franzens Universität Graz, Institut für Theoretische Physik
A-8010 Graz, Austria

ABSTRACT

I discuss our knowledge of the scalar sector of QCD and how it impacts the determination of the CKM angle α from the isospin analysis of $B \to \rho\pi$ decay.

1 Introduction and motivation

CP violation has been established experimentally in the K– and B–meson systems. In the Standard Model, this can be explained in terms of one single phase, which leads to complex entries in the CKM matrix. The unitarity of this matrix may be represented in terms of various triangles, one of them to be measured at the B–factories. Any violation of unitarity would be a signal of physiscs beyond the Standard Model. However, to achieve the required accuracy to really test the relation $\alpha + \beta + \gamma = \pi$, where α, β, and γ are the three

angles of the triangle, one has to be able to precisely calculate or eliminate the final–state interactions (FSI) of the mesons generated in the various B–decays (more precisely, it is the strong phase generated by the FSI associated with diagrams of the "wrong" weak phase that pose especial difficulty). Here, we will be concerned with the decay $B \to 3\pi$, because the isospin analysis possible in $B \to \rho\pi$ decay allows to extract $\sin(2\alpha)$ [1, 2]. Recent observations, however, have triggered the question about a possible "hadronic pollution" in the $\rho\pi$ phase space. In particular, the E791 collaboration has found that half of the rate of $D^- \to \pi^-\pi^+\pi^-$ decay goes via the $D^- \to \pi^-\sigma(500) \to \pi^-\pi^+\pi^-$ doorway state [3]. This measurement was also considered as further evidence for a light scalar–isoscalar meson, the elusive σ. Furthermore, it was shown in ref. [4] that the inclusion of this channel can improve the theoretical description of the ratio

$$\mathcal{R} = \frac{\mathrm{Br}(\bar{B}^0 \to \rho^\mp\pi^\pm)}{\mathrm{Br}(B^- \to \rho^0\pi^-)} = 2.7 \pm 1.2 \ , \tag{1}$$

measured at CLEO and BABAR. Note that $\mathcal{R} \simeq 6$ at tree level in naive factorization. Since there is on–going debate about the nature of the σ, we will address here the following questions:

* What do we know about the scalar sector of QCD?

* What is its impact on $B \to \rho\pi$ decay?

2 The scalar sector of QCD

The scalar–isoscalar sector of QCD is highly interesting because of its vacuum quantum numbers, and its direct relation to the quark mass terms (explicit chiral symmetry breaking), the related σ–terms, and so on. Its most distinct characteristics are the very strong final–state interactions, signaled e.g. by the rapidly rising isospin zero, S-wave $\pi\pi$ phase shift $\delta_0^0(s)$ or the observation that the scalar pion radius, $\langle r_S^2\rangle_\pi \simeq 0.6\,\mathrm{fm}^2$, is sizeably bigger than the corresponding vector (charge) radius, $\langle r_V^2\rangle_\pi \simeq 0.4\,\mathrm{fm}^2$. Note also that there is no direct experimental probe with such quantum numbers. Therefore, theoretical investigations using different tools have been employed to deepen our understanding of this sector, these are Chiral Perturbation Theory (CHPT), resummation schemes consistent with CHPT, unitarity, analyticity, ... (like e.g. the chiral

unitary approach [5]) and also dispersion relations. The following general results emerge: First, a **consistent** picture of the scalar (pion and kaon) form factors is obtained, and, second, all the light (non-strange and strange) scalar mesons are dynamically generated in a large class of resummation schemes (see e.g. ref. [6]), although this later topic is still vigorously debated[1]. For the impact on the $B \to \rho\pi$ decay, we fortunately only need the (non-strange) scalar form factor of the pion, $\Gamma_\pi(s)$ (or, equivalently, the $\sigma \to \pi\pi$ vertex function $\Gamma_{\sigma\pi\pi}(s)$), defined via

$$\langle 0|\hat{m}(\bar{u}u + \bar{d}d)|\pi^a(p)\pi^b(p')\rangle = \delta^{ab} M_\pi^2 \Gamma_\pi(s) = \mathcal{N}\,\Gamma_{\sigma\pi\pi}(s)\ , \quad s = (p+p)^2\ . \tag{2}$$

The scalar form factor is shown in fig. 1 for the various theoretical approaches mentioned above. We will use here the result of the chiral unitary approach [7]), which was successfully tested e.g. in $J/\Psi \to \phi\pi\pi(\bar{K}K)$ decays. It is worth to point out that the scalar form factor constructed in [7]) is systematically matched to the CHPT representation, and it embodies by construction the coupled channel $\pi\pi/\bar{K}K$ dynamics. It is also consistent with the dispersive results of ref. [8]). Most importantly for the later discussion, we remark that the form of the pion scalar form factor is very different from a Breit-Wigner (BW) form with a running width, as used e.g. in [3]), compare fig. 2. This apparent difference casts doubt on the recent conclusions of refs. [3, 4]). The situation is completely different for the pion vector form factor entering the $\rho\pi$ intermediate state - it can be described to good precision by a BW with running width. More generally, the vector form factor can be reconstructed from unitarity and analyticity and matched to CHPT. The resulting vertex function does not differ significantly from a BW with running width (see ref. [9]) for a detailed discussion on this point and corresponding figures).

3 Extending the isospin analysis of $B \to \rho\pi$ decay

Next, we wish to consider the impact of the $\sigma\pi$ channel on the isospin analysis of $B \to \rho\pi$. Since in the initial state the B-meson has isospin $I_i = 1/2$, and the final state $\rho\pi$ system has $I_f = 0, 1, 2$, transitions with $|\Delta I| = 1/2, 3/2, 5/2$

[1] Consequently, by "σ" we always mean a two–pion state with total isospin zero and in a relative S–wave state, $(\pi\pi)_S$, understanding its dynamical origin in the strong pionic FSI for these quantum numbers.

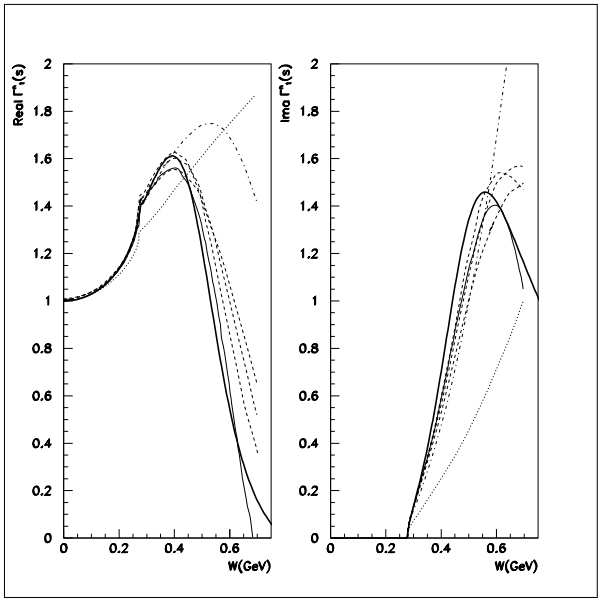

Figure 1: *Real (left) and imaginary part (right) of the non-strange scalar form factor of the pion. Solid line: chiral unitary approach as discussed in the text, dotted/dash-dotted line: CHPT to one/two loops, dashed line: dispersive results.*

are possible. If one parameterizes the corresponding amplitudes $a_{bc} \equiv A(B^0 \to \rho^b \pi^c)$ (with $a, b = \{+, 0, -\}$) by $A_{|\Delta I|, I_f}$, one gets

$$\begin{aligned} a_{+-} &= \frac{1}{2\sqrt{3}} \left[A_{3/2,2} + A_{5/2,2}\right] + \frac{1}{2} \left[A_{3/2,1} + A_{1/2,2}\right] + \frac{1}{\sqrt{6}} A_{1/2,0} \ , \\ a_{-+} &= \frac{1}{2\sqrt{3}} \left[A_{3/2,2} + A_{5/2,2}\right] - \frac{1}{2} \left[A_{3/2,1} + A_{1/2,2}\right] + \frac{1}{\sqrt{6}} A_{1/2,0} \ , \\ a_{00} &= -\frac{1}{\sqrt{3}} \left[A_{3/2,2} + A_{5/2,2}\right] + \frac{1}{\sqrt{6}} A_{1/2,0} \ , \end{aligned} \tag{3}$$

noting that $A(B^0 \to \pi^+\pi^-\pi^0) = f_+ \, a_{+-} + f_- \, a_{-+} + f_0 \, a_{00}$, where f_i is the form factor describing $\rho^i \to \pi\pi$. Because of CKM unitarity, there are two independent weak phases, a possible choice being

$$\frac{V_{ub}^* \, V_{ud}}{|V_{ub}^* \, V_{ud}|} = \exp(i\gamma) \ , \quad \frac{V_{tb}^* \, V_{td}}{|V_{tb}^* \, V_{td}|} = \exp(-i\beta) \ , \quad \alpha = \pi - \beta - \gamma \ , \tag{4}$$

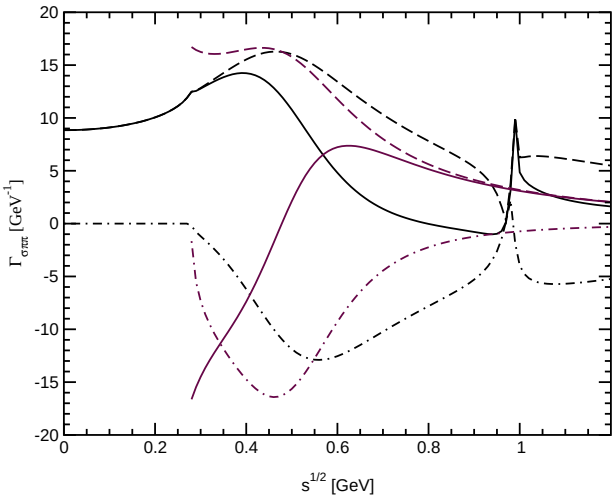

Figure 2: *The $\sigma \to \pi^+(p_+)\pi^-(p_-)$ form factor $\Gamma_{\sigma\pi\pi}$ as a function of $\sqrt{s}$, with $s = (p_+ + p_-)^2$. The real (solid line) and imaginary (dot-dashed line) parts of $\Gamma_{\sigma\pi\pi}$, as well as its modulus (dashed line), are shown. The curves which do not persist below physical threshold, $\sqrt{s} = 2M_\pi \sim 0.27\ GeV$, correspond to the form factor adopted in Ref.* [4], *whereas the curves which extend to $s = 0$ correspond to the form factor adopted here* [7]. *Both representations are normalized that their real parts agree at $\sqrt{s} = 0.478\ GeV$.*

leading to

$$\begin{aligned} e^{i\beta} a_{+-} &= T^{+-}\, e^{-i\alpha} + P^{+-} \ , \\ e^{i\beta} a_{-+} &= T^{-+}\, e^{-i\alpha} + P^{-+} \ , \\ e^{i\beta} a_{00} &= T^{00}\, e^{-i\alpha} + P^{00} \ , \end{aligned} \tag{5}$$

from which $\sin(2\alpha)$ can be deduced, having made the crucial assumption that the penguin is $|\Delta I| = 1/2$, so that

$$P^{00} = \frac{1}{2}(P^{+-} + P^{-+}) \ . \tag{6}$$

With this penguin assumption, one has 10 parameters, which can all be determined from a Dalitz plot analysis. As discussed in ref. [9], there are three different sources of isospin violation (IV) that could invalidate this analysis:

1) IV generates an additional amplitude of $|\Delta I| = 5/2$ character, 2) IV can distinguish the f_i, and 3) IV can generate penguins with $|\Delta I| = 3/2$. Some of these effects can be mitigated in an empirically driven way, as long as $A_{5/2,2}$ and $A_{3/2,2}$ share the same weak phase. However, non-$|\Delta I| = 1/2$ penguin effects, be they electroweak penguin contributions or contributions consequent to isospin-violating effects in the hadronic matrix elements of $|\Delta I| = 1/2$ operators, present an irreducible hadronic ambiguity from the viewpoint of this analysis (for a more detailed discussion, see ref. [9]). Note that this is quite different to the isospin analysis of $B \to \pi\pi$ decay [10]. Returning to the scalar sector, we remark that $\sigma\pi$ contributes preferentially to the $\rho^0\pi^0$ final state and thus can break the assumed penguin relation. However, $B \to \sigma\pi$ has definite transformation properties under CP, so that an extended isospin analysis is possible. Defining $a_{00}^\sigma = A(B^0 \to \sigma\pi^0)$, we have

$$e^{i\beta} a_{00}^\sigma = T_\sigma^{00} e^{-i\alpha} + P_\sigma^{00} \; . \tag{7}$$

T_σ^{00} and P_σ^{00} are unrelated to the parameters of Eq. (5), so that we gain four additional hadronic parameters. However, more observables are present as well. Including the scalar channel, we now have $A_{3\pi} \equiv A(B^0 \to \pi^+\pi^-\pi^0) = f_+ \, a_{+-} + f_- \, a_{-+} + f_0 \, a_{00} + f_\sigma \, a_{00}^\sigma$, where f_σ is the form factor describing $\sigma \to \pi^+\pi^-$. For this extended analysis to be useful, the σ has to contribute significantly to $B^0, \bar{B}^0$ decay. It is worth noting that any discernable presence of the $B \to \sigma\pi$ channel in the $B \to \rho\pi$ phase space falsifies the notion that the "nonresonant" background can be characterized by a single, constant phase across the Dalitz plot [11].

4 Evaluating $B \to \rho\pi$ in the presence of the $\sigma\pi$ channel

Our starting point is the effective $|\Delta B| = 1$ Hamiltonian for $b \to dq\bar{q}'$ decay

$$\mathcal{H}_{\rm eff} = \frac{G_F}{\sqrt{2}} \left[\sum_{j=u,c} \lambda_j \left(C_1 O_1^j + C_2 O_2^j \right) - \lambda_t \sum_{i=3}^{10} C_i O_i \right] \; , \tag{8}$$

with $\lambda_q = V_{qb} V_{qq}^\star$, V_{ij} an element of the CKM matrix and the operators are ordered such that the Wilson coefficients obey $C_1 \sim O(1)$, $C_1 > C_2 \gg C_{3,\ldots,10}$. We evaluate the resonance contributions to $B \to 3\pi$ decay by using a product

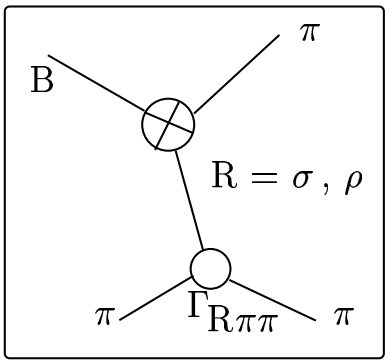

Figure 3: *Generic diagram for $B \to R\pi \to 3\pi$ decay, where $\Gamma_{R\pi\pi}$ denotes the corresponding strong vertex function, $R = \sigma, \rho$. The crossed vertex symbolizes the weak $B \to R\pi$ transition.*

ansatz, see fig. 3. For the requisite amplitudes, this means

$$A_R(B \to \pi^+\pi^-\pi) = \langle (R \to \pi^+\pi^-)\,\pi|\mathcal{H}_{\rm eff}|B\rangle = \underbrace{\langle R\pi\,|\mathcal{H}_{\rm eff}|B\rangle}_{\rm m.e.}\underbrace{\Gamma_{R\to\pi\pi}}_{\rm v.f.}\ , \quad (9)$$

where we compute the matrix element (m.e.) in factorization (including penguins) in the same way it was done in refs. [4, 12] for a crisp comparison (detailed formulae can be found in ref. [9]). To ascertain the impact of the $B \to \sigma\pi$ channel to $B \to \rho\pi$ decay, we combine the decay channels at the amplitude level, $\mathcal{M} = A_\sigma(B \to \pi^+\pi^-\pi) + A_\rho(B \to \pi^+\pi^-\pi)$, and then integrate over the relevant three-body phase space to compute the effective $B \to \rho\pi$ branching ratios. The main new ingredient is the vertex function (v.f.) for which we employ in the $\sigma\pi$ channel the scalar form factor discussed earlier and for the $\rho\pi$ mode the vector form factor from ref. [13]. In table 1 we display the effective branching ratios for $B \to \rho\pi$ decay computed at tree level (and also including penguins following ref. [12]). We find that at tree level $\mathcal{R} \simeq 5.5$, and the inclusion of penguin contributions lowers this value to $\mathcal{R} \simeq 5.1$. Neither this ratio nor the calculated branching ratios depend in any significant way on the various vector form factors employed. The $B \to \sigma\pi$ branching ratios are collected in table 2. The computed values of $\mathcal{R} \simeq 2.0 \ldots 2.6$ are consistent with the empirical value of $\mathcal{R}_{\rm exp} = 2.7 \pm 1.2$, albeit the errors are large. The reduction in $\mathcal{R}$ is mostly due to the effect of the $\sigma\pi$ channel on the B^- decay

Table 1: *Effective branching ratios (in units of* 10^{-6}*) for* $B \to \rho\pi$ *decay, computed at tree level. The numbers in parentheses include penguin contributions as well, after ref.* [12]. *"BW" denotes the use of the form factors of refs.* [4, 12], *whereas "RW" denotes the use of the vector form factor of ref.* [14]. *Finally, "*$*$*" denotes the use of the form factor advocated here* [9].

δ [MeV] (f.f.)	$\bar{B}^0 \to \rho^- \pi^+$	$\bar{B}^0 \to \rho^+ \pi^-$	$\bar{B}^0 \to \rho^0 \pi^0$	$B^- \to \rho^0 \pi^-$
200 (BW)	15.1 (14.7)	4.21 (4.24)	0.508 (0.497)	3.50 (3.68)
300 (BW)	16.4 (16.0)	4.74 (4.76)	0.918 (0.908)	3.89 (4.10)
200 (RW)	15.1 (14.8)	4.19 (4.21)	0.468 (0.463)	3.49 (3.68)
300 (RW)	16.4 (16.0)	4.69 (4.70)	0.835 (0.831)	3.87 (4.07)
200 ($*$)	15.3 (14.9)	4.26 (4.28)	0.473 (0.467)	3.49 (3.68)
300 ($*$)	16.4 (16.0)	4.75 (4.76)	0.865 (0.859)	3.85 (4.06)
δ [MeV] (f.f.)	$B^0 \to \rho^+ \pi^-$	$B^0 \to \rho^- \pi^+$	$B^0 \to \rho^0 \pi^0$	$B^+ \to \rho^0 \pi^+$
200 (BW)	15.1 (14.7)	4.21 (4.15)	0.508 (0.615)	3.50 (3.68)
300 (BW)	16.4 (16.0)	4.74 (4.67)	0.918 (1.02)	3.89 (4.10)
200 (RW)	15.1 (14.7)	4.19 (4.13)	0.468 (0.571)	3.49 (3.68)
300 (RW)	16.4 (15.9)	4.69 (4.62)	0.835 (0.935)	3.87 (4.07)
200 ($*$)	15.3 (14.8)	4.26 (4.20)	0.473 (0.576)	3.49 (3.68)
300 ($*$)	16.4 (15.9)	4.75 (4.68)	0.865 (0.963)	3.85 (4.06)

Table 2: Effective branching ratios (in units of 10^{-6}) for $B \to \sigma\pi$ and $B \to \rho\pi$ decay, computed at tree level. The form factors are defined as in Table 1.

δ (f.f.) [MeV]	$B^- \to \sigma\pi^-$	$B^- \to (\rho^0 + \sigma)\pi^-$	$\bar{B}^0 \to \sigma\pi^0$	$\bar{B}^0 \to (\rho^0 + \sigma)\pi^0$	$\mathcal{R}$
200 (BW)	2.97	6.16	0.0258	0.516	3.1
300 (BW)	5.17	8.61	0.0457	0.940	2.5
200 (RW)	2.97	6.19	0.0258	0.475	3.1
300 (RW)	5.17	8.62	0.0457	0.855	2.4
200 ($*$)	4.11	7.61	0.0396	0.508	2.6
300 ($*$)	7.01	10.7	0.0663	0.916	2.0

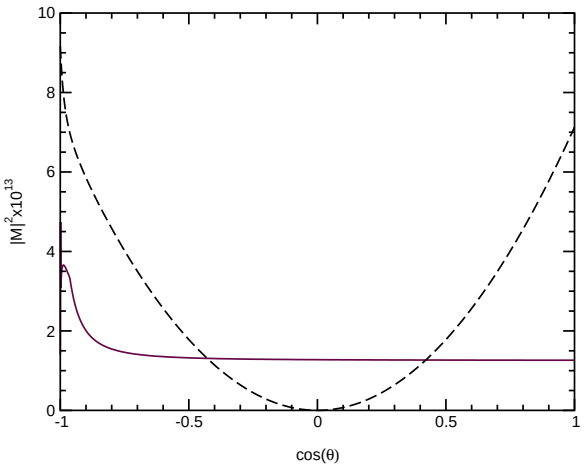

Figure 4: *Absolute square of the matrix element, $|M|^2$, for $B^- \to \rho^0\pi^-$ decay (dashed line), and for $B^- \to \sigma\pi^-$ decay (solid line), as a function of* $\cos\theta$ *at* $t = M_\rho^2$.

mode. Turning to $B \to \sigma\pi^0$ decay, we see that the contribution of the σ meson to $B^0(\bar{B}^0) \to \rho\pi$ decay is *much* smaller — with the scalar form factor we advocate, the effect is some 10%. Interestingly the σ has a tremendous impact on $B^- \to \rho^0\pi^-$ decay (very similar to the large effect in $D^- \to \pi^+\pi^-\pi^-$), and a relatively modest one on $\bar{B}^0 \to \rho^0\pi^0$ decay. Let us emphasize that we have realized our numerical analysis at tree level, so that the precise numbers but not the trends will change when a more refined analysis is performed. It is the relative size of the penguin contributions in $\bar{B}^0 \to \sigma\pi^0$ and $\bar{B}^0 \to \rho^0\pi^0$ decay which is of relevance to the isospin analysis to extract $\sin(2\alpha)$. The presence of the $\sigma\pi^0$ final state in the $\rho^0\pi^0$ phase space can break the assumed relationship, Eq. (6), between the penguin contributions in $\rho\pi$ and thus mimic the effect of isospin violation — alternatively we can expand the $\rho\pi$ analysis to include the $\sigma\pi$ channel. It is worth noting that the $\sigma\pi^0$ and $\rho^0\pi^0$ contributions can, to some measure, be distinguished. Certainly the $\sigma\pi^0$ and $\rho\pi^0$ contributions behave differently under the cut on the invariant mass of the $\pi^+\pi^-$ pair. Moreover, making a cut on the helicity angle θ, ought also be helpful in separating the ρ^0 and σ contributions. This is illustrated in fig. 4 for $B^- \to \rho^0/\sigma\,\pi^-$. The $\rho^0\pi$ contributions roughly follow a $\cos^2(\theta)$ distribution,

whereas the $\sigma\pi$ contributions are quite flat, save for the bump resulting from the u–channel contribution $\sim \Gamma_{\sigma\pi\pi}(u)$. Cutting on the helicity angle θ should also help disentangle the contributions from some of the intermediate B^* and B_0 resonances. Such type of terms were claimed to be of importance in ref. [12]. The contributions of these non–resonant intermediate states to the $\rho\pi$ channels has recently been scrutinized in ref. [15], where it was shown that the energy dependence of the intermediate heavy–meson propagator can lead to a drastic suppression of such contributions and thus the lowering of the value for $\mathcal{R}$ due to the σ persists in such a refined analysis. We also point out that an additional contribution to the phenomenological value of $\mathcal{R}$, realized through a diagram mediated by the $a_1^-(1260)$ meson, is proposed in ref. [16] (it might turn out to be insignificant in a more refined analysis for the same reasons just discussed for the B^*'s).

5 Summary and outlook

In this paper, we have scrutinized the role of the σ meson in $B \to \rho\pi \to 3\pi$ decay, understanding its dynamical origin in the strong pion-pion final state interactions in the scalar-isoscalar channel. The presence of the $\sigma\pi^0$ contribution in the $\rho^0\pi^0$ phase space is important in that it can break the assumed relationship between the penguin amplitudes, Eq. (6), consequent to an assumption of isospin symmetry. In this, then, its presence mimics the effect of isospin violation. The salient results of our investigation can be summarized as follows:

i) We have considered how SM isospin violation can impact the analysis to extract α in $B \to \rho\pi$ decay. Under the assumption that $|\Delta I| = 3/2$ and $|\Delta I| = 5/2$ amplitudes share the same weak phase, the presence of an additional amplitude of $|\Delta I| = 5/2$ character, induced by isospin-violating effects, does not impact the $B \to \rho\pi$ analysis in any way. This is in contradistinction to the isospin analysis in $B \to \pi\pi$. Thus the isospin-violating effects of importance are those which can break the assumed relationship between the penguin contributions, Eq. (6).

ii) The scalar form factor can be determined to good precision by combining the constraints of chiral symmetry, analyticity, and unitarity. The form factor we adopt describes the appearance of the $f_0(980)$ as well, so that

the shape of the $f_0(980)$ contribution in $B \to f_0(980)\pi \to 3\pi$, e.g., should serve as a test of our approach. We emphasize that the resulting scalar form factor is very different from the commonly used Breit-Wigner form with a running width. This is in stark contrast to the vector form factor, which is dominated by the ρ resonance. In that case, one can construct simple forms that fit the theoretical and empirical constraints.

iii) Remarkably, the impact of the $\sigma\pi$ channel on the ratio $\mathcal{R}$, cf. Eq. (1), is huge. The numbers we find for $\mathcal{R}$ are in agreement with the empirical ones, given its sizeable experimental uncertainty. This underscores the suggestion made, as well as improves the calculations done, in Ref. [4]. Our analysis is based on *consistent* scalar and vector form factors. This conclusion persists if one includes non–resonant B^*, B_0 intermediate states [15].

iv) On the other hand, the impact of the $\sigma\pi$ channel on the $B \to \rho\pi$ isospin analysis is merely significant. Varying the cuts on the $\pi\pi$ invariant mass and helicity angle θ should be helpful in disentangling the various contributions.

v) We have shown that one can expand the isospin analysis to include the $\sigma\pi$ channel because it has definite properties under CP. This may be necessary if varying the cuts in the $\pi\pi$ invariant mass and helicity angle θ are not sufficiently effective in suppressing the contribution from the $\sigma\pi^0$ channel in the $\rho^0\pi^0$ phase space.

This work is merely a first step in exploiting constraints from chiral symmetry, analyticity, and unitarity in the description of hadronic B decays. In particular, the contribution of the "doubly" OZI-violating strange scalar form factor and its phenomenological role in factorization breaking ought be investigated.

Acknowledgements

I am grateful to Susan Gardner for a very pleasant collaboration on the topics reported here and José Antonio Oller and Jusak Tandean for useful comments. I thank the organizers for their invitation and superbe organization.

References

1. H. J. Lipkin, Y. Nir, H. R. Quinn, and A. Snyder, Phys. Rev. D **44**, 1454 (1991).
2. A. E. Snyder and H. R. Quinn, Phys. Rev. D **48**, 2139 (1993).
3. M. Aitala *et al.* [E791 Collaboration], Phys. Rev. Lett. **86**, 770 (2001).
4. A. Deandrea and A. D. Polosa, Phys. Rev. Lett. **86**, 216 (2001).
5. J. A. Oller, E. Oset, and A. Ramos, Prog. Part. Nucl. Phys. **45**, 157 (2000).
6. M. Jamin, J. A. Oller, and A. Pich, Nucl. Phys. B **587**, 331 (2000).
7. Ulf-G. Meißner and J. A. Oller, Nucl. Phys. A **679**, 671 (2001).
8. J. F. Donoghue, J. Gasser, and H. Leutwyler, Nucl. Phys. B **343**, 341 (1990).
9. S. Gardner and Ulf-G. Meißner, Phys. Rev. D **65**, 094004 (2002).
10. S. Gardner, Phys. Rev. D **59**, 077502 (1999).
11. J. Charles, A. Le Yaouanc, L. Oliver, O. Pene, and J. C. Raynal, Phys. Lett. B **425**, 375 (1998); **433**, 441(E) (1998).
12. A. Deandrea, R. Gatto, M. Ladisa, G. Nardulli, and P. Santorelli, Phys. Rev. D **62**, 036001 (2000).
13. S. Gardner and H. B. O'Connell, Phys. Rev. D **57**, 2716 (1998); **62**, 019903(E) (1998)
14. P. F. Harrison and H. R. Quinn [BABAR Collaboration], editors, "The BaBar physics book: Physics at an asymmetric B factory," SLAC-R-0504.
15. J. Tandean and S. Gardner, arXiv:hep-ph/0204147.
16. N. Paver and Riazuddin, arXiv:hep-ph/0107330.

Frascati Physics Series Vol. XXVIII (2002), pp.169-182
HQ & L 2002 – Vietri s/m, May 27th - June 1st, 2002

TWO-BODY MODES OF B MESONS

Matthias Neubert*
F.R. Newman Laboratory for Elementary-Particle Physics
Cornell University, Ithaca, NY 14853, USA

ABSTRACT

The study of charmless two-body decays of B mesons is currently one of the hottest topics in B physics. QCD factorization provides the theoretical framework for a systematic analysis of such decays. A global fit to $B \to \pi K, \pi\pi$ branching fractions, combined with knowledge on $|V_{ub}|$, establishes the existence of a CP-violating phase in the bottom sector of the CKM matrix and tends to favor values of γ near 90°, somewhat larger than those suggested by the standard analysis of the unitarity triangle. A novel construction of the unitarity triangle is presented, which is independent of B–$\bar{B}$ and K–$\bar{K}$ mixing.

1 Introduction

Measurements of $|V_{ub}|$ in semileptonic decays, $|V_{td}|$ in B–$\bar{B}$ mixing, and $\mathrm{Im}(V_{td}^2)$ from CP violation in K–$\bar{K}$ and B–$\bar{B}$ mixing have firmly established the exis-

*Research supported by National Science Foundation Grant PHY-0098631

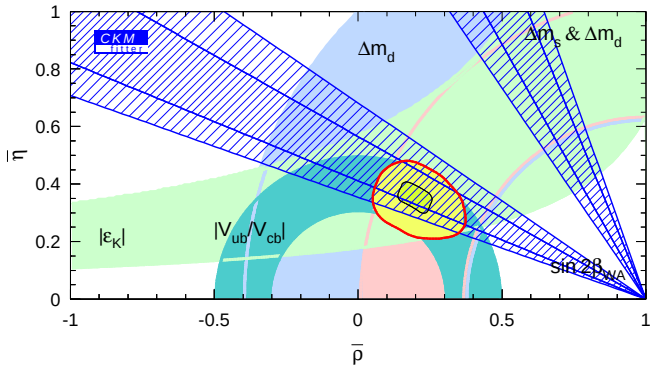

Figure 1: *Standard constraints on the apex* $(\bar\rho,\bar\eta)$ *of the unitarity triangle* [1].

tence of a CP-violating phase in the CKM matrix. The present situation, often referred to as the "standard analysis" of the unitarity triangle, is summarized in fig. 1. Three comments are in order concerning this analysis:

1. The measurements of CP asymmetries in kaon physics (ϵ_K and ϵ'/ϵ) and B–$\bar B$ mixing ($\sin 2\beta$) probe the imaginary part of V_{td} and so establish CP violation in the top sector of the CKM matrix. The CKM model predicts that the imaginary part of V_{td} is related, by three-generation unitarity, to the imaginary part of V_{ub}, and that those two elements are (to an excellent approximation) the only sources of CP violation in flavor-changing processes. In order to test this prediction, the next step must be to explore the CP-violating phase $\gamma = \arg(V_{ub}^*)$ in the bottom sector of the CKM matrix. In this talk I argue that the analysis of charmless hadronic B decays has by now established unambiguously that $\arg(V_{ub}^*) \neq 0$.

2. With the exception of the $\sin 2\beta$ measurement, the standard analysis is limited by large theoretical uncertainties, which dominate the widths of the various bands in the figure. These uncertainties enter via the calculation of hadronic matrix elements. I will discuss some novel methods to constrain the unitarity triangle using charmless hadronic B decays, which are afflicted by smaller hadronic uncertainties and hence provide powerful new tests of the Standard Model, which can complement the standard analysis.

3. With the exception of the measurement of $|V_{ub}|$ in semileptonic B decays, the standard constraints are sensitive to meson–antimeson mixing. Mixing amplitudes are of second order in weak interactions and hence might be most

susceptible to effects from physics beyond the Standard Model. The new constraints on $(\bar\rho,\bar\eta)$ discussed below allow a construction of the unitarity triangle that is over-constrained and independent of B–$\bar B$ and K–$\bar K$ mixing. It is in this sense orthogonal to the standard analysis.

The phase γ can be probed via tree–penguin interference in decays such as $B \to \pi K, \pi\pi$. Experiment teaches us that amplitude interference is sizable in these decays. Information about γ can be obtained not only from the measurement of direct CP asymmetries ($\sim \sin\gamma$), but also from the study of CP-averaged branching fractions ($\sim \cos\gamma$). The challenge is, of course, to gain theoretical control over the hadronic physics entering the tree-to-penguin ratios in the various decays.

2 QCD Factorization

Hadronic weak decays simplify greatly in the heavy-quark limit $m_b \gg \Lambda_{\rm QCD}$. The underlying physics is that a fast-moving light meson produced by a point-like source (the effective weak Hamiltonian) decouples from soft QCD interactions [2, 3, 4]. A systematic implementation of this color transparency argument is provided by the QCD factorization approach [5, 6]. This scheme makes rigorous predictions in the heavy-quark limit, some of which have been proven to all orders of perturbation theory [7]. One can hardly overemphasize the importance of controlling nonleptonic decay amplitudes in the heavy-quark limit. While a few years ago reliable calculations of such amplitudes appeared to be out of reach, we are now in a situation where hadronic uncertainties enter only at the level of power corrections suppressed by the heavy b-quark mass.

The workings of QCD factorization are illustrated in fig. 2. The graph on the left shows how in the familiar construction of the effective weak Hamiltonian hard gluon effects with virtualities $\mu \gg m_b$ can be calculated and factorized into Wilson coefficients $C_i(\mu)$. The graphs on the right illustrate how, in a similar way, hard gluon effects with $\mu \sim m_b$ can be calculated and factorized into perturbative hard-scattering kernels $T_{ij}(\mu)$. What remains after this step are factorized decay amplitudes, in which all gluon exchange between the emission meson at the "upper vertex" and the remaining hadronic system are integrated out. In the heavy-quark limit, such "nonfactorizable gluons" are hard because of color transparency. Note that this does not imply that nonleptonic amplitudes in the heavy-quark limit are perturbative. (In this respect, our approach

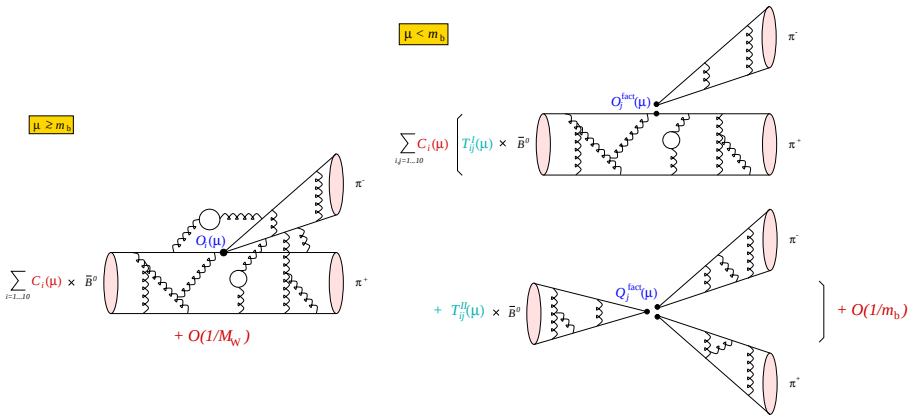

Figure 2: *Factorization of short- and long-distance contributions into running couplings and hadronic matrix elements. Left: Integrating out hard gluons ($k \sim M_W$) in the construction of the effective weak Hamiltonian. Right: Integrating out hard gluons ($k \sim m_b$) in the construction of the effective, factorized transition operator in QCD factorization.*

is more general that the pQCD scheme [8].) Important nonperturbative effects remain, which can be parameterized in terms of meson decay constants, $B \to M$ transition form factors, and meson light-cone distribution amplitudes. These quantities are an input to the factorization formula, ideally taken from experiment. Theoretical expressions for decay amplitudes obtained using the QCD factorization approach are complicated and depend on many input parameters. When discussing the theoretical uncertainties and limitations of this scheme it is important to distinguish between different classes of parameters. In order of phenomenological importance, these are Standard Model parameters ($\bar\rho$, $\bar\eta$, m_s, m_c, α_s), the renormalization scale (μ), hadronic quantities that can (at least in principle) be determined from data (decay constants, transition form factors), and hadronic quantities that can only indirectly be constrained by data (light-cone distribution amplitudes).

The most important question with regard to phenomenological applications of QCD factorization is that about the numerical size of power corrections. While the importance of the heavy-quark limit to the workings of factorization is evident from a comparison of nonfactorizable effects seen in kaon, charm and beauty decays [9], and while there is a lot of evidence (from spectroscopy, exclu-

sive semileptonic decays, and various inclusive decays) that power corrections are small at the b-quark scale, it is nevertheless important to address the issue of power corrections in a systematic way. Much effort has been devoted in the past few years to the study of power-suppressed effects, which in general violate factorization. The most important power corrections are proportional to the ratios $2m_K^2/(m_s m_b)$ or $2m_\pi^2/(m_q m_b)$, which are inversely proportional to light-quark masses. Such twist-3 corrections make up for a significant portion of the penguin amplitudes in B decays into light pseudoscalar mesons. It is important that these penguin contributions are calculable despite their power suppression and hence can be included reliably [6]. At the same order, there appear logarithmically divergent twist-3 corrections to the leading-twist hard spectator interactions. These corrections are universal, and their effect can be absorbed into a redefinition of a single hadronic parameter λ_B.

Perhaps the largest uncertainty from power corrections is due to weak annihilation contributions, for which both of the valence quarks of the initial B meson participate in the weak interactions [8, 10]. Annihilation amplitudes violate factorization and thus cannot be reliably computed using the QCD factorization approach. Although we find that with default parameter values the annihilation amplitudes are typically small, their effects can become sizable when the large model uncertainties in their estimate are taken into account [6]. Other types of power corrections, such as soft nonfactorizable gluon exchange, have been investigated using QCD sum rules [11] and the renormalon calculus [12, 13]. No large corrections of this type have been identified.

While it is a conceptual challenge to gain a better control over the leading power corrections to QCD factorization, perhaps using the framework of the soft-collinear effective theory [14, 15, 16], it is important that this approach makes many testable predictions. Their comparison with experimental data can teach us a lot about the importance of power-suppressed effects.

3 Testing Factorization in $B \to \pi K, \pi\pi$ Decays

Deriving constraints on the unitarity triangle from charmless hadronic B decays requires controlling the interference of tree and penguin topologies. This means that one must be able to predict not only the magnitudes of these contributions, but also their relative strong-interaction phase. Fortunately, the crucial aspects of such calculations can be tested using experimental data.

The magnitude of the leading $B \to \pi\pi$ tree amplitude can be probed in the decays $B^\pm \to \pi^\pm\pi^0$, which to an excellent approximation do not receive any penguin contributions. The QCD factorization approach makes an absolute prediction for the corresponding branching ratio [6],

$$\mathrm{Br}(B^\pm \to \pi^\pm\pi^0) = \left[5.3\,{}^{+0.8}_{-0.4}\,(\text{pars.}) \pm 0.3\,(\text{power})\right] \cdot 10^{-6} \times \left[\frac{|V_{ub}|}{0.0035}\,\frac{F_0^{B\to\pi}(0)}{0.28}\right]^2 ,$$

which compares well with the experimental result [17] $(4.9 \pm 1.1) \times 10^{-6}$. The theoretical uncertainties quoted are due to input parameter variations and to the modeling of power corrections. An additional uncertainty comes from the present error on $|V_{ub}|$ and the $B \to \pi$ form factor.

The magnitude of the leading $B \to \pi K$ penguin amplitude can be probed in the decays $B^\pm \to \pi^\pm K^0$, which to an excellent approximation do not receive any tree contributions. Combining it with the measurement of the tree amplitude just described, a tree-to-penguin ratio can be determined via the relation

$$\varepsilon_{\rm exp} = \left|\frac{T}{P}\right| = \tan\theta_C\,\frac{f_K}{f_\pi}\left[\frac{2\mathrm{Br}(B^\pm \to \pi^\pm\pi^0)}{\mathrm{Br}(B^\pm \to \pi^\pm K^0)}\right]^{1/2} = 0.205 \pm 0.025\,.$$

The experimental value of this ratio is in good agreement with the theoretical prediction [6] $\varepsilon_{\rm th} = 0.23 \pm 0.04\,(\text{pars.}) \pm 0.04\,(\text{power}) \pm 0.05\,(V_{ub})$, which is independent of form factors but proportional to $|V_{ub}/V_{cb}|$. This is a highly nontrivial test of the QCD factorization approach. Recall that when the first measurements of charmless hadronic decays appeared several authors remarked that the penguin amplitudes were much larger than expected based on naive factorization models. We now see that QCD factorization naturally reproduces the correct magnitude of the tree-to-penguin ratio. This observation also shows that there is no need to supplement the QCD factorization predictions in an ad hoc way by adding enhanced phenomenological penguin amplitudes, such as the "nonperturbative charming penguins" introduced in ref. [18].

QCD factorization predicts that most strong-interaction phases in charmless hadronic B decays are parametrically suppressed in the heavy-quark limit, because

$$\sin\phi_{\rm st} = O[\alpha_s(m_b), \Lambda_{\rm QCD}/m_b]\,.$$

This typically implies small direct CP asymmetries since, e.g., $A_{\rm CP}(\pi^+K^-) \approx -2\,|T/P|\sin\gamma\,\sin\phi_{\rm st}$. The suppression results as a consequence of systematic

cancellations of soft contributions, which are missed in phenomenological models of final-state interactions. In other schemes the strong-interaction phases are predicted to be larger, and therefore larger CP asymmetries are expected. Present data show no evidence for large direct CP asymmetries in charmless decays [17], but the errors are still too large to distinguish between different theoretical predictions. An important exception is the direct CP asymmetry for the decays $B \to \pi^\pm K^\mp$, which is already measured with high precision. The current world average [17], $A_{\rm CP}(\pi^+ K^-) = -0.05 \pm 0.05$, implies a rather small value of the corresponding strong-interaction phase, which is consistent with the expectation that this phase be suppressed in the heavy-quark limit. Specifically, for γ in the range between 60° and 90°, I obtain $\phi_{\rm st} = (8 \pm 10)^\circ$. Simple physical arguments suggest that the relevant strong-interaction phases in the decays $B \to \pi^\pm K^\mp$ and $B^\mp \to \pi^0 K^\mp$ should be very similar [19]. This observation will become important below.

4 Establishing CP Violation in the Bottom Sector

Various ratios of CP-averaged $B \to \pi K, \pi\pi$ branching fractions exhibit a strong dependence on γ and $|V_{ub}|$. It is thus possible to derive constraints on $\bar\rho$ and $\bar\eta$ from a global analysis of the data in the context of the QCD factorization approach, provided conservative error estimates for power corrections are included. A comprehensive discussion of such an analysis was presented in ref. [6], to which I refer the reader for details. The original result obtained in that paper is reproduced in the left plot in fig. 3. It reflects the status of the data as of spring 2001. The right plot shows an update of this analysis using the latest experimental data [17]. I have also updated two input parameters in order to take into account recent theoretical developments. The new analysis uses $m_s = (100 \pm 25)\,\text{MeV}$ at $\mu = 2\,\text{GeV}$, and $f_B = (200 \pm 30)\,\text{MeV}$. The values used in ref. [6] were $m_s = (110 \pm 25)\,\text{MeV}$ and $f_B = (180 \pm 40)\,\text{MeV}$.

The fit is excellent, which $\chi^2 = 0.5$ for three degrees of freedom. There is no problem in accounting for all of the experimental data simultaneously. The inclusion of model estimates of weak annihilation effects enlarges the allowed regions in the $(\bar\rho, \bar\eta)$ plane but is not required to fit the data. Leaving out all annihilation contributions, one still obtains a good fit ($\chi^2 = 0.7$) and similar best-fit values for the Wolfenstein parameters. The comparison of the two plots shown in the figure indicates the effect of the increase in experimental precision

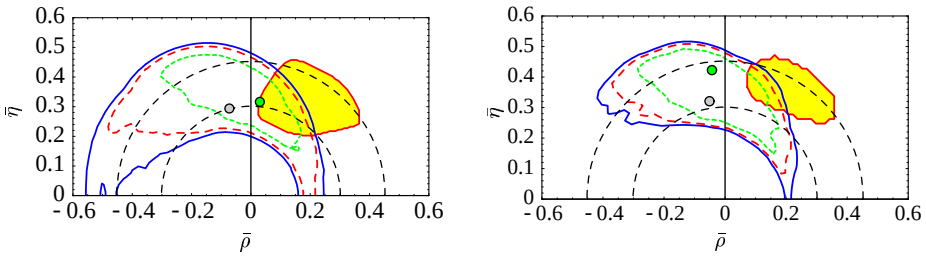

Figure 3: *95% (solid blue), 90% (dashed red) and 68% (short-dashed green) confidence level contours in the $(\bar{\rho},\bar{\eta})$ plane obtained from rare hadronic B decays (dark green dot = overall best fit; light gray dot = best fit for the default parameter set). The circled yellow region shows the result of the standard CKM fit. Left: status in spring 2001; right: update for summer 2002.*

between spring 2001 and summer 2002. The most important conclusion from this analysis is that, with the new data, the combination of results from rare hadronic B decays with the $|V_{ub}|$ measurement in semileptonic decays excludes $\bar{\eta} = 0$ and so establishes the existence of a CP-violating phase in the bottom sector of the CKM matrix.

The allowed regions obtained from the fit to charmless hadronic decays are compatible with the standard fit (shown by the yellow region), but tend to favor larger γ values. This tendency has been reinforced with the new data. The same trend is seen in an analysis that does not rely on QCD factorization but instead employs general amplitude parameterizations and flavor symmetries [20]. It is tantalizing to speculate about the possible origin of a (still hypothetical) disagreement between the allowed $(\bar{\rho},\bar{\eta})$ regions obtained from the standard analysis and from charmless hadronic B decays. A conventional explanation of such a discrepancy might be that the errors in lattice calculations of the relevant matrix elements for B_d–$\bar{B}_d$ and B_s–$\bar{B}_s$ mixing have been underestimated. In fact, in a recent paper the value $\xi = (f_{B_s}\sqrt{B_s})/(f_{B_d}\sqrt{B_d}) = 1.32 \pm 0.10$ was obtained [21], which is significantly larger than the result $\xi = 1.15 \pm 0.05$ used in previous analyses of the unitarity triangle. With such large ξ, values of γ in the vicinity of 90° are no longer excluded by the $\Delta m_s/\Delta m_d$ bound.

A more exciting possibility is, of course, to invoke New Physics to explain the discrepancy. Assume first that in charmless hadronic B decays one probes the true value of the CKM phase γ. In this case a discrepancy with the standard

analysis would most likely be due to a New Physics contribution to B–$\bar{B}$ mixing. For instance, there could be New Physics affecting B_s–$\bar{B}_s$ mixing. Eliminating the corresponding constraint from the standard analysis one finds that larger values of γ are allowed. This possibility will hopefully soon be checked, when B_s–$\bar{B}_s$ mixing will be explored at the Tevatron. Alternatively, there could be New Physics affecting B_d–$\bar{B}_d$ mixing. In this case one should eliminate the constraints arising from the measurements of Δm_d, $\Delta m_s/\Delta m_d$, and $\sin 2\beta$ from the standard analysis. Then only the constraints from K–$\bar{K}$ mixing and semileptonic B decays remain, which allow for large values of γ. A different possibility would be that the mixing amplitudes are unaffected by New Physics, but that there exist non-standard contributions to $b \to s$ or $b \to d$ FCNC transitions, e.g. from penguin and box diagrams involving the exchange of new heavy particles. (A more exotic model with light SUSY particles has also been considered [22].) In this case, γ measured in $B \to \pi K, \pi\pi$ decays would be a combination of the CKM angle and some new CP-violating phase. Many examples of New Physics models that could yield a significant additional phase have been explored in ref. [23]. A clean test of this possibility would be the measurement of the time-dependent CP asymmetry in $B \to \phi K_S$ decays, which in the Standard Model is due to the interference of a (real) $b \to s\bar{s}s$ penguin amplitude with the B_d–$\bar{B}_d$ mixing amplitude. If there was a New Physics phase $\phi_{\rm NP}$ of the penguin amplitude, then the CP asymmetry in $B \to \phi K_S$ would measure $\sin 2(\beta + \phi_{\rm NP})$, which when compared with the value of $\sin 2\beta$ measured in $B \to J/\psi\, K_S$ decays would reveal the existence of the phase $\phi_{\rm NP}$ [24]. Note that this strategy would not be invalidated even if there was a New Physics contribution to B_d–$\bar{B}_d$ mixing. In this case β would no longer be given by the CKM phase, but this effect would cancel out in the comparison of the two decay modes.

5 A Mixing-Independent Construction of The Unitarity Triangle

If the trend toward larger γ values revealed by the analysis of charmless hadronic B decays persists, one will want to check the compatibility with the standard analysis using measurements whose theoretical interpretation is "clean" in the sense that it only relies on assumptions that can be tested using experimental data. Here I propose a novel construction of the unitarity triangle (which I call the CP-b triangle, because it probes the CP-violating phase in the b

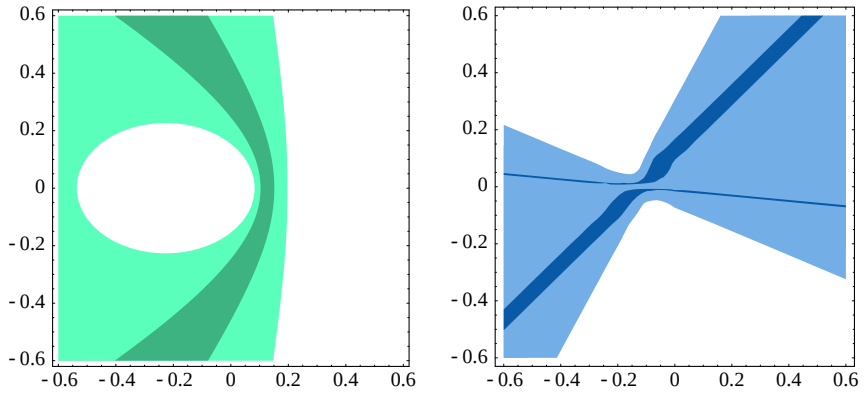

Figure 4: *New constraints in the $(\bar\rho,\bar\eta)$ plane used in the construction of the CP-b triangle (see text for explanation). Experimental errors are shown at 1σ. The dark central bands show the theoretical uncertainty, which in both cases is much smaller than the experimental errors. This shows the great potential of these methods once the data will become more precise.*

sector) which has this property, is over-determined, and can be performed using already existing data. Most importantly, this construction is insensitive to potential New Physics effects in B–$\bar B$ or K–$\bar K$ mixing. I will argue that the theoretical uncertainties limiting this construction are considerably smaller than for the standard analysis.

The first ingredient is the ratio $|V_{ub}/V_{cb}|$ extracted from semileptonic B decays, whose current value is $|V_{ub}/V_{cb}| = 0.090 \pm 0.025$. Several strategies have been proposed to determine $|V_{ub}|$ with a theoretical accuracy of about 10%, which would be a significant improvement. The second ingredient is a constraint derived from the ratio of the CP-averaged branching fractions for the decays $B^\pm \to \pi^\pm K_S$ and $B^\pm \to \pi^0 K^\pm$, using a generalization of the method suggested in ref. [25]. The experimental inputs to this analysis are the tree-to-penguin ratio $\varepsilon_{\rm exp} = 0.205 \pm 0.025$ mentioned earlier, and the ratio

$$R_* = \frac{\mathrm{Br}(B^+ \to \pi^+ K^0) + \mathrm{Br}(B^- \to \pi^- \bar K^0)}{2[\mathrm{Br}(B^+ \to \pi^0 K^+) + \mathrm{Br}(B^- \to \pi^0 K^-)]} = 0.78 \pm 0.11$$

of two CP-averaged $B \to \pi K$ branching fractions [17]. Without any recourse to QCD factorization this method provides a bound on $\cos\gamma$, which can be turned

into a determination of $\cos\gamma$ (for fixed value of $|V_{ub}|/V_{cb}|$) when information on the relevant strong-interaction phase ϕ is available. I have argued at the end of section 3 that the phase ϕ is bound by experimental data (and very general theoretical arguments) to be small, of order $(8\pm10)^\circ$. (In the future, this phase can be determined directly from the direct CP asymmetry in $B^\pm \to \pi^0 K^\pm$ decays.) It is thus conservative to assume that $\cos\phi > 0.8$, corresponding to $|\phi| < 37^\circ$. With this assumption, the corresponding allowed region in the $(\bar\rho, \bar\eta)$ plane was analysed in ref. [6], to which I refer the reader for details. The resulting constraint is shown in the first plot in fig. 4.

The third constraint comes from a measurement of the time-dependent CP asymmetry $S_{\pi\pi} = \sin 2\alpha_{\rm eff}$ in $B \to \pi^+\pi^-$ decays. The present experimental situation is unfortunately unclear, since the measurements by BaBar ($S_{\pi\pi} = -0.01 \pm 0.37 \pm 0.07$) and Belle ($S_{\pi\pi} = -1.21^{+0.38\,+0.16}_{-0.27\,-0.13}$) are inconsistent with each other [17]. The naive average of these results gives $S_{\pi\pi} = -0.64 \pm 0.42$ (with an inflated error). The theoretical expression for the asymmetry is

$$S_{\pi\pi} = \frac{2\,\mathrm{Im}\,\lambda_{\pi\pi}}{1+|\lambda_{\pi\pi}|^2}\,, \quad \text{where} \quad \lambda_{\pi\pi} = e^{-i\phi_d}\,\frac{e^{-i\gamma} + (P/T)_{\pi\pi}}{e^{+i\gamma} + (P/T)_{\pi\pi}}\,.$$

Here ϕ_d is the CP-violating phase of the B_d–$\bar B_d$ mixing amplitude, which in the Standard Model equals 2β. Usually, it is argued that for small P/T ratio the quantity $\lambda_{\pi\pi}$ is approximately given by $e^{-2i(\beta+\gamma)} = e^{2i\alpha}$, and so apart from a "penguin pollution" the asymmetry $S_{\pi\pi} \approx \sin 2\alpha$. Here I adopt a different strategy [6]. In order to become insensitive to possible New Physics contributions to the mixing amplitude, I use the experimental value $\sin\phi_d = 0.78\pm0.08$ [17] and write $e^{-i\phi_d} = \pm\sqrt{1-\sin^2\phi_d} - i\sin\phi_d$, with a sign ambiguity in the real part. (The plus sign is suggested by the standard fit of the unitarity triangle.) A measurement of $S_{\pi\pi}$ can then be translated into a constraint on γ (or $\bar\rho$ and $\bar\eta$), which remains valid even if the $\sin\phi_d$ measurement is affected by New Physics. The result obtained with the current experimental values and assuming $\cos\phi_d > 0$ is shown in the second plot in fig. 4. The resulting bands for $\cos\phi_d < 0$ are obtained by a reflection about the $\bar\rho$ axis. This follows because the expression for $S_{\pi\pi}$ is invariant under the simultaneous replacements $e^{-i\phi_d} \to -e^{i\phi_d}$ and $\gamma \to -\gamma$.

The two constraints in fig. 4 are, at present, limited by rather large experimental errors, while comparison with fig. 1 shows that the theoretical limitations are smaller than for the standard analysis. Yet, even at the present

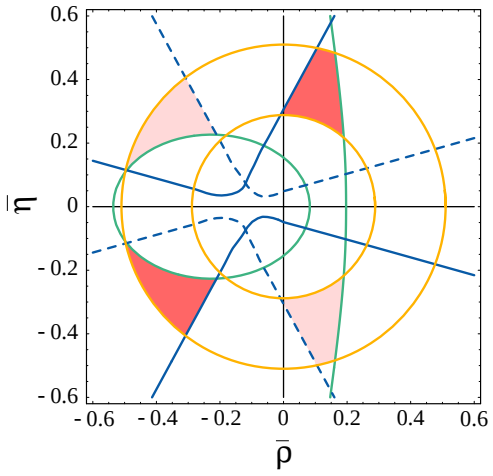

Figure 5: *Allowed regions in the* $(\bar{\rho},\bar{\eta})$ *plane obtained from the construction of the CP-b triangle. The dashed lines and light-shaded areas refer to* $\cos\phi_d < 0$.

level of accuracy it is interesting to combine the three constraints and construct the resulting allowed regions for the apex of the unitarity triangle. The result is shown in fig. 5. Note that the lines corresponding to the new constraints intersect the circles representing the $|V_{ub}|$ constraint at large angles, indicating that the three measurements used in the construction of the CP-b triangle give highly complementary information on $\bar{\rho}$ and $\bar{\eta}$. There are four allowed regions, two corresponding to $\cos\phi_d > 0$ (dark shading) and two to $\cos\phi_d < 0$ (light shading). If we use the information that the measured value of ϵ_K requires a positive value of $\bar{\eta}$, then only the two solutions in the upper half-plane remain. One of these regions (corresponding to $\cos\phi_d > 0$) is close to the standard fit, though once again somewhat larger γ values are preferred. (If only the BaBar result is used for $S_{\pi\pi}$, then this region is shifted toward yet larger values of γ.) I stress that this agreement is highly nontrivial, since with the exception of $|V_{ub}|$ none of the standard constraints are used in this construction. Interestingly, there is a second allowed region (corresponding to $\cos\phi_d < 0$) which would be consistent with the constraint from ϵ_K (see fig. 1) and the global analysis of charmless hadronic decays (see fig. 3), but inconsistent with the constraints derived from $\sin 2\beta$ and $\Delta m_s/\Delta m_d$. Such a solution would require a significant New Physics contribution to B–$\bar{B}$ mixing.

6 Outlook

After the by now precise measurement of $\sin 2\beta$, the study of charmless two-body modes of B mesons is presently the next hottest topic in B physics. QCD factorization provides the theoretical framework for a systematic analysis of hadronic B decay amplitudes based on the heavy-quark expansion. This theory has already passed successfully several nontrivial tests, and will be tested more thoroughly with more precise data.

A global fit to $B \to \pi K, \pi\pi$ decays establishes the existence of a CP-violating phase in the bottom sector of the CKM matrix and tends to favor values of γ near 90°, somewhat larger than the value suggested by the standard analysis of the unitarity triangle. If this trend were real, it would suggest several possibilities for new flavor physics beyond the Standard Model. In the future, the construction of the CP-b triangle will provide stringent tests of the Standard Model with small theoretical uncertainties.

References

1. A. Höcker, H. Lacker, S. Laplace and F. Le Diberder, Eur. Phys. J. C **21**, 225 (2001); see: http://www.slac.stanford.edu/ laplace/ckmfitter.html.
2. J. D. Bjorken, Nucl. Phys. Proc. Suppl. **11**, 325 (1989).
3. M. J. Dugan and B. Grinstein, Phys. Lett. B **255**, 583 (1991).
4. H. D. Politzer and M. B. Wise, Phys. Lett. B **257**, 399 (1991).
5. M. Beneke, G. Buchalla, M. Neubert and C. T. Sachrajda, Phys. Rev. Lett. **83**, 1914 (1999); Nucl. Phys. B **591**, 313 (2000).
6. M. Beneke, G. Buchalla, M. Neubert and C. T. Sachrajda, Nucl. Phys. B **606**, 245 (2001).
7. C. W. Bauer, D. Pirjol and I. W. Stewart, Phys. Rev. Lett. **87**, 201806 (2001).
8. Y. Keum, H. Li and A. I. Sanda, Phys. Lett. B **504**, 6 (2001); Phys. Rev. D **63**, 054008 (2001); Y. Keum and H. Li, Phys. Rev. D **63**, 074006 (2001).
9. M. Neubert and A. A. Petrov, Phys. Lett. B **519**, 50 (2001).

10. H. Y. Cheng and K. C. Yang, Phys. Rev. D **64**, 074004 (2001).

11. A. Khodjamirian, Nucl. Phys. B **605**, 558 (2001).

12. C. N. Burrell and A. R. Williamson, Phys. Rev. D **64**, 034009 (2001).

13. T. Becher, M. Neubert and B. D. Pecjak, Nucl. Phys. B **619**, 538 (2001); M. Neubert and B. D. Pecjak, JHEP **0202**, 028 (2002).

14. C. W. Bauer, S. Fleming, D. Pirjol and I. W. Stewart, Phys. Rev. D **63**, 114020 (2001); C. W. Bauer, D. Pirjol and I. W. Stewart, Phys. Rev. D **65**, 054022 (2002).

15. J. Chay and C. Kim, Phys. Rev. D **65**, 114016 (2002).

16. M. Beneke, A. P. Chapovsky, M. Diehl and T. Feldmann, preprint hep-ph/0206152.

17. I use the average of CLEO, BaBar and Belle data as compiled in the talks by R. Bartoldus, P. Dauncey, M. Hazumi, S. Rahatlu and E. Won presented at the Conference on *Flavor Physics and CP Violation*, Philadelphia, USA (May 16–18, 2002), to appear in the proceedings.

18. M. Ciuchini, E. Franco, G. Martinelli and L. Silvestrini, Nucl. Phys. B **501**, 271 (1997); M. Ciuchini, E. Franco, G. Martinelli, M. Pierini and L. Silvestrini, Phys. Lett. B **515**, 33 (2001).

19. M. Gronau and J. L. Rosner, Phys. Rev. D **59**, 113002 (1999).

20. R. Fleischer and J. Matias, preprint hep-ph/0204101, and private communication.

21. A. S. Kronfeld and S. M. Ryan, preprint hep-ph/0206058.

22. T. Becher, S. Braig, M. Neubert and A. L. Kagan, Phys. Lett. B **540**, 278 (2002).

23. Y. Grossman, M. Neubert and A. L. Kagan, JHEP **9910**, 029 (1999).

24. Y. Grossman and M. P. Worah, Phys. Lett. B **395**, 241 (1997).

25. M. Neubert and J. L. Rosner, Phys. Lett. B **441**, 403 (1998); Phys. Rev. Lett. **81**, 5076 (1998); M. Neubert, JHEP **9902**, 014 (1999).

Frascati Physics Series Vol. XXVIII (2002), pp.183-194
HQ & L 2002 – Vietri s/m, May 27th - June 1st, 2002

HADRONIC AND CHARMLESS B DECAYS AT BELLE

Chung-Hsiang Wang
(for the Belle Collaboration)
National Lien-Ho Institute of Technology, Taiwan

ABSTRACT

We have presented the results of hadronic and rare B decay analyses based on a large data sample collected with the Belle detector at the KEKB asymmetric e^+e^- collider. The decays of $B^+ \to D_{CP}K^+$, $B \to D^{0(*)}p\bar{p}$ and $B^+ \to D^{0(*)}K^+K^{0(*)}$ have been searched and the preliminary results have been reported. For charmless hadronic B decays, we have made the first observation of charmless baryonic decay $B^+ \to p\bar{p}K^+$. We also see strong evidence of $B^+ \to \eta K^+$ and $B^+ \to \eta\pi^+$, and observed the large decay $B^+ \to \omega K^+$. Preliminary results of improved measurements of the branching fractions for the decays $B \to K\pi$ and $\pi\pi$ are reported.

1 Introduction

One of the most important goals of experiments at B-factories is to precisely measure the sides and angles of the unitarity triangle in the Cabbibo-Kobayashi-

Maskawa matrix [1] (CKM) and check its consistency. Hadronic and charmless rare B decays play an important role for this. With more charmless B decays discovered, we can learn more on the penguin diagram decays, which is related to CP violation. An indication of new physics may arise from the unexpected large decay branching fractions or CP violation in B decays. Results of hadronic and charmless rare B decay analyses based on a large data sample are presented here. The data were collected with the Belle detector [2] at the KEKB asymmetric e^+e^- collider. [3]

2 Belle Detector

Belle is a general-purpose detector with a 1.5 T superconducting solenoid magnet. Charged particle tracking, covering 92% of the total center-of-mass (CM) solid angle, is provided by the Silicon Vertex Detector (SVD) consisting of three concentric layers of double-sided silicon strip detectors and a 50-layer Central Drift Chamber (CDC). Charged hadrons are distinguished by combining the responses from an array of Silica Aerogel Čerenkov Counters (ACC), a Time of Flight Counter system (TOF), and dE/dx measurements in the CDC. The combined response provides K/π separation of at least 2.5σ for laboratory momenta up to 3.5 GeV/c. Photons and electrons are detected in an array of 8736 CsI(Tl) crystals (ECL) located inside the magnetic field and covering the entire solid angle of the charged particle tracking system. The 1.5 T magnetic field is returned via an iron yoke, instrumented to detect muons and K_L mesons (KLM). The KLM consists of alternating layers of resistive plate chambers and 4.7 cm thick steel plates.

3 Analysis in General

In all the decay modes presented here, the continuum process
($e^+e^- \to q\bar{q}$) is the dominant background. Since $B\bar{B}$ events are spherical while the continuum events are jet-like, we apply cuts on various event shape variables (such as sphericity, thrust angle, Fox-Wolfram moments, and the production angle of B) to suppress the background. [4] K/π separation is performed by applying a cut on the likelihood ratio, $\mathcal{L}_{\rm K}/(\mathcal{L}_\pi + L_{\rm K})$, where $\mathcal{L}_{\rm K}$ ($\mathcal{L}_\pi$) is a kaon (pion) likelihood computed from information from the particle identification devices: specific ionization loss in the central drift chamber, photo-electron

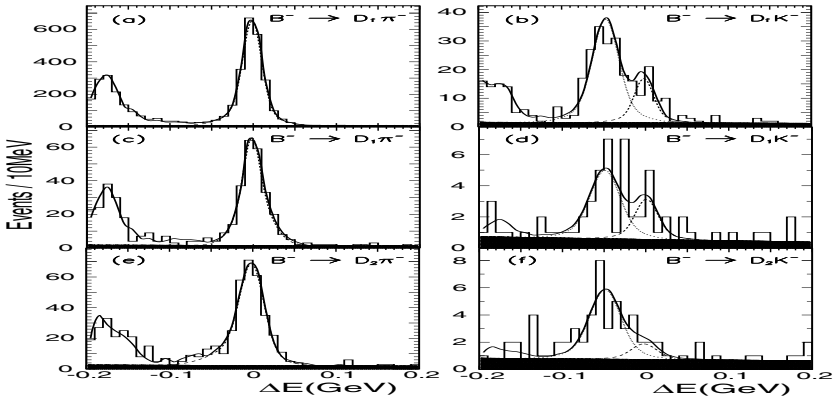

Figure 1: *ΔE distributions of $B \to D_{CP}\pi^-, D_{CP}K^-$ decays. The middle histograms are for $B \to D_1$ decays and the bottom ones are for $B \to D_2$ decays. The upper ones are for $B \to D_f$ decays, where D_f means $D^0 \to K^-\pi^+$ decays.*

yield in the aerogel Cherenkov counters, and time-of-flight. [2)]
B candidates are identified using two kinematic variables: beam constrained mass: $M_B = \sqrt{E^2_{beam} - p^2_B}$, and the energy difference: $\Delta E = E_B - E_{beam}$. Here E_{beam} is the beam energy, p_B and E_B are the momentum and energy of a reconstructed B candidate, respectively, where all variables are defined in the $\Upsilon(4S)$ rest frame. Charged conjugate is applied through in this note except for the direct CP violation search. The yields are obtained from either Maximum Likelihood fit or extended Maximun Likelihood fit on that variables. [5)] The signal distributions are obtained from signal Monte Carlo sample, while the background distributions are either from continuum Monte Carlo or data outside signal region.

4 B decays to Charm

4.1 $B^+ \to D_{CP}K^+$

In this analysis, we are looking for the charge asymmetry in $B^+ \to D_{1,2}K^+$ decays, where D_1 means K^+K^- and $\pi^+\pi^-$, D_2 means $K_s\pi^0, K_s\omega, K_s\phi, K_s\eta$ and $K_s\eta'$. The D_1 represent the "+" CP eigenstate, while D_2 represent

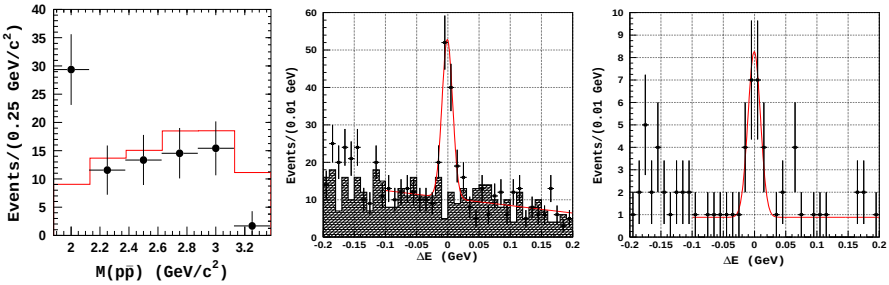

Figure 2: *$p\bar{p}$ invariant mass for $B \to D^0 p\bar{p}$(left) decays. ΔE distribution for $B \to D^0 p\bar{p}$(middle) and for $B \to D^{*0} p\bar{p}$(right) decays. Solid histogram is from the signal MC with $p\bar{p}$ generated in phase space.*

"$-$" CP eigenstate. The yields are obtained from fits on ΔE after event shape and KID cuts with M_B in the signal region. The data sample we used are 29.1 fb^{-1} on $\Upsilon(4S)$. The following relations are used to constrain the CP phase ϕ_3; $\mathcal{A}_{1,2} = \frac{\mathcal{B}(B^- \to D_{1,2} K^-) - \mathcal{B}(B^+ \to D_{1,2} K^+)}{\mathcal{B}(B^- \to D_{1,2} K^-) + \mathcal{B}(B^+ \to D_{1,2} K^+)} = \frac{2r \sin\delta' \sin\phi_3}{1 + r^2 + 2r \sin\delta' \sin\phi_3}$, $\mathcal{R}_{1,2} = \frac{\frac{\mathcal{B}(D_{1,2} K^-) + \mathcal{B}(D_{1,2} K^+)}{\mathcal{B}(D_{1,2} \pi^-) + \mathcal{B}(D_{1,2} \pi^+)}}{\frac{\mathcal{B}(D^0 K^-) + \mathcal{B}(D^0 K^+)}{\mathcal{B}(D^0 \pi^-) + \mathcal{B}(D^0 \pi^+)}} = 1 + r^2 + 2r \cos\delta' \cos\phi_3$, while $\delta' = \delta$ for D_1 and $= \delta + \pi$ for D_2.

The results of fitting are shown in Fig. 1. The preliminary results of the branching fractions in term of the ratio compared to the corresponding Cabiboo favor decays and the corresponding $\mathcal{A}_{1,2}$, $\mathcal{R}_{1,2}$ are $\mathcal{B}(D^0 K^-)/\mathcal{B}(D^0 \pi^-) = 0.094 \pm 0.009 \pm 0.007$, $\mathcal{B}(D_1 K^-)/\mathcal{B}(D_1 \pi^-) = 0.125 \pm 0.036 \pm 0.010$, $\mathcal{B}(D_2 K^-)/\mathcal{B}(D_2 \pi^-) = 0.119 \pm 0.028 \pm 0.006$, $\mathcal{A}_1 = +0.29 \pm 0.26 \pm 0.05$ ($-0.14 < \mathcal{A}_1 < 0.73$ @90%$C.L.$), $\mathcal{A}_2 = -0.22 \pm 0.24 \pm 0.04$ ($-0.67 < \mathcal{A}_2 < 0.23$ @90%$C.L.$), $\mathcal{R}_1 = 1.33 \pm 0.37 \pm 0.12$ and $\mathcal{R}_2 = 1.27 \pm 0.29 \pm 0.09$.

4.2 $B \to D^{(*)} p\bar{p}$

This belongs to the color suppressed decays with baryons. The D^0 is reconstructed through $K^-\pi^+, K^-\pi^+\pi^+\pi^-$ and $K^-\pi^+\pi^0$. The D^+ is reconstructed

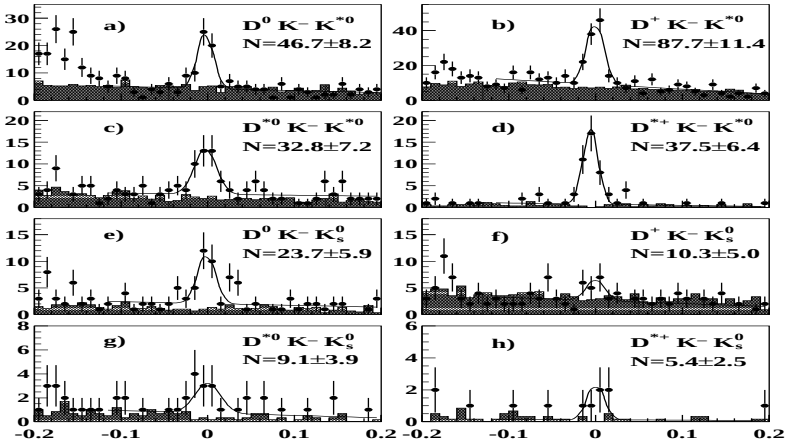

Figure 3: ΔE *distributions of* $B \to D^{(*)}K^-K^{0(*)}$ *decays.*

through $K^-\pi^+\pi^+$ D^* is reconstructed in $D^{*0} \to D^0\pi^0$ and $D^{*+} \to D^0\pi^+$. The yields are obtained from fits on ΔE after event shape and PID cuts with M_B in the signal region. The data sample we used are 29.4 fb^{-1} on $\Upsilon(4S)$. The total yields obtained are 90.0 for $\bar{B}^0 \to D^0 p\bar{p}$ and 20.3 for $\bar{B}^0 \to D^{*0} p\bar{p}$. The measured branching fractions are $\mathcal{B}(\bar{B}^0 \to D^0 p\bar{p}) = (1.18 \pm 0.15 \pm 0.17) \times 10^{-4}$, $\mathcal{B}(\bar{B}^0 \to D^{*0} p\bar{p}) = (1.20^{+0.33}_{-0.29}) \times 10^{-4}$. There aer no signals observed in $B^+ \to D^{+(*)} p\bar{p}$ decays. Their upper limit are $\mathcal{B}(B^+ \to D^+ p\bar{p}) < 0.13 \times 10^{-4}$ and $\mathcal{B}(B^+ \to D^{*+} p\bar{p}) < 0.22 \times 10^{-4}$ at 90% C.L. The fitting histograms are shown in Fig. 2. [6)]

4.3 $B \to D^{(*)}K^-K^{0(*)}$

This decays need $s\bar{s}$ production. We also veto the $B \to DD_s$ in this decays. The D is reconstructed in $D^0 \to K^-\pi^+$ and $D^+ \to K^-\pi^+\pi^+$ D^* is reconstructed in $D^{*0} \to D^0\pi^0$ and $D^{*+} \to D^0\pi^+$. The yields are obtained from fits on ΔE after event shape and PID cuts with M_B in the signal region. The data sample we used are 29.4 fb^{-1} on $\Upsilon(4S)$. The preliminary results are; $\mathcal{B}(D^0K^-K^{*0}) = (7.5\pm1.3\pm1.1)\times10^{-4}$, $\mathcal{B}(D^+K^-K^{*0}) = (8.8\pm1.1\pm1.4)\times10^{-4}$, $\mathcal{B}(D^{*0}K^-K^{*0}) = (14.0 \pm 3.1 \pm 2.6) \times 10^{-4}$, $\mathcal{B}(D^{*+}K^-K^{*0}) = (12.8 \pm 2.2 \pm 2.5) \times 10^{-4}$, and $\mathcal{B}(D^0K^-K^0) = (5.5 \pm 1.4 \pm 0.8) \times 10^{-4}$. The 90% C.L. up-

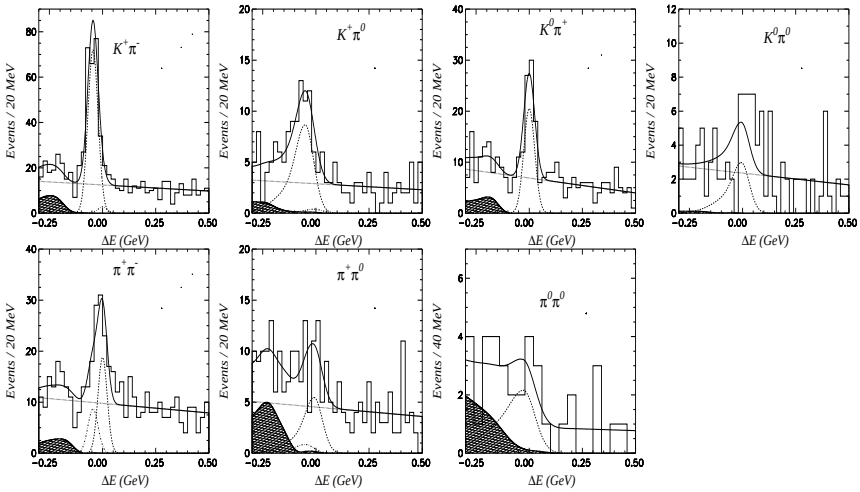

Figure 4: ΔE *distributions for* $B \to K\pi$ *and* $\pi\pi$ *decays.*

per limit are $\mathcal{B}(D^+K^-K^0) < 3.1 \times 10^{-4}$, $\mathcal{B}(D^{*0}K^-K^0) < 11.4 \times 10^{-4}$ and $\mathcal{B}(D^{*+}K^-K^0) < 4.9 \times 10^{-4}$. Fig. 3 show the ΔE distributions.

5 Charmless Rare B decays

5.1 $B \to K\pi, \pi\pi$

Various decays of $B \to K\pi$ and $\pi\pi$ can be used to extract strong and weak phase. The yields are obtained from fits on ΔE after event shape and PID cuts with M_B in the signal region. The data sample we used are 29.4 fb^{-1} on $\Upsilon(4S)$. The results are summarized in Table 1. Fig. 4 show the fit results. The charge asymmetry $\mathcal{A}_{CP}$ is defined as $\frac{N(\overline{B}\to\overline{f})-N(B\to f)}{N(\overline{B}\to\overline{f})+N(B\to f)}$. The results of $\mathcal{A}_{CP}$ is in Table 1 and there are no obvious charge asymmetry in those decays.

5.2 $B^+ \to \eta K^+, \eta\pi^+$

Large Branching fractions of $B \to \eta' K(B \to \eta K^*)$ to $B \to \eta' K^*(B \to \eta K)$ [7, 9, 10] show the effect of the interference between penguin and tree contributions. In this analysis, η is reconstructed through $\eta \to \gamma\gamma$ and $\eta \to \pi^+\pi^-\pi^0$ decays.

Table 1: *Branching fractions($\mathcal{B}$) and charge asymmetry $\mathcal{A}_{CP}$ of $B \to K\pi, \pi\pi$. The upper limit is at 90% C.L. The branching fractions and upper limit are in the unit of 10^{-5}.*

Mode	Yields	$\mathcal{B}$	$\mathcal{A}_{CP}$
$K^+\pi^-$	218 ± 18	$2.18 \pm 0.18 \pm 0.15$	$-0.06 \pm 0.08 \pm 0.01$
$K^+\pi^0$	58 ± 11	$1.25 \pm 0.24 \pm 0.12$	$-0.04 \pm 0.19 \pm 0.03$
$K^0\pi^+$	66 ± 10	$1.88 \pm 0.30 \pm 0.15$	$0.46 \pm 0.15 \pm 0.02$
$\pi^+\pi^-$	51 ± 11	$0.51 \pm 0.11 \pm 0.04$	-
$\pi^+\pi^0$	36 ± 11	$0.70 \pm 0.22 \pm 0.08$	$0.31 \pm 0.31 \pm 0.05$
$\pi^0\pi^0$	12 ± 6	< 0.56	-
$K^0\pi^0$	19 ± 8	$0.77 \pm 0.32 \pm 0.16$	-
K^0K^0	1 ± 3	< 1.3	-
K^+K^-	0 ± 2	< 0.05	-
K^+K^0	0 ± 2	< 0.38	-

Signal yields are obtained from extended unbinned maximum likelihood (ML) fits on the variables M_B and ΔE after event shape and PID cuts. The data sample we used are 29.4 fb^{-1} on $\Upsilon(4S)$. We have observed a large ηK^+ and π^+ signals. The preliminary results are listed in Table 2. The statistical significance(Σ) is defined as $\sqrt{-2\ln(\mathcal{L}(0)/\mathcal{L}_{\rm max})}$ where $\mathcal{L}_{\rm max}$ is the likelihood at the nominal signal yield and $\mathcal{L}(0)$ is the likelihood with the signal yield fixed to zero. The projections of fitting results for $B \to \eta K^+, \pi^+$ are shown in Fig. 5.

5.3 $B \to \omega K^+, \omega\pi^+$

In this analysis, candidate ω mesons are reconstructed from $\pi^+\pi^-\pi^0$ combinations where the CM momentum of the π^0 is required to be greater than 350 MeV/c to reduce the large combinatorial background from low energy photons. Signal yields are extracted using unbinned ML fit simultaneously for M_B and ΔE. The background functions include a combinatorial component and a component from other charmless B decays. Due to the possible mis-identification between K^- and π^-, we also include a component for feed-down from $\omega\pi^-$ to ωK^- fitting and vice versa. The fitted yields and the measured branching fractions are summarized in Table 2 The projections of the M_B and ΔE with the normalized signal and background PDFs are shown in Figure 6. We

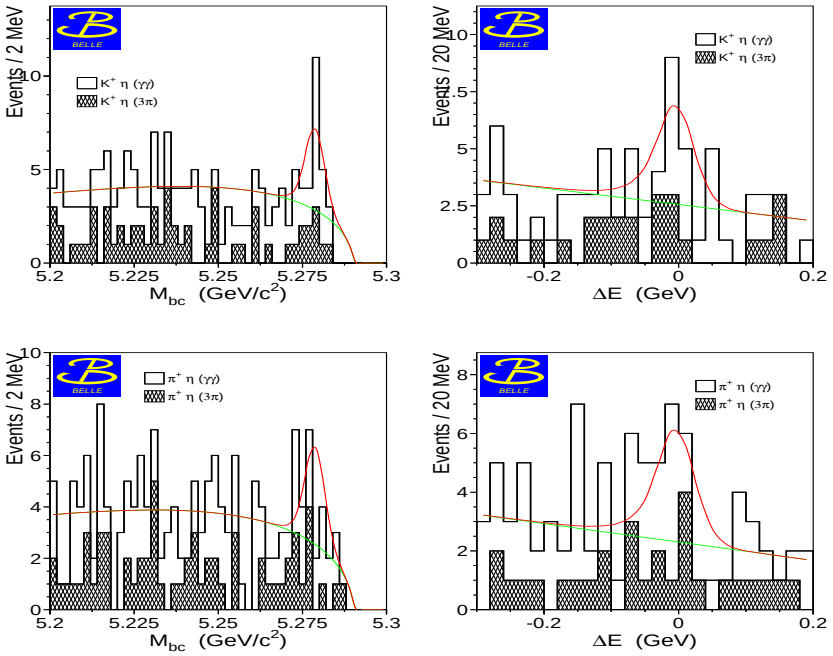

Figure 5: *Projection on M_B and ΔE from 2D ML fitting results for ηK^+(upper) and $\eta\pi^+$(bottom) with the expected signal and background function overlayed. The shaded area represents $\eta \to 3\pi$ decays.*

have observed the decay $B^\pm \to \omega K^\pm$ with 6.4σ significance. Our results on the $B^- \to \omega K^-$ and $\omega\pi^-$ branching fraction measurements disagree with the earlier ones from CLEO [8] and BABAR [9]. But the sum of the branching fractions of $B^- \to (\omega K^- + \omega\pi^-)$ is consistent with the CLEO's result.

5.4 $B \to p\bar{p}K, p\bar{p}\pi$

We have searched for the decay modes $B^+ \to p\bar{p}K^+$ and $B^0 \to p\bar{p}K^0_S$. These modes are expected to proceed mainly via $b \to s$ penguin diagrams. We also search for $B^+ \to p\bar{p}\pi^+$ which is expected to occur primarily via a $b \to u$ tree process. These baryonic modes can be used to either constrain or observe direct CP violation in B decay. [12] The combinations will be veto if the invariance mass of the proton anti-proton pair fall within the known chamonium states.

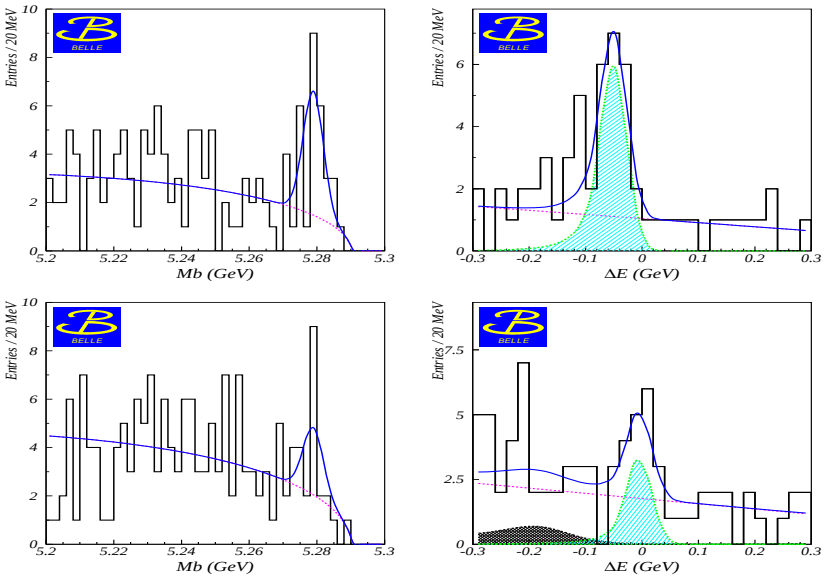

Figure 6: *Projection on M_B and ΔE from 2D ML fitting results for ωK^+(upper) and $\omega\pi^+$(bottom) with the expected signal and background function overlayed.*

In Figure 7, we show the ΔE distribution and M_B distribution for the signal candidates for $B \to p\bar{p}K^+$ decays. The fit to the ΔE distribution gives a yield of $42.8^{+10.8}_{-9.6}$ with a significance of 5.6σ. This is the first observation of a $b \to s$ transition with baryons in the final state. [11)]

We also examine the $M_{p\bar{p}}$ mass distributions for events in the ΔE, M_B signal region. The signal yield as a function of $p\bar{p}$ mass is shown in Figure 7. The distribution from a three-body phase space MC normalized to the area of the signal is superimposed. It is clear that the observed mass distribution is not consistent with three-body phase space but instead is peaked at low $p\bar{p}$ mass.

To avoid model dependence in the determination of the branching fraction for $p\bar{p}K^+$, we fit the ΔE signal yield in bins of $M_{p\bar{p}}$ and correct for the detection efficiency in each bin using a three-body phase space $B^+ \to p\bar{p}K^+$ MC model. We then sum the partial branching fractions in each bin to obtain $\mathcal{B}(B^+ \to p\bar{p}K^+) = (4.3^{+1.1}_{-0.9}(\text{stat}) \pm 0.5(\text{syst})) \times 10^{-6}$. A fit to the ΔE distributions to

Table 2: *Results of Combined branching fractions ($\mathcal{B}$) or 90% C.L. limit, significance (Σ) for $B \to \eta K^+, \eta\pi^+$ and $\omega K^- \omega\pi^-$.*

Mode	Signal Yields	Σ	$\mathcal{B}(10^{-6})$
$\eta_{\gamma\gamma}K^+$	$12.7^{+5.0}_{-4.2}$	4.3	$5.7^{+2.2}_{-1.9}$
$\eta_{\pi^+\pi^-\pi^0}K^+$	$4.2^{+3.1}_{-2.3}$	2.4	$4.6^{+3.4}_{-2.5}$
ηK^+	-	4.9	$5.3^{+1.8}_{-1.5} \pm 0.6$
$\eta_{\gamma\gamma}\pi^+$	$11.4^{+4.9}_{-4.1}$	3.8	$5.9^{+2.5}_{-2.1}$
$\eta_{\pi^+\pi^-\pi^0}\pi^+$	$4.0^{+3.1}_{-2.3}$	2.1	$4.8^{+3.7}_{-2.8}$
$\eta\pi^+$	-	4.3	$5.4^{+2.0}_{-1.7} \pm 0.6$
ωK^+	$19.7^{+5.4}_{-4.8}$	6.4	$9.9^{+2.7+0.7}_{-2.4-0.5}$
$\omega\pi^+$	$10.6^{+4.8}_{-4.5}$	3.3	$4.3 \pm 2.0 \pm 0.5 (< 8.2)$

$p\bar{p}K_s$ gives $6.4^{+4.4}_{-3.7}$ events and $p\bar{p}\pi^+$ gives $16.2^{+8.6}_{-8.0}$ events with significance of 2.1σ. Applying the Feldman-Cousins procedure, [13], we obtain an upper limit at 90% C.L. of $\mathcal{B}(B^0 \to p\bar{p}K^0) < 7.2 \times 10^{-6}$ and $\mathcal{B}(B^+ \to p\bar{p}\pi^+) < 3.7 \times 10^{-6}$.

6 Summary

We have observed and measured the branching fractions of CP phase related $B \to D_{CP}K$ decays. We have also made the first observation of charmless baryonic decay $B^+ \to p\bar{p}K^+$, the color suppressed baryonic decays $B \to D^{0(*)}p\bar{p}$, the three-body $B^0 \to D^{(*)}K^+K^{0(*0)}$ and obtain a strong evidence of $B^+ \to \eta K^+$ and $B^+ \to \eta\pi^+$. We also observed the decay $B^+ \to \omega K^+$ and measured the branching fractions for the decays $B \to K\pi$ and $\pi\pi$. By summer 2002 it is anticipated that Belle will have collected 90 fb^{-1} of data providing a rich sample to continue the search for rare B decays and measure CP violating effects in a variety of B decay modes.

7 Acknowledgements

We wish to thank the KEKB accelerator group for the excellent operation of the KEKB accelerator. We acknowledge support from the Ministry of Education, Culture, Sports, Science, and Technology of Japan and the Japan Society for the Promotion of Science; the Australian Research Council and the Australian Department of Industry, Science and Resources; the Department of Science and Technology of India; the BK21 program of the Ministry of Education of

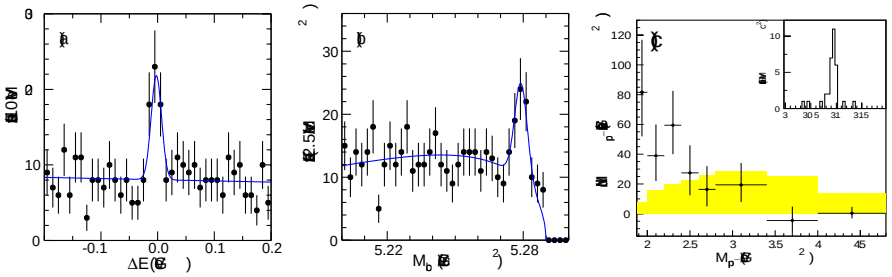

Figure 7: *(a) ΔE and (b) M_B distributions for $B^+ \to p\bar{p}K^+$ candidates. (c) The fitted yield divided by the bin size for $B^+ \to p\bar{p}K^+$ as a function of $M_{p\bar{p}}$. The distribution from non-resonant $B^+ \to p\bar{p}K^+$ MC simulation is superimposed. The inset shows the $M_{p\bar{p}}$ distribution for the $J/\psi K^+$ signal region by removing the charm veto.*

Korea and the CHEP SRC program of the Korea Science and Engineering Foundation; the Polish State Committee for Scientific Research under contract No.2P03B 17017; the Ministry of Science and Technology of Russian Federation; the National Science Council and the Ministry of Education of Taiwan; the Japan-Taiwan Cooperative Program of the Interchange Association; and the U.S. Department of Energy.

References

1. N. Cabibbo, Phys. Rev. Lett. **10**, 531 (1963); M. Kobayashi and T. Maskawa, Prog. Theor. Phys. **49**, 652 (1973).

2. Belle Collaboration, A. Abashian *et al.*, KEK Progress Report 2000-4 (2000), to appear in Nucl. Inst. and Meth. A.

3. KEKB B Factory Design Report, KEK Report 95-7 (1995), unpublished.

4. The shape variables used in this analysis differ among the modes. A typical example see Phys. Lett **B517**,309 2001.

5. The definition of extended Maximum LIkelihood fit is in Phys. Lett **B517**,309 (2001).

6. Belle Collaboration, K. Abe *et al.*, hep-ex/0205083, submitted to Phys. Rev. Lett.

7. CLEO Collaboration, D. Cronin-Hennessy *et al.*, Phys. Rev. Lett. **85**, 515 (2000).

8. CLEO Collaboration, C.P. Jessop *et al.*, Phys. Rev. Lett. **85**, 2881 (2000).

9. BABAR Collaboration, B. Aubert *et al.*, Phys. Rev. Lett. **87**, 221802 (2001).

10. See Prof. C.H. Wang's talk in Heavy Quarks and Leptons, Vietri, 2002 for the updated Belle results of $\eta' K$ and ηK^*.

11. Belle Collaboration, K. Abe *et al.*, Phys. Rev. Lett. **88**, 181803 (2002).

12. G. Eilam, M. Gronau, and J. Rosner, Phys. Rev. D **39**, 819 (1989).

13. G. J. Feldman and R. D. Cousins, Phys. Rev. D **57**, 3873 (1998).

Frascati Physics Series Vol. XXVIII (2002), pp.195-207
HQ & L 2002 – Vietri s/m, May 27th - June 1st, 2002

REVIEW OF RADIATIVE AND SEMILEPTONIC B DECAYS

Steven H. Robertson
Stanford Linear Accelerator Center

ABSTRACT

Recent experimental results on radiative and semileptonic B meson decays are described. Measurements of inclusive and exclusive $b \to s\gamma$ and $b \to s\ell^+\ell^-$ decays, and exclusive $B \to \rho\gamma$ and $B \to K\nu\bar{\nu}$ penguin decays are presented. The extraction of $|V_{cb}|$ from inclusive $B \to X_c\ell\nu$ decays and from exclusive $B \to D^*\ell\nu$ decays is also discussed.

1 Introduction

Radiative and semileptonic decays of B mesons are sensitive to a number of CKM matrix elements for which experimental measurements are needed to constrain the unitarity triangle describing CP-violation in the B meson system of the Standard Model (SM). In addition, radiative decays are expected to have significant sensitivity to new physics.

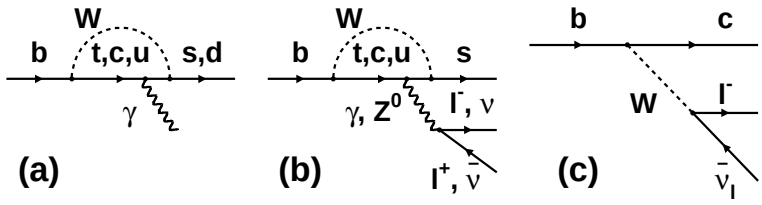

Figure 1: *Feynman diagrams for semileptonic and radiative B decays: (a) $b \to s\gamma$ and $b \to d\gamma$, (b) $b \to s\ell^+\ell^-, s\nu\bar{\nu}$, (c) $b \to c\ell\bar{\nu}$.*

Over the past few years there has been significant experimental progress in the study of these decays. This is due mainly to the large data sets ($\sim$ 50 M $B\bar{B}$ events) collected by the two asymmetric B factory experiments, Babar and Belle, but with significant contributions also from the CLEO experiment in spite of a somewhat smaller data sample. This review will discuss recent experimental results on radiative $b \to s\gamma$ and $b \to d\gamma$ decays, the related rare decays $b \to s\ell^+\ell^-, s\nu\bar{\nu}$ and the extraction of $|V_{cb}|$ from semileptonic B decays.

In a B factory environment $B\bar{B}$ events are produced at the $\Upsilon(4s)$ resonance. B meson candidates are reconstructed with the aid of two kinematic variables, $m_{ES} = \sqrt{E^{*2}_{beam} - p^{*2}_B}$ and $\Delta E = E^*_B - E^*_{beam}$, which define the reconstructed B mass and energy relative to the known beam energy, E^*_{beam}. Background from non-resonant $q\bar{q}$ ("continuum") is reduced by exploiting topological differences between the jet-like $q\bar{q}$ and spherically symmetric $B\bar{B}$ events using a combination of event-shape kinematic variables. Residual continuum backgrounds are generally estimated or explicitly subtracted using data collected for this purpose just below the $\Upsilon(4s)$ resonance.

2 Radiative B decays

Radiative B meson decays occur in the SM via effective flavour changing neutral currents mediated by so-called "penguin" loop diagrams, dominated by the t quark, as shown in figure 1a. The photon can be radiated from any of the charged lines associated with the b quark. Because the loop could potentially contain other heavy virtual particles, these decays can be used to constrain new physics at energies significantly beyond the B mass scale. Interference between the SM and non-SM processes can also potentially lead to CP-violating charge asymmetries as large as 20% [1]. Such asymmetries are small in the SM.

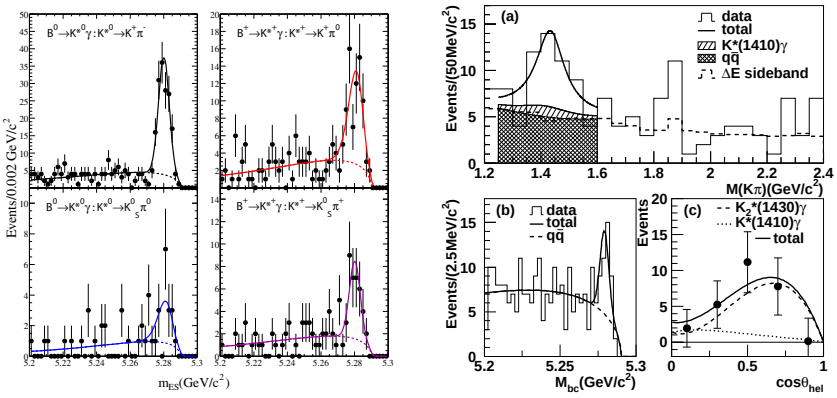

Figure 2: *(Left) Reconstructed m_{ES} of $B \to K^*(892)\gamma$ candidates obtained by Babar showing the parameterization of the combinatoric background and a signal peak at the B mass. (Right) $K\pi$ and B mass and helicity angle distributions, obtained by Belle, for $B \to K\pi\gamma$ candidates above the $K^*(982)$ mass.*

2.1 $B \to K^*(892)\gamma$

The decay $B \to K^*(892)\gamma$ provided the first evidence of the $b \to s\gamma$ process when it was observed by CLEO in 1993 [2]. This mode is now fairly well measured, with new published results from CLEO [3] and Babar [4] and a recent preliminary measurement from Belle [5] (see table 1). A $K^\pm$ or K^0_s and a $\pi^\pm$ or π^0 are selected for which the $K\pi$ combination is close to the expected $K^*(892)$ mass. These are combined with an energetic photon ($2.0\ \text{GeV} < E_\gamma < 2.8\ \text{GeV}$) to form the B meson candidate. The B mass distributions obtained by Babar are shown in the left side of figure 2. Backgrounds are predominantly from continuum $q\bar{q}$ events with a photon from ISR or π^0 or η decays. These are suppressed by a combination of event shape requirements and photon vetoes. The precision of the average of these measurements is now $\leq 10\%$ in both the charged and neutral modes.

Babar and Belle both look for CP-violating charge asymmetries, A_{CP}, by comparing the rate of $\bar{B} \to \bar{K}^*\gamma$ and $B \to K^*\gamma$, obtaining 90% confidence limits of $-0.179 < A_{CP} < 0.082$ and $-0.085 < A_{CP} < 0.149$ respectively.

Table 1: $B(B \to K^*(892)\gamma)$ *experimental results*

	$B^0 \to K^{*0}\gamma$	$B^+ \to K^{*+}\gamma$
CLEO	$(4.55 \pm 0.70 \pm 0.34) \times 10^{-5}$	$(3.76 \pm 0.86 \pm 0.28) \times 10^{-5}$
Babar	$(4.23 \pm 0.40 \pm 0.22) \times 10^{-5}$	$(3.83 \pm 0.62 \pm 0.22) \times 10^{-5}$
Belle (prelim)	$(4.08^{+0.35}_{-0.33} \pm 0.26) \times 10^{-5}$	$(4.92^{+0.59+0.38}_{-0.54-0.37}) \times 10^{-5}$
Combined	$(4.21 \pm 0.29) \times 10^{-5}$	$(4.23 \pm 0.42) \times 10^{-5}$

Table 2: *Experimental measurements of exclusive* $B \to X_s\gamma$ *for* X_s *mass above the* $K^*(892)$.

CLEO	$B(B \to K_2^*(1430)\gamma)$	$(1.66^{+0.59}_{-0.53} \pm 0.13) \times 10^{-5}$
Belle	$B(B \to K_2^*(1430)\gamma)$	$(1.5^{+0.6}_{-0.5} \pm 0.1) \times 10^{-5}$
	$B(B^+ \to K^+\pi^-\pi^+\gamma)$	$(2.4 \pm 0.5^{+0.4}_{-0.2}) \times 10^{-5}$
	$B(B^+ \to K^{*0}\pi^+\gamma)$	$(2.0^{+0.4}_{-0.2} \pm 0.2) \times 10^{-5}$
	$B(B^+ \to K^+\rho^0\gamma)$	$(1.0 \pm 0.5^{+0.2}_{-0.3}) \times 10^{-5}$
	$B(B^+ \to K^+\pi^-\pi^+\gamma$ non resonant)	$< 0.9 \times 10^{-5}$

2.2 Higher mass $B \to X_s\gamma$ modes

CLEO [3] and Belle [6] have both studied $B \to K\pi\gamma$ decays in which the mass of the $K\pi$ system is above the $K^*(892)$. CLEO reported an observation, now confirmed by a new measurement from Belle, of $B \to K_2^*(1430)\gamma$ in which the $K_2^*(1430)$ decays via $K_2^{*0} \to K^+\pi^-, K_s^0\pi^0$ or $K_2^{*+} \to K^+\pi^0, K_s^0\pi^+$. Contributions from $K_2^*(1430)$ and $K^*(1410)$ are distinguished by fitting the helicity angle distribution (shown in figure 2) of the $B \to K\pi\gamma$ candidates. The $K_2^*(1430)$ component is found to dominate. Belle has also considered the three-body X_s final state $K\pi\pi\gamma$ using a similar analysis method, and has found that it is dominated by resonant contributions from $K^*\pi$ and $K\rho$. The results are listed in table 2.

2.3 Inclusive $B \to X_s\gamma$

The inclusive $B \to X_s\gamma$ rate is more robust theoretically than the exclusive predictions since it is insensitive to non-perturbative long-distance QCD effects. It has been calculated at NLO to be $3.57 \pm 0.30 \times 10^{-4}$ for $E_\gamma > 1.6$ GeV [7]. Combining the measured branching ratios for the $K^*(892)\gamma$, $K_2^*(1430)\gamma$ and

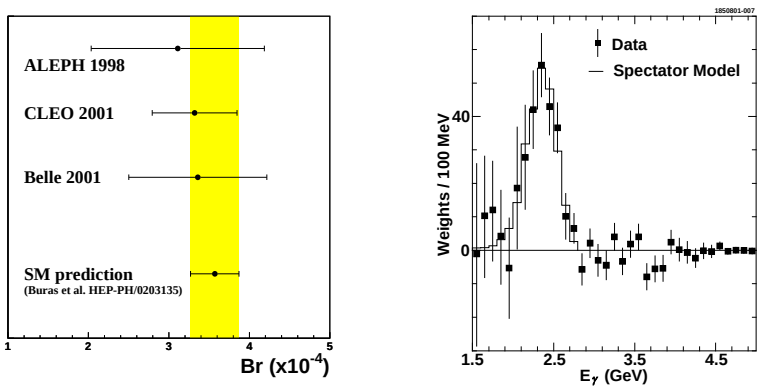

Figure 3: *(Left) Summary of inclusive $b \to s\gamma$ branching ratio measurements. The vertical band represents the SM expectation. (Right) The background-subtracted inclusive $b \to s\gamma$ photon energy spectrum obtained by CLEO.*

$K\pi\pi\gamma$ final states gives about a quarter of the predicted total $b \to s\gamma$ width.

Belle [8] and CLEO [9] have measured $B(B \to X_s\gamma)$ using a method in which the X_s system is reconstructed by combining a $K^{\pm}$ or K^0_s with up to four pions, including a maximum of one π^0. X_s candidates are combined with an energetic photon to form B candidates, which are then selected based on m_{ES} and ΔE. A significant continuum background which remains even after exploiting event-shape differences necessitates background subtraction using off-peak data. The CLEO and Belle inclusive $b \to s\gamma$ measurements along with an older ALEPH measurement [10], are summarized in figure 3 (left). The agreement with the SM prediction is good, leaving relatively little room for non-SM physics. The CLEO result, the most precise single measurement, is statistically limited while the Belle measurement was based on less than 10% of their present data statistics. This suggest that further improvements in this measurement can be expected in the near future.

CLEO has also studied the moments of the inclusive $b \to s\gamma$ photon energy spectrum [11], shown in figure 3 (right). The mean energy $\langle E_\gamma \rangle$ is approximately half the b quark mass, while the mean square width $\langle E_\gamma^2 \rangle - \langle E_\gamma \rangle^2$ is related to the b quark momentum in the meson. CLEO obtains $\langle E_\gamma \rangle = 2.346 \pm 0.032 \pm 0.011$ GeV and $\langle E_\gamma^2 \rangle - \langle E_\gamma \rangle^2 = 0.0226 \pm 0.0066 \pm 0.0020$ GeV^2 for the first and second moments, from which they extract the HQET parameter (in $\overline{MS}$, to order $1/m_B^3$ and $\beta_0\alpha_s^2$) $\bar{\Lambda} = 0.35 \pm 0.08 \pm 0.10$ GeV (see section 4.3).

Table 3: $B \to \rho\gamma$ *experimental results*

	$B(B^+ \to \rho^+\gamma)$	$B(B^0 \to \rho^0\gamma)$
Babar (prelim)	$< 2.8 \times 10^{-6}$	$< 1.5 \times 10^{-6}$
Belle (prelim)	$< 9.9 \times 10^{-6}$	$< 10.6 \times 10^{-6}$
CLEO	$< 13 \times 10^{-6}$	$< 17 \times 10^{-6}$

2.4 Exclusive $b \to d\gamma$

$b \to d\gamma$ transitions occur via radiative penguin diagrams similar to $b \to s\gamma$ (figure 1a). Although exclusive radiative decay branching ratios have large uncertainties, it has been argued [12] that these uncertainties largely cancel in the ratio $B(B \to \rho\gamma)/B(B \to K^*\gamma)$, given by

$$\frac{B(B \to \rho\gamma)}{B(B \to K^*\gamma)} = S_\rho \left|\frac{V_{td}}{V_{ts}}\right|^2 \left(\frac{1 - m_\rho^2/M^2}{1 - m_K^{*2}/M^2}\right)^3 \xi^2 \, (1 + \Delta R[\rho/K^*]) \qquad (1)$$

where $S_\rho = 1(1/2)$ for $\rho^{\pm(0)}$, $\xi = 0.76 \pm 0.06$ [13] is the ratio of the form factors and $\Delta R < 0.15$. This implies that the ratio $|V_{td}/V_{ts}|^2$ could be extracted from experimental measurements with $\sim 20\%$ theoretical uncertainty.

Experimentally $B(B \to \rho\gamma)$ is considerably more difficult than $B(B \to K^*\gamma)$ due to the smaller SM branching ratio, intrinsically higher backgrounds and the less stringent constraint imposed by the width of the ρ compared to the K^*. Babar has recently released a preliminary measurement [14] of $B(B \to \rho\gamma)$ which represents a considerable improvement over previous limits (see table 3) [15, 3]. The limit imposed on the ratio $|V_{td}/V_{ts}|$ by this measurement translates to a constraint on the B meson unitarity triangle, represented in figure 4 as a exclusion contour in the $\rho - \eta$ plane. A Babar result on $B(B \to \omega\gamma)$ using a similar method is expected soon.

3 Rare $b \to s\,\ell\bar{\ell}$ decays

The process $b \to s\,\ell\bar{\ell}$ proceeds via radiative penguin diagrams as shown in figure 1b with either a Z^0 or γ coupling to the charged leptons, or in the case of neutrinos, only a Z^0. W box diagrams also contribute.

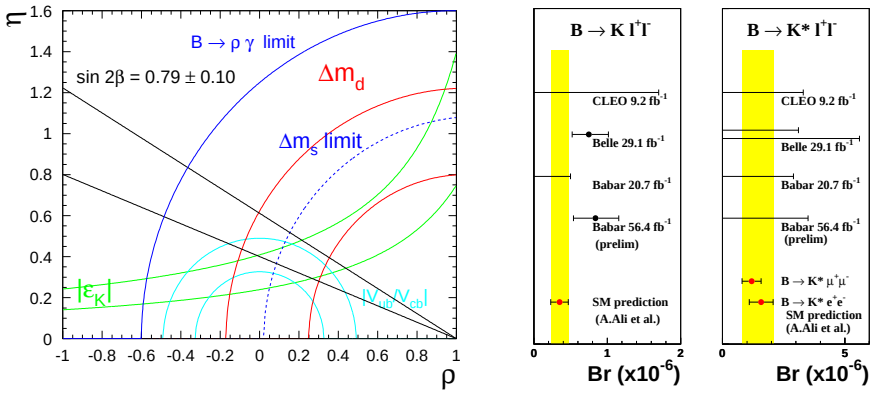

Figure 4: *(Left) The constraint on the $\rho - \eta$ plane imposed by the preliminary Babar $B \to \rho\gamma$, along with constraints from other measurements. (Right) Summary of $B \to K\ell^+\ell^-$ and $B \to K^*\ell^+\ell^-$ branching ratio measurements.*

3.1 $B \to K^{(*)}\ell^+\ell^-$

Belle reported an observation of $B \to K\ell^+\ell^-$ in 2001 [16] with a central value about a factor of two high compared with the SM expectation [17] and in apparent conflict with a recently published Babar result [18]. An update Babar preliminary result [19] with a significantly enlarged data sample now appears to confirm the Belle result, although no evidence was reported which would suggest that the published Babar result is invalid. $B \to K^*\ell^+\ell^-$ has yet to be observed, although experimental limits are now approaching the SM range. $B \to K^{(*)}\ell^+\ell^-$ results are summarized in figure 4 [20].

3.2 Inclusive $B \to X_s\ell^+\ell^-$

The theoretical predictions for inclusive $B \to X_s\ell^+\ell^-$ are more robust than for the exclusive modes. The branching ratios have been calculated at NNLO to be [17] $B(B \to X_s e^+e^-) = (6.89 \pm 1.01) \times 10^{-6}$ and $B(B \to X_s\mu^+\mu^-) = (4.14 \pm 0.70) \times 10^{-6}$. Belle has recently produced a preliminary measurement of this branching ratio [21] based on 43 fb^{-1} of data. The X_s system is identified using the same "pseudo-reconstruction" method as for the inclusive $B \to X_s\gamma$: a $K\pm$ or K^0_s is combined with up to four additional pions, of which a maximum of one may be a π^0. A signal is reported with a significance of 4.8σ on the combined $\ell = e, \mu$ mode with a branching ratio of $B(B \to X_s\ell^+\ell^-) = (7.1^{+1.6+1.4}_{-1.6-1.2}) \times 10^{-6}$.

3.3 $B^- \to K^- \nu\bar{\nu}$

The decay $B^- \to K^- \nu\bar{\nu}$ has a SM rate which is estimated to be $B(B^- \to K^- \nu\bar{\nu}) \simeq 4 \times 10^{-6}$ [22]. Babar has also recently produced a preliminary limit on this mode [23]. The previous best limit was $B^- \to K^- \nu\bar{\nu} < 2.4 \times 10^{-4}$ from CLEO [24]. The Babar analysis looks for a signature of a high momentum $K^\pm$ recoiling against a exclusively reconstructed $B^\pm \to D\ell\nu X$, where X represents possible photons or π^0s from from higher mass charm states. In contrast, the CLEO measurement used a reconstruction method based on hadronic B decays. Other than the reconstructed B and the signal kaon, no additional tracks and < 0.5 GeV of calorimeter energy are permitted in the event. A preliminary limit of $B^- \to K^- \nu\bar{\nu} < 9.4 \times 10^{-5}$ is obtained using 50.7 fb^{-1} of data. Although this limit is an order of magnitude above the SM expectation, the method shows promise of reaching the theoretically interesting region [22] $B(B \to K\nu\bar{\nu}) < 5 \times 10^{-5}$ in the future. The B factories have not yet reported results on the experimentally difficult inclusive $B \to X_s \nu\bar{\nu}$ mode.

4 Semileptonic decays and $|V_{cb}|$

Semileptonic B decays occur via tree level EW processes mediated by a $W^\pm$ as shown in figure 1c and are therefore sensitive to the CKM matrix elements $|V_{cb}|$ and $|V_{ub}|$. Only the favoured $b \to c$ mode is discussed here.

4.1 $|V_{cb}|$ from exclusive $B \to D^* \ell\nu$

The "classic" determination of $|V_{cb}|$ in semileptonic B decay involves extracting it from from the differential decay rate of exclusive $B \to D^* \ell\nu$ decays in the limit of zero recoil of the heavy quark. The differential rate

$$d\Gamma(B \to D^* \ell\nu)/dw \;\propto\; |V_{cb}|^2 \cdot |F_{D^*}(w)|^2 \tag{2}$$

is expressed in terms of the HQET variable w, defined as the scalar product of the B and D^* 4-velocities:

$$w = v_{\bar{B}} \cdot v_{D^*} = \frac{m_{\bar{B}}^2 + m_{D^*}^2 - q^2}{2 m_{\bar{B}} m_{D^*}}, \qquad q^2 = (p_{\bar{B}} - p_{D^*})^2 \quad . \tag{3}$$

The form factor $F_{D^*}(w)$ is precisely calculable in the limit $w = 1$ by exploiting HQS, and has been estimated to be 0.913 ± 0.042 [25]. Since there is little

phase space available at this limit, the entire $d\Gamma(B \to D^* \ell\nu)/dw$ spectrum is measured and $|V_{cb}| \cdot F_{D^*}(1)$ is obtained from an extrapolation of the fit to $w = 1$. $F(w)$ is constrained by dispersion relations and consequently is governed by a single shape parameter, ρ^2, corresponding to the slope at $w = 1$.

Recent experimental measurements available from CLEO [26], Belle [27] are summarized in table 4. At the B factories, the analysis proceeds by exclusively reconstructing the D^0 and D^* candidate and combining it with an identified lepton. Backgrounds from B decays are reduced using the kinematic variable

$$\cos\theta_{B-D^*\ell} = \frac{2E_B E_{D^*\ell} - m_B^2 - m_{D^*\ell}}{2|p_B||p^*_D\ell|} \quad , \tag{4}$$

which defines the angle between the B and the reconstructed $D^*\ell$ candidate. CLEO obtains the $D^*\ell\nu$ yield by fitting the $\cos\theta_{B-D^*\ell}$ distribution in bins of w. The result is shown in the left-hand plot of figure 5. The CLEO result is nominally the most precise single measurement, but shows a $\sim 3\sigma$ discrepancy relative to other analyses. This could potentially indicate correlated systematics in the LEP measurements, or other similar effects associated with Monte Carlo modeling, however it should also be noted that the combined results [28] are consistent at the level of $\sim 5\%$.

Table 4: *Experimental measurements of the product* $|V_{cb}| \cdot F(1)$

Experiment	$\lvert V_{cb}\rvert \cdot F(1)$
CLEO	$(4.31 \pm 0.13 \pm 0.18) \times 10^{-2}$
Belle	$(3.54 \pm 0.19 \pm 0.18) \times 10^{-2}$
LEP Combined	$(3.82 \pm 0.05 \pm 0.09) \times 10^{-2}$

4.2 $|V_{cb}|$ from inclusive $B \to X_c\ell\nu$ decays

The inclusive semileptonic width $\Gamma(B \to X_c\ell\nu)$ is calculated using HQET and can be expressed as an OPE in powers of $1/m_B$ schematically as

$$\Gamma(B \to X_c\ell\nu) \propto |V_{cb}|^2 \frac{G_F^2 m_B^5}{192\pi^3} \left(1 + f_1\left[\frac{\bar{\Lambda}, \alpha_s}{m_B}\right] + f_2\left[\frac{\bar{\Lambda}, \lambda_1, \lambda_2}{m_B^2}\right] + \mathcal{O}\left[\frac{1}{m_B^3}\right]\right) + ... \tag{5}$$

The $1/m_B$ term contains the perturbative expansion in α_s, and the parameter $\bar{\Lambda}$ which expresses the energy carried by the light quarks and gluons in the B

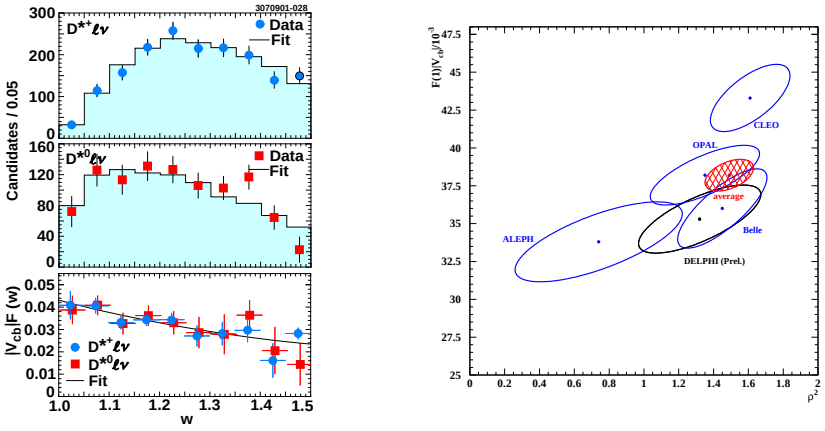

Figure 5: *(Left) CLEO $B \to D* \ell\nu$ data yield and fit as a function of w, and the extracted product $|V_{cb} \cdot F(w)|$. (Right) $|V_{cb} \cdot F(1)|$ vs the slope parameter ρ^2 and the combined fit to the LEP plus B factory data* [28].

meson. The parameters λ_1 and λ_2 are related to the average momentum of the b quark and the hyperfine interaction energy of the b quark spin with the light degree of freedom respectively, and enter at order $1/m_B^2$. Several additional parameters enter at order $1/m_B^3$. Extraction of $|V_{cb}|$ from the inclusive spectrum therefore requires knowledge of these parameters, as well as an underlying assumption of quark-hadron duality which introduces an additional unknown theoretical uncertainty.

4.3 Hadronic mass moments

CLEO has attempted to reduce the theoretical uncertainty on the extraction of $|V_{cb}|$ from inclusive $B \to X_c \ell\nu$ by constraining the HQET parameters $\bar{\Lambda}$ and λ_1 directly from experimental data [29]. This is accomplished by measuring the moments of the hadronic invariant mass spectrum in $B \to X_c \ell\nu$ decays and combining the results with data from the moments of the $b \to s\gamma$ photon energy spectrum. The inclusive hadronic mass spectrum is obtained indirectly by combining the identified lepton ℓ with the neutrino 4-vector obtained from the missing energy and momentum in the event. The mass of the hadronic system is estimated from $m_X^2 = m_B^2 + m_{\ell\nu}^2 - 2E_B E_{\ell\nu}$, where a small term $\sim P_B P_{\ell\nu} \cos\Theta_{B-\ell\nu}$ is neglected. The moments are extracted from a fit to the m_X^2 spectrum

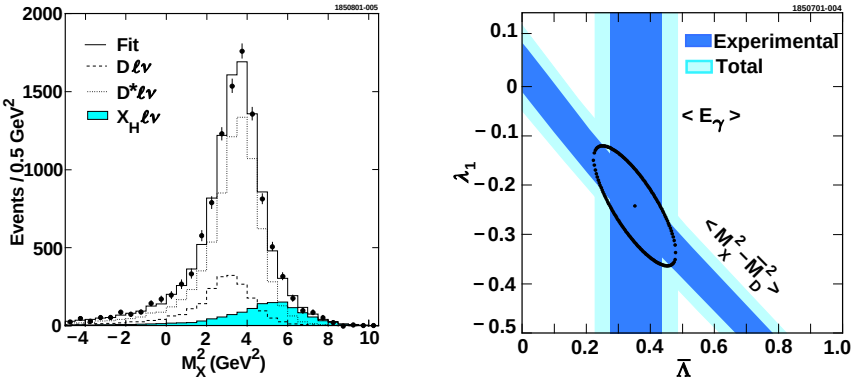

Figure 6: *Invariant mass squared, m_X^2, of the $B \to X_c \ell \nu$ hadronic system obtained by CLEO (left), and the allowed region of the $\bar{\Lambda} - \lambda_1$ plane.*

for the lepton momentum range $p_\ell \geq 1.5$ GeV/c, yielding $\langle m_X^2 - \bar{m}_D^2 \rangle = (0.251 \pm 0.066)$ GeV^2, and $\langle (m_X^2 - \langle m_X^2 \rangle)^2 \rangle = 0.576 \pm 0.170$ GeV^4 where $\bar{m}_D$ is the spin-averaged D meson mass. Uncertainties in the extracted moments are dominated by systematic errors associated with the simulation of the neutrino reconstruction. Appropriate expressions for the moments have been computed to order $\beta_0 \alpha_s^2$ and $1/m_B^3$ [30]. The first moment, $\langle m_X^2 - \bar{m}_D^2 \rangle$, defines an allowed region in the $\lambda_1 - \bar{\Lambda}$ plane (see figure 6). This can be combined with the result for $\bar{\Lambda}$ obtained from the previously described inclusive $b \to s\gamma$ measurement to constrain $\bar{\Lambda}$ and λ_1. CLEO obtains $\bar{\Lambda} = 0.35 \pm 0.07 \pm 0.10$ GeV and $\lambda_1 = -0.236 \pm 0.71 \pm 0.078$ where the errors are experimental and theoretical. Additional bands can be defined using the measurements of the second moments, but these are theoretically less robust. It should be noted that both CLEO [31] and DELPHI [32] have also very recently released preliminary measurements of $\bar{\Lambda}$ and λ_1 obtained from the moments of the lepton spectra in $B \to X_c \ell \nu$. Additional moments measurements are anticipated for summer 2002. CLEO extracts $|V_{cb}|$ using separate CLEO measurements of the $B(B \to X_c \ell \nu)$ and the ratio, f_{+-}/f_{00}, of the relative branching fractions of the $\Upsilon(4s)$ to B^+B^- and $B^0\bar{B}^0$, and the average $B^\pm$ and B^0 lifetimes [33], yielding $|V_{cb}| = (4.04 \pm 0.09 \pm 0.05 \pm 0.08) \times 10^{-2}$ where the first uncertainty is experimental, the second is due to the $\bar{\Lambda}$ and λ_1 determination, and the third represents theory errors from α_s scale and $1/m_B^3$ terms. Clearly there is still

some room for improvement of $B(B \to X_c \ell \nu)$, but it is worth noting that the $\bar{\Lambda}$, λ_1 determination has nearly equal contributions from theory and experimental errors, and in any case the theory error on $|V_{cb}|$ will soon dominate.

5 Conclusion

Numerous new experimental results have recently appeared on radiative and rare penguin B decays. Several exclusive channels have now been observed or have had stringent limits set, and inclusive modes, specifically $b \to s\gamma$ and $b \to s\ \ell^+\ell^-$, have been studied. Prospects also appear good for experimental extraction of HQET parameters from spectral moments, reducing the theory uncertainty on $|V_{cb}|$ extraction from inclusive semileptonic decays.

References

1. A. Kagan and M. Neubert, Phys. Rev. D **58** 094912 (1992).
2. R. Ammar *et al.*(CLEO Collab), Phys. Rev. Lett. **71**, 674 (1993).
3. T. E. Coan *et al.*(CLEO Collab), Phys. Rev. Lett. **84**, 5283 (2000).
4. B. Aubert *et al.*(Babar Collab), Phys. Rev. Lett. **88**, 101805 (2002).
5. A. Ishikawa, hep-ex/0205051 (2002).
6. S. Nishida *et al.*(Belle Collab), hep-ex/0205025 (2002).
7. A. J. Buras *et al.*hep-ph/0203135 (2002).
8. K. Abe *et al.*(Belle Collab), Phys. Lett. **B511**, 151 (2001).
9. S. Chen *et al.*(CLEO Collab), Phys. Rev. Lett. **87**, 251807 (2001).
10. R. Barate *et al.*(ALEPH Collab), Phys. Lett. **B429**, 169 (1998).
11. T. E. Coan *et al.*(CLEO Collab), Phys. Rev. Lett. **86**, 5661 (2001).
12. A. Ali and A. Ya. Parkhomenko, hep-ph/0105302, (2001).
13. A. Ali, V. Braun and H. Simma, Z. Phys. C **63**, 437 (1994).

14. H. Tanaka, "Rare B decays in Babar", XXXVII Rencontres de Moriond Electroweak Interactions and Unified Theories Les Arcs, March 9-16, 2002.

15. Y. Ushiroda, hep-ex/0104045 (2001).

16. K. Abe *et al.*(Belle Collab), Phys. Rev. Lett. **88**, 021801 (2002).

17. A. Ali *et al.*, hep-ph/0112300 (2002).

18. B. Aubert *et al.*, Phys. Rev. Lett. **88** 241801 (2002).

19. J. Walsh, "$B \to Kl^+l^-$ from BABAR", FPCP, May 16-18, 2002.

20. S. Anderson *et al.*(CLEO Collab), Phys. Rev. Lett. **87**, 181803 (2001).

21. K. Senyo, "$B \to Kl^+l^-$ from BELLE", FPCP, May 16-18, 2002.

22. G. Buchalla, G. Hiller and G. Isidori, Phys. Rev. **D63**, 014015 (2001).

23. P. Jackson, "A search for $B^+ \to K^+\nu\bar{\nu}$ ", DPF2002, Williamsburg, Virginia, May 24-28, 2002.

24. T. E. Browder *et al.*, Phys. Rev. Lett. **86** 2950 (2001).

25. M. Neubert in BaBar Physics Book, P. F. Harrison and H. R. Quinn (ed.), SLAC-R-504 (1998).

26. R. A. Briere *et al.*(CLEO Collab), hep-ex/0203032 (2002).

27. T. Nakadaira *et al.*(Belle Collab), Phys. Lett.B **526**, 247 (2002).

28. K. Ecklund, "V_{ub}, V_{cb} from semileptonic decays mini summary", FPCP, May 16-18, 2002.

29. D. Cronin-Hennessy *et al.*, Phys. Rev. Lett. **87**, 251808 (2001).

30. A. Falk, M. Luke and M. Savage, Phys. Rev. **D53**, 2491 (1996); *ibid*,**53**, 6316 (1996); A. Falk and M. Luke, Phys. Rev. *D57*, 424 (1998).

31. M. Artuso, "Lepton energy moments, OPE parameters, m_b and V_{cb}", DPF2002, Williamsburg, Virginia, May 24-28, 2002.

32. L. Salmi, "Study of Lepton Moments in $B \to X_c\ell\bar{\nu}$ Decays", DPF2002, Williamsburg, Virginia, May 24-28, 2002.

33. Particle Data Group, D. E. Groom *et al.*, Eur. Phys. J. C **15**, 1 (2000).

Frascati Physics Series Vol. XXVIII (2002), pp.209-219
HQ & L 2002 – Vietri s/m, May 27th - June 1st, 2002

SEMI-LEPTONIC AND WEAK-RADIATIVE DECAYS OF NEUTRAL HYPERONS. RECENT RESULTS AND EXPECTATIONS FOR THE NEAR FUTURE

Peter Marouelli
Institut für Physik, Johannes Gutenberg-Universität, 55099 Mainz, Germany

ABSTRACT

In recent years data samples from decays of neutral Hyperons have been collected by the KTeV experiment at Fermilab and the NA48 experiment at CERN. KTeV has observed the semi-leptonic decays $\Xi^0 \to \Sigma^+ e^- \bar{\nu}_e$ and $\Xi^0 \to \Sigma^+ \mu^- \bar{\nu}_\mu$ for the first time and published the branching ratio and the form factors for the first one. NA48 has started to analyse data from a 2001 test run and has found a few hundred events of the Ξ^0 beta decay. For the weak-radiative decays NA48 has found several hundred events for $\Xi^0 \to \Lambda\gamma$ and $\Xi^0 \to \Sigma^0\gamma$ in the data sample taken 1999. The asymmetry of $\Xi^0 \to \Lambda\gamma$ is under intensive study. KTeV has published an asymmetry and a branching ratio for the $\Xi^0 \to \Sigma^0\gamma$ decay. NA48/1 will continue the work of NA48 and will take an amount of data in 2002 which is one order of magnitude larger than KTeV.

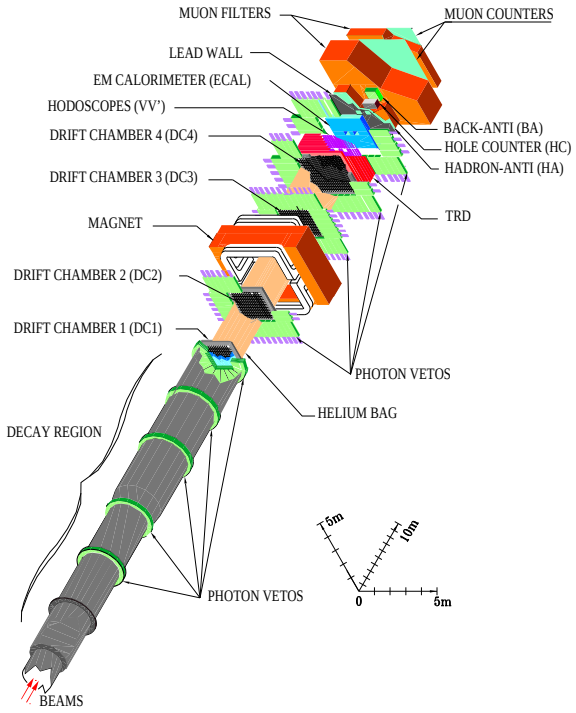

Figure 1: *The KTeV detector system (E799 configuration)*

1 The Experiments

The main purpose of both experiments was the measurement of the direct CP violation in neutral Kaon decays. Alongside this main purpose large samples of data on decays of neutral hyperons have been collected.

1.1 The KTeV Experiment

The KTeV experiment was located at the Fermi National Accelerator Laboratory using an 800 GeV proton beam from the Tevatron accelerator on a BeO target to produce neutral Kaons and Hyperons. The apparatus in the E799 configuration (vacuum beam) was used to observe rare K_L and hyperon decays in 1997 and 1999 [1)]. It consists of a charged particle spectrometer with two drift chambers upstream and two downstream of a spectrometer magnet, a CsI photon detector, a TRD (transition radiation detector) for electron and a

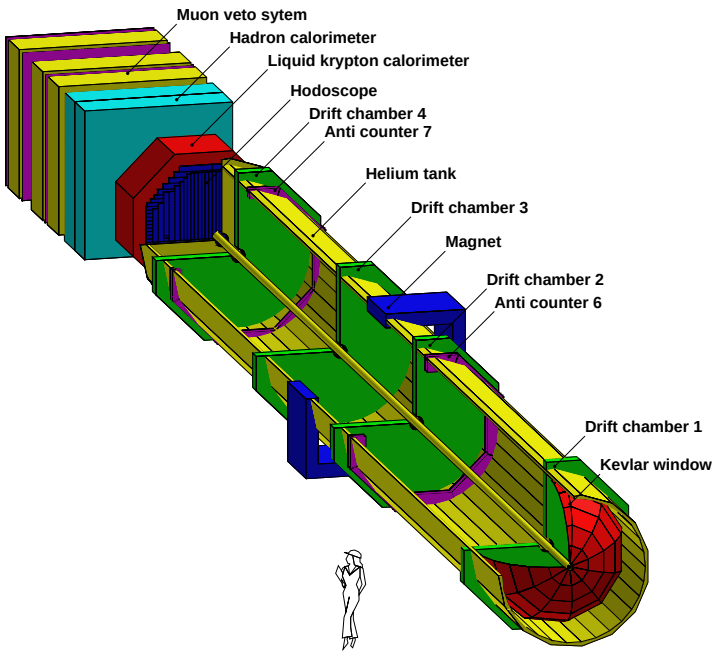

Figure 2: *The NA48 detector system*

muon detector for muon identification and several trigger hodoscopes and anticounters. The momentum resolution of the charged particle spectrometer is about 0.2% and the mass resolution less than 0.1 MeV/c^2. The photon detector consists of 3100 crystals of pure CsI with a position resolution of less than 1 mm. The average energy resolution of the system is better than 1% over most of the energy range of photons being detected. The TRD has a electron/pion rejection of 300 : 1 [2].

1.2 The NA48 Experiment

The NA48 experiment is located at CERN. Neutral Hyperons are produced together with K_S using a proton beam from the SPS accelerator onto a Be target. The proton energy has been lowered from 450 GeV in 1999 to 400 GeV for the data taken in 2001. The neutral Hyperons observed by NA48 are produced at the K_S target, so the data samples used for analyses are taken

during High Intensity K_S test runs in 1999 (48 hours) and 2001 (4 days).

The NA48 detector consists of a charged particle spectrometer, a liquid krypton electromagnetic calorimeter, a hadronic calorimeter, a muon detector, and trigger hodoscopes and anticounters. Like at KTeV the charged particles spectrometer consists of a spectrometer magnet and four driftchambers. The momentum resolution is better than 0.6%. The electromagnetic calorimeter contains 13500 cells of 2cm × 2cm size. The energy resolution was measured 1999 to be

$$\frac{\sigma(E)}{E} = \sqrt{\left(\frac{3.2\%}{\sqrt{E/\mathrm{GeV}}}\right)^2 + \left(\frac{0.090}{E/\mathrm{GeV}}\right)^2 + (0.4\%)^2} \qquad (1)$$

and the position resolution better than $5.4/\sqrt{E/\mathrm{GeV}}$ mm [3]. The hadron calorimeter is an iron sampling calorimeter. The muon detection system consists of three scintillator layers behind iron plates.

2 Semi-leptonic decays of the Ξ^0 hyperon

The matrix element M_0 for a semi-leptonic decay $A \to Bl\nu_l$ is given by [4]

$$M_0 = \frac{G_V}{\sqrt{2}}\bar{u}_B(W_\lambda^V + W_\lambda^A\gamma_5)u_A \times \bar{u}_e\gamma^\lambda(1+\gamma_5)v_\nu \qquad (2)$$

where

$$W_\lambda^V = f_1(q^2)\gamma_\lambda + \frac{f_2(q^2)}{M_A}\sigma_{\lambda\rho}q^\rho + \frac{f_3(q^2)}{M_A}q_\lambda \qquad (3)$$

$$W_\lambda^A = g_1(q^2)\gamma_\lambda + \frac{g_2(q^2)}{M_A}\sigma_{\lambda\rho}q^\rho + \frac{g_3(q^2)}{M_A}q_\lambda \qquad (4)$$

$$q_\lambda = (p_e + p_\nu)_\lambda = (p_A - p_B)_\lambda \qquad (5)$$

and G_V is a combination of the Fermi coupling constant and the corresponding CKM matrix element. f_1, f_2, g_1 and g_2 can be obtained by investigating the Ξ^0 beta decay, while f_3 and g_3 can only be measured in the $\Xi^0 \to \Sigma^+\mu^-\bar{\nu}_\mu$ channel because they are suppressed by a factor of m_l/M_A.

There are several predictions for the branching ratio and the form factors from the Cabibbo theory [5] ($SU(3)_f$) and attempts to break this symmetry, so from measurements information about the quality of these theories can be obtained.

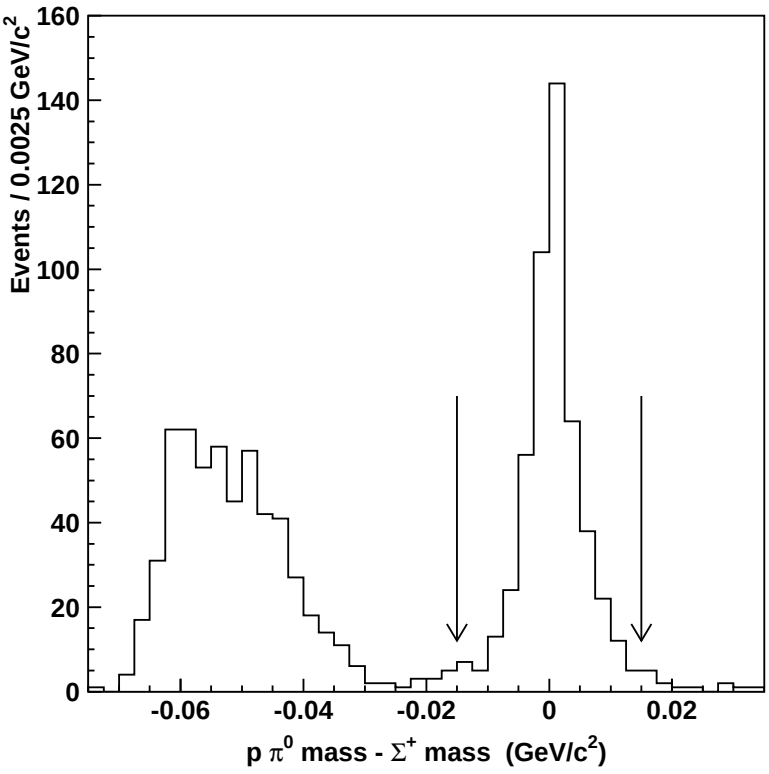

Figure 3: *The $\Sigma^+ \to p\pi^0$ mass peak from KTeV. The background on the left side is due to $\Xi^0 \to \Lambda\pi^0$ decays*

2.1 $\Xi^0 \to \Sigma^+ e^- \bar{\nu}_e$

This decay has been observed first by KTeV in the data taken 1997. In this data sample KTeV has found 626 events with a background of 60 ± 8 events. With these data a branching ratio of $(2.54 \pm 0.11 \pm 0.16) \times 10^{-4}$ has been obtained [2]. This value is still consistent with the prediction from exact $SU(3)_f$ symmetry, which is $(2.61 \pm 0.11) \times 10^{-4}$.

The KTeV collaboration has also published values for the form factor ratios g_1/f_1 and f_2/f_1 based on that data sample [6]. These are measured to

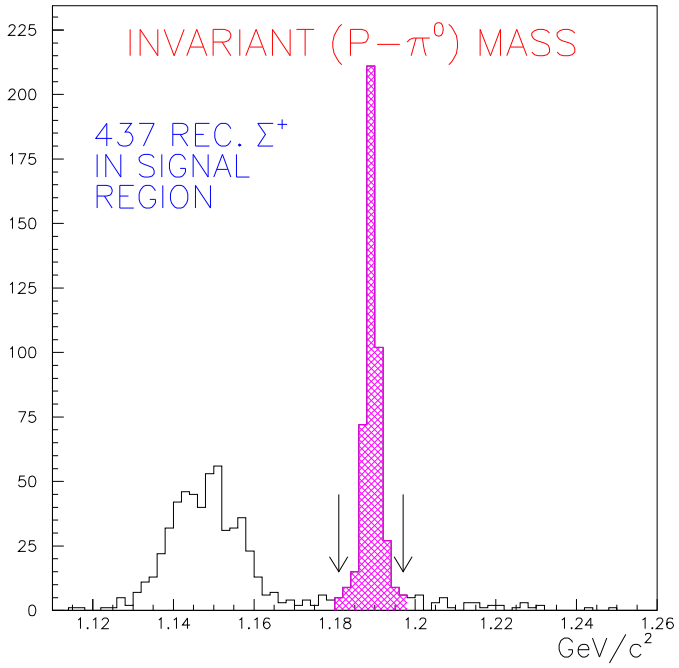

Figure 4: *The* $\Sigma^+ \to p\pi^0$ *mass peak from NA48.*

be

$$\frac{g_1}{f_1} = 1.32 \pm^{0.21}_{0.17_{\rm stat}} \pm 0.5_{\rm syst} \tag{6}$$

and

$$\frac{f_2}{f_1} = 2.0 \pm 1.2_{\rm stat} \pm 0.5_{\rm syst}. \tag{7}$$

These values are more consistent with the predictions from the Cabibbo theory than with the predictions from attempts to break the symmetry [7) 8)]. From the data taken 1999 the KTeV collaboration has also a sample of $\approx$ 2100 events $\Xi^0 \to \Sigma^+ e^- \nu_e$ but has so far not published any measurement based on that data sample.

NA48 has observed a preliminary number of 437 events $\Xi^0 \to \Sigma^+ e^- \nu_e$ in the data sample taken 2001. The Σ^+ mass peak is shown in Fig. 4. NA48 will continue to analyse these data and take more data in the dedicated High Intensity K_S experiment NA48/1 in 2002.

2.2 $\Xi^0 \to \Sigma^+ \mu^- \bar{\nu}_\mu$

This decay mode has also been observed for the first time in the KTeV data sample from 1997. With 5 events a branching ratio of $(3.5 \pm 1.5_{\text{stat}} \pm 0.8_{\text{syst}}) \times 10^{-6}$ has been obtained. In the data sample from 1999 approximately 10 final candidates were found [2].

With this decay a measurement of the form factors f_3 and g_3 is possible. For this task a few hundred events are needed, which may be the result of the efforts of NA48/1.

3 Weak radiative decays of the Ξ^0 hyperon

Weak radiative decays are a class of processes, which need all three fundamental interactions to occur. Therefore the theoretical models to describe these processes are the topic of controversial discussions for decades. Precise measurements of the decay asymmetries and branching ratios can be used to clarify the situation.

3.1 $\Xi^0 \to \Lambda\gamma$

At NA48 the analyses concentrate on the asymmetry in the $\Xi^0 \to \Lambda\gamma$ decay. The asymmetry is defined as a modification to the angular distribution of the emitted hadron in relation to the polarization of the original hadron. The situation is shown in Fig. 5. In principle the angular distribution of a polarized probe

$$\frac{dN}{d\cos\beta} = N_0(1 + \vec{P}_\Xi \cdot \hat{\Lambda}) = N_0(1 + \alpha_\Xi \cos\beta) \tag{8}$$

with the polarization vector $\vec{P}_\Xi$, the norm vector in direction of the emitted hadron $\hat{\Lambda}$ and the angle between the vectors β. For the NA48 experiment does not have a beam of polarized Ξ^0 hyperons, the consecutive decay $\Lambda \to p\pi^-$ is used to analyze the polarization. The Λ are emitted with the helicity α_Ξ. In the Λ rest frame this helicity is transferred to a polarization. Like the Ξ^0 decay the decay of the polarized Λ into p and π^- can be analyzed.

$$\frac{dN}{d\cos\Theta_\Lambda} = N_0(1 + \vec{P}_\Lambda \cdot \hat{p}) = N_0(1 + \alpha_\Lambda \alpha_\Xi \cos\Theta_\Lambda) \tag{9}$$

So in the Λ rest frame the combined asymmetry $\alpha_\Lambda \alpha_\Xi$ can be measured by measuring the angle between the emitted photon, which is equal to the direction

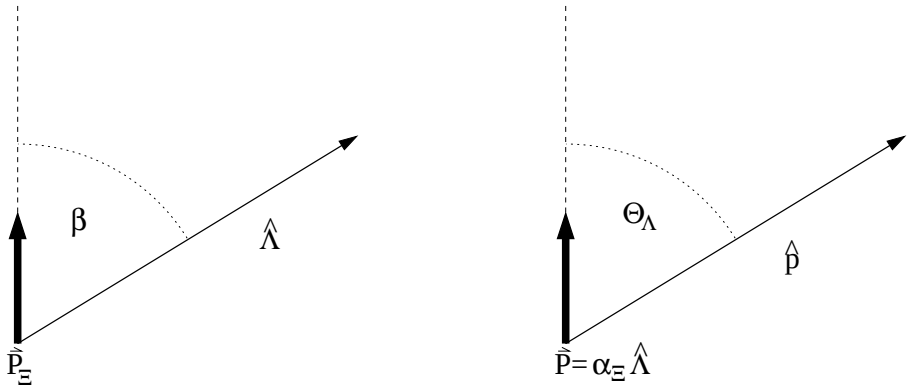

Figure 5: *Definition of the asymmetries in the* $\Xi^0 \to \Lambda\gamma$ *decay with* $\Lambda \to p\pi^-$

of the incoming Ξ^0, and the emitted proton. With the well known asymmetry [9] $\alpha_\Lambda = 0.642 \pm 0.013$ the asymmetry α_Ξ can be obtained.

To check this method, the well known asymmetry in the decay $\Xi^0 \to \Lambda\pi^0$ can be measured. The result [10] is consistent with the average value of previous mesurements $\alpha^{\rm PDG}_{\Xi^0\to\Lambda\pi^0} = -0.411 \pm 0.022$ [9]. A value for the asymmetry $\alpha_{\Xi^0\to\Lambda\gamma}$ will be published soon by the NA48 collaboration.

3.2 $\Xi^0 \to \Sigma^0\gamma$

For the decay $\Xi^0 \to \Sigma^0\gamma$ the KTeV collaboration has published a result for the asymmetry and the branching ratio [11]. The branching ratio was measured to be

$$\mathrm{BR}(\Xi^0 \to \Sigma^0\gamma) = (3.34 \pm 0.05_{\rm stat} \pm 0.09_{\rm syst}) \times 10^{-3} \qquad (10)$$

and the asymmetry parameter, which is defined the same way as in the decay $\Xi^0 \to \Lambda\gamma$, a value of

$$\alpha_{\Xi^0\to\Sigma^0\gamma} = -0.63 \pm 0.09 \qquad (11)$$

is published. These results are based on a data sample with 4045 signal events over an irreducible background of 804 events of the type $\Xi^0 \to \Lambda\pi^0$.

NA48 has found 380 signal events over 50 background events in the data sample taken 1999 (Fig. 6). The data taken 2001 are still analyzed.

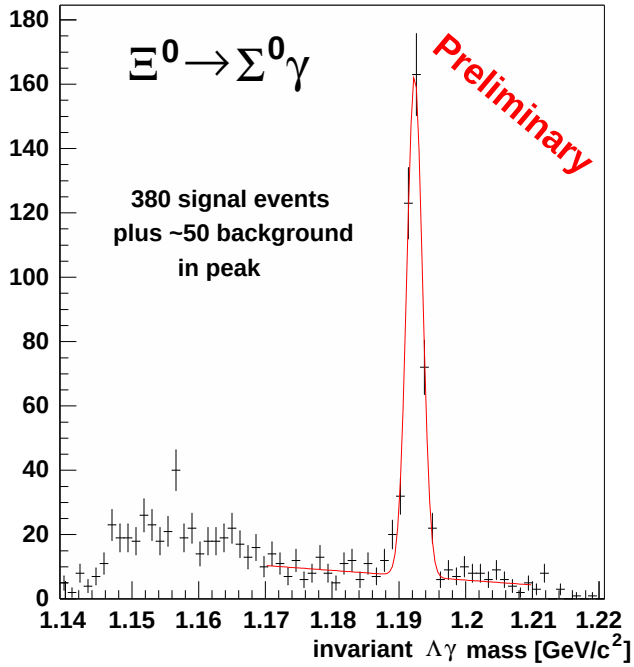

Figure 6: *Mass peak of the* Σ^0 *hyperons from the electromegnetic* $\Sigma^0 \to \Lambda\gamma$ *decay following a* $\Xi^0 \to \Sigma^0\gamma$ *decay observed by the NA48 experiment.*

4 Future Prospects with NA48/1

In 2002 the NA48/1 experiment will continue the work of NA48. NA48/1 is a dedicated K_S experiment, where also large amounts of hyperon data will be collected. The intensity of the proton beam will be increased to 400 times of the standard K_S intensity [12].

4.1 The Detector upgrade

To stand the expected data rate the detector and data acquisition systems have been upgraded.

The trigger system has been adjusted with special triggers for rare Kaon and Hyperon decays instead of the triggers used for the direct CP violation measurement. The readout of the electromagnetic calorimeter has been modi-

fied. The zero suppression, which was one of the bottlenecks has been moved from the front-end electronics to the DAQ PC farm to achieve a higher data rate. The network structure has been improved to get a better data throughput. Also a new system to pack two events of the electromagnetic calorimeter into one before sending it over the network has been implemented and tested. For the charged particle spectrometer a completely new readout has been developed, tested in 2001 and installed during the winter. For the data rate is expected to be much higher than in 2001 not all rawdata can be stored on tape. To reduce the amount of data, new filters for the third stage of the trigger system, the level 3 software filter, have been implemented and tested. Compared to the test in 2001 twice the trigger rate is expected.

4.2 Expectations for Data amounts

The high statistics will improve the measurements of the decays already considered and will allow new searches [13].

For both weak-radiative decays some 10^5 events are expected. With this data sample the branching ratios could be improved achieving a global error below 5%. It should also be possible to measure the asymmeties with an accuracy of the order of 15%.

For the beta decay 25000 events could be collected for a new consistency check of the $SU(3)_f$ symmetry and the Cabibbo model in hyperon decays. Also a new measurement of the Cabibbo angle should be possible. For the muonic channel $\Xi^0 \to \Sigma^+ \mu^- \bar{\nu}_\mu$ a few hundred events are expected. This would allow a measurement of the form factors f_3 and g_3.

The $\Delta S = 2$ transition $\Xi^0 \to p\pi^-$ has a present limit on the branching ratio of $4 \cdot 10^{-5}$ at 90% CL. This could be improved by at least a factor of 100.

5 Acknowledgements

I would like to thank Eric Ramberg from the KTeV collaboration for providing me with information about the results from KTeV.

References

1. D. A. Jensen, Weak Radiative Neutral Hyperon Decays in KTeV, Nuclear Physics B(Proc. Suppl.) 93 (2001) 22-25

2. Nickolas Solomey, Semi-leptonic, Weak-radiative and FCNC Decays of Hyperons and Kaons as a Window into Fundamental Processes, CERN Seminar, 15th October 2001.

3. A. Lai *et al.*, A precise measurement od the direct CP violation parameter Re(ε'/ε), Eur. Phys. J. C 22, 231-254 (2001)

4. A. Garcia and P. Kielanowski, The Beta Decay of Hyperons, Lecture Notes in Physics Vol. 222 (Springer-Verlag, Berlin, 1985).

5. N. Cabibbo, Phys. Rev. Lett. 10, 531 (1963)

6. A. Alavi-Harati *et al.*, First Measurement of Form Factors of the Decay $\Xi^0 \to \Sigma^+ e^- \bar{\nu}_e$, Phys. Rev. Lett. 87, 13, September 2001

7. P.G. Ratcliffe, Phys. Rev. D 59, 014038 (1999)

8. R. Flores-Mendieta *et al.*, Phys. Rev. D 58, 094028 (1998)

9. D.E. Groom *et al.* (Particle Data Group), Eur. Phys. J. C 15, 1-878 (2000)

10. Sven A. Schmidt, Die Zerfallsasymmetrie des radiativen Hyperonzerfalls $\Xi^0 \to \Lambda\gamma$, PhD thesis, Mainz, 2002 (in german)

11. A. Alavi-Harati *et al.*,A Measurement of the Branching Ratio and Asymmetry of the Decay $\Xi^0 \to \Sigma^0\gamma$, Phys. Rev. Let. 86, 3239-3243 (2001)

12. R. Fantechi, Future NA48 programs for hyperon rare decays and CP violation measurements, Nuclear Physics B(Proc. Suppl.) 93 (2001) 26-29

13. U. Koch, Future NA48 programs for hyperon rare decays and CP violation measurements, KEK Proceedings 2001-23, January 2002, 191-206

Frascati Physics Series Vol. XXVIII (2002), pp.223-244
HQ & L 2002 – Vietri s/m, May 27th - June 1st, 2002

RARE DECAYS OF B, D AND K MESONS

Gino Isidori
Theory Division, CERN, CH-1211 Geneva 23, Switzerland
INFN, Lab. Naz. di Frascati, Via E. Fermi 40, I-00044 Frascati, Italy

ABSTRACT

We present an overview of rare K, D and B decays. Particular attention is devoted to those flavour-changing neutral-current processes of K and B mesons that offer the possibility of new significant tests of the Standard Model. The sensitivity of these modes to physics beyond the Standard Model and the status of their experimental study are also discussed.[1]

1 Introduction

Why are we interested in rare decays? As a general rule, rare processes are particularly interesting when their suppression is associated to some, hopefully broken, conservation law. The most significant examples in this respect are

[1] Most of the material presented in these proceedings can also be found in Ref. 1.

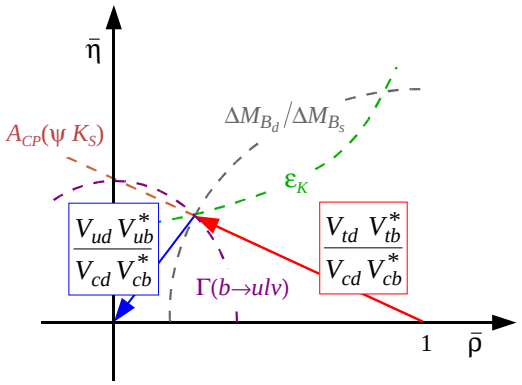

Figure 1: *Definition of the reduced CKM unitarity triangle, with the indication of the most significant experimental constraints currently available.*

proton decay and $\mu \to e\gamma$: processes completely forbidden within the Standard Model (SM) that, if observed, would represent an invaluable step forward in our understanding of fundamental interactions.

Conservation laws that so far appear unbroken can also be tested by means of heavy mesons. However, the most interesting perspectives in rare K, D and B decays are probably those opened by precision studies of flavour-changing neutral currents (FCNCs), or transitions of the type

$$q_i \to q_j + \begin{cases} \nu\bar{\nu} \\ \ell^+\ell^- \\ \gamma \end{cases} \qquad (1)$$

These processes are not completely forbidden within the SM, but are generated only at the quantum level because of the Glashow–Iliopoulos–Maiani (GIM) mechanism, and are additionally suppressed by the hierarchical structure of the Cabibbo–Kobayashi–Maskawa (CKM) matrix. FCNCs are thus particularly well suited to study the dynamics of quark-flavour mixing, within and beyond the SM. As a matter of fact, some of these processes (such as $K_L \to \mu^+\mu^-$) have played an important role in the historical formulation of the SM.

As discussed by many speakers at this conference, the CKM mechanism of quark-flavour mixing is in good agreement with all data available at present. The recent measurements of CP violation in the B_d system add a new piece of information that fits remarkably within the overall picture. One could therefore doubt about the need for new tests of the SM in the sector of (quark) flavour physics. However, there are at least two arguments why the present status

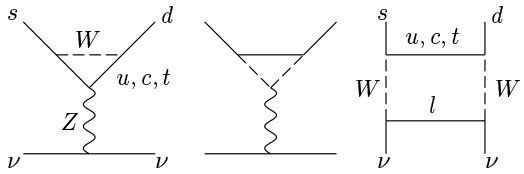

Figure 2: *One-loop diagrams contributing to the $s \to d\nu\bar{\nu}$ transition.*

cannot be considered conclusive and a deeper study of FCNCs is very useful:

- The information used at present to constrain the CKM matrix and, in particular, the unitarity triangle, is obtained only from charged currents (i.e. from tree-level amplitudes) and $\Delta F = 2$ loop-induced processes (see Fig. 1). In principle, rare K and B decays mediated by FCNCs could also be used to extract indirect information on the unitarity triangle. However, either because of experimental difficulties or because of theoretical problems, the quality of this information is very poor at present, with at least $\mathcal{O}(100\%)$ uncertainties. Since new physics could affect in a very different way $\Delta F = 2$ and $\Delta F = 1$ loop-induced amplitudes [e.g. with $\mathcal{O}(100\%)$ effects in the former and $\mathcal{O}(10\%)$ in the latter], it is mandatory to improve the quality of the FCNC information.

- Most of the observables used in the present fits, such as ϵ_K, $\Gamma(b \to u\ell\bar{\nu})$ or ΔM_{B_d}, suffer from irreducible theoretical errors at the 10% level (or above). In the perspective of reaching a high degree of precision, it would be desirable to base these fits only on observables with theoretical errors at the percent level (or below), such as the CP asymmetry in $B \to J/\Psi K_S$. As we shall see, a few rare K and B decays could offer this opportunity.

Motivated by the above arguments, most of this talk is devoted to K and B decays that offer the possibility of precision FCNC studies.

2 FCNCs in K decays: the golden $K \to \pi\nu\bar{\nu}$ modes

The $s \to d\nu\bar{\nu}$ transition is one of the rare examples of weak processes whose leading contribution starts at $\mathcal{O}(G_F^2)$. At the one-loop level it receives contributions only from Z-penguin and W-box diagrams, as shown in Fig. 2, or from pure quantum electroweak effects. Separating the contributions to the one-loop amplitude according to the intermediate up-type quark running inside the loop,

we can write

$$\mathcal{A}(s \to d\nu\bar{\nu}) = \sum_{q=u,c,t} V_{qs}^* V_{qd} \mathcal{A}_q \sim \begin{cases} \mathcal{O}(\lambda^5 m_t^2) + i\mathcal{O}(\lambda^5 m_t^2) & (q=t) \\ \mathcal{O}(\lambda m_c^2) + i\mathcal{O}(\lambda^5 m_c^2) & (q=c) \\ \mathcal{O}(\lambda \Lambda_{\rm QCD}^2) & (q=u) \end{cases} \qquad (2)$$

where V_{ij} denote the elements of the CKM matrix. The hierarchy of these elements would favour up- and charm-quark contributions; however, the *hard* GIM mechanism of the perturbative calculation implies $\mathcal{A}_q \sim m_q^2/M_W^2$, leading to a completely different scenario. As shown on the r.h.s. of (2), where we have employed the standard CKM phase convention ($\Im V_{us} = \Im V_{ud} = 0$) and expanded the V_{ij} in powers of the Cabibbo angle ($\lambda = 0.22$), the top-quark contribution dominates both real and imaginary parts. This structure implies several interesting consequences for $\mathcal{A}(s \to d\nu\bar{\nu})$:

a. it is dominated by short-distance dynamics, therefore its QCD corrections are small and calculable in perturbation theory;

b. it is very sensitive to V_{td}, which is one of the less constrained CKM matrix elements;

c. it is likely to have a large CP-violating phase;

d. it is very suppressed within the SM and thus very sensitive to possible new sources of quark-flavour mixing.

Short-distance contributions to $\mathcal{A}(s \to d\nu\bar{\nu})$, within the SM, can efficiently be described by means of a single effective dimension-6 operator:

$$Q_L^\nu = \bar{s}_L \gamma^\mu d_L \; \bar{\nu}_L \gamma_\mu \nu_L \; . \qquad (3)$$

Perturbative corrections to the Wilson coefficient of Q_L^ν have been calculated to high precision, [2] leading to a very accurate description of the partonic amplitude. In addition, the simple structure of Q_L^ν has two important advantages:

- The relation between partonic and hadronic amplitudes is quite accurate, since hadronic matrix elements of the $\bar{s}\gamma^\mu d$ current between a kaon and a pion are related by isospin symmetry to those entering K_{l3} decays, which are experimentally well known.

- The lepton pair is produced in a state of definite CP and angular momentum, implying that the leading SM contribution to $K_L \to \pi^0 \nu\bar{\nu}$ is CP-violating.

2.1 SM uncertainties

The dominant theoretical error in estimating the $K^+ \to \pi^+\nu\bar{\nu}$ rate is due to the subleading, but non-negligible charm contribution. Perturbative NNLO corrections in the charm sector have been estimated [2] to induce an error in the total rate of around 10%, which can be translated into a 5% error in the determination of $|V_{td}|$ from $\mathcal{B}(K^+ \to \pi^+\nu\bar{\nu})$. Recently, also non-perturbative effects introduced by the integration over charmed degrees of freedom have been analysed [3] and turns out to be within the error of NNLO terms. Finally, genuine long-distance effects associated to light-quark loops have been shown [4] to be negligible with respect to the uncertainties from the charm sector.

The case of $K_L \to \pi^0\nu\bar{\nu}$ is even cleaner from the theoretical point of view. Because of the CP structure, only the imaginary parts in (2) –where the charm contribution is absolutely negligible– contribute to $\mathcal{A}(K_2 \to \pi^0\nu\bar{\nu})$. Thus the dominant direct-CP-violating component of $\mathcal{A}(K_L \to \pi^0\nu\bar{\nu})$ is completely saturated by the top contribution, where QCD corrections are suppressed and rapidly convergent. Intermediate and long-distance effects in this process are confined only to the indirect-CP-violating contribution and to the CP-conserving one, which are both extremely small. [5] Taking into account the isospin-breaking corrections to the hadronic matrix element, [6] we can write an expression for the $K_L \to \pi^0\nu\bar{\nu}$ rate in terms of short-distance parameters, namely [2]

$$\begin{aligned}\mathcal{B}(K_L \to \pi^0\nu\bar{\nu})_{\rm SM} &= 4.16 \times 10^{-10} \\ &\times \left[\frac{\overline{m}_t(m_t)}{167\ {\rm GeV}}\right]^{2.30} \left[\frac{\Im(V_{ts}^* V_{td})}{\lambda^5}\right]^2 , \end{aligned} \tag{4}$$

which has a theoretical error below 3%.

The high accuracy of the theoretical predictions of $\mathcal{B}(K^+ \to \pi^+\nu\bar{\nu})$ and $\mathcal{B}(K_L \to \pi^0\nu\bar{\nu})$ in terms of modulus and phase of $\lambda_t = V_{ts}^* V_{td}$ clearly offers the possibility of very interesting tests of the CKM mechanism. A measurement of both channels would provide two independent pieces of information on the unitarity triangle, or a determination of $\bar{\rho}$ and $\bar{\eta}$. At present the SM predictions of the two $K \to \pi\nu\bar{\nu}$ rates are not extremely precise owing to the limited knowledge of λ_t. Taking into account all the indirect constraints, the allowed range is given by [2, 7]

$$\mathcal{B}(K^+ \to \pi^+\nu\bar{\nu})_{\rm SM} = (0.72 \pm 0.21) \times 10^{-10} \tag{5}$$

$$\mathcal{B}(K_L \to \pi^0\nu\bar{\nu})_{\rm SM} = (0.28 \pm 0.11) \times 10^{-10} \tag{6}$$

2.2 Beyond the SM: general considerations

As far as we are interested only in rare FCNC transitions, we can roughly distinguish the extensions of the SM into two big categories:

- *Models with minimal flavour violation*, or models where the only source of quark-flavour mixing is the CKM matrix (e.g. the two-Higgs-doublet model of type II, the constrained minimal supersymmetric SM, etc.). In this case non-standard contributions are severely limited by the constraints from electroweak data. However, we stress that the high-precision obtained by LEP and SLC at the Z peak (typically at the per mille level), refers to observables that receive tree-level contributions within the SM. The accuracy on the pure quantum electroweak effects barely reaches the 10% level. Thus even within this constrained scenario one can expect deviations at the 10%–30% level in observables such as $K \to \pi\nu\bar{\nu}$ rates. Detailed calculations performed within the flavour-constrained MSSM confirm this expectation. [8] In principle these effects could be detected, since they are above the intrinsic theoretical errors.

- *Models with new sources of quark-flavour mixing*, such as generic SUSY extensions of the SM, models with new generations of quarks, etc. On general grounds this category is the most natural one, since we expect some mechanism beyond the SM to be responsible for the observed flavour structure. Indeed the case of minimal flavour violation can be considered as a particular limit of this general category: the limit where the new sources of quark-flavour mixing appear only well above the electroweak scale.
  FCNCs could be dramatically affected by the presence of new sources of quark-flavour mixing, if the latter leads to overcoming the strong CKM hierarchy. This effect is potentially more pronounced in rare FCNC kaon decays, where the CKM structure implies an $\mathcal{O}(\lambda^5)$ suppression of the leading amplitude, than in B decays. This naive expectation is indeed explicitly realized in specific and consistent frameworks. In particular, within the non-constrained MSSM it is found [9] that $\mathcal{B}(K_L \to \pi^0\nu\bar{\nu})$ and/or $\mathcal{B}_{\mathrm{CPV-dir}}(K_L \to \pi^0 e^+ e^-)$ (to be defined later) could be enhanced over SM expectations up to one order of magnitude.

2.3 Experimental results and impact in the unitarity plane

The search for processes with missing energy and branching ratios below 10^{-10} is definitely a very difficult challenge, but has been proved not to be impossible. A strong evidence of $K^+ \to \pi^+\nu\bar{\nu}$ has been obtained by the E787 experiments at BNL, where two clean candidates have been observed. [10] The branching

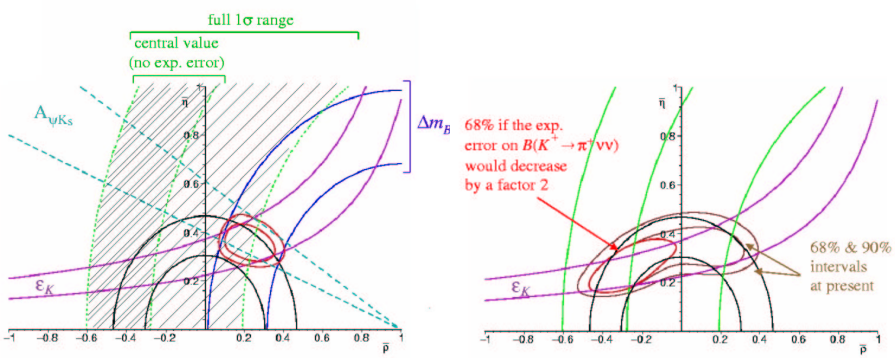

Figure 3: *Present impact of $K^+ \to \pi^+ \nu\bar{\nu}$ in the unitarity plane. The fit on the right panel do not include B_d–$\bar{B}_d$ data.* [7]

ratio inferred from this result is

$$\mathcal{B}(K^+ \to \pi^+ \nu\bar{\nu}) = \left(1.57 \,^{+\,1.75}_{-\,0.82}\right) \times 10^{-10} \ . \tag{7}$$

Although still compatible within the errors, the difference between the central values in Eqs. (7) and (5) opens interesting perspectives, as shown in Fig. 3. [7] The intriguing aspect of the central value in Eq. (7) is that is perfectly compatible with $\bar{\rho}$ and $\bar{\eta}$ constraints on ϵ_K and $|V_{ub}|$, but it favours a solution with $\bar{\eta} < 0$, which is in contradiction with $\Delta B = 2$ data. Thus the large central value of $\mathcal{B}(K^+ \to \pi^+ \nu\bar{\nu})$ is not necessarily a hint of new physics in the $s \to \nu\bar{\nu}$ amplitude, it could also be a hint of new physics in B_d–$\bar{B}_d$ mixing. This fascinating scenario will be explored by the upgrade of the the E787 experiment (BNL-E949) which, in three years of data taking, should collect about 10 events, at the SM rate, or about 20 events if the true rate coincides with the central value in Eq. (7).

Unfortunately the progress concerning the $K_L \to \pi^0 \nu\bar{\nu}$ is much slower. No dedicated experiment has started yet (contrary to the K^+ case) and the best direct limit is more than four orders of magnitude above the SM expectation. [11]

3 $K \to \pi\ell^+\ell^-$ and $K \to \ell^+\ell^-$

Similarly to $K \to \pi\nu\bar{\nu}$, short-distance contributions to $K \to \pi\ell^+\ell^-$ and $K \to \ell^+\ell^-$ are calculable with high accuracy and are highly sensitive to modulus and phase of λ_t. However, in these processes the size of long-distance contributions is usually much larger because of electromagnetic interactions. Only

in few cases (mainly in CP-violating observables) are long-distance contributions suppressed and is it then possible to extract the interesting short-distance information.

3.1 $K \to \pi\ell^+\ell^-$

Contrary to the $s \to \nu\bar{\nu}$ case, the GIM mechanism of the $s \to d\gamma^*$ amplitude is only logarithmic. As a result, the $K \to \pi\gamma^* \to \pi\ell^+\ell^-$ amplitude is completely dominated by long-distance dynamics and provides a large contribution to the CP-allowed transitions $K^+ \to \pi^+\ell^+\ell^-$ and $K_S \to \pi^0\ell^+\ell^-$. [12] This amplitude can be described in a model-independent way in terms of two form factors, $W_+(z)$ and $W_S(z)$, defined by [13]

$$i\int d^4x e^{iqx}\langle\pi|T\left\{J^\mu_{\rm em}(x)\mathcal{L}_{\Delta S=1}(0)\right\}|K_i\rangle\frac{W_i(z)}{(4\pi)^2}\left[z(p_K+p_\pi)^\mu-(1-r_\pi^2)q^\mu\right]\ ,$$

where $q = p_K - p_\pi$, $z = q^2/M_K^2$ and $r_\pi = M_\pi/M_K$. The two form factors are non singular at $z = 0$ and, because of gauge invariance, vanish to lowest order in chiral perturbation theory (CHPT). [12] Beyond lowest order two separate contributions to $W_i(z)$ can be identified: a non-local term, $W_i^{\pi\pi}(z)$, due to the $K \to 3\pi \to \pi\gamma^*$ scattering, and a local term, $W_i^{\rm pol}(z)$, which encodes the contributions of unknown low-energy constants (to be determined by data). At $\mathcal{O}(p^4)$ the local term is simply a constant, whereas at $\mathcal{O}(p^6)$ also a linear slope in z arises. Note that already at $\mathcal{O}(p^4)$ chiral symmetry alone does not help to relate W_S and W_+, or K_S and K^+ decays. [12]

Recent results on $K^+ \to \pi^+e^+e^-$ and $K^+ \to \pi^+\mu^+\mu^-$ by BNL-E865 [14] indicates very clearly that, owing to a large linear slope, the $\mathcal{O}(p^4)$ expression of $W_+(z)$ is not accurate enough. This should not be considered as a failure of CHPT, rather as an indication that large $\mathcal{O}(p^6)$ contributions are present in this channel. Indeed the $\mathcal{O}(p^6)$ expression of $W_+(z)$ seems to fit the data well. Interestingly, this is not only due to a new free parameter appearing at $\mathcal{O}(p^6)$, but it is also due to the presence of the non-local term. The evidence of the latter provides a really significant test of the CHPT approach.

Knowing $W_+(z)$, we can make reliable predictions about the CP-violating asymmetry between $K^+ \to \pi^+\ell^+\ell^-$ and $K^- \to \pi^-\ell^+\ell^-$ distributions. This asymmetry is generated by the interference between the absorptive contribution of $W_+(z)$ and the CP-violating phase of the $s \to d\ell^+\ell^-$ amplitude, dominated by short-distance dynamics. The integrated asymmetry for $M_{\ell^+\ell^-} \geq 2M_\pi$ is around 10^{-4}, within the SM, for both electron and muon modes. [13, 16] A measurement at the 10% level, consistent with zero, has recently been reported by the HyperCP Collaboration at Fermilab. [15] In the near future significant improvements can be expected by the charged-kaon extension of the NA48

experiment at CERN, although the sensitivity is likely to remain very far from SM expectations.

Similarly, also $K_S \to \pi^0\ell^+\ell^-$ decays are dominated by long-distance dynamics; however, in this case non-local terms are very suppressed. To a good approximation, the $K_S \to \pi^0 e^+e^-$ rate can be written as

$$\mathcal{B}(K_S \to \pi^0 e^+e^-) = 5 \times 10^{-9} \times a_S^2 \tag{8}$$

where a_S, defined by $W_S^{\rm pol}(0) = G_F m_K^2 a_S$, is expected to be $\mathcal{O}(1)$. The recent bound [17] $\mathcal{B}(K_S \to \pi^0 e^+e^-) < 1.4\times10^{-7}$ is still one order of magnitude above the most optimistic expectations, but a measurement or a very stringent bound on $|a_S|$ will soon arise from the K_S-dedicated run of NA48 and/or from KLOE at Frascati.

Apart from its intrinsic interest, the determination of $\mathcal{B}(K_S \to \pi^0 e^+e^-)$ has important consequences on the $K_L \to \pi^0 e^+e^-$ mode. Here the long-distance part of the single-photon exchange amplitude is forbidden by CP invariance and the sensitivity to short-distance dynamics in enhanced. The direct-CP-violating part of the $K_L \to \pi^0\ell^+\ell^-$ amplitude is conceptually similar to the one of $K_L \to \pi^0\nu\bar{\nu}$: it is calculable with high precision, being dominated by the top-quark contribution, [18] and is highly sensitive to non-standard dynamics. [9] This amplitude interfere with the indirect-CP-violating contribution induced by K_L–K_S mixing, leading to [13]

$$\mathcal{B}(K_L \to \pi^0 e^+e^-)_{\rm CPV} = 10^{-12}\times\left[15.3 a_S^2 \pm 6.8\frac{\Im\lambda_t}{10^{-4}}|a_S| + 2.8\left(\frac{\Im\lambda_t}{10^{-4}}\right)^2\right] \tag{9}$$

where the $\pm$ depends on the relative sign between short- and long-distance contributions, and cannot be determined in a model-independent way. Given the present uncertainty on $\mathcal{B}(K_S \to \pi^0 e^+e^-)$, at the moment we can only set a rough upper limit of 5.4×10^{-10} on the sum of all the CP-violating contributions to this mode, to be compared with the direct limit of 5.6×10^{-10} obtained by KTeV at Fermilab. [20]

An additional contribution to $K_L \to \pi^0\ell^+\ell^-$ decays is generated by the CP-conserving long-distance processes $K_L \to \pi^0\gamma\gamma \to \pi^0\ell^+\ell^-$. This amplitude does not interfere with the CP-violating one, and recent data on $K_L \to \pi^0\gamma\gamma$ (at small dilepton invariant mass) by NA48 indicate that it is very suppressed, with an impact on $\mathcal{B}(K_L \to \pi^0 e^+e^-)$ at the level of few$\times10^{-12}$ at most. [19]

At the moment there exist no definite plans to improve the KTeV bound on $\mathcal{B}(K_L \to \pi^0 e^+e^-)$. The future information on $\mathcal{B}(K_S \to \pi^0 e^+e^-)$ will play a crucial role in this respect: if a_S were in the range that maximizes the interference effect in (9), we believe it would be worths while to start a dedicated program to reach sensitivities of 10^{-12}.

3.2 $K_L \to \ell^+\ell^-$

Both $K_L \to \mu^+\mu^-$ and $K_L \to e^+e^-$ decays are dominated by the two-photon long-distance amplitude. The absorptive part of the latter is determined to good accuracy by the two-photon discontinuity and is calculable with high precision in terms of the $K_L \to \gamma\gamma$ rate. On the other hand, the dispersive contribution of the two-photon amplitude is a source of considerable theoretical uncertainties.

In the $K_L \to e^+e^-$ mode the dispersive integral is dominated by a large infrared logarithm [$\sim \ln(m_K^2/m_e^2)$], the coupling of which can be determined in a model-independent way from $\Gamma(K_L \to \gamma\gamma)$. As a result, $\Gamma(K_L \to e^+e^-)$ can be estimated with good accuracy [21] but is almost insensitive to short-distance dynamics.

The $K_L \to \mu^+\mu^-$ mode is certainly more interesting from the short-distance point of view. Here the two-photon long-distance amplitude is not enhanced by large logs and is almost comparable in size with the short-distance one, [2] sensitive to $\Re\lambda_t$. Actually short- and long-distance dispersive parts cancel each other to a good extent, since the total $K_L \to \mu^+\mu^-$ rate (measured with high precision by BNL-E871 [22]) is almost saturated by the absorptive two-photon contribution: [23]

$$\begin{aligned}
\mathcal{B}(K_L \to \mu^+\mu^-)^{\rm exp} &= (7.15 \pm 0.16) \times 10^{-9} \\
\mathcal{B}(K_L \to \mu^+\mu^-)^{\rm abs}_{2\gamma} &= \alpha^2 f\left(\frac{m_\mu}{m_K}\right) \mathcal{B}(K_L \to \gamma\gamma) = (7.00 \pm 0.18) \times 10^{-9}
\end{aligned}$$

The accuracy on which we can bound the two-photon dispersive integral determines the accuracy of possible bounds on $\Re\lambda_t$. A partial control of the $K_L \to \gamma^*\gamma^*$ form factor, which rules the dispersive integral, can be obtained by means of $K_L \to \gamma\ell^+\ell^-$ and $K_L \to e^+e^-\mu^+\mu^-$ spectra; additional constraints can also be obtained from model-dependent hadronic ansatze and/or perturbative QCD. [24, 25] Combining this information, significant upper bounds on $\Re\lambda_t$ (or lower bounds on $\bar\rho$) have recently been obtained, as shown in Fig. 4. The reliability of these bounds has still to be fully investigated, but some progress can be expected in the near future. The recent clarification of the discrepancy between $K_L \to \gamma e^+e^-$ and $K_L \to \gamma\mu^+\mu^-$ data in the extraction of the form factor is certainly an important step forward in this direction. [26] On the theoretical side, the extrapolation of the form factor in the high-energy region, which so far requires model-dependent assumptions, could possibly be limited by means of lattice calculations.

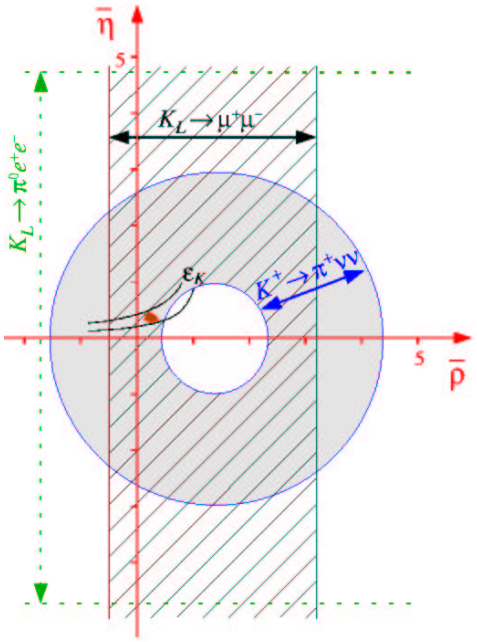

Figure 4: Present constraints in the $\bar{\rho}$–$\bar{\eta}$ plane from rare K decays (see text). The small dark region close to the origin denotes the constraints from B-physics and ϵ_K (see Fig. 1).

4 FCNCs in B decays: generalities

Inclusive rare B decays such as $B \to X_s\gamma$, $B \to X_s\ell^+\ell^-$ and $B \to X_s\nu\bar{\nu}$ are the natural framework for high-precision studies of FCNCs in the $\Delta B = 1$ sector. [27] Perturbative QCD and heavy-quark expansion [28] form a solid theoretical framework to describe these processes: inclusive hadronic rates are related to those of free b quarks, calculable in perturbation theory, by means of a systematic expansion in inverse powers of the b-quark mass.

The starting point of the perturbative partonic calculation is the determination of a low-energy effective Hamiltonian, renormalized at a scale $\mu = \mathcal{O}(m_b)$, obtained by integrating out the heavy degrees of freedom of the

theory. For $b \to s$ transitions –within the SM– this can be written as

$$\mathcal{H}_{\rm eff} = -\frac{G_F}{\sqrt{2}} V_{ts}^* V_{tb} \sum_{i=1}^{10,\ \nu} C_i(\mu) Q_i + \text{h.c.} \tag{10}$$

where $Q_{1\ldots6}$ are four-quark operators, Q_8 is the chromomagnetic operator,

$$Q_7 = \frac{e}{4\pi^2} \bar{s}_L \sigma_{\mu\nu} m_b b_R F^{\mu\nu} \tag{11}$$

$$Q_9 = \frac{e^2}{4\pi^2} \bar{s}_L \gamma^\mu b_L \bar{\ell} \gamma_\mu \ell \tag{12}$$

$$Q_{10} = \frac{e^2}{4\pi^2} \bar{s}_L \gamma^\mu b_L \bar{\ell} \gamma_\mu \gamma_5 \ell \tag{13}$$

and Q_ν is the $b \to s$ analogue of Q_L^ν in Eq. (3). Within the SM, the coefficients of all the FCNC operators (Q_7, Q_9, Q_{10} and Q_ν) receive a large non-decoupling contribution from top-quark loops at the electroweak scale. Nonetheless, the m_t dependence is not the same for all the operators, reflecting a different $SU(2)_L$-breaking structure, which can be affected in a rather different way by new-physics contributions.

The calculation of partonic rates then involves three distinct steps: i) the determination of the initial conditions of the Wilson coefficients at the electroweak scale; ii) the evolution by means of renormalization-group equations (RGEs) of the C_i down to $\mu = \mathcal{O}(m_b)$; iii) the evaluation of the QCD corrections to the matrix elements of the effective operators at $\mu = \mathcal{O}(m_b)$. The interesting short-distance dynamics that we would like to test enters only in the first step; however, the following two steps are fundamental ingredients to reduce and control the theoretical error. The status of these steps for the three main channels can be summarized as follows:

- $\underline{b \to s\gamma}$ As anticipated, QCD corrections play an important role in $b \to s\gamma$: the large logarithms generated by the mixing of four-quark operators with Q_7 enhance the partonic rate by a factor of almost three. Since the mixing of Q_7 with $Q_{1\ldots6}$ vanishes at the one-loop level, in this case a full treatment of QCD corrections beyond leading logarithms is a rather non-trivial task. This has been achieved thanks to the joint effort of several groups. [27] The only part of the SM calculation which has been performed by a single collaboration only is the three-loop mixing of Q_7 and $Q_{1\ldots6}$ (notably the most difficult step of the whole calculation). [29]

- $\underline{b \to s\ell^+\ell^-}$ Since Q_9 mixes with four-quark operators already at the one-loop level, in this case QCD corrections are even more important than for $b \to s\gamma$. This fact facilitates the NLO calculation, but enhances the relative importance of NNLO corrections. The latter have recently become

available for the initial conditions and (part of) the matrix elements. [30] Interestingly, the impact of QCD corrections is very limited in the axial-current operator Q_{10}, which also contributes to $b \to s\ell^+\ell^-$. This operator does not mix with four-quark operators and is completely dominated by short-distance contributions. Together with Q_ν, Q_{10} belongs to the theoretically clean $\mathcal{O}(G_F^2)$ hard-GIM-protected part of the effective Hamiltonian (10). Thus observables more sensitive to Q_{10}, such as the forward-backward lepton asymmetry, have a reduced QCD uncertainty and a strong sensitivity to possible non-standard phenomena.

$\underline{b \to s\nu\bar{\nu}}$ QCD corrections to the $b \to s\nu\bar{\nu}$ amplitude are the same as needed for the $s \to d\nu\bar{\nu}$ one, with the advantage that charm- and light-quark contributions are not CKM-enhanced and thus are completely negligible also in the real (CP-conserving) part. In other words, the only non-trivial step of the perturbative calculation for $b \to s\nu\bar{\nu}$ decays is the determination of the initial condition of C_ν, which is known with a precision around 1% within the SM.
The experimental upper limit

$$\mathcal{B}(B \to X_s\nu\bar{\nu}) < 6.4 \times 10^{-4} \tag{14}$$

has been announced this year by the ALEPH collaboration at LEP. [31] This has to be compared with a SM prediction [27] of about 3.5×10^{-5}. Similarly to $K \to \pi\nu\bar{\nu}$ decays, the $b \to s\nu\bar{\nu}$ transition can probe many new-physics scenarios [32] and deserve the maximum of attention. Hopefully, the gap between SM expectations and experimental limits could decrease in the next few years at B-factory experiments.

The three steps of the perturbative calculation can easily be transferred from the $b \to s$ case to the $b \to d$ one, although the structure of the effective Hamiltonian is richer in the latter, owing to the presence of two comparable CKM factors ($V_{td}^* V_{tb}$ and $V_{us}^* V_{ub}$). Being insensitive to V_{td}, $b \to s$ transitions are not interesting for precision tests in the $\bar{\rho}$–$\bar{\eta}$ plane; these processes are particularly useful to constrain (or even to detect) possible extensions of the SM. On the contrary, $b \to d$ transitions are very sensitive to $\bar{\rho}$ and $\bar{\eta}$, but are clearly disfavoured from the experimental point of view because of the additional $\mathcal{O}(\lambda^2)$ suppression.

5 $B \to X_{s,d}\gamma$

The inclusive $B \to X_s\gamma$ rate is the most significant information that we have at present on $\Delta B = 1$ FCNCs. New precise measurements have recently been

reported by CLEO at Cornell [33] and by BELLE at KEK. [34] Combining them with previous determinations, [23] the world average reads

$$\mathcal{B}(B \to X_s\gamma)^{\rm exp} = (3.23 \pm 0.42) \times 10^{-4} \tag{15}$$

On the theory side, non-perturbative $1/m_b$ corrections are well under control in the total rate. In particular, $\mathcal{O}(1/m_b)$ corrections vanish in the ratio $\Gamma(B \to X_s\gamma)/\Gamma(B \to X_c\ell\nu)$, and the $\mathcal{O}(1/m_b^2)$ ones are known and amount to few per cent. [28] The most serious problem of non-perturbative origin is related to the (unavoidable) experimental cut in the photon energy spectrum that prevents the measurement from being fully inclusive. [35] With the present cut by CLEO, [33] $E_\gamma > 2.0\,\text{GeV}$, this uncertainty is smaller but non-negligible with respect to the error of the perturbative calculation. The latter is around 10% and its main source is the uncertainty in the ratio m_c/m_b that enters through charm-quark loops. [36] According to a recent analysis of all the theoretical uncertainties, [36] the SM expectation is given by

$$\mathcal{B}(B \to X_s\gamma)_{\rm SM} = (3.73 \pm 0.30) \times 10^{-4}\,, \tag{16}$$

in good agreement with Eq. (15). Some comments are in order:

- The central value of the SM prediction in Eq. (16) is considerably higher than in all previous analyses since $\overline{m}_c(\mu)$ has been used, rather than the charm pole mass, in the ratio $m_c/m_b^{\rm pole}$ appearing in charm-quark loops. This choice is believed to minimize NNLO corrections. [36]

- The overall scale dependence is very small: for $\mu \in [m_b/2, 2m_b]$ the central value moves by about 1%. Therefore the error in Eq. (16) is an educated guess, whose dominant source is the variation of $\overline{m}_c(\mu)/m_b^{\rm pole}$ for $\mu \in [m_c, m_b]$ [note that the scale-independent ratio $\overline{m}_c(\mu)/\overline{m}_b(\mu)$ is well within this interval]. Additional uncertainties have been combined in quadrature; it is thus more appropriate to consider the r.h.s. of Eq. (16) as central value and standard deviation of a Gaussian distribution, rather than as a flat interval.

- Eq. (16) does not include the error induced by the extrapolation below the E_γ cut. This theoretical uncertainty is included in the experimental result and, for $E_\gamma^{\rm min} = 2.0$ GeV, is around 50% of the error in (16). It is worth while to stress that precise data on the photon spectrum (above the cut) could help to have a better control on this source of uncertainty. [35]

The comparison between theory and experiments in $\mathcal{B}(B \to X_s\gamma)$ is a great success of the SM and has led us to derive many significant bounds on possible

new-physics scenarios. Non-standard effects of $\mathcal{O}(1)$ are definitely excluded, resulting in stringent constraints of models with generic flavour structures, like the unconstrained MSSM. Deviations at the 10%–30% level, as generally expected within models with minimal flavour violation, are still possible, and improved measurements of $\mathcal{B}(B \to X_s\gamma)$ are certainly useful to further constrain this possibility. On the other hand, since the experimental error has reached the level of the theoretical one, it will be very difficult to clearly identify possible deviations from the SM, if any, in this observable.

Hopes to detect new-physics signals are still open via the CP-violating asymmetry

$$A_{\rm CP}^s = \frac{\Gamma(B \to X_s\gamma) - \Gamma(\bar{B} \to X_s\gamma)}{\Gamma(B \to X_s\gamma) + \Gamma(\bar{B} \to X_s\gamma)} \ . \tag{17}$$

This is expected to be below 1% within the SM, [37] but could easily reach $\mathcal{O}(10\%)$ values beyond the SM, even in the absence of large effects in the total $B \to X_s\gamma$ rate. The present measurement of $A_{\rm CP}^s$ is consistent with zero, but the sensitivity is still one order of magnitude above the SM level.

6 Inclusive and exclusive $b \to s\ell^+\ell^-$ transitions

The experimental search for FCNC decays of the B meson into a charged-lepton pair is just entering into an exciting era: preliminary evidences for all the three-body decays of the type $B \to (K, K^*) + (\mu^+\mu^-, e^+e^-)$ have been reported by BELLE and BABAR in the last few months. [38]

Similarly to the $b \to s\gamma$ case, the cleanest theoretical predictions are obtained for sufficiently inclusive observables. Non-perturbative $1/m_b$ corrections are well under control in the total rate and in the differential dilepton spectrum $d(\Gamma \to X_s\ell^+\ell^-)/ds$ (but for the end-point $s = M^2_{\ell^+\ell^-}/m_b^2 \approx 1$). Non-perturbative effects associated to charm-quark loops are very large for $M_{\ell^+\ell^-}$ in the region of the narrow $c\bar{c}$ resonances (see Fig. 5), but they are under control sufficiently far from this region. [39] As a result of these two effects, the cleanest predictions can be performed for $M^2_{\ell^+\ell^-} \lesssim 6\ {\rm GeV}^2$.

An important feature of $b \to s\ell^+\ell^+$ transitions is their sensitivity to the Wilson coefficients $C_{9,10}$. The latter could be strongly modified in several new-physics scenarios, without observable consequences on $b \to s\gamma$. As long as the basis of effective operators is the SM one, the purely perturbative dilepton spectrum can be written as

$$\frac{d}{ds}\Gamma(B \to X_s e^+e^-) \propto (1-s)^2 \\ \times \left\{ 4\frac{s+2}{s}\left|C_7\right|^2 + 12\Re\left[C_7^* C_9^{\rm eff}(s)\right] + (1+2s)\left(\left|C_9^{\rm eff}(s)\right|^2 + \left|C_{10}\right|^2\right)\right\} \ ,$$

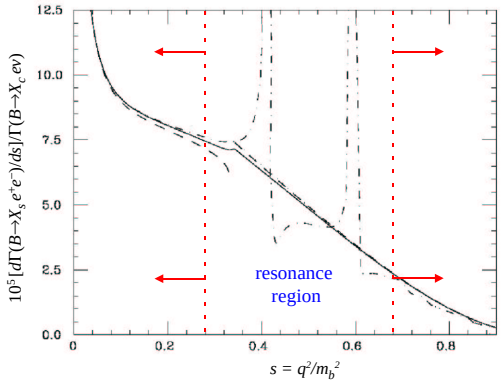

Figure 5: Dilepton spectrum of the inclusive $B \to X_s e^+ e^-$ decay within the SM. The full line denote the pure perturbative result (at fixed renormalization scale), dashed and dash-dotted lines correspond to estimates of non-perturbative $c\bar{c}$ effects. [39]

where $C_9^{\rm eff}(s)$ is an appropriate combination of C_9 and the Wilson coefficients of four-quark operators. [40] At very small s, the dominant contribution is that of C_7, enhanced by $1/s$; however, for $s \approx 0.1$ a rapid change of slope is expected because of the interference between C_7 and C_9 (see Fig. 5). Since this effect occurs in the theoretically clean part of the spectrum, it could be used to perform new high-precision tests of the SM. Even more interesting short-distance tests could be performed by means of the forward–backward asymmetry of the dilepton distribution.

The high-precision studies allowed by inclusive modes will certainly have to wait a few years because of experimental difficulties. On the other hand, three-body exclusive modes are certainly within the reach of B-factories. The recent data on $B \to (K, K^*) + (\mu^+\mu^-, e^+e^-)$ already led us to exclude some of the most exotic new-physics scenarios: [41] non-standard contributions to $C_{9,10}$ can be at most of the same order as that of the SM. Given this situation, it is difficult to detect possible deviations from the SM in the total exclusive rates, where the theoretical uncertainties are around 30% (or above). A much more interesting observable in this respect is provided by the lepton forward–

backward (FB) asymmetry. In the $B \to K^* \mu^+ \mu^-$ case this is defined as

$$A_{FB}(s) = \frac{1}{d\Gamma(B \to K^* \mu^+ \mu^-)/ds} \int_{-1}^{1} d\cos\theta \frac{d^2\Gamma(B \to K^* \mu^+ \mu^-)}{ds\ d\cos\theta} \mathrm{sgn}(\cos\theta) \ ,$$

where θ is the angle between μ^+ and B momenta in the dilepton centre-of-mass frame. Assuming that the leptonic current has only a vector (V) or axial-vector (A) structure, then the FB asymmetry provides a direct measure of the A–V interference. Indeed, at LO and employing the SM operator basis, one can write

$$A_{FB}(s) \propto \mathrm{Re}\left\{ C_{10}^* \left[s\ C_9^{\mathrm{eff}} + r(s) \frac{m_b C_7}{m_B} \right] \right\}$$

where $r(s)$ is an appropriate ratio of hadronic form factors. [42] The overall factor ruling the magnitude of $A_{FB}(s)$ is affected by sizeable theoretical uncertainties. Nonetheless, the position of the zero and the sign of $A_{FB}(s)$ provide a clear short-distance information.

6.1 $B_{s,d} \to \ell^+ \ell^-$

The purely leptonic decays constitute a special case among exclusive transitions. Within the SM only the axial-current operator, Q_{10}, induces a non-vanishing contribution to these processes. As a result, the short-distance contribution is not *diluted* by the mixing with four-quark operators. Moreover, the hadronic matrix element involved is the simplest we can consider, namely the B-meson decay constant

$$\langle 0 | \bar{q} \gamma_\mu \gamma_5 b | \bar{B}_q(p) \rangle = i p_\mu f_{B_q} \tag{18}$$

Reliable estimates of f_{B_d} and f_{B_s} are obtained at present from lattice calculations and in the future it will be possible to cross-check these results by means of the $B^+ \to \ell^+ \nu$ rate. Modulo the determination of f_{B_q}, the theoretical cleanliness of $B_{s,d} \to \ell^+ \ell^-$ decays is comparable to that of $K_L \to \pi^0 \nu \bar{\nu}$ and $B \to X_{s,d} \nu \bar{\nu}$.

Compared to their kaon counterparts ($K_L \to \mu^+ \mu^-$ and $K_L \to e^+ e^-$) $B_{s,d} \to \ell^+ \ell^-$ decays have the big advantage that the two-photon amplitude is completely negligible. However, the price to pay is a strong helicity suppression for $\ell = \mu$ (and $\ell = e$), or the channels with the best experimental signature. Employing the full NLO expression [2] of C_{10}, we can write

$$\mathcal{B}(B_s \to \mu^+ \mu^-)_{\mathrm{SM}} = 3.1 \times 10^{-9} \left(\frac{|V_{ts}|}{0.04} \right)^2 \left(\frac{f_{B_s}}{0.21\ \mathrm{GeV}} \right)^2 \left(\frac{\tau_{B_s}}{1.6\ \mathrm{ps}} \right)$$

$$\frac{\mathcal{B}(B_s \to \tau^+ \tau^-)_{\mathrm{SM}}}{\mathcal{B}(B_s \to \mu^+ \mu^-)_{\mathrm{SM}}} = 215 \ .$$

The corresponding B_d modes are both suppressed by an additional factor $|V_{td}/V_{ts}|^2 = (4.0 \pm 0.8) \times 10^{-2}$. The present experimental bound closest to SM expectations is the one obtained by CDF, at Fermilab, on $B_s \to \mu^+\mu^-$:

$$\mathcal{B}(B_s \to \mu^+\mu^-) < 2.6 \times 10^{-6} \quad (95\% \text{ CL}) \,,$$

which is still very far from the SM level. The latter will certainly not be reached before the LHC era.

As emphasized in the recent literature, [44)–46)] the purely leptonic decays of B_s and B_d mesons are excellent probes of a specific type of new-physics amplitudes, namely enhanced scalar (and pseudoscalar) FCNCs. Scalar FCNC operators, such as $\bar{b}_R s_L \bar{\mu}_R \mu_L$, are present within the SM but are absolutely negligible because of the smallness of down-type Yukawa couplings. On the other hand, these amplitudes could be non-negligible in models with an extended Higgs sector. In particular, within the MSSM, where two Higgs doublets are coupled separately to up- and down-type quarks, a strong enhancement of scalar FCNCs can occur at large $\tan\beta = v_u/v_d$. [44)] This effect would be practically undetectable in non-helicity-suppressed B decays and in K decays (because of the small Yukawa couplings), but could enhance $B \to \ell^+\ell^-$ rates by orders of magnitude, up to the present experimental bounds. [45), 46)] The search for these processes is therefore very interesting, even if we are still very far from the SM level. Experiments at hadron colliders, such as CDF or, in a long-term perspective, LHCb, are certainly advantaged in the search of $B_{s,d} \to \mu^+\mu^-$. B-factory experiments could try to complement the picture searching for $B_d \to \tau^+\tau^-$. [46)]

7 Other rare processes

7.1 FCNCs in D decays

The phenomenology of FCNCs with external up-type quarks, such as charm, is completely different from the examples discussed so far. [47)] In K and B decays the short-distance dominance of the clean SM transitions is ensured by the presence of the heavy top, which induces non-decoupling contributions growing with m_t [as explicitly shown in (2)]. A similar phenomenon cannot occur in $c \to u$ transitions, because of the simultaneous smallness of m_b and of the CKM factor $V_{cb}V_{ub}^*$. Even for $c \to u$ amplitudes with a hard GIM mechanism, the long-distance contribution dominates within the SM. As a result, FCNC D decays cannot be used to make precision tests of the CKM mechanism.

In cases where it is possible to put a firm upper bound on the long-distance contribution, FCNC D decays can be used to probe new-physics scenarios. This possibility has recently been discussed for $D \to P\ell^+\ell^-$, $D \to V\gamma$ and $D \to \gamma\gamma$

modes, [47, 48] where there is still a considerable gap between SM expectations and experimental limits. Note that only exotic non-standard scenarios can be probed by means of FCNC D decays. Indeed, to be clearly identified, the new-physics source should produce order-of-magnitude enhancements over a long-distance SM amplitude.

7.2 Lepton-flavour-violating modes

Decays like $K_L \to \mu e$, $K \to \pi\mu e$ (as well as similar D and B modes) are completely forbidden within the SM, where lepton flavour is conserved, but are also absolutely negligible if we simply extend the model by including only Dirac-type neutrino masses. A positive evidence of any of these processes would therefore unambiguously signal new physics, calling for non-minimal extensions of the SM.

In exotic scenarios, such as R-parity-violating SUSY or models with leptoquarks, the $q_i \to q_j \mu e$ amplitude can already be generated at tree level. In this case, even for high new-physics scales it is possible to generate lepton-flavour transitions close to the present experimental limits. In particular, the bound [49]

$$\mathcal{B}(K_L \to \mu e) < 4.7 \times 10^{-12} \,, \tag{19}$$

which is the most stringent limit on these types of transitions, let us put a bound on leptoquark masses above 100 TeV (assuming electroweak couplings).

In more conservative scenarios, such as the generic MSSM, where $q_i \to q_j \mu e$ transitions occur only at the one-loop level and the mechanisms for quark- and lepton-flavour mixing are separate, the rates for lepton-flavour-violating K, D and B decays are naturally well below the level of current experimental bounds.

8 Conclusions

Rare FCNC decays of K and B mesons provide a unique opportunity to perform high-precision tests of CP violation and flavour mixing, both within and beyond the SM.

The $B \to X_s\gamma$ rate represents the highest peak in our present knowledge of FCNCs: both experimental and theoretical errors have reached a comparable level of precision, around 10%, and the agreement between theory and data constitutes a highly non-trivial constraint for many extensions of the SM.

The lack of deviations from SM expectations in $\Gamma(B \to X_s\gamma)$ should not discourage the search for other rare FCNC observables. As emphasized several times during this talk, there are still several observables, such as the forward–backward asymmetry in $B \to K^*\ell^+\ell^-$ or the rates of $B \to \ell^+\ell^-$ and $K \to \pi\nu\bar{\nu}$

modes, where sizeable deviations from the SM are possible and are expected in specific new-physics models.

The measurement of observables with theoretical errors at the per-cent level, such as $\Gamma(K_L \to \pi^0 \nu\bar{\nu})$, $\Gamma(B \to X_s \nu\bar{\nu})$ and $\Gamma(B_{s,d} \to \mu^+\mu^-)$, is a very important long-term perspective. Even if new physics will first be discovered elsewhere, e.g. at future hadron colliders, the experimental study of such processes would still be very useful to investigate the flavour structure of any new-physics scenario.

Acknowledgements

I wish to thank the organisers for the invitation, and for choosing such a nice place for the conference!

References

1. G. Isidori, *Rare decays: Theory vs. experiments,* arXiv:hep-ph/0110255.
2. G. Buchalla and A. J. Buras, *Nucl. Phys.* B **548**, 309 (1999); M. Misiak and J. Urban, *Phys. Lett.* B **451**, 161 (1999).
3. A. F. Falk, A. Lewandowski and A. A. Petrov, *Phys. Lett.* B **505**, 107 (2001).
4. M. Lu and M. Wise, *Phys. Lett.* B **324**, 461 (1994).
5. G. Buchalla and G. Isidori, *Phys. Lett.* B **440**, 170 (1998); D. Rein and L.M. Sehgal, *Phys. Rev.* D **39**, 3325 (1989).
6. W.J. Marciano and Z. Parsa, *Phys. Rev.* D **53**, R1 (1996).
7. G. D'Ambrosio and G. Isidori, *Phys. Lett.* B **530**, 108 (2002).
8. A. J. Buras *at al.*, *Nucl. Phys.* B **592**, 55 (2001).
9. A. J. Buras *et al.*, *Nucl. Phys.* B **566**, 3 (2000).
10. S. Kettel, these proceedings.
11. J. Adams *et al.* [KTeV Collab.], *Phys. Lett.* B **447**, 240 (1999).
12. G. Ecker, A. Pich and E. de Rafael, *Nucl. Phys.* B **291**, 692 (1987).
13. G. D'Ambrosio, G. Ecker, G. Isidori and J. Portolés, *JHEP* **08**, 004 (1998).

14. R. Appel *et al.* [E865 Collab.], *Phys. Rev. Lett.* **83**, 4482 (1999). H. Ma *et al.* [E865 Collab.], *Phys. Rev. Lett.* **84**, 2580 (2000).

15. H. K. Park *et al.* [HyperCP Collab.] arXiv:hep-ex/0110033

16. A. Messina, *Phys. Lett.* B **538**, 130 (2002).

17. A. Lai *et al.* [NA48 Collab.], *Phys. Lett.* B **514**, 253 (2001).

18. A. J. Buras, M. E. Lautenbacher, M. Misiak and M. Munz, *Nucl. Phys.* B **423**, 349 (1994).

19. A. Lai *et al.* [NA48 Collab.], *Phys. Lett.* B **536**, 229 (2002); R. Wanke, these proceedings.

20. A. Alavi-Harati *et al.* [KTeV Collab.], *Phys. Rev. Lett.* **86**, 397 (2001).

21. G. Valencia, *Nucl. Phys.* B **517**, 339 (1998); G. Dumm and A. Pich, *Phys. Rev. Lett.* **80**, 4633 (1998).

22. D. Ambrose *et al.* [E871 Collab.], *Phys. Rev. Lett.* **84**, 1389 (2000).

23. D. E. Groom *et al.* [Particle Data Group], *Eur. Phys. J.* C **15**, 1 (2000).

24. L. Bergstrom, E. Masso and P. Singer, *Phys. Lett.* B **249**, 141 (1990).

25. G. D'Ambrosio, G. Isidori and J. Portolés, *Phys. Lett.* B **423**, 385 (1998).

26. T. Yamanaka, these proceedings.

27. For a recent review see e.g.: T. Hurth, arXiv:hep-ph/0106050; A. J. Buras, arXiv:hep-ph/0101336.

28. N. Uraltsev, these proceedings.

29. K. Chetyrkin, M. Misiak and M. Munz, *Phys. Lett.* B **400**, 206 (1997); **425**, 414 (1997) (E).

30. C. Bobeth, M. Misiak and J. Urban, *Nucl. Phys.* B **574**, 291 (2000); H.H. Asatrian, H.M. Asatrian, C. Greub and M. Walker, *Phys. Lett.* B **507**, 162 (2001); arXiv:hep-ph/0109140.

31. R. Barate *et al.* [ALEPH Collab.], *Eur. Phys. J.* C **19**, 213 (2001).

32. Y. Grossman, Z. Ligeti and E. Nardi, *Nucl. Phys.* B **465**, 369 (1996); **480**, 753 (1996) (E).

33. D. Cassel, these proceedings; S. Chen *et al.* [CLEO Collab.], arXiv:hep-ex/0108032.

34. H. Tajima, these proceedings. K. Abe *et al.* [BELLE Collab.], *Phys. Lett.* B **511**, 151 (2001).

35. A. L. Kagan and M. Neubert, *Eur. Phys. J.* C **7**, 5 (1999);

36. P. Gambino and M. Misiak, *Nucl. Phys.* B **611**, 338 (2001).

37. A. L. Kagan and M. Neubert, *Phys. Rev.* D **58**, 094012 (1998).

38. S. Robertson, these proceedings.

39. F. Krüger and L.M. Sehgal, *Phys. Lett.* B **380**, 199 (1996); G. Buchalla, G. Isidori and S. J. Rey, *Nucl. Phys.* B **511**, 594 (1998).

40. M. Misiak, *Nucl. Phys.* B **393**, 23 (1993); **439**, 461 (1993) (E); A. J. Buras and M. Munz, *Phys. Rev.* D **52**, 186 (1995).

41. A. Ali, E. Lunghi, C. Greub and G. Hiller, arXiv:hep-ph/0112300.

42. G. Burdman, *Phys. Rev.* D **57**, 4254 (1998).

43. F. Abe *et al.* [CDF Collab.], *Phys. Rev.* D **57**, 3811 (1998).

44. K. S. Babu and C. Kolda, *Phys. Rev. Lett.* **84**, ; (2000)

45. C. S. Huang, W. Liao, Q. S. Yan and S. H. Zhu, *Phys. Rev.* D **63**, 114021 (2001); **64**, 059902 (2001) (E). P. H. Chankowski and L. Slawianowska, *Phys. Rev.* D **63**, 054012 (2001). C. Bobeth, T. Ewerth, F. Kruger and J. Urban, *Phys. Rev.* D **64**, 074014 (2001).

46. A. Dedes, H. K. Dreiner and U. Nierste, arXiv:hep-ph/0108037; G. Isidori and A. Retico, arXiv:hep-ph/0110121.

47. See e.g.: G. Burdman, arXiv:hep-ph/9811457; G. Burdman, E. Golowich, J. L. Hewett and S. Pakvasa, *Phys. Rev.* D **52**, 6383 (1995); arXiv:hep-ph/0112235.

48. S. Fajfer, S. Prelovsek and P. Singer, arXiv:hep-ph/0106333; S. Fajfer, P. Singer and J. Zupan, *Phys. Rev.* D **64**, 074008 (2001); S. Fajfer, S. Prelovsek, P. Singer and D. Wyler, *Phys. Lett.* B **487**, 81 (2000).

49. D. Ambrose *et al.* [E871 Collab.], *Phys. Rev. Lett.* **81**, 5734 (1998).

Frascati Physics Series Vol. XXVIII (2002), pp.245-250
HQ & L 2002 – Vietri s/m, May 27th - June 1st, 2002

RARE DECAYS RECENT RESULTS FROM FOCUS (+THEORY)

Will E. Johns (for the FOCUS collaboration)
Department of Physics and Astronomy
Vanderbilt University
Nashville, TN USA

1 Introduction

The search for rare decays of charm particles is reaching a point where long range effects should be observable in the next few years. In order to perform the analysis of such small data sets, several techniques have become *de facto* standards in the last decade. In this talk, we will show new rare charm decay results from the FOCUS experiment. The analysis has been performed utilizing a bootstrap technique which we will describe below.

2 Technique

The FOCUS analysis technique has emphasized a careful approach to the treatment of backgrounds in a limited statistics analysis. The usual approach is to select cuts to optimize signal efficiency relative to background sidebands. This "blind" technique, where the signal region is masked off, can still lead to a

downward fluctuation of the sidebands relative to the masked off "signal" region and a more conservative limit on average.

Further, authors frequently use the technique outlined in reference [1] to calculate the confidence levels used in the calculation of their limits. The approach in [1] does not explicitly include fluctuations in the background. Indeed, the PDG [3] suggests presenting a measure of the experimental sensitivity in addition to the reported limit whenever experiments quote a result since none of the methods suggested [3], including [2], properly deal with fluctuations in the background and bias in selecting the data.

For our analysis, we chose a method [4] which includes the background fluctuations directly into the calculation of the likelihood. The probability of finding a signal rate μ and a background rate b given x events in a signal region and y events in background sidebands is described by:

$$P_{\mu,b}(x,y) = \frac{(\mu+b)^x e^{-(\mu+b)}}{x!} \; \frac{(\tau b)^x e^{-(\tau b)}}{y!}.$$

Where τ is the ratio of the number of background events in the sideband regions to the signal region. The τ is determined via Monte Carlo. Rolke and Lopez [4] have shown that this method for determining an upper limit provides better coverage than [1].

Methods presented by Rolke and Lopez have also been shown to reduce bias in the selection of optimal cuts [5]. Briefly, one uses the computed sensitivity on an ensemble of bootstrapped (sample with replacement) events from the data. The cuts chosen by each selected set in this manner are applied to a second, independent, bootstrapped sample. A sensitivity as well as an upper limit are computed from the second sample. The sensitivity and branching ratio quoted are the median values of the ensemble of results from the second bootstrap.

The data for the analyses presented in this talk were collected using the Wideband photoproduction experiment FOCUS during the 1996–1997 fixed–target run at Fermilab. The FOCUS detector is a large aperture, fixed–target spectrometer with excellent vertexing and particle identification used to measure the interactions of high energy photons on a segmented BeO target. The FOCUS beamline [6] and detector [7, 8] have been described elsewhere.

To provide a clean sample of D^+'s and D_s^+'s, we look for D's through the 3-body decay chain $D^+(D_s^+) \to h^\mp \mu^\pm \mu^+$ where the h represents a pion or a kaon. We use a cut grid based on kinematic variables and particle ID algorithm results that have been shown to be effective for other charm decays. The grid includes cuts on the significance of separation between the interaction and decay vertices (L/σ), the confidence level of the vertex fit of the decay vertex, the

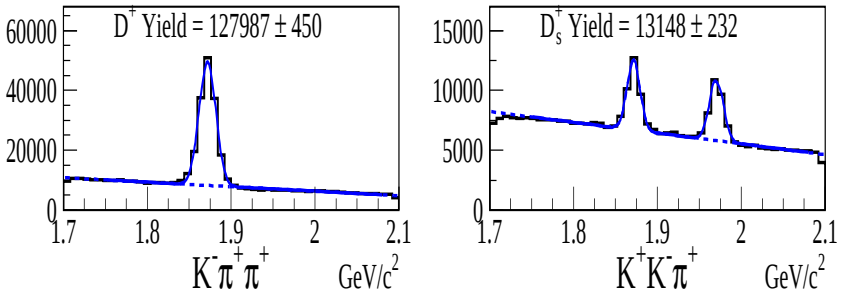

Figure 1: Modes used to normalize the rare decay modes. The yields are shown for the loosest cut grid combination.

confidence level that a particle is identified as a muon, the momentum of muon candidates, and Čerenkov likelihoods based on different particle hypotheses used to separate pions and kaons [8]. The normalizing modes used to compute the branching ratios for D^+ and D_s^+ are shown in Figure 1 for the loosest cuts in the grid.

3 Results and Systematic Checks

The dominant systematic effects in this analysis have been estimated to occur from the absolute branching ratios [9] used to calibrate the normalization modes. The systematic errors, which averaged about 7.6% for the D^+ modes and 27.6% for the D_s^+ modes, were added to the result using the technique outlined in [2]. As a check on the dual bootstrap, another technique was used that selected a unique cut *set* based on the results of the cut grid. The cuts used to determine the best sensitivities in the first bootstrap are examined for all modes and a best set is determined based on the most likely cut combination. This cut set is then applied to all modes *once* in the spirit of a more traditional "blind" analysis.

The results of the analysis are presented in Table 1 below. There is good agreement between the dual bootstrap, the sensitivity and the single cut systematic check. Note that the only mode where the result and the sensitivity show a marked difference is in $D^+ \to K^-\mu^+\mu^+$ which might indicate more contamination from $D^+ \to K^-\pi^+\pi^+$ than anticipated.

Decay Mode	Result	Sensitivity	Single Cut
$D^+ \to K^+\mu^+\mu^-$	9.2×10^{-6}	7.5×10^{-6}	11.8×10^{-6}
$D^+ \to K^-\mu^+\mu^+$	13.1×10^{-6}	4.8×10^{-6}	12×10^{-6}
$D^+ \to \pi^+\mu^+\mu^-$	8.8×10^{-6}	7.6×10^{-6}	7.5×10^{-6}
$D^+ \to \pi^-\mu^+\mu^+$	4.8×10^{-6}	5.6×10^{-6}	5.2×10^{-6}
$D_s^+ \to K^+\mu^+\mu^-$	3.6×10^{-5}	3.3×10^{-5}	3.8×10^{-5}
$D_s^+ \to K^-\mu^+\mu^+$	1.3×10^{-5}	2.1×10^{-5}	2.0×10^{-5}
$D_s^+ \to \pi^+\mu^+\mu^-$	2.6×10^{-5}	3.1×10^{-5}	1.8×10^{-5}
$D_s^+ \to \pi^-\mu^+\mu^+$	2.9×10^{-5}	2.3×10^{-5}	2.2×10^{-5}

Table 1: FOCUS results with incorporated systematic errors for the modes shown. Each number represents a 90% upper limit for the brancing ratio of the decay mode listed.

4 Comparisons to Experiment and Theory

In Figure 2 below, we show the FOCUS branching ratio limits for the dual bootstrap technique described in the text. Our results are a substantial improvement over previous results [12, 10] and FOCUS sets a new limit for the MSSM R-Parity violating prediction [13] for the branching ratio $D^+ \to \pi^+\mu^+\mu^-$ of 8.8×10^{-6} @ 90% C.L..

I am grateful to Daniel Engh for supplying all the FOCUS results presented in this note. I am also grateful to Gustavo Burdman and Paul Singer for their patience during several very useful conversations.

References

1. G. J. Feldman and R. D. Cousins, Phys. Rev. D **57**, 3873 (1998) [arXiv:physics/9711021].

2. R. D. Cousins and V. L. Highland, Nucl. Instrum. Meth. A **320**, 331 (1992).

3. F. James and R. Cousins, Eur. Phys. J. C **15**, 195 (2000).

4. W. A. Rolke and A. M. Lopez, Nucl. Instrum. Meth. A **458**, 745 (2001) [arXiv:hep-ph/0005187].

5. W. A. Rolke and A. M. Lopez, arXiv:hep-ph/0206139.

6. P. L. Frabetti *et al.*, Nucl. Instrum. Meth. A **329**, 62 (1993).

7. P. L. Frabetti *et al.* [E-687 Collaboration], Nucl. Instrum. Meth. A **320**, 519 (1992).

8. J. M. Link *et al.* [FOCUS Collaboration], Nucl. Instrum. Meth. A **484**, 270 (2002) [arXiv:hep-ex/0108011].

9. D. E. Groom *et al.* [Particle Data Group Collaboration], Eur. Phys. J. C **15**, 1 (2000).

10. E. M. Aitala *et al.* [E791 Collaboration], Phys. Lett. B **462**, 401 (1999) [arXiv:hep-ex/9906045].

11. E. M. Aitala *et al.* [E791 Collaboration], Phys. Rev. Lett. **86**, 3969 (2001) [arXiv:hep-ex/0011077].

12. P. L. Frabetti *et al.* [The E687 Collaboration], Phys. Lett. B **398**, 239 (1997).

13. G. Burdman, E. Golowich, J. Hewett and S. Pakvasa, arXiv:hep-ph/0112235.

14. S. Fajfer, S. Prelovsek and P. Singer, Phys. Rev. D **64**, 114009 (2001) [arXiv:hep-ph/0106333].

15. P. Singer and D. X. Zhang, Phys. Rev. D **55**, 1127 (1997) [arXiv:hep-ph/9612495].

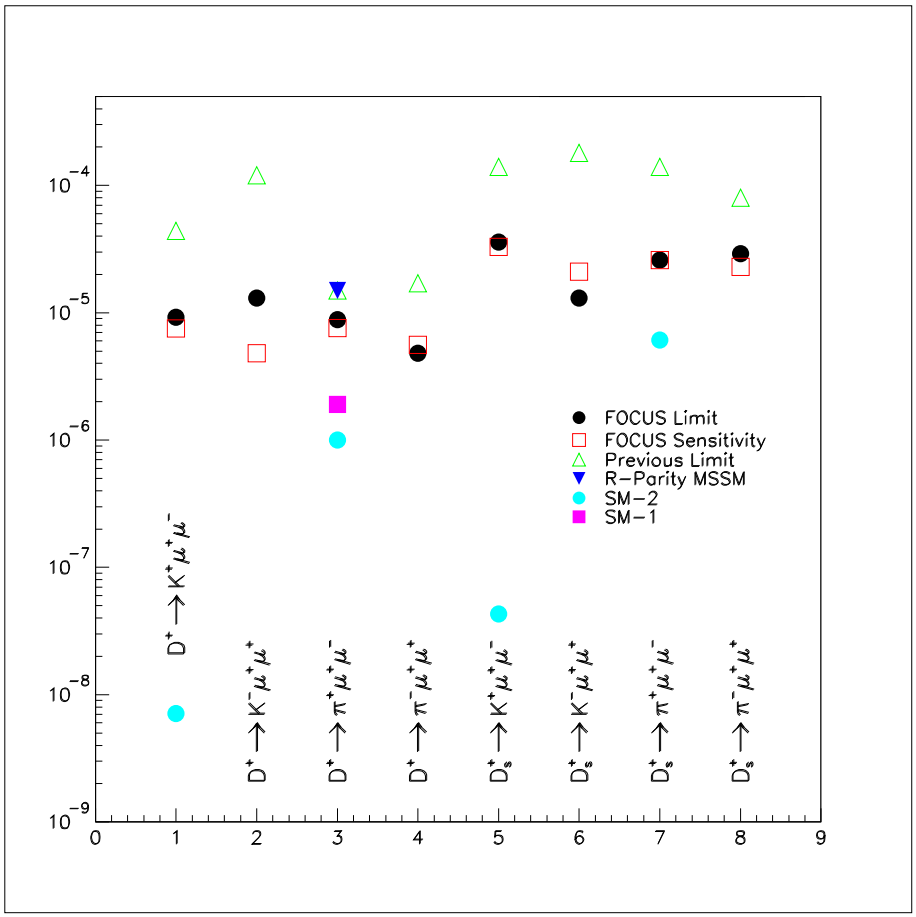

Figure 2: FOCUS results compared to other experiments and theory. The previous limits, except for the E687 $D^+ \to K^-\mu^+\mu^+$ [12] are from Fermilab experiment E791 [10]. The theory estimates come from [13] (R-Parity MSSM and SM-1) and [14] (SM-2). Note that the SM estimates from [13] use a formalism close to [15], and at present there is some discrepancy in the invariant M_{ll} mass behavior for the SM estimates in [13] and [14]. The results for four-body decays measured by E791 [11] are not shown.

Frascati Physics Series Vol. XXVIII (2002), pp.251-261
HQ & L 2002 – Vietri s/m, May 27th - June 1st, 2002

EXPERIMENTAL STATUS OF $K \to \pi\nu\overline{\nu}$

Steve H. Kettell
Brookhaven National Laboratory, Upton, NY 11973-5000 USA

ABSTRACT

The experimental program for the study of the rare kaon decays, $K \to \pi\nu\overline{\nu}$, is summarized. A review of recent results is provided along with a discussion of prospects for the future of this program. The primary focus of the world-wide kaon program is the two golden modes: $K^+ \to \pi^+\nu\overline{\nu}$ and $K_L^\circ \to \pi^\circ\nu\overline{\nu}$. The first step in an ambitious program to precisely measure both branching ratios has been successfully completed with the observation of two $K^+ \to \pi^+\nu\overline{\nu}$ events by E787. The E949 experiment is poised to reach an order of magnitude further in sensitivity and to observe ∼10 Standard Model events, and the CKM experiment should observe ∼100 SM events by the end of this decade. Limits on the neutral analog $K_L^\circ \to \pi^\circ\nu\overline{\nu}$ have been set by KTeV and within the next couple of years will be pushed by E391a. Measurements of the branching ratio should be made within the next 10 years by KOPIO, with a goal of ∼50 events, and at the JHF, with a goal of up to 1000 events.

1 Introduction

The primary focus in kaon physics today is the two golden modes: $K^+ \to \pi^+ \nu\overline{\nu}$ and $K_L^\circ \to \pi^\circ \nu\overline{\nu}$. These modes are interesting as there is essentially no theoretical ambiguity in extracting fundamental CKM parameters from measurements of the branching ratios [1, 2]. The intrinsic theoretical uncertainty in B($K^+ \to \pi^+ \nu\overline{\nu}$) is ~7% and is even smaller in B($K_L^\circ \to \pi^\circ \nu\overline{\nu}$), only ~2%; in both cases the hadronic matrix element can be extracted from the $K^+ \to \pi^\circ e^+ \nu_e$ (K_{e3}) decay rate.

The unitarity of the CKM matrix can be expressed as

$$V_{us}^* V_{ud} + V_{cs}^* V_{cd} + V_{ts}^* V_{td} = \lambda_u + \lambda_c + \lambda_t = 0$$

with the three vectors $\lambda_i \equiv V_{is}^* V_{id}$ converging to form a very elongated triangle in the complex plane. The length of first vector $\lambda_u = V_{us}^* V_{ud}$ is precisely determined from K_{e3} decay. The length of the third side $\lambda_t = V_{ts}^* V_{td}$ is measured by $K^+ \to \pi^+ \nu\overline{\nu}$ and the height of the triangle, $Im\lambda_t$, can be measured by $K_L^\circ \to \pi^\circ \nu\overline{\nu}$. Branching ratio measurements of the two $K \to \pi\nu\overline{\nu}$ modes, along with the well known K_{e3}, will completely determine the unitarity triangle.

Comparison of CKM parameters as measured from the golden $K \to \pi\nu\overline{\nu}$, $B_d^\circ \to \psi K_S^\circ$ and $\Delta M_{B_d}/\Delta M_{B_s}$ modes, provide the best opportunity to overconstrain the unitary triangle and to search for new physics. In particular, comparisons of

- $|V_{td}|$ from $K^+ \to \pi^+ \nu\overline{\nu}$ and from the ratio of the mixing frequencies of B_d and B_s mesons $\Delta M_{B_d}/\Delta M_{B_s}$ [2],
- β from B($K_L^\circ \to \pi^\circ \nu\overline{\nu}$)/B($K^+ \to \pi^+ \nu\overline{\nu}$) and from the time dependent asymmetry in the decay $B_d^\circ \to \psi K_S^\circ$ [3, 4]

offer outstanding opportunities to explore the Standard Model (SM) picture of *CP*–violation.

The SM prediction for the $K \to \pi\nu\overline{\nu}$ branching ratios are B($K^+ \to \pi^+ \nu\overline{\nu}$) $= (0.72 \pm 0.21) \times 10^{-10}$ and B($K_L^\circ \to \pi^\circ \nu\overline{\nu}$) $= (0.26 \pm 0.12) \times 10^{-10}$ [1]. In addition, an upper limit on B($K^+ \to \pi^+ \nu\overline{\nu}$) can be derived with small uncertainty from the current limit on B_s mixing; this limit is B($K^+ \to \pi^+ \nu\overline{\nu}$) $< 1.32 \times 10^{-10}$ [5].

2 $K^+ \to \pi^+ \nu\overline{\nu}$

The Alternating Gradient Synchrotron (AGS) as a high-energy physics (HEP) research facility has had a broad and rich program in kaon physics, culminating in the observation of two $K^+ \to \pi^+ \nu\overline{\nu}$ events by E787. With the recent successful commissioning of the Relativistic Heavy Ion Collider (RHIC), the primary role of the AGS has shifted to become an injector of heavy ions for RHIC. Nevertheless, the AGS remains the highest intensity proton synchrotron in the world and is designed to be available for ~20 hours/day when not filling RHIC, and as such retains an important role in the US HEP program. DOE and BNL have approved and agreed to fund one new HEP experiment to run at the AGS between RHIC fills: the E949 experiment seeks to make a precise measurement of the branching ratio B($K^+ \to \pi^+ \nu\overline{\nu}$). While DOE approved E949 to run for 60 weeks, the FY03 budget of the President of the United States does not include running for E949. At this point the E949 experiment will be terminated after only 12 weeks of running, unless the US Congress restores funding. The fate of the E949 experiment will not be known until Congress initiates and then completes the appropriations process between June and October of 2002.

The completion of the Main Injector (MI) at FNAL allows for the simultaneous operation of a fixed target program along with the Tevatron collider. The next step in the pursuit of $K^+ \to \pi^+ \nu\overline{\nu}$ will be the CKM experiment, which plans to use a modest fraction of the MI protons (5×10^{12}), extracted over a 1-second spill with minimal bunching of the proton beam, and will push the $K^+ \to \pi^+ \nu\overline{\nu}$ sensitivity to the current limits of theoretical precision.

2.1 E787

The first $K^+ \to \pi^+ \nu\overline{\nu}$ signal was observed in the 1995 data sample of the E787 experiment [6]. No new events were seen in the data sample from 1996–97 [7], and with a background of 0.08 ± 0.02 events and a signal of one event a branching ratio of B($K^+ \to \pi^+ \nu\overline{\nu}$) = $(1.5^{+3.4}_{-1.2}) \times 10^{-10}$ was measured. That event was in fact in a very clean region of the predefined $K^+ \to \pi^+ \nu\overline{\nu}$ signal region with a SM-signal to background ratio of 35. An analysis of the final E787 data sample from the 1998-99 run has recently been reported [8]. With a measured background of $0.066^{+0.044}_{-0.025}$, one new event was observed. The final plot of range vs. energy from the combined E787 1995–99 data sample for events passing all

other cuts is shown in Figure 1. The branching ratio, as determined from these

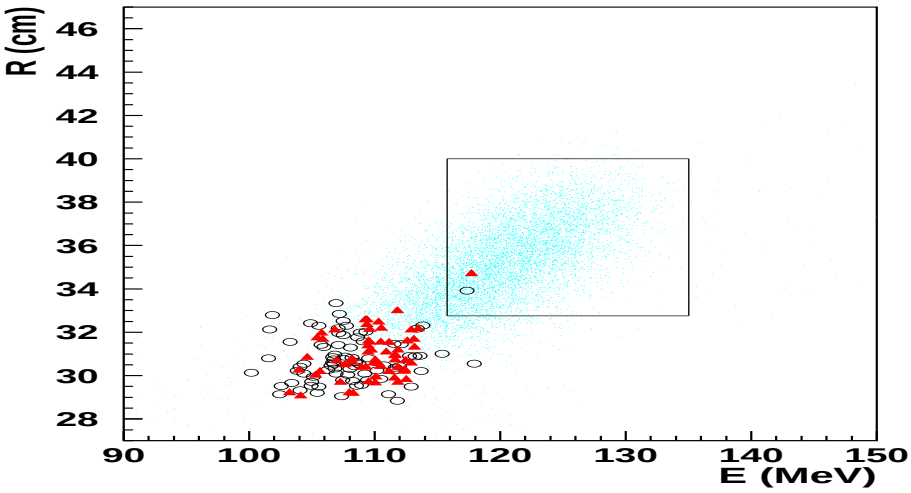

Figure 1: *Final E787 plot of range vs. energy for events passing all other cuts. The circles are for 1998 data and the triangles are for 1995–97 data. Two clean $K^+ \to \pi^+ \nu\overline{\nu}$ events are seen in the box. The remaining events are $K^+ \to \pi^+ \pi^\circ$ background. A $K^+ \to \pi^+ \nu\overline{\nu}$ Monte Carlo sample (dots) is overlayed on the data.*

two events, is

$$B(K^+ \to \pi^+ \nu\overline{\nu}\ ) = (1.57^{+1.75}_{-0.82}) \times 10^{-10}. \tag{1}$$

This branching ratio is a factor of two higher than expected in the SM and is higher than allowed by the current limit on B_s mixing. Of course, the uncertainty on the BR measurement is large due to limited statistics and new data from the E949 experiment are eagerly awaited.

The new event found in the 1998 data sample is in a relatively clean region of the accepted signal region: the SM signal to background ratio for this event is 3.6. An event display for this event, as well as the previous event, is shown in Figure 2.

Limits on $|V_{td}|$ and λ_t can be obtained (these are 1-σ limits except for $Im\lambda_t$ which is 90% CL),

$$\begin{aligned} 0.007 < \quad & |V_{td}| \quad < 0.030, \\ 2.9 \times 10^{-4} < \quad & |\lambda_t| \quad < 1.2 \times 10^{-3}, \end{aligned} \tag{2}$$

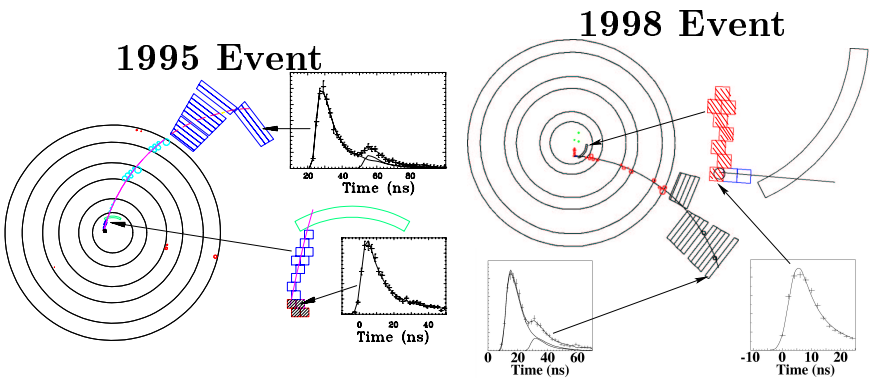

Figure 2: Graphical displays of the two $K^+ \to \pi^+ \nu\overline{\nu}$ events, discovered in the E787 data samples from 1995 and 1998. The display is an end view of the detector, with expanded views of the target region, and with views of the digitized pulses in the fiber where the kaon stopped and of the $\pi^+ \longrightarrow \mu^+$ decay signal in the scintillator where the pion stopped.

$$\begin{aligned} -0.88 \times 10^{-3} < \quad Re\lambda_t \quad &< 1.2 \times 10^{-3}, \\ Im\lambda_t \quad &< 1.1 \times 10^{-3}. \end{aligned}$$

Even with the large statistical error, this new measurement provides a non-trivial contribution to global fits of the CKM parameters [5]. The constraints on λ_t from this result are shown in Figure 3. The constraints from the other golden B modes, $\Delta M_{B_d}/\Delta M_{B_s}$ and $B^\circ_d \to \psi K^\circ_S$ are shown on the same plot. One can immediately see that $|\lambda_t|$ is tightly constrained to a narrow crescent by $K^+ \to \pi^+ \nu\overline{\nu}$ and $\Delta M_{B_d}/\Delta M_{B_s}$.

New data from the successor to E787, E949, will make a significant contribution to our knowledge of the CKM parameters.

In addition, E787 has searched for the decay $K^+ \to \pi^+ \nu\overline{\nu}$ in the pion kinematic region below the $K^+ \to \pi^+\pi^\circ$ ($K_{\pi 2}$) peak [9]. This region contains more of the $K^+ \to \pi^+ \nu\overline{\nu}$ phase space, but is complicated by a significant background from $K^+ \to \pi^+\pi^\circ$ decays with the π^+ scattering in the scintillating fiber target and shifting its kinematics into the search region. The data from the 1996 run of E787 has been analyzed (~20% of the entire E787 data sample). One event

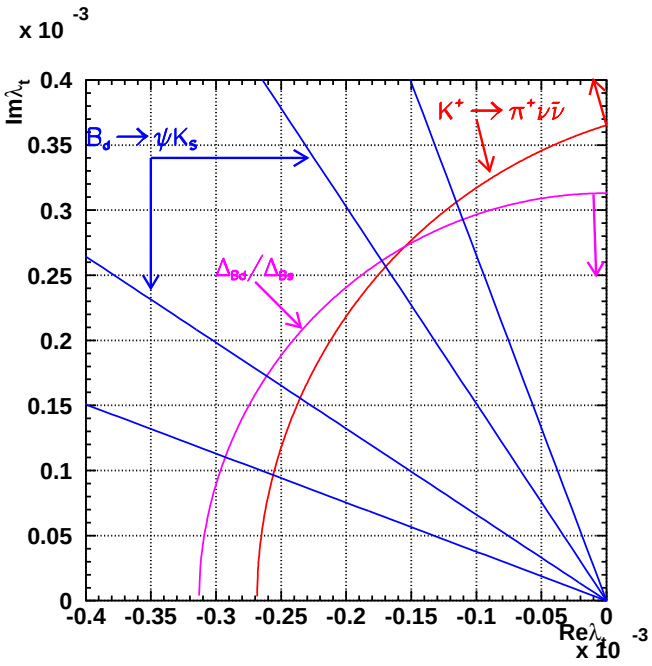

Figure 3: Constraints on λ_t from the golden modes. The experimental measurements for $B^\circ_d \to \psi K^\circ_S$ and $K^+ \to \pi^+ \nu\overline{\nu}$ are 90% CL limits and for $\Delta M_{B_d}/\Delta M_{B_s}$ is a 95% CL limit. The theoretical uncertainties in all of these modes are small. A measurement of $K^\circ_L \to \pi^\circ \nu\overline{\nu}$ will determine $Im\lambda_t$. (I have used $\Delta M_{B_s} < 14.6 ps^{-1}$, $0.56 < B(K^+ \to \pi^+ \nu\overline{\nu}\ ) < 3.89$ and $\sin(2\beta) = 0.79 \pm 0.13$.)

was observed in the search region, consistent with the background estimate of 0.73 ± 0.18. This implies an upper limit on $\mathrm{B}(K^+ \to \pi^+ \nu\overline{\nu}\ ) < 4.2 \times 10^{-9}$ (90% C.L.), and is consistent with the 2 events observed above the $K_{\pi 2}$ peak and the SM spectrum. Some additional reduction of the background levels in the remaining E787 data may be possible, but the major focus will shift to the new E949 experiment, which has significantly enhanced photon veto capabilities that will further suppress this background. In addition, the next experiment after E949, CKM at FNAL, will be essentially free of this background since there is no stopping target.

2.2 E949

E949 is an upgraded version of the E787 experiment, planning to capitalize on the full AGS beam to collect $K^+ \to \pi^+ \nu\overline{\nu}$ data at 14 times the rate of the E787 run in 1995. The new detector has substantially upgraded photon veto capabilities, enhanced tracking, triggering, monitoring, and DAQ capability, and will run at a higher AGS duty factor and a lower kaon momentum (with an increased fraction of stopped kaons). It has been designed to reach a sensitivity of at least 5 times beyond E787 and observe 5–10 SM events. The background level for E949 measurement of B($K^+ \to \pi^+ \nu\overline{\nu}$) above the $K_{\pi 2}$ peak is reliably projected from E787 data to be ~10% of the Standard Model signal.

E949 should see up to 10 SM events (or 20 events at the branching ratio measured by E787) within the next couple of years. This is an exciting opportunity to make a significant contribution to quark mixing and *CP*–violation that should be fully exploited. A history of the search for $K^+ \to \pi^+ \nu\overline{\nu}$ is shown in Figure 4.

2.3 CKM

The next step towards a precision measurement of B($K^+ \to \pi^+ \nu\overline{\nu}$) will be the CKM experiment at FNAL. CKM has been given scientific (Stage–1) approval by FNAL and could be running by 2007. CKM plans to use a novel technique for $K^+ \to \pi^+ \nu\overline{\nu}$: a decay in flight experiment, with redundant kinematic constraints from a conventional momentum spectrometer and a novel velocity spectrometer based on RICH counters. CKM expects to observe 100 SM signal events in a two year run, using the Main Injector simultaneously with the Tevatron. The background is expected to be ~10% of the SM signal, predominantly from $K^+ \to \pi^+ \pi^\circ$. A vacuum of 10^{-6} Torr is required to minimize backgrounds from kaon interactions in the decay volume. CKM will require less than 20% of the flux from the Main Injector, but will require a slow extracted spill of ~1 second duration. CKM will run with a 50 MHz 22 MeV/c beam with RF separators and about 70% K^+ purity. Figure 4 shows a projected measurement of B($K^+ \to \pi^+ \nu\overline{\nu}$) from CKM, assuming the current central value of the branching ratio.

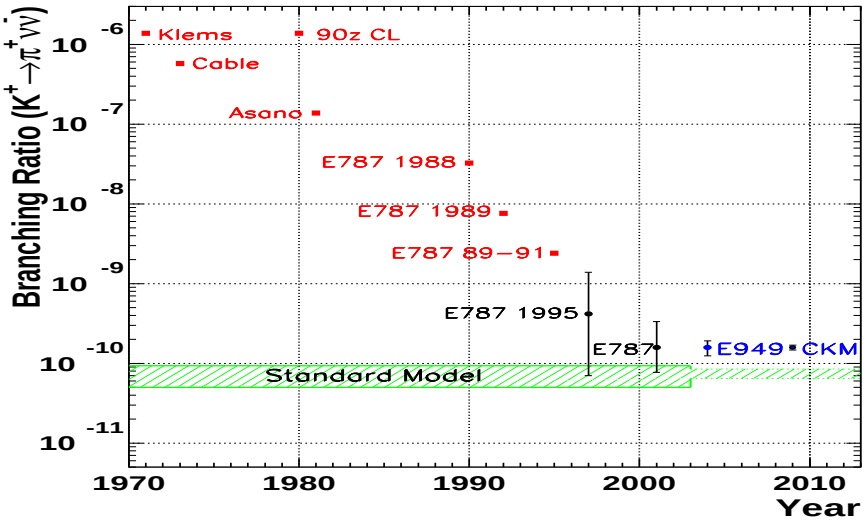

Figure 4: History of the search for $K^+ \to \pi^+ \nu\overline{\nu}$. The squares represent 90% CL limits, the dark circles are the E787 observation of $K^+ \to \pi^+ \nu\overline{\nu}$, and the projections of the current central value of the branching ratio to the proposed E949 and CKM sensitivities. The prediction from the SM is expected to narrow considerably once B_s°—$\overline{B_s^\circ}$ mixing has been observed.

3 $K_L^\circ \to \pi^\circ \nu\overline{\nu}$

The decay $K_L^\circ \to \pi^\circ \nu\overline{\nu}$ is even cleaner theoretically and is CP-violating. However, it is even more challenging experimentally as all of the particles involved are neutral.

Presently, the best limit on $K_L^\circ \to \pi^\circ \nu\overline{\nu}$ is derived in a model-independent way [10] from the E787 measurement of $K^+ \to \pi^+ \nu\overline{\nu}$:

$$\begin{aligned} B(K_L^\circ \to \pi^\circ \nu\overline{\nu}\,) &< 4.4 \times B(K^+ \to \pi^+ \nu\overline{\nu}\,) \\ &< 1.7 \times 10^{-9} \ \ (90\%\ \mathrm{CL}). \end{aligned} \tag{3}$$

Of course, it is desirable to observe this mode directly in order to extract a second constraint on the CKM matrix parameters. The current best direct limit is derived from a KTeV search for high transverse momentum π°'s decaying

via $\pi^\circ \to e^+e^-\gamma$. From the full 1997 data set, KTeV observed no events with an expected background of $0.12^{+0.05}_{-0.04}$ and set a 90%-CL limit [11] of

$$B(K_L^\circ \to \pi^\circ \nu\overline{\nu}\ ) < 5.9 \times 10^{-7}. \quad (4)$$

Due to the small $\pi^\circ \to e^+e^-\gamma$ branching ratio all future experiments plan to use the more copious $\pi^\circ \to \gamma\gamma$ mode. KTeV also made a search in this mode in a special one day test, with a highly collimated 'pencil' beam and observed one background event, most likely from a neutron interaction, and set a 90%-CL limit [12] of $\mathrm{B}(K_L^\circ \to \pi^\circ \nu\overline{\nu}\ ) < 1.6 \times 10^{-6}$.

3.1 E391

The next generation of $K_L^\circ \to \pi^\circ \nu\overline{\nu}$ experiments will start with E391a at the High Energy Accelerator Research Organization (KEK) which hopes to reach a sensitivity of 3×10^{-10}. This experiment will use a technique similar to KTeV, with a pencil beam, high quality calorimetry and very efficient photon vetos. This is the first experiment dedicated to searching for $K_L^\circ \to \pi^\circ \nu\overline{\nu}$ and aims to close the window for non-SM contributions to the decay. It will also serve as a test bed for the experimental techniques necessary to observe $K_L^\circ \to \pi^\circ \nu\overline{\nu}$ in future experiments. Beam tests were started in 2001 and the first data-taking run is scheduled for 2003. This experiment plans to eventually move to the Japanese Hadron Facility (JHF) in ~2007, and attempt to push to a sensitivity of $\mathcal{O}(1000)$ events.

3.2 KOPIO

The National Science Board of the National Science Foundation (NSF) has approved the construction of the two new large experiments at the BNL AGS: KOPIO and MECO, as components of the Rare Symmetry Violation Proposal (RSVP). RSVP is planned to be one of the next Major Research Equipment construction projects at the NSF.

The KOPIO experiment is designed to discover the $K_L^\circ \to \pi^\circ \nu\overline{\nu}$ decay and measure its branching ratio to ~20%. KOPIO will make use of a time-of-flight technique to measure the momentum of the K_L and will operate at a large targeting angle to improve the p_K resolution and soften the neutron spectrum to reduce π° hadroproduction. All possible aspects of the decay will be measured: the photon directions will be measured in a pre-radiator, the times and

energy will be precisely measured in a Shashlyk calorimeter, the time of the kaon's creation is determined by the proton bunch width from the AGS (~250 psec). KOPIO will have a substantial photon veto system and make the same sort of background measurements as E787, directly from the data, with two independent tools for attacking the major background, $K_L^\circ \to \pi^\circ\pi^\circ$, through both kinematics and photon veto. KOPIO expects to observe 50 SM events, with a background of 50%. This will allow a determination of $Im\lambda_t$ to 10%. KOPIO is expected to start data collection in ~2006.

4 Conclusion

The next decade will be an exciting time for improved understanding of *CP*-violation and quark mixing. It is quite likely that precise measurements of all four golden modes will be made: $B_d^\circ \to \psi K_S^\circ$ at the B-factories; $\Delta M_{B_d}/\Delta M_{B_s}$, most likely at the Tevatron; and $K \to \pi\nu\overline{\nu}$ at BNL, KEK and FNAL. These measurements will allow a precise determination of CKM parameters and provide a critical test of the SM picture of *CP*-violation.

5 Acknowledgements

I would like to thank Takao Inagaki, Bob Tschirhart, Taku Yamanaka, Takeshi Komatsubara, Shojiro Sugimoto, David Jaffe and Laurie Littenberg for discussions and/or comments on this paper. This work was supported in part under US Department of Energy contract #DE-AC02-98CH10886.

References

1. A. Buras, hep-ph/0101336 (2001); A. Buras and R. Fleischer, Phys. Rev. **D64**, 115010 (2001).
2. G. Bucahalla and A. Buras, Nucl. Phys. **B548**, 309 (1999).
3. G. Bucahalla and A. Buras, Phys. Lett. **B333**, 221 (1994); G. Bucahalla and A. Buras, Phys. Rev. **D54**, 6782 (1996); Y. Nir and M.P. Worah, Phys. Lett. **B423**, 319 (1998); S. Bergmann and G. Perez, JHEP **8**, 034 (2000).
4. Y. Grossman and Y. Nir, Phys. Lett. **B398**, 163 (1997).
5. G. D'Ambrosio and G. Isidori, hep-ph/0112135

6. S. Adler, *et al.*, Phys. Rev. Lett. **79**, 2204 (1997).
7. S. Adler, *et al.*, Phys. Rev. Lett. **84**, 3768 (2000).
8. S. Adler, *et al.*, Phys. Rev. Lett. **88**, 041803 (2002).
9. S. Adler, *et al.*, Phys. Lett. **B537**, 211 (2002).
10. Y. Grossman and Y. Nir, Phys. Lett. **B398**, 163 (1997).
11. A. Alavi-Harati *et al.*, Phys. Rev. **D61**, 072006 (2000).
12. J. Adams, *et al.*, Phys. Lett. **B447**, 240 (1999).

Frascati Physics Series Vol. XXVIII (2002), pp.263-272
HQ & L 2002 – Vietri s/m, May 27th - June 1st, 2002

RARE DECAY RESULTS FROM KTEV AND NA48

Taku Yamanaka
Physics Dept., Osaka University
1-1 Machikaneyama, Toyonaka, Osaka 560-0043 Japan

ABSTRACT

Recent results on rare kaon decays from Fermilab KTeV and CERN NA48 are summarized. The covered decay modes are: $K_L \to e^+e^-\gamma$, $K_L \to e^+e^-e^+e^-$, $K_L \to e^+e^-\mu^+\mu^-$, $\pi^0 \to e^+e^-e^+e^-$, $K_L \to \pi^+\pi^-e^+e^-$, $K_S \to \pi^+\pi^-e^+e^-$ and $K_S \to \pi^0e^+e^-$.

1 Introduction

The CERN NA48 and Fermilab KTeV experiments not only measure the CP violation parameter, $Re(\epsilon'/\epsilon)$, but also study various rare kaon decays. This is because both experiments use high flux neutral kaon beams and high performance detectors.

In this document, recent results on rare decays from both experiments are summarized. The $K_L \to e^+e^-\gamma$ and $K_L \to e^+e^-\mu^+\mu^-$ decays are tools to

understand the form factor of the kaon. The $\pi^0 \to e^+e^-e^+e^-$ decay is used to measure the form factor of π^0. The $K_L \to \pi^+\pi^-e^+e^-$ and $K_S \to \pi^+\pi^-e^+e^-$ are probes to observe CP violation in a kinematic distribution, and to measure form factors. The $K_S \to \pi^0 e^+e^-$ is necessary to untangle the CP violation effect in $K_L \to \pi^0 e^+e^-$ decay.

2 $K_L \to e^+e^-\gamma$

The $K_L \to e^+e^-\gamma$ and $K_L \to \mu^+\mu^-\gamma$ decays are probes for a long distance contribution in the kaon decays, since they proceed through $K_L \to \gamma^*\gamma$ where $\gamma^* \to \ell^+\ell^-$. This is important for extracting the CKM matrix element $|V_{td}|$ from the $K_L \to \mu^+\mu^-$ decay involving box and penguin diagrams. The $K_L \to \mu^+\mu^-$ decay is however, dominated by a process with two intermediate *real* photons, so this has to be subtracted based on $K_L \to \gamma\gamma$ measurement. In addition, the long distance contribution $K_L \to \gamma^*\gamma^{(*)} \to \mu^+\mu^-$ has to be subtracted, based on the $K_L \to e^+e^-\gamma$ and $K_L \to \mu^+\mu^-\gamma$ decay measurements.

The branching ratio of $K_L \to e^+e^-\gamma$ has been measured by NA48 to be $(10.6 \pm 0.2 \pm 0.2 \pm 0.4) \times 10^{-6}$ [1]. KTeV has collected 93.4k signal events, and recently gave $BR(K_L \to e^+e^-\gamma) = (10.13 \pm 0.04(stat) \pm 0.06(syst) \pm 0.29(ext.syst)) \times 10^{-6}$ (preliminary) [2] where the last external systematic error comes from the error on the branching ratio of $\pi^0 \to e^+e^-\gamma$.

The form factor [3] is measured by the M_{ee} distribution in the $K_L \to e^+e^-\gamma$ decay. However, for this measurement, one has to understand the effect of radiative corrections, since they also affect the M_{ee} distribution. KTeV has implemented the full and complete radiative corrections up to $O(\alpha^2)$ [4] in the Monte Carlo. In addition, one has to understand the amount of material in the beam because it also affects the ee mass resolution. One of the plots that KTeV showed to demonstrate such understanding is a track separation at the first drift chamber for $K_L \to e^+e^-\gamma$ and ee in the $K_L \to 3\pi^0$ decay where one of the π^0's decayed to $e^+e^-\gamma$. It shows that KTeV reproduces the distribution down to 2mm where the cut is applied. Figure 1 shows the M_{ee} distribution with the best fit result for the form factor, $\alpha_{K^*} = -0.192 \pm 0.011 \pm 0.009$ (preliminary) [2]. This is consistent with $\alpha_{K^*} = -0.160^{+0.026}_{-0.028}$ for $K_L \to \mu^+\mu^-\gamma$ decay measured by KTeV [5]. Current NA48's result for $K_L \to e^+e^-\gamma$ decay, $\alpha_{K^*} = -0.36 \pm 0.06 \pm 0.02$ [1], is 2.6 σ away from KTeV's new result, and a new result from NA48 with full data and complete radiative corrections is

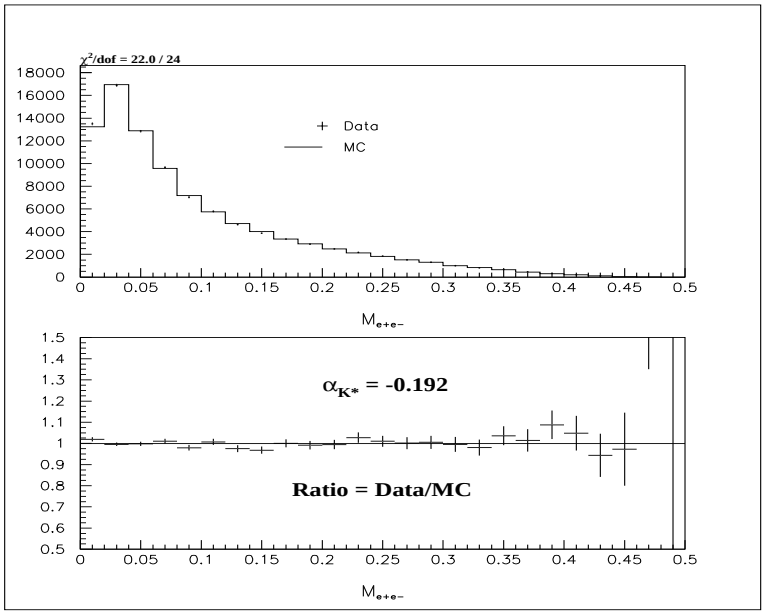

Figure 1: *Top figure shows the distribution of e^+e^- invariant mass for $K_L \to e^+e^-\gamma$ observed by KTeV. The dots show the data and the histogram show the Monte Carlo with the best fit α_{K^*}. Bottom figure shows the data/MC ratio.*

awaited.

3 $K_L \to e^+e^-\mu^+\mu^-$

The decay $K_L \to e^+e^-\mu^+\mu^-$ proceeds through two virtual photons, $K_L \to \gamma^*\gamma^* \to e^+e^-\mu^+\mu^-$. There are large variations between theoretical predictions of its branching ratio; 2.37×10^{-9} [6], $(1.63\pm0.07)\times10^{-9} \sim (3.67\pm0.15)\times10^{-6}$ depending on the amount of CP violating contribution [7], and $(1.3\pm0.2)\times10^{-9}$ [8].

Figure 2 shows the $ee\mu\mu$ invariant mass distribution observed by KTeV using 1997+1999 data. Based on 133 events in the signal region where 0.8 background events are expected, KTeV gave $BR = (2.61 \pm 0.23 \pm 0.18) \times 10^{-9}$ (preliminary) [9]. This result is consistent with their previous result, $BR =$

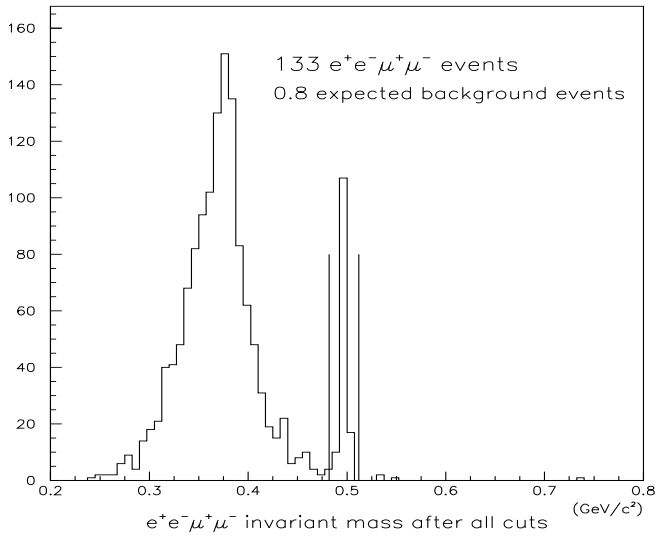

Figure 2: *The $e^+e^-\mu^+\mu^-$ invariant mass distribution for the KTeV 1997+1999 data. After all cuts, 133 events remain in the signal region.*

$(2.62 \pm 0.40 \pm 0.17) \times 10^{-9}$ [10] based on 43 events, and the first measurement, $BR = (2.9^{+6.7}_{-2.4}) \times 10^{-9}$ [11] based on one event. These results exclude some of the theoretical predictions shown above.

The ee and $\mu\mu$ mass distributions show a clear evidence for a non-trival form factor, and fits are in progress. During the conference, Isidori suggested to fit for a DIP form factor [12] α using $K_L \to e^+e^-\gamma$, and use its value as a constant when fitting for the other parameter, β, using $K_L \to e^+e^-\mu^+\mu^-$.

KTeV has looked at the angle (ϕ) between ee and $\mu\mu$ planes in the CMS frame, and found 63 events in the $\sin\phi\cos\phi > 0$ region and 70 events in the $\sin\phi\cos\phi < 0$ region. This is consistent with having no CP violating effects, as expected.

KTeV has also searched for lepton flavor violating decay, $K_L \to e^\pm e^\pm \mu^\mp \mu^\mp$. Based on no observed events, they set an upper limit $BR < 4.12 \times 10^{-11}$ (90% CL) (preliminary) [9] which is a factor 3 improvement over the previous result from KTeV [10].

4 $\pi^0 \to e^+e^-e^+e^-$

Just like $K_L \to e^+e^-\mu^+\mu^-$ and $K_L \to e^+e^-e^+e^-$, the decay $\pi^0 \to e^+e^-e^+e^-$ proceeds through two intermediate virtual photons, each converting to ee pair. KTeV has collected a total of 28k such events using $K_L \to 3\pi^0$ decays where one of the π^0's decayed to 4 electrons. They measured $BR(\ \pi^0 \to e^+e^-e^+e^-)/BR(\ \pi^0 \to \gamma\gamma) = (3.274 \pm 0.022 \pm 0.197) \times 10^{-5}$ (preliminary) [13]. This is consistent with the previous measurement back in 1962, $(3.18 \pm 0.30) \times 10^{-3}$, based on 146 events [14].

The analysis is under way to implement full radiative corrections and to fit for form factor and angular distributions.

5 $K_L \to \pi^+\pi^-e^+e^-$

The decay $K_L \to \pi^+\pi^-e^+e^-$ proceeds through $K_L \to \pi^+\pi^-\gamma^*$ where the γ^* internally converts to ee pair.

There are two major contributions; CP violating inner-bremsstrahlung where the γ^* is emitted from a pion, and CP conserving direct emission where the γ^* is emitted from the $K_L\pi^+\pi^-$ vertex. The interference between these contributions and the polarization of the γ^* which manifests itself by the ee plane, produces an asymmetry in the distribution of the angle ϕ between the $\pi\pi$ and ee planes. Using the current CP violation parameter, ϵ, the asymmetry between $\sin\phi\cos\phi > 0$ and < 0 is predicted to be about 14% [15].

The branching ratio was first measured by KTeV to be $(3.2 \pm 0.6 \pm 0.4) \times 10^{-7}$ based on 46 events [16], and a preliminary result, $(3.63 \pm 0.11 \pm 0.14) \times 10^{-7}$ (preliminary) was reported based on 1507.8 events using the 1997 data sample [17]. CERN NA48 has observed 1337 events in the signal region in the 1998+1999 data sample, as shown in Fig. 3. The signal to noise ratio is estimated to be 38. Based on this sample, they obtained $BR = (3.1 \pm 0.1 \pm 0.2) \times 10^{-7}$ (preliminary) [18]. KTeV now has 5056 ± 71 signal events on top of 185 background events in the full 1997+1999 data sample [19], and the analysis is in progress.

The asymmetry of the ϕ distribution was first measured by KTeV, as $A = (13.6 \pm 2.5 \pm 1.2)\%$ [20] based on the 1997 data. Using the data sample from 1998 and 1999 runs, NA48 recently measured $A = 13.9 \pm 2.7 \pm 2.0\%$ (preliminary) [18]. KTeV has also measured $A = 13.3 \pm 1.4(stat)\%$ (preliminary) based on

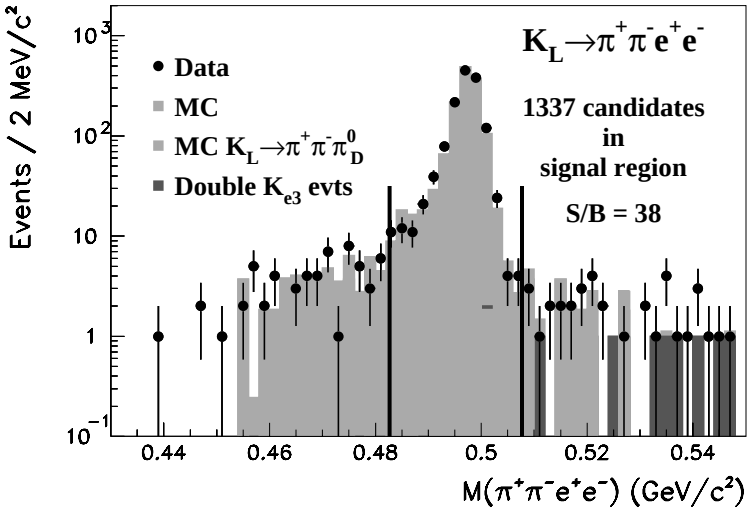

Figure 3: *The distribution of invariant mass of $\pi^+\pi^-e^+e^-$ observed by NA48 in the K_L beam. Dots show the data, and the histogram shows the Monte Carlo.*

the full data sample [19].

The form factors for the decay have been measured by KTeV using the 1997 data [20], and the full data sample is currently being analyzed.

6 $K_S \to \pi^+\pi^-e^+e^-$

The decay $K_S \to \pi^+\pi^-e^+e^-$ is similar to $K_L \to \pi^+\pi^-e^+e^-$ but it is dominated by the inner bremsstrahlung, since the CP violating direct emission is heavily suppressed. NA48 has observed these events for the first time, and measured $BR = (4.5 \pm 0.7 \pm 0.4) \times 10^{-5}$ based on 56 events in the 1998 data [21]. They have also shown that the ee invariant mass distribution is consistent with the inner bremsstrahlung. NA48 has recently analyzed data from 1998+1999 ϵ'/ϵ run and high intensity K_S run in 1999 for this decay mode. As shown in Fig. 4, they observed 921 events in the signal region, and measured $BR(K_S \to \pi^+\pi^-e^+e^-) = (4.3 \pm 0.2 \pm 0.3) \times 10^{-5}$ (preliminary) [18].

They have also looked at the distribution of the angle (ϕ) between the ee and $\pi\pi$ planes, and measured an asymmetry $A = (-0.2 \pm 3.4 \pm 1.4)\%$

(preliminary) [18] which is consistent with 0. Since the CP violating effect is negligible in this decay, the null asymmetry is an experimental evidence that the asymmetry due to final state interactions is negligible within the error.

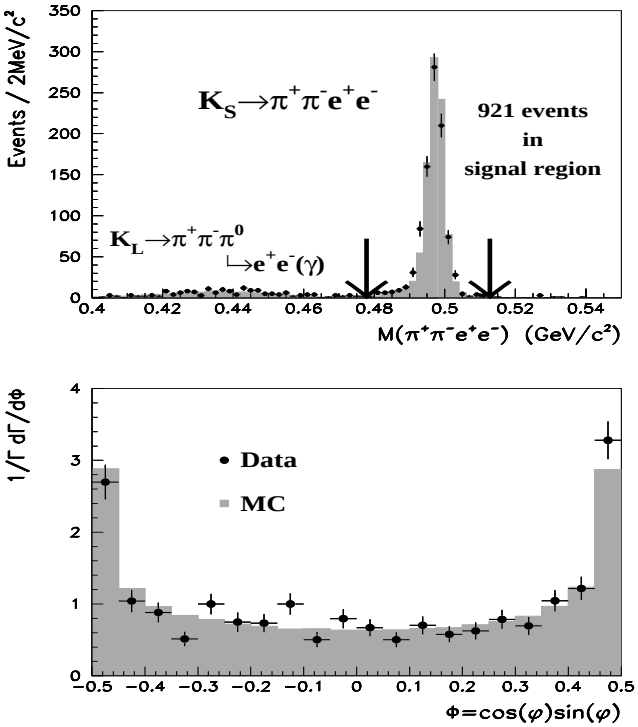

Figure 4: *The top figure shows the $\pi^+\pi^-e^+e^-$ invariant mass distributions for NA48 K_S beam. The dots show the data with 921 events in the signal region. The histogram shows the Monte Carlo. The bottom figure shows the distribution of* $\sin\phi\cos\phi$ *where ϕ is the angle between ee and $\pi\pi$ planes in the center of mass frame. Dots show the data, and the histogram shows the Monte Carlo. No evident asymmetry is observed.*

7 $K_S \to \pi^0 e^+ e^-$

One of the possible ways to measure the imaginary part of the CKM matrix, η, is to use $K_L \to \pi^0 e^+ e^-$. The $K_L \to \pi^0 e^+ e^-$ decay has several contributions;

direct CP violating penguin diagram, indirect CP violating amplitude with one virtual photon, and CP conserving amplitude with two virtual photons. In addition, SUSY penguin diagram could increase the branching ratio. In order to extract the direct CP violating contribution, one has to understand other contributions. The CP conserving contribution can be estimated from $K_L \to \pi^0\gamma\gamma$ decay measurements. The indirect CP violating amplitude can be directly measured from the branching ratio of $K_S \to \pi^0 e^+ e^-$.

NA48 had 40 hours of special K_S run in 1999 to searched for the decay, and set an upper limit, $BR(K_S \to \pi^0 e^+ e^-) < 1.4 \times 10^{-7}$ (90% CL) based on 0 observed events [22]. This limits the indirect CP violation contribution in the $K_L \to \pi^0 e^+ e^-$ branching ratio to $< 4 \times 10^{-10}$.

8 Future Prospects

NA48 will have a dedicated high intensity K_S run in 2002 by utilizing the existing K_S target station. Their original goal is to collect about ten $K_S \to \pi^0 e^+ e^-$ events, set better limits on $K_S \to 3\pi^0$ and $K_S \to \pi^+\pi^-\pi^0$ decays, increase the $K_S \to \gamma\gamma$ events by 2 orders of magnitude, increase the statistics for $K_S \to \pi^+\pi^- e^+ e^-$ events, and to study hyperon decays. This will be the most rich K_S program in the foreseeable future.

NA48 also has a plan to have a dedicated $K^\pm$ run. By splitting the charged kaons after the production target for tagging, and recombining them before the detector, they plan to compare the Dalitz plot between K^+ and $K^- \to \pi^\pm\pi^+\pi^-$ decays. The experiment has been approved, and it is under preparation.

KTeV has finished its data taking run, and they are analyzing the full data sample for various decay modes.

As covered by Steve Kettell in this conference, the CKM experiment at Fermilab is planning to collect one hundred $K^+ \to \pi^+\nu\overline{\nu}$ events decaying in flight to measure $|V_{td}|$. The experiment has been approved, and it is under preparation.

9 Summary

Besides the measurement of the CP violation parameter, ϵ'/ϵ, Fermilab KTeV and CERN NA48 experiments are producing many results on rare kaon decays.

With their high sensitivity, not only they are setting better limits on the real rare decay modes with $BR < O(10^{-10})$, they collect more than a hundred events for decay modes with $BR \sim O(10^{-9})$ such as $K_L \to e^+e^-\mu^+\mu^-$, and making accurate measurements on the semi-rare decays with $BR < O(10^{-5})$. These results on rare K_L decays will remain the best for the next decade, except for $K \to \pi\nu\overline{\nu}$ decays.

10 Acknowledgements

I would like to thank Rainer Wanke for providing me plots and information for preparing my talk.

References

1. V. Fanti *et al.*, Phys. Lett. **B 458**, 553 (1999).
2. J. Ladue, Presented at DPF2002, Williamsburg, VA, U.S.A. (2002).
3. L. Bergström, E. Massoò and P. Singer, Phys. Lett. 131 B, 229 (1983).
4. K.O. Mikaelian and J. Smith, Phys. Rev. **D 5**, 1763 (1972).
5. A. Alavi-Harati *et al.*, Phys. Rev. Lett. **87**, 071801 (2001).
6. C. Quigg, J.D. Jackson, unpublished, LBL preprint UCRL-18487 (1968).
7. Z. Uy, Phys. Rev. **D 43**, 802 (1991).
8. L. Zhang, J.L. Goity, Phys. Rev. **D 57**, 7031 (1998).
9. J. Hamm, Presented at DPF2002, Williamsburg, VA, U.S.A. (2002).
10. A.Alavi-Harati *et al.*, Phys. Rev. Lett. **87**, 111802 (2001).
11. P. Gu *et al.*, Phys. Rev. Lett. **76**, 4312 (1996).
12. G. D'Ambroisio, G. Isidori and J. Portolés, Phys. Lett. **B 423**, 385 (1998).
13. P. Toale, Presented at DPF2002, Williamsburg, VA, U.S.A. (2002).
14. N.P. Samios *et al.*, Phys. Rev. **126**, 1844 (1962).

15. L.M. Sehgal and M. Wanninger, Phys. Rev. **D 46**, 1035 (1992); *ibid.*, **D 46**, 5209 (E) (1992).

16. J. Adams it et al., Phys. Rev. Lett. **80**, 4123 (1998).

17. K. Senyo, Presented at EPS HEP99, Tampere, Finland (1999).

18. E. Mazzucato, Presented at International Conference on CP Violation, Ferrara, Italy (2000).

19. A. Golossanov, Presented at DPF2002, Williamsburg, VA, U.S.A. (2002).

20. A. Alavi-Harati it et al., Phys. Rev. Lett. **84**, 408 (2000).

21. A. Lai *et al.*, Phys. Lett. **B 496**, 137 (2000).

22. A. Lai *et al.*, Phys. Lett. **B 514**, 253 (2001).

Frascati Physics Series Vol. XXVIII (2002), pp.275-289
HQ & L 2002 – Vietri s/m, May 27th - June 1st, 2002

THEORY STATUS OF ε'/ε

Stefano Bertolini
INFN and SISSA, Via Beirut 4, I-34013 Trieste, Italy

ABSTRACT

I shortly review the present status of the theoretical calculations of ε'/ε and the comparison with the present experimental results. I discuss the role of higher order chiral corrections and in general of non-factorizable contributions for the explanation of the $\Delta I = 1/2$ selection rule and direct CP violation in kaon decays. Still lacking satisfactory lattice calculations, analytic methods and phenomenological approaches are helpful in understanding correlations among theoretical effects and experimental data. Substantial progress from lattice QCD is expected in the coming years.

1 Introduction

The results obtained in the last few years by the NA48 [1] and the KTeV [2] collaborations have marked a great experimental achievement, establishing some

35 years after the discovery of CP violation in the neutral kaon system [3] the existence of a much smaller violation acting directly in the decays:

$$\mathrm{Re}(\varepsilon'/\varepsilon) = \begin{cases} (15.3 \pm 2.6) \times 10^{-4} & (\mathrm{NA48}) \\ (20.7 \pm 2.8) \times 10^{-4} & (\mathrm{KTeV}). \end{cases} \quad (1)$$

The average of these results with the previous measurements by the NA31 collaboration at CERN and by the E731 experiment at Fermilab gives

$$\mathrm{Re}(\varepsilon'/\varepsilon) = (17.2 \pm 1.8) \times 10^{-4}. \quad (2)$$

While the Standard Model (SM) of strong and electroweak interactions provides an economical and elegant understanding of indirect (ε) and direct (ε') CP violation in term of a single phase, the detailed calculation of the size of these effects implies mastering strong interactions at a scale where perturbative methods break down. In addition, direct CP violation in $K \to \pi\pi$ decays arises from a detailed balance of two competing sets of contributions, which may hopelessly inflate the uncertainties related to the relevant hadronic matrix elements in the final outcome. All that makes predicting ε'/ε a complex and challenging task [4].

Just from the onset of the calculation the presence in the definition of ε'/ε , written as

$$\frac{\varepsilon'}{\varepsilon} = \frac{1}{\sqrt{2}} \left\{ \frac{\langle(\pi\pi)_{I=2}|\mathcal{H}_W|K_L\rangle}{\langle(\pi\pi)_{I=0}|\mathcal{H}_W|K_L\rangle} - \frac{\langle(\pi\pi)_{I=2}|\mathcal{H}_W|K_S\rangle}{\langle(\pi\pi)_{I=0}|\mathcal{H}_W|K_S\rangle} \right\} , \quad (3)$$

of given ratios of isospin amplitudes warns us of a longstanding and still unsolved theoretical "problem": the explanation of the $\Delta I = 1/2$ selection rule.

The $\Delta I = 1/2$ selection rule in $K \to \pi\pi$ decays is known since 45 years [5] and it states the experimental evidence that kaons are 400 times more likely to decay in the $I = 0$ two-pion state than in the $I = 2$ component ($\omega \equiv A_2/A_0 \simeq 1/22$). This rule is not justified by any symmetry argument and, although it is common understanding that its explanation must be rooted in the dynamics of strong interactions, there is up to date no derivation of this effect from first principle QCD.

Given the possibility that common systematic uncertainties may a-priori affect the calculation of ε'/ε and the $\Delta I = 1/2$ rule (see for instance the present difficulties in calculating on the lattice the "penguin contractions" for CP violating as well as for CP conserving amplitudes [6]) a convincing calculation

of ε'/ε must involve at the same time a reliable explanation of the $\Delta I = 1/2$ selection rule. Both observables indicate the need of large corrections to factorization in the evaluation of the four-quark hadronic transitions. Among these corrections Final State Interactions (FSI) play a substantial role. However, FSI alone are *not* enough to account for the large ratio of the $I = 0$ over $I = 2$ amplitudes. Other sources of large non-factorizable corrections are therefore needed for the CP conserving amplitudes [4, 8], which might affect the determination of ε'/ε as well. As a consequence, a self-contained calculation of ε'/ε should also address the determination of the $K \to \pi\pi$ rates.

2 OPE: an "effective" approach

The Operator Product Expansion (OPE) provides us with a very effective way to address the calculation of hadronic transitions in gauge theories. The integration of the "heavy" gauge and matter fields allows us to write the relevant amplitudes in terms of the hadronic matrix elements of effective quark operators and of the corresponding Wilson coefficients (at a scale μ), which encode the information about those dynamical degrees of freedom which are heavier than the chosen renormalization scale. According to the SM flavor structure the $\Delta S = 1$ transitions are effectively described by

$$\mathcal{H}_{\Delta S=1} = \frac{G_{\rm F}}{\sqrt{2}} V_{ud}\, V_{us}^* \sum_i \Big[z_i(\mu) + \tau\; y_i(\mu) \Big] Q_i(\mu) \;. \tag{4}$$

The entries V_{ij} of the 3×3 Cabibbo-Kobayashi-Maskawa (CKM) matrix describe the flavour mixing in the SM and $\tau = -V_{td}V_{ts}^*/V_{ud}V_{us}^*$. For $\mu < m_c$ ($q = u, d, s$), the relevant quark operators are:

$$\left.\begin{array}{rcl} Q_1 &=& (\overline{s}_\alpha u_\beta)_{\rm V-A}\,(\overline{u}_\beta d_\alpha)_{\rm V-A} \\ Q_2 &=& (\overline{s}u)_{\rm V-A}\,(\overline{u}d)_{\rm V-A} \end{array}\right\} \quad \text{Current-Current}$$

$$\left.\begin{array}{rcl} Q_{3,5} &=& (\overline{s}d)_{\rm V-A} \sum_q (\overline{q}q)_{\rm V\mp A} \\ Q_{4,6} &=& (\overline{s}_\alpha d_\beta)_{\rm V-A} \sum_q (\overline{q}_\beta q_\alpha)_{\rm V\mp A} \end{array}\right\} \quad \text{Gluon "penguins"} \tag{5}$$

$$\left.\begin{array}{rcl} Q_{7,9} &=& \frac{3}{2}\,(\overline{s}d)_{\rm V-A} \sum_q \hat{e}_q\,(\overline{q}q)_{\rm V\pm A} \\ Q_{8,10} &=& \frac{3}{2}\,(\overline{s}_\alpha d_\beta)_{\rm V-A} \sum_q \hat{e}_q (\overline{q}_\beta q_\alpha)_{\rm V\pm A} \end{array}\right\} \quad \text{Electroweak "penguins"}$$

Current-current operators are induced by tree-level W-exchange whereas the so-called penguin (and "box") diagrams are generated via an electroweak loop.

Only the latter "feel" all three quark families via the virtual quark exchange and are therefore sensitive to the weak CP phase. Current-current operators control instead the CP conserving transitions. This fact suggests already that the connection between ε'/ε and the $\Delta I = 1/2$ rule is by no means a straightforward one.

Using the effective $\Delta S = 1$ quark Hamiltonian we can write ε'/ε as

$$\frac{\varepsilon'}{\varepsilon} = e^{i\phi}\frac{G_{\rm F}\omega}{2|\epsilon|\,{\rm Re}\,A_0}\,{\rm Im}\,\lambda_t\ \left[\Pi_0 - \frac{1}{\omega}\,\Pi_2\right] \tag{6}$$

where

$$\begin{array}{rcl} \Pi_0 & = & \frac{1}{\cos\delta_0}\sum_i y_i\ {\rm Re}\langle Q_i\rangle_0\ (1-\Omega_{\rm IB}) \\ \Pi_2 & = & \frac{1}{\cos\delta_2}\sum_i y_i\ {\rm Re}\langle Q_i\rangle_2 \quad , \end{array} \tag{7}$$

and $\langle Q_i\rangle \equiv \langle\pi\pi|Q_i|K\rangle$. The rescattering phases $\delta_{0,2}$ can be extracted from elastic π-π scattering data [7] and are such that $\cos\delta_0 \simeq 0.8$ and $\cos\delta_2 \simeq 1$. Given that the phase of ε (θ_ε) is approximately $\pi/4$, as well as the difference $\delta_0 - \delta_2$, the ε'/ε phase $\phi = \frac{\pi}{2} + \delta_2 - \delta_0 - \theta_\varepsilon$ turns out to be consistent with zero. While $G_{\rm F}$, ω, $|\varepsilon|$ and ${\rm Re}\,A_0$ are precisely determined by experimental data, the first source of uncertainty that we encounter in eq. 6 is the value of ${\rm Im}\,\lambda_t \equiv {\rm Im}(V_{ts}^* V_{td})$, the combination of CKM elements which measures CP violation in $\Delta S = 1$ transitions. The determination of ${\rm Im}\,\lambda_t$ depends on B-physics constraints and on ε [9]. In turn, the fit of ε depends on the theoretical determination of B_K, the $\bar{K}^0 - K^0$ hadronic parameter, which should be self-consistently determined within every analysis. The theoretical uncertainty on B_K was in the past the main component of the final uncertainty on ${\rm Im}\,\lambda_t$. The improved determination of the unitarity triangle coming from B-factories and hadronic colliders [10] has weakened and will eventually lift the dependence of ${\rm Im}\,\lambda_t$ on B_K, allowing for an experimental measurement of the latter from ε . Within kaon physics, the decay $K_L \to \pi^0\nu\bar{\nu}$ gives the cleanest "theoretical" determination of ${\rm Im}\,\lambda_t$, albeit representing a great experimental challenge. At present, a typical range of values for ${\rm Im}\,\lambda_t$ is $(0.94 - 1.60)\times 10^{-4}$ [11].

We come now to the quantities in the square brackets. While the calculation of the Wilson coefficients is well under control, thanks primarily to the work done in the early nineties by the Munich [12] and Rome [13] groups, the evaluation of the "long-distance" factors in eq. 7 is the crucial issue for the ongoing calculations. The isospin breaking (IB) parameter $\Omega_{\rm IB}$, gives at the leading-order (LO) in the chiral expansion a *positive* correction to the A_2

amplitude (proportional to A_0 via the $\pi^0 - \eta$ mixing) of about 0.13 [14]. At the next-to-leading order (NLO) the full inclusion of the $\pi^0 - \eta - \eta'$ mixing lift the value of $\Omega_{\rm IB}$ to 0.16 ± 0.03 [15]. On the other hand, the complete NLO calculation of IB effects beyond the $\pi^0 - \eta - \eta'$ mixing (of strong and electromagnetic origin, among which the presence of $\Delta I = 5/2$ transitions) involves a number of unknown NLO chiral couplings and is presently quite uncertain. Dimensional estimates show that IB effects may be large and affect ε'/ε sizeably in both directions [16]. Although a partial cancellation of the indirect ($\Delta\omega$) and direct $\Delta\Omega_{\rm IB}$ NLO isospin breaking corrections in eq. 6 may reduce their final numerical impact on ε'/ε , we must await for further analyses in order to confidently assess their relevance. At present one may use $\Omega_{\rm IB} = 0.10 \pm 0.20$ [17, 18, 19] as a conservative estimate of the IB effects.

The final basic ingredient for the calculation of ε'/ε is the evaluation of the $K \to \pi\pi$ hadronic matrix elements of the quark operators in eq. 5. A simple albeit naive approach to the problem is the Vacuum Saturation Approximation (VSA), which is based on two drastic assumptions: the factorization of the four quark operators in products of currents and densities and the saturation of the intermediate states by the vacuum state. As an example:

$$\begin{aligned} \langle \pi^+\pi^- | Q_6 | K^0 \rangle \;\; &= \;\; 2\, \langle \pi^- | \overline{u}\gamma_5 d | 0 \rangle \langle \pi^+ | \overline{s} u | K^0 \rangle - 2\, \langle \pi^+\pi^- | \overline{d} d | 0 \rangle \langle 0 | \overline{s}\gamma_5 d | K^0 \rangle \\ &+ \; 2\, \left[\langle 0 | \overline{s} s | 0 \rangle - \langle 0 | \overline{d} d | 0 \rangle \right] \langle \pi^+\pi^- | \overline{s}\gamma_5 d | K^0 \rangle \end{aligned} \qquad (8)$$

The VSA does not exhibit a consistent matching of the renormalization scale and scheme dependences of the Wilson coefficients and it carries potentially large systematic uncertainties [4]. On the other hand it provides useful insights on the main features of the problem. A pictorial summary of the relative weights of the contributions of the various operators to ε'/ε , as obtained in the VSA, is shown in Fig. 1.

As we have already mentioned, CP violation involves loop-induced operators ($Q_3 - Q_{10}$). From Fig. 1 one clearly notices the potentially large cancellation among the strong and electroweak sectors and the leading role played by the gluonic penguin operator Q_6 and the electroweak operator Q_8. Tipical range of values for ε'/ε , obtained using the VSA, are shown in Fig. 2 together with the three most updated predictions available before 1999 (when the first KTeV and NA48 results became known) [20, 21, 27]. The fact that the cancellation among the strong and electroweak sectors turns out to be quite

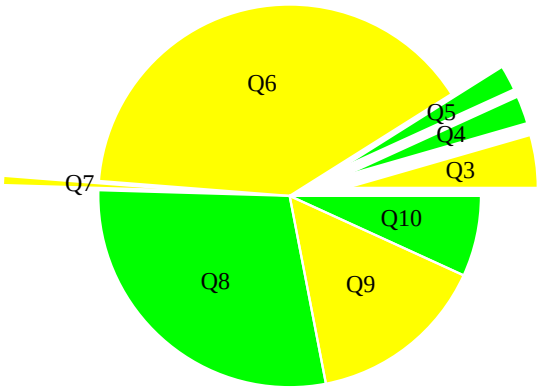

Figure 1: Anatomy of ε'/ε in the Vacuum Saturation Approximation. In light (dark) gray the positive (negative) contributions of the effective four-quark operators are shown with proportional weight.

effective (in the VSA) warns us about the possibility that the uncertainties in the determination of the relevant hadronic matrix elements may be largely amplified in the calculation of ε'/ε . It is therefore important to asses carefully the approximations related to the various parts of the calculations. In particular, the analysis of the problem suggests that factorization may be highly unreliable.

3 Beyond Factorization

The dark gray bars in Fig. 2 depict the results of three calculations of ε'/ε which are representative of approaches that (in principle) allow us to go beyond naive factorization. They are based from left to right on the large N_c expansion [20, 22], on lattice regularization [21, 23], and on phenomenological modelling of low-energy QCD (the chiral quark model) [24, 25, 26, 27].

The experimental and theoretical scenarios have changed substantially after the first KTeV data and the subsequent NA48 results. Fig. 3 shows the present experimental world average for ε'/ε compared with the revised or new theoretical calculations that appeared during the last year. Without entering into the details of the results (for a short summary see [28]) they all represent attempts to incorporate non-perturbative information into the

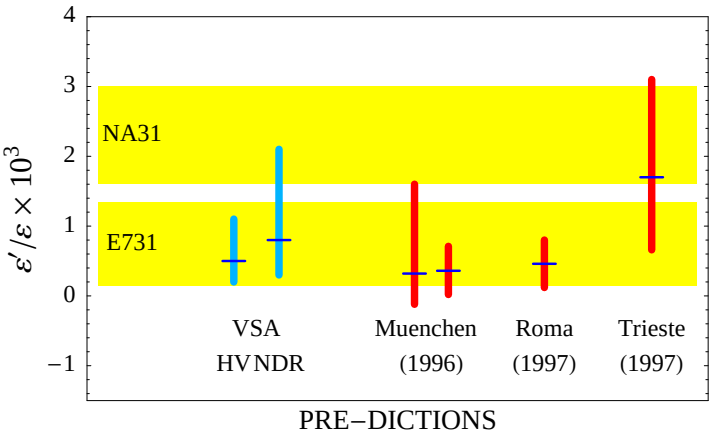

Figure 2: The 1-σ results of the NA31 and E731 Collaborations (early 90's) are shown by the gray horizontal bands. The old München, Roma and Trieste theoretical predictions for ε'/ε are depicted by the vertical bars with their central values. For comparison, the VSA estimate is shown using two renormalization schemes.

calculation of the hadronic matrix elements, whether their are based on the large N_c expansion (München [29], Dortmund [30], Beijing [31], Taipei [32], Valencia [33]), phenomenological modelling of low-energy QCD (Dubna [34], Trieste [27, 35], Lund [36]), QCD Sum Rules (Montpellier [37]) or, finally, on lattice regularization (Roma [6], CP-PACS [38], RBC [39]).

Overall most of the theoretical calculations are consistent with a non-vanishing positive effect in the SM (with the exception of the recent lattice results on which I will comment shortly).

At a closer look however, if we focus our attention on the central values, many of the predictions prefer the 10^{-4} regime, whereas only a few of them stand above 10^{-3}. Is this just "noise" in the theoretical calculations? Without entering the many details on which the estimates are based, most of the aforementioned difference can be explained in terms of a single effect: the different size of the hadronic matrix element of the gluonic penguin Q_6 as obtained in the various approaches. In turn, this can be understood in terms of sizeable higher order chiral contributions (NLO in the $1/N_c$ expansion) to the $I = 0$ amplitudes.

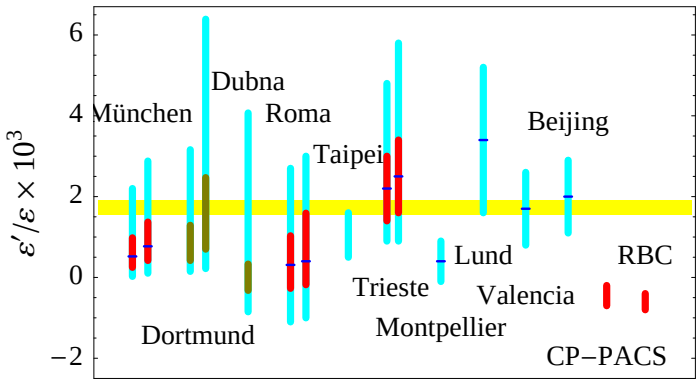

Figure 3: Recent theoretical calculations of ε'/ε are compared with the combined 1-σ average of the NA31, E731, KTeV and NA48 results ($\varepsilon'/\varepsilon = 17.2 \pm 1.8 \times 10^{-4}$), depicted by the gray horizontal band.

This effect was stigmatized well before the latest experimental round by the work of the Trieste group [26, 27], and appears clearly in the comparison of the leading $1/N_c$ and lattice results with the chiral quark model analysis in Fig. 2. The chiral quark model approach, together with the fit of the CP conserving amplitudes which normalizes phenomenologically the matching and the model parameters, allows us to carry the calculation of the hadronic matrix elements beyond the leading order in the chiral expansion (including the needed local counterterms). Non-factorizable chiral contributions (missing in the leading $1/N_c$ or lattice calculations) were shown to produce a substantial enhancement of the $I = 0$ transitions thus lifting the expectation of ε'/ε at the 10^{-3} level.

Since then a number of groups have attempted to improve the calculation of $K \to \pi\pi$ matrix elements in a model independent way. Table 3 presents a comparison of different calculations of the relevant matrix elements. Due to the leading role played by Q_6 and Q_8 we may write a simplified version of eq. 6,

$$\frac{\varepsilon'}{\varepsilon} \approx 13 \left(\frac{\Lambda^{(4)}_{\overline{MS}}}{340 \text{ MeV}} \right) \text{Im}\, \lambda_t \left[\frac{110 \text{ MeV}}{m_s \ (2 \text{ GeV})} \right]^2 \left[B_6(1 - \Omega_{\text{IB}}) - 0.4 B_8^{(2)} \right] , \quad (9)$$

which although "not be used for any serious analysis" [29] gives an effective and practical way to test and compare different calculations.

The B-factors $B_i \equiv \langle Q_i \rangle \,/\, \langle Q_i \rangle_{\rm VSA}$ represent a convenient parametrization of the hadronic matrix elements, albeit tricky, in that their values are in general scale and renormalization-scheme dependent, and a spurious dependence on the quark masses is introduced in the result whenever quark densities are involved. The latter is the case for the Q_6 and Q_8 penguins. As a consequence the VSA normalization may vary from author to author thus introducing systematic ambiguities. By taking the VSA matrix elements at the scale $\mu = 2$ GeV we obtain [4]

$$\begin{aligned} &\langle (\pi\pi)_2 | Q_8 | K^0 \rangle_{\rm VSA} = \sqrt{6}\, f\, m_K^4\, (m_s + m_d)^{-2} \simeq 1.1 \text{ GeV}^3 \,, \\ &\langle \pi\pi | Q_6 | K^0 \rangle_{\rm VSA} \,/\, \langle (\pi\pi)_2 | Q_8 | K^0 \rangle_{\rm VSA} = -2\sqrt{2}\, (f_K - f_\pi)/f_\pi \simeq -0.63 \,, \end{aligned} \tag{10}$$

where I have used $(m_s + m_d)(2 \text{ GeV}) = 110$ MeV and the chiral value $f = 86$ MeV for the octet decay constant.

It is known that B_6 and $B_8^{(2)}$ are perturbatively very weakly dependent on the renormalization scale [4]. Therefore it makes sense to compare the B's obtained in different approaches, where the matrix elements $\langle Q_i \rangle$ are computed at different scales. The results for the relevant penguin matrix elements coming from various approaches are collected in Table 3, paying care to normalizing the data in a homogeneous way (as far as detailed information on definitions and renormalization schemes was available).

As a guiding information, taking $\mathrm{Im}\,\lambda_t = 1.3 \times 10^{-4}$, the present experimental central value of ε'/ε is reproduced by $B_6\,(1 - \Omega_{\rm IB}) - 0.4\, B_8^{(2)} \approx 1$.

The most important fact is the first evidence of a signal in lattice calculations of $\langle \pi | Q_6 | K \rangle$, obtained by the CP-PACS [38] and RBC [39] collaborations. Both groups use the Domain Wall Fermion approach which allows to control the chiral symmetry on the lattice as a volume effect in a fifth dimension. This approach softens in principle the problem of large power subtractions which affects the lattice extraction of $I = 0$ amplitudes (penguin contractions). Still only the $\langle \pi | Q_i | K \rangle$ transition is computed on the lattice and LO chiral perturbation theory is used to extrapolate it to the physical amplitude. The two groups obtain comparable values of the Q_6 and Q_8 matrix elements leading both to a negative ε'/ε (and do not agree on the CP conserving $I = 0$ amplitude). On the other hand the calculations are at an early stage and do not include higher order chiral dynamics which may be responsible for the enhancement of $I = 0$ amplitudes (as large N_c approaches beyond LO and the Chiral Quark Model strongly suggest). The SPQcdR collaboration has reported a result for

Table 1: Comparison of various calculations of penguin matrix elements. The data marked by the star are rescaled by a factor $\sqrt{3/2}$, to account for a different definition of the isospin matrix elements.

Method	B_6 (NDR)	$B_8^{(2)}$ (NDR)	
Lattice (DWF, $K \to \pi$)	< 0.3	~ 0.9	CP-PACS [38]
Lattice (DWF, $K \to \pi$)	~ 0.4	~ 1	RBC [39]
Lattice ($K \to \pi + \chi$PT)	–	0.58 ± 0.06 *	APE [40]
Lattice ($K \to \pi + \chi$PT)	–	0.56 ± 0.07 *	SPQcdR [41]
Lattice ($K \to \pi\pi$)	–	0.64 ± 0.07 *	SPQcdR [41]
Large N_c+LMD (χ-limit)	–	2.6 ± 0.8 *	Marseille [42]
Dispersive+data (χ-limit)	–	2.5 ± 0.8 *	Amherst [43]
Dispersive+data (χ-limit)	–	1.4 ± 0.6	Lund [44]
Large N_c + data	1.0 ± 0.3	0.8 ± 0.2	Munich [29]
NLO $1/N_c$ CHPT	$1.5 \sim 1.7$	$0.4 \sim 0.7$	Dortmund [30]
NLO $1/N_c$ ENJL (χ-limit)	2.9 ± 0.5	1.5 ± 0.2	Lund [36]
NLO χQM + χPT	1.5 ± 0.4	0.84 ± 0.04	Trieste [27]
Large N_c + FSI	1.55 ± 0.10	0.92 ± 0.03	Valencia [33]

the Q_8 matrix element from direct calculation of the $K \to \pi\pi$ amplitude on the lattice. This result agrees with previous lattice data, albeit it does not yet include the chiral corrections relevant to quenching and to the extrapolation to the physical pion mass [41].

Among the analytic approaches important results have been obtained using data on spectral functions in connection with QCD sum rules and dispersive relations in the attempt to obtain model independent information on the relevant matrix elements. These approaches have produced as of today calculations of Q_8 (in the chiral limit) which are subtantially larger than the factorization (and lattice) results. While there is still disagreement among the different analysis, we must await the calculation of the Q_6 matrix element and a quantitative assessment of chiral breaking effects before drawing conclusions on these as well as lattice results.

Calculations which sofar have allowed for the determination of all relevant parameters, based on chiral perturbation theory and/or models of low-energy QCD, have shown the crucial role of higher order non-factorizable corrections

in the enhancement of the $I = 0$ matrix elements [27, 30, 33, 36]. Chiral loop corrections drive the final value of ε'/ε in the ballpark of the present data. However the calculation of higher order chiral effects cannot be fully accomplished in a model independent way due to the many unknown NLO local couplings. In the chiral quark model approach all needed local interactions are computed in terms of quark masses, meson decay constants and a few non-perturbative parameters as quark and gluon condensates. The latter are determined self-consistently in a phenomenological way via the fit of the CP conserving $K \to \pi\pi$ amplitudes, thus encoding the $\Delta I = 1/2$ rule in the calculation [26, 27]. The analysis shows that the role of local counterterms is subleading to the chiral logs when using the Modified Minimal Subtraction (as opposed to the commonly used Gasser-Leutwyler prescription). The phenomenological fit is crucial in stabilizing the numerical prediction [27]. The fact that the model parameters (quark and gluon condesates, constituent quark mass) turn out to be in the expected range, shows that the explicitly included chiral (and $1/N$ gluon condensate) corrections represent the largest non-factorizable effect.

Among higher order corrections FSI play a leading role. As a matter of fact, one should in general expect an enhancement of ε'/ε with respect to the naive VSA due to FSI. As Fermi first argued [45], in potential scattering the isospin $I = 0$ two-body states feel an attractive interaction, of a sign opposite to that of the $I = 2$ components thus affecting the size of the corresponding amplitudes. This feature is at the root of the enhancement of the $I = 0$ amplitude over the $I = 2$ one and of the corresponding enhancement of ε'/ε beyond factorization. An attempt to resum these effects in a model independent way has been worked out by the authors of ref. [33], using a dispersive approach a la Omnès-Mushkelishvili [46, 47]. Their analysis shows that resummation does not substantially modify the one-loop perturbative result and, as it appears from Table 3, a 50% enhancement of the gluonic penguin matrix element is found over the factorized result. However, the calculation suffers from a sistematic uncertainty due to the indetermination of the off-shell amplitude which is identified with the large N_c result [48]. Even when the authors in the most recent work match the dispersive resummation with the on-shell perturbative one-loop calculation, thus including $1/N_c$ effects, again a systematic uncertainty remains in the unknown polinomial parts of the local chiral counterterms. Therefore, a model-independent complete calculation of chiral loops

for $K \to \pi\pi$ is still missing.

Finally, it has been recently emphasized [49] that cut-off based approaches should pay attention to higher-dimension operators which become relevant for matching scales below 2 GeV and may represent one of the largest sources of uncertainty in present calculations. The results of refs. [43, 44] include these effects. The calculations based on dimensional regularization may be safe if phenomenological input is used in order to encode in the relevant hadronic matrix elements the physics at all scales (this is done in the Trieste approach).

In summary, while model dependent calculations suggest no conflict between theory and experiment for ε'/ε , a precise and "pristine" prediction of the observable is still quite ahead of us.

4 Outlook and Conclusions

Higher-order chiral corrections are taking the stage of $K \to \pi\pi$ physics. They are needed in order to asses the size of crucial parameters (as $\Omega_{\rm IB}$) and the effect of non-factorizable contributions in the penguin matrix elements.

Lattice, as a regularization of QCD, is *the* first-principle approach to the problem. However, lattice calculations still heavily depend on chiral perturbation theory [50]. Presently, very promising developments are being undertaken to circumvemt the technical and conceptual shortcomings related to the calculation of weak matrix elements [41, 51]. Among those are the Domain Wall Fermion approach [52] which allows us to decouple the chiral symmetry from the continuum limit, and the very interesting observation that the Maiani-Testa theorem [53] can be overcomed using the fact that lattice calculations are performed in finite volume [54], thus allowing for the direct calculation of the physical $K \to \pi\pi$ amplitude on the lattice. All these developments need a tremendous effort in machine power and in devising faster algorithms. Preliminary results for lattice calculations of both ε'/ε and the $\Delta I = 1/2$ selection rule are already available and others are currently under way [41].

In the meantime analytical and semi-phenomenological approaches have been crucially helpful in driving the attention of the community on some systematic short-comings of "first-principle" calculations. The amount of theoretical work triggered by the NA48 and KTeV data promises rewarding and perhaps exciting results in the forthcoming years.

References

1. A. Lai *et al.* , Eur. Phys. J. C **22**, 231 (2001); S. Giudici, these Proceedings.
2. A. Alavi-Harati *et al.* , Phys. Rev. Lett. **83**, 22 (1999); S. Giudici, in 1).
3. J.H. Christenson *et al.* , Phys. Rev. Lett. **13**, 138 (1964).
4. S. Bertolini, J.O. Eeg and M. Fabbrichesi, Rev. Mod. Phys. **72**, 65 (2000); A.J. Buras, *Erice School Lectures 2000*, hep-ph/0101336.
5. M. Gell-Mann and A. Pais, Proc. Glasgow Conf. , 342 (1955).
6. M. Ciuchini and G. Martinelli, Nucl. Phys. Proc. Suppl. **99B**, 27 (2001).
7. J. Gasser and U.G. Meissner, Phys. Lett. B **258**, 219 (1991); E. Chell and M.G. Olsson, Phys. Rev. D **48**, 4076 (1993).
8. J.-M. Gérard and J. Weyers, Phys. Lett. B **503**, 99 (2001); N.I. Kochelev and V. Vento, Phys. Rev. Lett. **87**, 111601 (2001).
9. M. Ciuchini *et al.* , JHEP **0107**, 013 (2001).
10. K. Kleinknecht, these Proceeedings.
11. A.J. Buras, Proc. *Kaon 2001* Conf., Pisa, Italy, hep-ph/0109197.
12. A.J. Buras *et al.* , Nucl. Phys. B **370**, 69 (1992); Nucl. Phys. B **400**, 37 (1993); Nucl. Phys. B **400**, 75 (1993); Nucl. Phys. B **408**, 209 (1993).
13. M. Ciuchini *et al.* , Phys. Lett. B **301**, 263 (1993); Nucl. Phys. B **415**, 403 (1994).
14. J. Gasser and H. Leutwyler, Nucl. Phys. B **250**, 465 (1985).
15. G. Ecker *et al.* , Phys. Lett. B **467**, 88 (2000).
16. S. Gardner and G. Valencia, Phys. Lett. B **466**, 355 (1999).
17. S. Gardner and G. Valencia, Phys. Rev. D **62**, 094024 (2000).
18. K. Maltman and C. Wolfe, Phys. Lett. B **482**, 77 (2000); Phys. Rev. D **63**, 014008 (2001).

19. V. Cirigliano, J.F. Donoghue and E. Golowich, Phys. Lett. B **450**, 241 (1999); Phys. Rev. D **61**, 093001 (2000); Phys. Rev. D **61**, 093002 (2000); Eur. Phys. J. C **18**, 83 (2000).

20. A.J. Buras, M. Jamin and E. Lautenbacher, Phys. Lett. B **389**, 749 (1996).

21. Ciuchini *et al.* , Z. Phys. C **68**, 239 (1995); Nucl. Phys. Proc. Suppl. **59**, 149 (1997).

22. W.A. Bardeen, A.J. Buras and J.M. Gerard, Nucl. Phys. B **293**, 787 (1987).

23. G. Martinelli, Proc. *Kaon 99* Conf., Chicago, USA, hep-ph/9910237.

24. S. Weinberg, Physica **A**, 96 (327)1979; A. Manhoar and H. Georgi, Nucl. Phys. B **234**, 189 (1984).

25. A. Pich and E. de Rafael, Nucl. Phys. B **358**, 311 (1991).

26. S. Bertolini *et al.* , Nucl. Phys. B **514**, 63 (1998).

27. S. Bertolini *et al.* , Nucl. Phys. B **514**, 93 (1998); Phys. Rev. D **63**, 056009 (2001).

28. S. Bertolini, Proc. *RADCOR 2000*, Carmel, USA, eConf C000911, hep-ph/0101212.

29. A.J. Buras, Proc. *Kaon 99* Conf., Chicago, USA, hep-ph/9908395.

30. T. Hambye *et al.* , Phys. Rev. D **58**, 014017 (1998); Nucl. Phys. B **564**, 391 (2000).

31. Yue-Liang Wu, Phys. Rev. D **64**, 016001 (2001).

32. H.Y. Cheng, Chin. J. Phys. **38**, 1044 (2000).

33. E. Pallante and A. Pich, Phys. Rev. Lett. **84**, 2568 (2000); Nucl. Phys. B **592**, 294 (2000); E. Pallante, A. Pich and I. Scimemi, Nucl. Phys. B **617**, 441 (2001).

34. A.A. Bel'kov *et al.* , hep-ph/9907335.

35. M. Fabbrichesi, Phys. Rev. D **62**, 097902 (2000).

36. J. Bijnens and J. Prades, JHEP **0006**, 035 (2000).

37. S. Narison, Nucl. Phys. B **593**, 3 (2001).

38. J. Noaki *et al.* , hep-lat/0108013.

39. T. Blum *et al.* , hep-lat/0110075.

40. A. Donini *et al.* , Phys. Lett. B **470**, 233 (1999).

41. G. Martinelli, Nucl. Phys. Proc. Suppl. **106**, 98 (2002), hep-lat/0112011.

42. M. Knecht, S. Peris and E. de Rafael, Phys. Lett. B **508**, 117 (2001); S. Peris, hep-ph/0204181.

43. V. Cirigliano, J.F. Donoghue, E. Golowich and K. Maltman, Phys. Lett. B **522**, 245 (2001).

44. J. Bijnens, E. Gamiz and J. Prades, JHEP **0110**, 009 (2001).

45. E. Fermi, Suppl. Nuovo Cim. **2**, 17 (1955).

46. N.I. Mushkelishvili, *Singular Integral Equations* (Noordhoff, Gronigen, 1953), p. 204; R. Omnès, Nuovo Cim. **8**, 316 (1958).

47. T.N. Truong, Phys. Lett. B **207**, 495 (1988); U. Meissner, in "Perspectives in Nucl. Physics at Intermediate Energies" 385-398, Trieste 1991.

48. A. J. Buras *et al.* , Phys. Lett. B **480**, 80 (2000); M. Buechler *et al.* , Phys. Lett. B **521**, 29 (2001).

49. V. Cirigliano, J.F. Donoghue and E. Golowich, JHEP **0010**, 048 (2000).

50. M. Golterman and E. Pallante, Nucl. Phys. Proc. Suppl. **106**, 335 (2002), hep-lat/0110183.

51. C.T. Sachrajda, Proc. *Lepton-Photon 2001*, Roma, Italy, hep-ph/0110304.

52. D. Kaplan, Phys. Lett. B **288**, 342 (1992).

53. L. Maiani and M. Testa, Phys. Lett. B **245**, 585 (1990).

54. L. Lellouch and M. Lüscher, Comm. Math. Phys. **219**, 31 (2001).

Frascati Physics Series Vol. XXVIII (2002), pp.291-297
HQ & L 2002 – Vietri s/m, May 27th - June 1st, 2002

EXPERIMENTAL STATUS OF $\mathcal{R}e(\epsilon'/\epsilon)$

Sergio Giudici
Scuola Normale Superiore and INFN sez. Pisa

ABSTRACT

The experimental status of the direct CP violation parameter $\mathcal{R}e(\epsilon'/\epsilon)$ of the neutral kaon system is reviewed. The experimental techniques adopted by the experiments KTEV and NA48 are briefly discussed. The current average value, $\mathcal{R}e(\epsilon'/\epsilon) = (17.2 \pm 1.8) \times 10^{-4}$, establishes direct CP violation beyond any doubt.

1 Introduction

Since its discovery in 1964 by Christenson, Cronin, Fitch and Turlay [1] in the decay $K_L \to \pi^+\pi^-$, the origin of CP violation has remained an enigma in particle physics for a long time. The $K^0 - \bar{K}^0$ system subsequently provided other experimental evidences of CP violating effects: the decay $K_L \to 2\pi^0$ [2], [3], the charge asymmetry in $K_L \to \pi^\pm e^\mp \nu$ [4] and $K_L \to \pi^\pm \mu^\mp \nu$ [5], the decay

$K_L \to \pi^+\pi^-\gamma$ [6] and, more recently, the asymmetry between the decay planes of $\pi^+\pi^-$ and e^+e^- in $K_L \to \pi^+\pi^-e^+e^-$ [7]. All these effects are successfully described by the mixing between K^0 and $\bar{K}^0$ strangeness eigenstates induced by a "super-weak" force as proposed by L. Wolfenstein [8] which is characterized by the mixing parameter ϵ. In this model the quantity ϵ is the ratio between the CP-violating to CP conserving amplitude for a given process of K_L and K_S. The Standard Model with three flavor generations can incorporate CP violation in a natural way in the weak interactions [9]. It is then possible that the CP-odd eigenstate $K_2 = (K^0 - \bar{K}^0)/\sqrt{2}$ can decay directly into a pion pair (direct CP violation). The parameter ϵ', describing direct CP violation, is proportional to the CP violating part of the $I = 2$ decay amplitude which is suppressed by the $\Delta I = 1/2$ rule. The "super-weak" model predicts $\epsilon' = 0$, while in the Kobayashi-Maskawa model ϵ' is in general not zero. The ratio between the CP-violating and CP conserving amplitudes are usually indicated by η_{00} and η_{+-} where the labels refer respectively to decay into a neutral or a charged pion pair. In term of ϵ and ϵ', η_{00} and η_{+-} read as:

$$\eta_{00} = \epsilon - 2\epsilon' \tag{1}$$

$$\eta_{+-} = \epsilon + \epsilon' \tag{2}$$

The size of ϵ' is suppressed with respect to ϵ so that in the limit $\epsilon' << \epsilon$ we have:

$$\frac{|\eta_{00}|^2}{|\eta_{+-}|^2} = 1 - 6 \times \mathcal{R}e(\epsilon'/\epsilon). \tag{3}$$

The phases of both ϵ' and ϵ are $\approx \frac{\pi}{4}$ so that $\mathcal{R}e(\epsilon'/\epsilon) \approx \epsilon'/\epsilon$.

2 First generation experiments

The quest for the ultimate high precision measurement of $\mathcal{R}e(\epsilon'/\epsilon)$ lasted several decades: in the 70's experiments achieved an accuracy on $\mathcal{R}e(\epsilon'/\epsilon)$ of about ten percent [10], [11], [12]; in the 80's experiments at BNL [13] and FNAL [14] were designed to reach an accuracy at the level of one percent and in the 90's E731 at FNAL and NA31 at CERN initiated the era of a less than per mille level accuracy.

Detectors employing wire chambers combined with calorimetry were conceived in order to determine the K^0 energy and decay vertex with the best precision allowed at that time. This is essential in order to define a common

phase space for all decay modes which are to be compared. A special feature of NA31 was a K_S beam mounted on a train which was moved along the beam direction covering a 50 m K_L decay region with K_S decays.

The final result of NA31 and E731 published in 1993 [15], [16] are "well known":

$$NA31 : \mathcal{R}e(\epsilon'/\epsilon) = (23 \pm 6.5) \times 10^{-4}$$

$$E731 : \mathcal{R}e(\epsilon'/\epsilon) = (7.4 \pm 5.9) \times 10^{-4}$$

The experimental situation was rather controversial: the NA31 result was only marginally in agreement with the contemporary predictions of the Standard Model while the E731 result was in the "right" range and it was compatible with the Superweak model ($\epsilon' = 0$).

3 Second generation: KTEV and NA48

In the 90's direct CP violation in neutral kaon has been studied at two fixed-target experiments, KTEV-Fnal and NA48-Cern. Both benefited from the experience gained with their predecessors, Na31 and E731 respectively, and from substantial upgrades in particle detection techniques. Both experiments measured the deviation from unity of the double ratio

$$R = \frac{\Gamma(K_L \to \pi^0\pi^0)}{\Gamma(K_S \to \pi^0\pi^0)} : \frac{\Gamma(K_L \to \pi^+\pi^-)}{\Gamma(K_S \to \pi^+\pi^-)} = 1 - 6 \times \mathcal{R}e(\epsilon'/\epsilon) \qquad (4)$$

by using double beam technique. This technique counts the decays from all four channels collected at the same time and under the same conditions and by exploiting the fact that biases affecting neutral and charged mode identically cancel out in the double ratio.

Fig. 1 shows the detector architecture of KTEV which is very similar to the one adopted by NA48. Charged pions are tracked by drift chambers and a spectrometer allows the momentum measurement. Both experiment make use of sophisticated electromagnetic calorimeter to detected final photons. A calorimeter consisting of 3100 blocks of pure cesium iodide (CsI) is used by KTEV [17] while the NA48 calorimeter is a quasi-homogeneous ionisation chamber, with liquid Kripton as active medium, segmented in $\sim$ 13000 cells [18]. Both detectors have similar resolutions, better then 1% for energy above 20 GeV, resulting in a $\sim$ 40 cm resolution on the longitudinal vertex. This

value has to be compared with a typical 100 m distance between the decay point and the detector. The main difference between the two experiments is the production mechanism of the K_S beam: in KTEV two Kaon beams are produced from a single target placed far enough so that only a small fraction of short-lived neutral particles (K_S and Λ) survives in the fiducial decay volume; the K_S are regenerated from one of the K_L beams by using a plastic regenerator fully instrumented to minimize the the scattered-kaon background to the coherently regenerated signal. In order to overcome the left-right bias, the regenerator moves from one beam to the other every minute. The regenerator converts the pure K_L beam to a mixed beam, $K_L + \rho K_S$, where ρ is the regeneration amplitude, $|\rho|$ is $\sim 3\%$. The double beam system of NA48 is shown in Fig. 2: the primary proton-beam impinges on a target ~ 120 m upstream the beginning of the fiducial decay volume. The charged component of outgoing particles is swept away by bending magnets. The neutral component is suitably collimated and forms the K_L beam. The non-interacting protons from the K_L target are directed onto a mechanically bent mono-crystal of silicon. A small fraction of protons is deflected following the crystalline planes, it is collimated and then passes through a counter (Tagger) which measures the time of the proton. A series of quadrupole transports the secondary proton beam to the K_S target where a system of sweeping magnets and collimators defines a neutral beam 6 m before the beginning of the decay volume. The decay spectrum of kaons of the K_L and K_S beam are very similar in the range 70-170 GeV, with an average energy of 110 GeV. In NA48 the two beams are quasi-collinear, being 0.6 mrad the angle between their axis, they converge at the detector and the maximum distance between the axis is 7.2 cm. The coincidence between the event time and a signal from the tagger allows to assign the event to the K_S beam. In KTEV the beams are parallel with 20 cm of separation, the K_S or K_L assignment is based on the vertexing of the track pair for the charged mode and on the 4-photon center of gravity for the neutral mode.

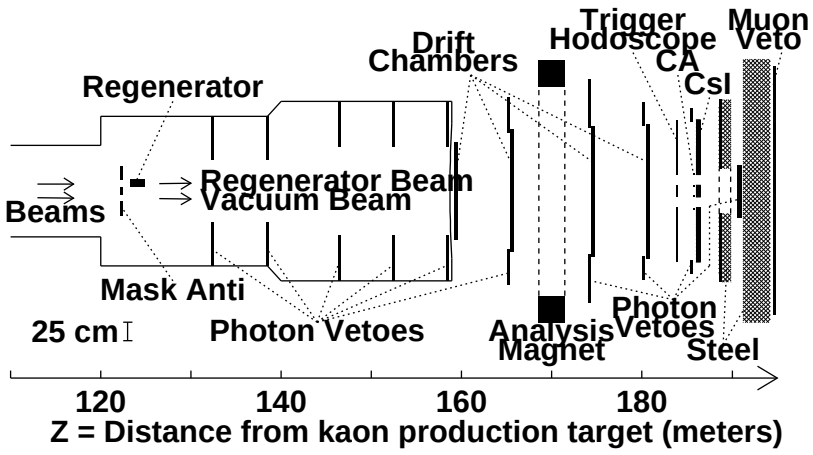

Figure 1: *A skematic drawing of the KTEV detector.*

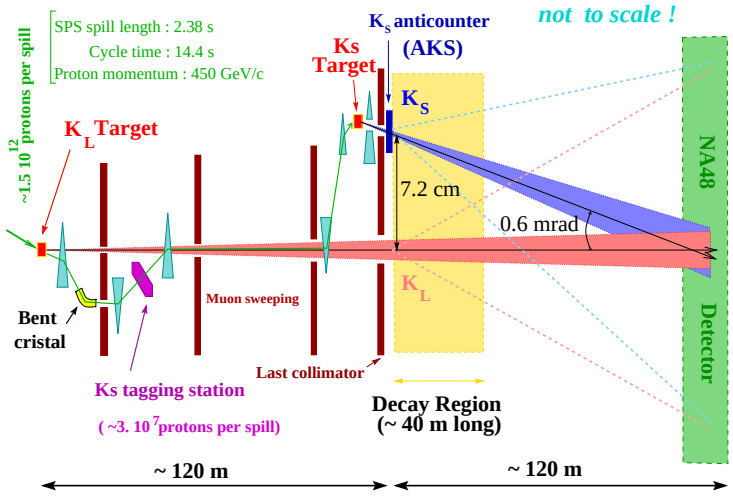

Figure 2: *Layout of the double beam system of NA48*

	year	$\mathcal{R}e(\epsilon'/\epsilon)$ (unit 10^{-3})	ref.
E731a	1988	3.2 ± 3.0	19)
NA31a	1988	3.3 ± 1.1	20)
E731	1993	0.7 ± 0.6	16)
NA31b	1993	2.0 ± 0.7	15)
KTEVa	1999	2.8 ± 0.4	21)
NA48a	1999	1.8 ± 0.7	22)
KTEVb	2001	2.07 ± 0.29	23)
NA48b	2001	1.50 ± 0.27	24)

Table 1: *Results on $\mathcal{R}e(\epsilon'/\epsilon)$ presented in the last 14 years*

4 Results and conclusions

Tab. 1 summarizes the experimental results on the direct CP violation parameter $\mathcal{R}e(\epsilon'/\epsilon)$ presented in the last 14 years. The final result of NA31, E731 and the latest result announced by NA48 and KTEV [1] gives the average

$$\boxed{\mathcal{R}e(\epsilon'/\epsilon) = (17.2 \pm 1.8) \times 10^{-4}}$$

which is $> 9\sigma$ above zero, and an acceptable confidence level for consistency is recovered ($\chi^2 = 5.5$ for 3 degrees of freedom). The latest results confirmed a non-zero and positive value of $\mathcal{R}e(\epsilon'/\epsilon)$. This is an important experimental result ruling out definitively the Superweak model and establishing direct CP violation beyond any doubt.

New result is expected from the analysis of the NA48 data collected during summer 2001 and similarly KTEV has to complete the analysis of the full statistics collected.

References

1. J.H. Christenson *et al*, Phys. Rev. Lett. **13**, 138 (1964).

2. M.Banner *et al*, Phys. Rev. Lett. **21**, 1103 (1968).

[1] The result labelled KTEVb is partially based on the same statistics analyzed in KTEVa therefore KTEVa is not included in the final average

3. I. Bugadov *et al*, Phys. Rev. Lett. **28B**, 215 (1968).
4. S. Bennett *et al*, Phys. Rev. Lett. **19**, 993 (1967).
5. D.E. Dorfan *et al*, Phys. Rev. Lett. **19**, 987 (1967).
6. E. Ramberg *et al*, Phys. Rev. Lett. **70**, 2525 (1993).
7. KTEV collaboration , Phys. Rev. Lett. **84**, 408 (2000).
8. L. Wolfenstein, Phys. Rev. Lett. **19**, 562 (1967).
9. M. Kobayashi and T. Maskawa, Prog. Theor. Phys. **49**, 652 (1973).
10. M. Holder it et al, Phys. Lett. **40B**, 141 (1972).
11. M. Banner it et al, Phys. Rev. Lett. **28**, 1597 (1972).
12. J.H. Christenson it et al, Phys. Lett. **43**, 1209 (1979).
13. J.K. Black *et al*, Phys. Rev. Lett. **54**, 1628 (1985)
14. R.H. Bernstein *et al*, Phys. Rev. Lett. **54**, 1631 (1985)
15. NA31 collaboration, Phys. Rev. Lett. **B317**, 233, (1993)
16. E731 collaboration, Phys. Rev. Lett. **70**, 1203, (1993)
17. A. Roodmann in: *Proceedings of the VII International Conference on Calorimetry in High Energy Physics*, (ed. E.Cheu) , 89, (World Scientific, Singapore, 1998)
18. G. Unal in: *Proceedings of the IX International Conference on Calorimetry in High Energy Physics*, **21**, 361, (Frascati Physics Series, 2000)
19. M. Woods *et al.*, Phys. Rev. Lett. **60**, 1695, (1988)
20. NA31 collaboration, Phys. Rev. Lett. **B206**, 169, (1988)
21. KTEV collaboration, Phys. Rev. Lett. **83**, 22, (1999)
22. NA48 collaboration, Phys. Rev. Lett. **B465**, 335, (1999)
23. A. Glazov , talk given at KAON 2001, International Conference on CP violation (Proceedings to be published)
24. NA48 collaboration, E.P.J **C22**, 231 (2001)

Frascati Physics Series Vol. XXVIII (2002), pp.301-301
HQ & L 2002 – Vietri s/m, May 27th - June 1st, 2002

EXTRA DIMENSIONS AND FLAVOUR PHYSICS *

John March-Russell
TH-Division, CERN, Geneva, Switzerland

* Written contribution not received

Frascati Physics Series Vol. XXVIII (2002), pp.303-313
HQ & L 2002 – Vietri s/m, May 27th - June 1st, 2002

FUTURE EXPERIMENTS AT HADRON MACHINES

Clara Matteuzzi
I.N.F.N. Milano and CERN

Dipartimento di Fisica G.Occhialini U2 Piazza della Scienza 3
20126 Milano

ABSTRACT

b-physics at hadron machines (Tevatron and LHC) is a challenging program which future dedicated experiments like BTeV and LHCb intend to perform with technical solutions which will be described. Several physics aspects of CP violation will be still left open by the B-factories, like all the B_s sector. The required statistics and spectroscopy of B particles necessary for an exhaustive study of the CP mechanism can only be realized at the hadron colliders, which provide large cross sections of $b\bar{b}$ pairs.

1 Introduction

In the recent past, a lot of informations on b-quark and B hadrons came from precise measurements performed at LEP [1], SLC and CLEO [2]. CDF, working at the Tevatron, also produced excellent quality results [3], demonstrating that hadron machines are a viable source of high statistics b-hadrons decays.

At present, we have witnessed B-factories working at the $\Upsilon(4s)$, at SLAC [4] and KEK [5], making precise measurements in the B_d sector.
The advantage of hadron machines is a very large cross section for $b\bar{b}$ pairs, which allows to collect large statistics even in very rare decay channels. At LHC about 10^{12} $b\bar{b}$ pairs are produced every year, of which 10^9 could be triggered and reconstructed. The most challenging aspects are clearly the trigger, and the identification of final state particles, in order to reconstruct the rare exclusive states, and assign through the tagging, the flavor of the b-hadron, where necessary.

2 The physics

An open problem of particle physics today is the CP violation mechanism. Cosmology tells us that the Standard Model does not predict the amount of CP violation necessary for the baryogenesis. The baryonic world in which we live needs more than what the CKM matrix expects. The main goal of future experiments must be the investigation of this mechanism. This will have two aspects: test up to a very high level of precision the consistency of the Standard Model and the CKM description of CP, and on the other hand, to measure very rare decays modes which could be affected by the existence of new particles. The additional loops or boxes through which the decays can take place could be probed by measuring the decay rate involved. At present there are already several measurements of the $\sin(2\beta)$, which is known to be different from zero (see in fig. 1 a compilation of the available results).
Putting together [6], [7] all the experimental measurements (see fig. 1 taken from reference [6]), and assuming the validity of the Standard Model, one can determine the expected value of β. If one compares the expected value obtained in this way, represented by the horizontal band in the figure 1 (left), with the direct measurements [8], one can conclude that the SM is consistent up to the level probed, which is the experimental error. For comparison, the dedicated experiments BTeV and LHCb will measure $\sin\beta$ with a precision of 0.02 in one year of running.
- *Measuring* α
Experimentally the simplest decay channel which is related to the angle α, $B\rightarrow \pi^+\pi^-$, is affected by a contamination of penguin diagrams which introduce a phase which must be disantangled from the weak phase one wants to

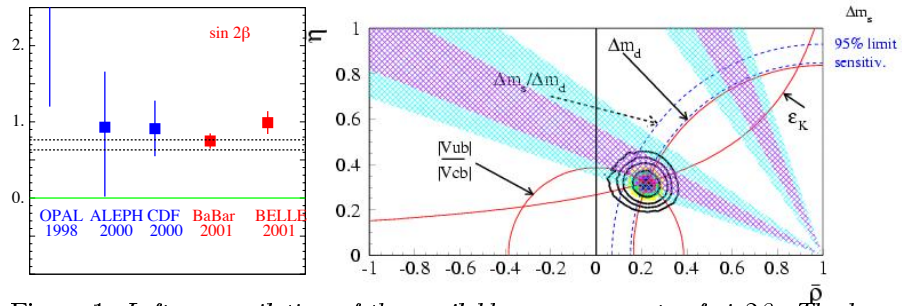

Figure 1: *Left:a compilation of the available measurements of sin2β. The horizontal band is the expected value from the Standard Model as estimated in* [6]. *Right:measurements of different parameters on the plane* (ρ, η) [6].

measure. Experimentally, the selection of this channel needs a high K/π separation capability to eliminate background from B$\to \pi K, KK$, while waiting for theoretical work or complete experimental measurements (samples of 10k-20k events per year will be available in the dedicated experiments) allowing to precisely estimate the amount of such contribution, other decays can be considered. A suggestion has been made [9] that the study of the decays of B^o into $\rho\pi$ is clean because of a cancelling effect in the sum of the amplitudes of the three possible charge states $\rho^-\pi^+$, $\rho^+\pi^-$ and $\rho^o\pi^o$. The Dalitz plot analysis then allows one to determine both $\sin(2\alpha)$ and $\cos(2\alpha)$ (cf. fig. 2: the signal events, expected to be of the order of 1000 per year are visible in the corners of the Dalitz plot). The precision on α could be of the order $3^o - 5^o$.

- *Measuring* γ

Also the angle γ can be measured from the decays of B$_s$ which are dominated by the transition $b \to u$. Examples are B$_s \to \rho^o K_o$, and B$\to D_s^{\pm} K^{\pm}$.

Similarly to B$\to \pi^+\pi^-$, the first decay is polluted by penguin contributions difficult to disantangle. The second decay allows one to access the angle γ through the measurement of the time dependent decay of $\bar{B}$ and B. The necessary performances of a detector to allow such a study are: a good trigger efficiency, excellent particle identification, good mass and proper time resolution. About 5k-10k events per year are expected in the dedicated experiments, reaching a sensitivity on γ which could be of the order of 10^o.

Other interesting channels are, for example: 1) B$\to D^{*\pm}\pi^{\pm}$, which is realated

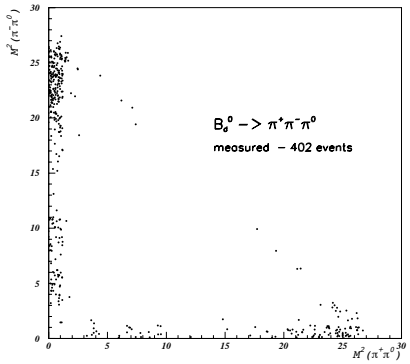

Figure 2: *Dalitz plot for $B \to \rho\pi$ from LHCb simulation.*

to $\gamma + 2\beta$ and requires therefore a measurement of the angle β. This should be available in the years 2006-2007 with a precision of $\sim$0.03 from B-factories. 2) $B_s^o \to J/\Psi\Phi$ related to the phase $2\delta\gamma$. 3) $B^- \to K^-\bar{D}^o$ and $B^+ \to K^+D^o$ [10], related to γ by measuring the decay rates in D^o and $\bar{D}^o$.

- *New Physics*

The existence of new particles expected in several extensions of the Standard Model could manifest itself through interference phenomena, modifying the contributions from loops or box diagrams (see for example [11]). Precise measurements of decays with very small branching ratios could be therefore a window on new physics.

An example is the decay $B^o \to \mu\mu(X)$. In fig. 3 it is shown the capability of identifying this decay in ATLAS.

3 The next generation of experiments

3.1 *General purpose Experiments*

At LHC, there will be two 'central detectors': ATLAS [12] and CMS [13] shown in fig. 4.

They cover a region of pseudorapidity $\eta < 2.5$ and the goal of their design is to discover Higgs and supersymmetric particles.

The features of the machine which they prefer are therefore a very high lu-

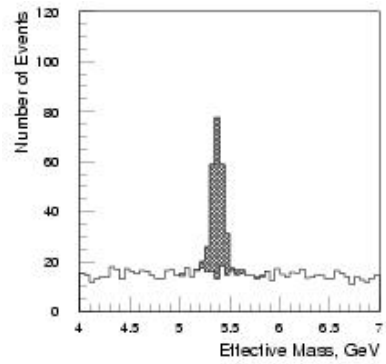

Figure 3: *The $\mu\mu$ invariant mass from the decay $B^o \to \mu\mu(X)$ in the ATLAS simulation.*

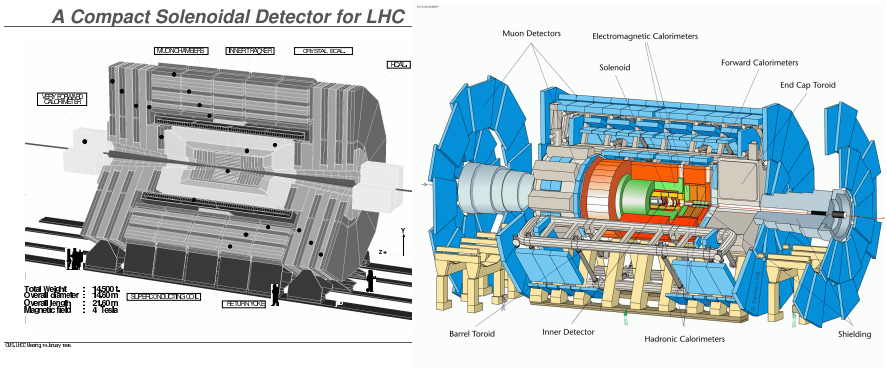

Figure 4: *The CMS (left) and ATLAS (right) detectors.*

minosity and the highest energy. The trigger is optimised to select high p_t particles. This setup implies that such experiments can do B-physics only in the initial phase of the machine commissioning, when the luminosity will not have reached the designed one (10^{34} cm^{-2} s^{-1}). At that stage, the multeplicity of primary interactions will be about 20, which makes it very difficult to associate correctly primary and secondary vertices.

The trigger designed in ATLAS and CMS expects to select high p_t (6-7 GeV for muons, and 12 GeV for electrons in CMS). This will allow, in the initial LHC stage, to study B channels [14] with intermediate states like J/Ψ or final states of the kind $B \to \mu^+\mu^-$. The limited possibility to identify particles is

Table 1: *Comparison of the caracteristics of Tevatron and LHC. IP1 and IP5 are the intersections housing ATLAS and CMS.*

	Tevatron	LHC
$\sqrt{s}$(TeV)	2	14
$\sigma_{b\bar{b}}$(mb)	0.1	0.5
$\sigma_{inelastic}$(mb)	60	80
σ_{total}(mb)	75	100
frequency(MHz)	7.6	40
bunch spacing(ns)	132	25
z size (cm)	30	5
luminosity($10^3$2 cm^{-2}s^{-1})	2	2.5
luminosity(IP1 and IP5)		10
number of interactions per bunch	2	0.5
number of interactions per bunch(IP1 and IP5)		20

also a serious limitation for these two detectors to study B-physics.

3.2 *Dedicated Experiments*

The two experiments BTeV at Tevatron and LHCb at LHC have been designed to measure the angles and sides of the CKM triangle, with many different decay channels. These dedicated experiments put great care in their design to the two crucial aspects of these difficult measurements: the trigger and the particle identification system. They will be described in the next sections.
The difference between the two machines, Tevatron and LHC, summarized in tab.1, gives a guide to the technical solutions adopted by the two detectors. The main features of the two experiments are summarized in tab.2.

3.2.1 The BTeV Detector

A new proposal [15] has been submitted by the BTeV collaboration. The detector is shown in fig. 5. It has been reduced from a double to a single-arm spectrometer.

The most ambitious part of the project is the trigger. The aim is to reduce the 7.6 MHz input rate at level 1, to 76 KHz at level 2. The final rate of data to be logged is planned to be about 3 KHz. Level 1 is based on the vertex detector, which consists of 30 stations (60 planes) containing

Table 2: *Technical characteristics of BTeV and LHCb.*

	BTeV	LHCb
Acceptance (mrad)	10-300	10-300
Vertex detector	Si pixel inside B field	Si strips
Magnet	2.6 Tm	3 Tm
Particle ID (RICH)	C_5F_{12} (liquid) C_4F_{10}	Aerogel + C_4F_{10} CF_4
Calorimeter	$PbWO_4$ (200 mrad)	Preshower+shashlik +Fe/scint.tiles
Muon	Proportional tubes (200 mrad)	MWPC+RPC

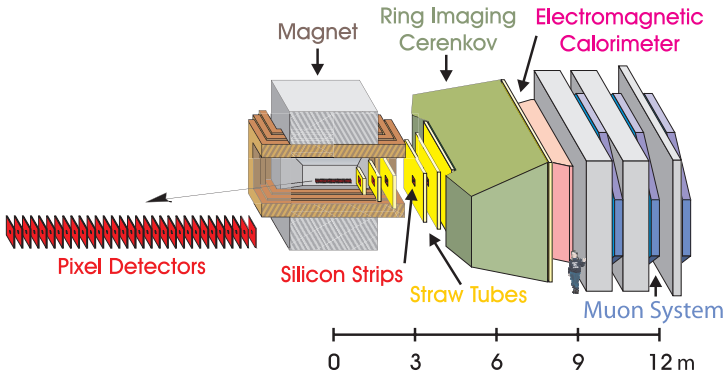

Figure 5: *The BTeV detector.*

a total of twenty two million pixels. The total area of silicon is 0.6 m^2 and the material sums up to 0.75 X_o. The geometry is vertical-horizontal, and the spatial resolution ranges between 5 and 10 μm according to the incident angle. The detector is inside the magnetic field, which allows the reconstruction of the particle momenta with a precision of about 20%. This is enough to discard low momentum particles, cleaning the reconstruction of the secondary vertices.

The trigger algorithms require substantial event buffering at each trigger level. BTeV will have more than a Terabyte of buffer memory, the average need being approximately 400 Gigabytes.

The particle identification (PID) is realized with RICHs detectors. The physics goal which sets the upper end of the momentum requirement is the separation

of the decay channels $B_d^o \to \pi^+\pi^-$, $B_d^o \to \pi^+K^-$, $B_s^o \to K^+K^-$. The low momentum requirement is defined by having high efficiency for tagging kaons from all B decays. Based on this, the range to be covered by a PID system is $3 < p < 70$ GeV. This goal is realized with a RICH having two radiators: one gaseous, C_4F_{10} (n=1.00138) and one liquid, C_5F_{12} (n=1.24). The Cerenkov angle from the latter is around 600 mrad, and the large ring is detected directly on an array of 3" diameter photomultipliers. The photons from C_4F_{10} are reflected from spherical mirrors and detected by HPDs.

3.2.2 The LHCb Detector

Fig. 6 shows the side view of the spectrometer. Some of its main characteristics are listed in table 2, compared to the technical choices proposed for BTeV.
The solutions adopted by LHCb for identifying particles [16)] and for triggering are different from those of BTeV. The PID system consists of RICH detectors based on 3 radiators: one solid, the aerogel with index of refraction n=1.03, and two gaseous, C_4F_{10} (n=1.00138), and CF_4 (n=1.0005). The first two cover roughly the range 2-50 GeV, and the last 30-150 GeV. In the case of LHCb, due to the higher energy of LHC, the momentum range over which the separation π/K/p is necessary is larger than in BTeV. The importance of the PID is illustrated, as an example, in fig. 7. It is clear that this channel, as many others, can be studied only if it will be well separated from background channels which tipically have much larger branching ratios.

LHCb plans to use only events with single interaction. The luminosity will be therefore kept to 2×10^{32} cm^{-2}s^{-1}, defocussing the beams at the LHCb intersection point. In these conditions, 30% of bunch crossings will have one proton-proton interaction, and 10% will have more than one.

The trigger of LHCb is based on high p_T leptons (with thresholds of 1 and 2.4 GeV for μ and electrons respectively), hadrons (with threshold at 3.4 GeV) and photons at the very first level (L0). At level 1, the 1 MHz having passed L0 are reduced to 40 KHz using secondary verteces reconstruction. Up to this level an efficiency of about 30% is mantained for the signal channels, and about 3% of minimum bias events are accepted. A scheme of L0 and L1 is given in fig. 6. The trigger Technical Design Report will be submitted early 2003.
The final amount of data to be logged is expected to be 200 Hz, at a rate of 20

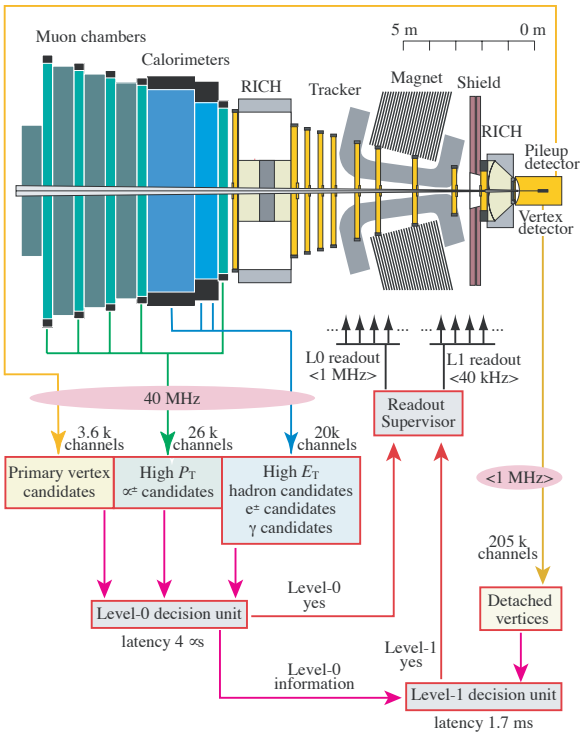

Figure 6: *The LHCb detector and the scheme of level 0 and level 1 trigger.*

Mbytes/s.

The vertex detector of LHCb [17] is made by Si strips, for a total of 0.32 m^2 of Si 200 μm thick, and with an R ϕ geometry. In total 21 stations are foreseen, for a total of 200k electronic channels. The material seen by a particle is in average 0.18 X_0. Two dedicated silicon planes located upstream of the vertex detector will be used to reconstruct the longitudinal position of the interaction vertices and reject events with more than one such vertices.

The LHCb project is well advanced, and the building phase going on at present, should finish in 2006, when the installation in pit 8 is planned.

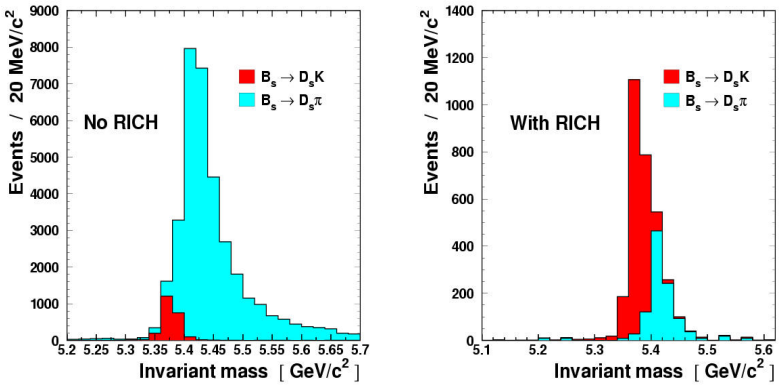

Figure 7: *The reconstruction of the decay channel $B \to D_s K$ with and without the RICH.*

4 Acknowledgements

I would like to thank the help of Daniele Pedrini in reviewing the BTeV project.

References

1. *Combined Results on b-hadrons Production and Decay Properties* CERN-EP 2001/050
2. see for example CLNS02/1789 CLEO02-9, CLNS02/1720 CLEO01-4
3. V.Papadimitriou FERMILAB-CONF-02/070-E
4. see for example BaBar Collaboration, B.Aubert et al., SLAC-PUB-9317, BaBar Collaboration, B.Aubert et al., SLAC-PUB-9293
5. see for example BELLE Collaboration, M.Yamauchi at ICHEP2002, Amsterdam july 2002
6. M.Ciuchini et al.,JHEP07, 13 (2001)
7. A.Hocker et al., Eur.Phys.J C21, 25(2001)
8. BaBar Collaboration, B.Aubrt et al., hep-ph/0203007
   BELLE Collaboration. K.Abe et al., hep-ph/0202027
   J.Tseng, FERMILAB-CONF-02/169-E

9. Snyder and H.Quinn, Phys. Rev.**D48**, 2139 (1993)

10. D.Atwood, I.Dunietz and A.Soni, Phys. Rev.Lett**78**, 3257 (1997)
M.Gronau and D.Wyler Phys. Lett.**B265**, 172 (1991)

11. W.J. Huo, hep-ph/0006110
J.Papavassiliou and A.Santamaria hep-ph/0008151
K.Agashe et al.,hep-ph/0105084
G.Buchalla et al.,hep-ph/0006136

12. W.W.Armstrong et al., ATLAS Technical Proposal CERN/LHCC 94-43 1994

13. G.L.Bayatran et al., CMS Technical Proposal CERN/LHCC 98-4 1998

14. CERN Yellow Report CERN-EP 2000/004
ATLAS Coll. CERN/LHCC 99-14 1999 and CERN/LHCC 99-15 1999

15. G.Y. Drobychev et al, Update to proposal for an Experiment to Measure Mixing, CP Violation and rare Decays in Charm and Beauty Particle Decays at the Fermilab Collider - BTeV (March 2002), **1**, 203 (North-Holland, Amsterdam, 1986).

16. LHCb Coll. CERN LHCC 2000-037 LHCb TDR3 September 2000

17. LHCb Coll. CERN LHCC 2001-011 LHCb TDR5 May 2001

Frascati Physics Series Vol. XXVIII (2002), pp.329-336
HQ & L 2002 – Vietri s/m, May 27th - June 1st, 2002

RESULTS OF B_d OSCILLATION AT BELLE EXPERIMENT

Tomonobu Tomura
(for the Belle collaboration)
Department of Physics, the University of Tokyo
7-3-1 Hongo, Bunkyo-ku, Tokyo 113-0033, Japan

ABSTRACT

We report measurements of the $B^0\overline{B}^0$ mixing parameter Δm_d using a 29.1 fb^{-1} data sample collected with the Belle detector at the KEKB asymmetric e^+e^- collider. Using pair-produced neutral B mesons at the $\Upsilon(4S)$ resonance, we identify the flavor of one neutral B meson in four different methods: inclusive leptons, partially reconstructed $D^*\pi$ events, fully reconstructed semi-leptonic B decays, and fully reconstructed hadronic B decays. The flavor of the accompanying B meson is determined from its decay products. We obtain the Δm_d value from the distribution of the time intervals between the two B meson decay points.

1 Introduction

In the Standard model, $B^0\overline{B}^0$ oscillation [1] occurs through second order weak interactions. Since the dominant contribution in the loop is t-quark exchange, the oscillation frequency Δm_d is related to one of the Cabibbo-Kobayashi-Maskawa (CKM) [1)] matrix elements V_{td}. Therefore, a measurement of Δm_d can be used to determine $|V_{td}|$, although theoretical uncertainties on the hadronic matrix elements currently limit the accuracy of $|V_{td}|$ determination. In addition, $B^0\overline{B}^0$ mixing is one of the sources of CP violation for B^0 decays, especially decays into CP eigenstates, and a good knowledge of Δm_d is important for precise measurements of CP asymmetries. Since the first observation of $B^0\overline{B}^0$ mixing [2)], Δm_d has been widely measured [3)]. Recently, asymmetric B-factory experiments have been providing more precise measurements of Δm_d [4, 5)].

In this report, we present measurements of Δm_d from the time evolution of opposite-flavor (OF; $B^0\overline{B}^0$) and same-flavor (SF; B^0B^0, $\overline{B}^0\overline{B}^0$) neutral B decays at the $\Upsilon(4S)$ resonance. In the absence of background and detector effects, the time-dependent probabilities of observing OF ($\mathcal{P}^{\rm OF}$) and SF ($\mathcal{P}^{\rm SF}$) states are given by

$$\mathcal{P}^{\rm OF}(\Delta t) = \frac{1}{4\tau_{B^0}} \exp\left(-\frac{|\Delta t|}{\tau_{B^0}}\right)[1+\cos(\Delta m_d \Delta t)], \quad (1)$$

$$\mathcal{P}^{\rm SF}(\Delta t) = \frac{1}{4\tau_{B^0}} \exp\left(-\frac{|\Delta t|}{\tau_{B^0}}\right)[1-\cos(\Delta m_d \Delta t)], \quad (2)$$

where τ_{B^0} is the B^0 lifetime, and Δt is the proper time difference between the two B meson decays. We assume that the decay width difference of two mass eigenstates of the B^0-$\overline{B}^0$ system is zero, since it is expected to be very small in the Standard Model [6)]. We report on the results using four different samples: inclusive dileptons, a partially reconstructed $D^{*\pm}\pi^{\mp}$ mode, fully reconstructed hadronic modes, and a fully reconstructed semi-leptonic mode.

2 Experimental apparatus

The analysis described here is based on a 29.1 fb^{-1} data sample, which contains 31.3×10^6 $B\overline{B}$ pairs (except for the dilepton analysis which is based on early

[1] In this report, we denote B^0_d by B^0.

data sample of 5.9 fb^{-1}), collected with the Belle detector [7] at the asymmetric-energy KEKB storage ring [8]. KEKB collides an 8.0 GeV electron beam with a 3.5 GeV positron beam, resulting in a center-of-mass system (cms) moving along the electron beam direction (z axis) with a Lorentz boost of $\beta\gamma = 0.425$. Since B mesons are nearly at rest in the $\Upsilon(4S)$cms, the proper time difference Δt can be approximated as $\Delta t \simeq \Delta z/(c\beta\gamma)$, where Δz is the distance between the decay vertices of the two B mesons in z (typically 200 μm).

The Belle detector consists of a three-layer silicon vertex detector (SVD), a 50-layer central drift chamber (CDC), an array of aerogel Cherenkov counters (ACC), time-of-flight scintillation counters (TOF), an electromagnetic calorimeter containing CsI(Tl) crystals (ECL), and 14 layers of 4.7 cm thick iron plates interleaved with a system of resistive plate counters (KLM). All subdetectors except the KLM are located inside a 3.4 m diameter superconducting solenoid which provides a 1.5 T magnetic field. The impact parameter resolutions for charged tracks are measured to be $\sigma_{xy}^2 = (19)^2 + (50/(p\beta\sin^{3/2}\theta))^2$ μm^2 in the plane perpendicular to the z axis and $\sigma_z^2 = (36)^2 + (42/(p\beta\sin^{5/2}\theta))^2$ μm^2 along the z axis, where $\beta = pc/E$, p and E are the momentum (GeV/c) and energy (GeV), and θ is the polar angle from the z axis.

3 Measurements of Δm_d

The measurements of Δm_d involve the reconstruction of the decay of a neutral B meson in a flavor-specific mode, the determination of the b-flavor of the accompanying (tagging) B meson, the reconstruction of the two decay vertices to determine Δt, and a fit of the Δt distribution taking into account Δt resolution and backgrounds to extract Δm_d. We use four methods to measure the Δm_d. Since each method uses nearly independent data sample and is expected to have different systematics, we can check the validity of the results.

3.1 Inclusive dilepton [4]

In the first method, we use high-momentum lepton pairs which are used for both flavor tagging and vertex reconstruction. In this analysis, we use an early data sample of 5.9 fb^{-1}. We identify the electrons using position, cluster energy, and shower shape in the ECL, dE/dx in the CDC, and hit information in the ACC. Muon selection is based on the response of the KLM. We reject events

containing leptons from J/ψ decays. In order to reduce secondary leptons and fakes from the same B and from the continuum, the opening angle between the leptons in the cms ($\theta^*_{\ell\ell}$) is required to satisfy $-0.8 < \cos\theta^*_{\ell\ell} < 0.95$. The vertex positions of leptons are determined from the intersection of the lepton tracks with the B decay vertex profile, which is estimated from the interaction point profile convolved with the average B flight length. The proper-time difference is calculated from the z coordinates of the two lepton vertices.

The value of Δm_d is extracted by simultaneously fitting the OF and SF distributions to the respective sums of contributions from all known signal and background sources. We perform a binned maximum likelihood fit to extract Δm_d. Using 5.9 fb^{-1} of data sample, we obtain

$$\Delta m_d = 0.463 \pm 0.008 \pm 0.016 \text{ ps}^{-1}.$$

The dominant sources of systematic errors are uncertainties in the ratios of the branching fractions of the $\Upsilon(4S)$ to charged and neutral B pairs (f_+/f_0) and the lifetimes of B^0 and B^+ (τ_{B^+}/τ_{B^0}).

3.2 Partially reconstructed $D^{*-}\pi^+$

In this method, $B^0 \to D^{*-}\pi^+$ decays (The inclusion of the charge conjugate decay modes is implied throughout this report) are reconstructed using only the fast pion (π_f) produced directly from the B^0 and the soft pion (π_s) from $D^{*-} \to \overline{D}{}^0\pi^-$. Here, we use a method based on reconstructing the D^0 missing mass. We select a π_f with cms momentum $2.05 < p^*_{\pi_f} < 2.45$ GeV/c and an oppositely charged π_s with a cms momentum of less than 0.45 GeV/c. The missing mass is then calculated assuming the B meson is at rest in the cms. We select events with missing mass larger than 1.85 GeV/c^2 as $D^{*-}\pi^+$ candidates. We require the ratio of the second to zeroth Fox-Wolfram moments [9] (R_2) to be less than 0.5 to reduce the continuum background.

In order to identify the flavor of the other B, we require an additional high momentum lepton with a cms momentum larger than 1.1 GeV/c. To reduce the background from incorrect tags (i.e. π_f and leptons from the same B), we further require $\cos\theta^*_{\ell\pi_f} > -0.8$ where $\theta^*_{\ell\pi_f}$ is the angle between a π_f and a lepton in the cms. We select 3686 OF (1213 SF) candidates with 73% (62%) purity after the missing mass cut and lepton-tag.

An unbinned maximum likelihood fit is performed to the OF and SF Δz distributions to extract Δm_d. We obtain

$$\Delta m_d = 0.505 \pm 0.017 \pm 0.020 \text{ ps}^{-1} \quad \text{(prelim.)}.$$

The dominant sources of systematic errors are uncertainties in the background fraction and the resolution function.

3.3 Fully reconstructed modes

We use fully reconstructed, self-tagged decay modes in two categories: hadronic decays ($D^{(*)-}\pi^+$, $D^{*-}\rho^+$) and semi-leptonic decay ($B^0 \to D^{*-}\ell^+\nu$).

For hadronic decays, B^0 mesons are fully reconstructed in the following decay modes: $B^0 \to D^-\pi^+$, $D^{*-}\pi^+$, and $D^{*-}\rho^+$. Neutral and charged D candidates are reconstructed in the following channels: $\overline{D}^0 \to K^+\pi^-$, $K^+\pi^-\pi^0$, $K^+\pi^-\pi^-\pi^+$, and $D^- \to K^+\pi^-\pi^-$. $D^{*-} \to \overline{D}^0\pi^-$ candidates are formed by combining a $\overline{D}^0$ candidate with a negatively charged soft pion. To reduce the continuum background, a selection based on R_2 and the angle between the thrust axes of the reconstructed and associated B mesons is applied mode by mode. We find 2269 $D^-\pi^+$, 2490 $D^{*-}\pi^+$, and 1901 $D^{*-}\rho^-$ events in the signal region with average purities of 86%, 81%, and 70%, respectively.

For $B^0 \to D^{*-}\ell^+\nu$, we use the same D^{*-} decay chains as for the hadronic modes. The D^{*-} candidates are combined with μ^+ or e^+ candidates having charge opposite to that of the D^{*-} candidate. Utilizing the small B momentum in the cms, we calculate $M^2_{\rm miss}$, the approximate missing mass squared in the cms, defined by $M^2_{\rm miss} \equiv (E_B^{\rm cms} - E_{D^*\ell}^{\rm cms})^2 - |\vec{p}_B^{\,\rm cms}|^2 - |\vec{p}_{D^*\ell}^{\,\rm cms}|^2$, where $E_B^{\rm cms}$ and $\vec{p}_B^{\,\rm cms}$ ($E_{D^*\ell}^{\rm cms}$ and $\vec{p}_{D^*\ell}^{\,\rm cms}$) are cms energy and momentum of B^0 (D^* and lepton system). Defining a product of the momenta of the B and the $D^*\ell$ system as $C \equiv 2|\vec{p}_B^{\,\rm cms}|\,|\vec{p}_{D^*\ell}^{\,\rm cms}|$, the cosine of the angle between $\vec{p}_B^{\,\rm cms}$ and $\vec{p}_{D^*\ell}^{\,\rm cms}$ is given by $\cos\theta_{B,D^*\ell} = -M^2_{\rm miss}/C$ due to the almost zero neutrino mass. We select $D^{*-}\ell^+\nu$ candidates by requiring $|\cos\theta_{B,D^*\ell}| < 1.1$. We find 16308 candidates with the overall signal fraction is estimated to be 81.4%.

Leptons, charged pions, and kaons that are not associated with the reconstructed B decay are used to identify the flavor of the accompanying B meson. We apply the same method used for the $\sin 2\phi_1$ measurement [10]. We use two parameters, q and r, to represent the tagging information. The first, q, corresponds to the sign of the b quark charge where $q = +1$ for $\overline{b}$

and hence B^0, and $q = -1$ for b and $\overline{B}^0$. The parameter r is an event-by-event, MC-determined flavor-tagging dilution factor that ranges from $r = 0$ for no flavor discrimination to $r = 1$ for unambiguous flavor assignment. It is used only to sort data into six intervals of r, according to flavor purity. The wrong-tag probabilities, w_l $(l = 1, 6)$, are determined directly from the data for the six classes. The total effective tagging efficiency is measured to be $\sum_l f_l(1 - 2w_l)^2 = 0.270 \pm 0.008(\mathrm{stat})^{+0.006}_{-0.009}(\mathrm{syst})$, where f_l is the fraction of the events in each class.

The vertex positions for the two B decays are reconstructed using tracks that have at least one three-dimensional coordinate determined from associated r-ϕ and z hits in the same SVD layer along with one or more additional z hits in the other layers. Each vertex position is required to be consistent with the B meson decay profile. We use the resolution function identical to the one used for the $\sin 2\phi_1$ measurement [10] for the semi-leptonic mode, while more elaborate one developed for the B lifetimes measurement [11] is used in the hadronic modes. We perform an unbinned maximum-likelihood fit to SF and OF Δt distributions simultaneously with Δm_d and w_l's as free parameters. (Δm_d is fixed at the world average value [12] when we determine w_l's.) We obtain

$$\Delta m_d = 0.521 \pm 0.017 \,^{+\,0.011}_{-\,0.014}\ \mathrm{ps}^{-1} \qquad \text{(prelim.)}$$

for hadronic modes and

$$\Delta m_d = 0.489 \pm 0.012 \,^{+\,0.011}_{-\,0.014}\ \mathrm{ps}^{-1} \qquad \text{(prelim.)}$$

for semi-leptonic mode.

Dominant sources of systematic errors for hadronic modes are uncertainties in the resolution function and the background components, including mixing. Those for the semi-leptonic mode are uncertainties in the effects of the backgrounds.

4 Conclusion

We have presented measurements of Δm_d using 29.1 fb^{-1} of data collected with the Belle detector at the $\Upsilon(4S)$ energy. We use four different method to measure the value of Δm_d, which enable us to increase the reliability of our result. Figure 1 shows the observed asymmetry for each mode as a function

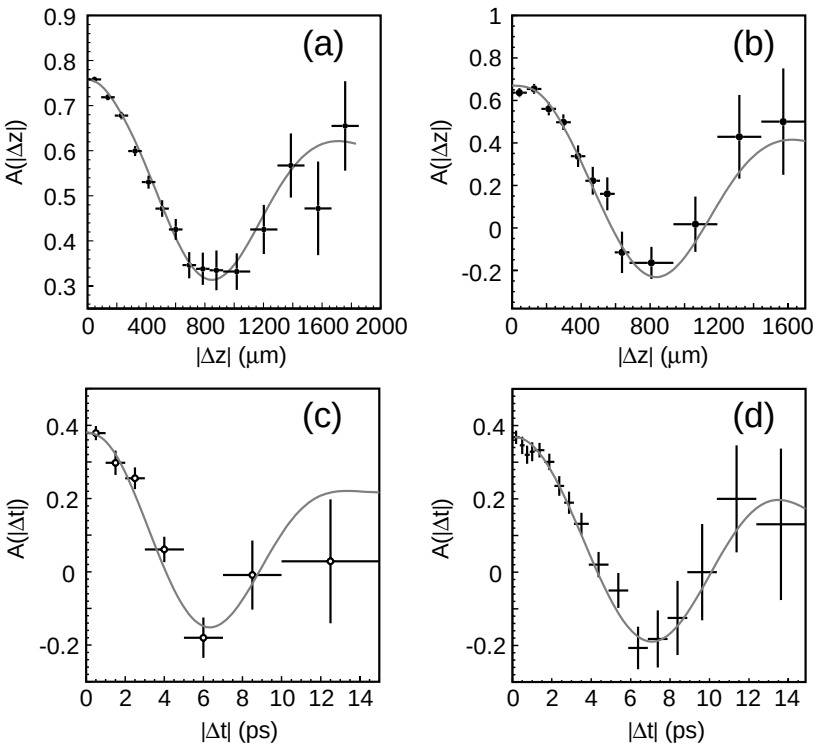

Figure 1: *Asymmetry as a function of the proper decay time difference for (a) dileptons, (b) partially reconstructed $B^0 \to D^*\pi$, (c) hadronic modes, and (d) semi-leptonic mode. Fit curves are also shown.*

of the proper decay time difference, together with the fit result. By combining the four measurements, taking into account the correlated systematic errors, we obtain

$$\Delta m_d = 0.490 \pm 0.006 \pm 0.009 \text{ ps}^{-1} \quad \text{(prelim.)}.$$

This result is consistent with past measurements [3], and has better precision than measurements at higher energies. Thus, it demonstrates the excellent capability of asymmetric B-factory for precise time-dependent measurements of B meson properties.

5 Acknowledgment

We would like to acknowledge the KEKB accelerator group for excellent operation of the collider. We would also like to thank the conference organizers for their hospitality.

References

1. M. Kobayashi and T. Maskawa, Prog. Theor. Phys. **49**, 652 (1973); N. Cabibbo, Phys. Rev. Lett. **10**, 531 (1963).
2. H. Albrecht *et al.*, ARGUS Collaboration, Phys. Lett. **B192**, 245 (1987).
3. B Oscillations Working Group, see `http://www.cern.ch/LEPBOSC/` and references therein.
4. K. Abe *et al.*, Belle Collaboration, Phys. Rev. Lett. **86**, 3228 (2001).
5. B. Aubert *et al.*, BaBar Collaboration, Phys. Rev. Lett. **88**, 221802 (2002); *ibid.*, Phys. Rev. Lett. **88**, 221803 (2002).
6. A. J. Buras, W. Slominski, and H. Steger, Nucl. Phys. **B245**, 369 (1984).
7. A. Abashian *et al.*, Belle Collaboration, Nucl. Instrum. Methods **A479**, 117 (2002).
8. E. Kikutani ed., KEK Preprint 2001-157 (2001), to appear in Nucl. Instrum. Methods **A**.
9. G. C. Fox and S. Wolfram, Phys. Rev. Lett. **41**, 1581 (1978).
10. K. Abe *et al.*, Belle Collaboration, Phys. Rev. Lett. **87**, 091802 (2001); hep-ex/0202027, submitted to Phys. Rev. **D**.
11. K. Abe *et al.*, Belle Collaboration, Phys. Rev. Lett. **88**, 171801 (2002).
12. D. E. Groom *et al.* (Particle Data Group), Eur. Phys. J. **C15**, 1 (2000).

Frascati Physics Series Vol. XXVIII (2002), pp.337-344
HQ & L 2002 – Vietri s/m, May 27th - June 1st, 2002

SIN 2β AND MIXING: RESULTS FROM B-FACTORIES

Stefania Ricciardi
Royal Holloway, University of London, Egham TW20 0EX, England, U.K.

ABSTRACT

First observation and subsequent more precise measurements of CP violation in the B meson system have been recently reported by experiments at asymmetric B-factories. Time-dependent measurements are performed by these experiments to study CP-violation and $B^0\overline{B}^0$ oscillation. Their results on the CP asymmetry amplitude, sin2β, and the $B^0\overline{B}^0$ mixing frequency, Δm_d, are reviewed.

1 Introduction

In the Standard Model of electroweak interaction the origin of CP violation is a non-zero complex phase in the three-generation CKM matrix [1)] which describes quark mixing. Since 1981 [2)] large CP-violating asymmetries have been predicted in the time distribution of B^0 decays to charmonium final states.

Asymmetries in experimentally easy-to-detect decays like $B^0 \to J/\psi K^0_S$ provide a direct measurement of $\sin 2\beta$, where $\beta = arg[-V_{cd}V^*_{cb}/V_{td}V^*_{tb}]$. However large samples of $B^0\overline{B}^0$ events ($> 10^7$) are necessary to unambiguosly observe CP violation and the first results [3] were statistically limited. Non-zero values of $\sin 2\beta$ with a significance higher than 4σ were published only 20 years later by dedicated experiments at asymmetric e^+e^- colliders, BaBar [4] at PEP-II and Belle [5] at KEKB. PEP-II and KEKB are high luminosity ($> 10^{33} cm^{-2} s^{-1}$) e^+e^- storage rings operating at the $\Upsilon(4S)$ resonance. A $B^0\overline{B}^0$ pair produced in an $\Upsilon(4S)$ decay evolves in a coherent P-wave state. The decay of one B meson to a self-tagging state, which distinguishes between B^0 and $\overline{B}^0$ at a certain time, projects the other B, at that time, onto the opposite flavor as a consequence of Bose symmetry. The probabilities for observing $B^0\overline{B}^0$, B^0B^0 and $\overline{B}^0\overline{B}^0$ pairs are oscillatory functions of Δt, the difference of time between the two B decays. This allows mixing frequencies and CP asymmetries to be determined if Δt is measured, if the flavor of the tagging B, B_{tag}, is ascertained and if the other neutral B decay, B_{rec}, is fully reconstructed. If B_{rec} is found in a flavor eigenstate ($B_{rec} = B_{flav}$), the mass difference between the neutral B mass eigenstates, Δm_d, can be measured from the time-dependent mixing asymmetry

$$A_{mixing}(\Delta t) \equiv \frac{h_+(\Delta t) - h_-(\Delta t)}{h_+(\Delta t) + h_-(\Delta t)} = cos(\Delta m_d \Delta t) \qquad (1)$$

where $h_+(h_-)$ is the decay rate for events with opposite(same) flavor for B_{flav} and B_{tag}.

If the fully reconstructed neutral B is found in a CP eigenstate ($B_{rec} = B_{CP}$), a time dependent CP-violating observable can be constructed

$$A_{CP}(\Delta t) \equiv \frac{f_+(\Delta t) - f_-(\Delta t)}{f_+(\Delta t) + f_-(\Delta t)} = \frac{2Im\lambda}{1+|\lambda|^2} sin(\Delta m_d \Delta t) - \frac{1-|\lambda|^2}{1+|\lambda|^2} cos(\Delta m_d \Delta t) \qquad (2)$$

measuring the decay rate asymmetry between B^0-tagged (f_+) and $\overline{B}^0$-tagged (f_-) events, where the complex parameter λ depends on both $B^0\overline{B}^0$ mixing and the decay amplitudes of B^0 and $\overline{B}^0$ to the common final state.

In the Standard Model, $\lambda = \eta_f e^{-2i\beta}$ for $b \to c\bar{c}s$ decays containing a charmonium state, where η_f is the CP eigenvalue of the final state. Therefore

for these decays the time-dependent CP violating asymmetry is

$$A_{CP}(\Delta t) = -\eta_f \sin 2\beta sin(\Delta m_d \Delta t) \tag{3}$$

and its amplitude is a direct measurement of $\sin 2\beta$.

2 Experimental aspects

Time dependent asymmetries are modified by detector effects and their measurement requires a determination of the experimental Δt resolution and the fraction of events, w, in which the tag assignement is incorrect. The observed amplitudes for the CP asymmetry in B_{CP} sample and the mixing asymmetry in the B_{flav} sample are reduced by the same factor $(1-2w)$ due to mistags. Since the Δt resolution is dominated by B_{tag}, as it will be mentioned later, the Δt distributions for the B_{CP} and the B_{flav} sample can be convoluted with a common Δt resolution function, $R(\delta t)$, where δt is the difference between the measured and true Δt value.

Neglecting the lifetime difference between mass eigenstates, and indicating the B^0 lifetime with τ, the observed decay rates can be written as

$$h_{\pm}(\Delta t) = \frac{e^{-|\Delta t|/\tau}}{4\tau}[1 \pm (1-2w)cos(\Delta m_d \Delta t)] \otimes R(\delta t) \tag{4}$$

for opposite flavor $(+)$ and same flavor $(-)$ signal events, and

$$f_{\pm}(\Delta t) = \frac{e^{-|\Delta t|/\tau}}{4\tau}[1 \pm \eta_f (1-2w) \sin 2\beta sin(\Delta m_d \Delta t)] \otimes R(\delta t) \tag{5}$$

for B^0 tagged $(+)$ and $\overline{B}^0$-tagged $(-)$ decays to CP eigenstates.

The Belle collaboration performs indepedent fits for the mistag fractions and $R(\delta t)$, extracting the first from the amplitude of the mixing asymmetry of the B_{flav} sample, and the second from a fit of charged and neutral B meson lifetimes. The BaBar collaboration performs a simultaneous fit to the B_{CP} sample and to the high statistics B_{flav} sample with $\sin 2\beta$, w and $R(\delta t)$ as free parameters. Both experiments fix Δm_d and τ to the PDG [6] value in the $\sin 2\beta$ fit.

In all cases the measurement of Δm_d, in addition to being of theoretical interest, has common elements with the analysis for the measurement of $\sin 2\beta$

and therefore it constitutes an essential validation test of the whole analysis chain, including flavor tagging, Δt determination and resolution.

2.1 Δt measurement

Neglecting the small B momentum in the $\Upsilon(4S)$ center of mass system, Δt can be determined by the $\Upsilon(4S)$ boost, $\beta\gamma$, and the measurement of the distance Δz between the two B decay vertices along the electron beam direction from

$$\Delta t = \Delta z / \beta\gamma c.$$

The average value for Δz is approximately 200 μm at KEKB where $\beta\gamma \approx 0.425$ and 260 μm at PEP-II where $\beta\gamma \approx 0.55$. The Δz resolution is dominated by the z position resolution for the B_{tag} vertex, which is tipically 140 - 170 μm on the B_{tag} side compared to about 70 μm on B_{rec} side.

3 $B^0\overline{B}^0$ mixing results

The $B^0\overline{B}^0$ mixing frequency Δm_d is determined with a simultaneous likelihood fit to the Δt distributions of opposite flavor ($B^0\overline{B}^0$) and same flavor (B^0B^0 or $\overline{B}^0\overline{B}^0$) events.

For fully-reconstructed B^0 decays to hadrons, BaBar has measured [7]

$$\Delta m_d = 0.519 \pm 0.016(stat) \pm 0.010(syst) ps^{-1}.$$

This is consistent with previous measurements from other experiments [6] and with other results from Belle and Babar, the most precise of which are based on a different technique and a dilepton data sample to give

$$\Delta m_d = 0.493 \pm 0.012(stat) \pm 0.009(syst) ps^{-1}$$

for Babar [8] and

$$\Delta m_d = 0.463 \pm 0.008(stat) \pm 0.016(syst) ps^{-1}$$

for Belle [9].

Including all these measurements, the new world average [10] is

$$\Delta m_d = 0.489 \pm 0.008$$

and it is dominated by the results from BaBar and Belle here reported.

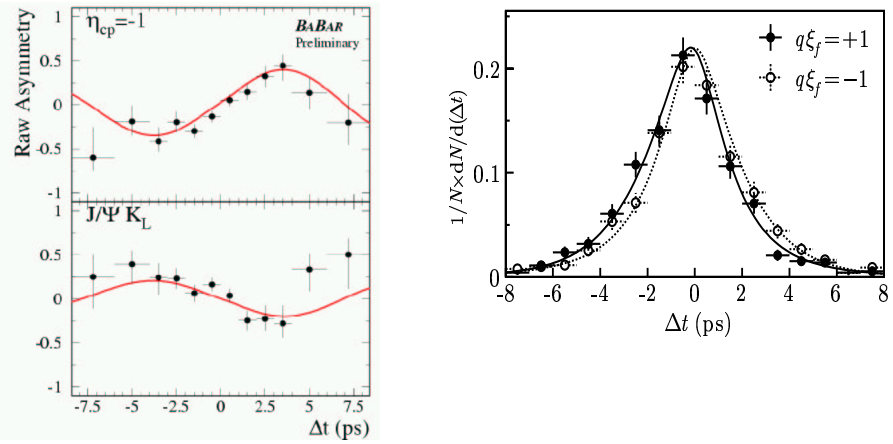

Figure 1: *On the left, raw asymmetry in the number of* B^0 *and* $\overline{B}^0$ *tags,* $(N_B^0 - N_{\overline{B}^0})/(N_B^0 + N_{\overline{B}^0})$*, as a function of* Δt *from Babar. The upper plot is for CP odd final states, the lower plot for the CP even* $J/\psi K_L^0$*. The solid curves represent the result of the combined fit which has determined the central* $\sin 2\beta$ *value (0.75). On the right,* Δt *distributions from Belle for the events with* $q\xi_f = 1$ *and* $q\xi_f = -1$*, where* ξ_f *is the CP eigenvalue and* $q = 1(-1)$ *for* B^0 *(*$\overline{B}^0$*) tag. The result of the global fit for* $\sin 2\beta = 0.82$ *is shown as solid and dashed curves respectively.*

4 $\sin 2\beta$ results with golden decay modes

From 62 million $B\overline{B}$ events collected between 1999 and 2001, which correspond to an integrated luminosity of approximately 56 fb^{-1}, the BaBar collaboration has measured [11]

$$\sin 2\beta = 0.75 \pm 0.09(stat) \pm 0.04(syst)$$

The B_{CP} sample used in this measurement consists of B mesons decaying to the final states $J/\psi K_S^0(K_S^0 \to \pi^+\pi^-, \pi^0\pi^0)$, $\psi(2S)K_S^0(K_S^0 \to \pi^+\pi^-)$, $\chi_{c1}K_S^0(K_S^0 \to \pi^+\pi^-)$, $J/\psi K^{*0}(K^{*0} \to K_S^0\pi^0, K_S^0 \to \pi^+\pi^-)$, and $J/\psi K_L^0$. The J/ψ and $\psi(2S)$ mesons are reconstructed through their decays to e^+e^- and $\mu^+\mu^-$; the $\psi(2S)$ is also reconstructed through its decay to $J/\psi\pi^+\pi^-$. The χ_{c1} is reconstructed in the decay mode $J/\psi\gamma$.

The observed time-dependent asymmetries for this B_{CP} data sample are shown in fig.1 (plots on the left).

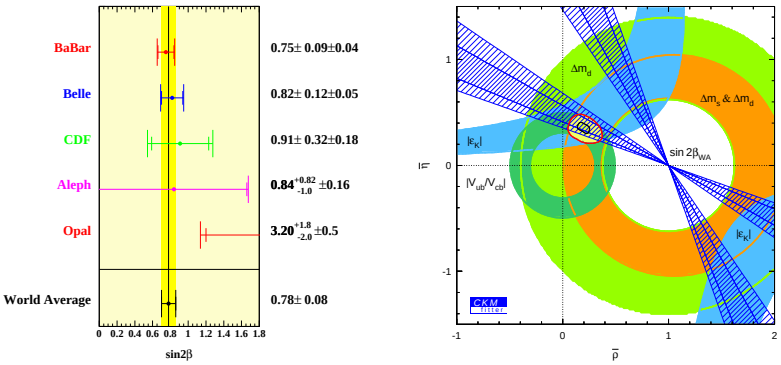

Figure 2: *On the left, most recent* $\sin 2\beta$ *results by experiment. On the right, present indirect constraints on the position of the apex of the Unitarity Triangle in the* $(\bar{\rho}, \bar{\eta})$ *plane, not including the* $\sin 2\beta$ *measurement. The fitting procedure is described in* [13]. *The* $\sin 2\beta$ *World Average is represented by the hatched regions, corresponding to one and two statistical standard deviations.*

The η_c K^0_S final state, with $\eta_c \to K^0_S K^{\pm}\pi^{\mp}$ and $\eta_c \to K^{\pm}K^{\mp}\pi^0$, has not been included in the global fit yet but the preliminary result for $\sin 2\beta$ with these purely hadronic decays, $\sin 2\beta = 0.43 \pm 0.46(\text{stat}) \pm 0.08(\text{syst})$ is consistent with other golden modes.

The final state in vector-vector decays like $B^0 \to J/\psi\ K^{*0}\ (\to K^0_S\ \pi^0)$ is a mixture of even and odd CP, depending on the relative orbital angular momentum of the J/ψ and K^{*0}. An angular analysis is performed to disantangle the two components.

The result from the Belle experiment [12], based on a luminosity of about 42 fb^{-1} and the same modes, including decays to η_c K^0_S, is

$$\sin 2\beta \ = \ 0.82 \ \pm \ 0.12(stat) \ \pm \ 0.05(syst)$$

The likelihood fit is overlaid to the observed Δt asymmetries in the plot on the right of fig. 1. Present $\sin 2\beta$ results and constraints on the Standard Model Unitarity Triangle are shown in fig.2.

For both experiments the dominant sources of systematic error are the parameterization of the Δt resolution function, possible differences in the mistag fractions between the B_{CP} and B_{flav} samples and uncertainties in the level, composition and CP asymmetry of the background.

By floating $|\lambda|$ in the fit to the $\eta_f = -1$ sample, which has high purity

and requires minimal assumptions on backgrounds, the BaBar collaboration has obtained

$$|\lambda| = 0.93 \pm 0.06(stat) \pm 0.02(syst)$$

consistent with Standard Model expectation of no direct CP violation.

5 sin2β results with other modes

As the size of the data sample increases, more tests of the Standard Model and independent measurements of sin2β with other decay modes can be performed.

An example is given by neutral B decaying to $D^{*\pm}D^{*\mp}$, where the leading sub-quark process is the Cabibbo-suppressed tree decay $b \to c\overline{c}d$ and the penguin contribution is expected to be small [14]. However no assumption is made on the penguin contribution by fitting for the sinus and cosinus coefficients in

$$A_{CP}(\Delta t) = Ssin(\Delta m_d \Delta t) + Ccos(\Delta m_d \Delta t)$$

and BaBar preliminary results are

$$S = -0.05 \pm 0.45 \pm 0.05$$

$$C = -0.12 \pm 0.30 \pm 0.05$$

Preliminary results by Belle on the CP asymmetry when the final state is $\eta' K^0_S$, a penguin-dominated decay mode ($b \to s\overline{s}d$), are

$$S = 0.27 \pm 0.54 \pm 0.07$$

$$C = 0.12 \pm 0.32 \pm 0.07$$

6 Conclusions and Outlook

Time-dependent measurements by experiments at B-factories allow the most precise measurements of the CP-violating amplitude sin2β and the $B^0\overline{B}^0$ mixing frequency, Δm_d. Present results on sin2β are consistent with the Standard Model predictions, as given by CKM global fits of indirect measurements, and have now reached a level of precision that offers significant constraint on the position of the apex of the Unitarity Triangle in the $(\bar{\rho}, \bar{\eta})$ plane.

Results on sin2β by BaBar and Belle are still limited by the data sample size and are expected to improve in the near future.

Over the next few years, indepedent measurements of the CP violation parameters with $b \to c\bar{c}d$ or $b \to s\bar{s}d$, if in disagreement with $\sin 2\beta$, can probe the effects of new physics beyond the Standard Model.

References

1. N. Cabibbo, Phys. Rev. Lett. **13**, 138 (1964); M. Kobayashi and T. Maskawa, Prog. Th. Phys. **49**, 652 (1973).
2. A.B. Carter and A. I. Sanda, Phys. Rev. **D23**, 1567 (1981); I.I. Bigi and A.I. Sanda, Nucl. Phys. **B193**, 85 (1981).
3. OPAL Collaboration, K. Ackerstaff *et al.*, Eur. Phys. Jour. **C5**, 379 (1998); CDF Collaboration, T. Affolder *et al.*, Phys. Rev. **D61**, 072005 (2000); Aleph Collaboration, Phys. Lett. **B492**, 259 (2000).
4. Babar Collaboration, B. Aubert *et al.*, Phys. Rev. Lett. **87**, 91801 (2001).
5. Belle Collaboration, K. Abe *et al.*, Phys. Rev. Lett. **87**, 091802 (2001).
6. Particle Data Group, D.E. Groom *et al.*, Eur. Phys. Jour. **C15**, 1 (2000).
7. Babar Collaboration, B. Aubert *et al.*, Phys. Rev. Lett. **88**, 221802 (2002).
8. Babar Collaboration, B. Aubert *et al.*, Phys. Rev. Lett. **88**, 221803 (2002).
9. K.Abe *et al.*, Belle Collaboration, Phys. Rev. Lett. **86**, 3228 (2001).
10. http://lepbosc.web.cern.ch/LEPBOSC/combined_results/PDG_2002.
11. Babar Collaboration, B. Aubert *et al.* contribution to 16th Les rencontres de Physique de la Vallee d'Aoste, la Thuile, Italy, March 2002, hep-ex/0203007.
12. T. Higuchi, for the Belle Collaboration, to appear in Proc. XXXVIIth Rencontres de Moriond QCD and Hadronic Interactions,Moriond, France, March 2002, hep-ex/0205020.
13. A. Höcker *et al.*, Eur. Phys. Jour. **C21**, 225 (2001). Many other analysis also available.
14. Y. Grossman and M.P. Worah, Phys. Lett. **B395**, 241 (1997).

Frascati Physics Series Vol. XXVIII (2002), pp.345-352
HQ & L 2002 – Vietri s/m, May 27th - June 1st, 2002

STATUS OF $D^0 - \overline{D}^0$ MIXING

Milind V. Purohit
Univ. of South Carolina, Columbia, SC 29212, USA
(on behalf of the BaBar collaboration)

ABSTRACT

In this talk we review the current status of the search for $D^0 - \overline{D}^0$ mixing. We begin with a brief overview of the physics of $D^0 - \overline{D}^0$ mixing, followed by an outline of the techniques used to search for it. Next, we summarize recent results from the E791, FOCUS, CLEO, Belle and BaBar experiments.

1 Physics of $D^0 - \overline{D}^0$ mixing

Because the D^0 and $\overline{D}^0$ decay into some common final states (such as K^+K^-, $\pi^+\pi^-$ etc.) one expects that they might mix just like the K^0 and $\overline{K}^0$ do. This is particularly true if the mixing amplitude is significant compared to the decay width. Calculations in the standard model using the box diagram indicate a mixing rate $r_{\rm mix} \sim 10^{-7}$ where $r_{\rm mix}$ is the rate at which decays occur via mixing, i.e.,

$$r_{\rm mix} \equiv \frac{\Gamma(D^0 \to \overline{D}^0 \to \overline{f})}{\Gamma(D^0 \to f)} \tag{1}$$

where f is some final state and $\overline{f}$ its CP conjugate. Note that there also could be CP violation [1] in mixing, i.e., $r_{\rm mix}(D^0 \to \overline{D}^0)$ may or may not equal $r_{\rm mix}(\overline{D}^0 \to D^0)$. [2]

The most common decays of the D^0 are the Cabibbo-allowed or "Right-Sign" (RS) decays such as $D^0 \to K^-\pi^+$. Similarly, "Wrong-Sign" (WS) decays such as $D^0 \to K^+\pi^-$ can occur due to Doubly-Cabibbo-Suppressed (DCS) amplitudes. It has been noted [3] that CP violation, which requires more than a single amplitude, is most likely to occur in the interference between the mixing and DCS amplitudes.

Interest in $D^0 - \overline{D}^0$ mixing stems mainly from the fact that $r_{\rm mix}$ is predicted to be so small in the Standard Model. Thus, observation of $r_{\rm mix}$ may be an indication of new physics beyond the standard model. [4] However, it has been pointed out by several authors [5] that even within the Standard Model it is possible to get $r_{\rm mix}$ as large as 0.001. Interest in this measurement is high although the theoretical situation is not completely clear and at this time observation of a signal may not imply physics beyond the standard model. However, any observation of a mixing signal is likely to cause a flurry of theoretical work to pin down the Standard Model contribution.

2 Analysis Formalism and Techniques

Expressions for the mixing rates typically use the parameters x and y, where $x \equiv \Delta m/\Gamma$ and $y \equiv \Delta\Gamma/2\Gamma$. Here $\Delta m \equiv m_1 - m_2$ and $\Delta\Gamma \equiv \Gamma_1 - \Gamma_2$ arise from the off-diagonal elements of the mass and decay matrices and are defined in terms of the mass eigenstates. The subscript "1" refers to the CP even state, such as the final state K^+K^- arising from D^0 decays. It is possible that there will be a strong phase difference δ between the RS and WS decays which then calls for use of rotated parameters

$$x' = x\cos\delta + y\sin\delta, \qquad y' = y\cos\delta - x\sin\delta \tag{2}$$

While ordinary decays proceed according to the familiar exponential time distribution, mixed decays obey a different distribution:

$$r_{\rm WS}(t) \sim [R_{\rm DCS} + \sqrt{R_{\rm DCS}} y' t + (x^2 + y^2) t^2] e^{-t/\tau} \qquad (3)$$

The constant term in square brackets corresponds to ordinary DCS decays, the quadratic term to purely mixing events and the linear term to the interference between the two. It is this time dependence that is essential in hadronic decays to isolate the mixing contribution to WS decays. Semileptonic decays do not get a contribution from DCS decays and are thus easier to analyze.

Experimentally, we distinguish between RS and WS decays in one of two ways. The method used by Mark III and CLEO-c is to produce $D\overline{D}$ pairs at the Ψ'' resonance, use one to tag the flavor and the other to study the WS decays. Another technique used by E691, E791, FOCUS, CLEO, BaBar, Belle and others is to tag the D^0 flavor at birth using only D^0's from D^{*+} decays and then use the final state to tag the flavor at the time of decay.

Measurement of $\Delta\Gamma$ or equivalently, of y, can be made by measuring the lifetime τ in a CP-even mode such as K^+K^- or $\pi^+\pi^-$ and comparing that to the lifetime in a copious mode such as $K^-\pi^+$, a mixture of CP-even and CP-odd. Thus, from a measurement of $\tau_{K\pi}$ and τ_{KK} one can obtain $y \approx (\tau_{K\pi}/\tau_{KK}) - 1$, an idea first suggested by Ted Liu. [6]

3 Recent Experimental Results

3.1 FOCUS

Some time ago there was a great deal of excitement because of the possible observation of a lifetime difference by FOCUS: in a sample of ~120,000 $K\pi$ decays and ~10,000 KK decays, they measured [7] a non-zero value for y:

$$y = (3.42 \pm 1.39 \pm 0.74)\%$$

which is an approximately 2.5σ signal. Also, FOCUS measured the total WS rate of

$$r_{\rm WS} = (0.405 \pm 0.085 \pm 0.025)\%$$

3.2 BaBar

BaBar results [9] on y are based on $\sim$ 58 fb^{-1} of data, while results on the WS rates are based on $\sim$ 23 fb^{-1} of data. There are approx. 158,000 $K\pi$ events,

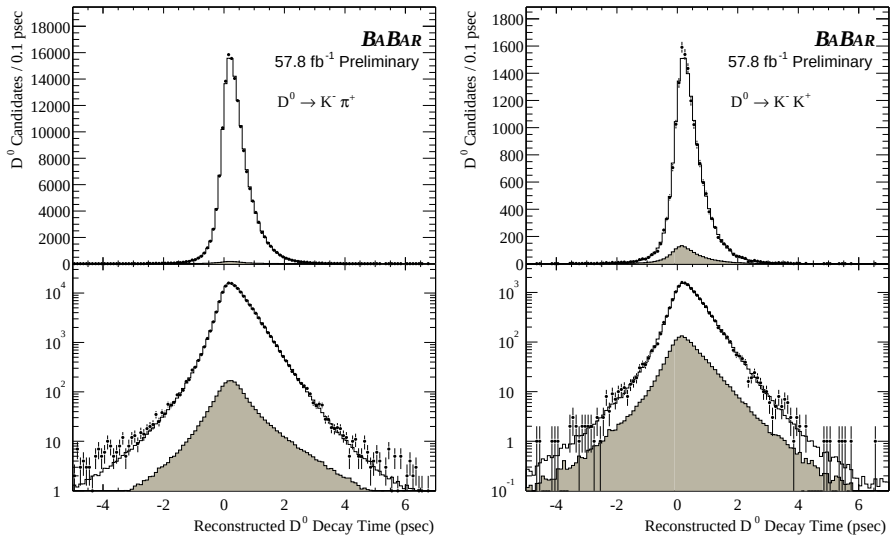

Figure 1: *BaBar lifetime distributions from ~58 fb^{-1} for $K\pi$ and KK candidates on linear and log scales.*

16,500 KK events and 8,360 $\pi\pi$ events from $D^{*\pm}$ decays. These have purity of 99.5%, 97.1%, and 92.4% respectively. The statistical errors on the lifetimes based on these samples are 1.3 fs, 4.4 fs and 6.5 fs respectively.

Although the lifetimes results are still blinded, the lifetime ratio has been measured and leads to $y = (1.4 \pm 1.0^{+0.6}_{-0.7})\%$. The statistical error is dominated by the KK mode while the systematic errors are still dominated by Monte Carlo statistics in that mode, giving hope for further improvement. Figure 1 shows the lifetime distribution for the KK candidates on a linear and a log scale.

The WS rate in the $K\pi$ mode has been measured to be $(0.38 \pm 0.04 \pm 0.02)\%$. Results on $D^0 - \overline{D}^0$ mixing are eagerly awaited.

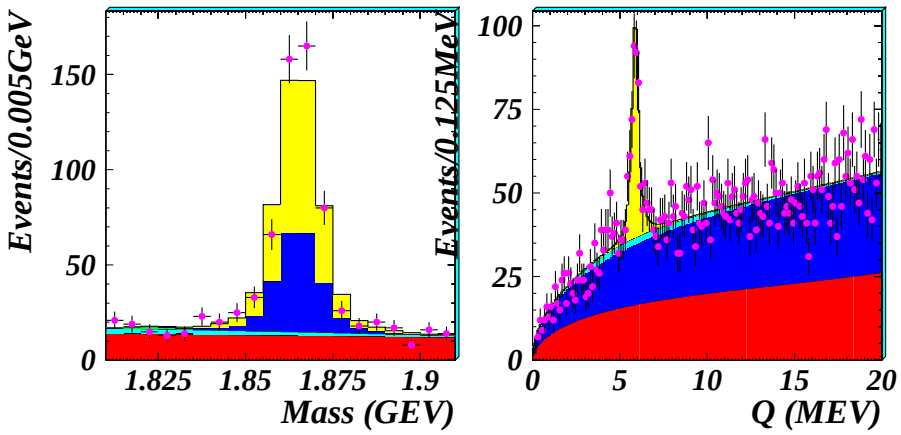

Figure 2: *The WS Belle M and Q distributions from ∼23 fb^{-1} for $K\pi$ and KK candidates.*

3.3 Belle

Belle results on y [10] based on $\sim$ 23 fb^{-1} of data using only KK decays and on the WS rate are shown in Figure 3. We see that even with less data than BaBar, they have similar errors - this is likely due to the looser cuts on Particle ID which are evident in the lower Signal / Background (S/B) ratio.

Their measurement of y yields $y = (-0.5 \pm 1.0^{+0.7}_{-0.8})\%$. The major systematic errors are from particle ID. Their preliminary measurement of the WS rate [11] in the $K\pi$ mode yields a rate of $(0.38 \pm 0.03 \pm 0.03)\%$. The second of the 0.03% errors is a preliminary estimate of the systematic error.

3.4 CLEO

CLEO is pursuing several analyses relevant to $D^0 - \overline{D}^0$ mixing. [12] In the $K^0_S\pi^+\pi^-$ mode they study the Dalitz plot of decays in which both the RS

($\overline{K}^0\pi^-\pi^+$, $K^{*-}\pi^+$) and the WS ($K^0\pi^+\pi^-$, $K^{*+}\pi^-$) signals occupy the same Dalitz plot. By a study of the time dependence they can extract the sign of x and the strong phase difference δ between RS and WS. Their efficiency across the plot is fairly constant and backgrounds are low ($\sim$1%). In their study they fit for the magnitudes and phases of 18 resonant and non-resonant amplitudes. At the 4.5σ level they observe WS decays and determine the phase difference δ to be $(3 \pm 14)^\circ$. They expect to use these data to measure also the sign of x.

Another analysis undertaken by CLEO is a study of the semileptonic WS decay $K^{*+}e^-\nu_e$. They observe 638 ± 51 RS decays and 0.00 ± 1.99 WS decay candidates. Interpreting the WS decays as signal leads to the measurement

$$r_{\rm mix} = (0.00 \pm 0.31 \pm 0.32)\%$$

which can be interpreted as the limit

$$r_{\rm mix} < 0.87\% \qquad \text{at the 95\% CL.}$$

4 Summary

Figure 3 shows the WS rates and y measurements from all recently reported measurements. The WS $K\pi$ rate is now clearly established as being a little over 1/3%. A non-zero value of y is not clearly established as of yet, but the errors are steadily getting better. Finally, results on $D^0 - \overline{D}^0$ mixing are eagerly awaited from BaBar, Belle and CLEO.

References

1. J. H. Christenson *et al*, Phys. Rev. Lett. **13**, 138 (1964).

2. A. Pais and S. B. Treiman, Phys. Rev. **D12**, 2744 (1975).

3. L. Wolfenstein, Phys. Rev. Lett. **75**, 2460 (1995) and G. Blaylock, A. Seiden and Y. Nir, Phys. Lett. **B355**, 555 (1995).

4. M. Leurer, Y. Nir and N. Seiberg, Nucl. Phys. **B420**, 468 (1994). See also A. Datta and D. Kumbhakar, Z. Phys. **C27**, 515 (1985) and Y. Nir, Nuovo Cimento **109A**, 991 (1996).

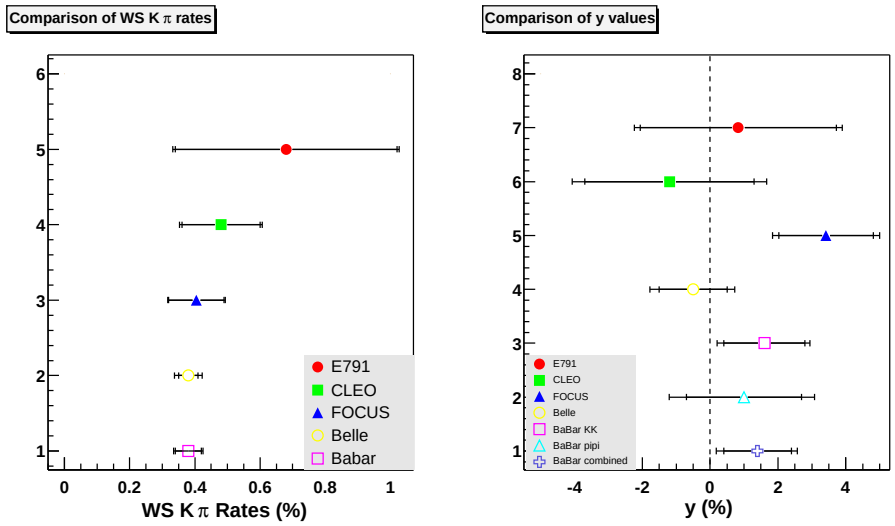

Figure 3: *Wrong Sign rates in the $K\pi$ mode and measurements of y from different experiments.*

5. For refined calculations of $r_{\rm mix}$ see H. Georgi, Phys. Lett. **B297**, 353 (1992), T. Ohl, G. Ricciardi, and E. H. Simmons, Nucl. Phys. **B403**, 605 (1993), L. Wolfenstein *ibid.* and A. Falk *et al.*, Phys. Rev. **D65**, 054034 (2002).

6. T. Liu, *Proceedings of the Workshop on the Future of High Sensitivity Charm Experiments: CHARM2000*, Batavia, IL, June 7-9, 1994. Harvard preprint HUTP-94-E021, 1994 and hep-ph/9408330.

7. J. M. Link *et al.*, Phys. Lett. **B485**, 62 (2000).

8. J. M. Link *et al.*, Phys. Rev. Lett. **86**, 2955 (2001).

9. A. Pompili, "Charm Mixing and Lifetimes at BaBar", in: Proc. of the XXXVII Rencontres de Moriond, "Electroweak Interactions and Unified Theories", 2002, to be published.

10. K. Abe *et al.*, Phys. Rev. Lett. **88**, 162001 (2002).

11. B. Yabsley, "Current charm Studies at Belle", presented at the APS Meeting of the DPF, Williamsburg, VA, 2002. See http://www.dpf2002.org/charm_quark_physics.cfm.

12. A. Smith, "Charm Physics in CLEO (mixing, CPV)", in: Proc. of the XXXVII Rencontres de Moriond, "QCD and Hadronic interactions", 2002, to be published.

Frascati Physics Series Vol. XXVIII (2002), pp.353-360
HQ & L 2002 – Vietri s/m, May 27th - June 1st, 2002

CP VIOLATION IN CHARM

Kevin Stenson
Dept of Physics & Astronomy, VU Station B 351807,
Vanderbilt University, Nashville, TN 37235 USA

ABSTRACT

Recent results on searches for CP and CPT violation in the charm sector are presented. These results include limits on direct CP violation in several channels from the FOCUS and CLEO experiments. The first reported search for CPT violation in charm, a preliminary result by the FOCUS collaboration, is also presented.

1 Charm CP Violation Introduction

CP violation is generally divided into three types: CP violation in mixing (indirect), CP violation in decay (direct), and CP violation in the interference between decay and mixing (indirect or direct). In all cases, CP violation occurs when the decay rate of a particle differs from that of its CP conjugate.

This requires contributions from two different CP violating terms with different phases. In addition, two CP conserving terms must also have different phases. The CP conserving phase shift is usually generated by QCD final state interactions. In the Standard Model (SM), two CP violating terms can come from tree level and penguin decays or Cabibbo favored and doubly Cabibbo suppressed decays. Extension to the Standard Model can introduce other CP violating terms which can interfere with the SM weak decays to generate CP violation.

In charm, mixing is very suppressed so at current experimental sensitivities, CP violation searches are generally searching for direct CP violation. One measures the CP violation rate by looking at the asymmetry:

$$A_{CP} \equiv \frac{\Gamma(D \to f) - \Gamma(\overline{D} \to \overline{f})}{\Gamma(D \to f) + \Gamma(\overline{D} \to \overline{f})} \quad (1)$$

In the fixed-target experiments E791 and FOCUS, the production mechanism gives rise to different numbers of produced particles and antiparticles. Therefore, these experiments normalize to another (copious) decay mode which is unlikely to exhibit CP violation.

2 Overview of Experiments

The most precise charm CP violation results come from the Fermilab fixed-target experiments E791 and FOCUS and the e^+e^- central detector, CLEO.

2.1 E791 and FOCUS experiments

E791 (FOCUS) took data at Fermilab during the fixed-target running of 1991–2 (1996–7). These experiments, like all modern fixed-target charm experiments are quite similar. Both sport silicon strip detectors in the vertex region to separate the charm production and decay vertices, a key requirement in separating signal from background. Following the silicon detectors are wire chambers and magnets which track and momentum analyze the decay products. Particle identification of charged hadrons is accomplished by the use of 2 (E791) or 3 (FOCUS) multi-cell threshold Čerenkov counters. Electromagnetic calorimeters identify electrons and photons while scintillation counters downstream of absorbing steel walls are used to identify muons. Both experiments used a hadron calorimeter to trigger on interesting events with high efficiency. The

targets in both experiments were segmented to allow charm decays in air. E791 used a 500 GeV/c π^- beam while FOCUS used a photon beam with an average energy of 180 GeV (for events with a reconstructed charm particle). The average charm momentum was around 60 GeV/c for both experiments. From a collection of 20 billion (6 billion) triggered events, E791 (FOCUS) fully reconstructed more than 200,000 (1,000,000) charm particles.

2.2 CLEO experiment

The CLEO experiment utilizes the CESR storage ring at Cornell which is a symmetric e^+e^- collider. The CLEO results presented here come from data taken at and near the $\Upsilon(4S)$, mostly from CLEO II.V (1996–9). Both CLEO II [1] and CLEO II.V [2] detectors use wire chambers for particle tracking and an excellent electromagnetic CsI calorimeter providing good reconstruction of photons, electron, and π^0's. These detectors are inside a 1.5 T axial magnetic field and surrounded by muon chambers. In CLEO II.V a silicon strip system near the beam was also present. The data presented here utilize 4.7–13.7 pb^{-1} of luminosity. Charm particles produced at CLEO generally have a momentum of a few GeV/c.

3 Direct CP Violation Results

3.1 Two-body decays

E791 [3], FOCUS [4], and CLEO [5] have all looked for CP violating behavior in the Cabibbo suppressed decays $D^0 \to K^+K^-$ and $D^0 \to \pi^+\pi^-$. These measurements, shown in Fig. 1 and tabulated in Table 1 are approaching the 1% level where non-Standard Model effects might show up.

Table 1: *Measurements of the CP asymmetry from $D^0 \to K^+K^-$, $\pi^+\pi^-$ decays.*

Expt	$A_{CP}(KK)$ (%)	$A_{CP}(\pi\pi)$ (%)
E791(98) [3]	$-1.0 \pm 4.9 \pm 1.2$	$-4.9 \pm 7.8 \pm 3.0$
FOCUS(00) [4]	$-0.1 \pm 2.2 \pm 1.5$	$4.8 \pm 3.9 \pm 2.5$
CLEO(02) [5]	$0.0 \pm 2.2 \pm 0.8$	$1.9 \pm 3.2 \pm 0.8$

FOCUS has recently published [6] results using the two-body decay modes $D^+ \to K^0_S\pi^+$, where Cabibbo favored and doubly Cabibbo suppressed ampli-

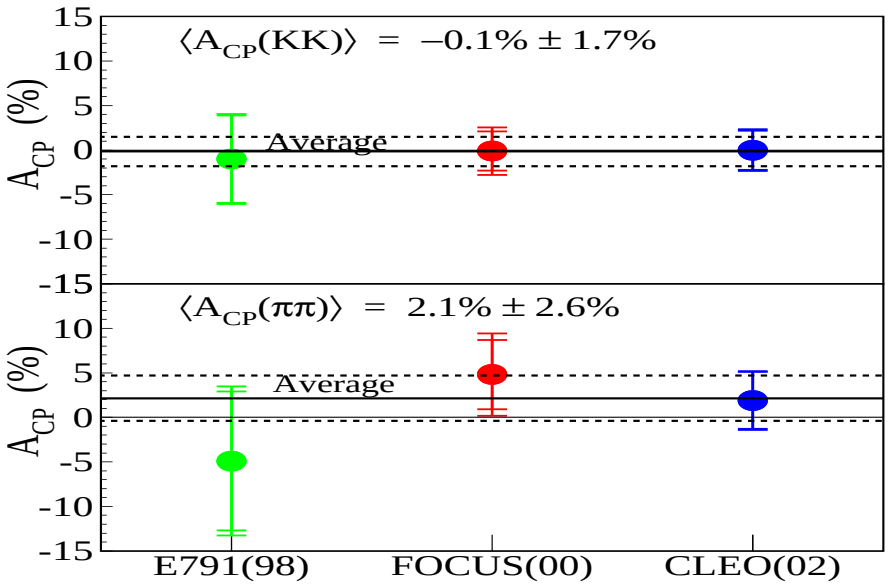

Figure 1: *Measurements of the CP asymmetry of* $D^0 \to K^+K^-$, $\pi^+\pi^-$ *decays.*

tudes can interfere and $D^+ \to K^0_S K^+$ which is a singly Cabibbo suppressed decay where interference between the tree and penguin diagrams can occur. These decay modes should also display a CP violation component due to CP violation in K^0 decays. As seen in Table 2, no evidence of CP violation was found which is consistent with the Standard Model for this level of sensitivity.

Table 2: *Measurements of the CP asymmetry from* $D^+ \to K^0_S K^+, K^0_S \pi^+$ *decays.*

CP Asymmetry	FOCUS
$A_{CP}(K^0_S\pi^+)$ w.r.t. $K^-\pi^+\pi^+$	$(-1.6\pm1.5\pm0.9)\%$
$A_{CP}(K^0_S K^+)$ w.r.t. $K^-\pi^+\pi^+$	$(6.9\pm6.0\pm1.8)\%$
$A_{CP}(K^0_S K^+)$ w.r.t. $K^0_S\pi^+$	$(7.1\pm6.1\pm1.4)\%$

3.2 Three-body decays

Searching for direct CP violation in three-body decays is significantly more complicated than two-body decays. One can look for CP violation by inte-

grating over phase space, by looking at quasi two-body decays by cutting on resonances, or by using a full Dalitz plot analysis of the charm and anticharm particle to look for discrepancies. FOCUS [4] and E791 [7] have both reported results for $D^+ \to K^-K^+\pi^+$. FOCUS reported $A_{CP} = (0.6 \pm 1.1 \pm 0.5)\%$ and plans to perform a CP violation Dalitz plot analysis in the future. E791 also reported results for the sub-resonances: $A_{CP}(\phi\pi^+) = (-2.8 \pm 3.6)\%$ and $A_{CP}(K^*K^+) = (-1.0 \pm 5.0)\%$.

As a byproduct of their Dalitz plot analysis of $D^0 \to K^-\pi^+\pi^0$ [8], CLEO measured

$$A_{CP} \equiv \int \frac{|M_{D^0}|^2 - |M_{\overline{D}^0}|^2}{|M_{D^0}|^2 - |M_{\overline{D}^0}|^2} dDP = (-3.1 \pm 8.6)\%, \qquad (2)$$

again consistent with zero.

4 CPT Violation Search

It is common knowledge that point particle Lorentz invariant field theories require CPT invariance [9]. However, some Standard Model extensions need not be Lorentz-invariant [10]. In fact, it might be possible to find evidence for strings which dominate at the Plank scale using data which exists today. Limits on CPT violation have been set using neutral K and B mesons (mixing interferometry). It is possible, however, for these effects to manifest at different levels in different flavors so a check in the charm system is also important.

4.1 CPT Violation Formalism

This analysis mostly follows the notation of Ref. [11]. First, the standard effective Hamiltonian is rewritten:

$$\Lambda = M - \frac{1}{2}i\Gamma \qquad \Longrightarrow \qquad \Lambda = \frac{1}{2}\Delta\lambda \begin{pmatrix} U+\xi & VW^{-1} \\ VW & U-\xi \end{pmatrix} \qquad (3)$$

where U, V, W, and ξ are complex and $\Delta\lambda = \Delta M - i\,\Delta\Gamma/2$. The parameter ξ is the CPT violating term. The time-dependent right-sign $D^0 \to f$ decay probability is given by:

$$\begin{aligned} P_f(t) = \frac{1}{2}|F|^2 e^{-\Gamma t} \big[&\left(1+|\xi|^2\right)\cosh\Delta\Gamma + \left(1-|\xi|^2\right)\cos\Delta M \\ &- 2\Re(\xi)\sinh\Delta\Gamma + 2\Im(\xi)\sin\Delta M \big]. \end{aligned} \qquad (4)$$

The time-dependent $\overline{D}^0 \to \overline{f}$ decay probability $\overline{P}_{\overline{f}}(t)$ is simply $P_f(t)$ with $\xi \to -\xi$ and $F \to \overline{F}$. From this, one can form an asymmetry for right-sign decays as:

$$A_{CPT}(t) \;=\; \frac{\overline{P}_{\overline{f}}(t) - P_f(t)}{\overline{P}_{\overline{f}}(t) + P_f(t)} \;=\; \frac{2\Re(\xi)\sinh\Delta\Gamma t - 2\Im(\xi)\sin\Delta M t}{(1+|\xi|^2)\cosh\Delta\Gamma t + (1-|\xi|^2)\cos\Delta M t}. \quad (5)$$

By Taylor expanding sin, sinh, cos, cosh to 1st order and switching to the standard mixing variables $x \equiv \Delta M/\Gamma$, $y \equiv \Delta\Gamma/2\Gamma$, one finds:

$$A_{CPT}(t) \;\approx\; [\Re(\xi)\, y - \Im(\xi)\, x)]\,\Gamma t \quad (6)$$

Given the measured limits on mixing and the lifetime range probed by the FOCUS experiment, this approximation is sufficiently accurate. Experimentally:

$$A_{CPT}(t') \;=\; \frac{N_{\overline{D}^0}(t') - N_{D^0}(t')}{N_{\overline{D}^0}(t') + N_{D^0}(t')}. \quad (7)$$

Therefore, measuring the slope of the lifetime ratio distribution immediately returns $[\Re(\xi)\, y - \Im(\xi)\, x]$.

4.2 Preliminary FOCUS CPT Violation Results

Figure 2 shows the invariant mass distribution for right-sign $D^0 \to K^-\pi^+$ decays. These decays have been tagged using the charge of the soft pion from $D^{*+} \to D^0\pi_s^+$ decays.

In Fig. 3, the ratio of $\overline{D}^0$ to D^0 as a function of reduced proper time, t', is plotted. The reduced proper time is defined by $t' \equiv (\ell - N\sigma_\ell)/(\beta\gamma c)$ where ℓ is the distance between the production and decay vertex, σ_ℓ is the calculated resolution on ℓ, and N is the minimum detachment cut applied. This has the effect of starting the clock at the moment at which the particle could first be reconstructed by the experiment (with the given detachment cut) and thus greatly reducing the amount of correction needed due to acceptance. The fit to Fig. 3 is the basis of the preliminary FOCUS result:

$$\Re(\xi)\, y \;-\; \Im(\xi)\, x \;\;=\;\; 0.0083 \pm 0.0065 \pm 0.0041 \quad (8)$$

The actual limit on the CPT violating parameter depends on mixing parameters; for example if $x = 0$ and $y = 1\%$ then $\Re(\xi) = 0.83 \pm 0.65 \pm 0.41$. The systematic errors were determined by exploring the effect of different absorption lengths in the Monte Carlo simulation, different selection criteria, and different sideband selections for the background subtraction.

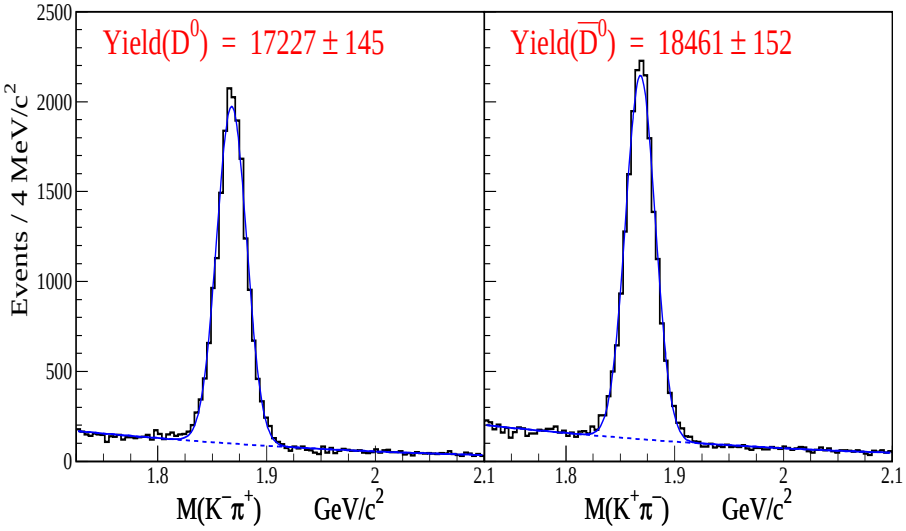

Figure 2: *Preliminary FOCUS mass plots of* $D^0 \to K^-\pi^+$ *for events which have a* D^* *tag.*

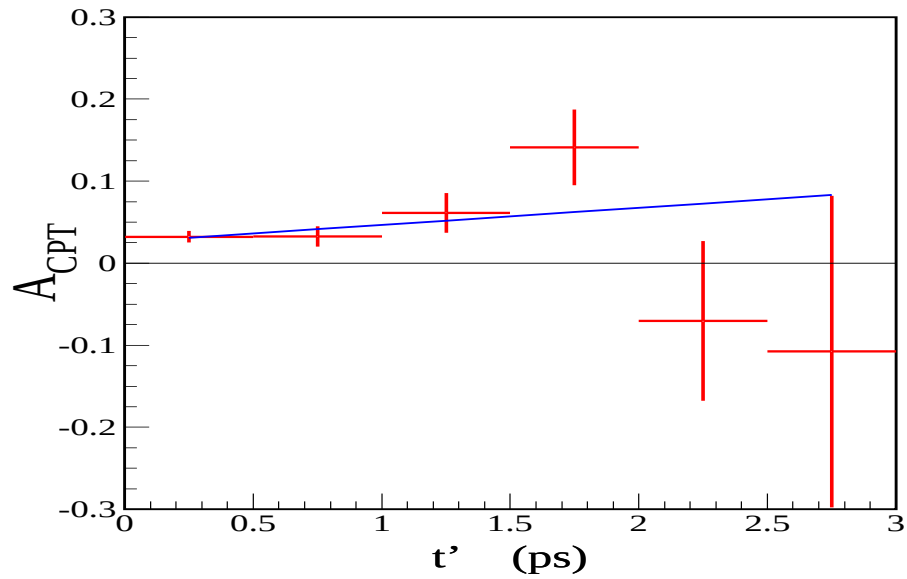

Figure 3: *Preliminary FOCUS fit to the ratio of* $\overline{D}^0$ *to* D^0 *as a function of reduced proper time,* t'.

5 Conclusion

Considerable progress is currently being made by FOCUS and CLEO in the search for direct CP violation in the charm system. Current limits are approaching the 1% level at which non-Standard Model effects might be seen. In the near future, BaBar and Belle should be able to probe even further in this exciting area. Following this, BTeV will also have an opportunity to search for CP violation in the charm sector with a sample of more than 1 billion reconstructed charm decays. In addition, the search for CPT violation is also being extended into the charm sector. Both types of searches have the potential to uncover exciting new physics.

References

1. Y. Kubota *et al.* (CLEO Collaboration), Nucl. Instrum. Meth. A **320**, 66 (1992).
2. T. Hill *et al.* (CLEO Collaboration), Nucl. Intrum. Meth. A **418**, 32 (1998).
3. E.M. Aitala *et al.* (E791 Collaboration), Phys. Lett. **B421**, 405 (1998).
4. J.M. Link *et al.* (FOCUS Collaboration), Phys. Lett. **B491**, 232 (2000).
5. S.E. Csorna *et al.* (CLEO Collaboration), Phys. Rev. D **65**, 031102 (2002).
6. J.M. Link *et al.* (FOCUS Collaboration), Phys. Rev. Lett. **88**, 041602 (2002).
7. E.M. Aitala *et al.* (E791 Collaboration), Phys. Lett. **B403**, 377 (1997).
8. S. Kopp *et al.* (CLEO Collaboration), Phys. Rev. D **63**, 092001 (2001).
9. R.G. Sachs, *The Physics of Time Reversal*, University of Chicago Press (1987).
10. V. Alan Kostelecký, Phys. Rev. D **64**, 076001 (2001), V. Alan Kostelecký, Phys. Rev. D **61**, 16002 (2000), D. Colladay and V. Alan Kostelecký, Phys. Rev. D **58** 116002 (1998), D. Colladay and V. Alan Kostelecký, Phys. Rev. D **55** 6760 (1997) and references therin.
11. V. Alan Kostelecký, Phys. Rev. D **64**, 076001 (2001).

Frascati Physics Series Vol. XXVIII (2002), pp.361-368
HQ & L 2002 – Vietri s/m, May 27th - June 1st, 2002

SEARCH FOR CP VIOLATION IN HYPERON DECAYS

Kenneth S. Nelson
University of Virginia, Charlottesville Va.
Representing the *HyperCP* Collaboration [1)]

ABSTRACT

The *HyperCP* experiment is searching for CP Violation in the decay sequence $\Xi^- \to \Lambda\pi^- \to p\pi^-\pi^-$ by comparing the angular distribution of the p with that of the $\overline{p}$ in the charge conjugate decay. A preliminary limit based on a small fraction of the data is reported.

1 Phenomenology of Non-Leptonic Hyperon Decays

The decays considered here are $\Xi^- \to \Lambda\pi^-$, $\Lambda \to p\pi^-$ and the charge conjugate decays. Since parity is not conserved in these weak decays the final state particles can be in either an S or P orbital state. Thus the decay can be described by three real quantities which are conventionally chosen to be; the partial decay rate $\Gamma \propto |S|^2 + |P|^2$ and two independent decay parameters

$$\alpha = \frac{2\mathrm{Re}(S^*P)}{|S|^2 + |P|^2} \quad \beta = \frac{2\mathrm{Im}(S^*P)}{|S|^2 + |P|^2} \ , \tag{1}$$

where S, P are the $\ell = 0, 1$ partial wave amplitudes. The parameter α quantifies $\mathcal{P}$ violation in the decay of a polarized hyperon through the angular distribution;

$$\frac{dN}{d\Omega} = \frac{1}{4\pi}(1 + \alpha \vec{\mathbf{P}} \cdot \hat{\mathbf{q}}) = \frac{1}{4\pi}(1 + \alpha P \cos\theta) \tag{2}$$

where $\vec{\mathbf{P}}$ is the polarization of the parent and $\hat{\mathbf{q}}$ is the momentum unit vector of the daughter baryon.

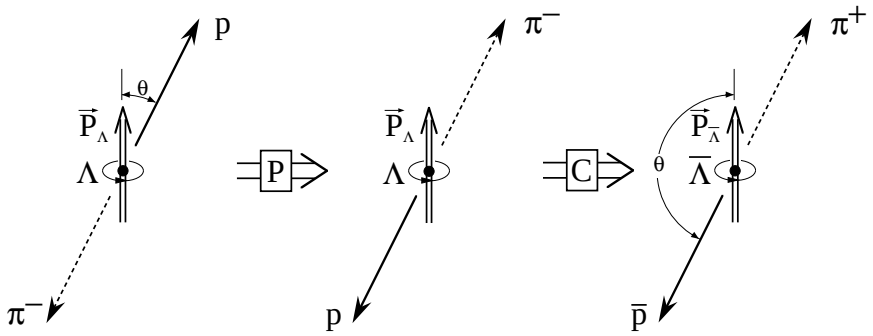

Figure 1: $\mathcal{P}$ *and* $\mathcal{C}$ *operations on* $\Lambda \to p\pi$.

A $\mathcal{CP}$ transformation of the decay of a polarized Λ is illustrated in fig. 1. The polar angle θ of the daughter proton relative to the parent polarization direction is mapped to $180° - \theta$. In the limit of $\mathcal{CP}$ invariance these two configurations have equal rates, which implies

$$\overline{\alpha} = -\alpha \ . \tag{3}$$

If the polarizations of parent Λ and $\overline{\Lambda}$ samples are exactly equal ($P = \overline{P}$) one can form a $\mathcal{CP}$ asymmetry observable given by

$$A = \frac{\alpha P + \overline{\alpha}\overline{P}}{\alpha P - \overline{\alpha}\overline{P}} = \frac{\alpha + \overline{\alpha}}{\alpha - \overline{\alpha}} \ . \tag{4}$$

The *HyperCP* experiment obtains Λ hyperons having precisely known polarization from *unpolarized* $\Xi^- \to \Lambda\pi^-$ decays. In this case $\vec{P}_\Lambda = \alpha_\Xi \hat{\Lambda}$, where $\hat{\Lambda}$ is the negative of the Ξ flight direction in the Λ rest frame. In the subsequent $\Lambda \to p\pi^-$ decay the angular distribution of the proton with respect to the polar axis defined by $\hat{\Lambda}$ is then

$$\frac{dN}{d\cos(\theta_{p\Lambda})} = 1 + \alpha_\Xi \alpha_\Lambda \cos(\theta_{p\Lambda}) \tag{5}$$

A similar expression is obtained for the $\overline{p}$ distribution stemming from $\overline{\Xi}^+$ decay. In the limit of $\mathcal{CP}$ conservation the slope of the $\overline{p}$ distribution in the $\overline{\Xi^+}$ decay is identical, by eqn. 3. The experimentally observed asymmetry then is

$$A_{\Xi\Lambda} \equiv \frac{\alpha_\Xi \alpha_\Lambda - \alpha_{\overline{\Xi}} \alpha_{\overline{\Lambda}}}{\alpha_\Xi \alpha_\Lambda + \alpha_{\overline{\Xi}} \alpha_{\overline{\Lambda}}} \approx A_\Xi + A_\Lambda \ , \tag{6}$$

where A_Ξ and A_Λ each have the form of eqn. 4.

2 Expectations

Donoghue et al. [2] have given a model independent approximate form for the decay asymmetry A in eqn. 4;

$$A \approx -\tan(\delta_P - \delta_S)\sin(\phi_P - \phi_S) \ , \tag{7}$$

where $\delta_{P,S}$ are the final state strong phase shifts for P and S waves with $\Delta I = 1/2$ and $\phi_{P,S}$ are the corresponding $\mathcal{CP}$ violating weak phases. The pion–nucleon phase shifts in $\Lambda \to p\pi^-$ have been measured [3] to be $\delta_P - \delta_S \approx 7°$. Since there is no experimental information on $\Lambda\pi$ scattering one must rely on theoretical estimates [4] which tend to favor small values. Consequently the asymmetry $A_{\Xi\Lambda}$ is thought to be dominated by the Λ decay. Predictions of A_Λ within the standard model range from 10^{-5} to 10^{-4}. Nevertheless, some SUSY models [5] can lead to A_Λ as large as $O(10^{-3})$ without an enhancement of ϵ'/ϵ.

At the present time the two best published limits on $\mathcal{CP}$ asymmetry in hyperon decays come from PS185 [6] at LEAR which measured $A_\Lambda = 0.013 \pm 0.022$ and E756 [7] at FNAL which found $A_{\Xi\Lambda} = 0.012 \pm 0.014$. Both of these experiments were limited by statistics. Being at the level of 1–2% neither of the measurements constrain current theory.

3 The *HyperCP* Experiment

The goal of the *HyperCP* experiment is a $O(10^{-4})$ sensitivity on $A_{\Xi\Lambda}$ which requires a sample on the order of 10^9 reconstructed Ξ^- and $\overline{\Xi}^+$ decays. Therefore, the primary considerations in the the design of the *HyperCP* spectrometer were that it be capable of operating at high rate and that it be simple in order to facilitate understanding potential biases at the level of the measurement. A

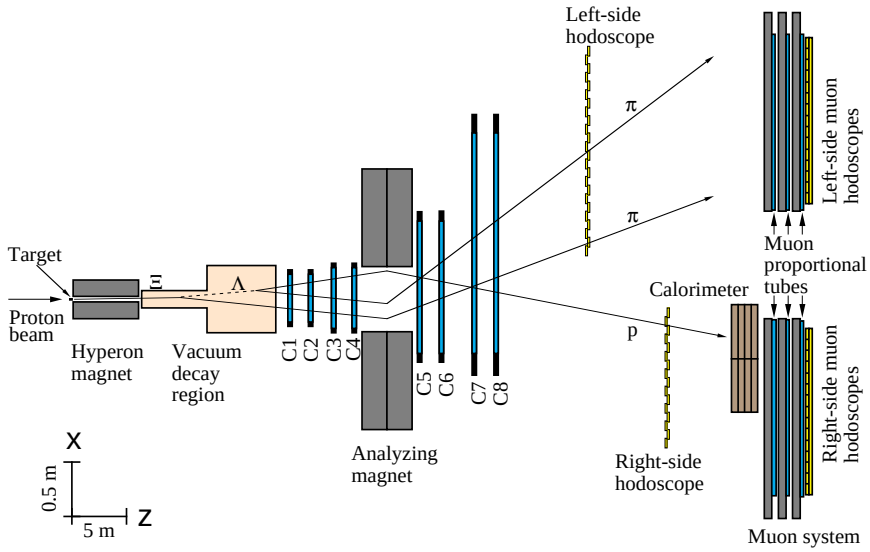

Figure 2: *Plan view of the Hyper$\mathcal{CP}$ spectrometer*

plan view of the apparatus is shown in figure 2 with the trajectories of Ξ decay particles superimposed.

An 800 Gev/c proton beam collided with targets of Cu, either 2cm or 6cm in length. The two target lengths were chosen to equalize the rates ($\approx$ 15 MHz) in the apparatus between Ξ^- and $\overline{\Xi}^+$ running. The forward produced particles were intercepted by a curved magnetized collimator whose entrance axis was colinear with the incoming beam in order to select an unpolarized sample of hyperons. Charged particles in the range of 120 GeV/c to 240 GeV/c were accepted by the collimator and emerged into a 13m long vacuum decay pipe. Following the decay pipe was a magnetic spectrometer consisting of MWPC's optimized for high rate operation, an analyzing magnet, segmented hodoscopes, a hadronic calorimeter and a muon system.

A simple and selective trigger was formed by a requiring a coincidence of one or more hits in each hodoscope on either side of the beam line. The calorimeter was used to suppress muon and secondary interaction backgrounds to this main trigger. The polarities of both the magnetic collimator and the analysis magnets were reversed between Ξ^- and $\overline{\Xi}^+$ running achieving a $\mathcal{CP}$ invariant trigger geometry. The final baryon (p or $\overline{p}$) was always deflected into

the calorimeter while the two pions were deflected to the hodoscope on the other side. A cycle of + and − runs was completed at least once per day.

The experiment took data in the 1997 and 1999 fixed target running periods at FNAL. From the total data set 4.6×10^8 $\overline{\Xi}^+$ and 2.0×10^9 Ξ^- decays have been reconstructed. The running conditions in the positive and negative modes were well matched as can be seen in the $p\pi\pi$ mass distributions in figure 3

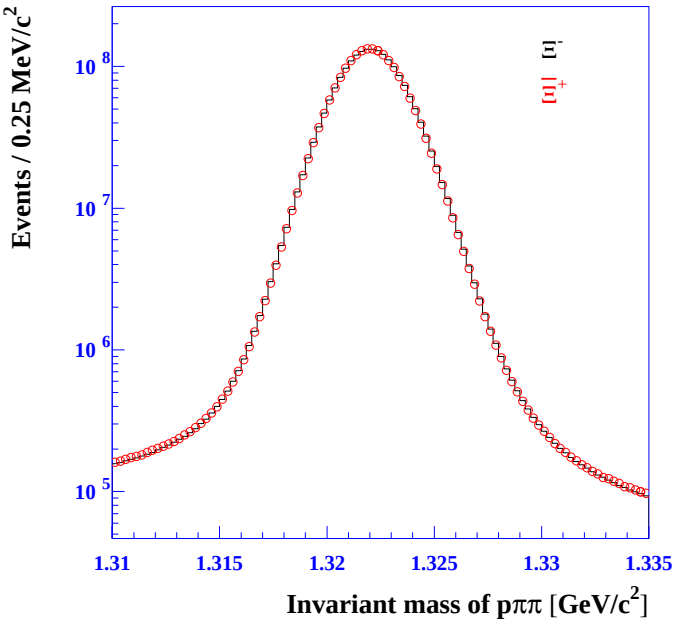

Figure 3: *The $p\pi\pi$ invariant mass during reconstruction*

4 Status of the Analysis

The asymmetry $A_{\Xi\Lambda}$ depends on a comparison of the slopes $\alpha_\Xi \alpha_\Lambda$ and $\alpha_{\overline{\Xi}} \alpha_{\overline{\Lambda}}$ of the angular distributions of the p and $\overline{p}$ in the Λ and $\overline{\Lambda}$ rest frames. Because the angular distribution is taken with respect to $\hat{\Lambda}$, which changes direction from event to event, the effect of biases which are fixed in space (*e.g.* a dead PWC wire) is diluted. Nevertheless, acceptance differences between Ξ^- and $\overline{\Xi}^+$ samples can lead to a false asymmetry. Two methods are being used to

overcome this effect to extract the asymmetry.

In the first a Hybrid Monte Carlo (HMC) technique (similar to that in ref. 7) is used to measure the acceptance of the spectrometer and correct for it. In the HMC technique a montecarlo, or *fake*, event is generated from an actual $\Xi \to \Lambda\pi \to p\pi\pi$ event observed in the data by replacing the p and π from the Λ decay with a p and π chosen from a uniform angular distribution. The p and π are then traced through a model of the apparatus, their trajectories are reconstructed and then subjected to the same selection criteria as the original event. If the fake event survives it is weighted by a function $W(\alpha_\Xi \alpha_\Lambda)$, where the product $\alpha_\Xi \alpha\Lambda$ is determined by minimizing the χ^2 difference between the angular distribution of real data events and weighted fake events. Figure 4 shows the evolution of the angular distribution from the raw data to the weighted HMC events. The quality of the fit is evident in the lower right plot of figure 4 which shows the ratio of the original data distribution to the weighted HMC distribution. The same procedure, including identical selection criteria, are applied to an $\overline{\Xi}^+$ sample to measure $\alpha_{\overline{\Xi}}\alpha_{\overline{\Lambda}}$. Finally the asymmetry follows from the difference according to eqn. 6. Systematic errors are evaluated using the data sample itself. For example, in modeling the apparatus the MWPC wire-by-wire efficiencies are varied according to their measured uncertainties to obtain the systematic error associated with imperfect knowlege of this aspect of the detector simulation. Other systematic difference effects which are considered are; polarization, rates, background, trigger efficiency uncertainty, B-field uncertainty and secondary interactions. Applying this procedure to a small sample of (15M Ξ^- and 30M $\overline{\Xi}^+$) events randomly distributed throughtout the 97-99 runs we obtain

$$A_{\Xi\Lambda} = [-7 \pm 12(\text{stat.}) \pm 6.2(\text{sys.})] \times 10^{-4} \; . \tag{8}$$

A second method, the weighting technique [8], weights events so as to force the Ξ^- and $\overline{\Xi}^+$ to samples to match in the 5-dimensional space defined by the momentum components and position of the $\Xi^-/\overline{\Xi}^+$ at the exit of the collimator. The slope difference $\alpha_\Xi \alpha_\Lambda - \alpha_{\overline{\Xi}}\alpha_{\overline{\Lambda}}$ is extracted from the ratio of the angular distribution of weighted events. By using MC Ξ decays overlaid on real events it has been demonstrated that the technique removes production distribution related biases while preserving the asymmetry input in the MC. This approach is still undergoing a course of refinement but so far it appears promising as a check of the HMC method.

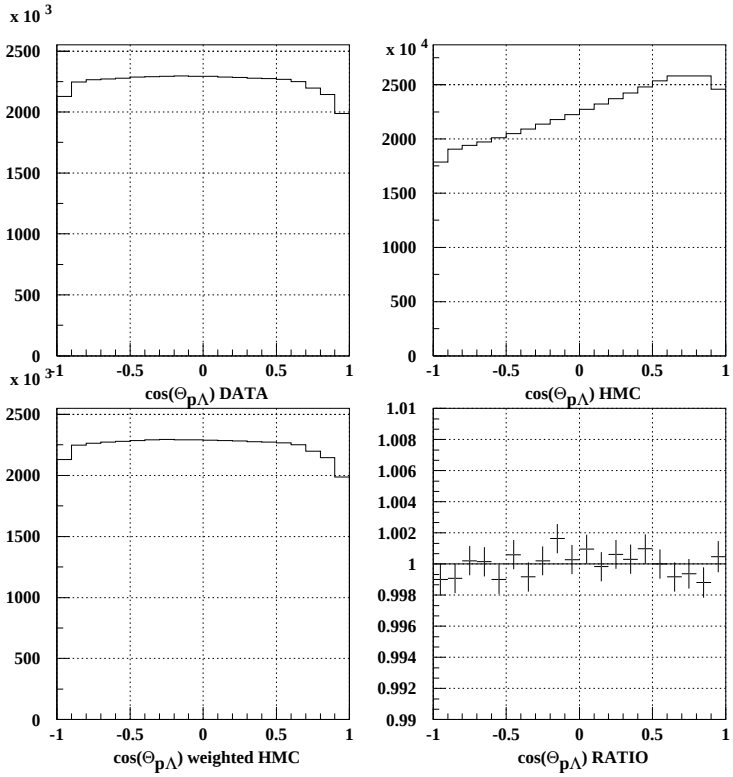

Figure 4: *Progression of HMC fitting procedure*

5 Conclusion

The HyperCP experiment has set a preliminary limit on $A_{\Xi}\Lambda$ at the 10^{-3} level using a small fraction of the total data sample. This limit is an order of magnitude better than current published values. Since the data itself has been used to establish systematic error estimates these will decrease as the full data sample is analyzed. The projected goal is an uncertainty in the asymmetry of $\delta A_{\Xi\Lambda} \sim 1.4 \times 10^{-4}$ which is within the range of some theoretical predictions.

References

1. A. Chan, Y.C. Chen, C. Ho, P.K. Teng (*Academia Sinica*); W.S. Choong, G. Gidal, Y. FU, P. Gu, T. Jones, K.B. Luk, P. Zyla, (*Berkeley and LBNL*); C. James, J. Volk, (*FNAL*); J. Felix, (*Guanajuato*); R.A. Burnstein, A. Chakravorty, D.M. Kaplan, L.M. Lederman, W. Luebke, D. Rajaram, H.A. Rubin, N. Solomey, Y. Torun, C.G. White, S.L. White, (*IIT*); N. Leros, J.P. Perroud, (*Lausanne*); H.R. Gustafson, M.J. Longo, F. Lopez, H.K. Park, (*Michigan*); K. Clark, C.M. Jenkins, (*South Alabama*); E.C. Dukes, C. Durandet, R. Godang, T. Holmstrom, M. Huang, L.C. Lu, K.S. Nelson, (*Virginia*)

2. J. Donoghue, X.G. He, and S. Pakvasa, Phys. Rev. **D34** (1986) 833.

3. L.D. Roper, R.M. Wright and B.T. Feld, Phys. Rev. **138** (1965) B190.

4. Recent predictions found in J. Tandean, A.W. Thomas and G. Valencia, Phys. Rev. **D64** (2001) 014005; U.G. Meissner and J.A. Oller, Phys. Rev. **D64** (2001) 014006.

5. X.G. He *et al*, Phys. Rev **D61** (2000) 071701(R).

6. P.D. Barnes *et al.,* Phys. Rev. **C 54** (1996) 1877.

7. K.B. Luk *et al.,* Phys. Rev. Lett. **85** (2000) 4860.

8. This is a refinement of the method found in N. Leros *et al.,* Nucl. Phys. **99** (*Proc. Suppl.*), 211 (2001).

Frascati Physics Series Vol. XXVIII (2002), pp.371-395
HQ & L 2002 – Vietri s/m, May 27th - June 1st, 2002

NEUTRINO OSCILLATIONS: STATUS AND PROSPECTS

G.L. Fogli,[1] E. Lisi,[1] A. Marrone,[1] D. Montanino[2] and A. Palazzo[1]
[1] *Dipartimento di Fisica and Sezione INFN di Bari*
[2] *Dipartimento di Scienza dei Materiali and Sezione INFN di Lecce*

ABSTRACT

The evidence for solar and atmospheric neutrino oscillations is analyzed, including the most recent SNO data, as well as the constraints on ν_e mixing coming from the CHOOZ reactor experiment. The regions of the mass-mixing parameter space compatible with the data are determined and their features discussed. The prospects of the future experiments are briefly examined.

1 Introduction

The most recent atmospheric neutrino data from the Super-Kamiokande (SK) experiment [1)] confirm an excellent agreement with the hypothesis of flavor oscillations in the $\nu_\mu \leftrightarrow \nu_\tau$ channel [2)]. Such hypothesis consistently emerges from all the SK data, i.e. sub-GeV e-like and μ-like events (SG$e, \mu$), multi-GeV e-like and μ-like events (MG$e, \mu$), and upward-going muon events (UPμ). As

well known, this result is also corroborated by independent atmospheric neutrino results from the MACRO [3] and Soudan-2 [4] experiments, as well as by the finalized upward-going muon data sample from the pioneering Kamiokande experiment. Oscillations in the $\nu_\mu \leftrightarrow \nu_\tau$ channel are also compatible with the negative results of the reactor experiment CHOOZ in the $\nu_e \leftrightarrow \nu_e$ channel [5]. Although two-flavor $\nu_\mu \leftrightarrow \nu_\tau$ oscillations represent the most economical explanation, however, particular interest is covered by the case of *dominant* $\nu_\mu \leftrightarrow \nu_\tau$ transitions plus *subdominant* $\nu_\mu \leftrightarrow \nu_e$ transitions, interpretation also consistent with the SK+CHOOZ data, that leads to a much richer three-flavor oscillation phenomenology for atmospheric ν's [6]. Accordingly, we discuss in Sec. 2 both atmospheric and solar neutrinos in a common 3ν oscillation framework.

In Sec. 3 we consider atmospheric ν data, including 55 data points from the SK experiment (79.5 kTy) [1]: the zenith distributions of sub-GeV events (SG e-like and μ-like, 10+10 bins), multi-GeV events (MGe,μ, 10+10 bins) and upward-going muons (stopping and through-going μ, 10+5 bins). We also include the rate of events in the CHOOZ reactor experiment (14 bins) [5].

Concerning solar neutrinos, discussed in Secs. 4 and 5, we simplify the approach, assuming the simplest scenario of two-family oscillations among active neutrinos. In this framework, we discuss how the data from the Homestake [7], SAGE [8], GALLEX/GNO [9, 10], Kamiokande [11], Super-Kamiokande [12], and Sudbury Neutrino Observatory (SNO) [13, 14, 15] experiments have consistently established that electron neutrinos emitted from the Sun [16] undergo flavor transitions to the other active states (ν_μ or ν_τ) and how neutrino oscillations [17], possibly affected by matter effects in the Sun or in the Earth [18], represent a beautiful explanation of such transitions.

2 Three-neutrino mixing and oscillations

The combined sources of evidence for neutrino flavor transitions coming from the solar ν problem and from the atmospheric ν anomaly demand an approach in terms of three-flavor oscillations among massive neutrinos (ν_1, ν_2, ν_3) [6, 19]. The three-flavor ν parameter space is then spanned by six variables:

$$\delta m^2 = m_2^2 - m_1^2, \quad (1)$$

$$m^2 = m_3^2 - m_2^2, \quad (2)$$

$$\omega = \theta_{12} \in [0, \pi/2], \quad (3)$$

$$\phi = \theta_{13} \in [0, \pi/2], \quad (4)$$

$$\psi = \theta_{23} \in [0, \pi/2], \quad (5)$$

$$\delta = \text{CP violation phase}, \quad (6)$$

where the θ_{ij} rotations are conventionally ordered as for the quark mixing matrix [20].

In the phenomenologically interesting limit $|\delta m^2| \ll |m^2|$, the two eigenstates closest in mass (ν_1, ν_2) are expected to drive solar ν oscillations, while the "lone" eigenstate ν_3 drives atmospheric ν oscillations. In such a limit (see [6, 19, 21] and refs. therein): *i*) the phase δ becomes unobservable; *ii*) the atmospheric parameter space is spanned by (m^2, ψ, ϕ); and *iii*) the solar ν parameter space is spanned by $(\delta m^2, \omega, \phi)$.

In other words, in the previous limit it can be shown that solar neutrinos probe the composition of ν_e in terms of mass eigenstates

$$\nu_e = U_{e1}\nu_1 + U_{e2}\nu_2 + U_{e3}\nu_3 \quad (7)$$

$$= c_\phi(c_\omega \nu_1 + s_\omega \nu_2) + s_\phi \nu_3 \quad (8)$$

in the parameter space

$$(\delta m^2, \omega, \phi) \equiv (\delta m^2, U_{e1}^2, U_{e2}^2, U_{e3}^2) \,, \quad (9)$$

where $U_{e1}^2 + U_{e2}^2 + U_{e3}^2 = 1$ for unitarity, whereas atmospheric (more generally, "terrestrial") neutrinos probe the flavor composition of ν_3,

$$\nu_3 = U_{e3}\nu_e + U_{\mu 3}\nu_\mu + U_{\tau 3}\nu_\tau \quad (10)$$

$$= s_\phi \nu_e + c_\phi(s_\psi \nu_\mu + c_\psi \nu_\tau) \quad (11)$$

in the parameter space

$$(m^2, \psi, \phi) \equiv (m^2, U_{e3}^2, U_{\mu 3}^2, U_{\tau 3}^2) \,, \quad (12)$$

where $U_{e3}^2 + U_{\mu 3}^2 + U_{\tau 3}^2 = 1$ for unitarity. The two unitarity constraints can be conveniently embedded [19] in two triangle plots (see Fig. 1), which describe the mixing parameter spaces for given δm^2 and m^2 for solar and atmospheric neutrinos, respectively. The only parameter common to the two triangles is $U_{e3}^2 = s_\phi^2$. [1]

[1] In the special case $\phi = 0$, the atmospheric and solar parameter spaces are decoupled into the two-family oscillation spaces $(\delta m^2, \omega)$ and (m^2, ψ).

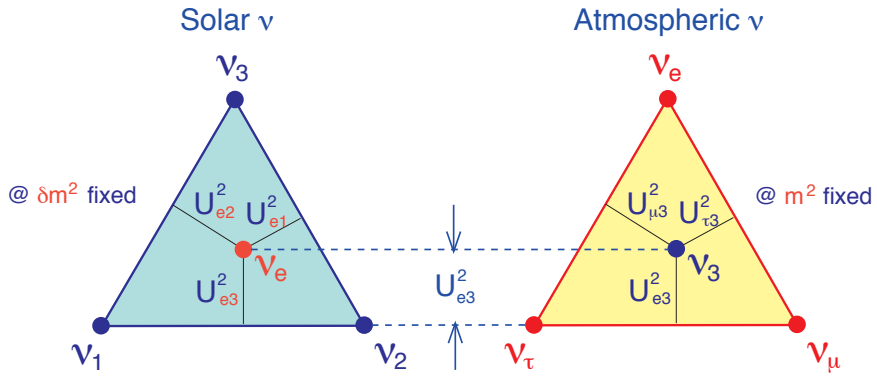

Figure 1: *Parameter spaces of solar and atmospheric neutrinos in the limit* $|\delta m^2| \ll |m^2|$, *for assigned* δm^2 *and* m^2. *The only common parameter is* $U^2_{e3} = s^2_\phi$.

3 Analysis of the atmospheric data

In this Section we report an updated analysis of the most recent SuperKamiokande data [1], and combine them with the limits coming from the CHOOZ experiment [5], by assuming the "standard" three-neutrino framework discussed in the previous Section. Details about our approach can be found in [6]. Constraints on the mass-mixing parameters are obtained through a χ^2 statistics, and are plotted in the atmospheric 3ν triangle described in Fig. 1.

Figure 2 shows the regions favored at 90% and 99% C.L. in the triangle plots, for five representative values of m^2. The CHOOZ data, which exclude a large horizontal strip in the triangle, appear to be crucial in constraining three-flavor mixing. Pure $\nu_\mu \leftrightarrow \nu_e$ oscillations (right side of the triangles) are excluded by SK and CHOOZ independently. The center of the lower side, corresponding to pure $\nu_\mu \leftrightarrow \nu_\tau$ oscillations with maximal mixing, is allowed in each triangle both by SK and SK+CHOOZ data. However, deviations from maximal ($\nu_\mu \leftrightarrow \nu_\tau$) mixing, as well as subdominant mixing with ν_e, are also allowed to some extent by SK data, but strongly constrained by the inclusion of the CHOOZ data. Such deviations from maximal 2ν mixing are now more constrained than in previous analyses [6].

Figure 3 shows the present tighter constraints on the mass parameter m^2 for unconstrained three-flavor mixing, with and without CHOOZ constraints.

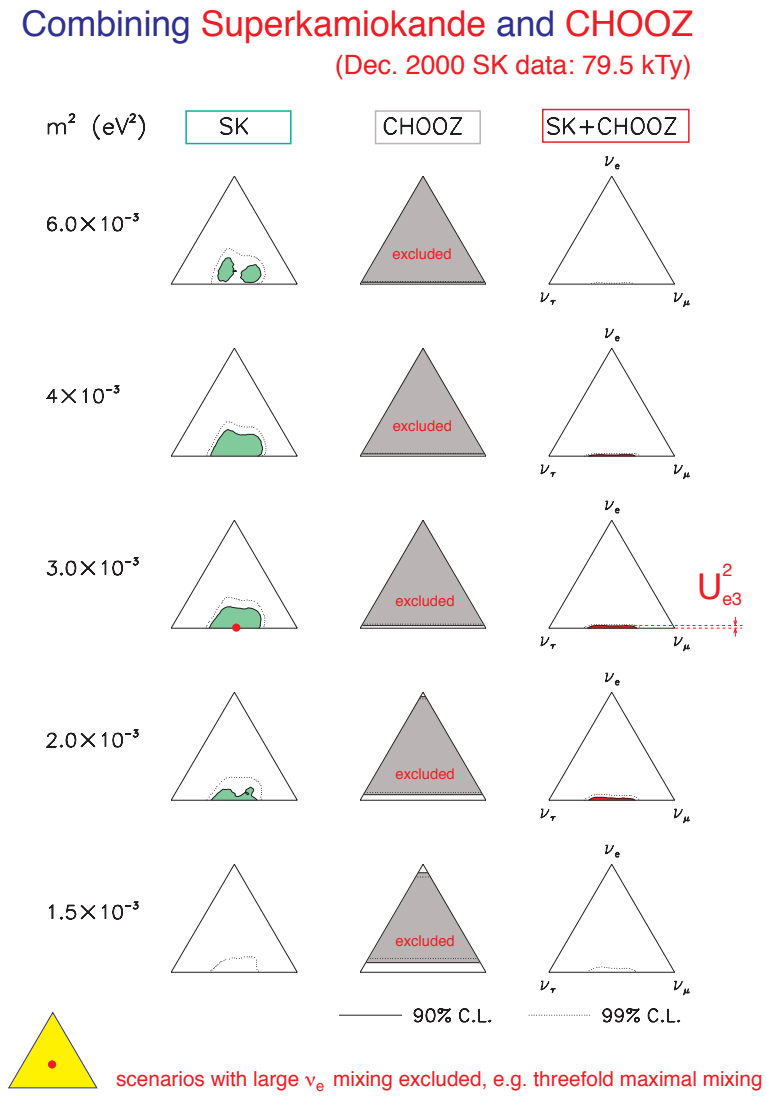

Figure 2: *Three-flavor analysis in the triangle plot, for five representative values of m^2. Left and middle column: separate analyses of Super-Kamiokande (79.5 kTy) and CHOOZ data, respectively. Right column: combined SK+CHOOZ allowed regions. The SK+CHOOZ solutions are very close to pure $\nu_\mu \leftrightarrow \nu_\tau$ oscillations, the allowed values of U^2_{e3} being very near to zero.*

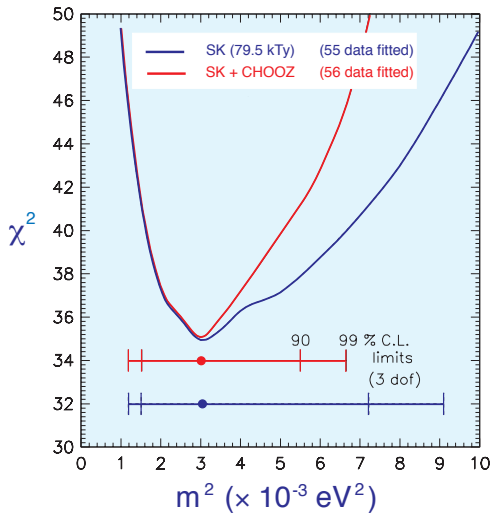

Figure 3: *90% and 99% C.L. bounds on the mass parameter m^2 for unconstrained 3ν mixing from SuperKamiokande atmospheric data, without and with CHOOZ data.*

The current best fit value is reached at $m^2 \sim 3.0 \times 10^{-3}$ eV^2, and is only slightly influenced by the inclusion of CHOOZ data. However, the upper bound on m^2 is significantly improved by including CHOOZ.

The impact of CHOOZ in constraining the mixing matrix element U_{e3}^2 is more clear in Fig. 4, where the 90% and 99% CL bounds on $U_{e3}^2 = \sin^2\phi$ are shown as a function of m^2, for unconstrained values of the angle ψ. It is seen that, when CHOOZ data are included, the element U_{e3}^2 cannot be larger than a few percent, the limits imposed by the SK data being considerably weaker ($\sin^2\phi < 0.4$).

Figure 5 shows the best-fit to the zenith distributions of SG and MG e, SG and MG μ, and UP (stopping and through-going) μ events, normalized to the no-oscillation rates in each bin. The best-fit cannot distinguish the effect coming from the inclusion of the CHOOZ constraint, since with or without the inclusion of the CHOOZ data the best fit is consistent with $U_{e3}^2 = \sin^2\phi = 0$.

In principle, a nonzero value of U_{e3}^2 at the best fit point is expected to induce to a slight excess in the MGe sample for $\cos\theta \to -1$. However, a significant reduction of the errors is needed to probe such possible distortions, which would be unmistakable signals of subdominant $\nu_\mu \to \nu_e$ oscillations.

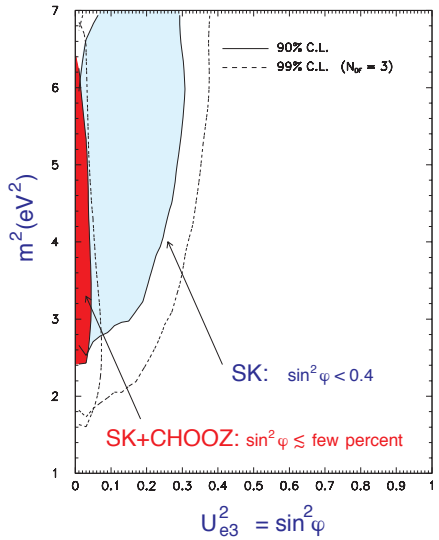

Figure 4: *Bounds on U^2_{e3} as a function of m^2 from SK data (79.5 kTy), with and without the finalized CHOOZ data.*

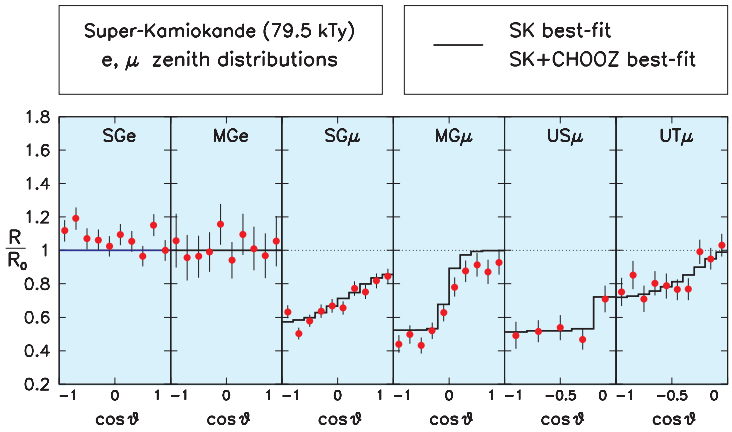

Figure 5: *SK zenith distributions of leptons at best fit. The best fit is consistent with $U^2_{e3} = \sin^2\phi = 0$, so we cannot appreciate the effect of including the CHOOZ constraint (the best fit with or without the CHOOZ data is the same).*

4 Solar neutrinos

The Sudbury Neutrino Observatory (SNO) experiment one year ago has presented the first measurements of the $\nu_e + d \to p + p + e^-$ reaction rate induced by ^{8}B solar neutrinos through charged currents (CC) [13]. The observed CC event rate, normalized to the latest standard solar model (SSM) prediction [22],

$$\mathrm{SNO/SSM} = 0.347 \pm 0.029 \ , \tag{13}$$

not only confirms the deficit of solar neutrino events previously observed by the chlorine [7], gallium [8, 9], and water-Cherenkov [11, 12] experiments, but provides [13] an evidence larger than 3σ for a $\nu_{\mu,\tau}$ contribution in the Super-Kamiokande (SK) measurement of the $\nu_x + e^- \to \nu_x + e^-$ reaction rate ($x = e, \mu, \tau$) in the equivalent energy range [12],

$$\mathrm{SK/SSM} = 0.459 \pm 0.017 \ . \tag{14}$$

The SK-SNO comparison can be made rigorously model-independent by making an appropriate choice for the SK energy threshold, as suggested in [23, 24] and discussed also in the SNO paper [13]. In this work we describe, following the path traced in [25], a three step approach to the SK-SNO comparison, where:

- First we present (Subsec. 1) an improved discussion of such model independent comparison, which, based on a detailed SNO detector specifications, confirms the $> 3\sigma$ evidence for a $\nu_{\mu,\tau}$ flavor component in the SK event sample;
- Then we assume (Subsec. 2) no oscillations into sterile neutrinos, and derive combined constraints on two free parameters: (i) the ratio f_B of the *true* ^{8}B ν flux from the Sun to the corresponding value predicted by the SSM, and (ii) the ν_e survival probability $\langle P_{ee} \rangle$ averaged over the SK-SNO response function. Such constraints confirm the SSM prediction for f_B, and strongly indicate an average ν_e flux suppression of about one third ($\langle P_{ee} \rangle \sim 1/3$).
- As next step (Subsec. 3), we assume the validity of the SSM, and perform an updated analysis of all the available solar neutrino data (including the

SNO event rate) in a 2ν active oscillation framework. Large mixing angle solutions are clearly preferred in the global fit, while the small-mixing one is not allowed at the 3σ level (99.73% C.L.) by the parameter estimation test.

4.1 First step: model independent approach, using the SK-SNO equivalence

An important characteristic of any solar neutrino experiment is the energy spectrum of parent neutrinos contributing to the collected event sample in the absence of oscillations—the so-called response function $\varrho(E_\nu)$ [26]. The response function basically folds the solar neutrino energy spectrum with the differential interaction cross section and with the detector threshold and energy resolution, and thus takes different forms for each experiment. However, it can be made equal in SK and SNO by an appropriate choice of the electron energy thresholds, as shown in [23, 24], on the basis of the *expected* SNO technical specifications.

By performing the comparison with the present SNO kinetic energy threshold ($T_e^{\rm SNO} \geq 6.75$ MeV) and energy resolution [13], we find the SK-SNO best agreement for a SK threshold $T_e^{\rm SK} \geq 8.6$ MeV [25] (instead of $T_e^{\rm SK} > 5$ MeV $- m_e$, for which the value in Eq. (14) is officially quoted [12]). Such "adjusted" threshold is in good agreement with the one estimated in the SNO paper, $T_e^{\rm SK} \geq 8.5$ MeV [13].

Figure 6 displays our calculations for the corresponding SK and SNO response functions to ^{8}B neutrinos, which appear to be in very good agreement with each other. Concerning the small shape difference in the first half of the response functions, we estimate [25] that the corresponding effect is, in the worst case, a factor of five smaller than the effect of the total SNO uncertainty in Eq. (13), so that we can safely take $\varrho_{\rm SK} = \varrho_{\rm SNO}$. With the adjustement of the SK threshold, the SK and SNO detectors are made equally sensitive to the incoming ^{8}B neutrinos. The possible small contribution of *hep* neutrinos (not shown in Fig. 6) does not spoil the SK-SNO equalization of response functions [24], as far as the *hep* flux is taken below the experimental upper limit provided by the latest SK spectral measurements [12].

Although there is no official number quoted yet by the SK collaboration for the SK/SSM value at $T_e^{\rm SK} \geq 8.6$ MeV, one can try to recover it from the published SK spectral data [12, 27]. We adopt the provisional SNO own

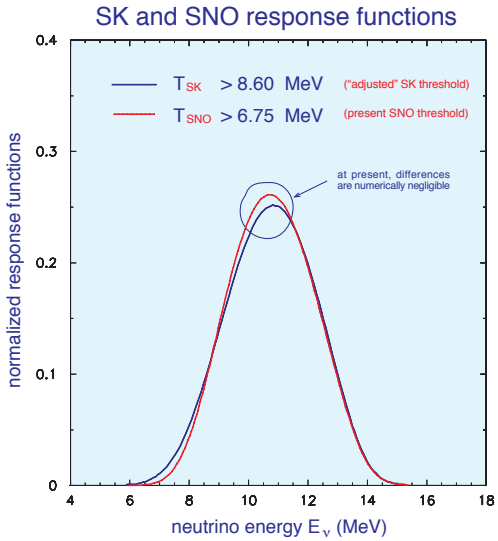

Figure 6: *Best-fit equalization of the SK and SNO response functions to* ^8B *neutrinos, as obtained by shifting the SK threshold to 8.6 MeV in electron kinetic energy.*

estimate [13], corresponding to take

$$\mathrm{SK/SSM} = 0.451 \pm 0.017 \ \ (T_e^{\mathrm{SK}} \geq 8.6 \ \mathrm{MeV}) \ , \tag{15}$$

which amounts to a small shift in the central value of the total SK rate. The attached SK error is assumed to be basically the same as in Eq. (14), since it should be dominated by systematic errors rather than by statistical uncertainties. Furthermore, the SK-SNO comparison is dominated by the (presently) larger SNO uncertainties, so that any (presumably small) official SK re-evaluation of the numbers in Eq. (15) is not expected to produce significant changes in the results discussed below.

For $\varrho_{\mathrm{SK}} = \varrho_{\mathrm{SNO}}$, the following relations hold *exactly* [23, 24]:

$$\mathrm{SNO/SSM} \ = \ f_B \langle P_{ee} \rangle \ , \tag{16}$$

$$\mathrm{SK/SSM} \ = \ f_B \langle P_{ee} \rangle + f_B \frac{\sigma_a}{\sigma_e} \langle P_{ea} \rangle \ , \tag{17}$$

where f_B is the ratio between the true (unknown) ^{8}B ν_e flux at the Sun and its SSM prediction [22], $\langle P_{ee} \rangle$ is the ν_e survival probability (energy-averaged over the common SK-SNO response function), $\langle P_{ea} \rangle$ is the averaged transition

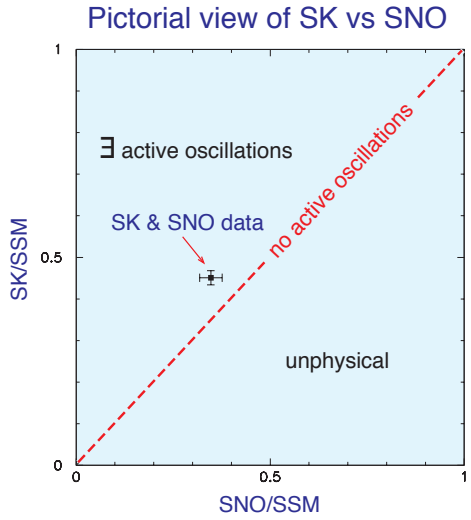

Figure 7: *Model-independent consequences of the SK and SNO results with equalized response functions: The data are well within the region where active neutrino transitions* $\nu_e \to \nu_{\mu,\tau}$ must *occur, and are* 3.1σ *distant from the diagonal line of "no active oscillations". This conclusion does not depend on either the standard solar model or the possible presence of additional transitions to sterile neutrinos. See the text for details.*

probability to active neutrinos ($\nu_a = \nu_{\mu,\tau}$), and σ_a/σ_e is the ratio of the (properly averaged [23, 24]) cross sections of ν_a and ν_e on electrons. We calculate $\sigma_a/\sigma_e = 0.152$ for $T_e^{\rm SK} \geq 8.6$ MeV. Notice that the above relations do not imply any assumption either on f_B, or on possible sterile neutrino oscillations, or on the functional form of $P_{ee}(E_\nu)$ or $P_{ea}(E_\nu)$, and thus they are *completely model-independent*.

From the above relations one can derive that SK/SSM $<$ SNO/SSM is always forbidden since it implies $\langle P_{ea} \rangle < 0$. Conversely, SK/SSM $>$ SNO/SSM is allowed only if $\langle P_{ea} \rangle > 0$. Figure 7 displays the above constraints at a glance. The SK+SNO experimental data are well within the region where there *must* be $\nu_e \to \nu_{\mu,\tau}$ transitions, independently of a possibly open [28] $\nu_e \to \nu_s$ channel. Only at more than 3σ (more precisely, at 3.1σ) the experimental data would hit the diagonal line which parametrizes the case of no $\nu_e \to \nu_{\mu,\tau}$ transitions

(corresponding to either no oscillations or pure $\nu_e \to \nu_s$ oscillations).

4.2 Second step: model independent approach excluding sterile neutrinos

The SNO results [13] and the model-independent analysis in the previous Section show that there is evidence for active neutrino transitions. Therefore, it is legitimate to explore the consequences of the *additional* hypothesis of *purely active* flavor transitions, corresponding to take $\langle P_{ea} \rangle = 1 - \langle P_{ee} \rangle$. In such a case, the SK-SNO relations in Eqs. (16) and (17) read

$$\text{SNO/SSM} = f_B \langle P_{ee} \rangle \,, \tag{18}$$

$$\text{SK/SSM} = f_B \langle P_{ee} \rangle + f_B \frac{\sigma_a}{\sigma_e} (1 - \langle P_{ee} \rangle) \,, \tag{19}$$

providing a system of two equations in the two unknowns f_B and $\langle P_{ee} \rangle$. By fitting the experimental values of SNO/SSM and SK/SSM given in Eqs (13) and (15), respectively, one can then determine the allowed ranges for f_B and $\langle P_{ee} \rangle$.

Figure 8 shows the contours of the allowed region in the ($\langle P_{ee} \rangle$, f_B) plane for $\chi^2 = \Delta\chi^2 = 1, 4$, and 9, whose *projections* onto the coordinate axes give the 1σ, 2σ, and 3σ separate ranges for f_B and $\langle P_{ee} \rangle$. The strong anticorrelation reflects the fact that a high ^{8}B flux can be partly compensated by a smaller survival probability, and viceversa. The projected 3σ range for f_B ($f_B = 1.03^{+0.50}_{-0.58}$) is in agreement with the SSM prediction (shown with its $\pm 1\sigma$ error band from [22], $f_B = 1^{+0.20}_{-0.16}$). On the other hand, the projected 3σ range for the average survival probability ($\langle P_{ee} \rangle = 0.34^{+0.61}_{-0.18}$), clashes with the standard electroweak model prediction of electron flavor conservation ($\langle P_{ee} \rangle = 1$) at more than 3σ. In the context of this figure, the standard model of the Sun appears clearly better satisfied than the standard model of electroweak interactions.

The results indicate that, in the case of generic active oscillations (i.e., no other assumption apart from $\langle P_{es} \rangle = 0$ in the range probed jointly by SK and SNO), the ν_e survival probability takes basically the lowest value allowed by pre-SNO experiments. It has been shown in [29] that the lowest values of $\langle P_{ee} \rangle$ (in the ^{8}B energy range) are typically reached within the so-called large mixing angle (LMA) solution to the solar neutrino problem, which may therefore be expected as favored. This will be confirmed by the analysis in the next section.

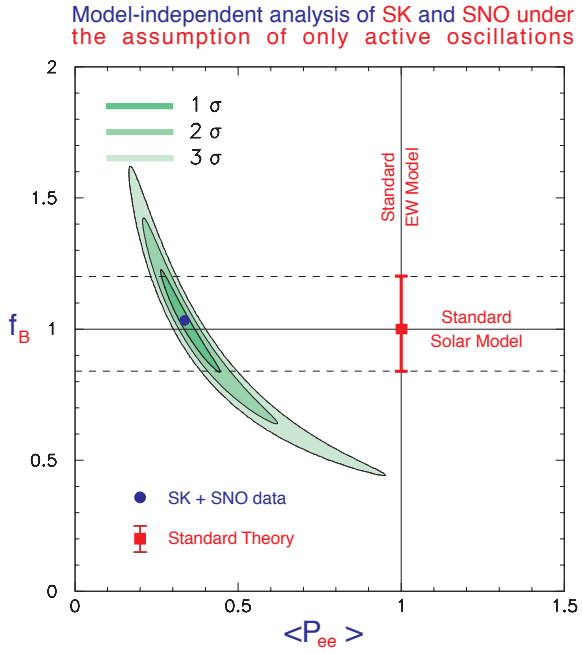

Figure 8: *Model-independent analysis of SK and SNO, assuming no oscillations into sterile states, in the plane charted by f_B (free factor multiplying the SSM ^8B neutrino flux) and $\langle P_{ee}\rangle$ (ν_e survival probability averaged over the SK-SNO response function). The contours of the allowed region (obtained for $\Delta\chi^2 =$ 1, 4, and 9) give, after projections onto the axes ($N_{\rm DF} = 1$), the separate 1σ, 2σ, and 3σ ranges for f_B and $\langle P_{ee}\rangle$. The f_B range is in good agreement with the SSM predictions (shown as a $\pm 1\sigma$ horizontal band), while the $\langle P_{ee}\rangle$ range is in $> 3\sigma$ disagreement with the standard electroweak model prediction of electron flavor conservation ($\langle P_{ee}\rangle = 1$).*

4.3 Third step: 2ν active oscillations assuming the SSM and including all the solar neutrino data

From the SNO results [13] and from the analysis in the previous Sections we have learned that: (i) There is evidence for active neutrino oscillations, and (ii) Assuming purely active ν oscillations, the SSM is confirmed and the ν_e survival probability should be $\sim 1/3$ in the SK-SNO energy range.

Let us now make two further assumptions about neutrino physics, namely,

that the ν fluxes from the Sun can be taken as predicted (with their uncertainties) by the SSM [22], and that active neutrino oscillations occur in an effective two-family framework. The latter hypothesis is totally correct if the mixing angle θ_{13} vanishes, and is accurate up to $O(\sin^2\theta_{13})$ corrections if $\theta_{13} > 0$. We have seen in the previous section that the joint analyses of SK atmospheric neutrino data [2] and of the CHOOZ reactor results [5] place stringent upper limits on θ_{13} [6, 30, 31]. Moreover, the CHOOZ data forbid large ν_e disappearance for neutrino square mass differences higher than $\sim 0.7 \times 10^{-3}$ eV^2, and thus they are also relevant to cut away the region of energy-averaged solar neutrino oscillations [31, 32, 33].

Therefore, we perform a 2ν analysis by adding the final CHOOZ spectral results [5] (14 bin, as discussed in [33]) to the usual solar neutrino data, and show then the results in the mass-mixing plane $(\delta m^2, \tan^2\omega)$, covering both octants in $\omega = \theta_{12}$ [34]. Since we are now assuming a specific functional form for $P_{ee}(E_\nu)$ (i.e., the one predicted by standard oscillation theory at any given mass-mixing point), the SK-SNO model-independent comparison becomes unimportant, and we can use the full SK rate given in Eq. (14) [12].

Concerning SNO, in this work we include the total CC rate [Eq. (13)] but not the published CC energy spectrum [13]. Notice that the present SNO spectrum information should be subdominant as compared to SK: actually, although one expects a SNO sensitivity to spectral deviations a factor of two larger than in SK [35], the current SNO spectral errors (both statistical and systematic) are more than a factor of two larger than in SK (and the published SNO event sample is an order of magnitude smaller than the SK one). Moreover, it is not easy to recover (from both the published SNO and SK data) the information needed to propagate *jointly*, on both the SK and SNO spectra. Therefore, we prefer to postpone the SNO spectrum analysis and its properly correlated combination with the SK spectrum to a future work. The total SNO CC rate is, however, already important by itself, and to appreciate its impact we show first the 2ν analysis *without* SNO for reference.

Figure 9 shows the results of the 2ν analysis using the three pre-SNO total solar neutrino rates (chlorine [7], combined gallium [8, 9], SK [12]) and the 14-bin CHOOZ data [5] (relevant to suppress the likelihood of the high-δm^2 region), as derived by drawing iso-$\Delta\chi^2$ contours (for $N_{\rm DF} = 2$) around the global χ^2 minimum. The fit in Fig. 9 favors the small-mixing angle (SMA)

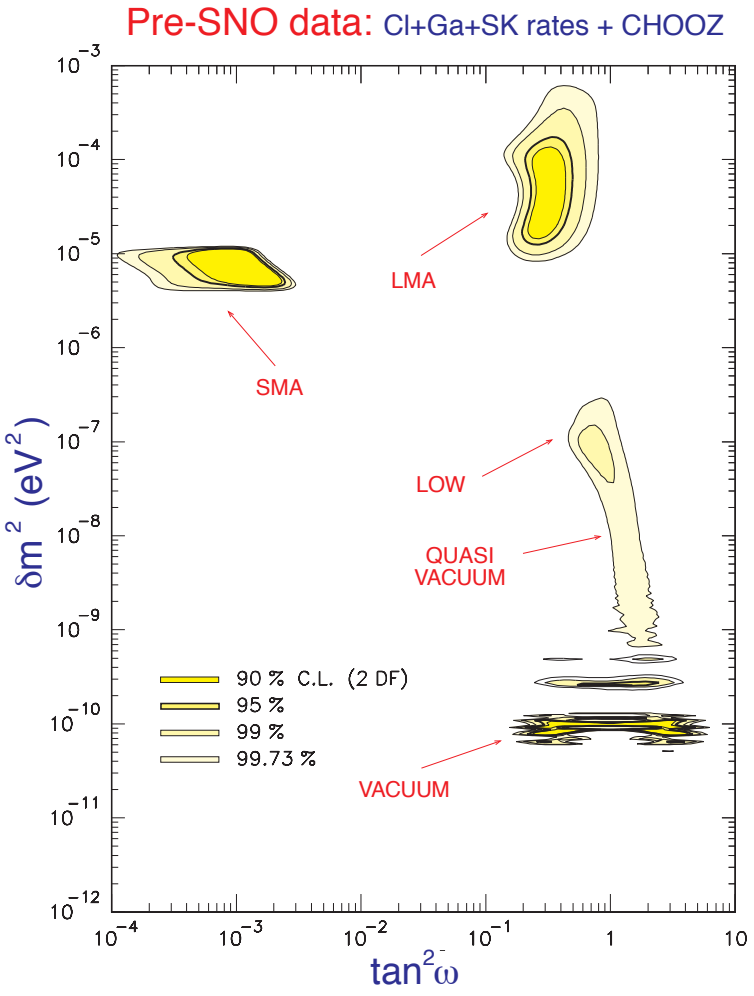

Figure 9: *Pre-SNO* 2ν *oscillation analysis of total neutrino event rates. CHOOZ data included. The regions shown in the figure are allowed at the 90, 95, 99, and 99.73% C.L. for the joint two-parameter estimation test, as obtained by drawing iso-*χ^2 *contours at* $\Delta\chi^2 = 4.61, 5.99, 9.21,$ *and 11.83 above the global minimum.*

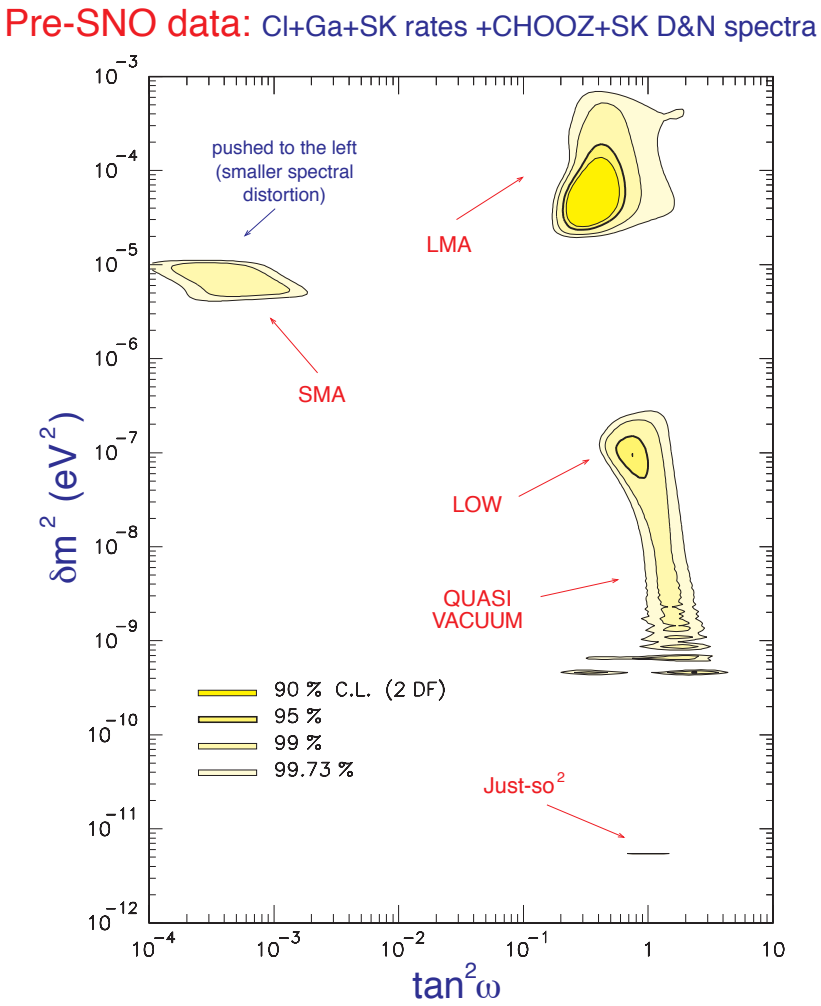

Figure 10: *Pre-SNO* 2ν *oscillation analysis of total neutrino event rates and of SK day-night energy spectra. CHOOZ data included.*

solution, as compared to the regions at $\tan^2\omega \sim O(1)$, usually referred to as large-mixing angle at high δm^2 (LMA) and at low δm^2 (LOW), extending down to the quasivacuum and vacuum oscillation (QVO and VO) regions.

Figure 10 shows the impact of the SK day-night spectral data [12] (19+19 bins minus one adjustable normalization factor), that cut away the vacuum solutions and also change the relative likelihood of the local SMA, LMA, and LOW best fits, favoring the LMA solution. Notice also that there is the trace of a small region allowed at 99.73% C.L. in the lowest δm^2 decade (the so-called Just-So^2 solution, see the first of Ref. [29] and references therein). Similar results have been largely discussed in the recent solar neutrino literature (see, e.g., [29, 12, 36, 37]), and we do not add further comments here.

Figure 11 is analogous to Fig. 9, but including the SNO CC rate [13]. The LMA (SMA) solution in Fig. 11 is enlarged (reduced) as compared to Fig. 9, due to the anticipated SNO preference for relatively small values of the ν_e average survival probability, which tend to favor the LMA case. The SMA solution tends to adapt itself to the low value of $\langle P_{ee}\rangle \sim 1/3$ by privileging its rightmost part (where the nonadiabatic ν_e suppression is stronger), and indeed the final compromise makes the SMA local fit comparable to the LMA one. However, in doing so, the SMA fit also privileges the part where spectral deviations are sizable, contrary to the SK day-night spectrum observations.

Indeed, the SMA solution disappears at $> 3\sigma$ when the SK day-night spectral data are included, as shown in Fig. 12 (analogous to Fig. 10, but including the SNO total CC rate). The "tension" between the total rate information (pushing the SMA to the right) and the SK spectrum (pushing the SMA to the left), which was already emerging from the latest SK data analysis [12], is now sufficiently strong to produce a significant decrease of the likelihood of the SMA solution. Since the SNO spectral data [13] (not included here) do not show any deviation from the standard shape within the (now large) errors, we may expect that the addition of such data in future analyses can only corroborate such trend.

The LMA solution appears clearly favored in the global fit, enhancing the hopes of interesting new physics at KamLand [38] and at future neutrino factories [39]. The LOW solution turns out to be slightly less favored then the LMA one, essentially because the gallium data prefer an increase of the ν_e survival probability at low energies, more easily provided in the LMA region

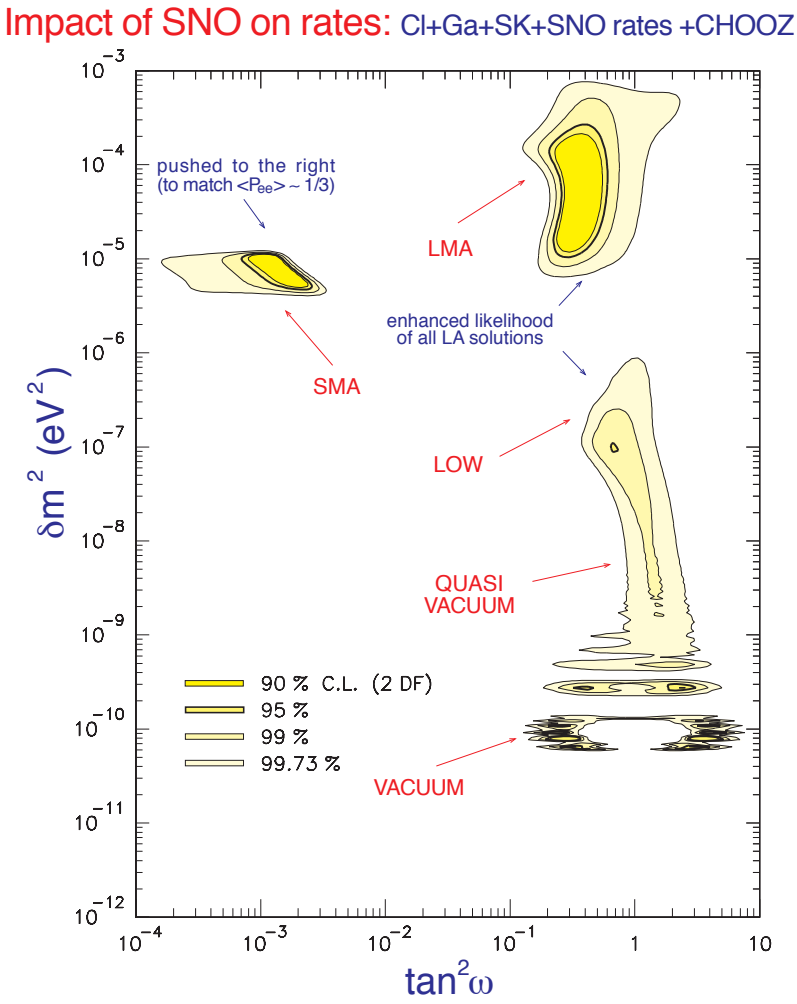

Figure 11: *Post-SNO 2ν oscillation analysis of total neutrino event rates. CHOOZ data included.*

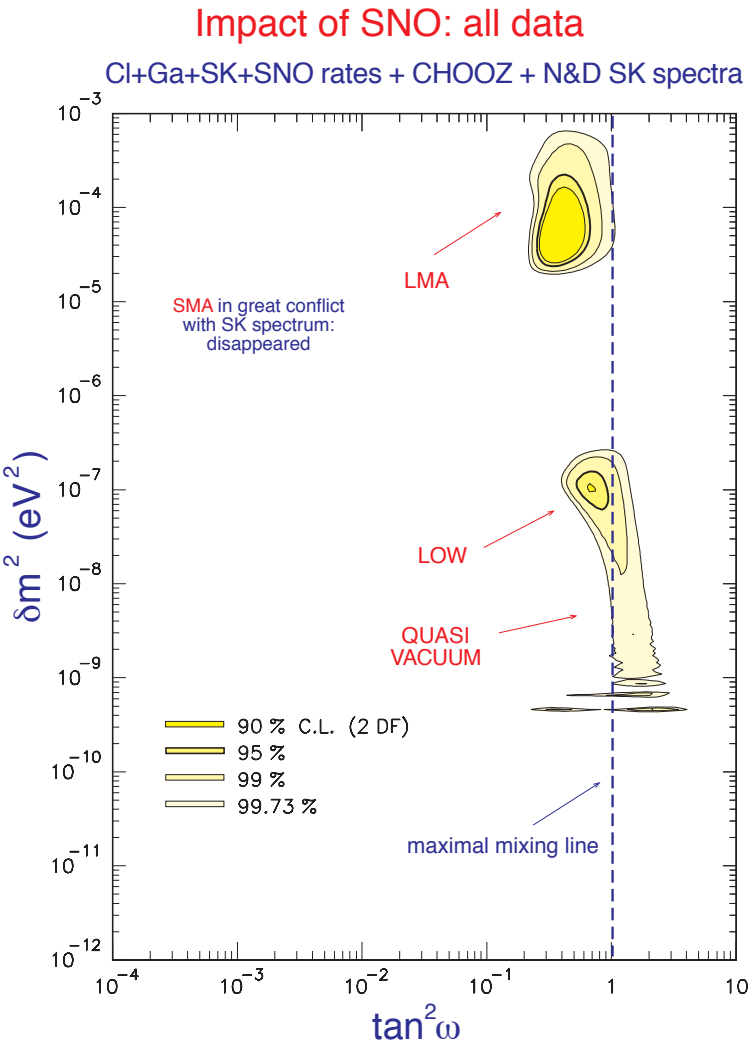

Figure 12: *Post-SNO* 2ν *oscillation analysis of total neutrino event rates and of SK day-night energy spectra. CHOOZ data included. Solutions at small mixing are highly disfavored. See the text for details.*

rather than in the LOW solution (see, e.g., [29]). However, the LOW solution is still in good shape, and should be tested through day-night earth matter effects in the BOREXINO experiment [40] or, with less sensitivity, through winter-summer matter effects after several years of data taking in the Gallium Neutrino Observatory (GNO) [41]. Notice that the LOW solution extends down to the quasivacuum oscillation [42] region, which might be probed in BOREXINO by pushing its time-variation sensitivity close to its upper limits [43].

5 Impact of the new solar neutrino data

Very recently the SNO eperiment has presented the first NC (and day-night) data [14, 15]. These data have enhanced the model-independent evidence for solar $\nu_e \to \nu_{\mu,\tau}$ transitions at $> 5\sigma$ [14], and have also strengthened the bounds on the oscillation parameters [15, 12, 46, 47].

In ref. [47] a thorough analysis of the current solar neutrino data is reported, in the context of two-flavor active neutrino oscillations. performing an accurate and exhaustive statistical treatment of both the input and the output information. Concerning the input, we analyze 81 observables, including the total event rate from the chlorine experiment, the total gallium event rate and its winter-summer difference, the 44 bins of the Super-Kamiokande (SK) energy-nadir electron spectrum, and the 34 day-night energy spectrum bins from the SNO experiment. At the same time, we carefully evaluate and propagate the effects of the 31 correlated systematic uncertainties.

Concerning the output information, we express the χ^2 analysis results in terms of "pulls," embedding the single contributions to the total χ^2 coming from both the observables and the systematics. The pull method, as compared to the (numerically equivalent) covariance matrix approach, is not only simpler and more advantageous, but also includes useful indications about the preferred variations of the neutrino fluxes with respect to their SSM predictions.

In the context of 2ν active oscillations, and with respect to the previous bounds in Fig. 12, it turns out that the latest data strongly favor the LMA solution, as shown in Fig. 13 (taken from [47]). However, it is not possible to rule out yet the LOW or QVO solutions at 3σ. The KamLAND experiment [38] will be decisive in this respect.

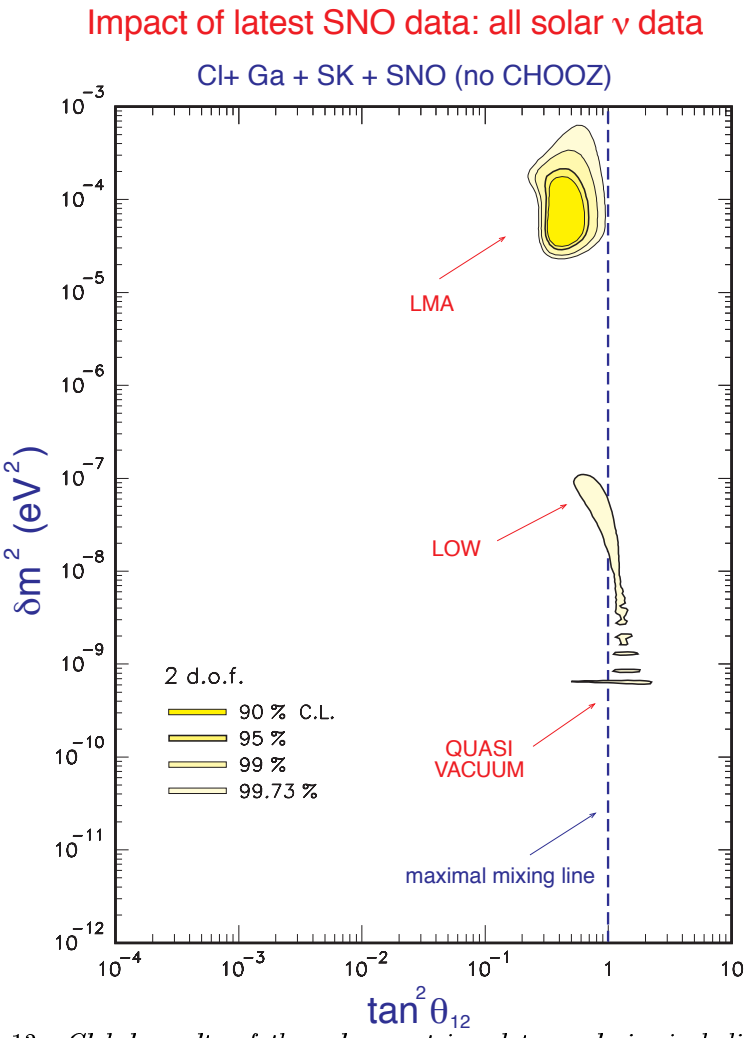

Figure 13: *Global results of the solar neutrino data analysis, including 81 observables and 31 sources of correlated systematics. The parameter space* $(\delta m^2, \tan^2\theta_{12})$ *refers to the scenario of* 2ν *oscillations among active states.*

Acknowledgments

We thank the organizers of the Heavy Quark & Leptons International Conference for kind hospitality. This work was supported in part by INFN and in part by the Italian *Ministero dell'Istruzione, Università e Ricerca* through the "Astroparticle Physics" research project.

References

1. C. McGrew, Superkamiokande Collaboration, Proceedings of the 9th International Workshop on Neutrino Telescopes, Venice, Italy, 2001 (U. of Padua press, Italy, 2001) Vol. I, p. 93.
2. SuperKamiokande Collaboration, S. Fukuda *et al.* Phys. Rev. Lett. **85**, 3999 (2000).
3. B.C. Barish for the Macro Collaboration in *Neutrino 2000*, Proceedings of the 19th Conference on Neutrino Physics and Astrophysics (Sudbury, Canada, 2000), Nucl. Phys. **B 91** (Proc. Suppl.) p. 141 (2001).
4. W.A. Mann for Soudan 2 Collaboration, in *Neutrino 2000* [3], p. 134.
5. CHOOZ Collaboration, M. Apollonio *et al.*, Phys. Lett. B **466**, 415 (1999).
6. G.L. Fogli, E. Lisi, A. Marrone, andG. Scioscia, Phys. Rev. D **59**, 033001 (1999).
7. K. Lande, P. Wildenhain, R. Corey, M. Foygel, and J. Distel, in *Neutrino 2000* [3] p. 50.
8. SAGE Collaboration, J. N. Abdurashitov *et al.*, astro-ph/0204245.
9. GALLEX Collaboration, W. Hampel *et al.*, Phys. Lett. B **447**, 127 (1999).
10. GNO Collaboration, T. Kirsten *et al.*, in *Neutrino 2002*, 20th International Conference on Neutrino Physics and Astrophysics (Munich, Germany, 2002), to appear in the Proceedings.
11. Kamiokande Collaboration, Y. Fukuda *et al.*, Phys. Rev. Lett. **77**, 168, 3 (1996).

12. Super-Kamiokande Collaboration, S. Fukuda *et al.*, hep-ex/0205075.

13. SNO Collaboration, Q. R. Ahmad *et al.*, Phys. Rev. Lett. **87**, 071301 (2001).

14. SNO Collaboration, Q. R. Ahmad *et al.*, nucl-ex/0204008.

15. SNO Collaboration, Q. R. Ahmad *et al.*, nucl-ex/0204009.

16. J. N. Bahcall, *Neutrino Astrophysics* (Cambridge University Press, Cambridge, 1989).

17. Z. Maki, M. Nakagawa, and S. Sakata, Prog. Theor. Phys. **28**, 870 (1962); B. Pontecorvo, Zh. Eksp. Teor. Fiz. **53**, 1717 (1968) [Sov. Phys. JETP **26**, 984 (1968)].

18. L. Wolfenstein, Phys. Rev. D **17**, 2369 (1978); S. P. Mikheev and A. Yu. Smirnov, Yad. Fiz. **42**, 1441 (1985) [Sov. J. Nucl. Phys. **42**, 913 (1985)]; V. D. Barger, K. Whisnant, S. Pakvasa, and R. J. Phillips, Phys. Rev. D **22**, 2718 (1980).

19. G.L. Fogli, E. Lisi, and D. Montanino, Phys. Rev. D **54**, 2048 (1996).

20. T.K. Kuo and J. Pantaleone, Rev. Mod. Phys. **61**, 937 (1989).

21. G.L. Fogli, E. Lisi, D. Montanino, and G. Scioscia, Phys. Rev. D **55**, 4385 (1997).

22. J.N. Bahcall, M.H. Pinsonneault and S. Basu, Astrophys. J. **555**, 990 (2001).

23. F.L. Villante, G. Fiorentini, and E. Lisi, Phys. Rev. D **59**, 013006 (1999).

24. G.L. Fogli, E. Lisi, A. Palazzo, and F.L. Villante, Phys. Rev. D **63**, 113016 (2001).

25. G.L. Fogli, E. Lisi, D. Montanino and A. Palazzo, Phys. Rev. D **64**, 093007 (2001).

26. B. Faïd, G.L. Fogli, E. Lisi, and D. Montanino, Phys. Rev. D **55**, 1353 (1997).

27. Super-Kamiokande Collaboration, S. Fukuda *et al.*, Phys. Rev. Lett. **86**, 5656 (2001).

28. V. Barger, D. Marfatia, and K. Whisnant, hep-ph/0106207.

29. J.N. Bahcall, P.I. Krastev, and A.Yu. Smirnov, J. of High Energy Phys. **5**, 15 (2001); Phys. Rev. D **63**, 053012 (2001); Phys. Rev. D **62**, 093004 (2000).

30. G.L. Fogli, E. Lisi, and A. Marrone, Phys. Rev. D **64**, 093005 (2001).

31. M.C. Gonzalez-Garcia, M. Maltoni, C. Peña-Garay, and J.W.F. Valle, Phys. Rev. D **63**, 033005 (2001).

32. G.L. Fogli, E. Lisi, A. Marrone, D. Montanino, and A. Palazzo, hep-ph/0104221.

33. G.L. Fogli, E. Lisi, and A. Palazzo, hep-ph/0105080.

34. G.L. Fogli, E. Lisi, and D. Montanino, Phys. Rev. D **54**, 2048 (1996).

35. G.L. Fogli, E. Lisi, and D. Montanino, Phys. Lett. B **425**, 341 (1998).

36. M.C. Gonzalez-Garcia, M. Maltoni, and C. Peña-Garay, Phys. Rev. D **64**, 093001 (2001).

37. D. Montanino, in *NOW 2000*, Proceedings of the 2nd Europhysics Neutrino Oscillation Workshop, (Conca Specchiulla, Italy, 2000), Nucl. Phys. B (Proc. Suppl.) **100**, p. 51 (2001).

38. A. Piepke for the Kamland Collaboration, in *Neutrino 2000* [3], p. 91.

39. E. Keil in *Neutrino 2000* [3], p. 239; H. Schellman, *ibidem*, p. 246; M.B. Gavela in *NOW 2000* [37], p. 175.

40. G. Ranucci for the BOREXINO Collaboration, in *Neutrino 2000* [3], p. 58.

41. G.L. Fogli, E. Lisi, D. Montanino, and A. Palazzo, Phys. Rev. D **61**, 073009 (2000).

42. A. Friedland, Phys. Rev. Lett. **85**, 936 (2000); G.L. Fogli, E. Lisi, D. Montanino, and A. Palazzo, Phys. Rev. D **62**, 113004 (2000); E. Lisi, A. Marrone, D. Montanino, A. Palazzo, and S.T. Petcov, Phys. Rev. D **63**, 093002 (2001).

43. A. De Gouvea, A. Friedland, and H. Murayama, Phys. Rev. D **60**, 093011 (1999).

44. J. Shirai [K2K Collaboration]: in *Neutrino 2002* [10].

45. M. Shiozawa [SK Collaboration]: in *Neutrino 2002* [10].

46. V. Barger, D. Marfatia, K. Whisnant, and B. P. Wood: hep-ph/0204253; P. Creminelli, G. Signorelli, and A. Strumia: JHEP **0105**, 052 (2001), hep-ph/0102234 v3; A. Bandyopadhyay, S. Choubey, S. Goswami, and D. P. Roy: hep-ph/0204286; J. N. Bahcall, M. C. Gonzalez-Garcia, and C. Pena-Garay: hep-ph/0204314; P. C. de Holanda and A. Y. Smirnov: hep-ph/0205241; A. Strumia, C. Cattadori, N. Ferrari, and F. Vissani, hep-ph/0205261

47. G. L. Fogli, E. Lisi, A. Marrone, D. Montanino and A. Palazzo: hep-ph/0206162

48. J. N. Bahcall, M. C. Gonzalez-Garcia and C. Pena-Garay: hep-ph/0204194

49. See also the first two refs. in [46]

50. See the "2+2 autopsy" in the second of Ref. [46]

51. J.W.F. Valle: in *Neutrino 2002* [10].

Frascati Physics Series Vol. XXVIII (2002), pp.397-411
HQ & L 2002 – Vietri s/m, May 27th - June 1st, 2002

REVIEW OF THE SOLAR NEUTRINOS PUZZLE

Aldo Ianni
INFN - Laboratori Nazionali del Gran Sasso,
S.S. 17bis km 18+910, I-67010 Assergi (AQ), Italy

ABSTRACT

Observation of solar neutrinos is offering a unique opportunity to go beyond the Standard Model of electroweak and strong interactions by studying the effect of matter upon neutrino propagation and non-standard neutrino properties. The longstanding solar neutrinos puzzle shows that neutrinos may undergo flavour transformations while travelling from the Sun to Earth and within the Earth, during the night hours, before being detected. In the paper solar neutrinos observations are reviewed. Implications of existing measurements are discussed.

1 Introduction

The Standard Model (SM) [1) 2)] of electroweak and strong interactions has successfully passed very precise tests at the 0.1% and 1% level. Nevertheless, the long-standing solar neutrinos puzzle is offering a unique opportunity to go beyond it as we show in this paper.

The Sun shines by transforming hydrogen into helium:

$$4H^+ + 2e^- \rightarrow^4 H^{++} + 2\nu_e + 26.73MeV. \quad (1)$$

According to the Standard Solar Model (SSM) [3] eq. 1 evolves through a number of nuclear reactions [4] and few of them produce a ν_e. The main source of solar neutrinos is: $p + p \rightarrow d + e^+ + \nu_e$. From this reaction, in particular, we learn that on average the ν_e carries an energy of about 0.2 MeV. So, taking into account that for about every 13 MeV the Sun produces a ν_e (see eq. 1), it is easy to show that solar neutrinos carry off about 1.5% of the total energy released per each cycle, i.e. every time hydrogen is converted into helium. Furthermore, the solar neutrinos flux on Earth can be estimated as $L/(13MeV) \approx 6.6 \cdot 10^{10}$ cm^{-2} s^{-1}, where $L = 8.6 \cdot 10^{11}$ MeV cm^{-2} s^{-1} is the solar luminosity at the current epoch. Other two importants reactions which produce neutrinos are: $^7Be + e^- \rightarrow^7 Li + \gamma + \nu_e$ with E_{ν_e}=0.86 MeV($\sim$90%) and E_{ν_e}=0.38 MeV($\sim$10%) together with $^8B \rightarrow^8 Be^* + e^- + \nu_e$ with $E_{\nu_e} \leq$ 15 MeV. In fig. 1 the solar neutrinos spectrum on Earth as predicted by the SSM is shown[1]. This figure shows, in particular, that solar neutrinos are mainly sub-MeV particles. The flux estimated above is enough to understand that detection of solar neutrinos on Earth is feasible with huge target mass detectors. As a matter of fact, the cross section for neutrino-electron elastic scattering, as an example, around 10 MeV is about 10^{-44} cm^2, so the expected rate for a kton target mass of H_2O is $N_t\phi\sigma \approx (3 \cdot 10^{32})(5 \cdot 10^5 \text{cm}^{-2}\text{s}^{-1})(10^{-44}\text{cm}^2) = 0.54\text{d}^{-1}$, where N_t is the number of target electrons, ϕ the neutrino flux (from fig. 1 around 10 MeV) and σ the cross section. Of course, in order to detect such a small signal, detectors must be located deep underground to reduce cosmic rays background.

Solar neutrinos have been detected since 1968 [5]. Their flux is measured to be smaller with respect to the SSM predictions. This deficit is known as the solar neutrinos puzzle. Over the past 34 years the solar neutrinos deficit has triggered the idea of neutrino flavour transformations in the leptons sector. This possibility, already confirmed at 5σ level, shows a physics beyond the SM. In the next future, solar neutrinos together with atmospheric neutrinos and neutrinos from accelerators will address a fundamental issue: determination of

[1] In fig. 1 are also reported neutrinos from the CNO chain. This chain in the Sun plays only a minor role

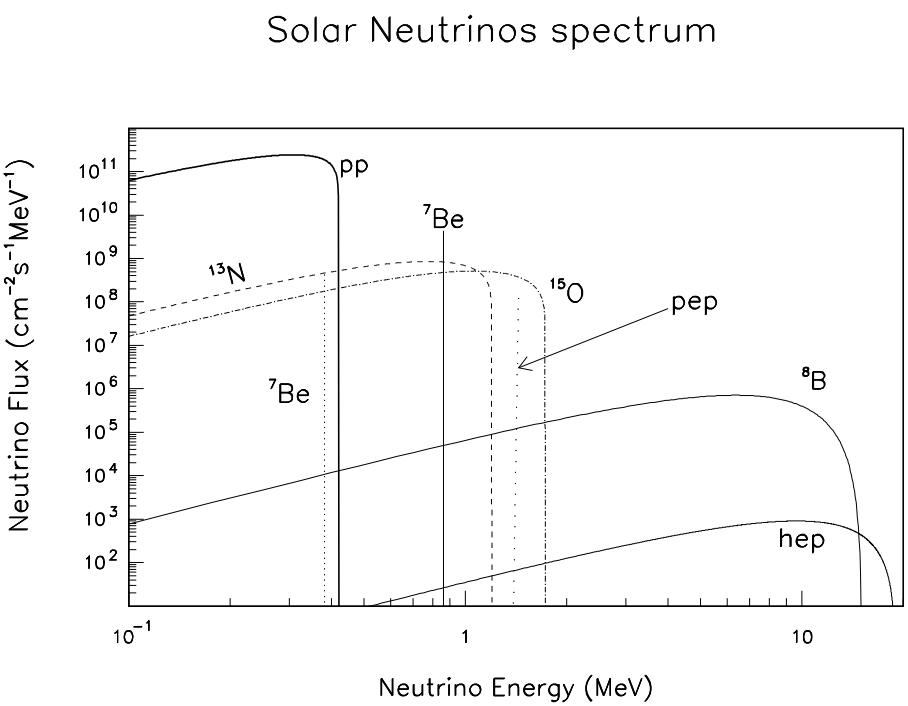

Figure 1: *Solar neutrinos spectrum on Earth.*

the neutrinos mixing matrix.

In this paper we are going to review and comment the solar neutrinos puzzle from the results of existing experiments. The plan of the paper is as follows. In Sec. 2 solar neutrinos observations are reviewed. In Sec. 3 implications of measurements are discussed. In Sec. 3 we draw our conclusions.

2 Solar neutrinos experiments

As of today 7 experiments have been able to measure solar neutrinos. Tab.1 shows the main features of the experiments[2]. Solar neutrinos detectors can be

[2]The Super-Kamiokande experiment has been stopped because of an accident which have destroyed about 60% of some 11,200 photomultipliers (PMTs). Data taking will be recovered by the end of 2002 with 47% of the PMTs.

Table 1: *Solar neutrinos experiments: summary of the main features.*

Experim.	Type	Fiducial mass (tons)	Threshold (MeV)	Start	Status
Cl-Ar	radioch.	135(^{35}Cl)	0.814	1968	stopped
Kamiokande	cherenkov	680(H_2O)	7.0	1985	stopped
SAGE	radioch.	23(^{71}Ga)	0.233	1990	running
Gallex	radioch.	12(^{71}Ga)	0.233	1991	upgraded into GNO
Super-Kamiokande (SK)	cherenkov	22,500(H_2O)	5.0	1998	stopped
GNO	radioch.	12(^{71}Ga)	0.233	1991	running
SNO	cherenkov	1000(D_2O)	5.0	1999	running

distinguished into two types: radiochemical experiments and real-time experiments.

In the radiochemical experiments one makes use of the inverse beta-decay reaction through $A^Z(\nu_e, e^-)A^{Z+1}$, where A^{Z+1} decays with half-life of the order of 10 days-1 month[3]. In the detector fiducial mass one accumulates the product nuclei. After the exposure these latter are removed by radiochemical separation and counted in a gas-filled proportional counter.

In tab. 1 the main parameters of the radiochemical experiments are reported. In the following we give a brief description of the experiments and refer the reader to dedicated papers [6) 7) 8) 9) 10) 11) 12)]. The Cl-Ar experiment has been the first to observe solar neutrinos. The detector is located in the Homestake gold mine in South-Dakota at a depth of 4,200 m.w.e. In the detector neutrinos interact with ^{37}Cl atoms via ^{37}Cl(ν_e, e^-)^{37}Ar. ^{37}Ar is radioactive and decays with a half-life of 35 days. Before starting a new run, a small amount (0.1-0.3 cm^3) of stable ^{36}Ar atoms are introduced in the C_2Cl_4. At the end of the exposure (35-50 days), Ar is extracted by flushing He for 20 hr. Since Ar is a noble gas, it is neither chemically nor physically attached to the Cl solution and can be easily removed. The Ar and He are separated by flushing the gas into a charcoal trap kept at the liquid nitrogen temperature. The Ar sample, within the charcoal, is later removed and counted. The number of ^{36}Ar atoms

[3]The threshold energy for radiochemical experiments is defined by the Q-value of the inverse beta-decay reaction.

measures the extraction efficiency. Background Ar atoms could be produced in the detector after spallation by ^{37}Cl(p, n)^{37}Ar, or by fast neutrons from rock walls or from (α, n) reactions. During each run the extraction efficiency of Ar atoms and the counting efficiency of the gas detector are measured and used to fit selected events by a maximum likelihood function which depends upon the activity of extracted ^{37}Ar atoms and the counter-sample background.

Gallex and SAGE make use of a ^{71}Ga target. The detection reaction is: ^{71}Ga(ν_e, e^-)^{71}Ge. ^{71}Ge atoms are radioactive with a half-life of 11 days. Gallex is located at the Gran Sasso underground Laboratory some 1,400 m below the Gran Sasso mount, while SAGE is located in the Baksan Underground Laboratory. Gallium experiments exploit a technique similar to the one used by the Cl-Ar detector for selecting and counting events but, of course, the extraction methods are different. The outstanding achievement of such experiments can be understood considering the fact that the extraction technique allow to measure few atoms against some 10^{30} target ones. Experimental procedures in Gallex and SAGE have been tested by a high intensity neutrino source (^{51}Cr). In particular, the Gallex one had a very high intensity at the level of 1.69 MCi. Source experiments showed an efficiency of the order of 90% for both Gallex and SAGE.

Real-time experiments aim to detect Cherenkov light in H_2O or D_2O. These experiments can measure in real time the energy (from the charge collected by each photomultiplier), the position and direction of the incoming neutrinos for the selected events (from the timing distribution of the hit photomultipliers and the Cherenkov cone). SK is located in the Kamioka mine 1,000 m below ground, while SNO in a nickel mine in Ontario at a depth of 2,000 m (6010 m.w.e.). In SK neutrinos are measured using the neutrino-electron elastic scattering interaction. In SNO neutrinos are detected by three processes: charge-current (CC) channel, $\nu_e + d \rightarrow p + e^- + p$ ($E_{thresh.}$=1.44 MeV), neutral-current (NC) channel, $\nu_e + d \rightarrow p + n + \nu_x$ ($E_{thresh.}$=2.22 MeV) and elastic-scattering. We notice that SNO offers a unique possibility to measure the total solar neutrinos flux in presence of flavour transformations through the NC channel, for the NC reaction is sensitive in the same way to all the active flavours. This is not possible in SK because the elastic-scattering is mainly sensitive to ν_e. In SK and SNO the main sources of background are ^{222}Rn in water, γ-rays from radioactivity, spallation products and induced radioac-

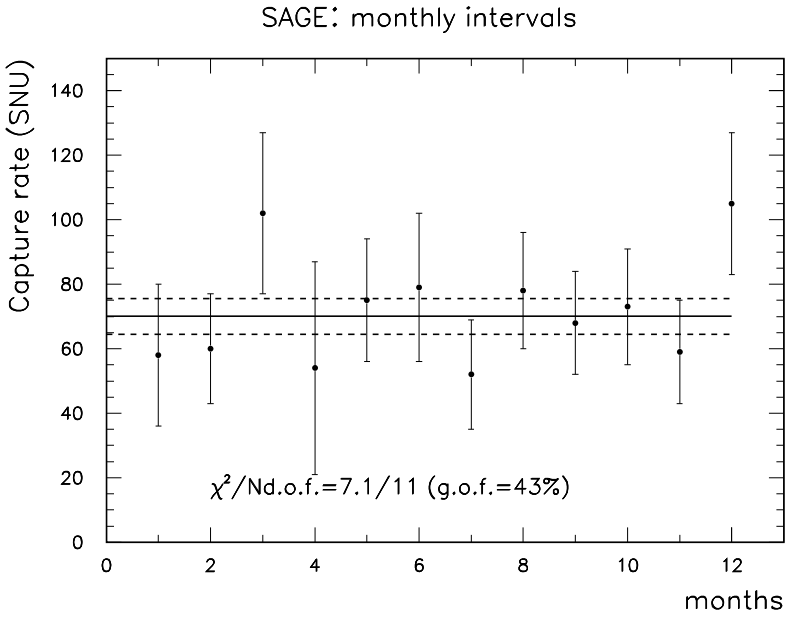

Figure 2: *SAGE data from 1990 to 2001 in monthly intervals. See text for details.*

tivity such as ^{16}O$(n,\ p)^{16}$N, where ^{16}N decays beta with Q_β=10.4 MeV and E_γ=6.1 MeV. Detectors simulation's reliability are tested by using artificial radioactive sources [12) 13)]. After data reduction signals are extracted exploiting a maximum likelihood fit. Background is separated by using few information such as the probability distributions against the angle between the direction of the incoming neutrino and that of the recoil electron[4], the event energy and reconstructed position within the detector. NC events in SNO are selected by measuring γ's after neutron capture on deuterium (E_γ=6.25 MeV) or by capture on ^{35}Cl, adding salt to the heavy water (E_γ=8.6 MeV). At the moment only results without salt are available. From tab. 1 it can be seen that existing experiments cover the most of the spectrum shown in fig. 1. Gallex/GNO and

[4]Both the elastic-scattering and CC channel have a directional sensitivity which allow to distinguish neutrinos interactions over background events.

Table 2: *Solar neutrinos experiments: summary of main results in terms of rates and fluxes. For radiochemical experiments rates are given in units of SNU (1 SNU = 10^{-36} captures/target atoms/sec.), for real time experiments, fluxes are given in units of 10^6 cm^{-2} s^{-1}. R is the measured value to the predicted one ratio. We also report the statistical significance of the solar neutrinos deficit in terms of number of σ's.*

Experim.	SSM	Measured	R	num. of σ's
Cl-Ar	$7.6^{+1.3}_{-1.1}$	2.56±0.23	0.34±0.06	3.7
Kamiokande	$5.05^{+1.01}_{-0.81}$	2.80±0.39	0.55±0.13	2.1
SK	$5.05^{+1.01}_{-0.81}$	2.40±0.10	0.48±0.09	2.5
Gallex+GNO	128^{+9}_{-6}	71±6	0.55±0.06	5
SAGE	128^{+9}_{-6}	71±6	0.55±0.06	5
SNO	$5.05^{+1.01}_{-0.81}$	CC:1.76±0.11	CC:0.35±0.07	CC:3.8
		NC:5.09±0.63	NC:1.01±0.23	NC:0.02

SAGE are sensitive to all solar neutrinos sources, while Cherenkov detectors to ^{8}B neutrinos. The Cl-Ar experiments was sensitive to ^{7}Be and ^{8}B neutrinos.

3 Implications of solar neutrinos measurements

Results of observations are summarized in tab. 2 in terms of rates and fluxes measurements. In the same table we also report SSM predictions [3] and the significance of the deficit per each experiment. A more precise evaluation of the solar neutrinos deficit significance is presented in [14]. In this paper a simultaneous fit of all the event rates results with arbitrary amplitudes for neutrinos fluxes, but undistorted spectra, gives a $\chi^2 \geq \chi^2_{min}$ probability for a non-neutrino oscillations scenario at the level of 10^{-5}. So, the possibility of solving the solar neutrinos deficit with a new solar physics seems poor. For this reason existing and future experiments are planning to study model independent measurements such as the charge current versus neutral current ratio, spectral distortion and regeneration of ν_e's within the Earth (an MSW effect [4]), seasonal variations due to the Earth's eccentricity, ϵ, and long term variations (correlation with the solar cycle). Existing experiments are already offering model independent information. The Gallex/GNO has measured a winter-summer asymmetry equal to -10.9±9.2 [15]. Using SAGE data [8], as an example, it is possible to study yearly and long term variations. In fig. 2

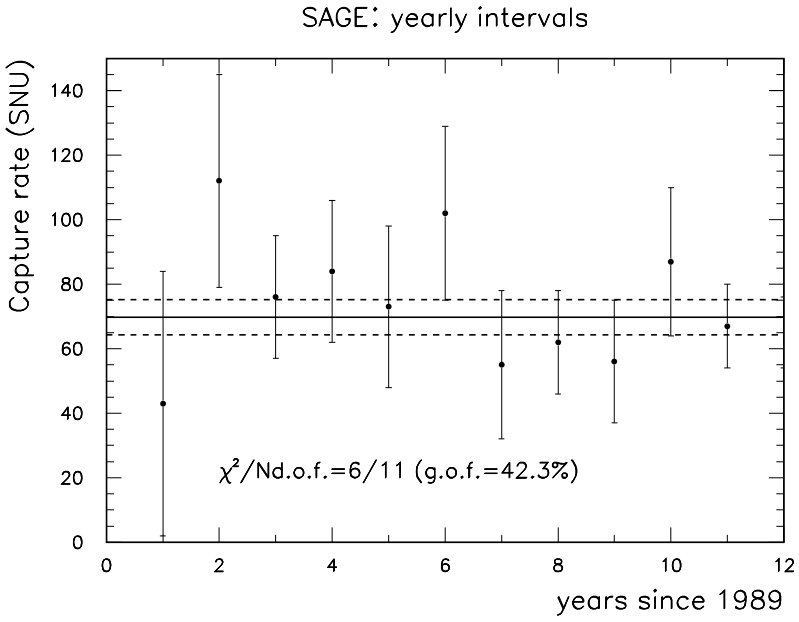

Figure 3: *SAGE data from 1990 to 2001 in yearly intervals. See text for details.*

and fig. 3 SAGE data are shown in monthly and yearly intervals, respectively. Fig. 2 and fig. 3 show that there is no evidence neither of seasonal nor long term variations from the SAGE data. Fits shown in these figures are the result of a χ^2 minimization with a constant suppression factor. Errors bands corresponde to 1σ. In SK data [9] it is also possible to look for day-night variations. If MSW transformations work for solar neutrinos then it is possible that a fraction of non-electron neutrinos are transformed back into electrons type while travelling within the Earth. So, an enhancement of the ν_e's signal is expected during the night hours. As a matter of fact SK measures such an effect but with a small statistical significance. The day-night asymmetry is defined as $A_{DN} = 2(\phi_N - \phi_D)/(\phi_N + \phi_D)$. SK measures $A_{DN} = 0.033 \pm 0.030$ which is only about 1σ away from zero. As far as seasonal variations in SK are concerned, in fig. 4 the 1258-days data set is combined in 8 bins during one year. Fig. 4 shows a χ^2 fit of the data set which takes into account the effect

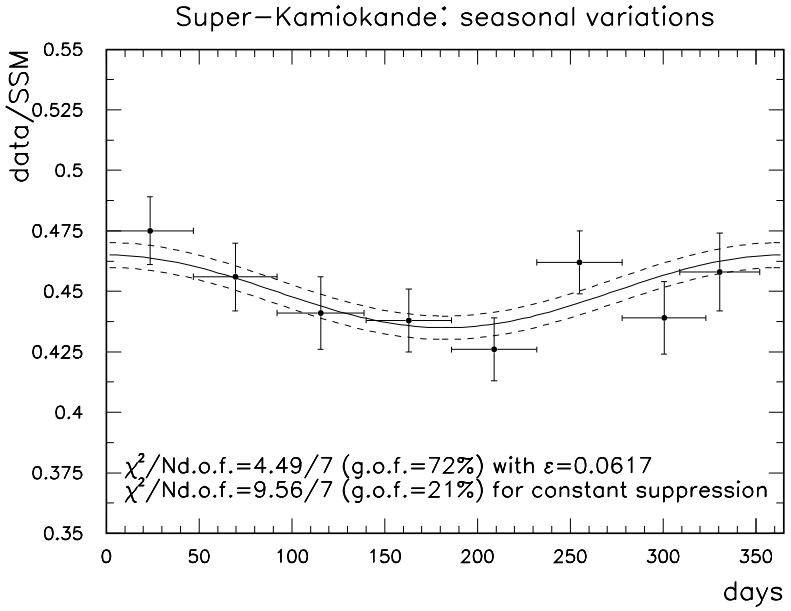

Figure 4: *Super-Kamiokande data combined to study seasonal variations. See text for details.*

of the Earth's eccentricity[5]. The agreement as shown is good. However, a fit with a flat distribution gives also a good result. So, we can conclude that SK data do not show any evidence of seasonal variations. This is also true for long term effects as reported in [9].

SNO data since one year has boosted the interpretation of the solar neutrinos deficit. Comparison of CC and elastic-scattering (ES) rates already shows that neutrinos are transforming into active flavours [11]. As a matter of fact the disagreement between CC and ES rates tells that oscillations to sterile neutrinos are strongly disfavoured [11]. Moreover, a comparison of the NC measured rate [12] and SSM prediction shows that the non-oscillations scenario is disfavoured at 5.5σ. In fig. 5 we report the flux of non-electron active neutrinos

[5]At first order in the eccentricity, ϵ, the Sun-Earth distance changes as $L(t) = L(1 - \epsilon \cos\alpha(t))$, where L=1 AU, α is the orbital phase and $0 \leq t \leq 2\pi$.

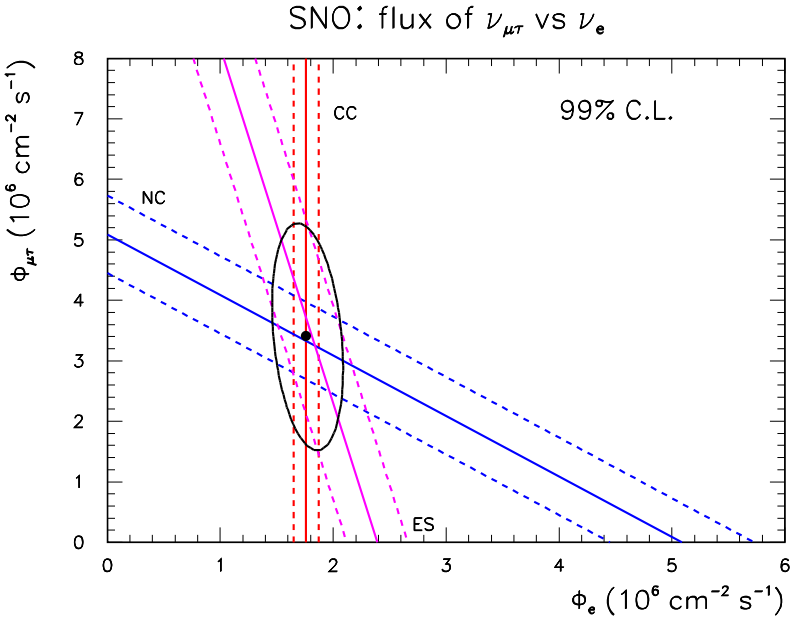

Figure 5: *SNO: measured flux for non-electron active neutrinos against measured electron neutrinos flux . See text for details.*

against the flux of electron neutrinos using only data from SNO. The flavour transformations to active neutrinos is evident. SNO has also measured a day-night asymmetry which is consistent with the SK result [16]. In particular, it is found $A_{DN}^{CC}(\%) = 14 \pm 6.3^{+1.5}_{-1.4}$ and $A_{DN}^{NC}(\%) = -20.4 \pm 16.9^{+2.4}_{-2.5}$, where as usual the first error is statistical and the second systematic. From these numbers it turns out that $A_{DN}^{\nu_e} = 7.0\% \pm 4.9\%(stat.)^{+1.3}_{-1.2}\%(sys.)$ for active-only models [16].

All observations reported above show that: solar neutrinos transform into active flavours while travelling from the Sun to Earth, that the transition probability is energy dependent since different regions of the spectrum in fig. 1 have different suppression factors (see tab. 2), that at energies greater than 5 MeV there are no seasonal variations and that there is a day-night asymmetry at the level of 7%. These experimental results find a good interpretation in the

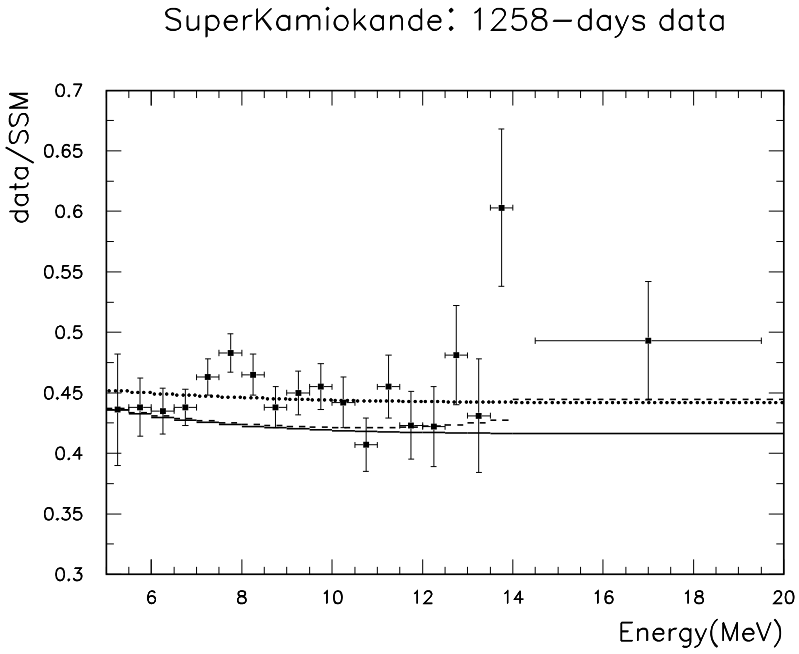

Figure 6: *Super-Kamiokande data against different scenarios. Solid line: LMA best-fit according to* [17] *with* f_B*=1.07. Dahsed line: LMA best-fit with* f_B*=1.07 and* f_{hep}*=12. Dotted line:* $\mu_\nu = 5 \cdot 10^{-12}\,\mu_B$ *with a constant suppression factor of 0.35 due to oscillations. See text for details.*

framework of neutrino oscillations. A so called global analysis of the solar neutrinos deficit in terms of neutrino oscillations [17] shows that observations can be explained by different sets of oscillations parameters, namely the large mixing angle (LMA), the low (LOW) and the vacuum (VAC) solution. In [17] it is shown that the yearly-average survival probability in the LMA solution (the most favoured [17]) has a small day-night effect and a suppression factor almost energy independent above 5 MeV. This behavour fits very well with what observed by SK and SNO. However, the LOW solution also predicts the same effects. Therefore, in order to distinguish between the two solution it will be necessary to measure sub-MeV neutrinos for at these energies the day-night for the LOW solution is much different than that for the LMA, as an example. This will be done in the next future by the Borexino experiment [18]

at the Gran Sasso Laboratory. Borexino is a real-time detector designed to study ^7Be neutrinos from the Sun. In Borexino a fiducial mass of 100 tons of organic scintillator (pseudocumene) will be used to search for solar neutrinos via neutrino-electron elastic scattering. The main innovation brought by Borexino has been the possibility to measure [19] very low level of ^{238}U and ^{232}Th contaminations in a 4-ton test detector. This small contamination (at the level of $\sim 10^{-16}$ g/g) allows to distinguish solar neutrinos over background on the basis of an off-line analysis and statistical subtractions. Moreover, the monoenergetic ^7Be neutrinos will give the experiment a strong potentiality to study seasonal variations and day-night effects (in the LOW solution scenario a day-night effect at the level of $23^{+10}_{-13}\%$ is predicted [17]).

4 Conclusions

In the previous section we have seen that, although we have evidence of neutrino oscillations, a solution to the solar neutrinos puzzle has still to come. We have also learnt from SNO that solar neutrinos are not missing. They have been transformed by a process we have to understand better. At the moment a running experiment, KamLand [20], has the potentiality to study neutrino oscillations in the range of the LMA solution. KamLand is a Borexino-like detector which observes $\bar{\nu}_e$'s LMA parameters, this might still leave room for some unpredicted sub-dominant effect in the solar neutrinos anomaly. The reason being the possibility of neutrino electromagnetic interactions within the Sun. As a matter of fact a non-zero mass for neutrinos could imply a non-zero magnetic moment [21], μ_ν. This kind of interaction has been taken into account to fit solar neutrinos data [22] using μ_ν at the level of 10^{-12} μ_B, which is consistent with astrophysical bounds [23]. In fig. 6, as an example, we show the SK data against different solutions. The solid line corresponds to a best fit using the LMA parameters from [17] [6] with f_B=1.07[7]. The dashed line corresponds to

[6] LMA best-fit parameters are: $\tan^2\theta = 0.42$ and $\delta m^2 = 5 \cdot 10^{-5}$ eV^2. Here θ is the mixing angle between the eigenstates which are manily involved in the oscillations, $\delta m^2 = m_2^2 - m_1^2$, where m_1 and m_2 are the neutrinos masses for the eigenstates m_1 and m_2, respectively.

[7] f_B is the best-fit value for the ^{8}B flux normalized to the SSM prediction

the same LMA parameters but with f_B=1.07 and f_{hep}=12[8]. The dotted line is for $\mu_\nu = 5 \cdot 10^{-12}\,\mu_B$ and a constant suppression factor due to oscillations equal to 0.35. The same data could be fitted using a flat distribution: suppression factor=0.45, $\chi^2/Ndof = 20.3/18$ (g.o.f.=32%). These results show that still a wide range of possibilites as sub-dominant effects could be possible in the solar neutrinos sector beyond the LMA solution. As stated above sub-MeV solar neutrinos experiment have a strong potentiality to search for such effects in the next years.

In this paper we have shown how strong is the opportunity to search for new physics with solar neutrinos. We have also shown that already a lot of information have been collected over the last 34 years by 7 experiments. A fundamental astrophysical parameter, the pp flux, can be already extrapolated from existing data [8)] and from SNO results it is possible to claim that neutrinos undergo flavour transformations. Therefore, the solar neutrinos anomaly already has brought us beyond the SM. However, we need new data, in particular, in the sub-MeV region to figure out how the mentioned transformation is happening and find out if any new non-standard neutrino property could be identified.

5 Acknowledgements

This work has been supported by INFN-LNGS. The author thanks the organizing committee for the pleasant atmosphere in the beautiful settings of Vietri sul mare.

References

1. S.L. Glashow, Nucl. Phys. **22**, 579 (1961). S. Weinberg, Phys. Rev. Lett. **19**, 1264 (1967). A. Salam, in *Elementary Particle Theory*, ed. by N. Svartholm 1969.

2. H. Fritzsch *et al*, Phys. Lett. B **47**, 365 (1973).

3. J.N. Bahcall *et al*, Astrophys. J. **555**, 990 (2001).

[8]Here f_{hep} has the same meaning of f_B but for hep neutrinos: $^3He + p \rightarrow ^4 He + e^+ + \nu_e$.

4. J.N. Bahcall in *Neutrino Astrophysics*, ed. by Cambridge University Press, Cambridge, 1989.

5. R. Davis *et al*, Phys. Rev. Lett. **20**, 1205 (1968).

6. B.T. Cleveland *et al*, Astrophys. J. **496** 505 (1998).

7. The Gallex collaboration, Phys. Lett. B **285**, 376 (1991). The Gallex collaboration, Phys. Lett. B **342**, 440 (1995). The Gallex collaboration, Phys. Lett. B **447**, 127 (1999).

8. The SAGE collaboration, astro-ph/0204245, submitted to Zh. Eksp. Teor. Fiz. (JETP).

9. The Super-Kamiokande collaboration, Phys. Rev. Lett. **86**, 5651 (2001).

10. M. Altman *et al*, Phys. Lett. B **447**, 127 (1999). C. Cattadori for the GNO collaboration in: Proc. TAUP 2001, LNGS sept. 2001, to be published in Nucl. Phys. B.

11. The SNO collaboration, Phys. Rev. Lett. **87**, 071301 (2001).

12. The SNO collaboration, nucl-ex/0204008.

13. The Super-Kamiokande collaboration, Nucl. Instrum. Methods Phys. Res. Sect. A **421**, 113 (1999).

14. J.N. Bahcall, Phys. Rev. C **65**, 025801 (2002).

15. T. Kirsten for the GNO collaboration in: Proc. Neutrino 2002, Munchen may 2002 to be published in Nucl. Phys. B.

16. The SNO collaboration, nucl-ex/0204009.

17. J.N. Bahcall *et al*, hep-ph/0204314.

18. The Borexino collaboration, Astrop. Phys. **16**, 205 (2002).

19. The Borexino collaboration, Astrop. Phys. **8**, 141 (1998).

20. A. Pieke, KamLand: a reactor neutrino experiment testing the solar neutrino anomaly, in: Proc. of the XIXth International Conference on Neutrino Physics and Astrophysics, 16-21 June 2000, Nucl. Phys. B **91** 105 (2001).

21. M.B. Voloshin *et al*, Sov. Phys. JETP **64**, 446 (1986).

22. J. Pulido, hep-ph/0112104.

23. G.G. Raffelt, Phys. Rev. Lett. **64**, 2856 (1990). V. Castellani and S. Degl'Innocenti, Astrophys. J. **402**, 574 (1993).

Frascati Physics Series Vol. XXVIII (2002), pp.413-426
HQ & L 2002 – Vietri s/m, May 27th - June 1st, 2002

ATMOSPHERIC NEUTRINOS IN 2002

Edward T. Kearns
Physics Department, Boston University, Boston, MA 02215, U.S.A.

ABSTRACT

In this talk, I will present a snapshot of key results regarding atmospheric neutrinos, as of the summer of 2002. I will review the evidence for neutrino oscillation, dominated by the large sample from Super-Kamiokande, but supported by confirmation from MACRO and Soudan 2. I will then review some of the more detailed inquiries made using Super-Kamiokande data such as alternative scenarios, three-flavor oscillation, and tau neutrino appearance.

1 Introduction

Atmospheric neutrinos are produced by the decay of pions, kaons, and muons in cosmic ray showers. They have provided a fortuitous laboratory for neutrino oscillations, where the oscillation probability:

$$P(\nu_a \rightarrow \nu_b) = sin^2 2\theta sin^2 \frac{1.27\Delta m^2 L}{E} \quad (1)$$

is probed over a wide range of L (10-10000 km) and E (0.5-100 GeV).

Two normalizing principles are used to understand the data. First, cosmic ray showers consist mostly of pions, which decay to $\mu + \nu_\mu$, and the μ decays to $e + \nu_\mu + \nu_e$, resulting in a flux ratio $(\nu_\mu/\nu_e) \sim 2$. This ratio grows to larger values at high energy, as the time-dilated muon may strike the ground before decaying (removing ν_e from the beam), but at all relevant energies the ratio is predicted to about 5% accuracy. The second principle is that at equal zenith and nadir angles the flux of high energy neutrinos must be nearly identical. Again, this is predicted with an accuracy of a few percent.

Before I review the experimental data, I should mention some developments in the neutrino flux calculation [1)], which is a key input to more detailed understanding of the data. First, there is new data providing clarity regarding the flux of primary cosmic rays, which is the starting point for these calculations. The BESS and AMS spectrometers have made new precision measurements [2), 3)] in the important range of 5-100 GeV/nucleon, with data in good agreement with each other whereas older measurements had fairly sizeable disagreements.

Second, increased computational power and the large Super-K data sample have motivated the transition from 1-dimensional calculations [4)], where the p_t of the daughter particles is neglected and every neutrino is assumed to follow the trajectory of the primary proton, to 3-dimensional calculations [5)]. In 3-dimensions, one should account for p_t as well as bending in the geomagnetic field. The first 3-D calculations showed a relatively surprising effect that turns out to play little if any role in oscillation studies. The effect is an enhanced neutrino flux at the horizon. Indeed, below $\sim$ 1 GeV, there is fairly sharp peaking as a function of zenith angle, as shown in Fig. 1. The central dip in the 1-D curve is caused by geomagnetic cutoff; the central enhancement in the 3-D curves overwhelms the cutoff. These effects are stronger with decreasing neutrino energy, but the lower the energy of the neutrino, the poorer is the correlation between the neutrino direction and that of the outgoing lepton. The net result is that the any structure at the horizon is washed out of the angular distributions of the lepton, as also shown in Fig. 1. The predicted shapes are nearly the same for each calculation. There are some differences in the overall normalization between the models, but in neutrino oscillation studies, the flux normalization is usually allowed to float as a free parameter.

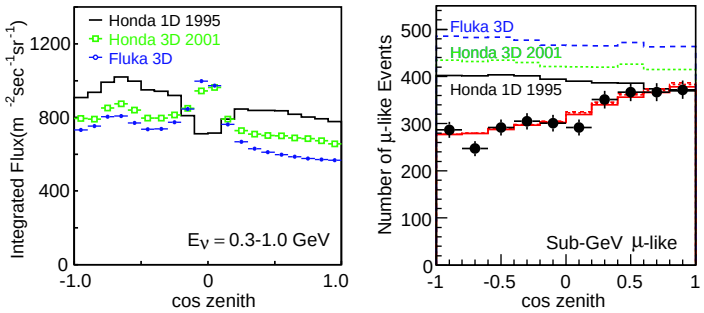

Figure 1: This figure compares 1-dimensional and 3-dimensional flux calculations for the Super-Kamiokande site. The left panel compares the integrated ν flux from 0.3 to 1 GeV as a function of zenith angle. The right panel shows the zenith distribution of μ-like data and Monte Carlo events in the Super-K analysis. The lower curves include ν-oscillation.

2 Evidence for Neutrino Oscillations

The evidence for neutrino oscillations [6] hinges on the two aforementioned normalizations of the atmospheric neutrino flux: that it should be composed of a well-predicted ratio of ν_μ to ν_e, and that it should be up-down symmetric at all zenith angles. To further cancel experimental systematic uncertainties, the flux ratio of ν_μ to ν_e is compared to a detailed Monte Carlo simulation by forming a double-ratio, R. For the sub-GeV sample of events ($E_\nu \lesssim 1.5$ GeV), the Super-Kamiokande analysis of 1489 days of data [7] shows:

$$R = \frac{(N_\mu/N_e)_{data}}{(N_\mu/N_e)_{m.c.}} = 0.688 \pm 0.016 \pm 0.050. \qquad (2)$$

The up-down asymmetry is expected to be zero for the multi-GeV muon sample ($E_\nu >\sim 1.5$ GeV), but is measured to be:

$$A = \frac{N_{up} - N_{down}}{N_{up} + N_{down}} = -0.303 \pm 0.030 \pm 0.004, \qquad (3)$$

whereas the asymmetry is consistent with zero for the multi-GeV electron sample and the multi-GeV muon Monte Carlo. The up-down asymmetry deviates from expectation by more than 10σ, essentially independent of any Monte Carlo input.

To estimate the parameters of neutrino oscillation, Super-K bins the single-ring ν_e and ν_μ events in energy and zenith angle (effectively path-length L). Additional ν_μ bins are also used: partially contained events where the muon exits the detector, multiple-ring events where the brightest ring is μ-like, or upward-going muons where the muon enters the detector from a neutrino interaction in the surrounding rock. Another category of multiple-ring events are selected where the brightest ring is e-like; these have an enhanced fraction of neutral current ($\simeq 35\%$). These bins play a negligible role in the $\nu_\mu \leftrightarrow \nu_\tau$ fits but are valuable in restricting alternative models involving sterile neutrinos or neutrino decay. In total, 155 bins are formed, too many to easily display. Figure 2 shows 95 bins in 10 zenith angle distributions, where some of the 155 bins have been combined. The data fits the prediction beautifully if a two-flavor $\nu_\mu - \nu_\tau$ oscillation is applied to the neutrino flux with $\sin^2 2\theta = 1$ and $\Delta m^2 = 3 \times 10^{-3}$ eV^2. The contours for this best fit are shown later, in Fig. 5.

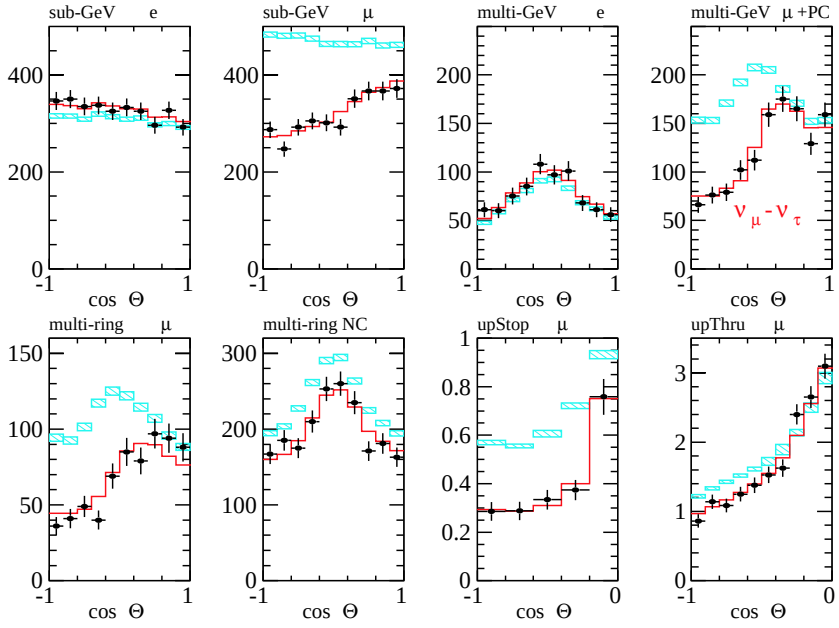

Figure 2: The zenith angle distribution for the atmospheric neutrinos used in the Super-Kamiokande oscillation analysis.

In the past, the value of R measured by iron calorimeters such as NUSEX [8] and Frejus [9] seemed to show little evidence for neutrino oscillations, compared to the contemporaneous water Cherenkov detectors Kamiokande and IMB. Currently, the Soudan 2 fine-grained iron tracking calorimeter in Minnesota, U.S.A., has recorded the largest data set [10] of contained atmospheric neutrino vertices using iron. They confirm the picture of atmospheric neutrino oscillation, with some quite different systematics such as geomagnetic location, target nucleus, and reconstruction technique. For their analysis of 5.9 kt·yrs of data, using a minimum momentum of 300 MeV/c, Soudan 2 reports $R = 0.71 \pm .09$, in agreement with the results from water Cherenkov experiments.

In addition, the Soudan 2 group exploits the good charged particle recognition of the detector to define a high resolution sample. The sample includes high energy quasi-elastics (single tracks), low energy quasi-elastics where the recoil proton from $\nu + n \rightarrow l + p$ is identified, and high energy multi-prong events. In each case, the neutrino direction is well determined, with approximately 25° angular resolution (for ν_μ) and resolution in $\log(L/E)$ of ~ 0.5. The data is binned by L/E and compared to Monte Carlo expectation for different oscillation parameters. Figure 3 shows the best agreement, found at $1 \times 10^{-2}\text{eV}^2$ and $\sin^2 2\theta = 0.97$. The apparent suppression of downward-going ν_μ ($\log(L/E) < 2.5$) explains the high value of Δm^2 compared to the Super-K best fit value. When uncertainties are incorporated, the 90% confidence interval for this fit does allow Δm^2 down to a few times 10^{-3}eV^2.

The MACRO detector is too coarsely grained and lightweight (4.7 kt) to effectively study contained interactions. However, it has a solid angle acceptance that rivals that of Super-Kamiokande, and is ideally suited to identify neutrino induced upward-going muons using time-of-flight. MACRO consists of a lower section filled with crushed rock absorber and an upper section that is hollow; both sections are instrumented with planes of streamer tube tracking. Fast timing is measured by tanks of liquid scintillator that surround the detector, and the plane between upper and lower sections is also a timing plane of liquid scintillator. The simplest analysis [11] is to measure the distortion in zenith angle flux for upward muons that pass completely through the detector; this is shown in the left panel of Fig. 4. These data demonstrate a best-fit to neutrino oscillation of $2.5 \times 10^{-3}\text{eV}^2$ and $\sin^2 2\theta = 1$, in perfect agreement with

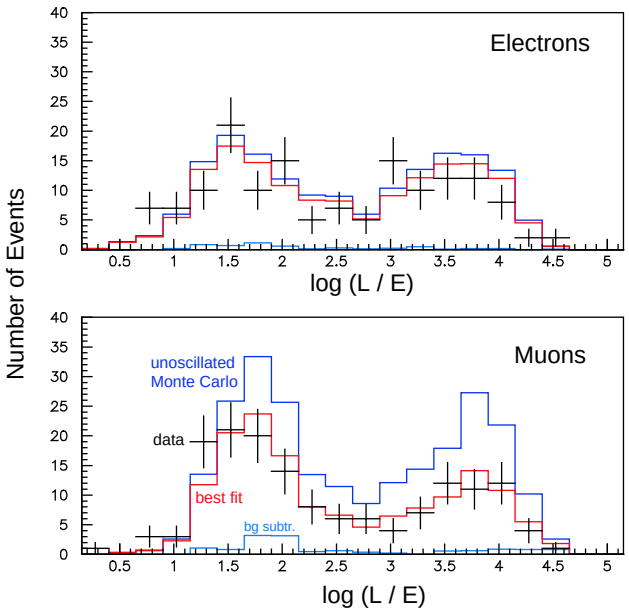

Figure 3: The L/E distribution for high resolution atmospheric neutrinos in the Soudan 2 analysis.

the Super-K result. MACRO has also studied the approximate energy distribution of these events (in four bins of 14, 35, 90, and 150 GeV) by considering the amount of multiple scattering [12]. This analysis shows consistency with neutrino oscillations, with the greatest ν_μ disappearance in the lowest energy bins.

MACRO also measures the rate of lower energy (~ 4 GeV) neutrino events that do not pass all of the way through the detector [13]. Internal upgoing events originate in the lower absorber but can be distinguished from downward stopping muons if they pass through two upper timing planes. In addition, there is a sample of internal downgoing events that start in the absorber and exit through the bottom. These have an indistinguishable topology from neutrino induced upward stopping muons. Fortunately, both of these topologies are neutrino induced, with similar parent energy distributions. The results for these samples are shown in the right panels of Fig. 4. These data also favor neutrino mixing in the range of 10^{-3} to 10^{-2}eV^2.

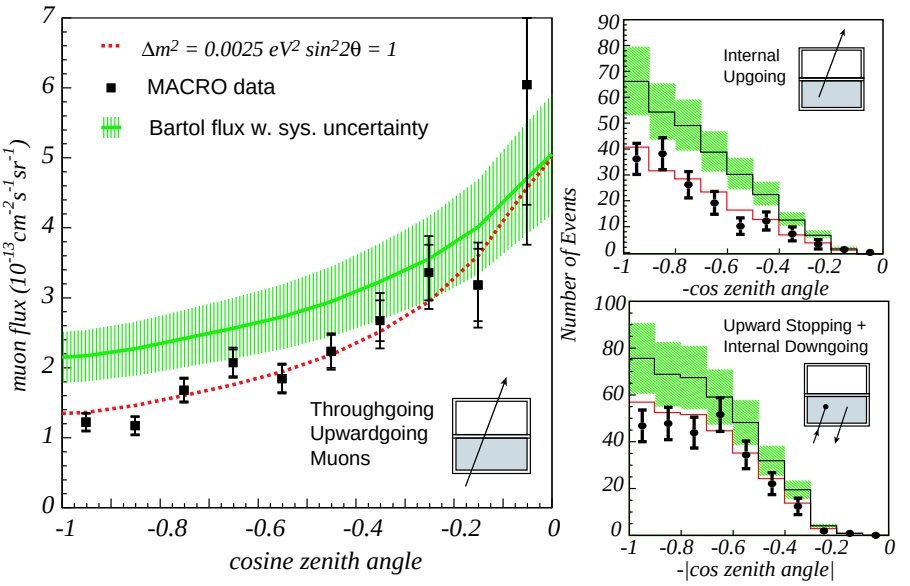

Figure 4: The zenith angle distribution for atmospheric neutrinos of various categories in the MACRO oscillation analysis.

Figure 5 shows the confidence intervals for the atmospheric neutrino analyses just described. The Super-Kamiokande, Soudan 2, and MACRO results are consistent with each other, with the Super-K result yielding the most significant and precise estimation of mass splitting and mixing angle. Despite the varied techniques of these three experiments, they do all rely upon atmospheric neutrinos, hence a further confirmation using a completely different neutrino source is desirable. The K2K experiment is the first long baseline experiment to probe neutrino oscillations with energy and flight distance comparable to atmospheric neutrinos. K2K uses a 98% pure ν_μ beam with mean energy 1.3 GeV that travels 250 km from KEK to the Super-K detector. The preliminary results from about one half of the planned running have recently been made public [14], and the contour from K2K is also overlayed in Fig. 5; the deepest minimum coincides exactly with the Super-Kamiokande best fit region.

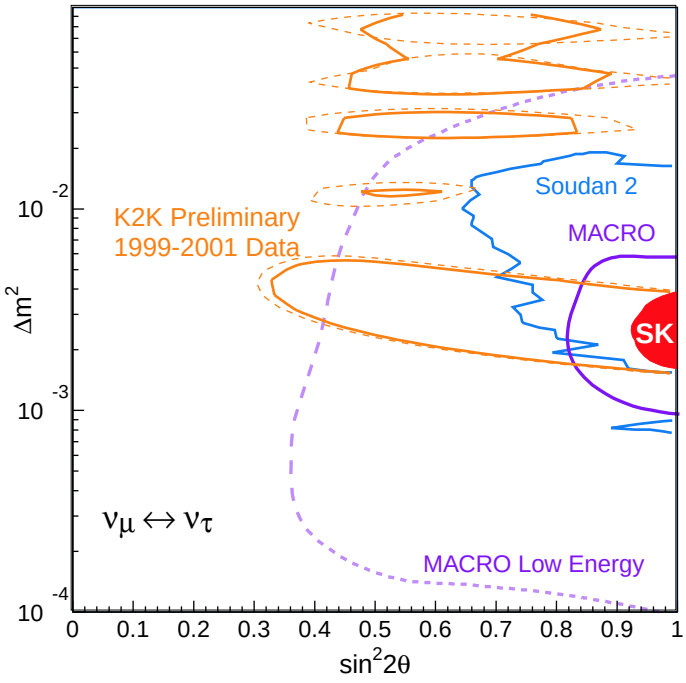

Figure 5: Confidence intervals for the parameters of atmospheric neutrino oscillation, as determined by several different experiments. The two similar contours for K2K reflect different treatment of systematic errors in the analysis.

3 Unlikely Alternatives

An important question is whether the Super-K atmospheric neutrino observations are only consistent with ν-oscillation or could alternatively be explained by neutrino decay [15], or other exotic ideas [16] such as violations of Lorentz invariance, flavor changing neutral currents etc. Table 1 summarizes the results of a fit to the Super-K data, again binned in by energy and zenith angle for fully- and partially-contained events, upward going muons, and multi-ring events. The multi-ring events are subdivided into charged current ν_μ and neutral current enhanced samples. The Monte Carlo sample used for $\nu_\mu \leftrightarrow \nu_\tau$ includes tau lepton appearance.

In Table 1 both the absolute χ^2 and the differences in χ^2 compared to the best fit of $\nu_\mu \leftrightarrow \nu_\tau$ oscillation are reported. In some cases, the functional form

Table 1: *Alternative fits to Super-Kamiokande atmospheric neutrino data.*

Mode	Functional Form	χ^2	$\Delta\chi^2$	σ
$\nu_\mu \leftrightarrow \nu_\tau$	$\sin^2 2\theta sin^2(1.27\Delta m^2 L/E)$	173.8	0.0	0.0
$\nu_\mu \leftrightarrow \nu_e$	$\sin^2 2\theta sin^2(1.27\Delta m^2 L/E)$	284.3	110.5	10.5σ
$\nu_\mu \leftrightarrow \nu_{sterile}$	$\sin^2 2\theta sin^2(1.27\Delta m^2 L/E)$	222.7	48.9	7.0σ
$L \times E$	$\sin^2 2\theta sin^2(\alpha LE)$	281.6	107.8	10.4σ
ν_μ decay	$\sin^4\theta + \cos^4\theta e^{-\alpha L/E}$	279.4	105.6	10.3σ
ν_μ decay	$\sin^2\theta + \cos^2\theta e^{-\alpha L/2E}$	194.0	20.2	4.5σ
ν_μ decoherence	$\frac{1}{2}\sin^2 2\theta(1 - e^{-\gamma L/E^2})$	184.3	10.5	3.2σ
No oscillation	-	427.4	252.4	15.9σ

of the transformation probability approaches that of the accepted hypothesis of pure $\nu_\mu \leftrightarrow \nu_\tau$. But in each case, there are typically several bins that constrain the alternative hypothesis. For example, matter effects suppress the oscillation probability for high energy μ-like bins (> 5 GeV $\times[\Delta m^2$ in units of $10^{-3}\text{eV}^2]$). For another example, neutral current events should disappear with sterile neutrinos or neutrino decay. By observing the differences in χ^2, one effectively ignores whichever bins are not sensitive to the differences in model. None of these pure alternatives fit the data very well; the decoherence model [17] is the most difficult to reject. Observation of an oscillatory minimum that is not washed out by L/E resolution would greatly assist in discrimination.

Clearly, one can generally include any exotic alternative as an admixture with "standard" neutrino oscillations. In fact, one is forced to consider both in the decay scenarios, where the neutrinos are required to have mass. For the important case of an admixture of sterile neutrino oscillation, Super-K has quoted limits on the allowable fraction of sterile neutrinos in a 4-neutrino scheme [18]. The $\nu_{sterile}$ mixture is found to be less than 20% (at 90% CL), with best fit to the Super-K data is at pure $\nu_\mu \leftrightarrow \nu_\tau$ mixing. Figure 6 shows the allowed region a function of the admixture fraction.

4 Three Flavor Oscillations

Having established nearly maximal $\nu_\mu \leftrightarrow \nu_\tau$ mixing as the explanation for the disappearance of atmospheric neutrinos, it is logical to search for a smaller component of mixing with ν_e. This is properly done in a 3-neutrino framework,

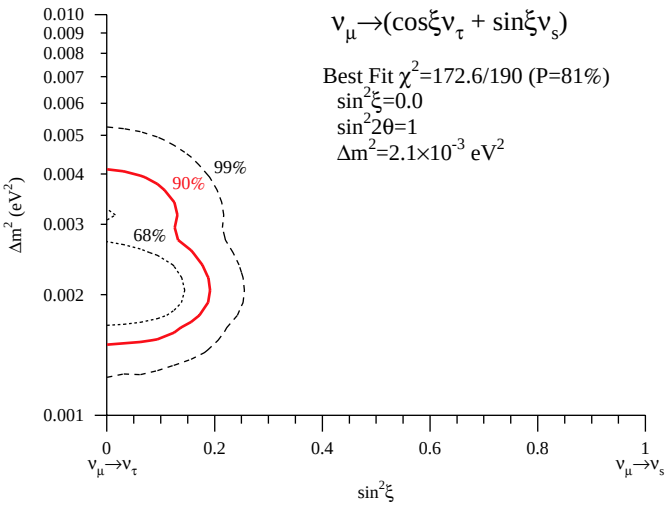

Figure 6: The allowed admixture of $\nu_{sterile}$ in a 4ν analysis of the Super-Kamiokande data.

where a 3×3 unitary matrix mixes the mass eigenstates with the flavor eigenstates. Because the earth is full of electrons, but devoid of free muons or tauons, a component of electron neutrino flavor passing through the earth may be enhanced by a matter effect resonance. The size of the resonant enhancement depends on neutrino energy and the pathlength through matter; therefore, this can potentially be observed by measuring a larger rate than expected in some narrow regions of zenith angle and energy. If one mass splitting dominates in scale over the other, as seems to be the case considering the likely results for solar neutrinos, the oscillation probabilities $P(\nu_e \leftrightarrow \nu_\mu)$, $P(\nu_\mu \leftrightarrow \nu_\tau)$, and $P(\nu_\tau \leftrightarrow \nu_e)$ may be expressed as functions of three parameters: two mixing angles (θ_{13}, θ_{23}) and the larger mass splitting Δm^2.

The Super-Kamiokande group has analyzed the sample of electron neutrino interactions with fine binning, but sees no deviation from the predicted rates. This null result is then turned into limits on the three mixing parameters, as shown by contours in Fig. 7. The left panel shows that the small fraction of ν_e appearance allowed by the data is consistent with the limit on ν_e disappearance from the Chooz [19] reactor experiment. In fact, the data is consistent with no ν_e mixing whatsoever.

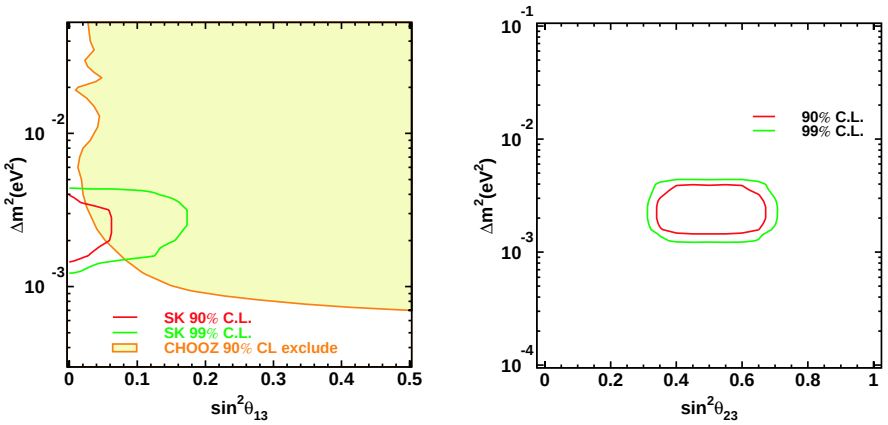

Figure 7: Contours for the mixing parameters of three active neutrinos, in the single dominant Δm^2 scenario, as allowed by 1489 days of Super-Kamiokande data.

5 Tau Appearance

If $\nu_\mu \leftrightarrow \nu_\tau$ oscillation is taking place, tau leptons should appear in the atmospheric neutrino flux. Most atmospheric ν_τ do not have more than the $\approx 3.5 GeV$ of energy needed to produce a τ lepton, however, in the large Super-K sample one does expect approximately 85 charged current ν_τ interactions. The events have many final state particles above Cherenkov threshold making exclusive reconstruction difficult, but a statistical analysis is possible. One preliminary analysis uses a neural network to select for characteristics of high p_t pion production, based on event variables such as number of rings, number of ring seeds, number-of-decay electrons, particle classification of the brightest ring, and so on.

For Δm^2 less than a few times $10^{-3}\mathrm{eV}^2$, it is expected that charged current tau appearance will only occur in the upward-going zenith bins. Therefore, the analysis is based on the up-down ratio of a sample selected for enhanced tau production, and the downward-going data may be used to check the performance of the neural network, as shown on the left of Fig. 8. This analysis has a 55% efficiency to save ν_τ interactions in the fiducial volume while keeping 4.5% of the background. After cuts, a fit is done to the zenith angle distribution with components for both the background and the expected tau appearance signal. The data and fit results are shown on the right of Fig. 8.

The best fit implies that the number of charged current ν_τ interactions was: $99 \pm 39_{stat} \pm 13_{\Delta m^2}{}^{+0}_{-15(3\nu)}$. The first systematic error comes from varying the assumed Δm^2 between 1 and 5 $\times 10^{-3} eV^2$ and the second comes from allowing three flavor oscillation at the CHOOZ limit. Although this is only a 2.3σ result, it shows that the Super-K data set is consistent with the expected rate of tau appearance.

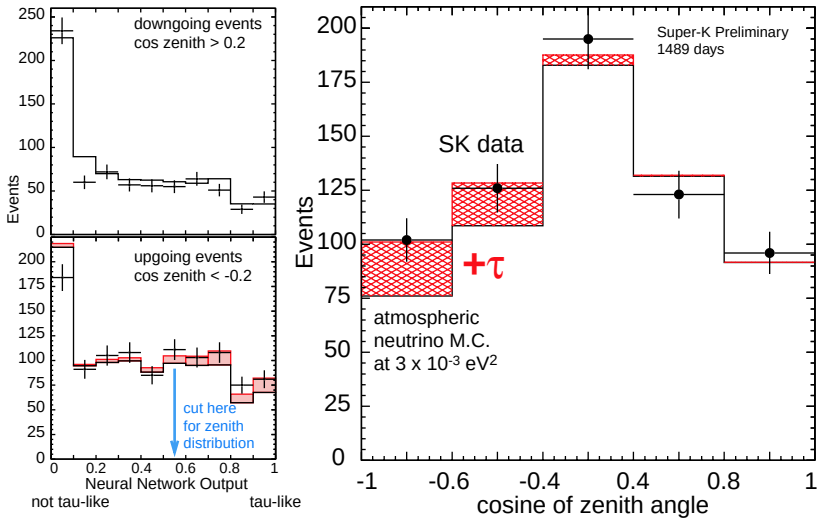

Figure 8: The left panels show the performance of the neural network identification. The right panel shows the zenith distribution of events selected as τ-like; the filled region shows the relative proportion of τ appearance that must be added to the atmospheric neutrino Monte Carlo to agree with the data.

6 Super-Kamiokande Accident and Reconstruction

On Nov 12, 2001 at 11:01 JST, a single photomultiplier on the bottom of the Super-Kamiokande tank imploded. At that time, the tank was 2/3 full of water; it was refilling after PMT replacement work in the preceding summer. The imploding tube caused a chain reaction that destroyed 6777 inner PMTs and 1100 outer PMTs. Subsequently, the collaboration made several studies to determine the mechanism of the chain reaction. A corrective measure was devised: the PMTs should be encased in a secondary shell consisting of a

transparent acrylic hemisphere over the photocathode and a fiberglass shell surrounding the rest of the tube. This enclosure is not intended to withstand static water pressure; instead, several small holes are placed in the shell. Then, if a PMT were to implode, water rushes into the resulting vacancy more slowly and a high pressure shock wave is not developed. This has been tested several times *in situ* up to the full level of the Super-K tank. The tests show that if the center tube of a grid of 3×3 tubes is imploded, the damage is contained within the protective vessel, and the eight surrounding tubes do not implode – even if they themselves are unprotected.

It will take several years to fabricate replacement photomultipliers for the inner detector. In the meantime, the detector is being recommissioned using the remaining tubes plus some spares to populate every other lattice point of the original photomultiplier tube array. This will be sufficient for nearly all research to continue, particularly the K2K long baseline experiment. The detector should be operational by the end of 2002.

7 Acknowledgements

I would like to thank the organizers of the Heavy Quarks and Leptons Workshop, particularly G. Cataldi. I am also thankful for assistance with the latest experimental results from M. Shiozawa, M. Goodman, and M. Spurio. Finally, I gratefully acknowledge support from the U.S. Department of Energy.

References

1. T.K. Gaisser and M. Honda, submitted to Ann.Rev.Nucl.Part.Sci. hep-ph/0203272

2. T. Sanuki *et al.*, Astrophys. J **533**, 1135 (2000).

3. J. Alcarez *et al.*. Phys. Lett. **B490**, 27 (2000).

4. M. Honda *et al.*, Phys. Rev. **D52**, 4985 (1995); M. Honda *et al.*, Phys. Lett. **B248**, 193 (1990).
   V. Agrawal *et al.*, Phys. Rev. **D53**, 1314 (1996); T.K. Gaisser and T. Stanev, Proc. 24th Int. Cosmic Ray Conf., Rome, Vol. 1, 694 (1995); G. Barr *et al.*, Phys. Rev. **D39**, 3532 (1989).

5. G. Battistoni *et al.*, Astropart. Phys. **12** 315, (2000);
P. Lipari, Astropart. Phys. **14** 153, (2000);
M. Honda *et al.*, Phys. Rev. **D64** 053011, (2001);
Y. Tserkovnyak *et al.*, Proc. 27th Intl. Cosmic Ray Conf. **3** 1218, (2001);

6. Y. Fukuda *et al.*, Phys. Rev. Lett. **81**, 1562 (1998).

7. M. Shiozawa, for the Super-Kamiokande collaboration, presentation at XXth Int. Conf. on Neutrino Physics and Astrophysics, Munich, (2002).

8. M. Aglietta *et al.*, Europhys. Lett. **8** 6111, (1989).

9. K. Daum *et al.*, Z. Phys. **C66**, 417 (1995).

10. W.W.M. Allison *et al.*, Phys. Lett. **B449**, 137 (1999);
M. Sanchez, Int. J. Mod. Phys. **A16S1B**, 727 (2001);
ibid, poster at XXth Int. Conf. on Neutrino Physics and Astrophysics, Munich, (2002). http://neutrino2002.ph.tum.de/pages/posters/B02.html

11. M. Ambrosio *et al.*, Phys. Lett. **B434**, 451 (1998);
M. Spurio, poster at XXth Int. Conf. on Neutrino Physics and Astrophysics, Munich, (2002). http://neutrino2002.ph.tum.de/pages/posters/B02.html

12. M. Ambrosio *et al.*, physics/0203018.

13. M. Ambrosio *et al.*, Phys. Lett. **B112**, 5 (2000).

14. K. Nishikawa, for the K2K collaboration, presentation at XXth Int. Conf. on Neutrino Physics and Astrophysics, Munich, (2002).

15. V. Barger *et al.*, Phys. Lett. **B462**, 109 (1999).

16. S.L. Glashow *et al.*, Phys. Rev. **D56**, 2433 (1997); G.L. Fogli *et al.*, Phys. Rev. **D60**, 053006 (1999); N. Fornengo *et al.*, Phys. Rev. **D65**, 013010 (2002).

17. E. Lisi, A. Marrone, and D. Montanino, Phys. Rev. Lett. **85**, 1166 (2000).

18. G.L. Fogli, E. Lisi, and A. Marrone, Phys. Rev. **D63**, 053008 (2001).

19. M. Apollonio *et al.*, Phys. Rev. **D61**, 012001 (2000).

Frascati Physics Series Vol. XXVIII (2002), pp.427-435
HQ & L 2002 – Vietri s/m, May 27th - June 1st, 2002

LONG BASELINE NEUTRINO EXPERIMENTS

Lionel Chaussard
Institut de Physique Nucléaire
Université Claude Bernard Lyon I
4 rue Enrico Fermi
F-69622 Villeurbanne cedex

ABSTRACT

We present a summary of the existing and foreseen experiments using standard neutrino beams, neutrino superbeams and neutrino factories, trying to show the physics potential of these experiments with respect to the study of neutrino oscillation.

1 Introduction: the need for man-made neutrino beams

The study of atmospheric and solar neutrinos have clearly shown a neutrino disappearance. SuperKamiokande has successfully demonstrated that the disappearance of atmospheric neutrinos is compatible with neutrino oscillations, with a preference for $\nu_\mu \to \nu_\tau$ transitions. The CHOOZ experiment has set up stringent limits on the hypothesis of $\nu_\mu \to \nu_e$ oscillations.

In order now to prove the oscillations, constrain the MNS unitarity triangle and in particular measure the CP violating phase and the θ_{13} mixing angle, controlled neutrino and antineutrino sources are needed. Neutrino beams can be produced in a "standard" way (K2K, CNGS): shooting protons on a target produces kaons and pions which decay into muons and neutrinos. The experiments on such beams will mainly control the sector of atmospheric neutrino oscillations. High intensity proton beams can be used to produce neutrino superbeams (JHF), which can be used as a staging step toward the measurement of solar neutrino oscillations. At last, muon storage rings could serve as neutrino factories in the far future in order to study matter effects and CP violation.

2 "Standard" neutrino beams

2.1 K2K [1) 2)]

An almost pure ν_μ beam is produced at KEK in Japan from 12 GeV protons shot on an Aluminium target. The neutrino beam has a low energy (1.3 GeV, so below the τ production threshold) and is directed to the SuperKamiokande water Cherenkov detector (22.5 kTons fiducial mass). A close detector composed of a 1 kTon (25 Tons fiducial mass) water Cherenkov tank completed with a scintillation fibre tracker and a μ range detector, placed at 300 m, allow to control the beam intensity, spectrum and composition. Data taking started in March 1999 and was stopped in November 2001 by the implosion of half of the 13000 photomultiplicators, restart is foreseen by the end of year 2002.

K2K is a "disappearance" experiment: from 4.8 10^{19} protons delivered on target (p.o.t.), $80.1^{+6.2}_{-5.4}$ fully contained events are expected in the far detector in the absence of oscillations ; only 56 events are seen. Using also a fit to the shape of the reconstructed neutrino energy spectrum, the oscillation parameters values are found to be consistent with the atmospheric neutrino results: the best fit value for $sin^2 2\theta$ is 1, and Δm^2 is found to be 2.8 10^{-3} eV^2 (with limits 1.5 - 3.9 x 10^{-3} eV^2 for $sin^2 2\theta = 1$ at 90% C.L.). The null oscillation probability is less than 1%. These results are already impressive, but one has to note that K2K will not cover the whole SuperKamiokande allowed region, even with the whole statistics it has been built for (10^{20} p.o.t., see fig. 1).

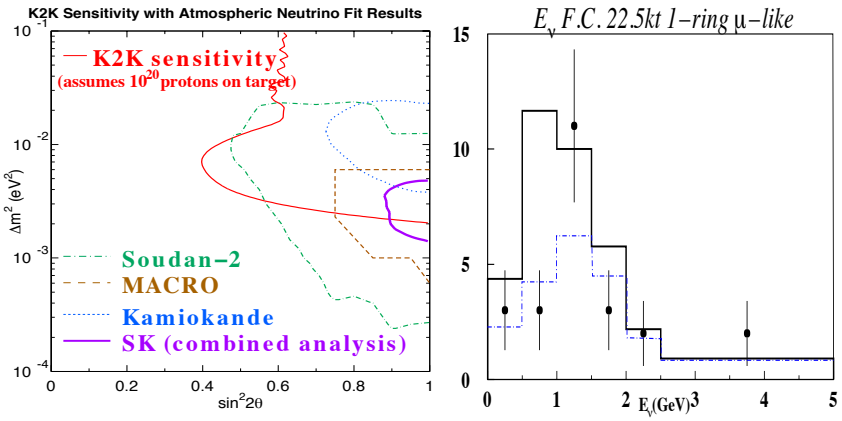

Figure 1: *Left: K2K sensitivity. Right: neutrino energy distribution for CC events, the dotted line corresponds to the spectrum expected with neutrino oscillations tuned to atmospheric results, the full line to the spectrum expected without oscillations.*

2.2 NuMI-MINOS [3)]

The NuMI beam will be a tunable 1 to 25 GeV ν_μ beam obtained from 120 GeV protons shot at FNAL on a graphite or Beryllium target. A close detector (approx. 1 kTon at 290 m) and a far detector (5.4 kTon at 730 km) will be used by the MINOS Collaboration to work in the disappearance mode. These two detectors will be tracking calorimeters, made of steel octogonal planes interleaved with sensitive planes of plastic scintillator strips. Light will be collected in the strips by wavelength shifting fibres and read at both ends by multianode photomultiplicators. The far detector should be operational by late 2003, the near detector should be completed and tested late 2004 and the beam commissioning is expected by end 2004 - early 2005.

In two years of data taking, MINOS should cover the whole region allowed by SuperKamiokande atmospheric results, with a sensitivity down to 8 10^{-4} eV^2 at maximal mixing. In case of oscillations, the study of dips position in the charged current energy distribution should allow a measurement of Δm^2 and $sin^2 2\theta$ (see fig. 2).

A study of the ratio of short (neutral currents) to long (charged cur-

rent) events should also allow some discrimination of $\nu_\mu \to \nu_\tau$ and $\nu_\mu \to \nu_e$ hypotheses.

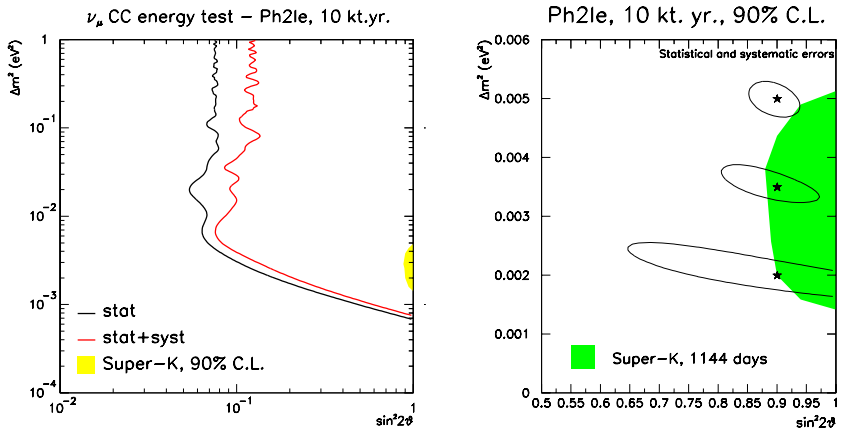

Figure 2: *Left: MINOS sensitivity. Right: example of measurements reachable by MINOS for $sin^2 2\theta = 0.8$ and several values of Δm^2.*

2.3 CNGS experiments

CERN foresees to produce a ν_μ beam [4) 5)] from 400 GeV protons shot out of the SPS on a graphite target. This beam, directed to the Gran Sasso laboratory (LNGS) 732 km away, is optimized for ν_τ appearance, with a 17 GeV mean energy. In the baseline option, 4.5 10^{19} p.o.t./year are expected. Civil engeneering has already started and first neutrinos should be produced in Spring 2006. Two detectors, OPERA and ICARUS, will be installed in the LNGS to study this beam.

2.3.1 OPERA [6) 7)]

OPERA wil be a massive lead/emulsion detector designed for ν_τ appearance. 56 lead plates (1 mm thick) and 56 emulsion sheets (two emulsion layers 50 μm thick each, on a 200 μm plastic base) will be arranged in a 4 inches x 5 inches brick. 52 x 64 bricks will be arranged in a wall, 31 walls will form a supermodule and two supermodules are foreseen for a 1.8 kTon detector. Neutrino interactions will occur in lead, and emulsions will be scanned to reconstruct

tracks. Planes of plastic scintillator strips *à la* MINOS will be interleaved between brick walls in order to trigger the experiment and allow to find the hit bricks which will be taken out by a robot for scanning. A muon spectrometer instrumented with resistive plate chambers will be placed downstream each supermodule to complete the analysis of the events. OPERA has been approved by CERN and LNGS commitees in February 2001, and detector construction is starting.

ν_τ charged current interactions should be signed almost background-free by the apparition of a τ track with a characteristic "kink" due to the τ decay (see tab. 1). The associated probability of a 3 σ significance for $\Delta m^2 = 2.5$ 10^{-3} eV^2 is greater than 99%. In the absence of signal, OPERA can cover the region corresponding to the atmospheric oscillation parameters, down to 10^{-3} eV^2. At last, OPERA has also a $\nu_\mu \rightarrow \nu_e$ appearance program.

Table 1: *Number of events seen in OPERA for a 5 years run.*

Δm^2 (10^{-3} eV^2)	N_τ	$N_{background}$
1.3	4	0.75
2.5	10	0.75
4.0	26	0.75

2.3.2 ICARUS [8)]

ICARUS is a project based on the use of 300 Tons liquid argon time projection chambers, which benefits from a full 3D event reconstruction. A first module has been mounted and tested in Pavia last year, two modules are on the way to be installed in the LNGS with a project of cosmic run early 2003 waiting for the CNGS beam.

The ν_τ appearance will be signed on the basis of an event-shape likelihood method, where visible and missing momenta play a major role (see fig. 3). The performances of ICARUS are similar to the performances of OPERA, provided that at least 10 modules 300 Tons each are set up. Yet, a 3 sigma effect will need a 40 kTon.year run. The ICARUS sensitivity to $\nu_\mu \rightarrow \nu_e$ oscillations may be a little bit better than in the case of OPERA.

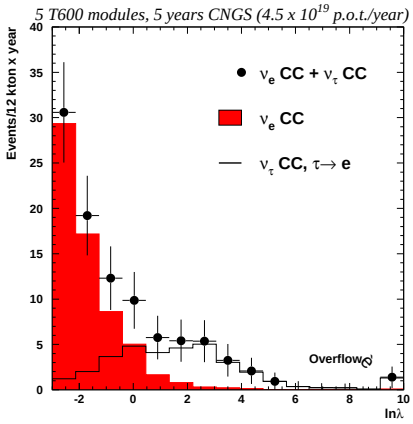

Figure 3: *ICARUS likelihood method to show out τ events in the $\tau \rightarrow e$ channel: for a cut at $ln(\lambda) > 2$, 13 events correspond to a ν_τ interaction, 0.7 event to ν_e background interaction.*

3 Superbeams

High luminosity neutrino beams can be produced by increasing the initial proton beam intensity. Detectors could then be placed off-axis in order to study low energy ν_μ and to reduce ν_e contamination. The corresponding physics program would be ν_μ disappearance and the study of $\nu_\mu \rightarrow \nu_e$ oscillations.

Several projects have been proposed in Japan, in Europe [9) 10)], and in the U.S.A. [11)], but only the Japanese JHF project has been approved yet. In a first phase of this project [12)], the 50 GeV PS situated in JAERI could deliver 3.3 10^{14} protons per 3.3 s cycle, corresponding to a 0.75 MW power. The induced 1 GeV neutrino beam would be directed to SuperKamiokande 295 km away. This first phase could start in 2007. In a second phase, the proton beam power would be increased to 4 MW and SuperKamiokande would be upgraded to HyperKamiokande (1000 kTon).

An order of magnitude could be reached in the atmospheric oscillation sector, with an error on Δm^2 of the order of 10^{-4} eV^2, and an error on $sin^2 2\theta$ around 0.01. In the sector of solar oscillations, a factor 20 could be gained with in particular a limit on $sin^2 2\theta_{13}$ of a few 10^{-3}. The CP violating phase could be measured down to approx. 20 degrees (if the LMA solution is confirmed).

4 Neutrino factories [13] [14] [15] [16] [17]

The ultimate neutrino source could be a muon storage ring. The idea is to start as usual from a proton beam shooting on a target, in order to produce pions and kaons that decay into muons and neutrinos. Then, instead of stopping every particle but the neutrinos, the muons are kept, rapidly cooled and reaccelerated to a few tens of GeV before being stored in a ring with long straight lines. The muon decays along these lines should produce well focused neutrino beams with high intensities and perfectly known composition. The goal is to obtain 10^{20} neutrinos per year. The main problems that are under study concern the targets that should support a high proton beam intensity, and the technology of fast cooling and reaccelerating of the muons. The first ν-factory will probably not be available before 2020.

Massive detectors could be placed at a few 10^3 km on the neutrino beams in order to solve the mass hierarchy ambiguity and measure the CP violating phase by the study of matter effects. As an example, fig. 4 presents the physics potential of neutrino factories compared to that of superbeams, showing that orders of magnitude could be gained [18].

5 Conclusion

Natural neutrino sources allowed physicists to discover neutrino disappearance. Man-made neutrino beams are now mandatory to constrain the mixing matrix. Appearance experiments like OPERA are in particular necessary to prove the $\nu_\mu \to \nu_\tau$ oscillation. Superbeams and neutrino factories could then allow to study $\nu_\mu \to \nu_e$ oscillations and CP violation in the neutrino sector.

References

1. K. Nakamura *et al*, Nucl. Phys. Proc. Suppl. **91**, 203 (2001).
2. S.H. Ahn *et al*, Phys. Lett. **B511**, 178 (2001).
3. MINOS Collaboration, NuMI-NOTE-GEN-0337 (1998).
4. G. Acquistapace *et al*, CERN 98-02, INFN/AE-98/05 (1998).
5. R. Bailey *et al*, CERN-SL/99-034(DI), INFN/AE-99/05 (1999).

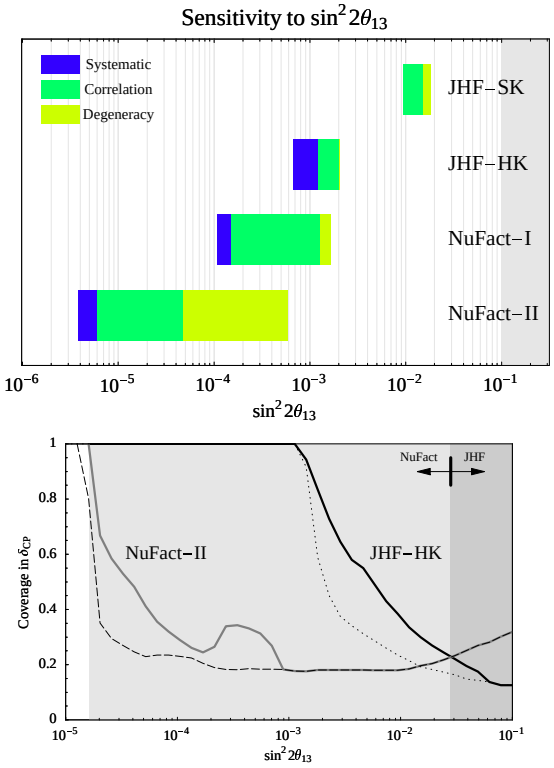

Figure 4: *Comparison of physics potentials of several superbeam scenarios and several neutrino factories scenarios (see [18] for details). First plot shows sensitivity to $sin^2 2\theta_{13}$. Second plot shows the sensitivity to the CP violating phase: 1 means 100% error measurement, 0 means perfect measurement.*

6. M. Guler *et al.*, CERN/SPSC 2000-028, SPSC/P318, LNGS P25/2000 (2000).

7. M. Guler *et al.*, CERN/SPSC 2001-025, SPSC/M668, LNGS-EXP 30/2001 Add. 1/01 (2001).

8. F. Arneodo *et al*, LNGS-EXP 13/89 add.2/01 (2001).

9. H. Minakata *et al*, Nucl. Phys. Proc. Suppl. **110**, 404 (2002).

10. M. Campanelli, hep-ex/0204004 (2002).

11. D.Beavis *et al*, hep-ex/0205040 (2002).

12. Y. Ytow *et al*, hep-ex/0106019 (2001).

13. S. Geer, hep-ph/0008155 (2000).

14. V. Barger *et al*, Phys. Lett. **B485**, 379 (2000).

15. S. Geer, hep-ph/0111016 (2001).

16. S. Geer, hep-ph/0111016 (2001).

17. T. Adams *et al*, hep-ph/0111030 (2001).

18. P.Huber *et al*, hep-ph/0204352 (2002).

tracks. Planes of plastic scintillator strips *à la* MINOS will be interleaved between brick walls in order to trigger the experiment and allow to find the hit bricks which will be taken out by a robot for scanning. A muon spectrometer instrumented with resistive plate chambers will be placed downstream each supermodule to complete the analysis of the events. OPERA has been approved by CERN and LNGS commitees in February 2001, and detector construction is starting.

ν_τ charged current interactions should be signed almost background-free by the apparition of a τ track with a characteristic "kink" due to the τ decay (see tab. 1). The associated probability of a 3 σ significance for $\Delta m^2 = 2.5$ 10^{-3} eV^2 is greater than 99%. In the absence of signal, OPERA can cover the region corresponding to the atmospheric oscillation parameters, down to 10^{-3} eV^2. At last, OPERA has also a $\nu_\mu \rightarrow \nu_e$ appearance program.

Table 1: *Number of events seen in OPERA for a 5 years run.*

Δm^2 (10^{-3} eV^2)	N_τ	$N_{background}$
1.3	4	0.75
2.5	10	0.75
4.0	26	0.75

2.3.2 ICARUS [8)]

ICARUS is a project based on the use of 300 Tons liquid argon time projection chambers, which benefits from a full 3D event reconstruction. A first module has been mounted and tested in Pavia last year, two modules are on the way to be installed in the LNGS with a project of cosmic run early 2003 waiting for the CNGS beam.

The ν_τ appearance will be signed on the basis of an event-shape likelihood method, where visible and missing momenta play a major role (see fig. 3). The performances of ICARUS are similar to the performances of OPERA, provided that at least 10 modules 300 Tons each are set up. Yet, a 3 sigma effect will need a 40 kTon.year run. The ICARUS sensitivity to $\nu_\mu \rightarrow \nu_e$ oscillations may be a little bit better than in the case of OPERA.

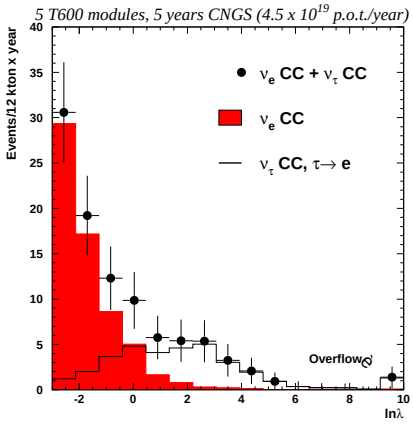

Figure 3: *ICARUS likelihood method to show out τ events in the $\tau \rightarrow e$ channel: for a cut at $ln(\lambda) > 2$, 13 events correspond to a ν_τ interaction, 0.7 event to ν_e background interaction.*

3 Superbeams

High luminosity neutrino beams can be produced by increasing the initial proton beam intensity. Detectors could then be placed off-axis in order to study low energy ν_μ and to reduce ν_e contamination. The corresponding physics program would be ν_μ disappearance and the study of $\nu_\mu \rightarrow \nu_e$ oscillations.

Several projects have been proposed in Japan, in Europe [9) 10)], and in the U.S.A. [11)], but only the Japanese JHF project has been approved yet. In a first phase of this project [12)], the 50 GeV PS situated in JAERI could deliver 3.3 10^{14} protons per 3.3 s cycle, corresponding to a 0.75 MW power. The induced 1 GeV neutrino beam would be directed to SuperKamiokande 295 km away. This first phase could start in 2007. In a second phase, the proton beam power would be increased to 4 MW and SuperKamiokande would be upgraded to HyperKamiokande (1000 kTon).

An order of magnitude could be reached in the atmospheric oscillation sector, with an error on Δm^2 of the order of 10^{-4} eV^2, and an error on $sin^2 2\theta$ around 0.01. In the sector of solar oscillations, a factor 20 could be gained with in particular a limit on $sin^2 2\theta_{13}$ of a few 10^{-3}. The CP violating phase could be measured down to approx. 20 degrees (if the LMA solution is confirmed).

4 Neutrino factories [13] [14] [15] [16] [17]

The ultimate neutrino source could be a muon storage ring. The idea is to start as usual from a proton beam shooting on a target, in order to produce pions and kaons that decay into muons and neutrinos. Then, instead of stopping every particle but the neutrinos, the muons are kept, rapidly cooled and reaccelerated to a few tens of GeV before being stored in a ring with long straight lines. The muon decays along these lines should produce well focused neutrino beams with high intensities and perfectly known composition. The goal is to obtain 10^{20} neutrinos per year. The main problems that are under study concern the targets that should support a high proton beam intensity, and the technology of fast cooling and reaccelerating of the muons. The first ν-factory will probably not be available before 2020.

Massive detectors could be placed at a few 10^3 km on the neutrino beams in order to solve the mass hierarchy ambiguity and measure the CP violating phase by the study of matter effects. As an example, fig. 4 presents the physics potential of neutrino factories compared to that of superbeams, showing that orders of magnitude could be gained [18].

5 Conclusion

Natural neutrino sources allowed physicists to discover neutrino disappearance. Man-made neutrino beams are now mandatory to constrain the mixing matrix. Appearance experiments like OPERA are in particular necessary to prove the $\nu_\mu \to \nu_\tau$ oscillation. Superbeams and neutrino factories could then allow to study $\nu_\mu \to \nu_e$ oscillations and CP violation in the neutrino sector.

References

1. K. Nakamura *et al*, Nucl. Phys. Proc. Suppl. **91**, 203 (2001).
2. S.H. Ahn *et al*, Phys. Lett. **B511**, 178 (2001).
3. MINOS Collaboration, NuMI-NOTE-GEN-0337 (1998).
4. G. Acquistapace *et al*, CERN 98-02, INFN/AE-98/05 (1998).
5. R. Bailey *et al*, CERN-SL/99-034(DI), INFN/AE-99/05 (1999).

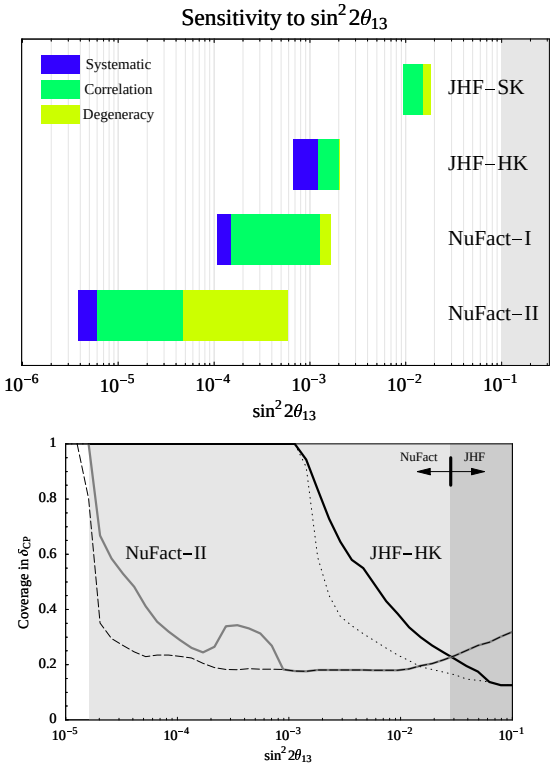

Figure 4: *Comparison of physics potentials of several superbeam scenarios and several neutrino factories scenarios (see [18] for details). First plot shows sensitivity to $sin^2 2\theta_{13}$. Second plot shows the sensitivity to the CP violating phase: 1 means 100% error measurement, 0 means perfect measurement.*

6. M. Guler *et al.*, CERN/SPSC 2000-028, SPSC/P318, LNGS P25/2000 (2000).

7. M. Guler *et al.*, CERN/SPSC 2001-025, SPSC/M668, LNGS-EXP 30/2001 Add. 1/01 (2001).

8. F. Arneodo *et al*, LNGS-EXP 13/89 add.2/01 (2001).

9. H. Minakata *et al*, Nucl. Phys. Proc. Suppl. **110**, 404 (2002).

10. M. Campanelli, hep-ex/0204004 (2002).

11. D.Beavis *et al*, hep-ex/0205040 (2002).

12. Y. Ytow *et al*, hep-ex/0106019 (2001).

13. S. Geer, hep-ph/0008155 (2000).

14. V. Barger *et al*, Phys. Lett. **B485**, 379 (2000).

15. S. Geer, hep-ph/0111016 (2001).

16. S. Geer, hep-ph/0111016 (2001).

17. T. Adams *et al*, hep-ph/0111030 (2001).

18. P.Huber *et al*, hep-ph/0204352 (2002).

tracks. Planes of plastic scintillator strips *à la* MINOS will be interleaved between brick walls in order to trigger the experiment and allow to find the hit bricks which will be taken out by a robot for scanning. A muon spectrometer instrumented with resistive plate chambers will be placed downstream each supermodule to complete the analysis of the events. OPERA has been approved by CERN and LNGS commitees in February 2001, and detector construction is starting.

ν_τ charged current interactions should be signed almost background-free by the apparition of a τ track with a characteristic "kink" due to the τ decay (see tab. 1). The associated probability of a 3 σ significance for $\Delta m^2 = 2.5$ 10^{-3} eV^2 is greater than 99%. In the absence of signal, OPERA can cover the region corresponding to the atmospheric oscillation parameters, down to 10^{-3} eV^2. At last, OPERA has also a $\nu_\mu \rightarrow \nu_e$ appearance program.

Table 1: *Number of events seen in OPERA for a 5 years run.*

Δm^2 (10^{-3} eV^2)	N_τ	$N_{background}$
1.3	4	0.75
2.5	10	0.75
4.0	26	0.75

2.3.2 ICARUS [8)]

ICARUS is a project based on the use of 300 Tons liquid argon time projection chambers, which benefits from a full 3D event reconstruction. A first module has been mounted and tested in Pavia last year, two modules are on the way to be installed in the LNGS with a project of cosmic run early 2003 waiting for the CNGS beam.

The ν_τ appearance will be signed on the basis of an event-shape likelihood method, where visible and missing momenta play a major role (see fig. 3). The performances of ICARUS are similar to the performances of OPERA, provided that at least 10 modules 300 Tons each are set up. Yet, a 3 sigma effect will need a 40 kTon.year run. The ICARUS sensitivity to $\nu_\mu \rightarrow \nu_e$ oscillations may be a little bit better than in the case of OPERA.

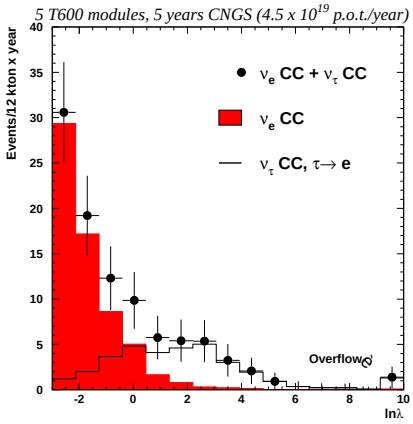

Figure 3: *ICARUS likelihood method to show out τ events in the $\tau \rightarrow e$ channel: for a cut at $ln(\lambda) > 2$, 13 events correspond to a ν_τ interaction, 0.7 event to ν_e background interaction.*

3 Superbeams

High luminosity neutrino beams can be produced by increasing the initial proton beam intensity. Detectors could then be placed off-axis in order to study low energy ν_μ and to reduce ν_e contamination. The corresponding physics program would be ν_μ disappearance and the study of $\nu_\mu \rightarrow \nu_e$ oscillations.

Several projects have been proposed in Japan, in Europe [9) 10)], and in the U.S.A. [11)], but only the Japanese JHF project has been approved yet. In a first phase of this project [12)], the 50 GeV PS situated in JAERI could deliver 3.3 10^{14} protons per 3.3 s cycle, corresponding to a 0.75 MW power. The induced 1 GeV neutrino beam would be directed to SuperKamiokande 295 km away. This first phase could start in 2007. In a second phase, the proton beam power would be increased to 4 MW and SuperKamiokande would be upgraded to HyperKamiokande (1000 kTon).

An order of magnitude could be reached in the atmospheric oscillation sector, with an error on Δm^2 of the order of 10^{-4} eV^2, and an error on $sin^2 2\theta$ around 0.01. In the sector of solar oscillations, a factor 20 could be gained with in particular a limit on $sin^2 2\theta_{13}$ of a few 10^{-3}. The CP violating phase could be measured down to approx. 20 degrees (if the LMA solution is confirmed).

4 Neutrino factories [13] [14] [15] [16] [17]

The ultimate neutrino source could be a muon storage ring. The idea is to start as usual from a proton beam shooting on a target, in order to produce pions and kaons that decay into muons and neutrinos. Then, instead of stopping every particle but the neutrinos, the muons are kept, rapidly cooled and reaccelerated to a few tens of GeV before being stored in a ring with long straight lines. The muon decays along these lines should produce well focused neutrino beams with high intensities and perfectly known composition. The goal is to obtain 10^{20} neutrinos per year. The main problems that are under study concern the targets that should support a high proton beam intensity, and the technology of fast cooling and reaccelerating of the muons. The first ν-factory will probably not be available before 2020.

Massive detectors could be placed at a few 10^3 km on the neutrino beams in order to solve the mass hierarchy ambiguity and measure the CP violating phase by the study of matter effects. As an example, fig. 4 presents the physics potential of neutrino factories compared to that of superbeams, showing that orders of magnitude could be gained [18].

5 Conclusion

Natural neutrino sources allowed physicists to discover neutrino disappearance. Man-made neutrino beams are now mandatory to constrain the mixing matrix. Appearance experiments like OPERA are in particular necessary to prove the $\nu_\mu \to \nu_\tau$ oscillation. Superbeams and neutrino factories could then allow to study $\nu_\mu \to \nu_e$ oscillations and CP violation in the neutrino sector.

References

1. K. Nakamura *et al*, Nucl. Phys. Proc. Suppl. **91**, 203 (2001).
2. S.H. Ahn *et al*, Phys. Lett. **B511**, 178 (2001).
3. MINOS Collaboration, NuMI-NOTE-GEN-0337 (1998).
4. G. Acquistapace *et al*, CERN 98-02, INFN/AE-98/05 (1998).
5. R. Bailey *et al*, CERN-SL/99-034(DI), INFN/AE-99/05 (1999).

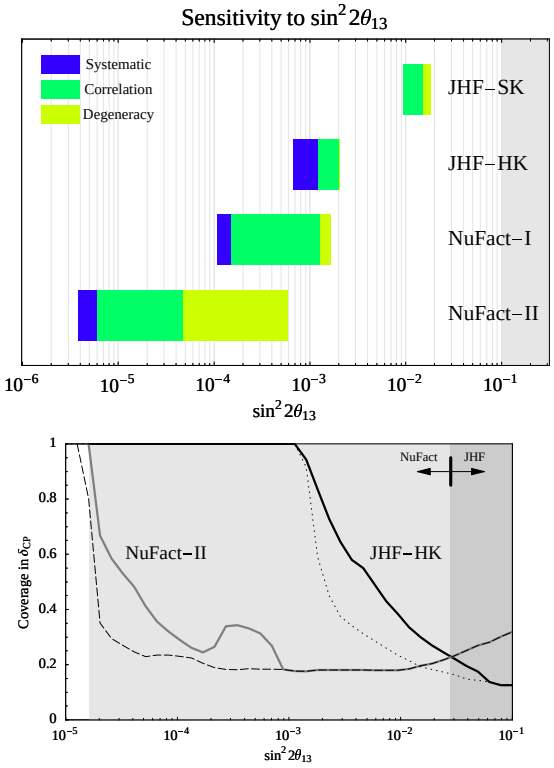

Figure 4: *Comparison of physics potentials of several superbeam scenarios and several neutrino factories scenarios (see [18] for details). First plot shows sensitivity to $sin^2 2\theta_{13}$. Second plot shows the sensitivity to the CP violating phase: 1 means 100% error measurement, 0 means perfect measurement.*

6. M. Guler *et al.*, CERN/SPSC 2000-028, SPSC/P318, LNGS P25/2000 (2000).

7. M. Guler *et al.*, CERN/SPSC 2001-025, SPSC/M668, LNGS-EXP 30/2001 Add. 1/01 (2001).

8. F. Arneodo *et al*, LNGS-EXP 13/89 add.2/01 (2001).

9. H. Minakata *et al*, Nucl. Phys. Proc. Suppl. **110**, 404 (2002).

10. M. Campanelli, hep-ex/0204004 (2002).

11. D.Beavis *et al*, hep-ex/0205040 (2002).

12. Y. Ytow *et al*, hep-ex/0106019 (2001).

13. S. Geer, hep-ph/0008155 (2000).

14. V. Barger *et al*, Phys. Lett. **B485**, 379 (2000).

15. S. Geer, hep-ph/0111016 (2001).

16. S. Geer, hep-ph/0111016 (2001).

17. T. Adams *et al*, hep-ph/0111030 (2001).

18. P.Huber *et al*, hep-ph/0204352 (2002).